JOURNAL OF BIOLOGICAL REGULATORS & HOMEOSTATIC AGENTS
Volume 34, No. 6, November - December, 2020

CONTENTS

Editorials

P. Conti, Al. Caraffa, C.E. Gallenga, R. Ross, S.K. Kritas, I. Frydas, A. Younes and G. Ronconi. Coronavirus-19 (SARS-CoV-2) induces acute severe lung inflammation via IL-1 causing cytokine storm in COVID-19: A promising inhibitory strategy 1971

M. Aslan Kayıran, A.S. Karadag and U. Wollina. Approach to skin malignancies in COVID-19 pandemic days 1977

Review article

R. Cardani, E.G. Bertoldo, A. Cerri, M. Picozzi, M.M. Corsi Romanelli and E. Callus. Establishment of a cardiac biobank in a Department of Pathology and Laboratory Medicine 1983

Original articles

S-Q. Ma, Y-C. Wang, Y. Li, X-Y. Li, J. Yang and Y-M. Sheng. LncRNA XIST promotes proliferation and cisplatin resistance of oral squamous cell carcinoma by downregulating miR-27b-3p 1993

A. Socha-Banasiak, S.G. Pierzynowski, P. Szczurek, J. Woliński, A. Wesołowska, E. Czkwianianc and K. Pierzynowska. Gut response to pasteurized donor human milk in a porcine model of the premature infant 2003

W-W. He, H-T. Ma, X. Guo, W-M. Wu, E-J. Gao and Y-H. Zhao. lncRNA SNHG3 accelerates the proliferation and invasion of non-small cell lung cancer by downregulating miR-340-5p 2017

Y. Jiang, WJ. Zhang, AM. Liang, GW. Lv, BD. Ma, H. Yue, L. Sun and H. Zhang. Cholesterol 24S-Hydroxylase overexpression increases the lipid droplet formation of human umbilical cord mesenchymal stem cells but does not affect adipocyte differentiation 2029

Y. Wang, R.-K. Zang and Y.-N. Du. HSA_CIRC_0004050 on proliferation and apoptosis of A549 cells through ERK/JNK signaling pathway 2037

HL. Li, PH. Han, DQ. Pan, G. Chen, XH. Lu and J- Li. LncRNA XIST regulates cell proliferation, migration and invasion of glioblastoma via regulating miR-448 and ROCK1 2049

W-P. Zhang, Y. Wang, D. Tan and C-G. Xing. Cystatin 2 leads to a worse prognosis in patients with gastric cancer 2059

R. Liu, Y. Li, D-X. Yang, M. Xu, Y-X. Yan, F-G. Zhou, Y-M. Liu, C. Xu, K. Zhao, G-Y. Jiang and M-W. Liu. Serum metabolic markers and metabolic pathways in rats with metabolomic cecal ligation and puncture-induced sepsis 2069

Letters to the Editor

JJ. Jin, LX. Xu, D. Zhang, CX. Wang, Z. Fan, TT. Xu, S. Wang and Y. Huang. Histological analysis of epidermal growth factor receptor gene mutation and clinical characteristics of advanced peripheral lung cancer 2079

T.-M. Qi, F.-R. Wang, C.-M. Fan, L.-M. Liu, J.-Y. Zhou, X.-C. Lin and A.-X. Suonan. Repairing effects of liraglutide on spinal cord injury in rats via PI3K/AKT/ENOS signaling pathway 2083

Y. Tai, J. Li, XH. Zhang, JF. Fu and J. Wang. Expression of ERR-α in ovarian cancer and endometrial carcinoma and its significance 2091

LL. Wang, X. Li, HT. Tian, Y. Sun and C. Sun. Comparison of effects of chloroprocaine and lidocaine epidural block on emergency response of gynecologic patients after pelvic surgery 2097

J. Zhang, CH. Wang, XJ. Liu, SF. Cheng, LH. Han and CL. Lv. Efficacy and safety analysis of dopamine combined with creatine phosphate sodium in the treatment of infantile pneumonia combined with heart failure 2103

W. Hameed, N. Sheikh, I. Liaqat, M. Mukhtar, A. Tayyab, F. Azam and R. Mehmood. Gene expression of *RAGE, HMGB1* and *BAX* as Genetic markers of diabetic myocardial infarction in population of Pakistan 2109

H. Liu, XR. Ding, YQ. Song, C. Jiang, XM. Zhong and HX. Hui. Neoadjuvant chemotherapy combined with concurrent chemoradiotherapy *versus* concurrent chemoradiotherapy alone on locally advanced nasopharyngeal carcinoma 2115

WH. Song, A. Liu, YF. Zhu[3], SY. Wang, XH. Yang and LN. Ma. Effects of butylphthalide on cognitive dysfunction and expression of superoxide dismutase and Smac in cortex of rats with chronic cerebral ischemia 2121

H-X. Li, J. Zhao, L. Liu, Y. Li, L-H. Yin, P. Fu and H-F. Li. Protective effect of sufentanil on skeletal muscle wasting in patients with sepsis 2127

Q. Wu, ZP. He, TQ. Chen, XB. Shen and PJ. Shi. Changes of related hormone levels in patients with acute coronary syndrome and their clinical significance 2131

XL. Sun, L. Sun, WX. Sun, XL. Zong. A comparative study of dexmedetomidine in combination with midazolam and dexmedetomidine alone for sedation during spinal anesthesia 2135

HL. Xue, ZK. Liu, LL. Wang, Z. Meng, JX. Du and YL. Li. Effect of general anesthesia combined with epidural anesthesia on cognitive function, stress response and NLR after radical mastectomy 2141

Z-F. Li, M-Y. Xu, D-H. Zhang, T-T. Gao, Z. Gao and H. Li. Effects of ulinastatin combined with octreotide on blood coagulation function, inflammatory factors and amylase in patients with severe acute pancreatitis 2147

YJ. He, DN. Yi, CF. Cai, CY. Zhu, WT. Zhan and L. Chen. Serum anti-Mullerian hormone level and its predictive value for pregnancy outcomes in women of late reproductive age 2153

XJ. Huang, Y. Yang, ZM. Deng, Y. Kuang, H. Shi, WY. Li and MY. Li. *Clostridium novyi* exhibits antitumor effect in mice transplanted with H22 hepatocarcinoma by down-regulation of hypoxia-inducible factor-1α 2159

HJ. He, DB. Xu, XY. Zheng, YQ. Yang, WP. Zheng and XL. Tao. Effects of prophylactic injection of methoxamine on pregnant women undergoing cesarean delivery using spinal anesthesia 2165

HY. Gong, ZY. Wang, YZ. Sui, JJ. Zhao, YY. Jing and M. Wang. Effects of dexmedetomidine combined with propofol on peri-anesthesia hemodynamics and postoperative sedation and analgesia in patients undergoing radical esophagectomy 2171

W. Chen, L. Wu, LF. Jiang, YQ. Hu, Y. Zhai, JH. Li, Y. Wu and N. Tang. Yifei Xuanfei Jiangzhuo Chinese bioformulation improves cognitive function in a murine model of vascular dementia – the implication of PI3K/AKT and Erk signalling pathway 2177

J. Han, M. Jiu and W-D. Fan. Investigating the relationship between peripheral blood eosinophils and myocardial infarction complicated by *Helicobacter pylori* infection 2185

Y. Li, JJ. Fu, YY. Sun, XD. Zhang and X. Geng. Exploring the role of serum fibroblast growth factor 21 in thyroid papillary carcinoma cells and its molecular mechanism 2191

LR. Tu, W. Li, J. Liu, XG. Song and HW. Xu. LncRNA LINC00847 contributes to hepatocellular carcinoma progression by acting as a sponge of miR-99a to induce E2F2 expression 2195

S. Zafiropoulou, M. Tirant, N. Van Thuong, A. Salimi, R. Sadoughifar and T. Lotti. Criolaser-assisted drug delivery in the treatment of refractory keloids 2205

NH. Ma, HM. Zhang, JX. Yang, ZJ. Sun, F. Yuan and XL. Qiu. Long noncoding RNA HOTAIR sponging miR-211 regulates cerebral ischemia-reperfusion injury 2209

WM. Hu, ZH. Shi, DY. Wu, SY. Ye, YJ. Xiang, C. Liu, JC. Chen and CL. Zeng. Effects of combined therapy of valsartan and rosuvastatin on patients with atrial fibrillation 2215

JL. Wang, YX. Yang, G. Xu and Q. Xu. Inhibitory effect of synthetic prostacyclin stimulants on liver fibrosis and related mechanisms 2221

ZY. Fang, HY. Yang, YQ. Ma, W. Wei and WY. Wu. Tamoxifen combined with sumer extract in the treatment of endometriosis in rats 2227

X.X. Gao, J.S. Bai and J.G. Qi. Diagnostic analysis of three-dimensional reconstruction of multi-slice spiral CT in the localization of ocular foreign bodies 2223

J. Tang, X.-Y. Xu, B.-L. Luo, L. Yang, X.-L. Zhang, Y.-D. Sun, Z.-Q. Hou and G. Yao. Potential role of lnc-PTGS2 in fibrosis progression after laminectomy via targeting EGR1 2237

Z-S. Gao, Y-C. Yuan, Q-M. Niu, J. Zhang, J-J. Zhao and L-P. Guo. Velocity vector imaging for assessing the heart function in pregnant women with gestational diabetes mellitus 2245

B. Meng, B. Li, YH. Zhao, JT. Wang and H. Zhang. Risk of acute kidney injury in myocardial infarction: New updates 2251

NX. Liu and QH. Li. LncRNA BC200 regulates neuron apoptosis and neuroinflammation via PI3K/AKT pathway in Alzheimer's disease 2255

DM. Xu, PH. Han, L. Chen, TT. Li, XH. Yang and R. Guo. Knockdown of MMP16 inhibits cell proliferation and invasion in chordoma *in vitro* 2263

Z-P. Qiu, L. Lin, N. Dai, J-J. Li, Q. Chi, Q-H. Liu, J. Zhu and H-H. Zhang. Flavonoid extract of hawthorn (*Crataegus oxyacantha* L.) fruit alleviates oxidative stress, inflammation and vascular dysfunction in L-NAME-induced hypertensive rats 2271

Q. Shang, S. Zhang and Y.D. Tang. Clinical analysis of percutaneous vertebroplasty in the treatment of osteoporotic vertebral compression fractures 2277

Y-F. He, N. Zhao, M-Y. Chen and L. Wei. Terminal differentiation-inducing non-protein coding RNA acted as a competitive endogenous RNA by sponging miR-31 and promoted nasopharyngeal carcinoma cell proliferation and invasion 2281

X-D. Zheng, Y-L. Bi, L-M. Zhang, Y-G. Xing, X-Z. Wang and Z-N. Wang. Analysis of ultrasonic diagnostic indexes of fetuses with coarctation of aorta 2289

AH. Li, YH. Gao, YM. Liu, YQ. Hu, H. Wei and SQ. Lv. Montelukast sodium combined with budesonide for cough variant asthma in children 2295

J.Y. Hou, X.N. Wang, G. Qiu, D.L. Gao and Y. Wang. Correlation between CT small airway parameters, T-lymphocyte subsets and MMP-9 level in patients with bronchial asthma 2299

X-Y. Duan, S-R. Lu, G-Q. Yan, R. Qiu and M-W. Liu. Diagnosis and treatment of two patients with novel coronavirus pneumonia combined with acute stress disorder 2305

JP. Li, R. Yan, PL. Ma, P. Fu, HT. Tian and LL. Wang. Effects of luteolin in different doses on the cardiomyocyte apoptosis in rats with myocardial ischemia reperfusion 2311

B. Huang, H. Luo and XB. Guo. High expression of KPNA2 promotes colorectal cancer development by activating the PI3K/AKT pathway 2317

A. Notarnicola, M. Baglioni, I. Covelli, FP. Bianchi, L. Moretti, G. Maccagnano and B. Moretti. Clinical experience of extracorporeal shockwave treatment on diaphyseal forearm non-union: effects on healing and bone density 2325

A. Chiesa, M. Mignani, C. Preda, F. Esposito, N. Buonocunto, AM. Genovesi and S. Cosola. Effectiveness of powder air polishing on natural and artificial dental surfaces: *in-vitro* study 2331

A. Scarano, D. Amuso, M. Amore, G. Ferraro, E. L. Iorio, A. Sbarbati, F. Lorusso and M. Petrini. Carboxytherapy with oxygen propulsion treatment of cellulite is more effective in women not affected by periodontal disease 2337

R. Saggini, T. Paolucci, A. Bramanti and R.G. Bellomo. A bioprogressive approach for post-acute rehabilitation in elderly COVID-19 survivors 2343

E. Maffezzoni, M. Notargiacomo, S. Agostini and M. Gelardi. Efficacy of a nasal spray containing N-acetylcysteine in hypertonic solution in the treatment of non-allergic chronic rhinitis with goblet cell metaplasia 2345

E. Buonamico, S. Dragonieri, P.I. Sciancalepore, P. Carratù, G.E. Carpagnano, O. Resta and M. Gelardi. Assessment of eosinophilic nasal inflammation in patients with severe asthma and nasal polyposis before and after six months of therapy with Benralizumab 2353

L. Pistelli, C. Sitzia, M. Carrara, S. Borlini, M. Tejada, G. Sammarco, C. Fulceri, R. Valaperta, P. Giubbilini, R. Rigolini, B. Rampoldi, M. Cornetta, S. Mazza, S.D. Corino, A. Pettinato, S. Ferrari, C. Paduraro, A. Moroni, B. Jance, E. Costa and M.M. Corsi Romanelli. Anti-SARS CoV2 antibody testing in healthcare workers: comparison between rapid-cassette tests, ELISA and CLIA methods 2359

E. Poggi, A. Giannattasio, M.E. Cartosio, R. Campus and G. Ciprandi. Primary care experience on Rinfodim 3® in children with recurrent respiratory infections 2365

D. Lucarelli, A. Stabilini, A. De Filippis, V. D'Avola, E. Mainardi. and L. Esposito. Orthodontic appliances in patients allergic to nickel 2375

C. Bertoldi, L. Generali, A. Forabosco, D. Zaffe, M. Ferrari and F. Narni. Extraction socket healing in leukemic patients: a preliminary radiographic evaluation 2379

L. Maiolino, I. La Mantia, C. Grillo, Ct. Grillo and G. Ciprandi. Dystrophic rhinitis: etiopathogenetic mechanisms and therapeutic strategy for functional recovery 2387

G. Galbiati, A. De Filippis, V. D'Avola, E. Mainardi and L. Esposito. Oral breathers and related malocclusion 2391

L. Giannini, L. Garavelli, E. Mainardi, A. De Filippis and L. Esposito. Obstructive sleep apnea syndrome 2395

N. Setaro, P. Luciani, L. Farinelli and A. Gigante. Conservative treatment of hip osteoarthritis; comparison between three medium/high molecular weight hyaluronic acid injections and two injections of HYADD®4: a randomized controlled double-blind study 2401

JOURNAL OF BIOLOGICAL REGULATORS & HOMEOSTATIC AGENTS Vol. 34, no. 6, 1971-1975 (2020)

EDITORIAL

Coronavirus-19 (SARS-CoV-2) induces acute severe lung inflammation via IL-1 causing cytokine storm in COVID-19: A promising inhibitory strategy

P. Conti[1], Al. Caraffa[2], C.E. Gallenga[3], R. Ross[4], S.K. Kritas[5], I. Frydas[6], A. Younes[7] and G. Ronconi[8]

[1]Postgraduate Medical School, University of Chieti, Chieti, Italy; [2]School of Pharmacy, University of Camerino, Camerino, Italy [3]Molecular Medicine, Department of Morphology, Surgery, Experimental Medicine, University of Ferrara, Ferrara, Italy; [4]University of Pennsylvania School of Veterinary Medicine, Philadelphia, PA, USA; [5]Department of Microbiology, University of Thessaloniki, Thessaloniki, Greece; [6]School of Veterinary Medicine, University of Thessaloniki, Thessaloniki, Greece; [7]Centro Medico "Mai più Dolore", Pescara, Italy; [8]Fondazione Policlinico Universitario A. Gemelli IRCCS, Università Cattolica del Sacro Cuore, Roma, Italy

Received September 20, 2020 – Accepted October 1, 2020

SARS-Cov-2 infection causes local and systemic inflammation mediated by pro-inflammatory cytokines and COX-2 eicosanoid products with metabolic dysfunction and tissue damage that can lead to patient death. These effects are primarily induced by interleukin (IL)-1 and IL-6, cytokines which are involved in the elevation of hepatic acute phase proteins and fever. IL-1 has a broad spectrum of biological activities and participates in both innate and acquired immunity. In infections, IL-1 induces gene expression and synthesis of several cytokines/chemokines in both macrophages and mast cells (MCs). The activation of MCs triggers the secretion of mediators stored in the granules, and the *de novo* synthesis of pro-inflammatory cytokines. In microorganism infections, the release of IL-1 macrophages acts on adhesion molecules and endothelial cells, leading to hypotension and septic shock syndrome. IL-1 activated by SARS-CoV-2 stimulates the secretion of IL-6 and TNF, a pro-inflammatory complex that can lead to cytokine storm and be deleterious both in the lung and systemically. In SARS-CoV-2 septic shock, severe metabolic cellular abnormalities occur which can lead to death. Here, we report that SARS-CoV-2 induces IL-1 in macrophages and MCs causing the induction of gene expression and activation of other pro-inflammatory cytokines. Since IL-1 is toxic, its production from ubiquitous MCs and macrophages activated by SARS-CoV-2 can also provoke both gastrointestinal and brain disorders. Furthermore, in these immune cells, IL-1 also elevates nitric oxide, and the release of inflammatory arachidonic acid products such as prostaglndins and thromboxane A2. All together these effects can generate cytokine storm and be the primary cause of severe inflammation with respiratory distress and death. Although IL-1 administered in low doses may be protective, when it is produced in high doses in infectious diseases it can be detrimental, therefore, IL-1 blockade has been studied in many human diseases including sepsis, resulting that blocking it is absolutely necessary. This definitely nurtures hope for a new effective therapeutic treatment. Recently, two interesting anti-IL-1 cytokines have been widely described: IL-37 and IL-1Ra. IL-37, by blocking IL-1, has been observed to have anti-inflammatory

Key words: IL-1; IL-6; cytokines; SARS-CoV-2; COVID-19; coronavirus-19; inflammation; immunity; virus; lung

Corresponding Author:
Prof. Pio Conti,
Postgraduate Medical School, University of Chieti,
Viale Unità d'Italia 73, Chieti, Italy
Tel./Fax: +39 0871 574136
e-mail: pconti@unich.it

0393-974X (2020)
Copyright © by BIOLIFE, s.a.s.
This publication and/or article is for individual use only and may not be further reproduced without written permission from the copyright holder.
Unauthorized reproduction may result in financial and other penalties
DISCLOSURE: ALL AUTHORS REPORT NO CONFLICTS OF INTEREST RELEVANT TO THIS ARTICLE.

action in rodents *in vivo* and in transfected cells. It has been reported that IL-37 is a very powerful protein which inhibits inflammation and its inhibition can be a valid therapeutic strategy. IL-37 is a natural suppressor of inflammation that is generated through a caspase-1 that cleaves pro-IL-37 into mature IL-37 which translocates to the nucleus and inhibits the transcription of pro-inflammatory genes; while IL-1Ra inhibits inflammation by binding IL-1 to its IL-1R receptor. We firmly believe that blocking IL-1 with an anti-inflammatory cytokine such as IL-37 and/or IL-1Ra is an effective valid therapy in a wide spectrum of inflammatory disorders including SARS-CoV-2-induced COVID-19. Here, we propos for the first time that IL-37, by blocking IL-1, may have an important role in the therapy of COVID-19.

In December 2019, a new SARS-CoV-2 virus was found to be the causative agent of coronavirus disease-19 (COVID-19), an acute respiratory distress syndrome (1). Last February, the Food and Drug Administration (FDA) announced a state of emergency for the severe COVID-19 disease induced by SARS-CoV-2 coronavirus-2. This is a highly transmissible and pathogenic virus that caused the pandemic that threatens the world population with potential degree of mortality (2). The pandemic is a global health crisis, with a high morbidity that engages health systems in diagnosis and treatment. SARS-CoV-2 belongs to a family of heterogeneous microorganisms capable of infecting many animals including humans. It can cause severe infections of the airways including lungs, and provoking cough, systemic inflammation, muscle aches, headaches and other symptoms (3). Additionally, it has recently been reported in thousands of patients that brain fog afflicts Covid survivors by impeding their ability to work and function in daily life. This occurs mainly in people who are not seriously ill and had no previous illness. The cause of this dementia is still unclear, although it can be attributed to inflammation of the blood vessels of the brain induced by pro-inflammatory cytokines such as interleukin (IL)-1, IL-6 and tumor necrosis factor (TNF). Today, it is well-known that COVID-19 patients who are sicker may die from breathing difficulties due to the accumulation of edematous fluid in the lungs, and fibrosis (4).

Therapies based on the reduction of pro-inflammatory cytokines in COVID-19 and reduction of viral load is very important. Furthermore, preventing coronavirus-19 from entering the cells is one of the first therapeutic approaches, but also targeting IL-1 in COVID-19 pneumonia represents a rational and strategic intervention. Moreover, it is important to remember that in ubiquitous mast cells IL-1 is a strong inducer of IL-6 which is also a pro-inflammatory cytokine (5). Therefore, antibodies that can bind IL-6 can have a plausible blocking mechanism of action by reducing the severity of an advanced COVID-19 episode, especially if they can be administrated at the initial symptoms (6). However, a combination therapy with a cocktail of anti-virus and anti-inflammatory cytokines may be able to fight to SARS-CoV-2 infection more effectively.

IL-1 is the main cytokine that plays an important role in the TH1 response and innate immunity, and has the ability to induce other pro-inflammatory cytokines such as IL-6 and TNF. The maturation of IL-1 occurs through the cleavage by caspase-1. By inhibiting IL-1 with the IL-1 converting enzyme (ICE), suppression of this cytokine is achieved, an effect that can provoke immunosuppressive innate response and inhibition of inflammation.

Macrophages and COVID-19

Macrophages are immune phagocytic cells derived from blood monocytes, that play an important role in innate and adaptive immunity. Macrophages are activated by microorganisms, including pathogenic coronavirus. Activated macrophages engulf and kill the virus; these activities cause the secretion of harmful

pro-inflammatory cytokines that can induce a cytokine storm that can lead to patient death. IL-1 is mainly produced by activated mononuclear phagocytes the principal function of which is to mediate host inflammatory responses (7). The IL-1 receptor (IL-1R) domain in innate immune cells and Toll-Like receptors (TLRs) respond to microorganisms, including SARS-CoV-2, triggering an immune response. Microorganisms are recognized by the 11 human TLRs via leucine enzyme, resulting in signal transmission within the cell (8). Both IL-1R and TLRs recruit MyD88 causing the initiation of signal transduction. Therefore, IL-1R and TLR share similar functions and properties. Hence, blocking the IL-1 receptor or neutralizing TLRs cause an inhibition of inflammation, including that provoked by SARS-CoV-2, with therapeutic activity. In addition, caspase-1 is the intracellular cysteine protease that cleaves the immature IL-1 inactive precursor to active mature cytokines; therefore, inhibiting caspase-1 may also be beneficial in SARS-CoV-2 infection and inflammation (9). Blocking the IL-1 receptor with the IL-1 receptor antagonist (IL-1Ra) can slow viral inflammation, and reduce signs, symptoms, and progression of COVID-19 disease (10).

Mast cells (MCs)

MCs are effector cells with innate immune responses, present in all vascularized tissues, and represent the sentinels of innate immunity (11). MCs are IgE-dependent and traditionally intervene in allergic diseases by producing stored chemical mediators, but they can also participate in the defense against invading pathogens, such as viruses, by generating pro-inflammatory cytokines (12). Therefore, MCs activated by coronavirus-19 release histamine, proteases, arachidonic acid products (thromboxane A2), and numerous cytokines, such as IL-1, IL-6 and others (13). During acute infectious attack induced by SARS-CoV-2, MCs also intervene among the immune cells which contribute to increasing inflammation of the tissues, both in the initial phase with the production of chemical mediators, and later with the generation of pro-inflammatory cytokines (4). These cytokines together with others, such as TNF, IL-18 and

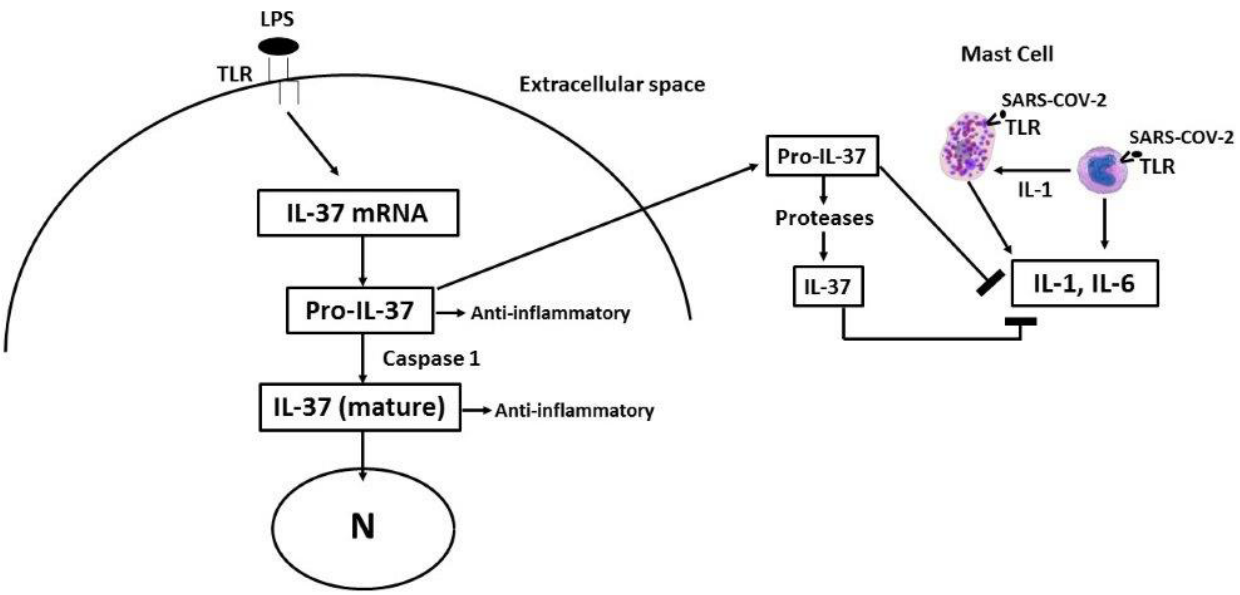


Fig. 1. *IL-1 released by mast cell and macrophage SARS-COV-2 activation induces IL-6 as well as causing cytokine storm which can be inhibited by IL-37.*

IL-33, can trigger strong reactions in the lungs attributable to the cytokine storm, resulting in toxic shock syndrome with falling blood pressure and patient death (14).

MCs also participate in septic shock where they produce TNF and IL-1 which act synergistically to induce hypotension in COVID-19 (9). Endotoxic shock, a hemodynamic decompensation, can occur after SARS-CoV-2 infection and then during COVID-19, with a systemic response and damage to microvascularization, reduced vascular flow, and increased leukocyte adhesiveness (14). However, the systemic inflammation triggered by SARS-CoV-2 causes tissue damage, cell death, and acute organ dysfunction, including lung.

Selective inhibition of MCs and their products can decrease SARS-CoV-2-induced acute tissue inflammation which can be one more tool to save the lives of COVID-19 patients (4). Activated MCs by multivalent antigen triggers early secretion of granule-stored chemical mediators, as well as late de novo synthesis of cytokines, including IL-6 (15). In COVID-19, IL-1 is one of the most important pro-inflammatory compounds which stimulate MCs to release newly synthesized IL-6 (in the absence of degranulation), aggravating inflammation. Inhibiting IL-1 and IL-6 would have a therapeutic benefit that could reduce not only the symptoms, but also the mortality of patients infected by SARS-CoV-2.

Interleukin-37

IL-37, formerly called IL-1 family member 7, is a natural cytokine with anti-inflammatory activity, whose overexpression in epithelial cells and macrophages suppresses the production of pro-inflammatory cytokines, including IL-1 (16). Therefore, IL-37 is a cytokine which can inhibit or even prevent a broad spectrum of inflammatory models (17). IL-37, one of the newest members of the IL-1 family cytokines, is a fundamental suppressor of innate and acquired immunities (18). In experimental models, IL-37 suppresses IL-1 and other related cytokines, an effect that can lead one to think that this cytokine may have clinical therapeutic implications (19). This anti-inflammatory cytokine has been reported to be generated by different tissues and cells such as macrophages, circulating monocytes, dendritic cells, B lymphocytes, and plasma cells (20). Activation of TLR or IL-1R with pro-inflammatory stimuli leads to the endogenous synthesis of the IL-37 precursor (pro-IL-37) and the activation of caspase-1 with consequent cleavage of the IL-37 precursor (21). From these reactions, mature IL-37 is formed which, associated with phosphorylated Smad-3, moves to the nucleus and is subsequently secreted by the cell together with the pro-IL37 form, both biologically active (22). In the exogenous synthesis of mature IL-37, cytoplasmic endocellular pro-IL-37 is secreted out of the cell and, through a still unknown protease, transforms into mature IL-37 with anti-inflammatory activity (22). IL-37 is applicable where inhibition of anti-inflammatory cytokines is ineffective; although this cytokine is used only in laboratory experiments and is not yet commercially available.

Here, we propose that IL-37, a strong inhibitor of IL-1, could have a therapeutic effect on COVID-19 patients through the inhibition of pro-inflammatory cytokines.

REFERENCES

1. Zou L, Ruan f, Huang MX, et al. sars-cov-2 viral load in upper respiratory specimens of infected patients. N Engl J Med 2020 Mar 19; 382(12):1177-79.
2. Pavan K. Bhatraju, Bijan J, et al. Covid-19 in critically ill patients in the Seattle region - Case series. N Engl J Med 2020; NEJMoa2004500. Published online 2020 Mar 30. doi: 10.1056/NEJMoa2004500.
3. Kai L, Sirois P, Ai-Guo D, Liao DF. SARS-CoV-2 Infected cases with untraceable epidemic origin: its values, identification and tcm treatment in preventing recurrence. Digital Chinese Medicine 2020 Jun; 3(2):133-38.
4. Conti P, Gallenga CE, Tetè G, et al. How to reduce the likelihood of coronavirus-19 (CoV-19 or SARS-CoV-2) infection and lung inflammation mediated by IL-1. J

Biol Regul Homeost Agents 2020; 34(2):333-38.

5. Kandere-Grzybowska K, Letourneau R, Kempuraj D, et al. IL-1 induces vesicular secretion of IL-6 without degranulation from human mast cells. J Immunol 2003; 171(9):4830-36.
6. Saha A, Sharma AR, Bhattacharya M, Sharma G, Lee SS, Chakraborty C. Tocilizumab: A therapeutic option for the treatment of cytokine storm syndrome in COVID-19. Arch Med Res 2020; 51(6):595-97.
7. Wakabayashi G, Cannon JG, Gelfand JA, et al. Altered interleukin-1 and tumor necrosis factor production and secretion during pyrogenic tolerance to LPS in rabbits. Am J Physiol 1994; 267(1 Pt 2):R329-36.
8. Dinarello CA. Overview of the IL-1 family in innate inflammation and acquired immunity. Immunol Rev 2018; 281(1):8-27.
9. Conti P, Caraffa A, Gallenga CE, et al. Coronavirus-19 (SARS-CoV-2) induces acute severe lung inflammation via IL-1 causing cytokine storm in COVID-19: a promising inhibitory strategy. J Biol Regul Homeost Agents 2020; 34(6).
10. Powers NE, Swartzwelter B, Marchetti C, et al. PASylation of IL-1 receptor antagonist (IL-1Ra) retains IL-1 blockade and extends its duration in mouse urate crystal-induced peritonitis. J Biol Chem 2020; 295(3):868-82.
11. Galli SJ, Kalesnikoff J, Grimbaldeston MA, Piliponsky AM, Williams CM, Tsai M. Mast cells as "tunable" effector and immunoregulatory cells: recent advances. Annu Rev Immunol 2005; 23:749-86.
12. Barrett NA, Austen KF. Licensed to Ill: IL-9 Generation in immature mast cells permits food-elicited anaphylaxis. Immunity. 2015; 43(4):626-28.
13. Conti P, Caraffa A, Gallenga CE, et al. Coronavirus-19 (SARS-CoV-2) induces acute severe lung inflammation via IL-1 causing cytokine storm in COVID-19: a promising inhibitory strategy. J Biol Regul Homeost Agents 2020; 34(6).
14. Dinarello CA. The proinflammatory cytokines interleukin-1 and tumor necrosis factor and treatment of the septic shock syndrome. J Infect Dis 1991; 163(6):1177-84.
15. Kandere-Grzybowska K, Kempuraj D, Cao J, Cetrulo CL, Theoharides TC. Regulation of IL-1-induced selective IL-6 release from human mast cells and inhibition by quercetin. Br J Pharmacol 2006; 148(2):208-15
16. Dinarello CA. The IL-1 family of cytokines and receptors in rheumatic diseases. Nat Rev Rheumatol 2019; 15(10):612-32.
17. Tsilioni I, Patel AB, Pantazopoulos H, Berretta S, Conti P, Leeman SE, Theoharides TC. IL-37 is increased in brains of children with autism spectrum disorder and inhibits human microglia stimulated by neurotensin. Proc Natl Acad Sci U S A 2019; 116(43):21659-65.
18. Papathanasiou E, Conti P, Carinci F, Lauritano D, Theoharides TC. IL-1 Superfamily members and periodontal diseases. J Dent Res. 2020 Aug 6:22034520945209.
19. Cavalli G, Koenders M, Kalabokis V, et al. Treating experimental arthritis with the innate immune inhibitor interleukin-37 reduces joint and systemic inflammation. Rheumatology (Oxford); 55(12):2220-29.
20. Henry CJ, Casás-Selves M, Kim J, et al. Aging-associated inflammation promotes selection for adaptive oncogenic events in B cell progenitors. J Clin Invest. 2015; 125(12):4666-80.
21. Conti P, Lauritano D, Caraffa A, Gallenga CE, Kritas SK, Ronconi G, Martinotti S. Microglia and mast cells generate proinflammatory cytokines in the brain and worsen inflammatory state: Suppressor effect of IL-37. Eur J Pharmacol 2020; 875:173035.
22. Cavalli G, Dinarello CA. Suppression of inflammation and acquired immunity by IL-37. Immunol Rev 2018; 281(1):179-90.

JOURNAL OF BIOLOGICAL REGULATORS & HOMEOSTATIC AGENTS Vol. 34, no. 6, 1977-1982 (2020)

EDITORIAL

Approach to skin malignancies in COVID-19 pandemic days

M. Aslan Kayıran[1], A.S. Karadag[1] and U. Wollina[2]

[1]Departments of Dermatology, Istanbul Medeniyet University, School of Medicine, Goztepe Training and Research Hospital, Istanbul, Turkey; [2]Department of Dermatology and Allergology, Städtisches Klinikum Dresden, Academic Teaching Hospital of the Technical University, Dresden, Germany

Received June 5, 2020 – Accepted July 15, 2020

COVID-19 pandemic emerged as a condition that changed our entire life and led us to develop new perspectives on diseases. Cancers are generally additional risk factors for COVID-19, and this has implications also for skin cancer patients. Those patients require special attention, due to situations such as an increased risk of infection as a result of visiting the hospital for treatment. It is imperative that the diagnosis and treatment of patients who have a cancer that progresses rapidly, such as malignant melanoma, high-risk squamous cell carcinoma and a high risk of metastasis, are delayed. Due to the relatively long-lasting nature of basal cell carcinoma and, as almost no metastasis would be expected, its treatment may be postponed, except for those that occur in areas such as the eyes and mouth. Diagnosis and treatment of skin cancers is a process that requires many procedures. Throughout this process, physicians should take appropriate precautions that are sufficient to protect both the patient and themselves in the best way without leading to any delay in the procedures.

The COVID-19 pandemic has taken over the world very quickly, creating a crisis environment that seriously affects health, economy, and social life. This infection first appeared in Wuhan city of the Hubei province of China in December 2019, and spread to the whole world in a short time (1). COVID-19 has been shown to progress severely and even cause death in patients with comorbidities, one of which is cancer. In 5.6-8% of patients who died, COVID-19 was found to have been accompanied by cancer (1, 2). Due to the pandemic we are facing, patients apply less to outpatient clinics and they are encouraged to stay at home, except for urgent problems. This situation may lead to problems in the diagnosis and treatment of skin cancers that are progressing chronically and are not considered urgent as they do not cause any symptoms in patients. Thus, it has been addressed in this article how one should approach the skin cancers during the COVID-19 pandemic, from the perspectives of both the patients and the dermatologists.

Cancer patients and skin cancers in the COVID-19 population

Studies conducted on COVID-19 revealed that COVID-19 is most frequently accompanied by preexisting lung cancer followed by esophagus and breast cancers (3). In the analysis of Chinese mainland COVID-19, cancer was associated with more severe symptoms of COVID-19, including admission to the intensive care unit and invasive ventilation and a death rate of 39% *vs* 8% in patients without cancer (4).

Key words: COVID-19 pandemic; skin cancer; cancer therapy; dermoscopy; dermatology

Corresponding Author:
Professor Dr. Uwe Wollina,
Department of Dermatology and Allergology,
Städtisches Klinikum Dresden, Academic Teaching Hospital of the Technical University,
Friedrichstrasse 41, 01067 Dresden, Germany
e-mail: uwe.wollina@klinikum-dresden.de

0393-974X (2020)
Copyright © by BIOLIFE, s.a.s.
This publication and/or article is for individual use only and may not be further reproduced without written permission from the copyright holder.
Unauthorized reproduction may result in financial and other penalties
DISCLOSURE: ALL AUTHORS REPORT NO CONFLICTS OF INTEREST RELEVANT TO THIS ARTICLE.

The fact that the cancer patients have a mean age higher than the normal population (63.1 *vs* 48.7 years), as well as a higher rate of comorbidities, may explain the severe course they can have in COVID-19 disease. If the person has received an antitumor treatment, such as chemotherapy and radiotherapy within 14 days, or has undergone cancer surgery or is a stage IV cancer patient, the possibility of developing COVID-19 infection increases further (5). In one study, 28.6% of cancer patients were infected with COVID-19 while receiving treatment at hospital (2). No specific attributions were made to the skin cancer patients in these aforementioned studies (6). Retrospective studies that are to be conducted on the incidence and course of COVID-19 in skin cancer patients will be useful.

Dermoscopy examination during the pandemic period

Dermoscopy examination is almost indispensable for dermatologists in patients suspected of skin cancer; nonetheless, it is performed in close contact with the patient. Is it safe for both dermatologists and patients during the pandemic period? It has been determined that SARS-CoV-2 can live on plastic, metal, glass, paper, wood and PVC surfaces for 1-5 days (7).

It should be taken into consideration that the surfaces of dermoscopes can become contaminated, considering that they are made of glass and metal. For this reason, some precautions must be taken before and after the dermoscopy examination. It is recommended that the patient enters the examination room alone, if possible, wearing a mask and washing his/her hands properly before and after the examination. The dermatologist should wear personal protective equipment (PPE) and wash his/her hands before and after the examination. The dermoscope should be wiped clean with 70% isopropyl alcohol for at least 1 minute before use. It is recommended that the area that is to be examined is also cleaned in the same way with alcohol. Non-contact dermoscope should be preferred if possible (8). If a non-contact dermoscope is not available, the surface of the dermoscope that contacts the patient can be wrapped with plastic film or disposable covers. A glass surface such as a slide or a thin plastic layer can be placed on the area, and the examination can be made through this slide or layer (8, 9). After the examination, the dermoscope and the areas on the patient that have come into contact with the dermoscope should be wiped again with alcohol (9). Whenever possible, computerized dermoscopy should be preferred over hand dermoscopes. In this way, the doctor can complete the examination by projecting the image of the lesion onto the screen, without the need for directly touching the patient, removing the visor or approaching the patient. If a computerized dermoscope is not available, mobile phone cases that are fitted to mobile phones and compatible with dermoscopes would also be useful for the dermatologist to see the lesion on the phone screen. However, taking into consideration that coronaviruses can also be detected on the mobile phone, it is necessary to clean the mobile phone before and after the examination by wiping it with 70% isopropyl alcohol for 1 minute, to use the mobile phone with cling film, to change this film after each examination, and to pay attention to hand hygiene (7).

Issues that lie ahead of COVID-19, skin cancer patients and dermatologists

It is always recommended to perform a biopsy in skin cancer patients and confirm the diagnosis before the treatment. However, there are no reports as to how to proceed in pandemic periods, which takes into account the risk of infection through aerosol in biopsy. How should the routine biopsy procedures be conducted during pandemic periods? Is there an additional advantage in verifying the diagnosis by biopsy in patients who are already diagnosed of having cancer by examination or dermoscopy? In the event of an underdiagnosis, a misdiagnosis or a false treatment, there is a risk of being sued regardless of whether the reason for not conducting a biopsy is attributed to the pandemic period or not. Especially in cases of risky area lesions, cases that require extensive resection or limb loss, in cases where malignant melanoma (MM), Merkel cell carcinoma (MCC) and high-risk squamous cell carcinoma (SCC) are suspected, the diagnosis should be confirmed by performing a punch or shave biopsy. When a case that can rapidly

metastasize is suspected, such as MM or MCC, performing an excisional biopsy will be useful in terms of both diagnosis and treatment if the lesion is small (10).

After the diagnosis is confirmed, it should be decided whether the skin cancer requires surgery. If the answer is yes, the next decision to be made is elective or urgent surgery. If there is a non-surgergical alternative such as cryotherapy, topical 5% imiquimod or topical 5% 5-fluorouracil, in patients with small and superficial basal cell carcinoma, this should be discussed with the patient. Electrodessication, curettage and laser treatments may be risky in terms of the spread of the particles, which has been proven for hepatitis B virus, human immunodeficiency virus and human papillomavirus, although transmission of SARS-CoV-2 by surgical smoke has not yet been confirmed (11). Having received radiotherapy in the last 14 days aggravates COVID-19 disease and increases the mortality rate (5). Therefore, it would be appropriate to postpone radiotherapy in basal cell carcinoma (BCC) and non-high-risk SCC patients (10). The Centers for Disease Control and Prevention recommends the physicians to use an N95 mask when carrying out aerosol generating procedures (12). Spray cryotherapy may scatter particles on the applied surface and cause COVID-19 to be transmitted. Therefore, contact cryotherapy is relatively safer in BCC unless there is no N95 mask. It is necessary to be more careful when dealing with regions near the hands, face, eyes and mucosae, where particles can be found more frequently, as they are risky in terms of contamination (7, 13).

Before interventional procedures, such as cryotherapy and biopsy, the area, where the procedure is to be applied should be cleaned with 70% isopropyl alcohol, the operating physician should use PPE and perform hand disinfection with an alcohol-based disinfectant before and after the procedure. Sterile protective gloves should be used. Unless necessary, nobody other than the patient and the doctor should be in the operating room to reduce the risk of infection. The room must be well ventilated. During the 2003 epidemic of Severe Acute Respiratory Syndrome, no contamination was observed in healthcare workers who used gloves, masks and gowns, and who washed their hands on a regular basis (14). During COVID-19 pandemic, it is recommended to use N95/FFP2/FFP3 type mask, goggles/visor and apron during risky interventions. At the beginning of the epidemic, nosocomial transmission was detected in 41% of patients in Wuhan, 26% of whom went into intensive care, whereas 4.3% of them died (1). Extra care should be taken to prevent nosocomial transmission in such interventions.

Skin cancers that require surgical intervention

The fact that BCC is a relatively long-lasting disease and that metastasis is not expected may be an advantage in the case of a pandemic. After the diagnosis is made, the patient and the doctor must decide together whether the surgery has to be

Table I. *Tumor drugs and special risks during COVID 10 pandemic*

Compound	Special risk	Reference
Temozolomide 2020	Lymphopenia	Tanriverdi
CHOP and other 2020	Severe cytopenias including	Zic et al.
Cytotoxic drugs 2020	febrile neutropenia	Russell et al.
Alemtuzumab Fludarabine		
Ipilimumab 2020	In 3-5% severe neutropenia	Kattan et al.

delayed. However, surgical intervention should not be postponed for areas such as around the eyes and the mouth where excision become more difficult as the tumor grows. As the operation date gets further delayed, anxiety and depression may develop in the patient; for this reason, some authors have reported that the surgery should not be delayed for more than 21 days even in elective cases (15).

Surgery should never be postponed in fast-spreading skin cancers such as MM, or SCC with involvement of the head-neck region and mucosae (10). In such cases, the best treatment option is total excision of the lesion (15). Delaying surgery in these patients may worsen progonis and increase the difficulty of an optimal treatment. Mortality, increased morbidity, recurrence and metastasis may be observed (16). Skin cancers that require urgent surgery are MM, MCC, advanced and high-risk SCCs and BCCs that settle in critical areas such as around the eyes. SCCs with perineural invasion and poor differentiation, which are larger than 4 cm in diameter and which have spread to deep and subcutaneous tissues are considered as high risk (17).

COVID-19 diagnostic tests should be performed before surgery. Mortality and morbidity rates were found to be high in COVID-19 cases that underwent elective surgeries, even during the incubation period. In such cases, operations on COVID-19 positive cases can be postponed until they test negative (18). It is appropriate to carry out the surgery in negative-pressure operating rooms, where ventilation is good, provided that all the involved personnel use PPE, and that the patient is administered local anesthesia, if possible. If there is no negative-pressure operating rooms, the procedure can be carried out in high-efficiency particulate air filtered rooms. It would also be useful to prolong the time between surgeries to ventilate the room for at least half an hour (18).

Targeted and immune therapy in advanced skin cancer

During the pandemic, risks and benefits might be considered from another viewpoint than in normal life. Cancer patients in need of chemotherapy or radiotherapy should be treated in a protected environment. There should be a risk stratification of cancer patients before treatment: (I) patients with newly diagnosed cancer or suspected cancer; (II) patients on active therapies; (III) patients in remission and on follow-up (19). Early identification of symptoms that are suspicious of an infection with SARS-CoV-2 is necessary. These patients should be treated in a COVID-19 cancer facility. No visits should be allowed for the cancer patients. Multidisciplinary tumor boards should use either web-based meetings or – if not possible – should limit the participants to the lowest possible number.

Systemic treatment should be considered as a treatment option in advanced tumor stages to prolong survival in the presence of metastasis (20). There is no clear information on how to proceed with those skin cancer patients (MM, MCC, metastatic SCC and BCC, cutaneous lymphoma and sarcoma patients) undergoing targeted therapy or immunotherapy during pandemic conditions such as COVID-19 (21). The decision about the possible benefits and harm of treatment should be made together with the patients, irrespective of whether the patient has tested positive or negative for COVID-19. The Italian Association of Medical Oncology recommends to not stop treatment as much as possible and to take decisions based on the biological character and clinic of the tumor (21). It should be considered that antitumor therapies might increase the risk of intensive care and mortality in COVID-19 patients. The risk differs for various available medical drugs: some examples are listed in Table I (22-24). Preliminary data suggest that cancer patients on immune checkpoint inhibitors do not pose a higher risk for COVID-19 in general of for a more severe course of COVID-19 (25). If possible, a swab test is recommended for patients who are to receive systemic therapy, in a similar fashion to the patients undergoing surgical treatment (21). If these patients are to continue receiving these treatments, they must be strictly isolated even if they tested negative for COVID-19. If the results of the swap tests come up positive, it would be appropriate to skip one treatment cycle, even if they are asymptomatic (21).

Palliative treatments have to be considered in patients in the terminal stage. It should be taken into consideration that these patients are less likely

to survive even in intensive care conditions if they become infected with COVID-19 (15, 26).

CONCLUSION

Cancers constitute a risk factor for transmission of infection during the COVID-19 pandemic and they are also a factor for worsening of the prognosis. However, the studies conducted did not reveal sufficient data as to whether skin cancers are one of these comorbid cancers. Among skin cancers, patients with MM, MCC and high-risk SCC may be at risk. BCCs that progresses slowly have a relatively good prognosis. This is different for those in high-risk areas such as the H-zone of the face where delay of diagnosis and treatment is unacceptable. However, the diagnosis and treatment of skin cancers such as MM, MCC and high-risk SCC is urgent and should not be neglected. This is a process that requires the performance of many procedures such as dermoscopy, biopsy, cryotherapy and dermatosurgery. In short, physicians should not delay the performance of these procedures, but at the same time protect both the patient and themselves in the best way.

REFERENCES

1. Wu Z, McGoogan JM. Characteristics of and important lessons from the Coronavirus Disease 2019 (COVID-19) outbreak in China: summary of a report of 72 314 cases from the chinese center for disease control and prevention. JAMA 2020; 323:1239-42.
2. Richardson S, Hirsch JS, Narasimhan M, et al. Presenting characteristics, comorbidities, and outcomes among 5700 patients hospitalized with COVID-19 in the New York City area. JAMA 2020; 323:2052-59.
3. Zhang L, Zhu F, Xie L, et al. Clinical characteristics of COVID-19-infected cancer patients: a retrospective case study in three hospitals within Wuhan, China. Ann Oncol 2020; 31(7):894-901.
4. Liang W, Guan W, Chen R, et al. Cancer patients in SARS-CoV-2 infection: a nationwide analysis in China. Lancet Oncol 2020; 21:335-37.
5. Sidaway P. COVID-19 and cancer: what we know so far. Nat Rev Clin Oncol 2020; 17:336.
6. Moujaess E, Kourie HR, Ghosn M. Cancer patients and research during COVID-19 pandemic: a systematic review of current evidence. Crit Rev Oncol Hematol 2020; 150:102972.
7. Kampf G, Todt D, Pfaender S, Steinmann E. Persistence of coronaviruses on inanimate surfaces and their inactivation with biocidal agents. J Hosp Infect 2020; 104:246-51.
8. Jakhar D, Kaur I, Kaul S. Art of performing dermoscopy during the times of coronavirus disease (COVID-19): simple change in approach can save the day! [published online ahead of print, 2020 Mar 29]. J Eur Acad Dermatol Venereol 2020; 10.1111/jdv.16412.
9. Mun JH, Park SM, Ko HC, et al. Prevention of possible cross-infection among patients by dermoscopy: a brief review of the literature and our suggestion. Dermatol Pract Concept 2013; 3:33-34.
10. Der Sarkissian SA, Kim L, Veness M, Yiasemides E, et al. Recommendations on dermatologic surgery during the COVID-19 pandemic [published online ahead of print, 2020 Apr 10]. J Am Acad Dermatol 2020; S0190-9622(20)30610-1.
11. Do MH, Minkis K, Petukhova TA, Lipner SR. Recommendations for personal protective equipment and smoke evacuation for dermatologic surgeries amid the COVID-19 crisis [published online ahead of print, 2020 May 15]. Dermatol Ther 2020; e13592.
12. Centers for disease control and prevention. information for healthcare professionals about Coronavirus (COVID-19). 2020; https://www.cdc.gov/coronavirus/2019-nCoV/hcp/index.html. Accessed 5/2/2020.
13. World Health Organization. Considerations for quarantine of individuals in the context of containment for coronavirus disease (‍COVID-19)‍: interim guidance, 19 March 2020. World Health Organization. https://apps.who.int/iris/handle/10665/331497. License: CC BY-NC-SA 3.0 IGO.
14. Seto WH, Tsang D, Yung RW, et al. Effectiveness of precautions against droplets and contact in prevention of nosocomial transmission of severe acute respiratory syndrome (SARS). Lancet 2003; 361:1519-20.

15. Wollina U. Challenges of Covid-19 Pandemic for dermatology. Dermatol Ther 2020; 10.1111/dth.13430. doi: 10.1111/dth.13430 [Epub ahead of print].
16. Xiao R, Ward MC, Yang K, et al. Increased pathologic upstaging with rising time to treatment initiation for head and neck cancer: a mechanism for increased mortality. Cancer 2018; 124:1400-14.
17. Clayman GL, Lee JJ, Holsinger FC, et al. Mortality risk from squamous cell skin cancer. J Clin Oncol 2005; 23:759-65.
18. Lei S, Jiang F, Su W, Chen C, et al. Clinical characteristics and outcomes of patients undergoing surgeries during the incubation period of COVID-19 infection. EClinicalMedicine 2020; 100331. doi:10.1016/j.eclinm.2020.100331 [Epub ahead of print].
19. Curigliano G, Cardoso MJ, Poortmans P, et al. Recommendations for triage, prioritization and treatment of breast cancer patients during the COVID-19 pandemic Breast 2020; 52:8-16.
20. Hanna TP, Evans GA, Booth CM. Cancer, COVID-19 and the precautionary principle: prioritizing treatment during a global pandemic. Nat Rev Clin Oncol 2020; 17:268-70.
21. Conforti C, Giuffrida R, Di Meo N, Zalaudek I. Management of advanced melanoma in the COVID-19 era. Dermatol Ther 2020; doi:10.1111/dth.13444 [Epub ahead of print].
22. Tanriverdi O. Lymphopenia that may develop in patients treated with temozolomide and immune control check-point inhibitor may be a high risk for mortality during the COVID-19 outbreak. Med Oncol 2020; 37:51.
23. Zic JA, Ai W, Akilov OE, Carter JB, et al. United States Cutaneous Lymphoma Consortium recommendations for treatment of cutaneous lymphomas during the COVID-19 pandemic. J Am Acad Dermatol 2020; S0190-9622(20)30662-9. doi:10.1016/j.jaad.2020.04.049 [Epub ahead of print].
24. Kattan J, Kattan C, Assi T. Do checkpoint inhibitors compromise the cancer patients' immunity and increase the vulnerability to COVID-19 infection? Immunotherapy 2020; 12:351-54.
25. Yekedüz E, Dursun B, Aydın GÇ, et al. Clinical course of COVID-19 infection in elderly patient with melanoma on nivolumab [published online ahead of print, 2020 May 19]. J Oncol Pharm Pract. 2020;1078155220924084. doi:10.1177/1078155220924084.
26. Ueda M, Martins R, Hendrie PC, et al. Managing cancer care during the COVID-19 pandemic: agility and collaboration toward a common goal. J Natl Compr Canc Netw 2020; 18:366-69

REVIEW

Establishment of a cardiac biobank in a Department of Pathology and Laboratory Medicine

R. Cardani[1], E.G. Bertoldo[2], A. Cerri[3,4], M. Picozzi[4], M.M. Corsi Romanelli[5,6] and E. Callus[2,5]

[1]BioCor Biobank, UOC SMEL-1 of Clinical Pathology, IRCCS-Policlinico San Donato, San Donato Milanese, Milan, Italy; [2]Clinical Psychology Service, IRCCS Policlinico San Donato, San Donato Milanese, Italy; [3]Scientific Directorate, IRCCS Policlinico San Donato, San Donato Milanese, Italy; [4]Center for Clinical Ethics (CREC), Insubria University, Varese, Italy; [5]Department of Biomedical Sciences for Health, University of Milan, Milan, Italy; [6]UOC SMEL-1 of Clinical Pathology, IRCCS Policlinico San Donato, San Donato Milanese, Milan, Italy

Received March 12, 2020 - Accepted October 8, 2020

Biobanks are considered to be important resources of Departments of Pathology and Laboratory Medicine allowing the clarification of relevant disease mechanisms and the improvement of the diagnosis, prognosis, and treatment of both pediatric and adult cardiovascular diseases. To successfully establish a cardiovascular biobank, it is important to consider the public opinion and views on it and the factors involved in the willingness of the public to participate in the donation of genetic material. The literature was systematically reviewed to identify the attitude and willingness of patients affected by congenital and acquired heart disease to participate in biobanking research. Six relevant studies were identified in which it was indicated that psychosocial and demographic characteristics, as well as the patient's medical condition, could influence patient and family members' attitudes and willingness to participate in research. In both congenital and acquired heart diseases, participation in biobank research activities was higher if patients and their families were approached when hospitalized, but not during the acute moment of their illness. Other quantitative and qualitative studies are required to improve patient and family participation in these research initiatives.

The great advancement made in the field of molecular biology and the sequencing of the human genome has led to a deeper understanding of the molecular basis of human diseases, thus entering in the era of personalized medicine. Despite the enormous and invaluable contribution of animal models in the understanding of both physiology and disease pathogenesis, human tissue sampling has become imperative for fulfilling the potential promise of personalized medicine. Therefore, it has become necessary to create infrastructures in which the processing, handling and storage of biological samples, as well as the management of the associated clinical information take place. During the past few decades, there has been an increased interest in the field of public health from researchers and scientists, which has led pathologists and biochemists to create human biological biobanks with the objective of increasing the knowledge about genetic, behavioural and environmental determinants of many diseases,

Key words: biobank; pathology and laboratory medicine; cardiovascular diseases; willingness; attitude

Corresponding Author:
Prof. Massimiliano Marco Corsi Romanelli, MD PhD
UOC SMEL-1 of Clinical Pathology,
IRCCS Policlinico San Donato,
Piazza E. Malan 1, 20097 San Donato Milanese, Milan, Italy
Tel.: +39 02 52774662
e-mail: mmcorsi@unimi.it

0393-974X (2020)
Copyright © by BIOLIFE, s.a.s.
This publication and/or article is for individual use only and may not be further reproduced without written permission from the copyright holder.
Unauthorized reproduction may result in financial and other penalties
DISCLOSURE: ALL AUTHORS REPORT NO CONFLICTS OF INTEREST RELEVANT TO THIS ARTICLE.

supporting the development of new drugs and therapies and improving quality of life.

In 2008, the Biobanking and Biomolecular Resources Research Infrastructure (BBMRI) was established as a pan European research infrastructure and biobank network with the aim to support high quality biomolecular and medical research. The structure of the BBMRI network is represented as a "disturbed hub and spoke scheme" where the various biobanks, biomolecular resources and specialized technology centres are connected via their specific hub (Fig. 1). BBMRI has defined a generally accepted classification of biobanks, which distinguishes between only two major biobank formats with several subtypes characterized by distinct and complementary scientific value: population-based and disease-oriented biobanks (1). Population-based biobanks (longitudinal population-based biobanks, population isolates, and twin registries) collect samples and epidemiological/clinical data from volunteers without specific inclusion or exclusion criteria and aim to mirror the status of the general population (2). Disease-oriented biobanks (biobanks of tissue samples and clinical data also referred to as disease oriented or clinical biobanks) collect samples from patients suffering from a specific clinical condition with the aim of contributing to diagnostics, basic science research, drug and therapy development of specific diseases (3).

Numerous collections of biological material established all over the world are constituted especially from the donations of the patients and their families who, generously, have collaborated and continue to collaborate for the development of research. Thus, it is necessary to establish some regulations to address the practice of researchers also to promote interdisciplinary collaboration and a rigorous methodology, adhering with Ethical Committee requirements. The development of genetic and genomic technologies, the proliferation of databases containing large amount of genotypic and phenotypic data and wide-spread data sharing among institutions have led to the need to develop best practices for addressing ethical, legal and social issues (ELSI) of biobanking, thus protecting the participants in biobanking research (4, 5).

Biobanks and the Departments of Pathology and Laboratory Medicine

One of the most common way for biobanks to acquire specimens is to obtain residual or "leftover" specimens originally collected for clinical care from hospitals, clinical laboratories and pathology departments. For over two hundred years, pathological institutes have collected human tissue samples for histopathological analysis and further research. Thus, collections of paraffin embedded tissue samples may be considered the predecessor of today's biobanks. Moreover, in pathology and laboratory medicine as well as in biobanks, the pre-analytical phase, consisting in the preparation of the biological material for the subsequent analyses, impacts enormously on the results obtained from experiments. In biobanks, the pre-analytical phase consists of working according to standard operating procedures (SOPs) which are essential in modern laboratory medicine to obtain high quality samples, especially in the era of precision medicine. For all these reasons in most of the medical centres, biobanks are usually associated to Departments of Pathology and Laboratory Medicine and they have become an important component of the routine practice of pathology (6).

Biobank for cardiovascular research

Cardiovascular diseases (CVD) are the major cause of human morbidity and mortality worldwide, accounting for 45% of all deaths in European countries in 2016 (7) and almost a third of deaths worldwide (8). According to recent epidemiological information, despite continual improvements in preventive therapies, in Italy cardiovascular mortality represents 37% of all deaths (9) which has a huge impact on public health and on economic resources. The potential of cardiac tissue banking in cardiovascular research has long been recognized. The genetic susceptibility to CVD will be understood clearly when combined with genomics, proteomics and genotyping; hence, the potential of existing DNA biobanks and registries will help in finding answers to the genetic conundrum in CVD (10, 11). Furthermore, as highlighted in the BioHEART-CT cohort study, complex network and machine

learning approaches will be applied to biological and clinical datasets to identify new biomarkers for early diagnosis and to suggest new targeted therapeutics (12). Accordingly, there are major efforts worldwide to professionalize biobanks, including consenting and governance, biospecimens, risk factor and related data, informatics and linkage to electronic health records, in order to provide high quality preservation and storage of biological samples with a potential scientific impact in the era of personalized medicine and drug treatment (11, 13-16).

Within this study area, clinical care for patients with congenital heart disease (CHD) should require more consideration. Indeed, these patients have an increased risk of diverse adverse outcomes including arrhythmia, hypertension, heart failure etc. In order to facilitate the biomarker research in adults with CHD and associated diagnoses, a protocol to collect, process, and store biospecimens from adults has been developed (17).

A major advantage of a cardiovascular biobank is that it allows to conduct research on large sample sizes collected with standardized procedures combined with extensive phenotypic and genotypic data. In fact, several institutions all over the world have established human heart tissue biobanks. In 2017, an association for cardiovascular research was established in Italy as a result of the funding support received from the Italian Ministry of Health. The Cardiology Network includes 19 institutes, which represent excellence in the cardiovascular field, with the obvious advantage of collecting a large number of samples from diseased and healthy participants and thus strongly supporting the scientific progress towards personalized medicine in the area of heart disease. For the long term success of a biobank project it is important to know what the public opinion about these infrastructures is and the public willingness to participate. The theory of reasoned action (TRA), originally introduced in the field of Social Psychology, has been widely used to explain individuals' behaviour in health contexts (18, 19). The theory postulates that individuals' behavioural intention is influenced by their attitude and subjective norm, and that this in turn influences behaviour (Fig. 2). The research assessing attitude toward the consent process and widespread data is limited, however, a number of issues to be assessed have been identified: public knowledge and public views on biobanks, willingness to donate and to agree to sample storage, donors' motivation, perceived benefits and risks, influence of credibility and trust in research institutions, trust toward biobanks (20-24). The aim of this review is to explore the literature and to assess the general attitude of public to donate their biological samples linked with health information and to participate in cardiac research. Understanding patients' perceptions and characteristics can help in developing the best practices for biobanking in the fields of cardiovascular diseases.

METHODS

The authors analysed the theoretical background in the current literature about biobanks in cardiac patients in order to identify the characteristics and attitudes of patients affected by cardiovascular diseases (CVD) and to design an efficient protocol to assess the social attitudes towards the creation of a cardiac biobank in accordance with systematic review guidelines (25).

A systematic review of the literature was conducted in the database of PubMed using a combination of key words: "biobank", "biobanking", "social attitudes", "participation in the research", "cardiology", "cardiac surgery", "congenital heart disease", "adolescents", "heart failure", "cardiovascular", "myocardial infarction", "coronary artery disease". For the selection of the keywords, we have taken into consideration the keywords utilized in previous systematic reviews (20, 26). The initial search, carried out in September 2019 for all studies available from 2009, identified 497 studies, which were then selected on the inclusion criteria of keywords, English language and time of research. Papers, which were not in English, were excluded, as well as those with titles or abstracts not pertinent to the focus of this study. Finally, only 6 relevant studies regarding the attitude and willingness of patients affected by CVD to participate in biobanking were found (Fig. 3; Table I).

RESULTS

The results of the literature review show that there

is a lack of data regarding the social attitude and participation toward biobanking of patients affected by cardiovascular diseases. Among the 6 selected studies, 1 study investigated the opinion of biobank participants to be informed about unexpected genetic findings (27), 2 studies regarded participation of pediatric and adolescent patients with childhood–onset heart diseases (CHD) in biobanking (28, 29), 1 study assessed the attitudes and willingness of parents of CHD children to donate their children's biospecimens for future research (30), 1 study investigated the reasons why cardiovascular patients decline to participate and to enrol in a biobank (31), and 1 study proposed a methodology to explore the attitude of patients from a tertiary cardiology centre about participating in biomarker-based clinical trials (32).

The study of Haukkala et al. (27) on patients who experienced the process of receiving the long QT syndrome unexpected genetic information shows that participants mainly had positive experiences in the process and thought that genetics results should be returned to participants, in particular if they could be life-saving information.

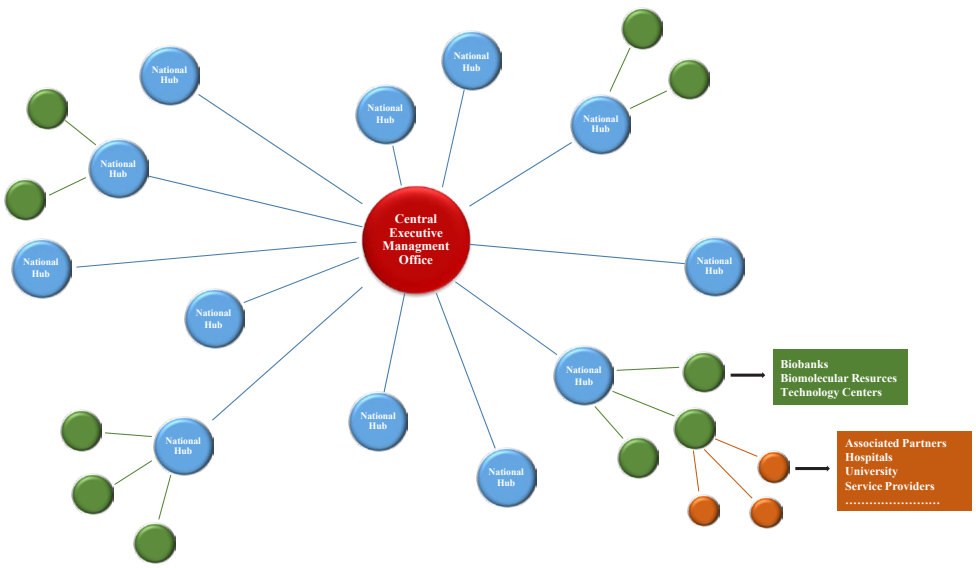


Fig. 1. *The distributed "hub and spoke" structure of BBMRI*

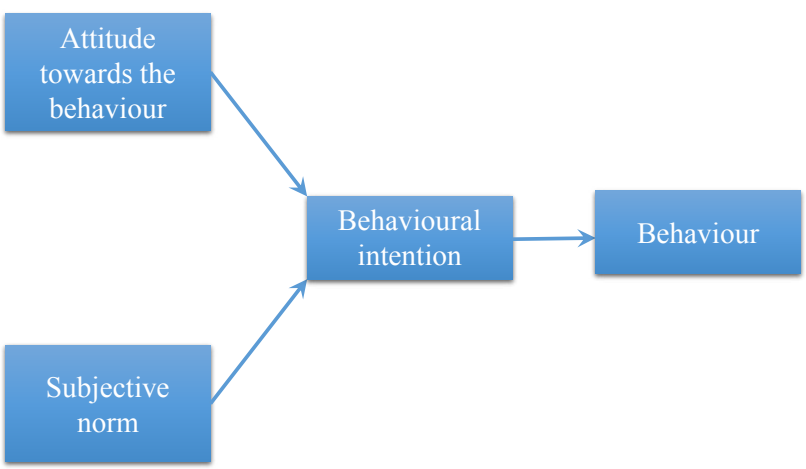


Fig. 2. *Diagram of the relationships in the Theory of the Reasoned Action*

Regarding the opinion and participation in biorepositories of pediatric and adolescent patients affected by cardiac diseases and their parents, two interesting studies were conducted in Canada (28, 29). When it comes to pediatric patients (2-16 years) participation in biobanking, pediatric consent rate was similar to that observed in the adult cohort and it was 100% for parents of CHD children (29). A high willingness to donate biological material has been observed in adolescents (14-18 years) who were in hospital and in their parents (28). However, a less altruistic approach toward pediatric biobanking was seen in adolescents surveyed in school settings and their parents. It is interesting to note that several features influenced pediatric or adolescent participation, including age, race, and the invasiveness of the procedure performed to obtain the biological sample. In addition, it seems that disease severity has a great impact on biobanking attitude. In adult vulnerable patients with cardiovascular disease presenting acute symptoms, critical diagnoses, emergency admissions and diminished capacity to comprehend, the 2 primary themes which emerged from explanations when declining to contribute to

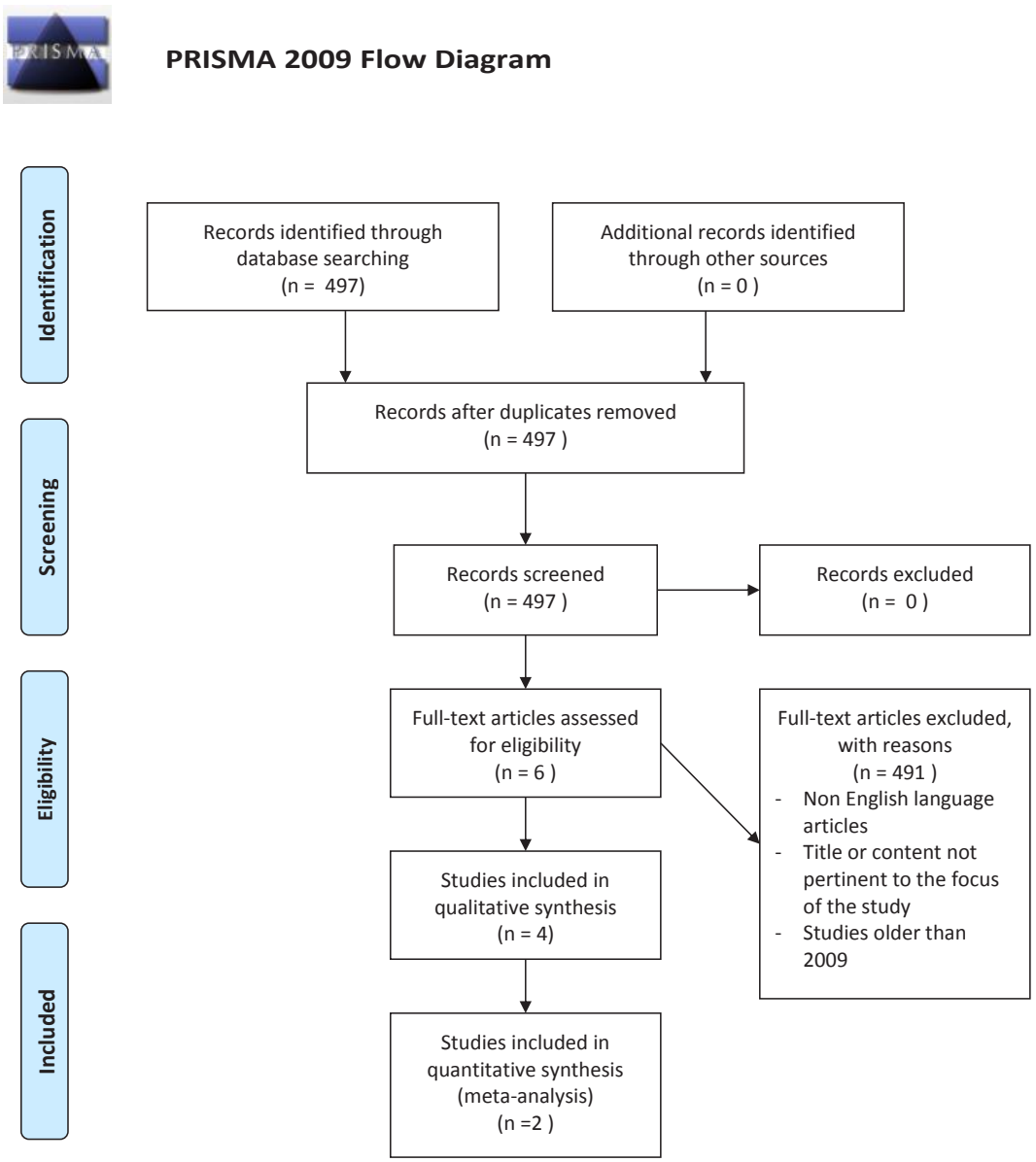


Fig. 3. *PRISMA flow-diagram of the systematic review (34). For more information, visit www.prisma-statement.org*

Table I. *Results of literature search on the social attitude and participation toward biobanking of patients affected by cardiovascular diseases*

Authors	Year	Country	Type of Study	Sample	Study description
Haukkala A et al. (27)	2013	Finland	Cross sectional study; questionnaires and interviews	27	How biobank study participants, who were found to have long QT syndrome (LQTS), a potentially life-threatening but treatable cardiac arrhythmia condition, experienced the process of disclosure of unexpected results and referral to health care.
Kong CC et al. (28)	2015	Canada	Exploratory survey	423	This survey assesses the opinion of adolescents (aged 14 - 18 years), both healthy and in the hospital clinic setting, and their parents regarding biobank participation and related subjects. In particular, willingness to donate biospecimens, appropriate age of assent and the perceived importance of reconsent when they reach the age of majority.
Papaz, T et al. (29)	2012	Canada	Longitudinal Research	3637	The study identifies specific barriers to pediatric participation in biorepositories relative to adults, and proposes strategies to improve ethical and responsible participation of pediatric-aged patients in large-scale genomics and biorepository-driven research without significantly increasing research burden for affected families.
Qiu S et al. (30)	2018	China	Exploratory survey	319	In this study, the aim is to examine factors that may influence Chinese parents' willingness to donate their children's biospecimens in pediatric wards. This may improve the participants' understanding and enhance participants' engagement in biospecimen donation. Furthermore, the authors try to determine whether willingness differed by parents' demographic and children's disease-based characteristics and to get an idea of parents' attitudes toward their children's participation in the consent for biospecimen research.
Williams, PH et al. (31)	2013	USA	Qualitative study	568	A qualitative study was conducted to explore 568 cardiac care patients' explanations of why they declined to contribute their samples to a future genomic research biobank.
Micheu, MM et al. (32)	2018	Romania	Descriptive, prospective and longitudinal single centre study	333	The research's aim is to explore the attitude of patients admitted in a Romanian tertiary cardiology center to take part in biomarker-based clinical trials. Variable assessed are demographics, medical history, attitudes toward biomarker-based clinical trials and trust in medical researchers.

research biobanking initiatives were intrusion and autonomy (31). Patients thought that the process was too intrusive considering their present illness status or hospitalization. Similar findings were found in parents of children with CHD who presented a lower consent rate when approached during situations of high stress, such as cardiac surgery or catheterization (29). Adult patients often give broad consent for the use of their tissues and blood specimens in research projects; however, little is known about the parent willingness to donate their children's biospecimens to be stored for future research. A study conducted

in China to assess attitudes and willingness of parents of children with CHD regarding donating biospecimens for future research, revealed that nearly 70% of parents were willing to donate, the most important motivation being that doing so might help other children. The willingness to donate was positively influenced by parents having a higher education level and the children's hospitalization history and negatively influenced by the potential physical discomfort for the children. The majority of the parents wanted to receive the research results related to their children's biospecimens (30).

CONCLUSIONS

The literature considered indicates that it is crucial to consider patient and family member psychosocial and demographic characteristics which can influence their attitudes and willingness to participate in research and provide consent to donate biological samples. Specific patient characteristics linked to their medical condition and the moment in patient healthcare trajectory (for example diagnosis, hospital admittance for intervention and follow-up) need to be considered.

In studies regarding cardiac disease (both congenital and acquired), patients who were hospitalized and their family members donated their biological samples more willingly than other patients who were not hospitalized in that moment. However, those who were hospitalized during the acute/critical phase of their illness did not feel that it was an appropriate moment to be approached for biological sample donation. There are also studies showing the opinions, feelings and attitudes of parents and their willingness to donate their children's biospecimens for use in pediatric research and for a hypothetical pediatric biobank. These studies confirm the need for specific policies dedicated to this kind of biobank, highlighting several variables which may influence the parents' opinions and decisions towards the donation, such as the nature of disease, younger age, race and the location of consent.

The consideration of all these elements will allow to structure efficient and tailor-made interventions aimed at educating specific patient populations, and to increase patient and family member participation in research and the probability to donate their biological samples. Finally, a multidisciplinary collaboration, which involves professional figures who can take into consideration these peculiarities, linked also to the psychosocial and ethical aspects, is highly recommended (33).

ACKNOWLEDGEMENTS

This study was supported by the Italian Ministry of Health (bando Conto Capitale CC-2016-2365501 Cat. B -PRV- CARDIO) and partially supported by Ricerca Corrente funding from Italian Ministry of Health to IRCCS-Policlinico San Donato. The funders had no role in study design, data collection and analysis, decision to publish, or preparation of the manuscript

REFERENCES

1. Asslaber M, Zatloukal K. Biobanks: transnational, European and global networks. Brief Funct Genomic Proteomic 2007; 6:193-201.
2. Swede H, Stone CL, Norwood AR. National population-based biobanks for genetic research. Genet Med 2007; 9:141-49.
3. Reza M, Cox D, Phillips L, et al. MRC Centre Neuromuscular Biobank (Newcastle and London): Supporting and facilitating rare and neuromuscular disease research worldwide. Neuromuscul Disord 2017; 27:1054-64.
4. Campbell LD, Astrin JJ, DeSouza Y, et al. The 2018 Revision of the ISBER Best Practices: Summary of Changes and the Editorial Team's Development Process. Biopreserv Biobank 2018; 16:3-6.
5. Ferioli E, Picozzi M. La conservazione del materiale biologico finalizzato alla ricerca scientifica: questioni giuridiche e riflessioni etiche sulle biobanche. Medicina e Morale 2011; 60:1-32.
6. Andry C, Duffy E, Moskaluk CA, McCall S, Roehrl MHA, Remick D. Biobanking—Budgets and the role of pathology biobanks in precision medicine. Acad Pathol 2017; 4:1-8.
7. Townsend N, Wilson L, Bhatnagar P, Wickramasinghe K, Rayner M, Nicholset M. Cardiovascular disease in Europe: epidemiological update 2016. Eur Heart J 2016; 37:3232-45.

8. DALYs GBD, Collaborators H, Murray CJ, Barber RM, Foreman KJ, et al. Global, regional, and national disability-adjusted life years (DALYs) for 306 diseases and injuries and healthy life expectancy (HALE) for 188 countries, 1990-2013: quantifying the epidemiological transition. Lancet 2015; 386:2145-91.
9. Giampaoli S, Palmieri L, Donfrancesco C, et al. Cardiovascular health in Italy. Ten-year surveillance of cardiovascular diseases and risk factors: Osservatorio Epidemiologico Cardiovascolare/ Health Examination Survey 1998-2012. Eur J Prev Cardiol 2015; 22:9-37.
10. Jayasinghe SR, Mishra A, Van Daal A, Kwan E. Genetics and cardiovascular disease: Design and development of a DNA biobank. Exp Clin Card 2009; 14:33-37.
11. Littlejohns TJ, Sudlow C, Allen NE, Collins R. UK Biobank: opportunities for cardiovascular research. Eur Heart J 2019; 40:1158-66.
12. Kott KA, Vernon ST, Hansen T, et al. Biobanking for discovery of novel cardiovascular biomarkers using imaging-quantified disease burden: protocol for the longitudinal, prospective, BioHEART-CT cohort study. BMJ open 2019; 9:e028649.
13. Mercuri A, Turchi S, Borghini A, et al. Nitrogen biobank for cardiovascular research. Curr Cardiol Rev 2013; 9:253-59.
14. Olson JE, Bielinski SJ, Ryu E, Winkler EM, Takahashi PY, Pathak J, Cerhan JR. Biobanks and personalized medicine. Clin Genet 2014; 86:50-55.
15. Scholtes VP, de Vries JP, Catanzariti LM, D P V de Kleijn, F L Moll, G J de Borst, G Pasterkamp. Biobanking in atherosclerotic disease, opportunities and pitfalls. Curr Cardiol Rev 2011; 7:9-14.
16. Vegvari A, Welinder C, Lindberg H, Fehniger TE, Marko-Varga G. Biobank resources for future patient care: developments, principles and concepts. J Clin Bioinforma 2011; 1:24.
17. Opotowsky AR, Loukas B, Ellervik C, et al. Design and Implementation of a Prospective Adult Congenital Heart Disease Biobank. World J Pediatr Congenit Heart Surg 2016; 7:734-43.
18. Fishbein M, Ajzen I. Belief, attitudes, intention and behavior: An introduction to theory and research. Reading MA: Addison-Wesley, 1975.
19. Dewi TK, Zein RA. Predicting Intention Perform Breast Self-Examination: Application of the Theory of Reasoned Action. Asian Pac J Cancer Prev 2017; 18(11):2945-2952.
20. Domaradzki J, Pawlikowski J. Public Attitudes toward Biobanking of Human Biological Material for Research Purposes: A Literature Review. Int J Environ Res Public Health 2019; 16:2209.
21. Lemke AA, Wolf WA, Hebert-Beirne J, Smith ME. Public and biobank participant attitudes toward genetic research participation and data sharing. Public Health Genomics 2010; 13:368-77.
22. Porteri C, Pasqualetti P, Togni E, Parker M. Public's attitudes on participation in a biobank for research: an Italian survey. BMC Med Ethics 2014; 15:81.
23. Pulley JM, Brace MM, Bernard GR, Masys DR. Attitudes and perceptions of patients towards methods of establishing a DNA biobank. Cell Tissue Bank 2008; 9:55-65.
24. Tozzo P, Fassina A, Caenazzo L. Young people's awareness on biobanking and DNA profiling: results of a questionnaire administered to Italian university students. Life Sci Soc Policy 2017; 13:9.
25. Perestelo-Pérez L. Standards on how to develop and report systematic reviews in Psychology and Health. Int J Clin Health Psychol 2013; 13:49-57.
26. Ronksley PE, Brien SE, Turner BJ, Mukamal KJ, Ghali WA. Association of alcohol consumption with selected cardiovascular disease outcomes: a systematic review and meta-analysis. BMJ 2011; 342:d671.
27. Haukkala A, Kujala E, Alha P, Salomaa V, Koskinen S, Swan H, Kääriäinen H. The return of unexpected research results in a biobank study and referral to health care for heritable long QT syndrome. Public Health Genomics 2013; 16:241-50.
28. Kong CC, Tarling TE, Strahlendorf C, Dittrick M, Vercauteren SM. Opinions of adolescents and parents about pediatric piobanking. J Adolesc Health 2016; 58:474-80.
29. Papaz T, Safi M, Manickaraj AK, et al. Factors influencing participation in a population-based biorepository for childhood heart disease. Pediatrics 2012; 130:e1198-205.
30. Qiu S, Song Y, Wang J, et al. Factors That Affect Chinese Parents' Willingness to Donate Children's Biospecimens in Pediatric Research. Biopreserv

Biobank 2018; doi: 10.1089/bio.2018.0051.
31. Williams PH, Nemeth LS, Sanner JE, Frazier LQ. Thematic analysis of cardiac care patients' explanations for declining contribution to a genomic research-based biobank. Am J Crit Care 2013; 22:320-27.
32. Micheu MM, Udrea OM, Popa OM, et al. The Attitude of Patients from a Romanian Tertiary Cardiology Center as Regards Participation in Biomarker-Based Clinical Trials - Survey Methodology. J Med Life 2018; 11:320-27.
33. Picozzi M, Nicoli F, Pegoraro R. The devolopment of clinical ethics in Italy and the birth of the "Document of Trento". Clinical Ethics 2017; 12:24-30.
34. Moher D, Liberati A, Tetzlaff J, Altman DG, The PRISMA Group. Preferred Reporting items for Systematic Reviews and Meta-Analyses: The PRISMA Statement. PLoS Med 2009; 6(7):e1000097.

LncRNA XIST promotes proliferation and cisplatin resistance of oral squamous cell carcinoma by downregulating miR-27b-3p

S-Q. Ma[1*], Y-C. Wang[2*], Y. Li[3], X-Y. Li[4], J. Yang[5] and Y-M. Sheng[6]

[1]Department of Oral and Maxillofacial Surgery, The People's Hospital of Zhangqiu Area, Jinan, Shandong Province, China; [2]Department of Pharmacy, Yantaishan Hospital, Yantai, Shandong Province, China; [3]Interventional Vascular Department, The People's Hospital of Zhangqiu Area, Jinan, Shandong Province, China; [4]Department of Nutriology, The People's Hospital of Zhangqiu Area, Jinan, Shandong Province, China; [5]Department of Clinical Laboratory, The People's Hospital of Zhangqiu Area, Jinan, Shandong Province, China; [6]Department of Emergency, Qingdao Hospital of Traditional Chinese Medicine, Qingdao Hiser Medical Group, Qingdao, Shandong Province China

Received April 16, 2020 – Accepted October 9, 2020

[*]These Authors contributed equally to this work

Chemotherapy resistance has become a major obstacle to effective treatment of human cancer. This study aimed to investigate the effect of lncRNA XIST on cell proliferation and cisplatin (CDDP) of oral squamous cell carcinoma (OSCC). RT-qPCR and Western blot analysis were used to detect mRNA and protein expression. CCK-8 and flow cytometry assays were explored to evaluate CDDP sensitivity in OSCC cells. The relationship between lncRNA XIST and miR-27b-3p was confirmed by luciferase reporter assay. The results showed that lncRNA XIST was upregulated in OSCC tissues, cell lines, and CDDP-resistant OSCC cells. Functionally, upregulation of lncRNA XIST promoted cell proliferation, enhanced CDDP resistance, and inhibited apoptosis in OSCC cells. In addition, lncRNA XIST acts as a molecular sponge for miR-27b-3p in OSCC. Downregulation of miR-27b-3p partially reversed the tumor suppression effect and CDDP chemosensitivity of XIST knockdown in CDDP-resistant OSCC cells. In conclusion, lncRNA XIST promotes cell proliferation and enhances resistance to CDDP in OSCC by downregulating miR-27b-3p.

Oral squamous cell carcinoma (OSCC) is the most common malignant tumor in oral cancer. In addition to local hyperplasia and erosion of surrounding tissues leading to dysfunction, OSCC also frequently undergoes lymphatic metastasis in the corresponding lymphatic drainage area of the neck (1). OSCC is therefore a major threat to human health. Today, moderately and poorly differentiated OSCC can be treated with radical radiotherapy and chemotherapy. For moderate and highly differentiated OSCC, surgery is the mainstay, and postoperative adjuvant radiotherapy or chemotherapy (2). As an effective adjuvant therapy for patients with OSCC, the efficacy of chemotherapy is largely affected by cancer cell resistance (3). Cisplatin (CDDP) is a platinum-based anticancer drug that can be used in a variety of human cancers, and drug resistance often limits its clinical application in OSCC (4). Therefore, it is of great significance to explore effective targets for the treatment and CDDP chemoresistance of OSCC.

Key words: LncRNA XIST; cisplatin; proliferation; oral squamous cell carcinoma; miR-27b-3p

Corresponding Author:
Dr Yongmei Sheng,
Department of Emergency,
Qingdao Hospital of Traditional Chinese Medicine,
Qingdao Hiser Medical Group, No. 4 Renmin Road,
Shibei District, Qingdao, 266033, Shandong Province, China
Tel.: +86 0532-83777009
e-mail: ebz3tz@163.com

0393-974X (2020)
Copyright © by BIOLIFE, s.a.s.
This publication and/or article is for individual use only and may not be further reproduced without written permission from the copyright holder.
Unauthorized reproduction may result in financial and other penalties
DISCLOSURE: ALL AUTHORS REPORT NO CONFLICTS OF INTEREST RELEVANT TO THIS ARTICLE.

Long non-coding RNA (lncRNA) is a type of transcript greater than 200 nucleotides in length, which can regulate various physiological and pathological processes of human cancers. The functions of lncRNAs have been identified in OSCC, such as TUG1 and CASC9 (5, 6). In particular, it is reported that lncRNA HOXA11-AS promote cell proliferation and cisplatin resistance in OSCC by inhibiting the expression of miR-214-3p (7). However, the functions of some lncRNAs remain vastly incomplete in OSCC. X inactive-specific transcript (XIST) is the lncRNA encoded by the XIST gene and is responsible for the inactivation of X chromosome in mammals. Previous studies have shown that lncRNA XIST was upregulated in retinoblastoma and glioma (8, 9). Functionally, lncRNA XIST promoted the development of laryngeal squamous cell carcinoma through sponging miR-125b-5p (10). In addition, lncRNA XIST promoted the chemoresistance of breast cancer cells to doxorubicin by sponging miR-200c-3p (11). Upregulation of lncRNA XIST was associated with CDDP resistance in non-small cell lung cancer (NSCLC) by downregulating miR-144-3p (12). However, the effect of lncRNA XIST on OSCC tumorigenesis and CDDP resistance is unknown. Therefore, this study aims to explore the function of lncRNA XIST in OSCC.

In addition, miR-27b-3p was found to be a potential target of lncRNA XIST. The regulatory mechanism of miR-27b-3p has been extensively investigated in human diseases. For example, downregulation of miR-27b-3p has been found in NSCLC and diabetic nephropathy (13, 14). Functionally, downregulation of miR-27b-3p contributed to malignant behavior of gastric cancer cells by targeting GSPT1 (15), and miR-27b-3p was involved in the resistance of human thyroid cancer cells to doxorubicin (16). Importantly, it has been reported that miR-27b can inhibit OSCC resistance to cisplatin drugs (17). However, the interaction between lncRNA XIST and miR-27b-3p in OSCC is still unknown. Therefore, the regulatory mechanism of lncRNA XIST/miR-27b-3p was investigated in OSCC. At the same time, the effect of lncRNA XIST on cell proliferation and CDDP resistance in OSCC was also investigated. This study may provide a novel target for the treatment and CDDP chemoresistance of OSCC.

MATERIALS AND METHODS

OSCC tissues and cell lines

Clinical tissues were collected from 27 patients diagnosed with OSCC in Qingdao Hospital of Traditional Chinese Medicine, Qingdao Hiser Medical Group. All patients with OSCC signed and provided informed consents. All samples were frozen in liquid nitrogen and then were stored at -80°C until further use. This study was approved by the Institutional Ethics Committee of Qingdao Hospital of Traditional Chinese Medicine, Qingdao Hiser Medical Group.

Human oral keratinocyte cell line HOK and OSCC cell lines (CAL-27, SCC-9) were obtained from the American Tissue Culture Collection (ATCC; Manassas, VA, USA). The cisplatin-resistant cell line CAL-27-CDDP is produced by its parental cell line CAL-27 through gradually giving incremental doses of cisplatin administration in the cell culture medium (18). These cells were cultured in DMEM medium containing 10% FBS (Invitrogen, Carlsbad, CA, USA) and incubated at 37°C in a humidified atmosphere with 5% CO_2.

Cell transfection

XIST overexpression vector and siRNA or miR-27b-3p mimics and inhibitor were purchased from RiboBio (Guangzhou, China). These plasmids and oligonucleotides were transfected into CAL-27 cells using lipofectamine 2000 reagent (Invitrogen).

RT-qPCR

TRIzol reagent (Invitrogen) was used to collect total RNA in OSCC tissues or cells. First-strand cDNA was synthesized using 1 μg total RNA and miScript reverse transcription kit (Qiagen, Dusseldorf, Germany). The expression of XIST and miR-27b-3p was quantified on the ABI 7900 system (Applied Biosystems, USA) by miScript SYBR-Green PCR kit (Qiagen). GAPDH or U6 snRNA was used as an internal control. The $2^{-\Delta\Delta Ct}$ method was used to calculate their relative expression of XIST and miR-27b-3p. The primer sequences were the following: GAPDH forward, 5'-ACA ACT TTG GTA TCG TGG AAG G-3', and reverse, 5'-GCC ATC ACG CCA CAG

TTT C-3'; XIST forward,5'-AAT GAC TGA CCA CTG CTG GG-3', and reverse, 5'-GTG TAG GTG GTT CCC CAA GG-3'; miR-27b-3p forward: 5'-GCG CAG TTC ACA GTG GCT AA-3', Reverse: 5'-AGT GCG TGT CGT GGA GTC G-3'; U6 forward: 5'-GCT TCG GCA GCA CAT ATA CTA AAA T-3' and reverse, 5'-CGC TTC ACG AAT TTG CGT GTC AT-3'.

Cell proliferation and drug sensitivity determination

The cisplatin resistance and cell proliferation were quantified by CCK-8 assay. For drug sensitivity analysis, transfected CAL-27 cells were exposed to CDDP in a concentration range from 0 to 160 μmol/L for 48 h. Half maximal inhibitory concentration (IC50) was calculated using GraphPad Prism Version 5.0 Software. For cell proliferation, transfected CAL-27 cells (3×10^3) were cultured in 96-well plates for 48 h. Next, these cells were incubated with 10 μL CCK-8 reagents (Beyotime) for 2 h. Finally, the absorbance value at 450 nm was measured by a microplate reader (Bio-Rad, Hercules, CA, USA).

Cell apoptosis

Fluorescein isothiocyanate (FITC) Annexin V Apoptosis Detection Kits (Invitrogen) was used for apoptosis. Firstly, the transfected CAL-27 and CAL-27-CDDP cells were incubated for 48 h. Next, apoptotic cells were stained with 5 μL of Annexin V-FITC/PI in the dark for 15 min. Finally, the apoptotic rate was evaluated by FACSan flow cytometry (BD Biosciences, San Jose, CA, USA).

Dual luciferase reporter assay

The pGL3 plasmid with wt-XIST or mut-XIST was transfected into CAL-27 cells containing miR-27b-3p mimics. After 48 h of incubation, luciferase activity was measured by a dual-luciferase reporter assay system (Promega, USA).

Western blot assays

RIPA buffer (Beyotime, Shanghai, China) was used to extract whole protein. Equal amounts of protein were separated by 10% SDS-PAGE and transferred to a polyvinylidene fluoride membrane (PVDF, Millipore, USA). After blocking in 5% non-fat milk for 1 h, the PVDF membranes were incubated with primary antibodies against Bax, BCL2, and GAPDH (Santa Cruz Biotechnology, Dallas, TX, USA) at 4°C overnight. Next, the membranes were incubated with a horseradish peroxidase (HRP)-conjugated secondary antibody at room temperature for 1 h. Finally, the protein was detected using the ECL system (Millipore, USA).

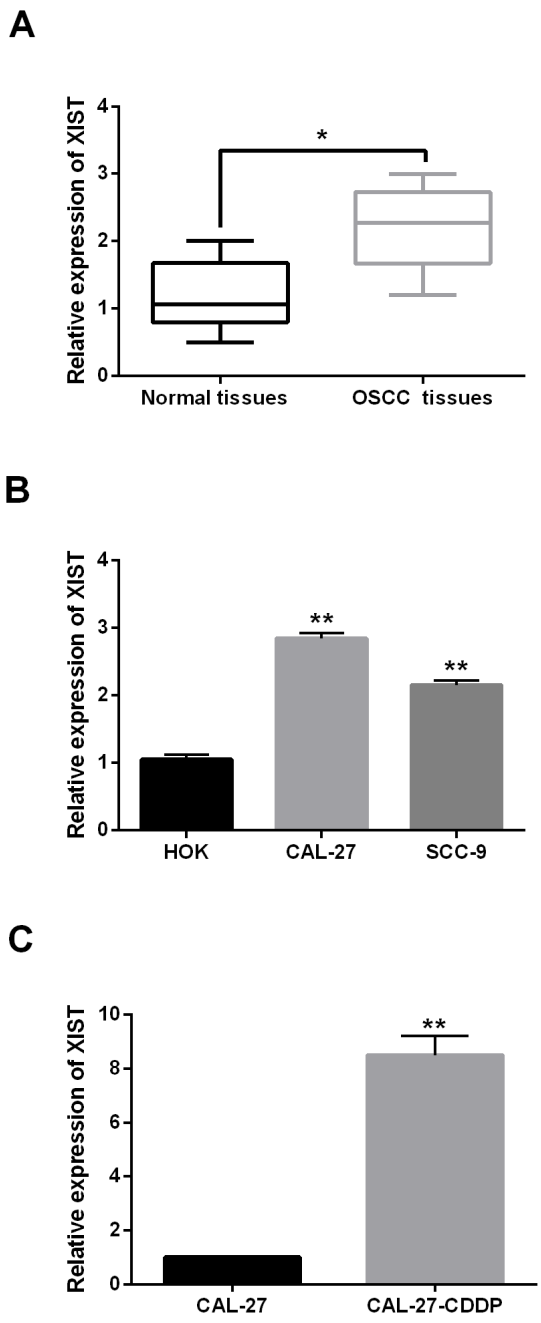


Fig. 1. *LncRNA XIST expression is increased in OSCC and CAL-27-CDDP cells **A.**) LncRNA XIST expression in OSCC tissues and normal tissues. **B**) LncRNA XIST expression in normal human oral keratinocyte cell line (NHOK) and OSCC cell lines (CAL-27, SCC-9). C) LncRNA XIST expression in CAL-27 and CAL-27-CDDP cells *P <0.05, ** P <0.01*

Statistical analysis

Data are presented as mean ± standard deviation (SD). Student's *t*-test or one-way analysis of variance (ANOVA) was used to compare the differences between two or more groups. The difference of $P < 0.05$ was statistically significant.

RESULTS

LncRNA XIST expression is increased in OSCC and CAL-27-CDDP cells

To explore the role of lncRNA XIST in OSCC, abnormal expression of lncRNA XIST was detected in OSCC tissues and cells. RT-qPCR showed that lncRNA XIST in OSCC tissues was upregulated compared with normal tissues ($P < 0.05$, Fig. 1A). At the same time, we found that the expression of lncRNA XIST expression in OSCC cell lines CAL-27 and SCC-9 was higher than that in human oral keratinocyte cell line HOK ($P < 0.01$, Fig. 1B). Next, lncRNA XIST expression was detected in CAL-27-CDDP cells to explore its involvement in OSCC resistance to CDDP. The results showed that the expression of lncRNA XIST in CAL-27-CDDP cells was increased compared to the corresponding parental cells ($P < 0.01$, Fig. 1C). These results indicate that lncRNA XIST may be involved in the progression of OSCC and CDDP resistance.

LncRNA XIST promotes proliferation and inhibits CDDP susceptibility of OSCC cells

Next, XIST siRNA was transfected into CAL-27 and CAL-27-CDDP cells. RT-qPCR showed that XIST expression was reduced by its siRNA in CAL-27 and CAL-27-CDDP cells compared with the negative control groups ($P < 0.01$, Fig. 2A). CCK-8 assay was then used to evaluate the effect of XIST on cell proliferation. The results showed that knockdown of XIST inhibited cell proliferation in CAL-27 and CAL-27-CDDP cells ($P < 0.01$, Fig. 2B). In addition, downregulation of XIST led to a reduction in CDDP resistance in CAL-27-CDDP cells, which was manifested by a lower IC50 value (P

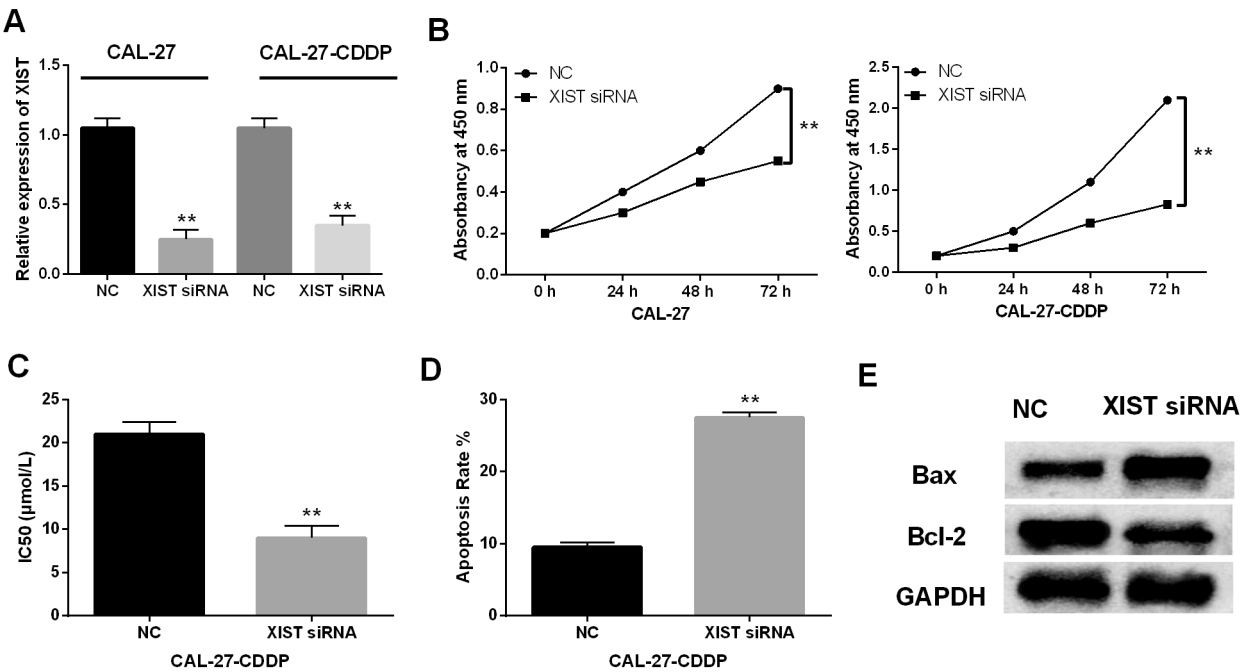


Fig. 2. *LncRNA XIST promotes proliferation and inhibits CDDP susceptibility of OSCC cells. **A**) RT-qPCR assays were used to confirm the efficiency of XIST siRNA. **B**) The effect of XIST siRNA on cell proliferation in CAL-27 and CAL-27-CDDP cells. **C**) The effect of XIST siRNA on CDDP resistance was assessed by computing IC50 value. **D**) The effect of XIST siRNA on cell apoptosis was detected in CAL-27-CDDP treated with 5 μmol/L CDDP. **E**) The effect of XIST siRNA on protein expression of Bax/BCL2 **P <0.01*

< 0.01, Fig. 2C). Flow cytometry analysis showed that downregulation of XIST significantly induced CDDP-induced apoptosis in CAL-27-CDDP cells (P < 0.01, Fig. 2D). To further verify this conclusion, the effect of XIST on the expression of apoptosis-related genes (Bax and Bcl-2) was also detected in CAL-27-CDDP cells treated with CDDP. We found that knockdown of XIST enhanced the protein expression of proapoptosis gene Bax and reduced the expression of anti-apoptosis gene Bcl-2 (Fig. 2E). Briefly, upregulation of XIST promotes cell proliferation and enhances the CDDP resistance of OSCC cells.

LncRNA XIST acts as a molecular sponge for miR-27b-3p

Then, miR-27b-3p is predicted to be a potential target of lncRNA XIST in starBase version 2.0 (http://starbase.sysu.edu.cn/, Fig. 3A). Dual luciferase reporter assay showed that miR-27b-3p mimics reduced the luciferase activity of wt-XIST in CAL-27 cells, but had little effect on that of mut-XIST (P < 0.01, Fig. 3B). This indicates that lncRNA XIST can directly bind to miR-27b-3p. Next, the expression level of miR-27b-3p was detected in OSCC tissues. We found that miR-27b-3p in OSCC tissues was downregulated compared to normal tissues (P < 0.01,

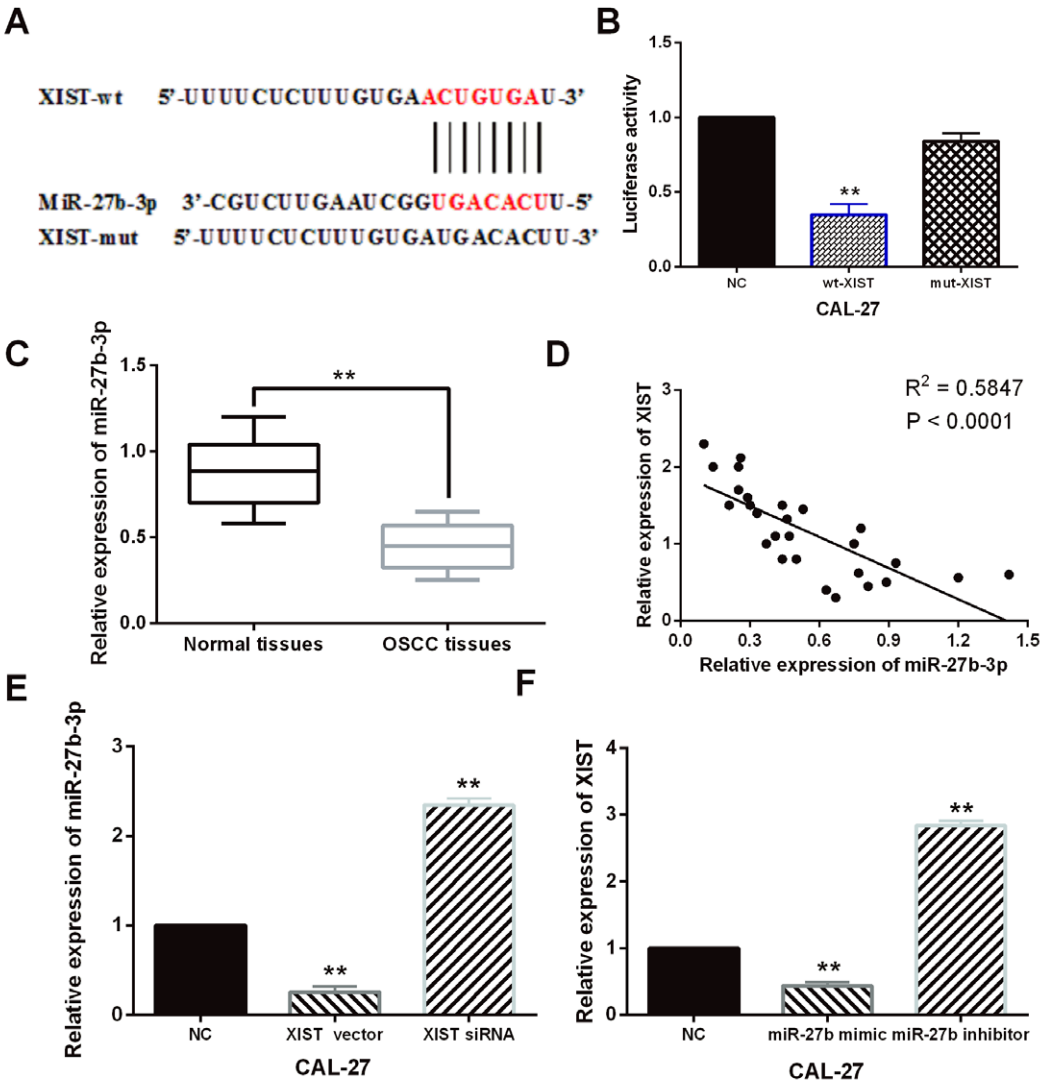


Fig. 3. *LncRNA XIST acts as a molecular sponge of miR-27b-3p. **A**) The binding sites between XIST with miR-27b-3p. **B**) Luciferase reporter assay (C) MiR-27b-3p expression in OSCC tissues and normal tissues. **D**) A negative correlation between XIST and miR-27b-3p expression in OSCC tissues. **E**) MiR-27b-3p expression in CAL-27 cell with XIST siRNA and vector. **F**) XIST expression in CAL-27 cells containing miR-27b-3p mimics or inhibitor **P <0.01*

Fig. 3C). LncRNA XIST was negatively correlated with miR-27b-3p expression in OSCC tissues ($P < 0.01$, Fig. 3D). Consistently, miR-27b-3p expression was also reduced by XIST vector and promoted by XIST siRNA in CAL-27 cells ($P < 0.01$, Fig. 3E). At the same time, overexpression of miR-27b-3p inhibited XIST expression, while downregulation of miR-27b-3p promoted XIST expression in CAL-27 cells ($P < 0.01$, Fig. 3F). Collectively, lncRNA XIST acts as a molecular sponge for miR-27b-3p in OSCC.

MiR-27b-3p partly reverses the effect of lncRNA XIST on proliferation, CDDP susceptibility and apoptosis in CDDP-resistant OSCC cells

To verify whether lncRNA XIST regulates OSCC tumorigenesis by mediating miR-27b-3p, XIST siRNA or XIST siRNA + miR-27b-3p inhibitor was transfected into CAL-27-CDDP cells. RT-qPCR showed that the decreased expression of XIST induced by its siRNA was restored by miR-27b-3p inhibitor (Fig. 4A). CCK-8 assay showed that downregulation of miR-27b-3p weakens the inhibitory effect of XIST siRNA on cell proliferation in CAL-27-CDDP cells (Fig. 4B). In addition, XIST siRNA induced sensibility of CAL-27-CDDP cells to CDDP was attenuated by downregulation of miR-27b-3p (Fig. 4C). We also found that the increase in apoptotic rate induced by XIST downregulation was abrogated by miR-27b-3p downregulation in CAL-27-CDDP cells (Fig. 4D). Meanwhile, the increased expression of Bax and decreased expression of Bcl-2 induced by XIST siRNA was restored by

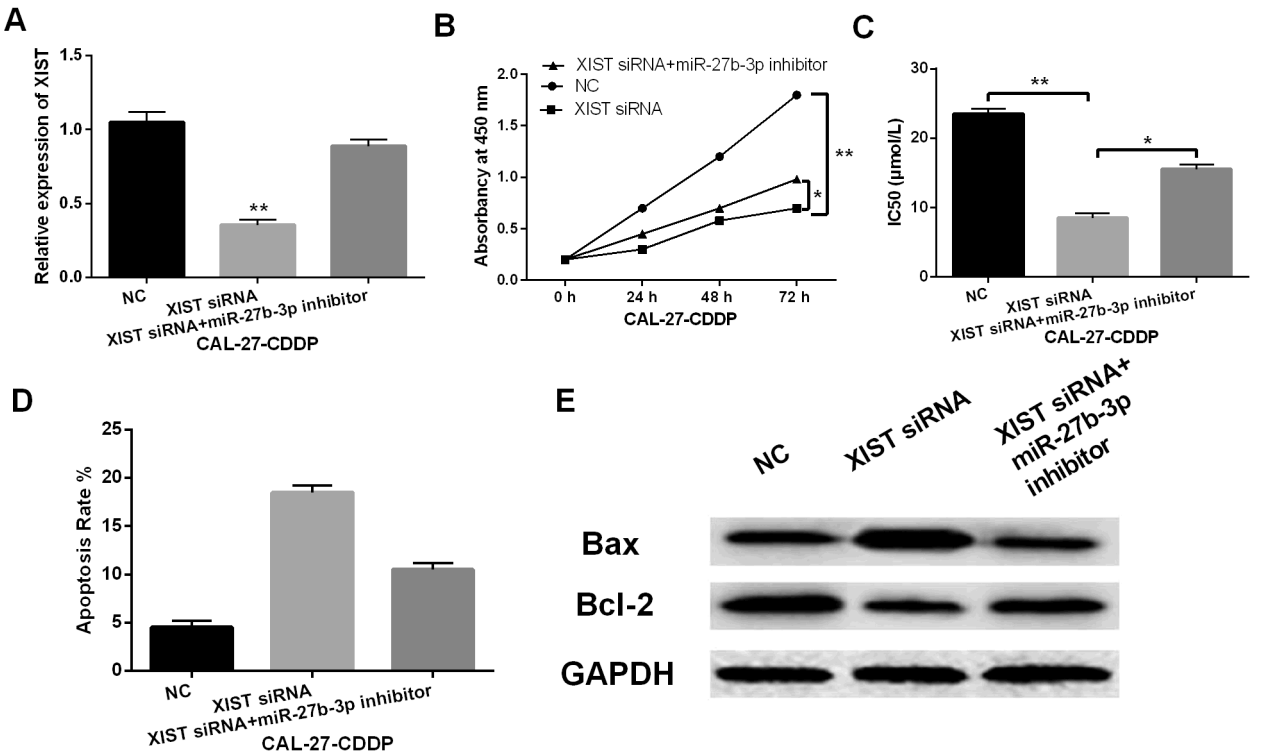


Fig. 4. *MiR-27b-3p partly reverses the effect of lncRNA XIST on proliferation, CDDP susceptibility and apoptosis in CDDP-resistant OSCC cells.* ***A****) lncRNA XIST expression in CAL-27-CDDP cells with XIST siRNA or XIST siRNA + miR-27b-3p inhibitor.* ***B****) Cell proliferation in CAL-27-CDDP cells with XIST siRNA or XIST siRNA + miR-27b-3p inhibitor.* ***C****) The CDDP sensitivity was detected by calculating IC50 value in CAL-27-CDDP cells with XIST siRNA or XIST siRNA + miR-27b-3p inhibitor.* ***D****) Cell apoptosis in CAL-27-CDDP cells with XIST siRNA or XIST siRNA + miR-27b-3p inhibitor.* ***E****) Western blot assays of Bax and BCL2 expression in CAL-27-CDDP cells with XIST siRNA or XIST siRNA + miR-27b-3p inhibitor *P <0.05, ** P <0.01*

downregulation of miR-27b-3p in CAL-27-CDDP cells (Fig. 4E). In summary, lncRNA XIST regulates cell viability and CDDP sensitivity in OSCC by making miR-27b-3p sponge.

DISCUSSION

An increasing number of studies have shown that lncRNAs play important roles in the progression of OSCC. For example, RNA interference of lncRNA HOTAIR inhibited autophagy and promoted apoptosis and sensitivity to CDDP in OSCC (19). lncRNA UCA1 promoted OSCC cell proliferation and CDDP resistance by inhibiting miR-184 expression (20). The present study also confirmed that lncRNA XIST promoted cell proliferation and enhanced resistance to CDDP in OSCC by downregulating miR-27b-3p. Specifically, lncRNA XIST was upregulated in OSCC tissues, cell lines, and CDDP-resistant OSCC cells. Moreover, upregulation of lncRNA XIST promoted cell proliferation, enhanced CDDP resistance and inhibited apoptosis in OSCC. These results imply that lncRNA XIST acts as an oncogene in the pathogenesis of OSCC.

Consistent with our results, upregulation of lncRNA XIST was also found in nasopharyngeal carcinoma (21) and cervical cancer (22). Functionally, knockdown of XIST has been reported to inhibit cell proliferation and induce apoptosis in laryngeal squamous cell carcinoma (23). Knockdown of lncRNA XIST enhanced the chemosensitivity of NSCLC cells to CDDP by inhibiting autophagy (24). Xu et al. has also found that silencing of lncRNA XIST inhibited cell growth and promoted chemosensitivity to CDDP in NSCLC (25). These findings are similar to our results in the present study, indicating that lncRNA XIST promoted the development of OSCC and CDDP resistance. In addition, lncRNA XIST was found to promote the resistance of human lung adenocarcinoma cells to CDDP through the let-7i/BAG-1 axis (26). In this study, lncRNA XIST was found to act as a molecular sponge for miR-27b-3p in OSCC. Downregulation of miR-27b-3p partially reversed the tumor suppression effect and CDDP chemosensitivity of XIST knockdown in CDDP-resistant OSCC cells which indicates that miR-27b-3p can inhibit OSCC tumorigenesis and enhanced CDDP chemosensitivity in OSCC.

Previous studies have shown that miR-27b-3p is involved in the pathogenesis of human cancers. In particular, downregulation of miR-27b-3p was detected in NSCLC (27) and endometrial cancer (28). Functionally, miR-27b-3p inhibited cell proliferation, migration and invasion in colorectal cancer (29). Downregulation of miR-27b-3p can enhance tamoxifen resistance in breast cancer (30). More importantly, it has been reported that miR-27b can inhibit the CDDP resistance of OSCC, increase apoptosis, and inhibit the proliferation of OSCC cells (17). These studies are consistent with our results. In addition, upregulation of LINC01234 was found to promote the development of NSCLC by inhibiting the expression of miR-27b-3p (31). Here, we also found that lncRNA XIST promoted OSCC tumor formation by downregulating miR-27b-3p.

In summary, lncRNA XIST was upregulated in OSCC tissues, cell lines, and CDDP-resistant OSCC cells. Functionally, lncRNA XIST promoted cell proliferation and enhanced resistance to CDDP in OSCC by downregulating miR-27b-3p. This research can help us better understand the regulatory mechanism of lncRNA XIST in OSCC and provide new therapy targets for OSCC.

REFERENCES

1. Villa A, Akintoye SO. Dental management of patients who have undergone oral cancer therapy. Dent Clin North Am 2018; 62:131-42.
2. Carr AB. Oral cancer therapy may influence survival of dental implants. J Evid Based Dent Pract 2011; 11:124-26.
3. Ferreira JA, Peixoto A, Neves M, Gaiteiro C, Santos LL. Mechanisms of cisplatin resistance and targeting of cancer stem cells: Adding glycosylation to the equation. Drug Resist Updat 2015; 24:34-54.
4. Luo SD, Yi-Ju C, Chien-Ting L, et al. Osteopontin involves cisplatin resistance and poor prognosis in oral squamous cell carcinoma. Biomed Res Int 2015:1-13.
5. Liu S, Liu LH, Hu WW, Wang M. Long noncoding RNA TUG1 regulates the development of oral squamous cell carcinoma through sponging miR-

524-5p to mediate DLX1 expression as a competitive endogenous RNA. J Cell Physiol 2019; 234:20206-16.
6. Yang Y, Chen D, Liu H, Yang K. Increased expression of lncRNA CASC9 promotes tumor progression by suppressing autophagy-mediated cell apoptosis via the AKT/mTOR pathway in oral squamous cell carcinoma. Cell Death Dis 2019; 10:41.
7. Wang X, Li H, Shi J. LncRNA HOXA11-AS promotes proliferation and cisplatin resistance of oral squamous cell carcinoma by suppression of miR-214-3p expression. Biomed Res Int 2019; 2019:8645153.
8. Wang Y, Sun D, Sheng Y, Guo H, Meng F, Song T. XIST promotes cell proliferation and invasion by regulating miR-140-5p and SOX4 in retinoblastoma. World J Surg Oncol 2020; 18:49.
9. Luo C, Quan Z, Zhong B, et al. lncRNA XIST promotes glioma proliferation and metastasis through miR-133a/SOX4. Exp Ther Med 2020; 19:1641-48.
10. Liu C, Lu Z, Liu H, Zhuang S, Guo P. LncRNA XIST promotes the progression of laryngeal squamous cell carcinoma via sponging miR-125b-5p to modulate TRIB2. Biosci Rep 2020; 40:4.
11. Zhang M, Wang F, Xiang Z, Huang T, Zhou WB. LncRNA XIST promotes chemoresistance of breast cancer cells to doxorubicin by sponging miR-200c-3p to upregulate ANLN. Clin Exp Pharmacol Physiol 2020; 47:1464-72.
12. Tian LJ, Wu YP, Wang D, et al. Upregulation of long noncoding RNA (lncRNA) X-Inactive specific transcript (XIST) is associated with cisplatin resistance in non-small cell lung cancer (NSCLC) by downregulating microRNA-144-3p. Med Sci Monit 2019; 25:8095-104.
13. Wang X, Xu Y, Zhu YC, et al. LncRNA NEAT1 promotes extracellular matrix accumulation and epithelial-to-mesenchymal transition by targeting miR-27b-3p and ZEB1 in diabetic nephropathy. J Cell Physiol 2019; 234:12926-33.
14. Chen Z, Chen X, Lu B, et al. Up-regulated LINC01234 promotes non-small-cell lung cancer cell metastasis by activating VAV3 and repressing BTG2 expression. J Hematol Oncol 2020; 13:7.
15. Zhang C, Zou Y, Dai DQ. Downregulation of microRNA-27b-3p via aberrant DNA methylation contributes to malignant behavior of gastric cancer cells by targeting GSPT1. Biomed Pharmacother 2019; 119:109417.
16. Xu Y, Han YF, Ye B, Zhang YL, Dong JD, Zhu SJ, Chen J. miR-27b-3p is involved in doxorubicin resistance of human anaplastic thyroid cancer cells via targeting peroxisome proliferator-activated receptor gamma. Basic Clin Pharmacol Toxicol 2018; 123:670-77.
17. Liu B, Cao G, Dong Z, Guo T. Effect of microRNA-27b on cisplatin chemotherapy sensitivity of oral squamous cell carcinoma via FZD7 signaling pathway. Oncol Lett 2019; 18:667-73.
18. Ghosh RD, Ghuwalewala S, Das P, et al. MicroRNA profiling of cisplatin-resistant oral squamous cell carcinoma cell lines enriched with cancer-stem-cell-like and epithelial-mesenchymal transition-type features. Sci Rep 2016; 6:23932.
19. Wang X, Liu W, Wang P, Li S. RNA interference of long noncoding RNA HOTAIR suppresses autophagy and promotes apoptosis and sensitivity to cisplatin in oral squamous cell carcinoma. J Oral Pathol Med 2018; 47:930-37.
20. Fang Z, Zhao J, Xie W, Sun Q, Wang H, Qiao B. LncRNA UCA1 promotes proliferation and cisplatin resistance of oral squamous cell carcinoma by sunppressing miR-184 expression. Cancer Med 2017; 6:2897-908.
21. Zhao CH, Bai XF, Hu XH. Knockdown of lncRNA XIST inhibits hypoxia-induced glycolysis, migration and invasion through regulating miR-381-3p/NEK5 axis in nasopharyngeal carcinoma. Eur Rev Med Pharmacol Sci 2020; 24:2505-17.
22. Liu X, Xie S, Zhang J, Kang Y. Long noncoding RNA XIST contributes to cervical cancer development through targeting miR-889-3p/SIX1 axis. Cancer Biother Radiopharm 2020; 1557-8852.
23. Cui CL, Li YN, Cui XY, Wu X. lncRNA XIST promotes the progression of laryngeal squamous cell carcinoma by sponging miR-144 to regulate IRS1 expression. Oncol Rep 2020; 43:525-35.
24. Sun W, Zu Y, Fu X, Deng Y. Knockdown of lncRNA-XIST enhances the chemosensitivity of NSCLC cells via suppression of autophagy. Oncol Rep 2017; 38:3347-54.
25. Xu X, Zhou X, Chen Z, Gao C, Zhao L, Cui Y. Silencing of lncRNA XIST inhibits non-small cell lung cancer growth and promotes chemosensitivity to cisplatin. Aging (Albany NY) 2020; 12:4711-26.

26. Sun J, Pan LM, Chen LB, Wang Y. LncRNA XIST promotes human lung adenocarcinoma cells to cisplatin resistance via let-7i/BAG-1 axis. Cell Cycle 2017; 16:2100-07.
27. Sun W, Zhang L, Yan R, Yang Y, Meng X. DLX6-AS1LncRNA promotes the proliferation, invasion, and migration of non-small cell lung cancer cells by targeting the mir-27b3p/ GSPT1 axis. Onco Targets Ther 2019; 12:3945-54.
28. Liu L, Hu J, Yu T, You S, Zhang Y, Hu L. miR-27b-3p/MARCH7 regulates invasion and metastasis of endometrial cancer cells through Snail-mediated pathway. Acta Biochim Biophys Sin (Shanghai) 2019; 51:492-500.
29. Chen Y, Chen G, Zhang B, Liu C, Yu Y, Jin Y. miR-27b-3p suppresses cell proliferation, migration and invasion by targeting LIMK1 in colorectal cancer. Int J Clin Exp Pathol 2017; 10:9251-61.
30. Zhu J, Zou Z, Nie P, et al. Downregulation of microRNA-27b-3p enhances tamoxifen resistance in breast cancer by increasing NR5A2 and CREB1 expression. Cell Death Dis 2016; 7:e2454.
31. Chen Z, Chen X, Lu B, et al. Up-regulated LINC01234 promotes non-small-cell lung cancer cell metastasis by activating VAV3 and repressing BTG2 expression. J Hematol Oncol 2020; 13:7.

Gut response to pasteurized donor human milk in a porcine model of the premature infant

A. Socha-Banasiak[1], S.G. Pierzynowski[2,3,4], P. Szczurek[5], J. Woliński[6], A. Wesołowska[7], E. Czkwianianc[1] and K. Pierzynowska[2,4,6]

[1]Department of Gastroenterology, Allergology and Pediatrics, Polish Mother's Memorial Hospital-Research Institute, Lodz, Poland; [2]Department of Biology, Lund University, Lund, Sweden; [3]Department of Medical Biology, Institute of Rural Health, Lublin, Poland; [4]Consortium SGP+Group, Trelleborg, Sweden; [5]Department of Animal Nutrition and Feed Science, National Research Institute of Animal Production, Balice, Poland; [6]Department of Animal Physiology, The Kielanowski Institute of Animal Physiology and Nutrition, Polish Academy of Sciences, Jablonna, Poland; [7]Laboratory of Human Milk and Lactation Research at Regional Human Milk Bank in Holy Family Hospital, Medical University of Warsaw, Department of Medical Biology, Warsaw, Poland

Received May 14, 2020 – Accepted October 14, 2020

This study investigated the tolerance and safety of pasteurized donor human milk (PDHM) given either alone or together with commercially-used supplements in a porcine model of premature infants. A porcine model, mimicking human neonates at 30-32 weeks of gestational age, was used. The 7-day experiment was performed on 20 piglets. After birth, the piglets were infused with porcine immunoglobulins via the umbilical artery and surgically fitted with a stomach port. The piglets were then randomized into five groups and fed either PDHM, different variants of fortified PDHM or 'raw' human milk (RHM). Preterm piglets fed PDHM showed signs of gastrointestinal intolerance. Four piglets across the various PDHM-fed groups died, none of them were from the group fed PDHM supplemented with long-chain polyunsaturated fatty acids (LC PUFA). In all groups fed PDHM, macroscopic features of enterocolitis were observed, however, these pathological gut changes were less manifested in piglets receiving PDHM supplemented with LC PUFA. The piglets fed RHM had no specific signs of gut damage. The poor tolerance to PDHM suggests changes in milk composition caused by the Holder pasteurization. The supplementation with LC PUFA probably improves tolerance to PDHM.

Considering all the immunological and nutritional benefits of breast milk, the best way to feed preterm infants is with their own mother's milk (OMM) (1). Early enteral nutrition (EN) is preferable to total parenteral nutrition (TPN) due to the decreased risk of complications (i.e. sepsis, vascular catherization and other adverse effects of TPN) (2). Although various feeding strategies have been proposed for premature infants, the results of studies concerning the optimal timing for the introduction of EN and the safety of using donor milk fortifiers (DMF) are controversial (3, 4).

However, literature and clinical data indicate a decreased risk of necrotizing enterocolitis (NEC) and sepsis in preterm neonates fed with OMM, thus strong efforts to promote lactation are being made (5). Although premature infants have higher nutritional

Key words: milk pasteurization; milk fortification; preterm piglets; preterm infants

Corresponding Author:
Dr Kateryna Pierzynowska,
Department of Biology, Lund University, Solvegatan 35,
22362 Lund, Sweden
Tel.: +46 73 387 96 26
Fax: +46 (0) 462222 42 06
e-mail: katerina.goncharova@biol.lu.se

0393-974X (2020)
Copyright © by BIOLIFE, s.a.s.
This publication and/or article is for individual use only and may not be further reproduced without written permission from the copyright holder.
Unauthorized reproduction may result in financial and other penalties
DISCLOSURE: ALL AUTHORS REPORT NO CONFLICTS OF INTEREST RELEVANT TO THIS ARTICLE.

requirements in comparison to those born at term, their mothers' milk at the usual feeding volumes is not rich enough in macro- and micronutrients, including long chain polyunsaturated fatty acids (LC PUFA). Therefore, fortification of human milk is recommended to ensure the optimal growth and development of preterm neonates (6). Moreover, when OMM is not available or not sufficient in quantity, pasteurized donor human milk (PDHM) is a recommended alternative (7). Although milk pasteurization, via the Holder method, guarantees the destruction of bacteria and viruses, the high temperatures which the milk is exposed to also leads to a considerable reduction in the levels of important immune molecules, enzymes, hormones and other biologically active compounds (8-10). Moreover, it was previously shown that pasteurization increases casein resistance to infant digestion (11). The negative influence of the Holder pasteurization process on the composition of donor human milk (DHM) may contribute to impaired growth and development of preterm infants (12, 13).

The above facts encouraged us to continue with research focused on investigating the safety of PDHM and human milk fortification in the case of prematurity. Therefore, the general aim of this study was to test pasteurized human milk variants: PDHM *vs* PDHM enriched with LC PUFA *vs* PDHM supplemented with commercial fortifiers in a model of premature human infants. Considering the similarities between preterm piglets and human infants including body size, immaturity of the gastrointestinal tract and impaired respiratory, nutritional, immunological, and metabolic status after birth, the current study made use of an established preterm porcine model supplemented with immunoglobulins intravenously. Intravenous immunoglobulin supplementation increases the similarities between preterm piglets and human neonates at approximately 30-32 weeks of gestational age (14).

MATERIALS AND METHODS

Animals

The present study was performed in strict accordance with the recommendations in the Guide for the Care and Use of Laboratory Animals of the National Institutes of Health. All efforts were made to minimize animal suffering. The study was approved by the Second Local Ethics Committee for Animal Experimentation in Warsaw, Poland (approval no. WAW2/15/2017).

The study made use of 20 piglets (Polish synthetic line 990, male: 11, female: 9) delivered by caesarean section, from two sows inseminated by the same boar semen, 8 days before full gestation (107 days, 93% gestation, corresponding to 30-32 weeks human gestation). All piglets that were delivered were used in the study. During the experiment, piglets were maintained on a 12-hour day-night cycle, with lights on from 06.00-18.00 (6am-6pm). In order to ensure the proper development of the preterm piglets immediately after delivery, they were infused with porcine immunoglobulins (Ig) (1540 mg/kg bwt – 25 ml of sterile Ig preparation/kg bwt) via the umbilical artery (15). After delivery, the sucking reflex was absent in the animals. The insertion and maintaining of orogastric tubes were recognized as procedures which cause more suffering for animals than the insertion of gastric tubes. Jugular vein catheters and gastric ports were inserted under isoflurane anesthesia, in aseptic conditions. After a long incision (5 cm), the stomach was isolated and a gastric port catheter (Silastic, Laboratory Tubing 508-002, Dow Corning, Auburn MI, USA) was implanted via the *curvatura major* and fixed with purse string catgut sutures (KRUUSE Chromic Catgut, USP 4-0; Kruuse Svenska AB, Uppsala, Sweden). The abdomen was then stitched up using 3 layers of sutures, absorbable sutures for the muscle layers and non-absorbable sutures for the skin (Silon Monofil 2/0; CHIRANA, Prague, Czech Republic). Ampicillin (250-500 mg, Doktacillin, Astra Läkemedel, Södertalje, Sweden) was administrated at the incision site. A jugular vein catheter (Silastic, Laboratory Tubing 508-001, Dow Corning, Auburn MI, USA) for infusions was also implanted during the same anaesthesia (14). After surgery, all piglets received a 5% glucose infusion via the jugular vein catheter, at a rate of ~3 mL/h, for a period of 8 hours. Enteral feeding via the stomach port was initiated immediately following the first initial 8-h period after surgery. Parenteral nutrition was not used.

The piglets were individually housed in special sampling cages for preterm piglets, equipped with heating pads to maintain a temperature of 35-37°C. The humidity in the room was ~60%. Piglets were allowed to move around freely within their cages and had visual contact

with each other. The health status of the piglets and their feeding tolerance were monitored daily throughout the study period.

Study design and enteral feeding

A total of 20 piglets were randomized into 5 groups fed with different variants of milk feeds for a period of 7 days. Piglets were fed every 2 hours. The milk feeds were freshly prepared and heated to 37ºC each time before being administered to the piglets. During the first day after birth, the piglets were fed between 2-5 mL every 2 h (depending on the piglet's body weight, piglets <1kg - 2mL, piglets >1kg - 5mL). From the second day, the volume of milk was adjusted to the piglets' body weight, caloric requirements and health status. The daily target volume of milk ingested by the piglets according to the ESPGHAN recommendation was at least 135 mL/kg/day (1). The different experimental groups (n = 4 each) were as follows:

1. PDHM: Pasteurized donor human milk, thawed after freezing (-20°C), obtained from a local milk bank (Warsaw, Poland).
2. PDHM+LC PUFA: PDHM enriched with Arachidonic acid (ARA) (Raw oil/TG-ARA, Lot 6700003994, Nu-Chek Prep, USA) and Docosahexaenoic acid (DHA) (Raw oil/TG-DHA, Lot 880 000 4666, Nu-Chek Prep, USA).
3. PDHM+LC PUFA+PF: PDHM enriched with ARA and DHA, supplemented with powder fortifier (Enfamil Human Milk Fortifier, Mead Johnson, USA).
4. PDHM+LC PUFA+LF: PDHM enriched with ARA and DHA, supplemented with liquid fortifier (Similac Human Milk Fortifier hydrolyzed protein concentrated liquid, Abbott, USA).
5. RHM: Raw human milk (non-pasteurized human donor milk), thawed after freezing (-20°C), obtained from the same local milk bank as the PDHM (Warsaw, Poland) – control group.

All samples of PDHM were pooled prior to administration to ensure that each experimental group received a representative aliquot. Details of the milk feed preparations are presented in Table I.

Feeding tolerance observations

Feeding tolerance observations were based on visual identification of the general health of the piglets, as well as on the identification of potential symptoms including abdominal distention, vomiting, abnormal stool consistency, blood in the stool and abnormal autopsy findings. Visual observations of the piglets were classified descriptively based on the following:

Days 2-4. General well-being of piglets: playful, alert "+"; not playful or not alert "0".

Days 4-7 scoring. 1) Unwillingness to stand. 2) Cold limbs. 3) Abdominal distension. 4) Dehydration syndrome (dry skin, dry oral mucosa and/or no passing of urine). 5) Vomiting.

The piglets were assessed for the above-mentioned abnormalities every 2 hours before the feeding procedure.

Stool observations were also performed and the presence of meconium was noted. The consistency of the faeces was assessed using the Brussels Infant and Toddler Stool Scale (BITSS) (16):

type 1 - "separate hard lumps"
type 2 - "lumpy and sausage-like"
type 3 - "sausage-shaped with cracks on the surface"
type 4 - "stool in the form of a smooth, soft sausage"
type 5 - "soft blobs with clear-cut edges" or "loose stools"
type 6 - "mushy consistency"
type 7 - "entirely liquid consistency with no solid pieces".

Post-mortem examination and euthanasia

Piglets which died during the study and those euthanized with sodium pentobarbiturate (100 mg/kg) at the end of experiment were examined *post-mortem*. The autopsies of the animals that died during the experiment were performed within the same day. The gastrointestinal tract was examined for pathological abnormalities, especially features of necrotizing enterocolitis (NEC) (intestinal edema and hemorrhage, intestinal pneumatosis).

Statistical analysis

Data are expressed as mean ± standard deviation (SD). All analyses were carried out using Prism, version 8 (GraphPad Software, Inc, San Diego, CA,USA). To assess data distribution, a Shapiro-Wilk normality test was performed. An ANOVA followed by a Tukey post-hoc test or Kruskal-Wallis test for non-Gaussian distributed data was used to assess statistical differences between groups. Differences were considered significant if $p \leq 0.05$.

RESULTS

Body weight gain and milk feeding volume/energy

Baseline characteristics of piglets associated

with growth and milk intake are presented in Table II. Body weight gain during the first week of life was observed in piglets from both the PDHM+LC PUFA+PF and PDHM groups. Piglets in all other groups displayed a moderate decline in body weight (less than 15%) over the first week of life. Feeding volume increased slowly from an initial 70 mL/kg/day (day 2) to 110 mL/kg/day on the last day of the study (day 7). There were no statistical differences in mean volume milk intake among the groups.

Daily observations on the well-being and overall health of the piglets

Between day 2 and day 4 general well-being scores were recorded for most of the piglets. On day 3 a decrease in vitality was observed in individual piglets from the PDHM, PDHM+LC PUFA+PF and RHM groups. A decrease in vitality was also observed in piglets from the PDHM+LC-PUFA+PF group on day 4. Almost all piglets had distended abdomens after the volume of milk was increased

Table I. *Supplementation details for each group.*

	Preparation (volumes/amounts were scaled to meet needs)	**volume**
PDHM	PDHM (mL)	QS
PDHM +LC PUFA	ARA oil - 42% ARA (μL)	302
	DHA oil - 43% DHA (μL)	206
	PDHM - (mL)	100
PDHM +LC PUFA+PF	ARA oil - 42% ARA (μL)	302
	DHA oil - 43% DHA (μL)	206
	PF (No. of packets)	4
	PDHM (mL)	100
PDHM +LC PUFA+LF	ARA oil - 42% ARA (μL)	362
	DHA oil - 43% DHA (μL)	247
	LF (No. of packets)	4
	PDHM (mL)	100
RHM	RHM (mL)	QS

QS – quantum satis, PDHM- pasteurized donor human milk, LC PUFA - long chain polyunsaturated fatty acids, ARA-Arachidonic acid, DHA - Docosahexaenoic acid, PF-powder fortifier, LF- liquid fortifier, RHM-raw human milk.

Table II. Baseline characteristics of piglets, body weight gain and milk intake during the 7-day study period.

Groups	Sex	Initial BW (g)	Final BW (g)	BW gain (g)	Food volume (mL/kg/day)	Food energy (kcal/kg/day)
PDHM	2M, 2F	1349 ± 187	1390 ± 221	41	88.1 ± 11.9	61.7 ± 8.31
PDHM+LC PUFA	3M, 1F	1250 ± 295	1160 ± 214	-90	92.7 ± 17.0	68.6 ± 12.6
PDHM+LC PUFA+PF	1M, 3F	1318 ± 169	1445 ± 7	127	88.9 ± 17.1	78.2 ± 15.0
PDHM+LC PUFA+LF	3M, 1F	1463 ± 162	1430 ± 113	-33	91.6 ± 16.2	88.9 ± 15.7
RHM	2M, 2F	1157 ± 287	1123 ± 198	-34	93.8 ± 14.8	65.7 ± 10.3

Data are mean values±SD for each group. BW - body weight, PDHM- pasteurized donor human milk, LC PUFA - long chain polyunsaturated fatty acids, PF-powder fortifier, LF- liquid fortifier, RHM – raw human milk, M - males, F- females.

to 95 mL/kg/day on day 4. On days 5-7, an inability/unwillingness to stand (especially in piglets from the PDHM+LC PUFA group), cold limbs (in piglets from the PDHM, PDHM+LC PUFA+PF, PDHM+LC PUFA+LF groups), abdomen distension (in most of the piglets except for those from the RHM group) were observed. The total number of abnormalities observed between day 4 and day 7, including an unwillingness to stand, cold limbs, abdominal distension, dehydration syndrome and vomiting, was highest for piglets from the PDHM, PDHM+LC PUFA+PF and PDHM+LC PUFA+LF groups (scores 42, 39 and 26, respectively). On the other hand, piglets from the RHM and PDHM+LC PUFA groups had the lowest total scores (2 and 8, respectively) (Table III).

After delivery, all piglets passed meconium. From day 4 some piglets started passing watery stools (type 7 according to the BITSS scale). This abnormality was noted mainly in piglets from the groups fed PDHM. Bloody diarrhea was observed in some of the piglets from the PDHM, PDHM+LC PUFA+PF and PDHM+LC PUFA+LF groups. Almost all of the piglets from the PDHM+LC PUFA+LF group and a half of the piglets from the PDHM+LC PUFA group passed no faeces except for

Table III. *Daily observation on the overall well-being of the piglets during the 7-day study period.*

Groups	Piglet #	Day 2	Day 3	Day 4	Day 5	Day 6	Day 7	Total# recorded^	Totals number recorded/group
PDHM	1	+	0	+1,2,3	D	D	D	9	42
	2	+	+	+	3	1,3	3	9	
	3	+	+	+,3	3	3	3	7	
	4	+	+	+,3	1,2,3	2,3	3	17	
PDHM+LC PUFA	1	+	+	+,3	1	-	-	1	8
	2	+	+	+,3	1	1	1	3	
	3	+	+	+,3	1	-	-	2	
	4	+	+	+,3	1	-	-	2	
PDHM +LC PUFA+PF	1	+	+	+,3	1,2,3	1,2,3,4,5	D	29	39
	2	+	+	+,3	3	-	3	6	
	3	+	0	0,2,3	D	D	D	D	
	4	+	+	+,3	-	-	3	4	
PDHM+LC LUFA+LF	1	+	+	+	2,3	1,2,3,4,5	D	13	26
	2	+	+	+,3	-		3	4	
	3	+	+	+,3	-	-	3	4	
	4	+	+	+,3	-	-	3	5	
RHM	1	+	+	+,3	-	-	-	0	2
	2	+	0	+,3	-	-	3	2	
	3	+	+	+	-	-	-	0	
	4	+	+	+	-	-	-	0	

+: positive well-being (playful, alert); 0: not playful, alert; ^Refers to a total count of the number of time points between days 4-7 that one of the numbered items was observed/recorded.

1: unwilling to stand; 2: cold limbs; 3: abdominal distension; 4: dehydration syndrome; 5: vomiting; PDHM: pasteurized donor human milk; LC PUFA: long chain polyunsaturated fatty acids; PF: powder fortifier; LF: liquid fortifier; RHM: row human milk.

meconium. Only piglets in the RHM group passed stools that were considered normal for neonates (type 5/6 according to the BITSS scale) throughout the whole experimental period (Table IV).

During the study period two piglets died on day 4 (one from the PDHM group and another from the PDHM+LC PUFA+PF group). Prior to their death, the piglets were lethargic and had passed no stools except for the meconium. The piglet from the PDHM group presented with an unwillingness to stand, cold limbs and abdominal distension. The second piglet had advanced bowel distention. No vomiting was observed. Two piglets from the groups that obtained fortified milk (PDHM+LC PUFA+PF and PDHM+LC PUFA+LF) died on day 7. These piglets were lethargic, unwilling to stand, had cold limbs, abdominal distension and features of dehydration syndrome. The piglets were passing watery, bloody stools. From day 6 vomiting was also observed in these piglets.

Post-mortem examination

All piglets that died during the experimental period had clinical symptoms of NEC (Table III, Table IV). Various abnormalities were observed upon autopsy of the piglets that died on day 4. In case of the piglet from the PDHM group, features of classical enterocolitis (large intestine and distal part of ileum with advanced hemorrhages) were noted (Fig. 1 a, b). Macroscopic examination of piglet number 3 (PDHM+LC PUFA+PF group) indicated extensive hemorrhage of the stomach (Fig. 1c). Intestinal

Table IV. *Summary of piglet stool quality records during the 7-day study period.*

Groups	Piglet #	First abnormal stool observed (day of study period)	Stools according to BITSS scale
PDHM	1	-	Died on Day 4
	2	7	7
	3	5	7 with blood
	4	-	No stools after meconium
PDHM+LC PUFA	1	5	7
	2	-	5
	3	-	No stools after meconium
	4	-	No stools after meconium
PDHM+LC PUFA+PF	1	5	7 with blood/died on Day 7
	2	-	5
	3	-	Died on Day 4
	4	-	No stools after meconium
PDHM+LC PUFA+LF	1	4	7 with blood/died on Day 7
	2	-	No stools after meconium
	3	-	No stools after meconium
	4	-	No stools after meconium
RHM	1	-	5/6
	2	-	5
	3	-	5/6
	4	-	5

The days on which the piglets started passing pathological stools are noted in the table. "-" – means no stools were passed after the meconium or that the piglets were passing normal stools (type 5) throughout the experiment period.
PDHM: pasteurized donor human milk; LC PUFA: long chain polyunsaturated fatty acids; PF: powder fortifier; LF: liquid fortifier; RHM: raw human milk.

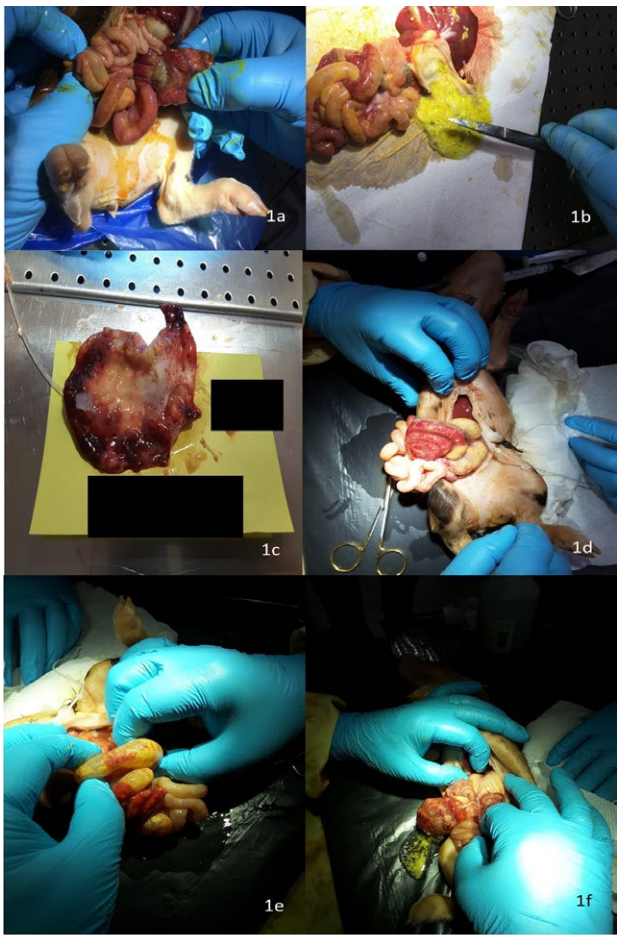


Fig. 1. *Post-mortem examination of piglets that died on day 4 and day 7. Piglets that died on day 4 of the 7-day study period: Piglet No.1 from the PDHM group (**a, b**); Piglet No. 3 from the PDHM+LC PUFA+PF group (**c**). Piglets that died on day 7 of the 7-day study period: Piglet No. 1 from the PDHM+LC PUFA+PF group (**d, e**); Piglet No. 1 from the PDHM+LC-PUFA+LF group (**f**).*

edema and hemorrhage of the colon with a bloody stool in the intestinal cavity were also observed. In the case of the two piglets from the PDHM+LC PUFA+PF and PDHM+LC-PUFA LF groups, features of enterocolitis (huge hemorrhagic areas of the colon) were noted (Fig. 1 d, e, f). Moreover, gas was observed within the bowel wall in the colon of the piglet from the PDHM+LC PUFA+LF group. In the stomach of all of the piglets that died during the experimental period, yellow, jelly-like content with a lot of mucus was observed (Fig. 1b). Bleeding from the upper part of the digestive system, as well as bloody mucus in the stomach, was observed in the piglets from the PDHM+LC PUFA+PF group.

A summary of the macroscopic observations made during *post-mortem* examination of the piglets that died during the experiment, as well as those euthanized at the end of the study is shown in Table V. Abnormal gastric content (gummy, jelly like, with mucus) was generally observed in all the piglets, except those in the RHM group. Additionally, bloody mucus was observed in the stomach of the piglets that were euthanized from the PDHM and PDHM+LC PUFA+PF groups. Piglets from the RHM group had normal, physiological stomach content (normal, soft, cheese-like type digesta). Macroscopic features of enterocolitis were observed in piglets from the PDHM, PDHM+LC PUFA+PF and PDHM+LC PUFA+LF groups (Fig. 2). Almost all the piglets had intestinal edema in different

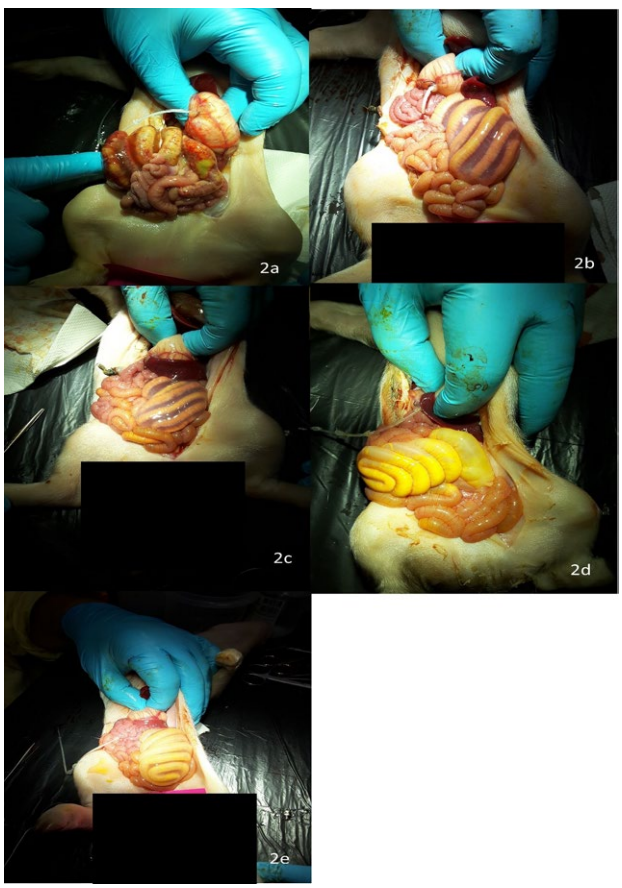


Fig. 2. *Examples of autopsy examination of euthanized piglets. Pig No. 4 from the PDHM group (a); Pig No. 4 from the PDHM+LC PUFA+PF group (**b**); Pig No. 4 from the PDHM+LC PUFA+LF group (**c**); Pig No. 1 from the PDHM+LC PUFA group (**d**); Pig No. 2 from the RHM group (**e**).*

stages which could be described as either slight (S) or large (L). Moreover, in some of the piglets the presence of small areas of intestinal hemorrhage was observed (groups: PDHM, PDHM+LC PUFA+PF, PDHM+LC PUFA+LF). Pneumatosis intestinalis was noted in the two piglets from the PDHM group. In the piglets from the RHM and PDHM+LC PUFA groups, only intestinal edema was detected. The respiratory tract of almost all of the piglets displayed features of immature lung development. The results of the *post-mortem* examination of the piglets that died during the 7-day study period and those that were euthanized at the end of the 7-day study period are shown in Fig. 1 and Fig. 2, respectively.

DISCUSSION

The current study aimed to compare the gastrointestinal effects of PDHM alone, PDHM supplemented with fat rich in LC PUFA and PDHM supplemented with LC PUFA with either liquid or powder fortifiers, in a porcine model of preterm infants. Our results may suggest some adverse effects of the traditional milk pasteurization process. This is of meaningful clinical importance since prematurity is accompanied by a general immaturity of the gastrointestinal tract, and thus the development of a milk feed that is well-tolerated by premature neonates is one of the major challenges in neonatology.

Almost all of the piglets displayed an intolerance to the milk feed, except for those in the RHM group. The feeding volume was below the targeted milk feed intake of 135 mL/kg/day (1). As a consequence, body weight gain of the piglets was generally low. However, it should be noted that due to the very

Table V. *Results of the post-mortem examination of the piglets.*

Groups	Piglet #	Stomach content	Intestinal Edema	Pneumatosis	Hemorrhage within gastrointestinal tract	Heart	Lungs	Day on which piglet died
PDHM	1	2	L	-	X			4
	2	2	S	-	-		I	
	3	2	L	X	-		I	
	4	3	L	X	X		I	
PDHM+LC PUFA	1	2	-	-	-		I	
	2	2	S	-	-			
	3	2	L	-	-		I	
	4	2	S	-	-		I	
PDHM+LC PUFA +PF	1	3	L	-	X			7
	2	2	L	-	-		I	
	3	3	S	-	X	hypertrophy	I	4
	4	2	S	-	X		I	
PDHM+LC PUFA +LF	1	2	L	X	X			7
	2	2	-	-	-			
	3	2	S	-	-		I	
	4	2	L	-	-		I	
RHM	1	1	S	-	-		I	
	2	1	-	-	-		I	
	3	1	S	-	-		I	
	4	1		-	-		I	

Stomach content classifications: 1) normal, soft, cheese-like digesta; 2) gummy, jelly-like, with mucus; 3) gummy, jelly-like, with bloody mucus

S: slight intestinal edema; L: large intestinal edema; Lungs: I-immature respiratory tract; PDHM: pasteurized donor human milk; LC PUFA: long chain polyunsaturated fatty acids, PF: powder fortifier; LF: liquid fortifier, RHM: raw human milk

short experimental period (7 days), we did not expect significant increases in the piglets' body weight at the end of the study. The less than 15% loss of body weight observed in some groups, seems to be a physiological phenomenon during the first week of life (17). The slight body weight gain in the PDHM and PDHM+LC PUFA+PF groups may be as a result of the significantly higher mass of digesta in the gastrointestinal tract (18). Previous studies comparing the effects of OMM and DHM on the general development of preterm neonates are scarce. However, some authors showed that PDHM does not promote the growth and development of preterm neonates as efficiently as OMM (13, 19).

DHM is usually prepared using the Holder pasteurization method (62.5°C for 30 minutes), which may have an adverse effect on the intestinal health of neonates and their resistance against bacterial infections (13). Similar observations were made in the present study using a porcine model of prematurity, where significant signs of the development of NEC were observed. Holder pasteurization may modify the physical properties of milk proteins, such as casein, and inactivate physiologically important molecules including erythropoietin and IL-10, which may lead to gastrointestinal intolerance and decreased protective effect of human milk against NEC (8, 9). Moreover, the Holder pasteurization process may decrease the antioxidant capacity of human milk, which may be important in the context of protection of immature infants against intestinal inflammation (13). In an observational study which focused on the analysis of the transcriptome in exfoliated epithelial intestinal cells from preterm infants, OMM was more efficient in inducing a differential expression of specific genes that may contribute to a more efficient response to a pro-oxidant challenge early in the postnatal period, compared to DHM (20). Moreover, it was shown that feeding with OMM is associated with a favorable gut microbiome colonization with a greater presence of *Bifidobacteriaceae* compared to that observed in preterms fed with DHM (21). The negative impact of the Holder pasteurization to milk composition encourages to search the new methods to better preserve the nutritional and biological properties of human milk, while assuring at least the same microbiological safety. The techniques include High-Temperature-Short-Time (HTST) pasteurization, High Pressure Processing (HPP), and Ultraviolet-C (UV-C) irradiation which are under tests (22).

It should be noted that thermally modified casein, after Holder pasteurization, becomes difficult to digest by pepsin (11). Thus, forms of insoluble conglomerates with milk fat remain in the stomach, as was clearly observed on autopsy in our piglets. These insoluble conglomerates may injure the gut mucosa, when they eventually pass into the small intestine, since they are not easily digested and serve as substrates for bacteria overgrowth which would cause bleeding and inflammation within the intestine. This theory seemed to be confirmed by the results of the present study, since jelly-type globules of undigested milk were observed in the stomach of all piglets fed PDHM, sometimes together with bloody mucus. This may suggest that these jelly-like conglomerates are not easily digested and thus could not be easily evacuated from the stomach of the preterm piglets. Poor PDHM tolerance, in comparison to RHM, was also confirmed by clinical observation of the piglets. All groups of preterm piglets fed PDHM displayed symptoms such as the unwillingness to stand, cold limbs, abdominal distension or dehydration syndrome more frequently compared to those in the RHM group. Moreover, only the piglets fed RHM passed normal stools, even though the RHM was from a foreign species - human. It would be interesting to repeat the study using similarly treated sow milk in preterm piglets. Upon *post-mortem* examination of the piglets that were euthanized following the 7-day study period, only in piglets from the RHM and PDHA+LC PUFA groups were features of pneumatosis and/or intestinal hemorrhage not detected.

Upon learning that feeding exclusively with OMM may not be sufficient to meet the needs of preterm infants, various efforts have been made to develop liquid or powder human milk fortifiers (23). Milk fortification is even more essential in the case of preterm neonates fed with PDHM due to the late lactational stage of the donor milk, which is less concentrated in nutrients than early milk

(24). Literature encourages starting human milk fortification when the volume reaches 50-100 mL/kg/d (6). In the current study, the milk fortification was started at the beginning of enteral feeding and was related to both the study aim and the assessment of food tolerance in premature neonates right after birth and throughout the short duration of the experiment. Although "Individualized Fortification" to optimize nutrient intake is now being recommended by the European Milk Bank Association, the "Standard Fortification" is still the most utilized regimen in neonatal intensive care units (6).

In the present study, bovine milk-based fortifiers, both in liquid and powder form, were used. The type of milk fortifier determines its nutritional composition. However, a study performed on a group of 150 preterm human infants showed no differences in the tolerance of preterm infants to liquid and powder milk fortifiers (25). No differences in the general health and well-being of the piglets (activity, symptoms) were observed between the groups fed PDHM with liquid fortifier and those fed PDHM with powder fortifier. However, upon analysis of stool consistency and frequency of defecation, an interesting phenomenon was observed. Almost all the piglets from the group supplemented with a liquid milk fortifier (with casein hydrolysate) did not pass any stools except for meconium.

It should be noted that the gastrointestinal tract of newborn pigs is probably even more immature (gut opening). Piglets born naturally only acquire the capacity to digest diets other than OMM much later (26). Moreover, during the study, the parenteral nutrition was not used to avoid the necessity of extension of the experimental period. The animals obtained the daily increased volume of the foreign species milk that may lead to gastrointestinal intolerance. On the other hand, our previous experiment showed no significant adverse effect of early enteral nutrition in the similar increase milk amounts (14).

During *post-mortem* examination, differences in the incidence of gastrointestinal hemorrhage and pneumatosis intestinalis among the groups were detected. Pneumatosis intestinalis, pathognomonic for NEC, was observed only in one piglet from the group fed PDHM+LC-PUFA LF and in two piglets from the PDHM group. Areas of intestinal hemorrhage were noted in both groups fed with fortified PDHM (liquid and powder). However, two piglets from the group fed PDHM+LC PUFA+PF died before the end of the 7-day study period. Potential side effects associated with the use of bovine milk-based fortifiers have been previously described (2, 23) and the use of human milk-based fortifiers are preferable over the bovine milk-based fortifiers due to the reduced mortality and morbidity of newborns (27). It has been shown that neonates exclusively receiving a human milk-based diet (OMM or DHM with human milk-based fortifier) have significantly lower rates of NEC compared to those fed preterm formula or human milk with a bovine milk-based fortifier (5, 27). Additionally, the use of PDHM with a bovine milk-based fortifier did not reduce the rates of NEC and other infections in a group of extremely premature infants when compared to preterm formula as a substitute for OMM (28). Unfortunately, in many countries, including Poland, human milk-based fortifiers are not available.

In the current study, the milk feeds were all supplemented with LC PUFA (DHA/ARA), except for the PDHM and RHM groups. DHA/ARA are essential to ensure proper growth, as well as brain and retinal development, including proper signal transduction, neurotransmission and neurogenesis (29). Infant formulas, as well as PDHM lack active bile salt-stimulated lipase (BSSL) leading to fat malabsorption including that of the crucial LC PUFAs - DHA/ARA. For these reasons, the FDA has recommended that infant formulas be supplemented with DHA and ARA at levels comparable to that found in human milk (29). However, the DHA and ARA in infant formulas, as well as in the milk feeds used in the present study, are not in the form of free fatty acids but rather as triglycerides, which could make the supplementation relatively ineffective since, as previously mentioned, infant formulas lack lipase making the neonate unable to digest lipids efficiently. Preterm infants obtain not more than 50% of the DHA that is normally accreted *in utero* (30). In the case of preterm piglets, another limitation for DHA/ARA absorption is the level

of plasma immunoglobulins. In a recent study on newborn, agammaglobulinemic pigs, Pierzynowska et al. (31) showed that ARA/DHA absorption is positively correlated with IgG level in the blood. Our piglets received a preparation of Ig directly after their delivery by caesarean section, ensuring the level of IgG was similar to those measured in full term piglets after gut closure. Considering the results of clinical observations and autopsy, we believe that the initial treatment with the Ig preparation improved DHA/ARA absorption, even though it was offered in the form of LC PUFA, which in turn improved the tolerance of the piglets to PDHM. Moreover, it was previously shown on the rat model that LC PUFA may indicate the protective properties on enterocytes by inhibition of intestinal platelet-activating factor receptor (PAFR) and Toll-like receptor (TLR) 4 gene expressions which are the key factors involved in experimental NEC pathogenesis (32). In our study, the piglets fed exclusively with RHM and piglets from the PDHM+LC-PUFA group revealed no severe symptoms of gastrointestinal inflammation.

Our results should however be interpreted with care due to the limited number of animals per group, although it has been previously shown that the porcine preterm model used in this study corresponds to preterm human neonates. The immunoglobulin infusion after birth should assure appropriate growth and development of the animals also in the case of prematurity (14).

In conclusion, it should be emphasized that the RHM was well-tolerated by the premature piglets, even though it is essentially from a foreign (human) species. The poor tolerance of piglets to pure PDHM and PDHM supplemented with fortifiers, suggests that the changes in milk composition which occur during the pasteurization process and the possible adverse effects of the post-Holder milk fortification process require further research. However, treatment with Ig and supplementation of the PDHM milk with LC PUFA may ameliorate the negative effects of pasteurization on the porcine model.

ACKNOWLEDGEMENTS

The authors would like to express their thanks to Dr Janine Donaldson for her constructive feedback and valuable input with regards to the writing of the manuscript.

The present study was supported by grants from Consorcium SGP + Group, Trelleborg, Sweden and The Royal Physiographic Society of Lund, Sweden.

REFERENCES

1. Agostoni C, Buonocore G, Carnielli VP, et al. ESPGHAN Committee on Nutrition. Enteral nutrient supply for preterm infants: commentary from the European Society of Paediatric Gastroenterology, Hepatology and Nutrition Committee on Nutrition. J Pediatr Gastroenterol Nutr 2010; 50:85-91.
2. Dutta S, Singh B, Chessell L, et al. Guidelines for feeding very low birth weight infants. Nutrients 2015; 7:423-42.
3. Jain S, Mukhopadhyay K, Jain V, Kumar P. Slow versus rapid enteral feed in preterm neonates with antenatal absent end diastolic flow. J Matern Fetal Neonatal Med 2016; 29:2828-33.
4. Choi A, Fusch G, Rochow N, Fusch C. Target fortification of breast milk: predicting the final osmolality of the feeds. PLoS One 2016; 11(2):e0148941.
5. Cristofalo EA, Schanler RJ, Blanco CL, et al. Randomized trial of exclusive human milk versus preterm formula diets in extremely premature infants. J Pediatr 2013; 163:1592-5.
6. Arslanoglu S, Boquien CY, King C, et al. Fortification of human milk for preterm infants: update and recommendations of the European Milk Bank Association (EMBA) working group on human milk fortification. Front Pediatr 2019; 22:7:76.
7. Arslanoglu S, Corpeleijn W, Moro G, et al. ESPGHAN Committee on Nutrition. Donor human milk for preterm infants: current evidence and research directions. J Pediatr Gastroenterol Nutr 2013; 57:535-42.
8. Untalan PB, Keeney SE, Palkowetz KH, Rivera A, Goldman AS. Heat susceptibility of interleukin-10 and other cytokines in donor human milk. Breastfeed Med 2009; 4:137-44.
9. Baro C, Giribaldi M, Arslanoglu S, et al. Effect of two pasteurization methods on the protein content of

human milk. Front Biosci (Elite Ed) 2011; 3:818-29.
10. Henderson TR, Fay TN, Hamosh M. Effect of pasteurization on long chain polyunsaturated fatty acid levels and enzyme activities of human milk. J Pediatr 1998; 132:876-8.
11. Dupont D, Mandalari G, Mollé D, et al. Food processing increases casein resistance to simulated infant digestion. Mol Nutr Food Res 2010; 54:1677-89.
12. Casper C, Carnielli VP, Hascoet JM, et al. rhBSSL improves growth and LCPUFA absorption in preterm infants fed formula or pasteurized breast milk. J Pediatr Gastroenterol Nutr 2014; 59:61-69.
13. Hård AL, Nilsson AK, Lund AM, Hansen-Pupp I, Smith LEH, Hellström A. Review shows that donor milk does not promote the growth and development of preterm infants as well as maternal milk. Acta Paediatr 2019; 108:998-1007.
14. Socha-Banasiak A, Pierzynowski S, Woliński J, et al. The pig as a model for premature infants - the importance of immunoglobulin supplementation for growth and development. J Biol Regul Homeost Agents 2017; 31:87-92.
15. Goncharova K, Arevalo Sureda E, Wolinski J, Lozinska L, Weström B, Pierzynowski SG. Importance of maternal immunoglobulin transfer for cognitive function and neuronal plasticity – study on newborn piglet model. Plos One 2017**;** 28 2(6):e0180002.
16. Vandenplas Y, Szajewska H, Benninga M, et al. BITSS Study Group. Development of the Brussels Infant and Toddler Stool Scale ('BITSS'):protocol of the study. BMJ Open 2017; 7:e014620.
17. Anchieta LM, Xavier CC, Colosimo EA, Souza MF. Weight of preterm newborns during the first twelve weeks of life. Braz J Med Biol Res 2003; 36:761-70.
18. Moößeler A, Schwarzmaier T, Gregory PC, Piechotta M, Beyerbach M, Kamphues J. Pancreatic exocrine insufficiency affects not only digestibility of nutrients and growth, but also body composition and endocrinological parameters –study on piglets used as a model for children. Pancreat Disord Ther 2015; 5:S5.
19. Lund A, Löfqvist C, Pivodic A, Lundgren, P, Hård AL, Hellström A, Hansen-Pupp I. Unpasteurised maternal breast milk is positively associated with growth outcomes in extremely preterm infants. Acta Paediatrica 2019;10.1111.
20. Parra-Llorca A, Gormaz M, Lorente-Pozo S, et al. Impact of donor human milk in the preterm very low birth weight gut transcriptome profile by use of exfoliated intestinal cells. Nutrients 2019; 11:2677
21. Parra-Llorca A, Gormaz M, Alcántara C, Cernada M, Nuñez-Ramiro A, Vento M, Collado MC. Preterm gut microbiome depending on feeding type: significance of donor human milk. Front Microbiol 2018; 9:1376.
22. Moro GE, Billeaud C, Rachel B, et al. Processing of donor human milk: update and recommendations from the European Milk Bank Association (EMBA). Front Pediatr 2019;7:49.
23. Koletzko B, Poindexter B, Uauy R. Nutritional care of preterm infants: scientific basis and practical guidelines. World Rev Nutr Diet Basel 2014; 110:215-27.
24. Valentine CJ, Morrow G, Reisinger A, Dingess KA, Morrow AL, Rogers LK. Lactational stage of pasteurized human donor milk contributes to nutrient limitations for infants. Nutrients 2017; 9:302.
25. Moya F, Sisk PM, Walsh KR, Berseth CL. A new liquid human milk fortifier and linear growth in preterm infants. Pediatrics 2012; 130:e928-35.
26. Sangild PT, Thymann T, Schmidt M, Stoll B, Burrin DG, Buddington RK. Invited review: the preterm pig as a model in pediatric gastroenterology. J Anim Sci 2013; 91:4713-29.
27. Sullivan S, Schanler RJ, Kim JH, et al. An exclusively human milk-based diet is associated with a lower rate of necrotizing enterocolitis than a diet of human milk and bovine milk-based products. J Pediatr 2010; 156:562-67.
28. Schanler RJ, Lau C, Hurst NM, Smith EO. Randomized trial of donor human milk versus preterm formula as substitutes for mothers' own milk in the feeding of extremely premature infants. Pediatrics 2005; 116:400-406.
29. Martin CR, Cheesman A, Brown J, Makda M, Kutner AJ, DaSilva D. Factors Determining optimal fatty acid absorption in preterm infants. J Pediatr Gastroenterol Nutr 2016; 62:130-36.
30. Lapillonne A, Groh-Wargo S, Gonzalez CH, Uauy R. Lipid needs of preterm infants: updated recommendations. J Pediatr 2013; 162:37-47.
31. Pierzynowska K, Wolinski J, Weström B, Jazwiec R, Shmigel H, Pierzynowski SG. Absorption of

Polyunsaturated Fatty Acid (PUFA) is related to IgG blood levels of neonatal pigs during the first 48 hours postpartum. J Immunol Res 2020; 6,2020:3813250.

32. Lu J, Jilling T, Li D, Caplan MS. Polyunsaturated fatty acid supplementation alters proinflammatory gene expression and reduces the incidence of necrotizing enterocolitis in a neonatal rat model. Pediatr Res 2007;61:427-32.

lncRNA SNHG3 accelerates the proliferation and invasion of non-small cell lung cancer by downregulating miR-340-5p

W-W. He[1, 2], H-T. Ma[1], X. Guo[2], W-M. Wu[2], E-J. Gao[2] and Y-H. Zhao[2]

[1]Department of Thoracic Surgery, The First Affiliated Hospital of Soochow University, Suzhou City, Jiangsu, China; [2]Department of Thoracic Surgery, Shanghai Jiaotong University Affiliated No 6th People's Hospital, Shanghai, China

Received June 22, 2020 – Accepted October 29, 2020

Small nucleolar RNA host genes (SNHGs) as a subset of long non-coding RNAs (lncRNAs) act critical roles in tumor progression. The present study aimed to elucidate the role and mechanisms of SNHG3 in non-small cell lung cancer (NSCLC). The correlation of SNHG3/miR-340-5p/HOXA10 with the clinicopathological features and outcomes in NSCLC was analyzed by TCGA cohort. *In vitro* and *in vivo* functional experiments were conducted to assess the role of SNHG3 in NSCLC cells. Bioinformatic analysis and luciferase gene reporter were used to estimate the interaction between miR-340-5p and SNHG3/HOXA10 3'UTR. The effects of SNHG3 and (or) miR-340-5p on HOXA10 expression were detected by qRT-PCR and Western blot analysis. As a consequence, the elevated expression of SNHG3 and HOXA10 or lowered expression of miR-340-5p was related to the lymph node infiltration, distant metastases and unfavorable prognosis in NSCLC. Ectopic expression of SNHG3 boosted the proliferation and invasion of NSCLC cells *in vitro* and *in vivo*, whereas downregulation of SNHG3 reversed these effects. Moreover, SNHG3 could bind with miR-340-5p and reduce its expression levels, and miR-340-5p attenuated SNHG3-induced tumor proliferation and HOXA10 expression in NSCLC cells. Our findings unveiled that SNHG3 might be an oncogenic factor in NSCLC by downregulating miR-340-5p.

Lung cancer ranks the first leading cause of cancer-related deaths in China and contributes to a tremendous threat to human health (1). Non-small cell lung cancer (NSCLC) accounts for 80% of lung cancer cases and approximately75% of the patients with NSCLC are diagnosed at an advanced stage due to tumor invasiveness and metastases (2). Accumulating data have shown that the dysregulation of long noncoding RNAs (lncRNAs) is involved in the pathogenesis and progression of NSCLC (3-5), therefore, identification of the novel lncRNAs may provide potential targets for NSCLC.

Small nucleolar RNA host gene 3 (SNHG3) as an oncogenic lncRNA plays vital roles in cancer progression. It has been reported that SNHG3 is upregulated in a variety of cancers such as osteosarcoma (OS) (6), acute myeloid leukemia (AML) (7), clear cell renal cell carcinoma (CCRCC) (8), gastric cancer (GC) (9), oral squamous cell carcinoma (10), and thyroid carcinoma (11). In addition, elevated SNHG3 expression indicates a correlation with tumor size (6), lymph node metastasis (11) and poor prognosis (6-9) in cancer patients, and boosts the growth, invasion, metastasis and glycolysis metabolism, but blocks

Key words: SNHG3; miR-340-5p; proliferation; invasion; non-small cell lung cancer

Corresponding Author:
Dr. Hai-Tao Ma,
Department of Thoracic Surgery,
The First Affiliated Hospital of Soochow University,
No. 188 Shizi Road,
Suzhou City, Jiangsu 215006, China
e-mail: mahaitao2019@163.com

0393-974X (2020)
Copyright © by BIOLIFE, s.a.s.
This publication and/or article is for individual use only and may not be further reproduced without written permission from the copyright holder.
Unauthorized reproduction may result in financial and other penalties
DISCLOSURE: ALL AUTHORS REPORT NO CONFLICTS OF INTEREST RELEVANT TO THIS ARTICLE.

the cell apoptosis in multiple cancer cells (7-12). Mechanical investigations show that SNHG3 acts by regulating TOP2A (8) and MED18 (9) in CCRCC and GC or sponging miR-196a-5p in OS (6), miR-758-3p/SRGN in AML (7), miR-214-3p/PSMD10 in thyroid carcinoma (11) and miR-330-5p in breast cancer (12). These studies suggest that SNHG3 can modulate gene expression and miRNAs to participate in carcinogenesis.

Previous reports showed that SNHG3 can enhance the proliferation and migration of NSCLC by regulating IL-6/JAK2/STAT3 signaling (13, 14). However, the clinical prognosis and molecular mechanisms of SNHG3 in NSCLC remain unknown. In the present study, high expression of SNHG3/HOXA10 or low expression of miR-340-5p was linked to the lymph node infiltration or distant metastases, and acted as a prognostic factor of poor prognosis in NSCLC. Ectopic expression of SNHG3 promoted the proliferation and invasion of NSCLC by downregulating miR-340-5p.

MATERIALS AND METHODS

Clinical samples

The expression levels of SNHG3, HOXA10, miR-340-5p, miR-186-5p, miR-196a-5p, miR-135b-5p, miR-139-5p, miR-326, miR-135a-5p, miR-758-3p, miR-330-5p, miR-216a-5p, miR-196b-5p and miR-182-5p as well as the prognostic data of NSCLC patients (n = 515) were acquired from The Cancer Genome Atlas (TCGA) RNA sequencing dataset (https://genome-cancer.ucsc.edu/). Ethical approval for this study was obtained from the Ethics Committee of The First Affiliated Hospital of Soochow University.

Materials

Normal lung epithelial cells BEAS-2B and NSCLC cell lines (SPC-A1, A549, NCI-H23 and NCI-H460) were stored in our laboratory. Lentiviruses mediated si-SNHG3 (GCACACTGTGTTGGTGGTTATATTA) or si-NC (GCATGTCGTTGGG TGTATTAACTTA), SNHG3 plasmids and control group as well as miR-340-5p mimic and inhibitor were purchased from GenePharma (Shanghai, China).

Cell transfection

SPC-A1 and A549 cells were cultured in DMEM medium supplemented with 10% heat-inactivated FBS, 100U/ml of penicillin, and 100 μg/ml of streptomycin. Cells in this medium were placed in a humidified atmosphere containing 5% CO2 at 37°C. When SPC-A1 and A549 cells reached 60-80% confluence, they could be used for transfection with si-SNHG3/si-NC or SNHG3/control plasmids, and cultured at 37°C and 5% CO2 for 4 h.

Quantitative RT-PCR (qRT-PCR) analysis

To measure the expression of SNHG3, miR-340-5p and HOXA10 in NSCLC cell lines, qRT-PCR analysis was conducted. Total RNA was extracted by TRIzol (Invitrogen) or a High Pure miRNA isolation kit (Roche) according to the manufacturer's protocol. Reverse transcription was carried out by a PrimeScript RT Reagent Kit or a TaqMan MicroRNA Reverse Transcription kit (Life Technologies). The amplification of cDNA was implemented by SYBR Premix Ex Taq (TaKaRa). The primer sequences are listed as follows: SNHG3: Forward 5'-CAGTGGTCGCTTCTTCTCCTT-3', Reverse: 5'-GGCATGAAATGCACCTCAAT-3'; miR-340-5p: Forward 5'-AAUCAGUCUCAUUGCUUUAUAA-3', Reverse: 5'-CAAATTCGTGAAGCGTTCCATAT-3'; HOXA10: Forward 5'- GGCAAAGAGTGGTCGGAAGAAGCG-3', Reverse: 5'- AACCAGCCCTGCACA GATGTAACGG-3'. GAPDH or U6 gene was used as an endogenous control.

Western blot analysis

SPC-A1 and A549 cell lines were harvested and extracted using lysis buffer (Tris-HCl, SDS, Mercaptoethanol, Glycerol). Cell extracts were boiled for 5 min in loading buffer and then an equal amount of cell extracts were separated on 12% SDS-PAGE gels. Separated protein bands were transferred into polyvinylidene fluoride (PVDF) membranes. The primary antibodies against PCNA (ab13969, abcam), MMP2 (ab97779, abcam) and HOXA10 (720220, Invitrogen) were diluted (1:1000) according to the instructions and incubated overnight at 4°C. A detailed description of the Western blotting was conducted as previously described (3).

MTT and Transwell assays

MTT and Transwell assays were carried out as previously described (3).

Dual-luciferase reporter assay

SPC-A1 and A549 cells were seeded into 24-well

plates. After 24 h incubation, a luciferase report vector PRL-TK-pMIR containing WT or Mut SNHG3 3'UTR was co-transfected with miR-340-5p mimic or inhibitor into SPC-A1 and A549 cells. 48 h after transfection, luciferase activities were measured by a Dual-luciferase Reporter System (Promega).

In-vivo tumorigenesis

Male nu/nu nude mice (4-6 week, n = 5) were provided by Shanghai Experimental Animal Research Center. A tumor xenograft model was constructed by being subcutaneously injected by si-SNHG3 or si-NC transfected SPC-A1 cells. After 5 weeks, the tumor size was measured and the tumor samples were collected. The tumor volume was obtained according to the formula: length × width$^2/_2$.This protocol was approved by the Animal Ethics Committee of The First Affiliated Hospital of Soochow University.

H&E staining and immunochemistry analysis

H&E staining and Immunochemistry (IHC) analysis of Ki-67 (#12202, Cell Signaling) index were performed as previously reported (3).

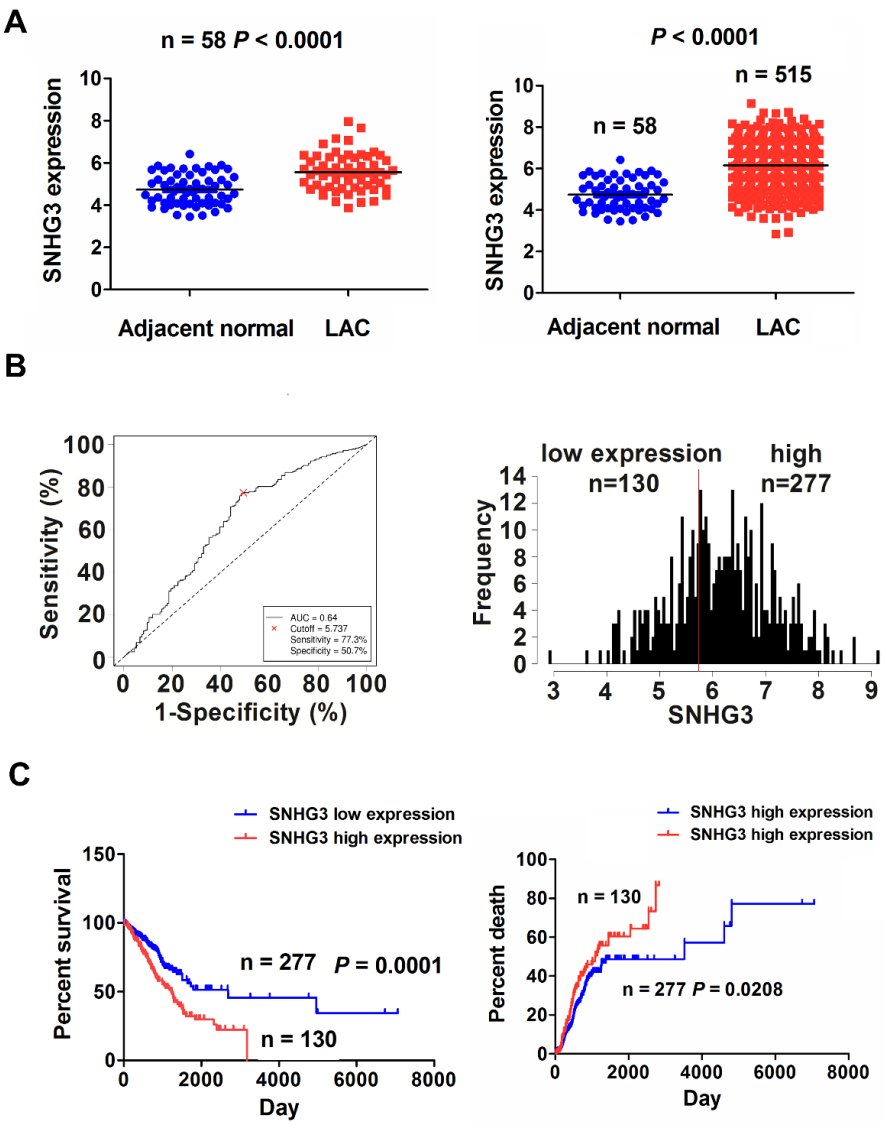


Fig. 1. *Elevated expression of SNHG3 was associated with poor survival and tumor recurrence in NSCLC.* ***A****) TCGA analysis of the expression levels of SNHG3 in paired and unpaired NSCLC tissue samples.* ***B****) The cutoff value of SNHG3 was obtained by ROC curve in NSCLC and divided the patients into high and low SNHG3 expression groups.* ***C****) Kaplan-Meier analysis of the correlation of high or low SNHG3 expression with the poor survival and tumor recurrence in NSCLC patients.*

Statistical analysis

Statistical analyses were carried out by SPSS 20.0 (IBM, SPSS, Chicago, IL, USA) and GraphPad Prism 7.0. Student's *t*-test, *Chi*-squared and Analysis of Variance were used to assess the statistical significance for the comparisons between the two groups. Survival or recurrence curves were acquired by the Kaplan-Meier and log-rank test. Univariate analysis and multivariate models were established by a Cox proportional hazards regression model. $P < 0.05$ had a statistical significance.

RESULTS

Elevated expression of SNHG3 was an independent factor of poor prognosis in patients with NSCLC

The expression of SNHG3 was assessed in NSCLC tissue samples from the TCGA cohort, which indicated that SNHG3 expression was dramatically upregulated in paired (n = 58) and unpaired NSCLC tissues (n = 515, Fig. 1A). In the light of SNHG3 expression levels, the patients' survival time and survival status, a cutoff value (5.737) of SNHG3 was gained in NSCLC patients by using a cutoff Finder (http://molpath.charite.de/cutoff/load.jsp), and divided the patients into high and low SNHG3 expression groups (Fig. 1B). High expression of SNHG3 was associated with lymph node infiltration in NSCLC patients. Kaplan-Meier analysis showed that the patients with high SNHG3 expression harbored a lower survival rate and a higher recurrence rate as compared with those with low SNHG3 expression (Fig. 1C).

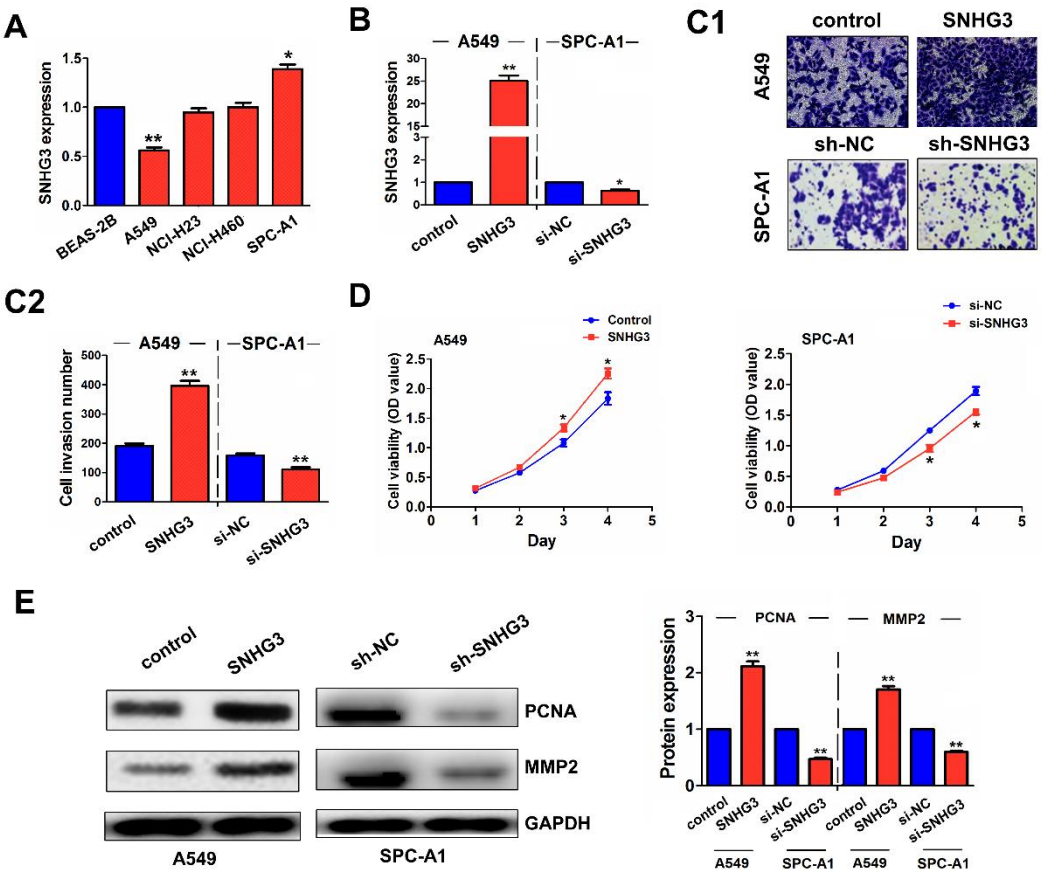


Fig. 2. *SNHG3 enhanced the proliferation and invasion of NSCLC cells.* ***A****) qRT-PCR analysis of the expression levels of SNHG3 in multiple NSCLC cell lines.* ***B****) qRT-PCR analysis of the overexpression efficiency of SNHG3 plasmids in A549 or si-SNHG3 in SPC-A1 cell line.* ***C****) Transwell analysis of the effects of SNHG3 overexpression or knockdown on cell invasion in A549 or SPC-A1 cells.* ***D****) MTT analysis of the effects of SNHG3 overexpression or knockdown on cell proliferation in A549 or SPC-A1 cells.* ***E****) Western blot analysis of the effects of SNHG3 overexpression or knockdown on PCNA and MMP2 expression in A549 or SPC-A1 cells. The data are presented as the mean± SD. *P<0.05; **P<0.01.*

SNHG3 enhanced the proliferation and invasion of NSCLC cells

The expression of SNHG3 was detected in NSCLC cell lines by qRT-PCR, which indicated that SNHG3 harbored an increased expression in SPC-A1 cell line but a reduced expression in A549 cell line as compared with the BEAS-2B cell line (Fig. 2A). The overexpression efficiencies of SNHG3 plasmids in A549 or knockdown efficiencies of si-SNHG3 in SPC-A1 were determined by qRT-PCR analysis (Fig. 2B). Functional experiments showed that restored SNHG3 expression facilitated the cell invasion and viability as compared with the control group, but silencing SNHG3 had the opposite effects (Fig. 2C, D). Western blot analysis showed that SNHG3 increased the expression of PCNA and MMP2 in A549 cells, but downregulation of SNHG3 reduced their expression in SPC-A1 cells (Fig. 2E).

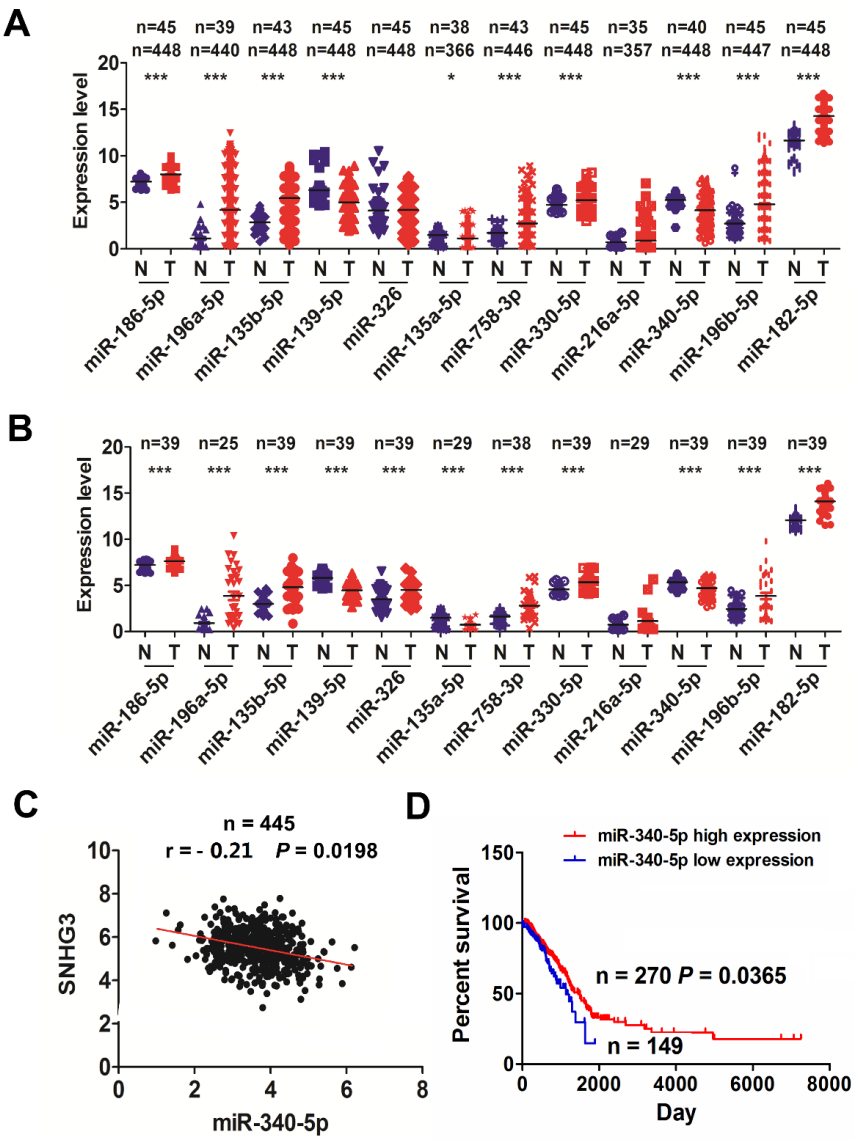


Fig. 3. *High expression of miR-340-5p was associated with a favorable survival in patients with NSCLC.* ***A, B****) TCGA analysis of the expression levels of 12 miRNAs in unpaired and paired NSCLC tissues.* ***C****) Pearson correlation analysis of the correlation of SNHG3 with miR-340-5p expression in NSCLC tissues.* ***D****) Kaplan-Meier analysis of the association of high or low miR-340-5p expression with overall survival in NSCLC patients.*

Low expression of miR-340-5p was associated with poor survival in NSCLC patients

In terms of the high stringency, starBasev2.0 (http://starbase.sysu.edu.cn/starbase2 /index.php) was used to identify 12 miRNAs which may bind with SNHG3, among which miR-340-5p/-135a-5p/139-5p indicated a dramatically decreased expression in unpaired (Fig. 3A) and paired (Fig. 3B) NSCLC tissues as compared with the adjacent normal tissues. Pearson correlation analysis demonstrated that miR-340-5p possessed a negative correlation with SNHG3 expression in NSCLC tissues (Fig. 3C). A cutoff value (3.687) of miR-340-5p was obtained and divided the patients into high and low miR-340-5p expression groups. Low expression of miR-340-5p was positively associated with distant metastases in patients with NSCLC. Kaplan-Meier analysis indicated that the patients with low miR-340-5p expression harbored

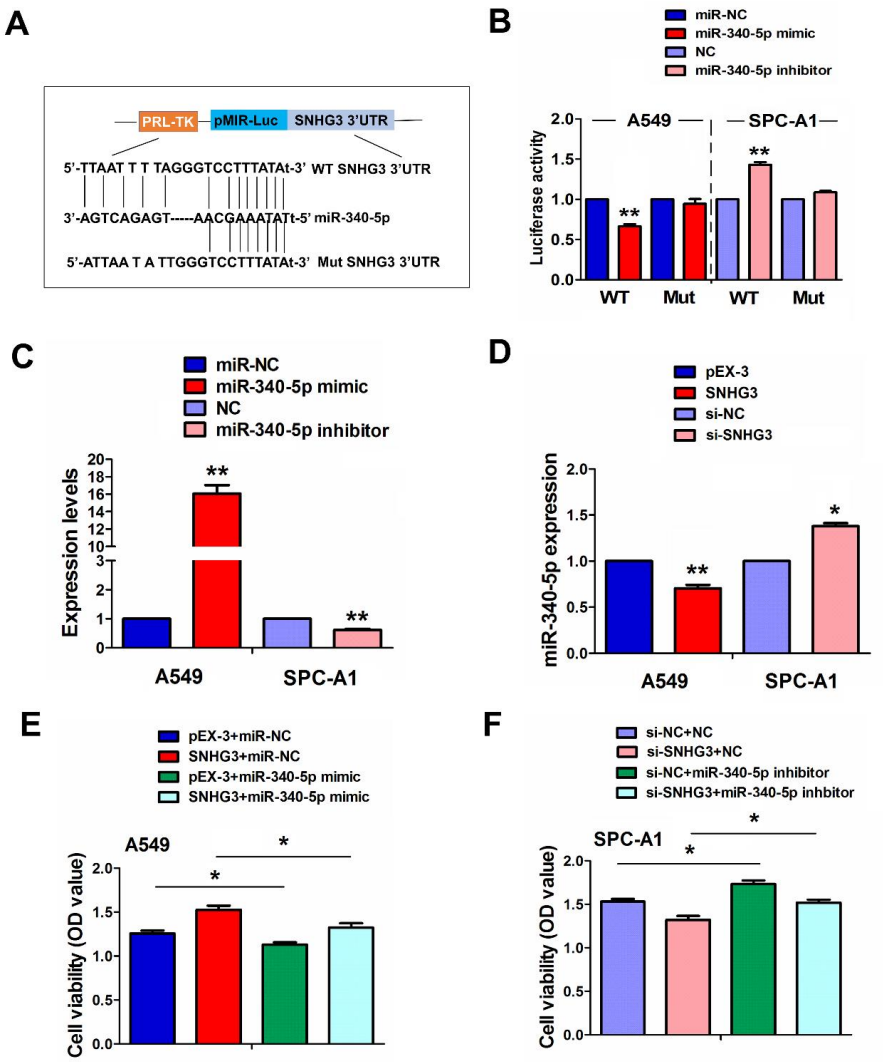


Fig. 4. *SNHG3 could bind with miR-340-5p in NSCLC cells.* ***A****) The binding sites between miR-340-5p and WT or Mut SNHG3 3'UTR.* ***B****) The effects of miR-340-5p mimic or inhibitor on the luciferase activity of WT or Mut SNHG3 3'UTR in A549 or SPC-A1 cell line.* ***C****) qRT-PCR analysis of the overexpression or knockdown efficiency of miR-340-5p mimic or inhibitor in A549 or SPC-A1 cell line.* ***D****) qRT-PCR analysis of the effects of SNHG3 overexpression or knockdown on miR-340-5p expression in A549 or SPC-A1 cell line.* ***E, F****) MTT analysis of the cell proliferation after co-transfection with miR-340-5p mimic and SNHG3 plasmids in A549 or miR-340-5p inhibitor and si-SNHG3 in SPC-A1 cell line. The data are presented as the mean± SD. *P<0.05, **P<0.01.*

a worse survival as compared with those with high miR-340-5p expression (Fig. 3D).

SNHG3 could bind with miR-340-5p expression in NSCLC cells

The binding sites between miR-340-5p and WT or Mut SNHG3 3'UTR are shown in Fig. 4A. After WT or Mut SNHG3 3'UTR was co-transfected with miR-340-5p mimic into A549 or miR-340-5p inhibitor into SPC-A1 cells, miR-340-5p weakened the luciferase activity of WT SNHG3 3'UTR in A549 cells, but its inhibitor had an opposite effect. miR-340-5p mimic or inhibitor had no effects on that of Mut SNHG3 3'UTR as compared to the control group (Fig. 4B). The overexpression efficiency of miR-340-5p mimic in A549 or the knockdown efficiency of miR-340-5p inhibitor in SPC-A1 was determined by qRT-PCR analysis (Fig. 4C). In addition, ectopic SNHG3 expression inhibited the expression of miR-340-5p, while silencing SNHG3 increased its expression (Fig. 4D). Moreover, after the co-transfection with SNHG3 plasmids and miR-340-5p mimic into A549 or si-SNHG3 and miR-340-5p inhibitor into SPC-A1 cells, miR-340-5p mimic suppressed the proliferation and attenuated the proliferation promoting effect of SNHG3 in A549 cell line (Fig. 4E), but miR-340-5p inhibitor displayed an opposite effect (Fig. 4F).

High expression of HOXA10 was an independent prognostic factor of poor survival in patients with NSCLC

The targets of miR-340-5p (n = 8) were screened

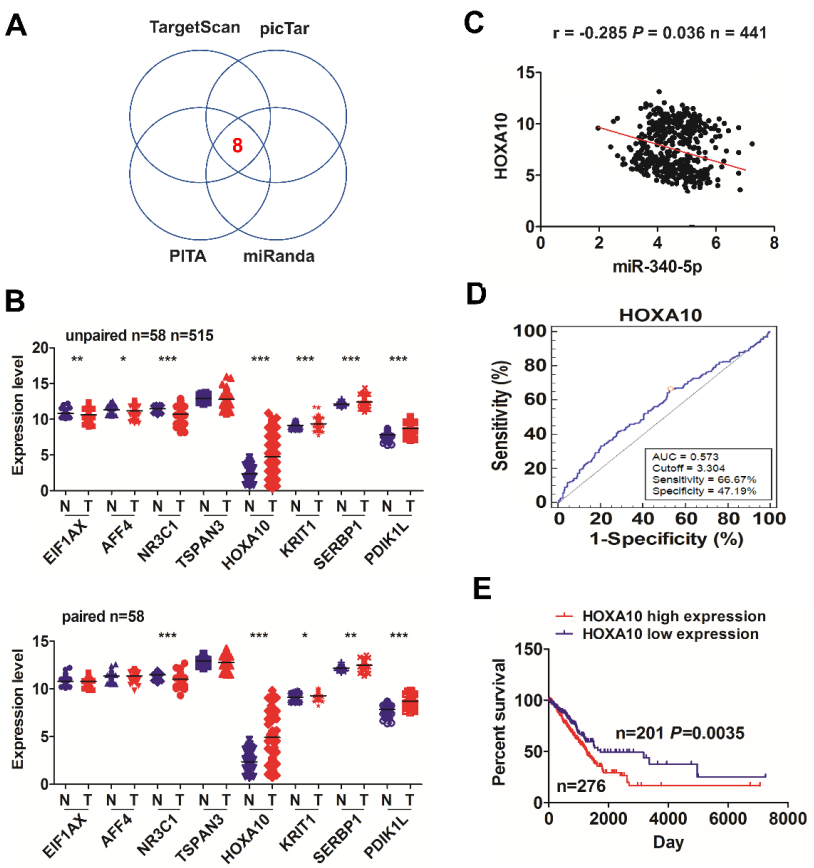


Fig. 5. *Upregulation of HOXA10 expression was associated with a poor survival in NSCLC patients.* ***A)*** *Identification of 8 targets of miR-340-5p by four prediction tools.* ***B)*** *TCGA analysis of the expression levels of these 8 target genes in unpaired and paired NSCLC tissues.* ***C)*** *Pearson correlation analysis of the correlation of HOXA10 with miR-340-5p expression in NSCLC tissues.* ***D)*** *The cutoff value of HOXA10 was obtained by ROC curve in NSCLC.* ***E)*** *Kaplan-Meier analysis of the association of high or low HOXA10 expression with overall survival in patients with NSCLC.*

by using starBasev2.0 (http://starbase.sysu.edu.cn/starbase2 /index.php) (Fig. 5A), among which HOXA10, KRIT1, SERBP1 and PDIK1L indicate an extreme upregulation in unpaired and paired NSCLC tissues (Fig. 5B). Pearson correlation analysis indicated that HOXA10 exhibited a negative correlation with miR-340-5p in NSCLC tissues (Fig. 5C).

The cutoff value (3.304) of HOXA10 in NSCLC was acquired (Fig. 5D), and divided the patients into high and low HOXA10 expression groups. HOXA10 expression was associated with distant metastases in NSCLC. Kaplan-Meier analysis revealed that the patients with high HOXA10 expression harbored a poorer survival as compared with those with low HOXA10 expression (Fig. 5E).

MiR-340-5p reversed SNHG3-induced HOXA10 expression in NSCLC cells

The binding sites between miR-340-5p and WT or Mut HOXA10 3'UTR are demonstrated in Fig. 6A. To verify whether miR-340-5p can bind with HOXA10 3'UTR, WT or Mut HOXA10 3'UTR was transfected with miR-340-5p mimic into A549 or its inhibitor into SPC-A1 cells, and miR-340-5p mimic reduced the

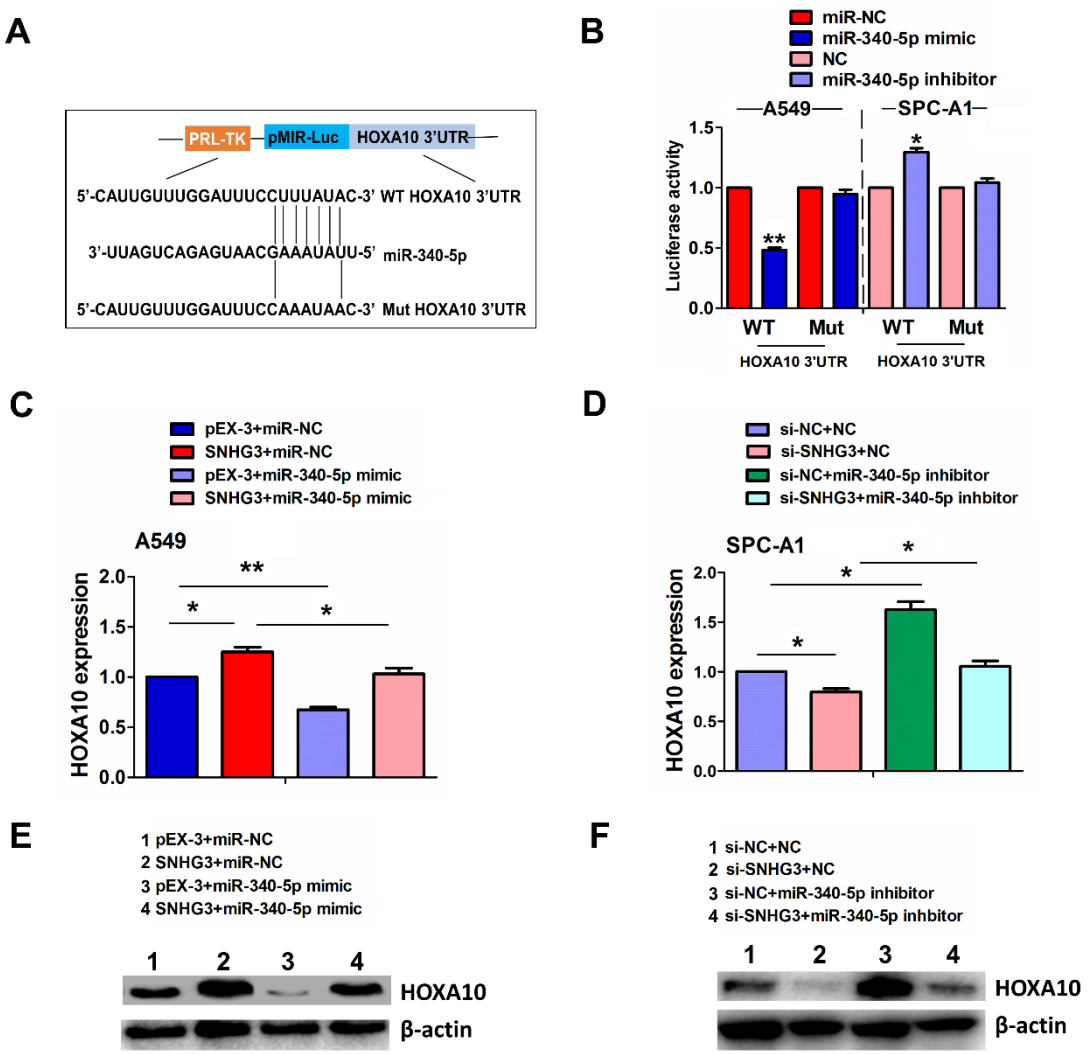


Fig. 6. *miR-340-5p counteracted SNHG3-induced HOXA10 expression in NSCLC cells. A) The binding sites between miR-340-5p and WT or Mut HOXA10 3'UTR.* ***B****) The effects of miR-340-5p mimic or inhibitor on the luciferase activity of WT or Mut HOXA10 3'UTR in A549 or SPC-A1 cell line.* ***C, D****) qRT-PCR and (****E, F****) Western blot analysis of the HOXA10 expression after co-transfection with miR-340-5p mimic and SNHG3 plasmids in A549 or miR-340-5p inhibitor and si-SNHG3 in SPC-A1 cell line. The data are presented as the mean± SD. *P<0.05; **P<0.01.*

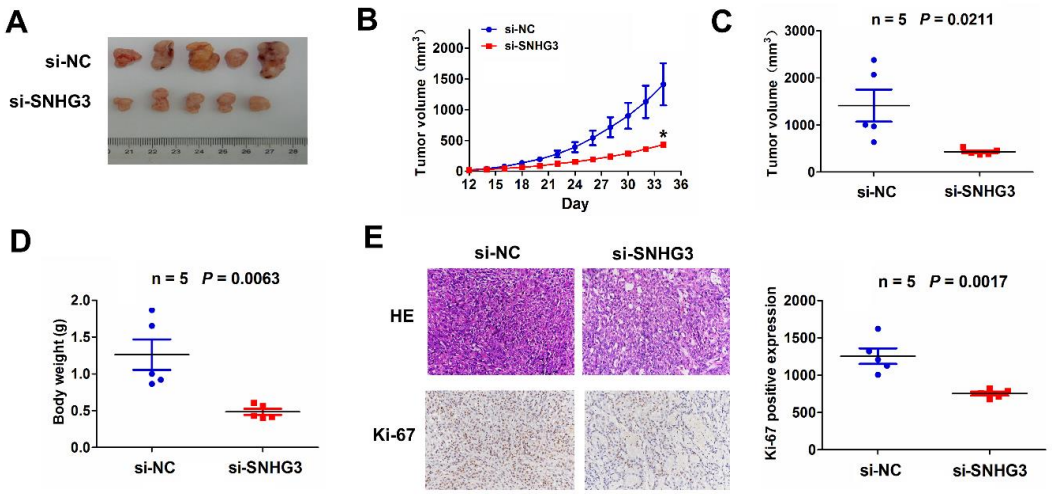


Fig. 7. *SNHG3 knockdown inhibited the tumorigenesis of NSCLC.* ***A, B****) The tumor size was detected every three days and the tumor growth curve was indicated in si-SNHG3 and si-NC groups.* ***C, D****) The tumor volume and weight were measured in si-SNHG3 and si-NC groups.* ***E****) HE staining of the tumor cell number and IHC analysis of the Ki-67 index in si-SNHG3 and si-NC groups.*

luciferase activity of WT HOXA10 3'UTR in A549 cells, but its inhibitor showed an opposite effect. miR-340-5p mimic or inhibitor exerted no effects on that of Mut HOXA10 3'UTR as compared to the control group (Fig. 6B). Additionally, after co-transfection with SNHG3 plasmids and miR-340-5p mimic into A549 or si-SNHG3 and miR-340-5p inhibitor into SPC-A1 cells, qRT-PCR (Fig. 6 C, D) and Western blot analysis (Fig. 6 E, F) indicated that miR-340-5p downregulated HOXA10 expression and attenuated SNHG3-induced HOXA10 expression in A549 cells, but miR-340-5p inhibitor indicated an opposite effect.

Knockdown of SNHG3 suppressed the tumorigenesis of NSCLC

The comparison of tumor size between control and si-SNHG3 groups is indicated in Fig. 7A. The tumor growth was inhibited in si-SNHG3 transfected SPC-A1 cells as compared with the control group (Fig. 7B). After an investigation for three weeks, the tumor volume and weight were lowered in the si-SNHG3 group as compared with those in the control group (Fig. 7C, D). HE staining showed that the number of tumor cells in the si-SNHG3 group was reduced as compared with the control group, and IHC analysis indicated that Ki-67 index was lowered by silencing SNHG3 as compared with the control group (Fig. 7E).

DISCUSSION

Increasing evidence has indicated that upregulated SNHG3 expression is related to the tumor metastasis and poor prognosis in various cancers (6-9, 11). Previous study showed that increased expression of SNHG3 is associated with an unfavorable survival in NSCLC (14). Coinciding with this study, large sample data from a TCGA cohort showed that SNHG3 was upregulated in 515 unpaired and 58 pair-matched NSCLC tissues. Upregulation of SNHG3 was associated with lymph node metastases and acted as an independent prognostic factor of poor survival and tumor recurrence in patients with NSCLC.

SNHG3 acts as an oncogene in a variety of malignant tumors including NSCLC (7-14). Herein, in consistence with previous reports (13, 14), silencing SNHG3 suppressed the growth and invasion of NSCLC cells *in vitro* and *in vivo*, but its overexpression displayed the opposite effects. PCNA and MMP2 can

be used to assess the tumor proliferation and invasion in NSCLC (15). In the present study, silencing SNHG3 reduced PCNA and MMP2 expression and overexpressing SNHG3 increased their expression. Our studies suggested that SNHG3 might act as a proliferation-promoting factor in NSCLC.

SNHG3 can sponge miRNAs to promote tumorigenesis and invasion (6, 7, 11, 12). Herein, SNHG3 was found to bind with miR-340-5p and have a negative correlation with miR-340-5p in NSCLC cells. Additionally, lncRNA HAND2-AS1 or MCM3AP-AS1 also sponges miR-340-5p to participate in the proliferation of ovarian cancer (16) and lung cancer (17).

It is known that miR-340-5p suppresses the growth, invasiveness and stemness maintenance in glioblastoma, OS and NSCLC by Wnt/β-catenin signaling (18-20), but favors cell viability and colony formation in thyroid cancer (21). In the present study, miR-340-5p expression was decreased and indicated a favorable survival in patients with NSCLC. Homeobox A10 (HOXA10) can facilitate the proliferation and invasion in NSCLC (22). In our present study, HOXA10 was identified as a direct target of miR-340-5p and indicated a poor survival in patients with NSCLC. Moreover, miR-340-5p reversed SNHG3-induced cell proliferation and HOXA10 expression. Our findings indicated that SNHG3 acted by regulating miR-340-5p/HOXA10 axis in NSCLC.

In brief, our findings revealed that upregulation of SNHG3 was associated with lymph node metastasis and acted as an independent prognostic factor of poor survival in NSCLC patients. SNHG3 promoted the growth and invasion of NSCLC cells by downregulating miR-340-5p.

REFERENCES

1. Chen W, Zheng R, Zhang S, et al. Cancer incidence and mortality in China, 2013. Cancer Lett 2017; 401:63-71.
2. Zhou F, Geng J, Xu S, et al. FAM83A signaling induces epithelial-mesenchymal transition by the PI3K/AKT/Snail pathway in NSCLC. Aging (Albany NY) 2019; 11(16):6069-88.
3. Wu W, Zhao Y, Gao E, et al. LncRNA DLEU2 accelerates the tumorigenesis and invasion of non-small cell lung cancer by sponging miR-30a-5p. J Cell Mol Med 2020; 24(1):441-50.
4. Yang J, Qiu Q, Qian X, et al. Long noncoding RNA LCAT1 functions as a ceRNA to regulate RAC1 function by sponging miR-4715-5p in lung cancer. Mol Cancer 2019; 18(1):171.
5. Pang L, Cheng Y, Zou S, Song J. Long noncoding RNA SNHG7 contributes to cell proliferation, migration, invasion and epithelial to mesenchymal transition in non-small cell lung cancer by regulating miR-449a/TGIF2 axis. Thorac Cancer 2020; 11(2):264-76.
6. Chen J, Wu Z, Zhang Y. LncRNA SNHG3 promotes cell growth by sponging miR-196a-5p and indicates the poor survival in osteosarcoma. Int J Immunopathol Pharmacol 2019; 33:2058738418820743.
7. Peng L, Zhang Y, Xin H. lncRNA SNHG3 facilitates acute myeloid leukemia cell growth via the regulation of miR-758-3p/SRGN axis. J Cell Biochem 2020; 121(2):1023-31.
8. Zhang C, Qu Y, Xiao H, et al. LncRNA SNHG3 promotes clear cell renal cell carcinoma proliferation and migration by upregulating TOP2A. Exp Cell Res 2019; 384(1):111595.
9. Xuan Y, Wang Y. Long non-coding RNA SNHG3 promotes progression of gastric cancer by regulating neighboring MED18 gene methylation. Cell Death Dis 2019; 10(10):694.
10. Liu Z, Tao H. Small nucleolar RNA host gene 3 facilitates cell proliferation and migration in oral squamous cell carcinoma via targeting nuclear transcription factor Y subunit gamma. J Cell Biochem 2020; 121(3):2150-58.
11. Sui G, Zhang B, Fei D, Wang H, Guo F, Luo Q. The lncRNA SNHG3 accelerates papillary thyroid carcinoma progression via the miR-214-3p/PSMD10 axis. J Cell Physiol 2020; 235:6615-24.
12. Li Y, Zhao Z, Liu W, Li X. SNHG3 Functions as miRNA sponge to promote breast cancer cells growth through the metabolic reprogramming. Appl Biochem Biotechnol 2020; 191:1084-99.
13. Liu L, Ni J, He X. Upregulation of the long noncoding RNA SNHG3 promotes lung adenocarcinoma proliferation. Dis Markers 2018; 2018:736716.
14. Shi J, Li J, Yang S, et al. LncRNA SNHG3 is activated

by E2F1 and promotes proliferation and migration of non-small-cell lung cancer cells through activating TGF-β pathway and IL-6/JAK2/STAT3 pathway. J Cell Physiol 2020; 235(3):2891-2900.

15. Yang CC, Chang CK, Chang MT, Shyur LF. Plant galactolipid dLGG suppresses lung metastasis of melanoma through deregulating TNF-α-mediated pulmonary vascular permeability and circulating oxylipin dynamics in mice. Int J Cancer 2018; 143(12):3248-61.
16. Chen J, Lin Y, Jia Y, et al. LncRNA HAND2-AS1 exerts anti-oncogenic effects on ovarian cancer via restoration of BCL2L11 as a sponge of microRNA-340-5p. J Cell Physiol 2019; 234(12):23421-36.
17. Li X, Yu M, Yang C. YY1-mediated overexpression of long noncoding RNA MCM3AP-AS1 accelerates angiogenesis and progression in lung cancer by targeting miR-340-5p/KPNA4 axis. J Cell Biochem 2020; 121(3):2258-67.
18. Kim S, Choi JY, Seok HJ, Park MJ, Chung HY, Bae IH. miR-340-5p suppresses aggressiveness in glioblastoma multiforme by targeting Bcl-w and Sox2. Mol Ther Nucleic Acids 2019; 17:245-55.
19. Rongxin S, Pengfei L, Li S, Xiaochen J, Yihe H. MicroRNA-340-5p suppresses osteosarcoma development by down-regulating the Wnt/β-catenin signaling pathway via targeting the STAT3 gene. Eur Rev Med Pharmacol Sci 2019; 23(3):982-91.
20. Lu G, Zhang Y. MicroRNA-340-5p suppresses non-small cell lung cancer cell growth and metastasis by targeting ZNF503. Cell Mol Biol Lett 2019; 24:34.
21. Zhao P, Ma W, Hu Z, Zhang Y, Zhang S, Wang Y. Up-regulation of miR-340-5p promotes progression of thyroid cancer by inhibiting BMP4. J Endocrinol Invest 2018; 41(10):1165-72.
22. Hou J, Wang Y, Zhang H, Hu Y, Xin X, Li X. Silencing of LINC00461 enhances radiosensitivity of lung adenocarcinoma cells by down-regulating HOXA10 via microRNA-195. J Cell Mol Med 2020; 24:2879-90.

Cholesterol 24S-Hydroxylase overexpression increases the lipid droplet formation of human umbilical cord mesenchymal stem cells but does not affect adipocyte differentiation

Y. Jiang[1], WJ. Zhang[1], AM. Liang[1], GW. Lv[1], BD. Ma[2], H. Yue[2], L. Sun[2] and H. Zhang[1]

[1]Department of Neurosurgery, Zhengzhou Central Hospital affiliated Zhengzhou University, Zhengzhou, China; [2]Center of Stem Cell and Regenerative Medicine, Zhengzhou Central Hospital affiliated Zhengzhou University, Zhengzhou, China

Received July 16, 2020 – Accepted October 8, 2020

Dysregulation of the adipo-osteogenic differentiation balance of mesenchymal stem cells (MSCs), which are common progenitor cells of adipocytes and osteoblasts, has been associated with many pathophysiologic diseases, such as obesity, osteopenia, and several neurodegenerative disorders. Growing evidence suggests that lipid metabolism is crucial for maintaining stem cell homeostasis and cell differentiation, however, the detailed underlying mechanisms are largely unknown. In this study, we demonstrate that CYP46A1 genes are key determinants of MSC increasing lipid droplet formation. Brain cholesterol is synthesized *in situ* and cannot cross the blood–brain barrier: to be exported from the central nervous system into the blood circuit, excess cholesterol must be converted to 24S-hydroxycholesterol by the cholesterol 24-hydroxylase encoded by the CYP46A1 gene. To address this issue, we used an adeno-associated virus (AAV) gene transfer strategy to increase CYP46A1 expression in order to investigate the consequences on the human mesenchymal stem cell (hU-MSCs). CYP46A1 expression was assessed with Western blotting and quantitative reverse transcription PCR. We found that CYP46A1 expression was increased during adipogenesis, and treatment with exogenous CYP46A1 increased adipogenesis. Thus, we hypothesize that CYP46A1 overexpression in hU-MSCs would significantly enhance cholesterol turnover in the brain of hypoxic-ischemic encephalopathy (HIE). CYP46A1 can potentially serve as a specific target to modify the therapeutic and biological effects of hU-MSCs on HIE patients.

Mesenchymal stem cells (MSCs) are multipotent progenitor cells capable of differentiation into several types of mesenchymal cells, such as osteoblasts, adipocytes, and chondrocytes (1, 2). The differentiation commitment of MSCs is exquisitely regulated. In particular, adipo-osteogenic balance is reciprocally maintained. Adipogenic factors, such as peroxisome proliferator-activated receptor γ (PPARγ) and miR-204, inhibit osteoblastic differentiation; conversely, osteogenic regulators, including runt-related transcription factor 2 (Runx2), show anti-adipogenic effects (3). Dysregulation of this balance is linked to pathophysiologic states. In particular, increased marrow fat content, caused by a shift in the MSC lineage commitment to adipocytes rather than osteoblasts, has been observed and contributes to pathogenesis of various bone diseases (4). Although each lineage-specific factor is needed for fate determination, the exact governing mechanism is not clearly defined. Several stem cell fate-

Key words: CYP46A1; HIE; mesenchymal stem cells; adipocyte differentiation

Corresponding Author:
Dr. Hui Zhang,
Zhengzhou Central Hospital
Affiliated Zhengzhou University,
No. 16, Tongbai Road,
Zhongyuan, Zhengzhou 450007, China
e-mail: 528zhanghui@sina.com

0393-974X (2020)
Copyright © by BIOLIFE, s.a.s.
This publication and/or article is for individual use only and may not be further reproduced without written permission from the copyright holder.
Unauthorized reproduction may result in financial and other penalties
DISCLOSURE: ALL AUTHORS REPORT NO CONFLICTS OF INTEREST RELEVANT TO THIS ARTICLE.

determining factors have been newly discovered, and this information provides new insight into the differentiation and treatment of metabolic bone diseases (5, 6).

There is a growing body of evidence of a strong association between abnormalities in brain cholesterol homeostasis (especially high concentrations in neurons) and several neurodegenerative disorders, including Alzheimer's disease, Huntington's disease and Parkinson's disease (7). However, there has been no experimental demonstration that increased cholesterol concentrations in neurons may result in neurodegeneration *in vivo*. Cholesterol does not freely cross the intact blood–brain barrier and nearly all cholesterol in the adult brain is synthesized *in situ* by astrocytes. Only 0.02% of the cholesterol in the adult brain undergoes a turnover each day and thus most is metabolically inert (8). The cholesterol abundance in the central nervous system (CNS) depends primarily on local synthesis and efflux. However, cholesterol cannot be exported directly from the brain; it is converted to 24S-hydroxycholesterol by cholesterol 24-hydroxylase (encoded by the CYP46A1 gene), a highly conserved cytochrome P450 enzyme, which can be exported across the blood–brain barrier (BBB) and is metabolized into bile acids in the liver. The BBB is a highly selective, semi-permeable membrane composed of specialized endothelial cells held together by tight junctions. It is somewhat surprising that MSCs can cross the BBB unassisted, particularly as MSCs can be involved in maintaining the BBB. Small numbers of MSCs can cross the intact BBB (9). Recent *in vitro* studies suggest that oxidative stress and endogenous neurotransmitters upregulate CYP46A1, with glutamate eliciting the highest increase in CYP46A1 activity (10). These are well-accepted mechanisms that are associated with brain damage in neonatal hypoxic-ischemic encephalopathy (HIE), the clinical syndrome of brain dysfunction in newborns with few tools for diagnosis and intervention. Studies on regulation of cholesterol homeostasis in the developing brain, as well as its disturbance after HIE at early postnatal stage, would allow for a better understanding of lipid disorders and their involvement in HIE gray and white matter injury (11).

In the present study, we found that CYP46A1 expression was increased during adipogenesis, and treatment with exogenous CYP46A1 increased adipogenesis. These results show the novel molecular mechanism of the adipo-osteogenic differentiation balance and suggest a new therapeutic option for treating neurological diseases.

MATERIALS AND METHODS

All lipid-containing media were freshly prepared and not reused. Dexamethasone, 3-isobutyl-1-methylxanthine (IBMX), rosiglitazone, indometacin, insulin, ascorbic-2-phosphate, puromycin, d,l-threo-1-phenyl-2-decanoylamino-3-morpholino-1-propanol (PDMP), Oil Red O, and Alizarin red S were purchased from Sigma Aldrich. β-Glycerophosphate was purchased from USB Corp. BODIPY™

Human umbilical-derived mesenchymal stem cells

hU-MSCs were isolated from the umbilical cord of 5 healthy donors. The experimental design was approved by the Institutional Ethics Committee (Zhengzhou Central Hospital, Henan, China). Samples were obtained from donors after they provided informed consent according to the Helsinki Declaration of 1975, as revised in 2013. The samples were washed with phosphate-buffered saline (PBS) and minced and digested at 37°C for 1 h with 2% of type I collagenase (Gibco, Life Technologies, Madrid, Spain). Tissue remains were filtered through a 100 µm cell strainer (BD Biosciences Durham, NC, USA). Cells were then washed with DMEM/HAM F12 (Sigma-Aldrich, St. Louis, MO, USA) containing penicillin and streptomycin (1%), seeded onto tissue culture flasks ($1\text{-}2 \times 10^6$ cells/mL) in DMEM/HAM F12 medium with penicillin and streptomycin (1%), supplemented with 15% extracellular vesicle-free human serum, and incubated at 37°C in a 5% CO_2 atmosphere. Human serum was obtained from whole-blood donations of AB-blood-group-typed donors according to the criteria of Valencia Transfusion Centre. To eliminate the extracellular vesicle fraction, serum was centrifuged during 18 h at 120,000 ×g and 4°C using a SW-28 swinging-bucket rotor (Beckman Coulter, CA, USA). When cells reached semiconfluence, culture plates were washed and the ASC phenotype confirmed by flow cytometry (Cytoflex, Beckman, USA) using specific

antibodies, anti-CD73-PE, anti-CD90-APC, anti-CD105-APC-A750, anti-CD34, CD45, CD11b, CD19, HLA-DR-FITC (Biolegend, USA), and measuring cellular viability with propidium iodide.

Stably expressing SensGFP-CYP46A1

The lentivirus vector containing the SensGFP-CYP46A1 reporter was purchased from Genechem (Shanghai, China). Stably expressing SensGFP-CYP46A1 were selected by the treatment of puromycin (2μg/ml). After the different treatments, the cells were fixed and then analyzed using fluorescence microscopy (Olympus BX51, Japan).

RNA extraction and qRT-PCR

Total RNA was isolated from tissues or cell lines using Trizol reagent (Invitrogen, USA). RNA was reversed transcribed into cDNAs using the PrimeScript™ one stepRT-PCR kit (TaKaRa, China) according to the manufacturer's protocol. The mRNA level was measured using the SYBR® Premix DimmerEraser™ kit (TaKaRa, China) and the ABI7500 system (Applied Biosystems, USA). The relative mRNA expression change was calculated by using $2^{-\Delta\Delta}$Ct method and the β-actin was used as an internal control for normalization. The primer sequences are listed in Table I.

Western blot

Each group of MSCs in 10 cm dishes were washed with cold phosphate-buffered saline (PBS) and incubated with RIPA containing 1 mM phenylmethylsulfonyl fluoride, followed by cell scraping and centrifugation. The nuclear protein was isolated as recommended by the manufacturer (Beyotime, Shanghai, China). After measuring protein concentration with the bicinchoninic acid (BCA) assay, 40 μg total protein containing loading buffer was separated by SDS-PAGE and transferred to PVDF membranes. The membranes were immersed in 5% non-fat milk for 2 h to block non-specific antigen and then incubated with primary antibodies (CYP46A1, 1:1000) overnight at 4°C. After incubation with secondary antibodies (1:2000), an enhanced chemiluminescence detection system (PerkinElmer, USA) with an ECL reagent was used to expose proteins on the membrane. A semi-quantitative analysis of protein bands was performed using AlphaEaseFC 4.0 software.

Adipogenic induction and Oil red O stain

Before inducing differentiation, hU-MSCs were grown to confluence. Adipogenic differentiation was induced by culturing hU-MSCs for 4 days in adipogenic induction medium (AIM, 10% FBS, 1 μmol/L dexamethasone, 0.5 mmol/L IBMX, 1 μmol/L insulin, and 1 μmol/L rosiglitazone in α-MEM). After 4 days, the cells were cultured in α-MEM containing only 10% FBS and 1 μmol/L insulin, and the medium was changed every 2 days. Differentiated adipocytes were stained with Oil Red O as an indicator of intracellular lipid accumulation. In

Table I. *qPCR primer sequences*

Gene		Sequences (5′–3′)	Product size (bp)
CYP46A1	forward	AGAAGTATGGTCCTGTTGTA	20
		ACATTCAGACACCA AGCC	18
GAPDH	forward	CAACGGGAAACCCATCACCA	20
		ACGCCAGTAGACTCCACGACAT	22

Primer sequences for CYP46A1 and GATPDH. GATPDH: Glyceraldehyde phosphate dehydrogenase

brief, cells were washed twice with PBS and fixed with 4% paraformaldehyde for 1 h at 4°C. After two washes in distilled water, cells were stained for 1 h in freshly diluted Oil Red O solution (six parts Oil Red O stock solution and four parts H2O; Oil Red O stock solution is 0.5% Oil Red O in isopropanol) at 4°C.The stain was then removed and cells were washed twice with distilled water. Images of cells stained with Oil Red O were obtained with Olympus IX71 microscope and DP71 camera.

Statistical analysis

Statistical assay was performed using GraphPad Prism 7.0. All data in this study are shown as the mean ± Standard Error of Mean (SEM) of three independent experiments. The significance of the differences in mean values between and within multiple groups was examined by one-way ANOVA followed by Duncan's multiple range test. P value < 0.05 was considered as statistically significant.

RESULTS

Characterization of hU-MSCs

Isolated cells obtained after enzymatic treatment of Wharton's jelly displayed a fibroblast-like appearance during the first 3 days of culture. The

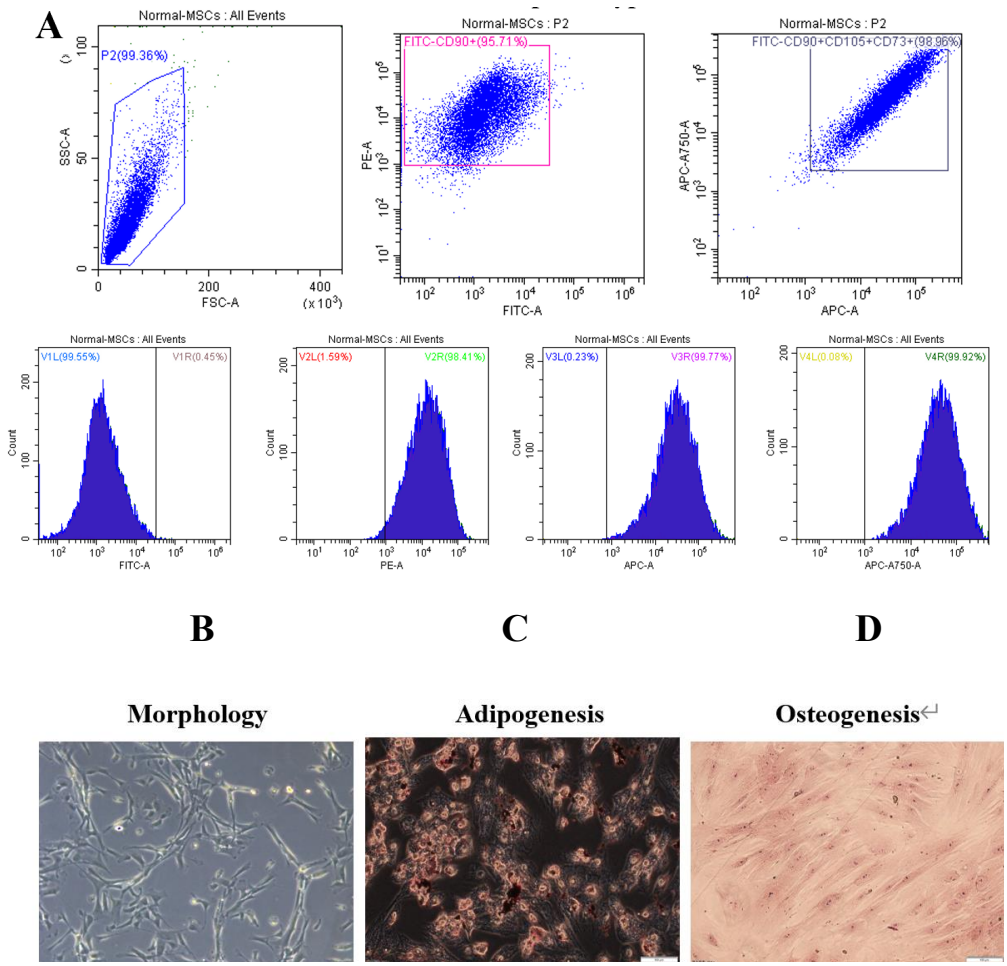


Fig. 1. *Morphology, immunophenotype, adipocyte and osteoblast differentiation of hU-MSCs.* ***A****) Mean fluorescence intensity (MFI) of CD34, CD45, CD11b, CD19, HLA-DR, CD73, CD90 and CD105 was determined on hU-MSCs by flow cytometric analysis.* ***B****) Representative micrographs depict morphology of hU-MSCs. (Scale bars indicate 100 mm).* ***C****) hU-MSCs were cultured in adipogenic medium for 21 days, and adipogenic differentiation was indicated by oil red O staining.* ***D****) hU-MSCs were cultured in osteogenic medium for 21 days, and osteoblast differentiation was indicated by Von Kossa staining for calcium phosphate.*

majority of cells were flat with a wide cytoplasm within stress fiber patterns inside. Contamination of culture with hematopoietic cells was excluded by absence of CD34, CD45, CD11b, CD19 and HLA-DR (Fig. 1A). Morphology of the cells changed with a higher level of confluence; the cytoplasm became narrower, and stress fibers were less apparent (Fig. 1B). Flow cytometry confirmed MSC signature of hU-MSCs at the fourth passage with a high expression of CD90, CD73 and CD105.

hU-MSCs adipogenic differentiation was shown by formation of intracytoplasmic lipid droplets stained with Oil Red O (Fig. 1C). Nevertheless, the hU-MSCs response to adipogenic induction was heterogeneous because cells did not all display this phenotype and because of the disparity in number and size of lipid droplets per cell. Osteogenic differentiation was also achieved by formation of clusters of small polygonal cells (Fig. 1D). These bone nodules were a site of calcium mineralization, as shown by Alizarin Red and von Kossa stains and tetracycline incorporation.

Overexpression of CYP46A1 in hU-MSCs

hU-MSCs were first plated on Matrigel-coated dishes and transfected with lentivirus encoding

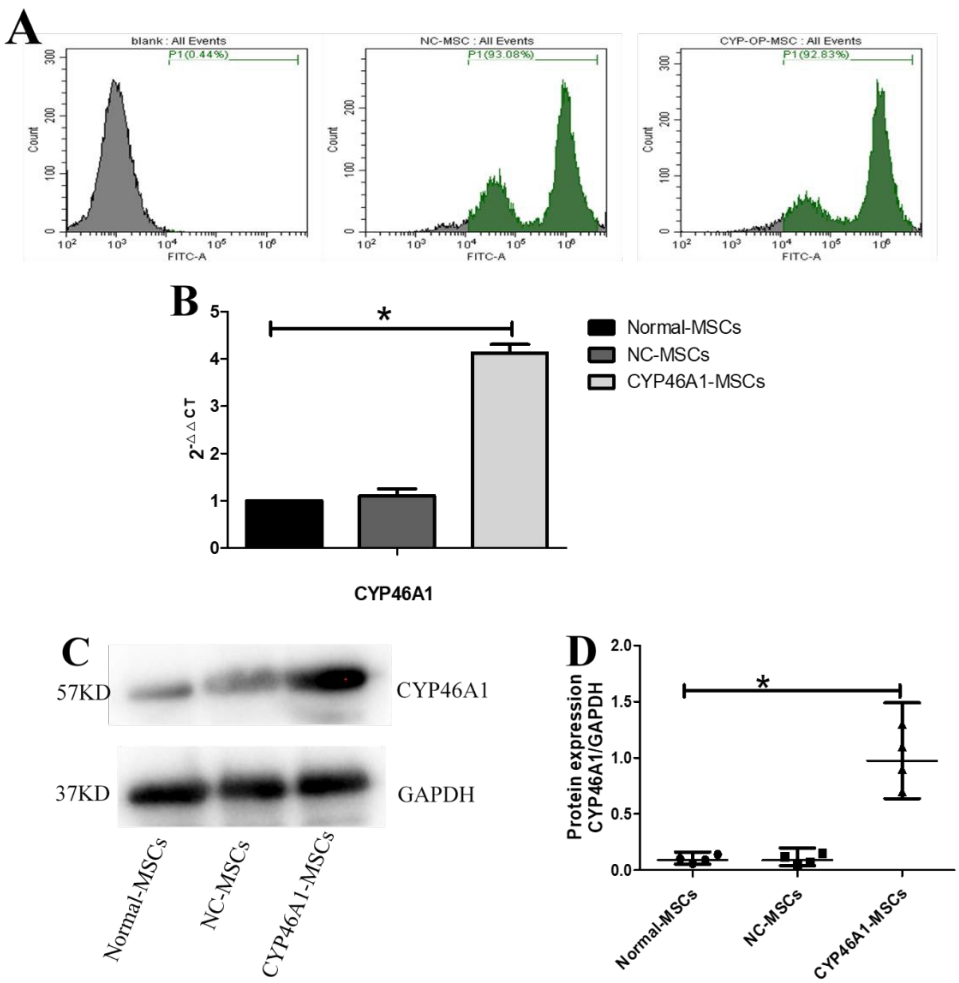


Fig. 2. *hU-MSCs were transduced with lentivirus encoding CYP46A1. **A)** Flow cytometric plot of GFP expression in hU-MSCs after 12 days of transduction. **B)** qRT-PCR results for expression of total RNA CYP46A1 in hU-MSCs. **C)** Western blot results for expression of total proteins of CYP46A1 in hU-MSCs. **D)** The optical density of CYP46A1/GAPDH was analyzed. Data represent mean±95% CI, *P<0.05, n=4.*

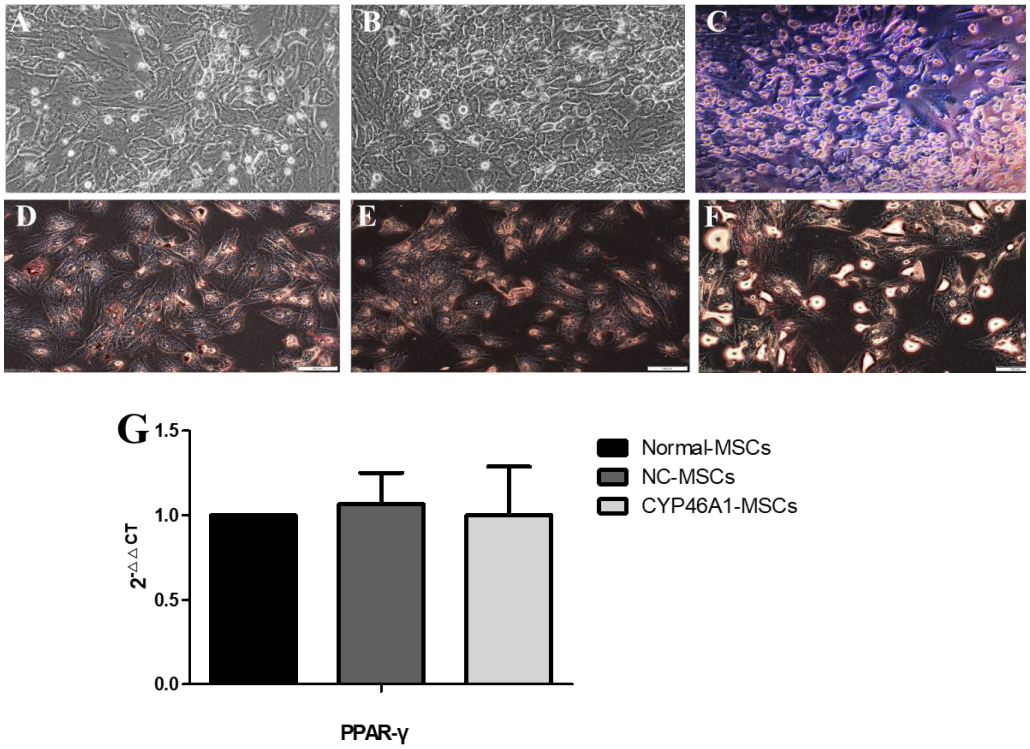


Fig. 3. *CYP46A1 increased the lipid droplet formation but did not affect adipocyte differentiation.* ***A****) Normal-MSCs were induced in adipogenic medium for 21 days; a lot of lipid droplets can be seen.* ***B****) NC-MSCs* ***C****) CYP46A1-MSCs.* ***D****) Normal-MSCs (****E****) and NC-MSCs (****F****) were induced in adipogenic medium, and adipogenic differentiation was indicated by oil red O staining. CYP46A1–MSCs (****G****) qRT-PCR for lipoprotein lipase gene. The expression of PPAR-γ was detected in induced adipocytes of each group. GAPDH was performed as a control.*

the CYP46A1 protein and cultured with 2 μg/mL puromycin and 10% FBS. After 12 days, about 92.83% of CYP46A1 lentivirus transfected hU-MSCs were GFP^+ as shown by flow cytometry analysis, suggesting high transduction efficiency (Fig. 2A). Expression of CYP46A1 gene was confirmed at both mRNA and protein levels by qRT-PCR (Fig. 2B) and Western analyses 12 days after transduction (Fig. 2 C, D). The results are expressed as mean ± SD. *$P \leq 0.05$. Representative example of four experiments.

Adipogenic differentiation of Normal/NC/CYP46A1–MSCs

For adipogenic differentiation, lipid-laden cells appeared after 3–4 days. After 3 weeks, more than 60% of each group of MSCs differentiated into adipocytes that were stained with Oil red O (Fig. 3 D-F), and a lot of lipid droplets could be seen (Fig. 3C).Our results indicated that CYP46A1 did not affect the mRNA expressions of PPAR-γ($P<0.05$, respectively) (Fig. 3G).

DISCUSSION

Present mainly in the brain, CYP46A1 catalyzes the hydroxylation of cholesterol into 24S-HC to eliminate surplus cholesterol from the brain, and thereby has an important role in maintenance of cholesterol homeostasis (12). CYP46A1 protein expression is low until 1 week after birth in mice and gradually increases to reach a steady level around 3 weeks. In humans, it reaches the adult level at around 3 years of age. This allows deposition of nearly all cholesterol at an early age to assist in the rapid expansion of the brain and myelin, and in the removal of redundant cholesterol as the animal matures. Thus, we hypothesize that CYP46A1 overexpression in hU-MSCs would significantly enhance cholesterol turnover in brain of HIE (13).

HIE is a neonatal neurological condition caused by anoxic or ischemic brain injury in the perinatal period. Current treatment for HIE is prompt resuscitation, administration of supportive measures to prevent hyperthermia and hypoglycemia, treatment and control of subclinical seizures, and therapeutic hypothermia within the first few hours after birth to minimize the condition's effects. Animal models of HIE have found that MSC administration improves the functional outcomes of affected animals. These therapeutic actions are believed to be due to a combination of the MSC capacity to suppress inflammation, release of neurotropic factors, and increase angiogenesis, as discussed above. MSC administration also reduced the number of seizures and increased long term potentiation (LTP) in animal models of HIE, supporting the MSCs being protective against the electrical effects of HIE. Similar trials have begun also in human patients, using autologous umbilical cord-derived MSCs (14, 15) (others registered on clinicaltrials.gov).

In this study we therefore used an adeno-associated virus gene transfer strategy to increase CYP46A1 expression in order to investigate the consequences on the human mesenchymal stem cell. Our results confirm that cholesterol 24S-Hydroxylase overexpression can increase the lipid droplet formation of human umbilical cord mesenchymal stem cells but not affect adipocyte differentiation. This suggests that our observations are relevant to the future safe clinical application in perinatal brain injury of CYP46A1-MSCs. However, activation of CYP46A1 may have more specialized roles than just removing cholesterol from the central nervous system. Future work is required to gain better insight into cholesterol homeostasis in the developing brain before considering clinical practice.

ACKNOWLEDGEMENT

This study was funded by Henan province medical science and technology project (No. LHGJ20191045)

REFERENCES

1. Rocha-Ferreira E, Hristova M. Plasticity in the neonatal brain following hypoxic-ischaemic injury. Neural Plast 2016; 2016:4901014
2. Barkhuizen M, Vles JS, et al. 25 years of research on global asphyxia in the immature rat brain. Neurosci Biobehav Rev 2017; 75:166-82.
3. Azzopardi D, Strohm B, Marlow N, et al. Effects of hypothermia for perinatal asphyxia on childhood outcomes. N Engl J Med 2014; 371(2):140-49
4. Oppliger B, Joerger-Messerli M, Mueller M, et al. Intranasal delivery of umbilical cord-derived mesenchymal stem cells preserves myelination in perinatal brain damage. Stem Cells Dev 2016; 25(16):1234-42.
5. . Katsuda T, Kosaka N, Takeshita F, et al. The therapeutic potential of mesenchymal stem cell-derived extracellular vesicles. Proteomics 2013; 13(10-11):1637-53
6. Zhang B, Shen L, Shi H, et al. Exosomes from human umbilical cord mesenchymal stem cells: identification, purification, and biological characteristics. Stem Cells Int 2016; 2016:1929536.
7. Wang K, Jiang Z, Webster KA, et al. Enhanced cardioprotection by human endometrium mesenchymal stem cells driven by exosomal MicroRNA-21. Stem Cells Transl Med 2017; 6(1):209-22
8. Mead B, Tomarev S. Bone marrow-derived mesenchymal stem cells-derived exosomes promote survival of retinal ganglion cells through miRNA-dependent mechanisms. Stem Cells Transl Med 2017; 6(4):1273-85
9. Shamas-Din A, Kale J, Leber B, et al. Mechanisms of action of Bcl-2 family proteins. Cold Spring Harb Perspect Biol 2013; 5(4):a008714.
10. Hu B, Chen S, Zou M, et al. Effect of extracellular vesicles on neural functional recovery and immunologic suppression after rat cerebral apoplexy. Cell Physiol Biochem 2016; 40(1-2):155-62.
11. Doeppner TR, Herz J, Gorgens A, et al. Extracellular vesicles improve post-stroke neuroregeneration and prevent postischemic immunosuppression. Stem Cells Transl Med 2015; 4(10):1131-43
12. Xin H, Li Y, Buller B, et al. Exosome-mediated transfer of miR-133b from multipotent mesenchymal stromal cells to neural cells contributes to neurite outgrowth. Stem Cells 2012; 30(7):1556-64.
13. Zhuang X, Xiang X, Grizzle W, et al. Treatment of

brain inflammatory diseases by delivering exosome encapsulated antiinflammatory drugs from the nasal region to the brain. Mol Ther 2011;19(10):1769-79

14. Lavrnja I, Smiljanic K, Savic D, et al. Expression profiles of cholesterol metabolism-related genes are altered during development of experimental autoimmune encephalomyelitis in the rat spinal cord. Sci Rep 2017; 7:2702.
15. Wu H, Li Z, Yang X, et al. SBDPs and Tau proteins for diagnosis and hypothermia therapy in neonatal hypoxic ischemic encephalopathy. Exp Ther Med 2017; 13:225-29.

HSA_CIRC_0004050 on proliferation and apoptosis of A549 cells through ERK/JNK signaling pathway

Y. Wang*, R.-K. Zang*and Y.-N. Du

Department of Radiation Oncology, The Affiliated Yantai Yuhuangding Hospital of Qingdao University, Yantai, China

Received September 3, 2020 – Accepted October 19, 2020

*These Authors contributed equally to this work

The aim of this study was to **screen the differentially expressed circular ribonucleic acid (circRNA) in non-small cell lung cancer (NSCLC) and explore its functional mechanism. Differentially expressed circRNAs in tumor tissues of NSCLC patients were detected via gene microarray and reverse transcription-quantitative polymerase chain reaction (RT-qPCR). The associaton between their expressions and the clinical phenotypes was explored combined with clinical data. The effect of overexpression of hsa_circ_0004050 on the proliferation of A549 cells was detected via cell counting kit-8 (CCK-8) assay and CFSE assay. The effect of overexpression of hsa_circ_0004050 (human circular ribonucleic acid_0004050) on the apoptosis of A549 cells was detected using the Annexin V-FITC/PI kit. Then the direct-acting miRNAs of hsa_circ_0004050 were screened using bioinformatics software and luciferase reporter assay, and the direct targets of miR-1233-3p were explored using bioinformatics software and luciferase reporter assay combined with RT-qPCR and Western blotting. The effects of overexpression of miR-1233-3p or knockdown of dual specificity phosphatase 9 (DUSP9) on the cell proliferation and apoptosis affected by overexpression of hsa_circ_0004050 were detected. Western blotting was performed to detect the effects of hsa_circ_0004050 on the extracellular signal-regulated kinase (ERK)/c-Jun N-terminal kinase (JNK) signaling pathway. The expression of hsa_circ_0004050 was significantly lower in tumor tissues than that in para-carcinoma tissues in NSCLC patients. The expression of hsa_circ_0004050 was significantly correlated with TNM stage, tumor size and lymph node metastasis. The results of survival analysis showed that the survival time of patients with a high expression of hsa_circ_0004050 was obviously prolonged. According to the results of phenotype assay, hsa_circ_0004050 could promote apoptosis and inhibit proliferation of A549 cells. In terms of its mechanism, hsa_circ_0004050 could markedly increase the protein expression of DUSP9 via targeting miR-1233-3p in A549 cells, thereby inhibiting the ERK/JNK signaling pathway. Hsa_circ_0004050 may serve as a potential therapeutic target for NSCLC or a biomarker for the diagnosis of NSCLC in the future.**

According to epidemiological research, lung cancer is one of the most common types of cancer around the world, accounting for 11.6% of the total, which has the highest mortality rate (18.4%) among all cancer types (1). Non-small cell lung cancer (NSCLC) is the most important type of lung

Key words: hsa_circ_0004050, ERK/JNK signaling pathway, cell proliferation, apoptosis, A549 cell lines

Corresponding Author:
Yuanna Du, MM
Department of Radiation Oncology,
The Affiliated Yantai Yuhuangding Hospital
of Qingdao University, No 20, Yuhuangding Road,
Zhifu District, Yantai, Shandong, 264000, China
Tel.: 86015315159466
e-mail: yuyuan19970119@163.com

0393-974X (2020)
Copyright © by BIOLIFE, s.a.s.
This publication and/or article is for individual use only and may not be further reproduced without written permission from the copyright holder.
Unauthorized reproduction may result in financial and other penalties
DISCLOSURE: ALL AUTHORS REPORT NO CONFLICTS OF INTEREST RELEVANT TO THIS ARTICLE.

cancer, representing 85% of the total. In the past few decades, with the clinical application of new treatment methods (including immunotherapy and various tyrosine kinase inhibitors), the survival rate of NSCLC patients has been greatly improved, but the cure and survival rates are still low, with a 5-year survival rate below 20% (2). There is a lack of reliable biomarkers for early diagnosis and targets for drug development due to the insufficient understanding of the underlying pathological mechanism of NSCLC, thus leading to a low survival rate of patients.

Circular ribonucleic acids (circRNAs) were discovered by Sanger in 1976, which, unlike ordinary linear RNAs, have a closed loop structure, making them more resistant to endogenous exonuclease and more stable in an endogenous environment (3). CircRNAs have a variety of functional mechanisms. For example, they can act as competitive endogenous RNAs (miRNA sponge) to relieve the inhibition of miRNAs on related mRNAs. They can also affect the expressions of related RNAs through the RNA-RNA or RNA-protein interaction, ultimately regulating gene expression at a variety of levels, and exerting a wide range of biological functions. Based on these mechanisms, a large number of research results have shown that circRNAs play important roles in tumorigenesis and cancer progression (4-7). However, the functional roles of a large number of circRNAs in NSCLC remain unknown. DUSP is a member of the MAPK family and contains at least 10 catalytically active enzymes (15). DUSP9, also known as MAPK4, has an important function of dephosphorylating p-ERK and p-JNK via targeting the MAPK signaling pathway, thereby inhibiting the MAPK signaling pathway (16). The pro-apoptotic and anti-apoptotic effects of ERK and JNK on NSCLC cells have long been recognized.

In the present study, the differentially expressed circRNAs in NSCLC tissues and para-carcinoma tissues were screened using high-throughput gene microarray and reverse transcription-quantitative polymerase chain reaction (RT-qPCR), the association between the expression level of the differentially expressed circRNA and the clinical phenotypes was explored, and its functional role and mechanism were investigated at the *in vitro* level. The results showed that hsa_circ_0004050 played an important role in the progression of NSCLC, which suppressed the mitogen-activated protein kinase (MAPK) signaling pathway via targeting the miR-1233-3p/dual specificity phosphatase 9 (DUSP9) axis, thereby inhibiting proliferation and promoting apoptosis of A549 cells. Therefore, hsa_circ_0004050 may be used as a new therapeutic target for NSCLC.

MATERIALS AND METHODS

Patients and tumor tissue sampling

This study was approved by the Ethics Committee of The Affiliated Yantai Yuhuangding Hospital of Qingdao University, and all participants signed the informed consent. The patients pathologically diagnosed with NSCLC before surgery were enrolled, while those who underwent radiotherapy, chemotherapy or other therapies before operation were excluded, so as to avoid the influence of drugs and other therapies on the circRNA expression profile. In this study, a total of 56 patients who underwent surgical treatment in our hospital from February 2015 to January 2020 were enrolled, and NSCLC tissues and para-carcinoma tissues were collected during the operation. Then the tissue samples were immediately stored in liquid nitrogen at -80°C.

Gene microarray assay

Total RNA was isolated from 3 cases of NSCLC tissues and the corresponding para-carcinoma normal tissues, and treated with RNase-R kits (Epicentre, Inc., Madison, Wisconsin, USA) according to the manufacturer's instructions, so as to remove linear RNAs. Then the RNA was subjected to hybridization assay using Arraystar-Human-CircRNA Microarray (Arraystar Inc., Rockville, MD, USA), washed and fixed, followed by treatment of hybridized microarrays with an Agilent scanner G2505C (Agilent Technologies, Santa Clara, CA, USA). Finally, differentially expressed circRNAs in NSCLC tissues and para-carcinoma tissues were screened ($p<0.05$ and Fold change >2).

Cell culture And transfection

NSCLC cell lines (A549) and pulmonary epithelial cell line (BEAS-2B) were purchased from the American Type

Culture Collection (ATCC) (Manassas, VA, USA). and were cultured with Dulbecco's modified Eagle medium (DMEM) (Gibco, Rockville, MD, USA) containing 10% fetal bovine serum (FBS) (Gibco, Rockville, MD, USA) and 1% penicillin-streptomycin in a humidified incubator with 5% CO_2 at 37°C.

The sequences of hsa_circ_0004050 were cloned into PLCDH-cir vectors (Ribobio, Guangzhou, China) to construct hsa_circ_0004050 overexpression lentiviral vectors. MiR-1233-3p mimic, miR-1233-3p inhibitor and miR-negative control (NC) were purchased from GenePharma (Shanghai, China). DUSP9 was knocked down using sh-RNA. The cells were transfected strictly according to the manufacturer's instructions of the kits.

Cell counting kit-8 (CCK-8) assay

The effects of different treatment methods on cell proliferation were detected via CCK-8 assay. A549 cell lines were inoculated into a 96-well plate (5000 cells/well) in a 5% CO_2 humid environment at 37°C for 24, 48 and 72 h. Then 10% (V/V) CCK-8 solution (Dojindo, Mashikimachi, Japan) was added into each well at a specific time point at 37°C. 4 h later, the absorbance was measured at 490 nm using an FLx800 Fluorescent Microplate Reader (BioTek, Biotek Winooski, VT, USA) at 24, 48 and 72 h.

CFSE assay

The effects of different treatment methods on cell proliferation were further detected using CFSE reagents (Life Technologies-Molecular Probes, Grand Island, NY, USA). The treated A549 cells were incubated with CFSE (10 nM) for 30 min and washed with complete medium. 72 h later, flow cytometry was performed.

Apoptosis assay

At 72 h after transfection, the cells were trypsinized, washed with phosphate buffered saline (PBS) for 3 times, and re-suspended in binding buffer, followed by staining using Annexin V-fluorescein isothiocyanate (FITC)/propidium iodide (PI) kits (BD Biosciences, Franklin Lakes, NJ, USA). Then the cells were washed twice with PBS (Invitrogen, Carlsbad, CA, USA) and detected using a FACSCalibur flow cytometer (BD Biosciences, Franklin Lakes, NJ, USA). The data were analyzed using FlowJo.

RT-qPCR

The total RNA was extracted from the cultured cells strictly according to the manufacturer's instructions of TRIzol kits (Invitrogen, Carlsbad, CA, USA). The purity and concentration of total RNA were detected using a spectrophotometer (Thermo Fisher Scientific, Waltham, MA, USA). Then RT-qPCR was performed using RT kits (TaKaRa, Tokyo, Japan) and SYBR Green PCR Master Mix (TaKaRa, Tokyo, Japan) on the CFX96 detection system (Bio-Rad, Hercules, CA, USA). With glyceraldheyde 3-phosphate dehydrogenase (GAPDH) as an internal reference, the relative expression of RNA was calculated using delta-delta CT ($2^{-\Delta\Delta Ct}$). The primer sequences used are shown in Table I.

Western blotting

The total protein was extracted from differently treated cells using radioimmunoprecipitation assay (RIPA) buffer (Beyotime, Shanghai, China), and its concentration was quantified using the bicinchoninic acid (BCA) kit (Thermo Scientific Pierce, Waltham, MA, USA). Then the total protein was separated via 10% sodium dodecyl sulphate-polyacrylamide gel electrophoresis (SDS-PAGE), transferred onto a polyvinylidene fluoride (PVDF) membrane (Millipore, Billerica, MA, USA) via semi-dry transfer process, sealed with tris-buffered saline (TBS) containing 5% skim milk for 1 h, and incubated with primary antibodies (1:1000, Abcam, Cambridge, MA, USA) at 4°C overnight. The next day, the protein was incubated again with horseradish peroxidase (HRP)-labeled secondary antibodies (1:2000, Abcam, Cambridge, MA, USA) in the dark for 2 h. Finally, the protein bands were visualized using enhanced chemiluminescence (ECL) kits (Pierce, Rockford, IL, USA).

Luciferase reporter assay

Based on the prediction results using bioinformatics software, the potential sequences (wild-type and mutant-type) binding to miR-1233-3p in hsa_circ_0004050 were cloned into pmirGLO vectors (Promega, Madison, WI, USA). A549 cells were co-transfected with pmirGLO-circ_0001946-WT reporter genes or pmirGLO-circ_0001946-MUT reporter genes and miR-1233-3p mimic or miR-NC using Lipofectamine™ 2000 in strict accordance with the manufacturer's instructions of the kits. 48 h later, luciferase reporter assay was performed

using a dual luciferase reporter assay system (Promega, Madison, WI, USA).

Statistical analysis

Statistical Product and Service Solutions (SPSS) 17.0 software (SPSS, Inc., Chicago, IL, USA) was used for statistical analysis. Data were expressed as mean ± standard deviation. Each independent experiment was repeated for at least 3 times. Differences were analyzed using Student's *t*-test or one-way analysis of variance. The correlation was analyzed via Pearson correlation analysis. The overall survival rate of NSCLC patients was analyzed using Kaplan-Meier method and log-rank test. $P<0.05$ was considered to be statistically significant.

RESULTS

Expression of hsa_circ_0004050 declined in NSCLC tissues

To screen the key circRNAs in the pathological process of NSCLC, differentially expressed circRNAs in NSCLC tissues and para-carcinoma tissues were screened via gene microarray ($p<0.05$ and Fold change >2) (Fig. 1A). Then 5 differentially expressed circRNAs significantly down-regulated in the 2 kinds of tissues were found via RT-qPCR, among which hsa_circ_0004050 was down-regulated most significantly (Fig. 1B). To further explore the association between hsa_circ_0004050 and NSCLC, 56 NSCLC patients were divided into high-expression group and low-expression group based on the mean expression of hsa_circ_0004050. As shown in Table II, the expression of hsa_circ_0004050 was significantly associated with TNM stage, tumor size and tumor metastasis in NSCLC patients. According to the Kaplan-Meier survival analysis, the survival time of patients in the high-expression group was obviously prolonged compared with that in the low-expression group (Fig. 1C).

Table I. *Primer sequences*

Primer	Primer sequence (5'-3')
hsa_circ_0004050	5'-ACCGAACATGAACATCAGCA-3'
	5'-AAACTTCGGTTGTCAGCTTCA-3'
hsa_circ_0003786	5'-TGCACAAGTTGCTAGCCTCA-3'
	5'-TCCCCAGTGGCTACTACCAT-3'
hsa_circ_0001424	5'-GCCTGGATGACTCTGAGGAG-3'
	5'-CTTTCTGCTGTGCCAAGTCA-3'
hsa_circ_0127271	5'-GCCTGGATGACTCTGAGGAG-3'
	5'-TTAACTTGCCTCCTCCTTGC-3'
hsa_circ_0004929	5'-TTTCCCCAACTTTGAGCATC-3'
	5'-TCTTCCAGTACAGCCCATCC-3'
DUSP9	5'-AGAAGCTGCGAGAGGAAGGCTA-3'
	5'- CAGCAAGGCTGGTCTCACACAG-3'
miR-1233-3p	5'-TGAGCCCTGTCCTCCC-3'
	5'- GAACATGTCTGCGTATCTC-3'
GAPDH	5'- CGCTTCGGCAGCACATATACTA-3'
	5'-CGCTTCACGAATTTGCGTGTCA-3'

Overexpression of hsa_circ_0004050 inhibited proliferation of A549 cells

To further detect the biological function of hsa_circ_0004050 in NSCLC, RT-qPCR was performed. The results showed that the expression of hsa_circ_0004050 obviously declined in A549 cells compared with that in BEAS-2B cells, and there was a statistically significant difference ($P<0.05$) (Fig. 2A).

In addition, the results of RT-qPCR revealed that the expression of hsa_circ_0004050 in A549 cells obviously increased in the hsa_circ_0004050 overexpression group, so further functional experiments could be carried out (Fig. 2B). The results of CCK-8 and CFSE assays showed that the proliferation rate of A549 cells in the hsa_circ_0004050 overexpression group was obviously lower than that in the hsa_circ_0004050 NC group (Fig. 2 C, D). The above findings indicate that overexpression of hsa_circ_0004050 can effectively inhibit the proliferation of A549 cells.

Overexpression of hsa_circ_0004050 promoted apoptosis of A549 cells

To further detect the effect of hsa_circ_0004050 overexpression on the apoptosis of A549 cells, flow cytometry was performed. It was found that the apoptosis rate was markedly higher in the hsa_circ_0004050 overexpression group than that

in the hsa_circ_0004050 NC group (Fig. 3A). In addition, the results of Western blotting manifested that the active caspase-3 and active caspase-9 protein expressions were markedly higher in the hsa_circ_0004050 overexpression group than those in the hsa_circ_0004050 NC group, with statistically significant differences (Fig. 3B). It can be seen that overexpression of hsa_circ_0004050 can promote the apoptosis of A549 cells.

Hsa_circ_0004050 suppressed expression of miR-1233-3p

A large number of studies have shown that

Table II. *Correlation between hsa_circ_0004050 expression and clinical characteristics of patients with NSCLC (n=56)*

Clinical index	hsa_circ_0004050 expression		*P*
	High-expression group	Low-expression group	
TNM stage			
Negative	19	7	0.0003
Positive	9	21	
Lymph node metastasis			
Yes	3	17	0.002
No	25	11	
Tumor size			
≥3 cm	10	23	0.00001
≤3 cm	18	5	

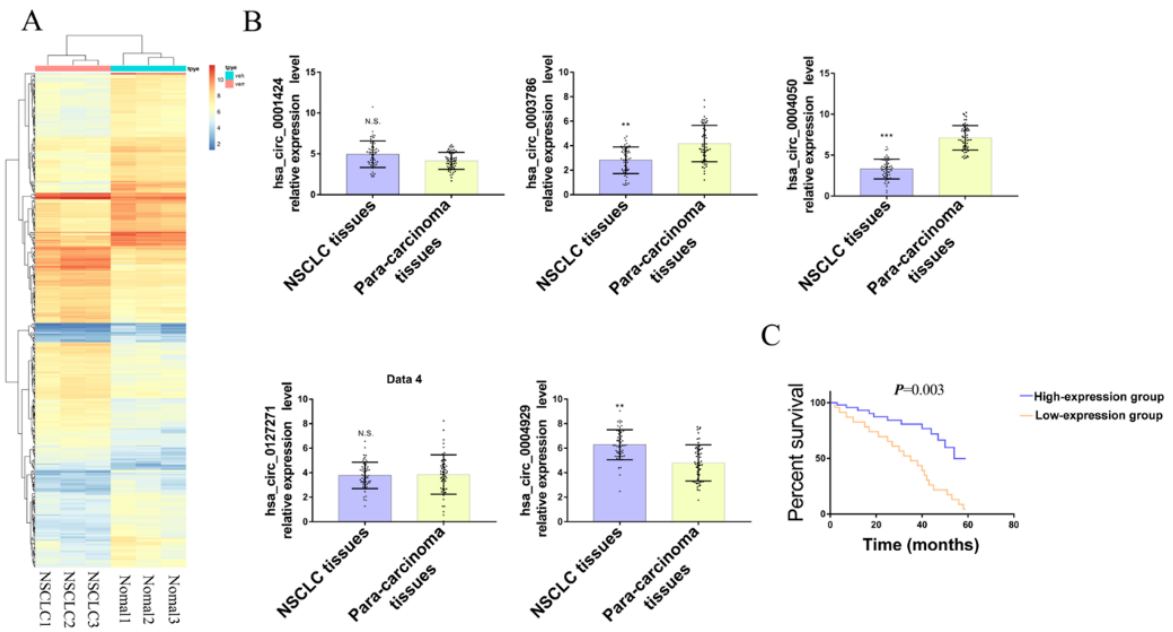


Fig. 1. *Expression of hsa_circ_0004050 declined in NSCLC tissues. **A**) Differentially expressed circRNAs in 3 cases of NSCLC tissues and para-carcinoma tissues screened via gene microarray. **B**) 5 differentially expressed circRNAs in the 2 kinds of tissues verified via RT-qPCR. **C**) Kaplan-Meier survival analysis in high-expression group and low-expression group.*

circRNAs can regulate the gene expression through interaction with miRNAs. Based on this, therefore, the mechanism of hsa_circ_0004050 in inhibiting proliferation and promoting apoptosis of A549 cells was explored. It was predicted using bioinformatics that miR-1233-3p might be the target of hsa_circ_0004050, and the potential binding sites between them are shown in Fig. 4A. The results of RT-qPCR manifested that the expression of miR-1233-3p evidently declined in A549 cells in the hsa_circ_0004050 overexpression group (Fig. 4B). Moreover, a significant negative correlation between hsa_circ_0004050 and miR-1233-3p was found via RT-qPCR and Pearson correlation analysis (Fig. 4C). Finally, the results of luciferase reporter assay manifested that miR-1233-3p mimic could evidently reduce the luciferase activity in A549 cells transfected with wild-type hsa_circ_0004050 plasmids compared with that in cells transfected with mutant-type hsa_circ_0004050 plasmids (Fig. 4D). It can be confirmed that miR-1233-3p is the direct target of hsa_circ_0004050 in A549 cells.

Hsa_circ_0004050 increased DUSP9 protein expression via targeting miR-1233-3p

Furthermore, the functional mechanism of hsa_circ_0004050 in affecting the A549 cell phenotype via targeting miR-1233-3p was explored. First, it was pointed out by bioinformatics prediction that DUSP9 was the direct target of miR-1233-3p, and the matched sequences are shown in Fig. 5A. Then the results of RT-qPCR manifested that the DUSP9 mRNA expression was distinctly lower in the miR-1233-3p mimic group than that in the miR-NC group, while it was distinctly higher in the miR-1233-3p inhibitor group, and there were statistically significant differences (Fig. 5B). Similarly, the results of Western blotting showed that the DUSP9 protein expression in A549 cells was distinctly decreased by miR-1233-3p mimic but distinctly increased by miR-1233-3p inhibitor (Fig. 5C). The wild-type and mutant-type DUSP9 3'-UTR sequences are shown in Fig. 5D. Finally, it was found in luciferase reporter assay that miR-1233-3p mimic could greatly lower the luciferase activity in A549 cells transfected with wild-type DUSP9 3'-UTR sequences compared with that in cells transfected with mutant-type DUSP9 3'-UTR sequences (Fig. 5E).

Hsa_circ_0004050 inhibited proliferation and promoted apoptosis of A549 cells via targeting miR-1233-3p/DUSP9 axis

The results of CCK-8 assay pointed out that, compared with that in the hsa_circ_0004050 overexpression group, the proliferation rate of A549 cells remarkably rose in the hsa_circ_0004050

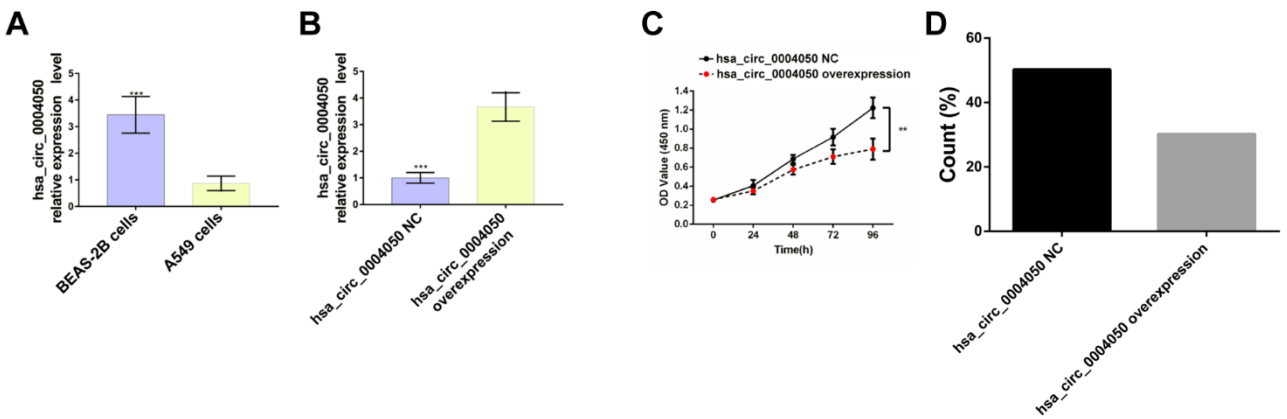


Fig. 2. *Overexpression of hsa_circ_0004050 inhibited proliferation of A549 cells.* ***A)*** *Difference in hsa_circ_0004050 expression between BEAS-2B and A549 cells detected via RT-qPCR.* ***B)*** *Relative expression of hsa_circ_0004050 in A549 cells in hsa_circ_0004050 overexpression group and hsa_circ_0004050 NC group detected via RT-qPCR.* ***C)*** *Effect of overexpression of hsa_circ_0004050 on proliferation of A549 cells detected via CCK-8 assay.* ***D)*** *Effect of overexpression of hsa_circ_0004050 on proliferation of A549 cells detected via CFSE assay.*

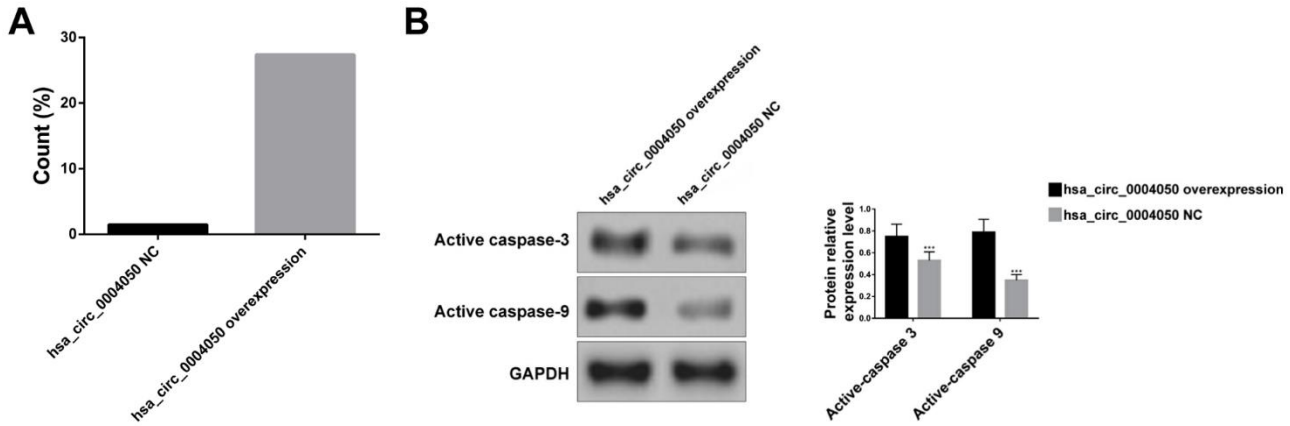


Fig. 3. *Overexpression of hsa_circ_0004050 promoted apoptosis of A549 cells.* ***A)*** *Effect of hsa_circ_0004050 overexpression on apoptosis of A549 cells determined using flow cytometry.* ***B)*** *Effect of hsa_circ_0004050 overexpression on apoptosis-related proteins in A549 cells determined using Western blotting.*

A

TargetScan miRNA predictions								
CircRNA Mirbase ID	CircRNA (Top) - miRNA (Bottom) pairing	Site Type	CircRNA Start	CircRNA End	3' pairing	local AU	position	TA
hsa_circ_0004050 (5' ... 3') hsa-miR-1233 (3' ... 5')	GUCAGUAGUGAAGAUAGGGCUCC GACGCCCUCCUGUCCCGAGU	7mer-m8	220	226	0.003	-0.002	-0.031	-0.001

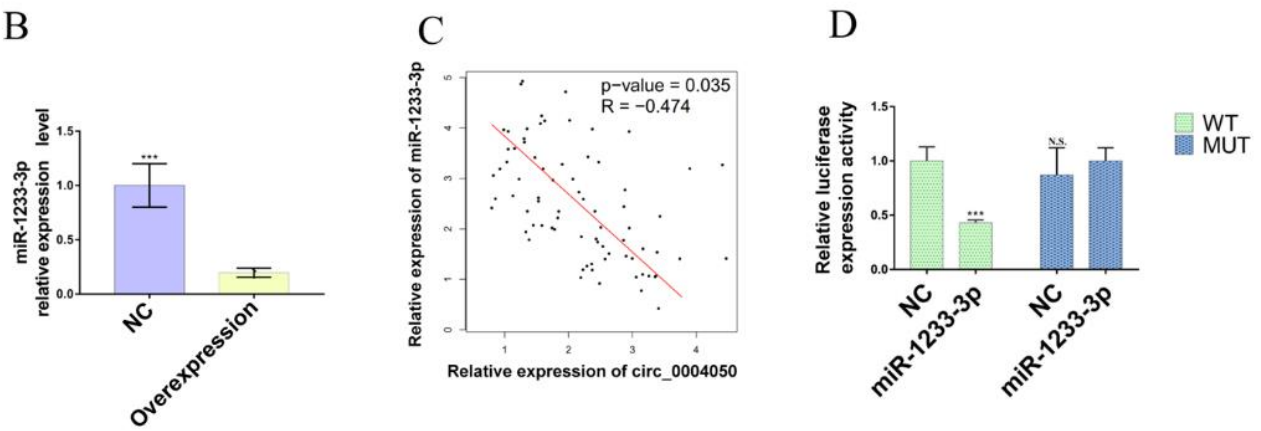


Fig. 4. *Hsa_circ_0004050 suppressed expression of miR-1233-3p.* ***A)*** *Direct binding sites between hsa_circ_0004050 and miR-1233-3p predicted using TargetScan software.* ***B)*** *Effect of overexpression of hsa_circ_0004050 on expression of miR-1233-3p in A549 cells detected via RT-qPCR.* ***C)*** *Correlation between hsa_circ_0004050 and miR-1233-3p in NSCLC tissues.* ***D)*** *Interaction between hsa_circ_0004050 and miR-1233-3p detected via luciferase reporter assay.*

overexpression + miR-1233-3p mimic group and the hsa_circ_0004050 overexpression + sh-DUSP9 group, showing statistically significant differences (Fig. 6A). The same results were also obtained in CFSE assay (Fig. 6B). Then it was confirmed using Annexin V-FITC/PI double staining that the apoptosis rate of A549 cells remarkably declined in the hsa_circ_0004050 overexpression + miR-1233-3p mimic group and the hsa_circ_0004050 overexpression + sh-DUSP9 group compared with that in the hsa_circ_0004050 overexpression group (Fig. 6C).

Hsa_circ_0004050 suppressed extracellular signal-regulated kinase (ERK)/c-Jun N-terminal kinase (JNK) signaling pathway via targeting miR-1233-3p/DUSP9 axis

According to the results of Western blotting, the protein expressions of phosphorylated (p)-ERK1/2/ERK1/2 and p-JNK/JNK were greatly lower in the hsa_circ_0004050 overexpression group than those in the NC group, while they were much higher in the hsa_circ_0004050 overexpression + miR-1233-3p mimic group and the hsa_circ_0004050 overexpression + sh-DUSP9 group than those in

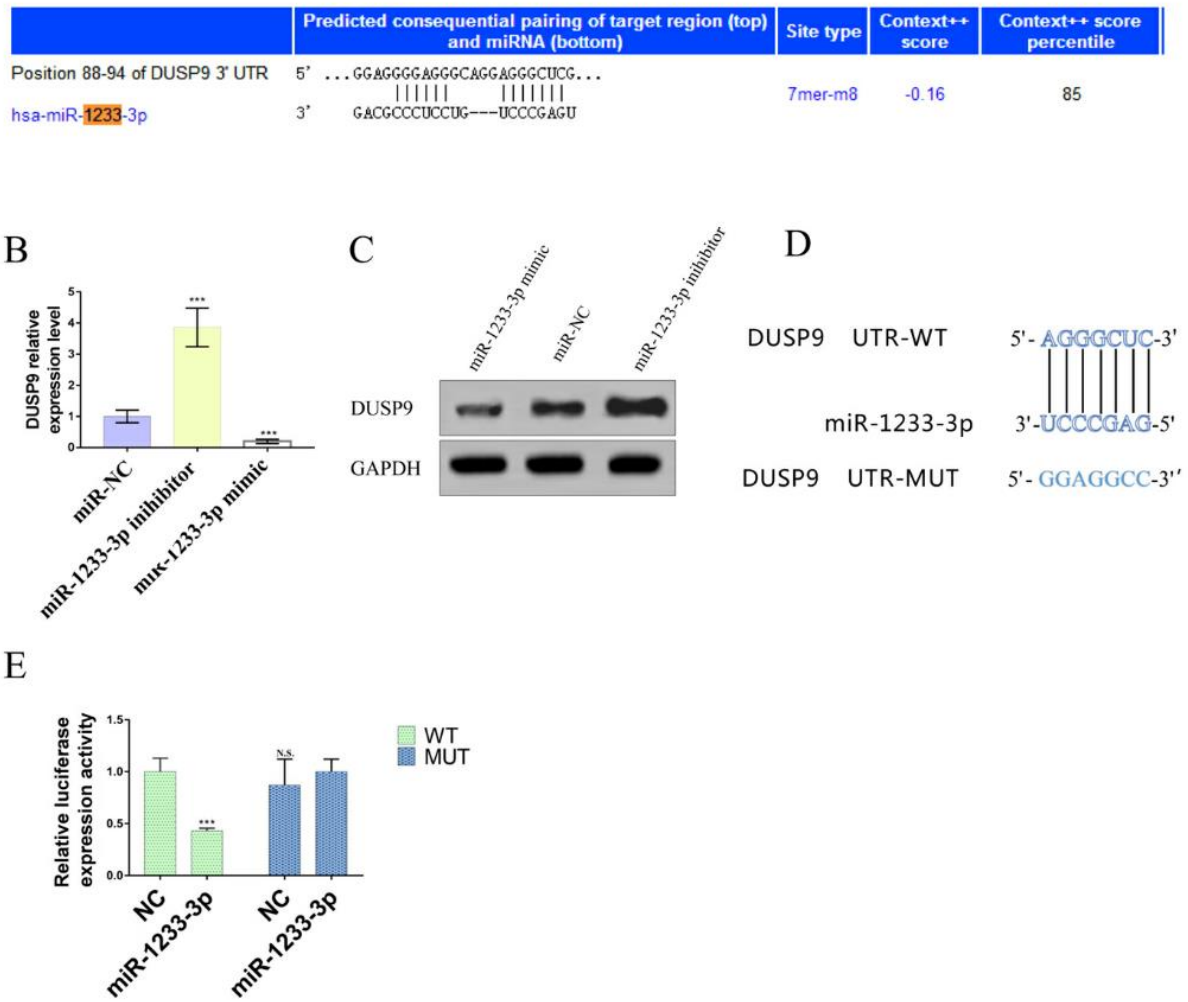


Fig. 5. H*sa_circ_0004050 increased DUSP9 protein expression via targeting miR-1233-3p.* ***A****) Potential binding sites between miR-1233-3p and DUSP9 predicted using bioinformatics software.* ***B****) Effect of miR-1233-3p level on DUSP9 mRNA expression determined using RT-qPCR.* ***C****) Effect of miR-1233-3p level on DUSP9 protein expression determined using Western blotting.* ***D****) Wild-type and mutant-type DUSP9 3'-UTR sequences.* ***E****) Interaction between miR-1233-3p and DUSP9 explored using luciferase reporter assay.*

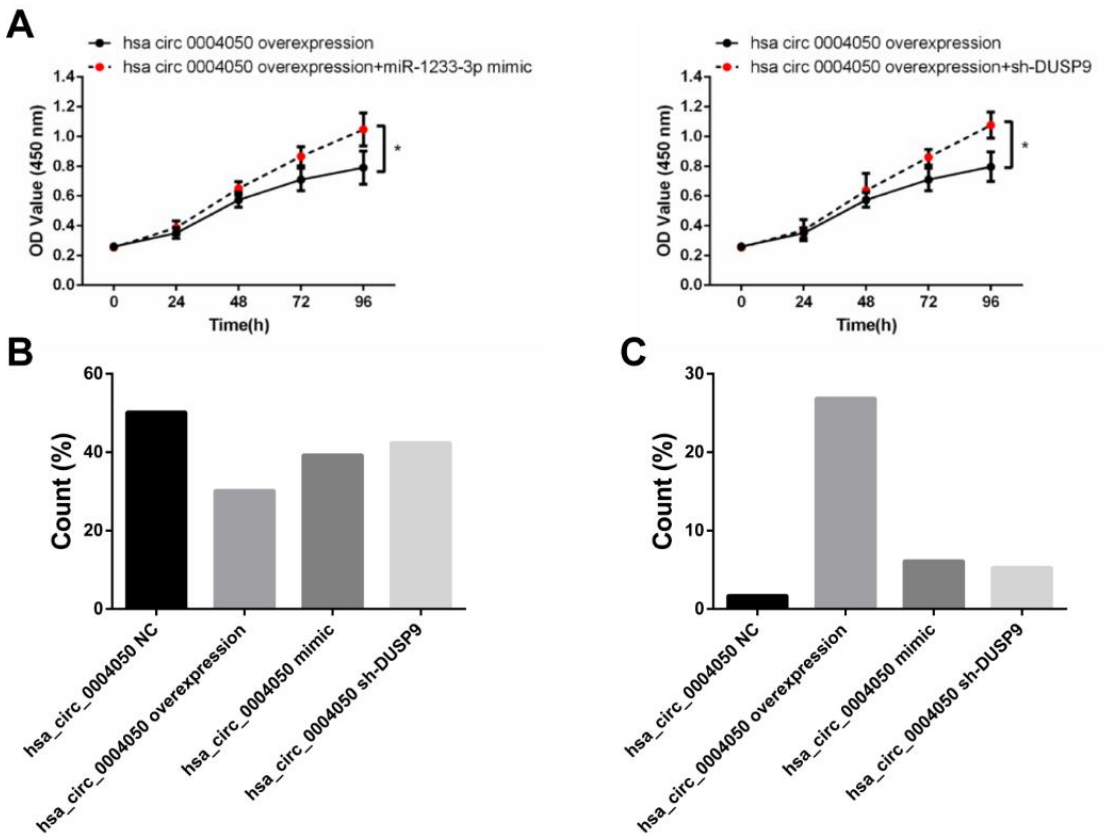


Fig. 6. *Hsa_circ_0004050 inhibited proliferation and promoted apoptosis of A549 cells via targeting miR-1233-3p/DUSP9 axis.* ***A****) Effects of miR-1233-3p overexpression and DUSP9 knockdown on proliferation of A549 cells detected through CCK-8 assay.* ***B****) Effects of miR-1233-3p overexpression and DUSP9 knockdown on proliferation of A549 cells detected through CFSE assay.* ***C****) Effects of miR-1233-3p overexpression and DUSP9 knockdown on proliferation of A549 cells detected through Annexin V-FITC/PI double staining.*

the hsa_circ_0004050 overexpression group, and the differences were statistically significant (Fig. 7). These results demonstrate that hsa_circ_0004050 suppresses the ERK/JNK signaling pathway via targeting the miR-1233-3p/DUSP9 axis.

DISCUSSION

CircRNAs are widely distributed in mammalian cells, whose expression, conservatism and stability are superior to those of lncRNAs and miRNAs (8). Due to the excellent biophysical properties and the key regulatory roles in tumor cell proliferation, apoptosis, migration, invasion and epithelial-mesenchymal transition, circRNAs have become a research hotspot in the field of cancer at present (9-11). Therefore, circRNAs have the potential to become biomarkers for the diagnosis or treatment of tumors (12). However, the functions and potential mechanisms of most circRNAs in NSCLC remain unknown.

In the present study, the results of gene microarray assay and RT-qPCR showed that the expression of hsa_circ_0004050 significantly declined in NSCLC tissues compared with that in para-carcinoma tissues. Moreover, the results of analysis of clinical samples revealed that the decreased expression of hsa_circ_0004050 had an obvious association with TNM stage, tumor size and tumor metastasis in NSCLC patients. More importantly, the Kaplan-Meier survival analysis manifested that there was a significant positive correlation between hsa_circ_0004050 expression and survival time of patients. It can be seen that hsa_circ_0004050 is remarkably associated with the prognosis of NSCLC patients.

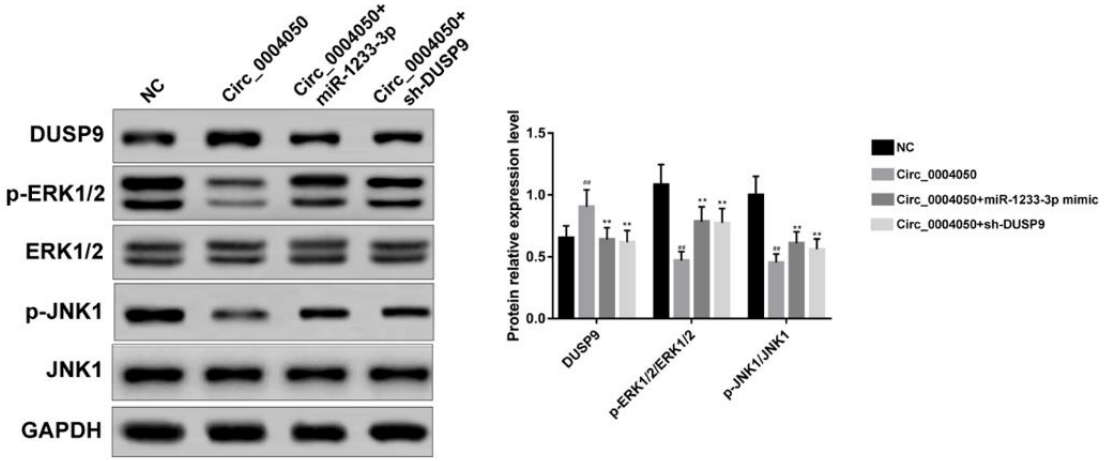


Fig. 7. *Hsa_circ_0004050 suppressed ERK/JNK signaling pathway via targeting miR-1233-3p/DUSP9 axis. Effects of hsa_circ_0004050, miR-1233-3p and DUSP9 on ERK/JNK signaling pathway detected using Western blotting.*

Hsa_circ_0004050 is significantly associated with the survival time, TNM stage, tumor size and tumor metastasis in NSCLC patients. There are numerous reports showing that the abnormal expression of circRNAs is greatly related to the imbalance of biological functions of tumor cells. For example, Wan et al. (13) pointed out that circRNA-ITCH can inhibit the proliferation of NSCLC cells via suppressing the Wnt/β-catenin signaling pathway. In addition, Wang et al. (14) argued that hsa_circ_0008305 can inhibit TGF-β-induced epithelial-mesenchymal transition through regulating the TIF1γ protein expression in NSCLC. Therefore, the effects of hsa_circ_0004050 expression on proliferation and apoptosis of A549 cells were further explored at the *in vitro* level in this study. The results demonstrated that A549 cells had a weakened proliferation ability and an enhanced apoptosis ability after overexpression of hsa_circ_0004050. The findings indicate that hsa_circ_0004050 serves as a tumor suppressor in NSCLC.

It has been proved previously in a large number of studies that circRNAs bind to miRNAs to act as a molecular sponge during the progression of tumors, thereby relieving the inhibition of miRNAs on corresponding target mRNAs. Therefore, whether hsa_circ_0004050 plays a role as a cancer suppressor gene through the circRNA-miRNA-mRNA axis was further explored in this study. First, it was confirmed that hsa_circ_0004050 was a molecular sponge of miR-1233-3p in A549 cells. However, the interaction between hsa_circ_0004050 and miR-1233-3p in tumors has not been clarified yet. In addition, the results of luciferase reporter assay showed that DUSP9 was the direct target of miR-1233-3p. Furthermore, according to the results of rescue assay, the weakened proliferation and enhanced apoptosis of A549 cells induced by hsa_circ_0004050 overexpression could be partially reversed by miR-1233-3p overexpression or DUSP9 knockdown. It can be inferred that the miR-1233-3p/DUSP9 axis is an important player in the progression of NSCLC regulated by hsa_circ_0004050. To sum up, hsa_circ_0004050 inhibits the progression of NSCLC through the miR-1233-3p/DUSP9 axis.

According to a large number of studies, DUSP9 plays an important role in the occurrence and development of a variety of tumors, such as colon cancer, liver cancer and gastric cancer (16, 17). In this study, the results manifested that DUSP9 could negatively regulate the ERK1/2 and JNK signaling pathways. Knocking down DUSP9 could reverse the inhibitory effect of overexpression of hsa_circ_0004050 on the ERK and JNK signaling pathways. As seen from the above results, hsa_circ_0004050 can regulate the DUSP9/ERK/JNK signaling pathway.

In conclusion, hsa_circ_0004050 raises the protein expression of DUSP9 via targeting miR-1233-3p, thereby inhibiting the ERK1/2 and JNK signaling pathways. The results demonstrate that hsa_circ_0004050 may be used as a new biomarker for the diagnosis or treatment of NSCLC.

REFERENCES

1. Ramalingam SS, Vansteenkiste J, Planchard D, et al. Overall survival with osimertinib in untreated, EGFR-mutated advanced NSCLC. N Engl J Med 2020; 382:41-50.
2. Arbour KC, Riely GJ. Systemic therapy for locally advanced and metastatic non-small cell lung cancer: a review. JAMA 2019; 322:764-74.
3. Qi Y, Zhang B, Wang J, Yao M. Upregulation of circular RNA hsa_circ_0007534 predicts unfavorable prognosis for NSCLC and exerts oncogenic properties in vitro and in vivo. Gene 2018; 676:79-85.
4. Ebbesen KK, Hansen TB, Kjems J. Insights into circular RNA biology. Rna Biol 2017; 14:1035-45.
5. Vo JN, Cieslik M, Zhang Y, et al. The landscape of circular RNA in cancer. Cell 2019; 176:869-81.
6. Zhang S, Zeng X, Ding T, Guo L, Li Y, Ou S, Yuan H. Microarray profile of circular RNAs identifies hsa_circ_0014130 as a new circular RNA biomarker in non-small cell lung cancer. Sci Rep 2018; 8:2878.
7. Zheng Q, Bao C, Guo W, et al. Circular RNA profiling reveals an abundant circHIPK3 that regulates cell growth by sponging multiple miRNAs. Nat Commun 2016; 7:11215.
8. Salzman J. Circular RNA expression: its potential regulation and function. Trends Genet 2016; 32:309-16.
9. Chen J, Li Y, Zheng Q, et al. Circular RNA profile identifies circPVT1 as a proliferative factor and prognostic marker in gastric cancer. Cancer Lett 2017; 388:208-19.
10. Du WW, Fang L, Yang W, Wu N, Awan FM, Yang F, Yang BB. Induction of tumor apoptosis through a circular RNA enhancing Foxo3 activity. Cell Death Differ 2017; 24:357-70.
11. Xu L, Zhang M, Zheng X, Yi P, Lan C, Xu M. The circular RNA ciRS-7 (Cdr1as) acts as a risk factor of hepatic microvascular invasion in hepatocellular carcinoma. J Cancer Res Clin Oncol 2017; 143:17-27.
12. Meng J, Chen S, Han JX, et al. Twist1 regulates vimentin through Cul2 circular RNA to promote EMT in hepatocellular carcinoma. Cancer Res 2018; 78:4150-62.
13. Wan L, Zhang L, Fan K, Cheng ZX, Sun QC, Wang JJ. Circular RNA-ITCH suppresses lung cancer proliferation via inhibiting the Wnt/beta-catenin pathway. Biomed Res Int 2016; 2016:1579490.
14. Wang L, Tong X, Zhou Z, et al. Circular RNA hsa_circ_0008305 (circPTK2) inhibits TGF-beta-induced epithelial-mesenchymal transition and metastasis by controlling TIF1gamma in non-small cell lung cancer. Mol Cancer 2018; 17:140.
15. Lu H, Tran L, Park Y, Chen I, Lan J, Xie Y, Semenza GL. Reciprocal regulation of DUSP9 and DUSP16 expression by HIF1 controls ERK and p38 MAP kinase activity and mediates chemotherapy-induced breast cancer stem cell enrichment. Cancer Res 2018; 78:4191-202.
16. Luo J, Luo X, Liu X, Fang Z, Xu J, Li L. DUSP9 suppresses proliferation and migration of clear cell renal cell carcinoma via the mTOR pathway. Onco Targets Ther 2020; 13:1321-30.
17. Wu F, Lv T, Chen G, Ye H, Wu W, Li G, Zhi F-C. Epigenetic silencing of DUSP9 induces the proliferation of human gastric cancer by activating JNK signaling. Oncol Rep 2015; 34:121-28.

LncRNA XIST regulates cell proliferation, migration and invasion of glioblastoma via regulating miR-448 and ROCK1

HL. Li[1], PH. Han[2], DQ. Pan[3], G. Chen[4], XH. Lu[4] and J. Li[5]

[1]Emergency Department, Weifang People's Hospital, Weifang, China; [2]Department of Encephalopathy, Traditional Chinese Medical Hospital of Huangdao Distict, Qingdao, China; [3]No.1 Department of Neurology, Qingdao Central Hospital, Qingdao University, Qingdao, China; [4]Department of Clinical Laboratory, Weifang People's Hospital, Weifang, China; [5]Emergency Department, Qingdao Hospital of Traditional Chinese Medicine, Qingdao Hiser Medical Group, Qingdao, China

Received September 15, 2020 – Accepted November 25, 2020

Long non-coding ribonucleic acids (lncRNAs) have been recognized as markers in several cancers and play important roles in glioblastoma (GBM). But the role of lncRNA X inactive-specific transcript (XIST) in GBM and its possible mechanisms are rarely studied in depth. This study was conducted to explore the detailed roles of XIST in cell proliferation, migration, and invasion of GBM. Expressions of XIST, miR-448, and ρ-associated coiled-coil containing protein kinase 1 (ROCK1) were detected by qRT-PCR or Western blot in A172 and U251 cells. The interactions among XIST, miR-448 and ROCK1 were verified through luciferase reporter assay and RNA immunoprecipitation (RIP) assay. Cell Counting Kit-8 (CCK-8) assay and Transwell assay were introduced to detect how XIST knockdown, miR-448 overexpression, or along with ROCK1 overexpression affect cellular malignancy of GBM cells. XIST and ROCK1 were up-regulated while miR-448 expression was decreased in GBM cells. XIST knockdown or miR-448 overexpression could dramatically inhibit GBM cell proliferation, migration, and invasion. Moreover, XIST negatively regulated miR-448 expression through the function as competing endogenous RNA (ceRNA), thus leading to the up-regulation of ROCK1, one miR-448 target gene. Moreover, ROCK1 overexpression could reverse the suppression of XIST knockdown or miR-448 upregulation on cellular malignancy. In brief, the effects of XIST may promote cellular malignancy of GBM through miR-448/ROCK1 axis, which will provide new understanding of GBM pathogenesis and progression.

GBM is the most common primary central nervous system tumor with poor prognosis and relatively low survival (1, 2). Therefore, how to improve its prognosis has become the direction of clinical research for many years. However, the pathogenesis of GBM is various and complex, and further study is necessary. Giving patients more precise treatment, and finding more effective combination treatment regimens will be the new direction for GBM treatments.

LncRNAs are non-coding regulatory RNAs with transcripts over 200 nucleotides in length (3). Dysregulation of lncRNAs has been confirmed to be associated with cancers and has become a new prognostic indicator, chemotherapy response marker and target of cancer therapy (4-7). LncRNAs

Key words: XIST; ROCK1; miR-448; glioblastoma; cellular malignancy

Corresponding Author:
Dr Jie Li,
Emergency Department,
Qingdao Hospital of Traditional Chinese Medicine,
Qingdao Hiser Medical Group, No.4 Renmin Road,
Shibei District, Qingdao 266033, China
e-mail: zhuofawvmss31121@163.com

0393-974X (2020)
Copyright © by BIOLIFE, s.a.s.
This publication and/or article is for individual use only and may not be further reproduced without written permission from the copyright holder.
Unauthorized reproduction may result in financial and other penalties
DISCLOSURE: ALL AUTHORS REPORT NO CONFLICTS OF INTEREST RELEVANT TO THIS ARTICLE.

could affect cancer progression by regulating cell proliferation, angiogenesis, apoptosis, invasion and metastasis (3, 8). Although a large number of lncRNAs have been confirmed to be implicated in GBM progression and development, the specific mechanism still need further study (9, 10).

XIST is dysregulated in various human cancers (11, 12). Aberrant expression of XIST may affect gene expression and heterochromatin stability, which may play a crucial role in cancer pathology (11). XIST has been confirmed to be significantly up-regulated in GBM (13, 14). XIST participated in chemoresistance, survival time, angiogenesis and tumor growth by targeting certain miRNAs and their target genes in GBM, such as miR-29c, miR-137, miR-152 and miR-429 (13-16). However, the specific mechanisms of XIST in GBM remain unclear and still need more investigation.

Our study suggested XIST was significantly upregulated in GBM cells. Suppression of proliferation, migration, and invasion were observed in GBM cells after XIST knockdown or miR-448 overexpression. ROCK1 could directly target miR-448. Furthermore, ROCK1 overexpression could reverse the suppression of XIST knockdown or miR-448 upregulation on cellular malignancy. XIST upregulation might contribute to GBM cell proliferation, migration and invasion via competitively binding to miR-448, upregulating ROCK1. It improves the new understanding of the functions and the possible mechanisms of XIST in GBM, providing new targets for molecular therapy.

MATERIALS AND METHODS

Cell culture and transfection

A172 and U251, two human GBM cells and normal human astrocyte cell line (NHA) were purchased from Shanghai Institute of Biosciences Cell Resource Center and cultured in DMEM (Invitrogen, Carlsbad) media containing 10% fetal bovine serum (FBS) at 37°C with 5% CO_2.

Cells were seeded in 6-well plates with 2×10^5/well. siXIST (small interfering RNA directed against human XIST), opXIST (XIST-overexpressing plasmid) and opROCK1 (ROCK1-overexpressing plasmid) were ligated into the pcDNA3.1 vector (GenePharma, Shanghai, China) respectively. MiR-448 mimics and control were obtained from GenePharma (Shanghai, China). The transient transfection was performed by Lipofectamine 2000 (Invitrogen, USA).

CCK-8 assay

Cell proliferation was measured by CCK-8 assay. Cells of each group were inoculated in a 96-well plate with 5×10^3 cells/well. 10 μL CCK-8 reagents (Dojindo Laboratory, Japan) were added and then cultured for another 2 h at 37°C. The spectrophotometric absorbance at 450 nm was detected at 1, 2, 3, and 4 days, respectively, after transfection of each group.

Transwell assay

Transwell chamber (Corning, NY, USA) was used to detect cell migration and invasion. Cells (5×10^4) were cultured in upper chambers Matrigel-coated (for assessment of cell invasion) or Matrigel-uncoated (for assessment of cell migration) and serum-free medium, 700 μL medium containing 15% FBS was added in the lower chamber as the chemoattractant. Finally, the cells on the outer layer were fixed. Then, 20% Giemsa solution was used to stain cells. Five random fields were selected for cell counts using an inverted microscope (CK2, Olympus).

Bioinformatic analysis

The Starbase v3.0 (http://starbase.sysu.edu.cn/index.php) was used to search for the binding site of miR-448 and XIST. TargetScan (http://www.targetscan.org/) was used to predict the potential targets of miR-448.

Dual luciferase activity assay

Cells were seeded in 24-well plates with 3×10^4 cells/well. Luciferase reporter vector of XIST and ROCK1 containing the wild-type (XIST-wt and ROCK1-wt) or mutated-type (XIST-mut and ROCK1-mut) were obtained from GeneChem (Shanghai, China). GBM cell lines were co-transfected with miR-448 mimics and reporter vectors using Lipofectamine 2000 (Invitrogen, USA). Luciferase activity was measured by the Dual-Luciferase Reporter Assay kit (Promega, USA) at 48 h after transfection.

RIP assay

RIP kit (Millipore, USA) was used to perform RIP

assay. A172 and U251 cell lines were lysed by RIP lysis buffer, respectively. Magnetic beads were added to cell lysate (100 µl), and then incubated with Ago2 or IgG antibody (Abcam, MA, USA) in RIP buffer at 4°C overnight. Precipitated RNAs were isolated, and XIST and miR-448 expressions were detected.

QRT-PCR

Total RNAs were isolated from the cells by Trizol reagent (Invitrogen, USA) following the manufacturer's instructions. The cDNA template was synthesized by reverse transcription with Reverse Transcription Kit (Takara, Tokyo, Japan) using a PCR instrument. QRT-PCR reactions were practiced with SYBR Green (Takara) and performed with ABI 7300 System. U6 or GAPDH was used as endogenous control. The $2^{-\Delta\Delta Ct}$ method was used to calculate the relative expressions of XIST, miR-448, and ROCK1. Primers are listed in Table I.

Western blot assay

Total proteins were extracted using RIPA buffer with phenylmethanesulfonyl fluoride (PMSF) and separated by 10% SDS-PAGE. The bands were transferred onto polyvinylidene difluoride (PVDF) membranes. Subsequently, they were probed with primary antibodies (ROCK1 and GAPDH antibodies, 1:1,000 dilution, Abcam, USA) after blocking. Membranes were then probed with HRP-conjugated secondary antibodies. Finally, bands were visualized after incubation with chromogenic substrate using enhanced chemiluminescence (ECL).

Statistical analysis

Data were presented as the mean ± SD. GraphPad Prism 5.0 software (San Diego, USA) analyzed differences between groups using Student's *t*-test. $P<0.05$ was the criterion of statistical significance.

RESULTS

XIST and ROCK1 were upregulated while miR-448 was downregulated in A172 and U251 cells

XIST, miR-448, and ROCK1 expressions were detected in A172 and U251 cells. The findings indicated that expressions of XIST and ROCK1 were higher in A172 and U251 cells than NHA cells (Fig. 1 A, C, D). However, miR-448 had an obvious

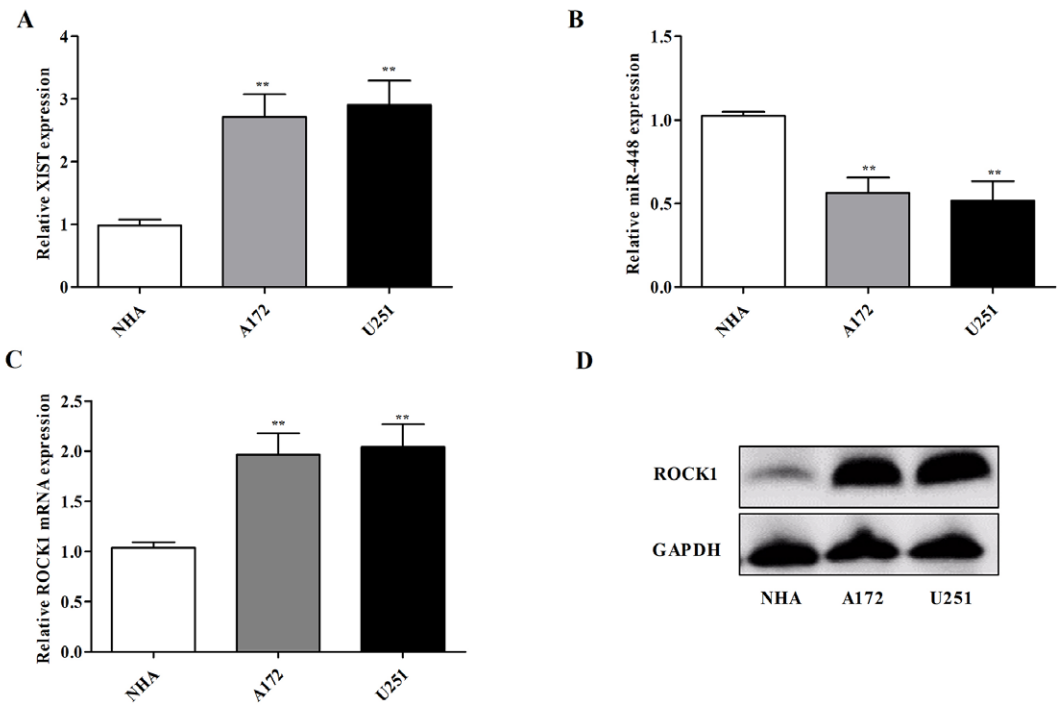


Fig. 1. *Expressions of XIST, miR-448 and ROCK1 were examined by qRT-PCR or Western blot in GBM cells.* ***A****) Expression of XIST in GBM cells.* ***B****) MiR-448 expression in GBM cells.* ***C, D****) ROCK1 was up-regulated in GBM cells. **P < 0.01, compared with NHA cells.*

Table I. *Primer sequences for real-time fluorescence quantification PCR*

Gene	Primer sequences
GAPDH	Forward primer: 5′-ACGCTGCATGTGTCCTTAG-3′
	Reverse primer: 5′-GAGCCTCTTATAGCTGTTTG-3′
U6	Forward primer: 5′-CTCGCTTCGGCAGCACA-3′
	Reverse primer: 5′-AACGCTTCACGAATTTGCGT-3′
XIST	Forward primer: 5′-AATGACTGACCACTGCTGGG-3′
	Reverse primer: 5′-GTGTAGGTGGTTCCCCAAGG-3′
miR-448	Forward primer: 5′-TTATTGCGATGTGTTCCTTATG-3′
	Reverse primer: 5′-ATGCATGCCACGGGCATATACACT-3′
ROCK1	Forward primer: 5′-AGGAAGGCGGACATATTAGTCCCT-3′
	Reverse primer: 5′-AGACGATAGTTGGGTCCCGGC-3′

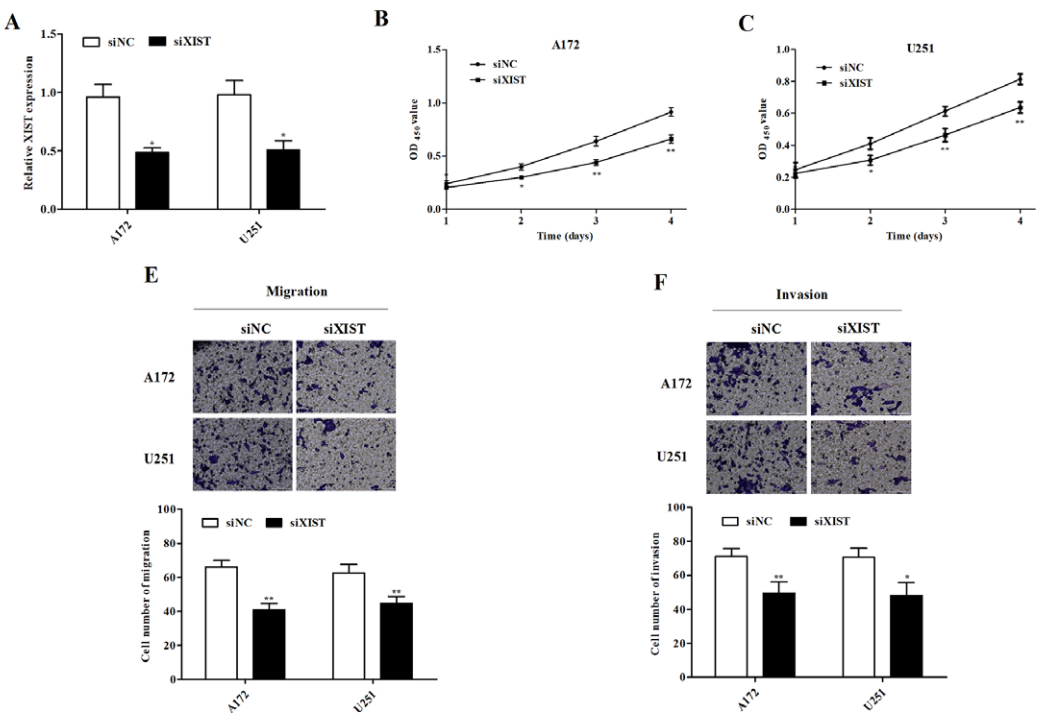


Fig. 2. *XIST knockdown suppressed A172 and U251 cell proliferation, migration and invasion in vitro.* ***A****) Expression of XIST in GBM cells transfected with siXIST or siNC.* ***B, C****) XIST knockdown inhibited cell proliferation.* ***D, E****) XIST knockdown inhibited cell migration and invasion (200X). *P < 0.05, **P < 0.01, compared with siNC group.*

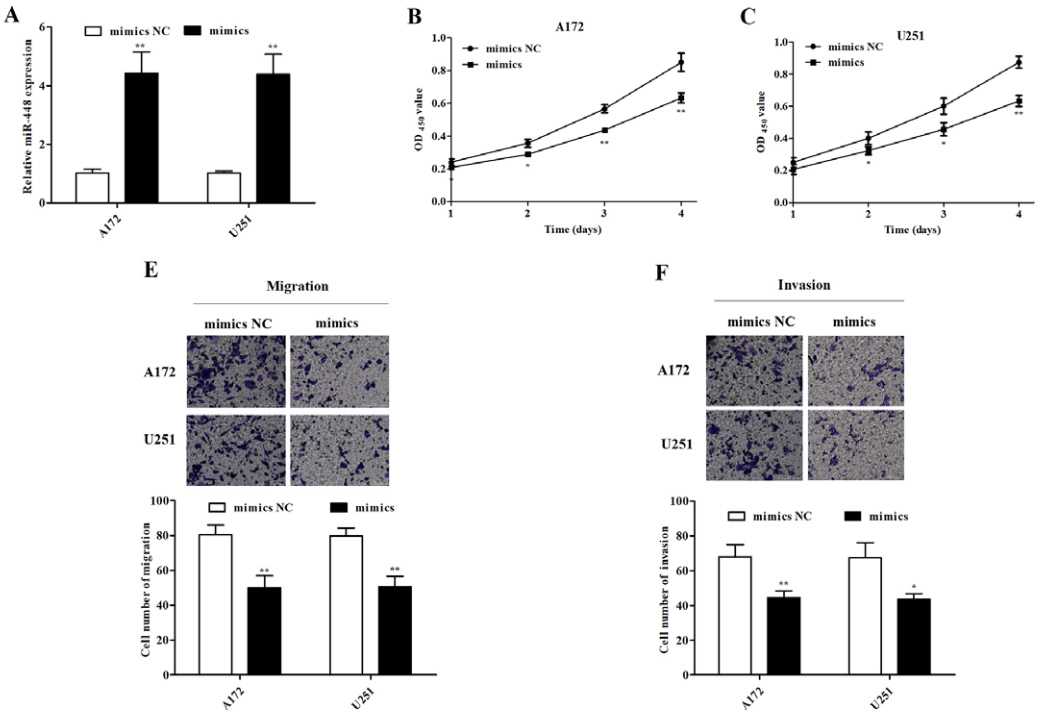


Fig. 3. *MiR-448 overexpression suppressed A172 and U251 cell proliferation, migration and invasion in vitro.* ***A)*** *Expression of miR-448 in GBM cells transfected with miR-448 mimics or mimics NC.* ***B, C)*** *miR-448 overexpression inhibited cell proliferation.* ***D, E)*** *miR-448 overexpression inhibited cell migration and invasion (200X). *P < 0.05, **P < 0.01, compared with mimic NC group.*

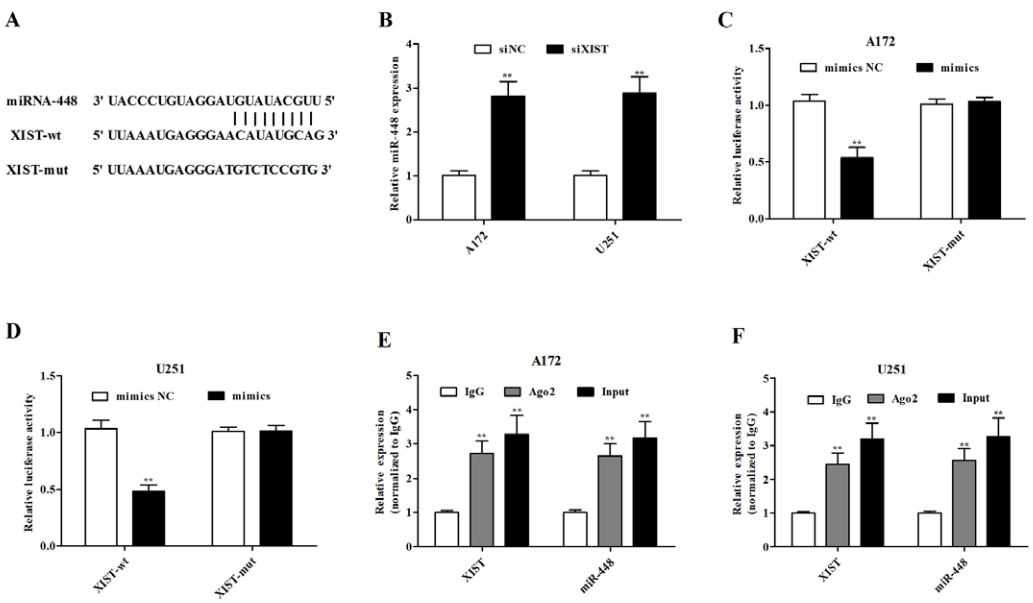


Fig. 4. *XIST functioned as an endogenous sponge to downregulate miR-448 by competitively binding to miR-448.* ***A)*** *Putative binding sites between XIST and miR-448.* ***B)*** *MiR-448 expression in GBM cells transfected with siXIST or siNC.* ***C, D)*** *The luciferase activity was measured by dual-luciferase reporter assay.* ***E, F)*** *MiR-448 and XIST expressions in RIP assay. **P < 0.01, compared with siNC, mimic NC or IgG group.*

upregulation in A172 and U251 cells *versus* NHA cells (Fig. 1B). These results suggested that aberrant expressions of XIST, miR-448 and ROCK1 may be related to GBM progression.

XIST knockdown or miR-448 overexpression suppressed cell proliferation, migration, and invasion in A172 and U251 cells

To explore the functions of XIST and miR-448 in the progression of GBM, siXIST or miR-448 mimic was transfected into A172 and U251 cells, respectively. XIST expression was obviously decreased in siXIST group compared with siNC (Fig. 2A), while miR-448 expression was obviously increased in the mimic group compared with mimics NC group in GBM cells (Fig. 3A). Moreover, proliferation of GBM cells was significantly suppressed in siXIST (Fig. 2 B, C) or miR-448 mimics (Fig. 3 B, C) group compared with siNC or mimics NC group. Cell migration and invasion were also effectively reduced in GBM cells transfected with siXIST (Fig. 2 D, E) or miR-448 mimics (Fig. 3 D, E) in Transwell assay. Therefore, we suggested that XIST and miR-448 have a relationship to cellular malignancy in GBM.

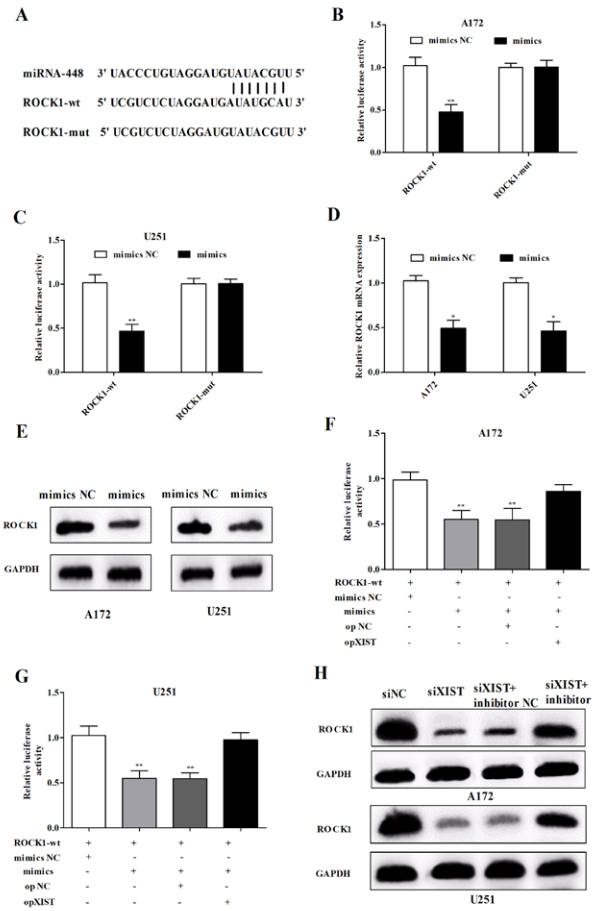


Fig. 5. *XIST regulated ROCK1 expression by competitively binding to miR-448.* ***A)*** *Putative binding sites between miR-448 and ROCK1.* ***B, C)*** *The luciferase activity was measured by dual-luciferase reporter assay.* ***D, E)*** *ROCK1 was downregulated in cells transfected with miR-448 mimics.* ***F, G)*** *The relative luciferase activity was detected in cells with ROCK1-wt and mimics NC, ROCK1-wt and miR-448, or in combination with opNC or opXIST.* ***H)*** *The protein level of ROCK1 in A172 and U251 cells transfected with siNC, siXIST, siXIST and inhibitor NC, or siXIST and inhibitor. *P < 0.05, **P < 0.01, compared with NC group.*

XIST targeted miR-448 and negatively regulated its expression

LncRNAs which were confirmed as ceRNAs could bind to miRNAs and liberate the target RNA transcripts (17). To explore the regulator mechanisms of XIST, the prediction of target sites between XIST and miR-448 was performed by StarBasev3.0 (Fig. 4A). And the miR-448 expression was explored in GBM cells after XIST knockdown. We observed that miR-448 expression was significantly increased in cells transfected with siXIST (Fig. 4B). Thus, we hypothesized that XIST may act as a ceRNA of miR-448 in GBM cells. As expected, the luciferase activity was obviously decreased in A172 and U251 cells with XIST-wt and mimics co-transfection while XIST-mut and mimic co-transfection failed to affect luciferase activity (Fig. 4 C, D). It is suggested that XIST could directly interact with miR-448 in A172 and U251 cells. In order to further validate the relationship of XIST and miR-448, RIP assay was performed with antibody against Ago2. XIST and miR-448 were enriched in Ago2 group cell extracts (Fig. 4 E, F). Collectively, these results implied that XIST could directly target miR-448 as a ceRNA and negatively regulate its expression.

ROCK1 was a target gene of miR-448

To further explore the molecular regulation mechanism of XIST and miR-448, bioinformatic analysis was performed to explore miR-448 potential targets in GBM cells. ROCK1 was

predicted as a miR-448 target gene and the binding sites were analyzed by TargetScan (Fig. 5A). In order to confirm the prediction of bioinformatics, we conducted a luciferase reporter assay. Luciferase activity was significantly reduced in ROCK1-wt and mimic co-transfection cells compared with NC and ROCK1-wt co-transfection, and the co-transfection of mimics and ROCK1-mut did not affect luciferase activity (Fig. 5 B, C). Moreover, the expression of ROCK1 was measured in cells with miR-448 mimics. Overexpression of miR-448 effectively suppressed the ROCK1 expression in GBM cells (Fig. 5 D, E). These data confirmed that ROCK1 directly targeted and negatively regulated miR-448. Additionally, the suppression effect of miR-448 mimics on the luciferase activity of the ROCK1-wt was abated by the co-transfection of miR-448 mimics and opXIST (Fig. 5 F. G). Meanwhile, the effect of XIST knockdown or miR-448 inhibitor on ROCK1 protein expression was analyzed**.** Expression of ROCK1 was apparently decreased in A172 and U251 cells transfected with siXIST, which were obviously counteracted when miR-448 inhibitor was co-transfected (Fig. 5H). Collectively, these results demonstrated that XIST could positively regulate ROCK1 by inhibiting miR-448 expression.

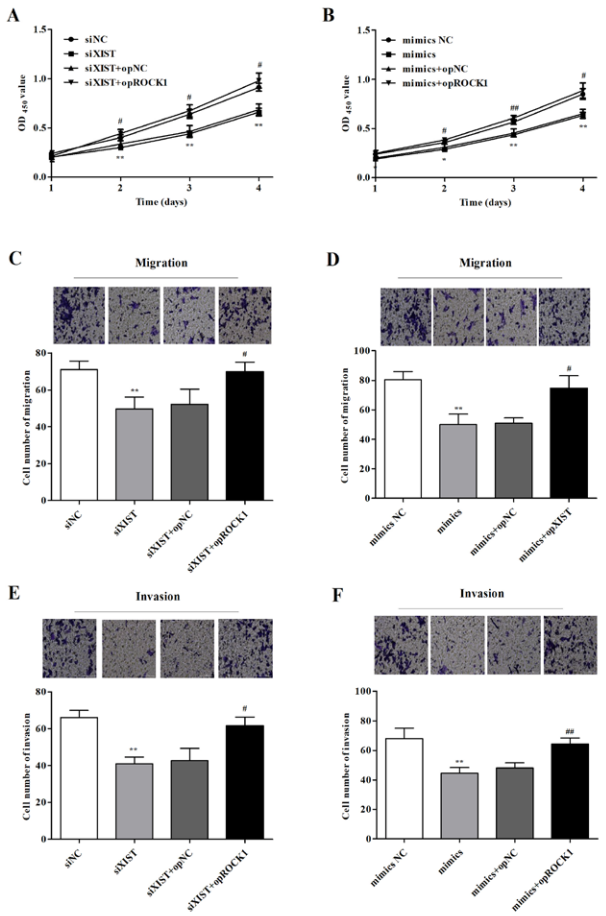


Fig. 6. *ROCK1 overexpression could overturn XIST knockdown or miR-448 overexpression induced suppressive role on cell proliferation, migration and invasion of GBM cells.* ***A, C, E****) A172 cells proliferation, migration and invasion (200X) after transfected with siNC, siXIST, siXIST and opNC, or siXIST and opROCK1.* ***B, D, F****) A172 cells proliferation, migration and invasion (200X) after transfected with mimics NC, miR-448 mimics, miR-448 mimics and opNC, or miR-448 mimics and opROCK1. *P < 0.05, **P < 0.01, #P < 0.05, ##P < 0.01, compared with NC or mimics+opNC group.*

XIST/miR-448/ROCK1 axis regulated GBM cell proliferation, migration and invasion

Based on the findings of the above experiments, we inferred the XIST-miR-448-ROCK1 regulatory axis may be associated with the development of GBM. To validate this hypothesis, CCK-8 and Transwell assay were performed by transfecting siXIST or miR-448 mimics in combination with opROCK1 into A172 cells. As expected, the results showed that miR-448 overexpression or XIST knockdown significantly suppressed cell proliferation, migration, and invasion in A172 cells, while ROCK1 overexpression abrogated these effects (Fig. 6). It is suggested that XIST could promote cellular malignancy by competitively binding to miR-448, up-regulating ROCK1, and thus promoting the progression of GBM.

DISCUSSION

Glioblastomas (GBM) is the most malignant glioma among astrocytic tumors with high mortality (18, 19). Despite tremendous efforts in GBM diagnosis and treatment, the 5-year survival rate is still less than 5% (2). Therefore, exploration of potential molecular mechanisms of GBM development is crucial for GBM diagnosis and treatment. LncRNAs could mediate gene expression, and impact tumor development, progression and therapy (8). As potential biomarkers in

cancer, lncRNAs are particularly important in malignant transformation, recurrence and prognosis of GBM (20, 21). Many lncRNAs have been validated as oncogenic or tumor suppressors in GBM, such as NEAT1, SOX2OT, H19, MEG3, TUNA, XIST (17). However, the specific regulatory mechanisms of lncRNAs in GBM have not been investigated. Therefore, exploration of potential molecular mechanisms of lncRNA in GBM might contribute to the development of novel targets.

XIST, which affects X chromosome inactivation, is an extensively studied oncogenic lncRNA that is necessary for the viability of many GBM cells (12, 22). For instance, Wang et al. found that highly expressed XIST exerts oncogenic functions by promoting cell proliferation in human GBM cells (23). The present study found XIST was upregulated in GBM cells compared to NHA cells according to qRT-PCR analysis. XIST knockdown inhibited GBM cell proliferation, migration and invasion, which confirmed XIST may affect GBM progression. We suggest that XIST, which may act as an oncogene, could benefit GBM development and progression by its upregulation.

LncRNAs, as ceRNAs, exerted a crucial role in biology and pathology of cancers by binding to miRNAs and indirectly regulated mRNAs (17). For instance, PVT1 could up-regulate HK2 expression as a ceRNA of miR-143 to promote gallbladder cancer cell proliferation and metastasis (24). HULC promoted cell proliferation of colon cancer via the miR-613/RTKN (25), and XIST function as an endogenous sponge of miR-137 to up-regulate Rac1 which is a target gene of miR-137, thus promoting glioma cell proliferation (23). In this study, XIST and miR-448 expressions were detected, and a reverse expression trend of these in GBM cells were observed. Also, we revealed that XIST contained binding site to miR-448 according to the bioinformatic analysis. Luciferase reporter and RIP assay confirmed that XIST directly interacted with miR-448. Taken together, XIST could competitively bind to and negatively regulate miR-448 as a sponge.

In several human cancers, miR-448 was confirmed to be abnormally expressed (26-29). ROCK1, which is a serine/threonine kinase, plays vital roles in cancers (30). ROCK1 could change the status of the cytoskeleton to affect cell invasion and migration, and is highly expressed in cancer cells (31-35). Su et al. found that miR-448 could inhibit cell proliferation by downregulating CTTN in glioma (36). Zhang et al. manifested that suppressing ROCK1 expression could inhibit cell proliferation and invasion in glioma (37). Wu et al. demonstrated that miR-448 inhibit retinoblastoma progression by targeting ROCK1 (29). In order to explore whether XIST could negatively regulate miR-448 as ceRNA to liberate its target mRNA, miR-448 target gene ROCK1 which was upregulated in GBM cells was selected for further experiments. ROCK1 was confirmed as a target gene of miR-448 by bioinformatic analysis and luciferase reporter assay. More importantly, XIST overexpression reversed luciferase activity of ROCK1-wt repressed by miR-448 mimics, and XIST knockdown dramatically decreased ROCK1 expression while miR-448 inhibitor reversed the effect. We propose that XIST could regulate ROCK1 expression via negatively regulating miR-448. Furthermore, ROCK1 overexpression prominently overturned the suppressive effect of XIST knockdown or miR-448 overexpression on cellular malignancy, suggesting that the XIST-miR-448-ROCK1 axis may involve in GBM progression.

Taken together, the data revealed that XIST promoted cellular malignancy of GBM via regulating miR-448 and ROCK1, which is conducive to a better understanding of the lncRNA-miRNA-mRNA regulatory network in GBM. However, animal experiments were not performed in the function of XIST, miR-448 and ROCK1 *in vivo*. In addition, the possible other miRNAs or associated genes and mechanisms of XIST were not studied thoroughly. Therefore, further studies should be performed to explore the mechanisms of XIST in GBM.

In brief, XIST was highly expressed and could act as ceRNA to bind to miR-448, leading to ROCK1 derepression of miR-448 target gene ROCK1 in GBM cells. XIST exerted its facilitating effects on GBM cellular malignancy *in vitro* through miR-448/ROCK1 axis, which provides new diagnostic, prognostic and therapeutic targets for GBM.

REFERENCES

1. Thakkar JP, Dolecek TA, Horbinski C, Ostrom QT, Lightner

DD, Barnholtz-Sloan JS, Villano JL. Epidemiologic and molecular prognostic review of glioblastoma. Cancer Epidem Biomar Prev 2014; 23:1985-96.
2. Davis ME. Glioblastoma: overview of disease and treatment. Clin J Oncol Nurs 2016; 20:S2-8.
3. Fang Y, Fullwood MJ. Roles, functions, and mechanisms of long non-coding RNAs in cancer. Genom Proteom Bioinf 2016; 14:42-54.
4. Ellis BC, Molloy PL, Graham LD. CRNDE: A long non-coding rna involved in cancer, neurobiology, and development. Front Genet 2012; 3:270.
5. Han P, Li JW, Zhang BM, et al. The lncRNA CRNDE promotes colorectal cancer cell proliferation and chemoresistance via miR-181a-5p-mediated regulation of Wnt/beta-catenin signaling. Mol Cancer 2017; 16:9.
6. Youness RA, Gad MZ. Long non-coding RNAs: Functional regulatory players in breast cancer. Noncoding RNA Res 2019; 4:36-44.
7. Garzon R, Ranganathan P. Long Noncoding RNAs and Cancer. John Wiley & Sons, Ltd 2014; DOI: 10.1002/9780470015902.a0025252.
8. Xiong XD, Ren X, Cai MY, Yang JW, Liu X, Yang JM. Long non-coding RNAs: An emerging powerhouse in the battle between life and death of tumor cells. Drug Resist Updat 2016; 26:28-42.
9. Shao M, Liu W, Wang Y. Differentially expressed LncRNAs as potential prognostic biomarkers for glioblastoma. Cancer Genet 2018; 226-227:23-29.
10. Balci T, Yilmaz Susluer S, Kayabasi C, Ozmen Yelken B, Biray Avci C, Gunduz C. Analysis of dysregulated long non-coding RNA expressions in glioblastoma cells. Gene 2016; 590:120-22.
11. Weakley SM, Wang H, Yao Q, Chen C. Expression and function of a large non-coding RNA gene XIST in human cancer. World J Surg 2011; 35:1751-6.
12. Yang Z, Jiang X, Jiang X, Zhao H. X-inactive-specific transcript: A long noncoding RNA with complex roles in human cancers. Gene 2018; 679:28-35.
13. Yao Y, Ma J, Xue Y, et al. Knockdown of long non-coding RNA XIST exerts tumor-suppressive functions in human glioblastoma stem cells by up-regulating miR-152. Cancer Lett 2015; 359:75-86.
14. Du P, Zhao H, Peng R, Liu Q, Yuan J, Peng G, Liao Y. LncRNA-XIST interacts with miR-29c to modulate the chemoresistance of glioma cell to TMZ through DNA mismatch repair pathway. Biosci Rep 2017; 37: BSR20170696.
15. Cheng Z, Li Z, Ma K, et al. Long Non-coding RNA XIST promotes glioma tumorigenicity and angiogenesis by acting as a molecular sponge of miR-429. J Cancer 2017; 8:4106-16.
16. Rynkeviciene R, Simiene J, Strainiene E, et al. non-coding RNAs in glioma. Cancers (Basel) 2018; 11:17.
17. Pop S, Enciu AM, Necula LG, Tanase C. Long non-coding RNAs in brain tumours: Focus on recent epigenetic findings in glioma. J Cell Mol Med 2018; 22:4597-610.
18. Hambardzumyan D, Bergers G. Glioblastoma: defining tumor niches. Trends Cancer 2015; 1:252-65.
19. Delgado-Lopez PD, Corrales-Garcia EM. Survival in glioblastoma: a review on the impact of treatment modalities. Clin Transl Oncol 2016; 18:1062-71.
20. Kiang KM, Zhang XQ, Leung GK. Long Non-Coding RNAs: The key players in glioma pathogenesis. Cancers (Basel) 2015; 7:1406-24.
21. Toraih EA, El-Wazir A, Hussein MH, Khashana MS, Matter A, Fawzy MS, Hosny S. Expression of long intergenic non-coding RNA, regulator of reprogramming, and its prognostic value in patients with glioblastoma. Int J Biol Markers 2019; 34:69-79.
22. Malissovas N, Ninou E, Michail A, Politis PK. Targeting long non-coding RNAs in nervous system cancers: new insights in prognosis, diagnosis and therapy. Curr Med Chem 2019; 26:5649-63.
23. Wang Z, Yuan J, Li L, Yang Y, Xu X, Wang Y. Long non-coding RNA XIST exerts oncogenic functions in human glioma by targeting miR-137. Am J Transl Res 2017; 9:1845-55.
24. Chen J, Yu Y, Li H, et al. Long non-coding RNA PVT1 promotes tumor progression by regulating the miR-143/HK2 axis in gallbladder cancer. Mol Cancer 2019; 18:33.
25. Dong Y, Wei MH, Lu JG, Bi CY. Long non-coding RNA HULC interacts with miR-613 to regulate colon cancer growth and metastasis through targeting RTKN. Biomed Pharmacother 2019; 109:2035-42.
26. Lv Y, Lei Y, Hu Y, Ding W, Zhang C, Fang C. miR-448 negatively regulates ovarian cancer cell growth and metastasis by targeting CXCL12. Clin Transl Oncol 2015; 17:903-9.
27. Wu X, Tang H, Liu G, Wang H, Shu J, Sun F. miR-448 suppressed gastric cancer proliferation and

invasion by regulating ADAM10. Tumour Biol 2016; 37:10545-51.
28. Li B, Ge L, Li M, Wang L, Li Z. miR-448 suppresses proliferation and invasion by regulating IGF1R in colorectal cancer cells. Am J Transl Res 2016; 8:3013-22.
29. Wu S, Ai N, Liu Q, Zhang J. MicroRNA448 inhibits the progression of retinoblastoma by directly targeting ROCK1 and regulating PI3K/AKT signalling pathway. Oncol Rep 2018; 39:2402-12.
30. Wei L, Surma M, Shi S, Lambert-Cheatham N, Shi J. Novel insights into the roles of Rho kinase in cancer. Arch Immunol Ther Exp (Warsz) 2016; 64:259-78.
31. Amano M, Nakayama M, Kaibuchi K. Rho-kinase_ ROCK_ a key regulator of the cytoskeleton and cell polarity. Cytoskeleton 2010; 67:545-54.
32. Morgan-Fisher M, Wewer UM, Yoneda A. Regulation of ROCK activity in cancer. J Histochem Cytochem 2013; 61:185-98.
33. Maskey N, Li D, Xu H, et al. MicroRNA-340 inhibits invasion and metastasis by downregulating ROCK1 in breast cancer cells. Oncol Lett 2017; 14:2261-67.
34. Shahana M, Altaf AD, Sharanjot S, et al. MicroRNA-1280 Inhibits invasion and metastasis by targeting ROCK1 in bladder cancer. PloS one 2012; 7:e46743.
35. Shin JY, Kim YI, Cho SJ, et al. MicroRNA 135a Suppresses lymph node metastasis through down-regulation of ROCK1 in early gastric cancer. PloS one 2014; 9:e85205.
36. Su H, Lin Z, Peng W, et al. MiR-448 downregulates CTTN to inhibit cell proliferation and promote apoptosis in glioma. Eur Rev Med Pharmacol Sci 2018; 22:3847-54.
37. Zhang P, Lu Y, Liu XY, Zhou YH. Knockdown of Rho-associated protein kinase 1 suppresses proliferation and invasion of glioma cells. Tumour Biol 2015; 36:421-8.

Cystatin 2 leads to a worse prognosis in patients with gastric cancer

W-P. Zhang[1*], Y. Wang[1*], D. Tan[1] and C-G. Xing[2]

[1]Department of General Surgery, Ruijin Hospital/Lu Wan Branch, School of Medicine, Shanghai Jiaotong University, Shanghai, P. R. China; [2]Department of General Surgery, The Second Affiliated Hospital of Soochow University, Suzhou, Jiangsu, P. R. China

Received May 20, 2020 – Accepted September 16, 2020

[*]These Authors contributed equally to this work

Despite the amazing progress in the treatment of gastric cancer (GC), it is still the third leading cause of cancer death in the world. This study explored the key genes that are related to the prognosis and pathogenesis of GC. Data from the cancer genome atlas (TCGA) and Oncomine were applied to evaluate the expression of cystatin 2 (CST2) in GC samples. Kaplan-Meier plotter was carried out to detect the overall survival of GC patients with different expression levels of CST2. Gene Set Enrichment Analysis (GSEA) was carried out to investigate the functions and pathways connected with CST2 expression. Quantitative real-time polymerase chain reaction (qPCR) and Western blot assays were used to assess CST2 expression. The biological properties of GC cells were assessed with the support of cell proliferation and Transwell assays. Important proteins involved in the regulation of CST2 in GC cell behaviors were evaluated by Western blot. Through analysis of the database, we found that CST2 expression was significantly upregulated in GC samples and actively related to GC patients' poor outcomes. Importantly, the analysis of GSEA showed that GST2 expression was closely connected with the proliferation and migration of cells, as well as the TGF-β1 signaling pathway. In addition, biological assays illustrated that over-expression of CST2 strengthened the activity and metastasis of GC cells. After the upregulation of CST2, the expression of cyclin D1, N-cadherin, vimentin, TGF-β1, and Smad4 increased, and E-cadherin expression decreased. Our findings revealed that over-expression of CST2 enhanced the growth, migration, and invasion of GC cells through modulating the epithelial-mesenchymal transition (EMT) and TGF-β1 signaling pathway, affording a possible biomarker for the treatment of GC.

Gastric cancer (GC), one of the most common malignant tumors worldwide, has a complex onset, and is the result of the combined action of internal and external causes (1). Although the incidence of GC is decreasing, it still accounts for more than 1 million newly diagnosed cases and 850,000 deaths worldwide each year (2). The high mortality rate is primarily the result of the late manifestation; the early stages of GC are asymptomatic or have nonspecific symptoms. The survival rate at diagnosis relies on the phase of GC (3). While surgery is currently the primary treatment option, more than 50% of patients still relapse after

Key words: gastric cancer; CST2; cyclin D1; E-cadherin; TGF-β1; Smad4

Corresponding Author:
Dr Chungen Xing,
Department of General Surgery,
The Second Affiliated Hospital of Soochow University,
No.1055, Sanxiang Road,
Suzhou, Jiangsu, 215000 China
e-mail: darvid0610@sina.com

0393-974X (2020)
Copyright © by BIOLIFE, s.a.s.
This publication and/or article is for individual use only and may not be further reproduced without written permission from the copyright holder.
Unauthorized reproduction may result in financial and other penalties
DISCLOSURE: ALL AUTHORS REPORT NO CONFLICTS OF INTEREST RELEVANT TO THIS ARTICLE.

radical resection. Excellent screening methods for early detection are the best approach to decreasing the mortality rate. Endoscopy is uncommon in the community due to its side effects, including perforation, aspiration pneumonia, and bleeding (4). Therefore, there is an urgent need to find biomarkers for the early detection of GC.

Cystatin 2 (CST2) is an endogenous protease inhibitor and belongs to the superfamily of cystatins. CST2 plays a crucial role in epithelial barrier and immunomodulatory processes (5). A previous study revealed that CST2 might be as a crucial factor in the relapse of eosinophilic chronic rhinosinusitis and allergic rhinitis through the interplay with several factors, including infection, fibroblasts, and the suppression of allergen-related histamine release (6). In addition, CST2 was highly upregulated in subjects with both mild and moderate asthma compared with healthy subjects (7). Interestingly, CST2 was shown to be overexpressed in patients with hepatocellular carcinoma (8). Through analysis of the TCGA database, Wang et al. revealed that CST2 was highly expressed in GC (9). Although CST2 was discovered more than 30 years ago, research on its function has been limited (10), especially in gastric cancer, therefore, further exploration into the effects of CST2 in GC is urgent.

Our results revealed that CST2 was profoundly upregulated in the GC samples and was connected with poor prognosis in GC patients. Importantly, CST2 upregulation strengthened the viability and aggressiveness of the GC cells by elevating the progression of the epithelial-mesenchymal transition (EMT) and the TGF-β1 signaling pathway. Our findings offer a potential novel biomarker for the treatment and prognosis of gastric cancer and revealed the underlying mechanism of CST2 in GC development.

MATERIALS AND METHODS

Data acquisition and analysis

Data from the TCGA (https://cancergenome.nih.gov/) dataset, which included 375 GC tumor samples and 32 normal samples, were used to assess the expression of CST2 in GC. Data from the Oncomine (http://www.oncomine.org) database, which covered 26 cases of GC tissues and 31 cases of normal samples, were applied to detect CST2 expression in GC. A total of 324 cases of GC samples with complete clinical data were used to analyze the correlation between CST2 expression and clinical features. Analysis of the 208555_x_at database by the Kaplan-Meier (KM) plotter revealed that the overall survival and the first progression and post-progression survival differed among GC patients with different expression of CST2. Gene Set Enrichment Analysis (GSEA) was used to explore the functions and pathways related to CST2 expression.

Cell culture and treatment

Human GC cell lines AGS, SGC-7901, and BGC-823 were obtained from the Chinese Academy of Science Cell Bank (Shanghai, China), and the normal cell GSE-1 was acquired from ATCC (USA). All cell lines were cultured in RPMI-1640 medium supplemented with 10% fetal bovine serum, 100 U/mL penicillin, and 0.1 mg/mL streptomycin at 37°C, 5% CO_2.

si-CST2#1(5'-GAGTATAACAAGGCCACTGAA-3'), si-CST2#2 (5'- TAATCGAGGGTGGCATCTATG-3'), si-con (5'-CGAACUCACUGGUCUGACC-3'), pcDNA3.1-CST2, and pcDNA3.1 were commercially provided by Sangon (Shanghai, China) and transfected into GC cells with the support of Lipofectamine 2000 (Invitrogen, USA) to regulate CST2 expression.

RNA extraction and quantitative real-time PCR (qPCR)

Total RNA was isolated from GC cells using Trizol (Invitrogen, USA) and then reverse transcribed into cDNA using a GoScript™ RT kit (Promega Corporation). qPCR was carried out utilizing SYBR Fast qPCR mix (Invitrogen, USA) to evaluate the CST2 expression level. The qPCR program was run using the following steps: 95°C for 5 min; 40 cycles, including 9°C for 30 sec, 60°C for 45 sec, and 72°C for 1 min and with extension at 72°C for 10 min. The relative expression level of CST2 was evaluated via the $2^{-\Delta\Delta CT}$ method and normalized to GAPDH. All sequences used are shown below:

CST2: forward: 5'-CTCATCAGCCACTGGAAAGGCA-3', reverse: 5'- GACTCGTGAAGTCAGCCTGAAAC-3';
GAPDH: forward: 5'-TGTGTCCGTCGTGGATCTGA-3', reverse: 5'-CCTGCTTCACCACCTTCTTGA-3'.

Western blot

Cultured GC cells were lysed in radio immuno precipitation assay (RIPA) buffer. Proteins were isolated on a 12.5% SDS-PAGE and electro-transferred onto a polyvinylidene difluoride (PVDF) membrane. After blocking with 5% skim milk, the membrane was incubated at 4°C overnight with primary antibodies, including anti-cyclin D1 (1:500), E-cadherin (1:1000), N-cadherin (1:1000), vimentin (1:1000), TGF-β1 (1:1000), and Smad4 (1:1000). After rinsing with TBST, the membrane was incubated with secondary antibody at room temperature for 1.5 h. Visualization was performed using ECL reagents and developed on a film.

Cell proliferation analyses

The proliferation of GC cells was examined with the help of the cell counting kit-8 (CCK-8). Firstly, the treated cells were seeded in 96-well plates and cultured under the above condition. The activity of the cells was calculated every 24 h in line with the supplier's recommendations. Before each test, 15 μL of CCK-8 reagent was loaded into the well and incubated with the cells for 1.5 h at 37°C in an incubator. Afterward, the optical density was measured at a wavelength of 450 nm, and GraphPad Prism 6.0 was used to draw the proliferation curve.

Cell invasion and migration assays

Transwell chambers were applied to evaluate the invasion and migration abilities of the GC cells. For the invasion assay, chambers were pre-coated with matrigel matrix (RPMI 1640: matrigel matrix=6:1). A total of 5,000 cells were seeded in the top well with serum-free medium, while complete medium supplemented with 10% FBS was loaded in the lower well. After a 24-h incubation, the cells in the top well were obliterated lightly with a cotton swab. The cells that had invaded the bottom surface of the membrane were fixed with paraformaldehyde and stained with crystal violet. The invading cells were counted under a light microscope. The steps in the migration assay were similar to the invasion experiment, except that matrigel was not required.0

Statistical analysis

Results were processed with SPSS software (version 22.0; SPSS, Inc.). The survival rates of GC patients were assessed under the support of the Kaplan-Meier (KM) plotter and the log-rank test was used for comparison. Numerical data are shown as the mean ± standard deviation (SD). Statistical comparisons between the two groups of normalized values were analyzed utilizing the Student's *t*-test. Statistical comparisons among multiple groups of normalized data were analyzed using one-way analysis of variance followed by Dunnett's post hoc test. A P-value less than 0.05 indicated a statistically significant difference.

RESULTS

High expression of CST2 correlated positively with a poor prognosis of GC patients

Firstly, we evaluated the expression of CST2 in GC samples based on the data from the TCGA and Oncomine databases. The data from TCGA containing 375 tumor samples and 32 normal samples indicated that CST2 was highly expressed in GC tissues compared with normal tissues (Fig. 1A, $P<0.0001$). Consistent with the results from TCGA, CST2 expression in GC tissues from the Oncomine database was also profoundly upregulated (Fig. 1B, $P<0.0001$). By KM plotter analysis, we discovered that the overall survival of GC patients was poor in the group with high CST2 expression (Fig. 1C, $P=0.026$). Analysis of the 208555_x_at database by the KM plotter revealed that the overall survival, first progression, and post-progression survival of GC patients in the high CST2 expression group were lower than the low expression group (Fig. 1 D–F, $P<0.01$). The clinical correlation analysis showed that CST2 expression was connected with the grade and lymph node metastasis in patients with GC (Table I). The findings illustrated that high expression of CST2 appeared in patients with GC, and was positively correlated with GC patients' poor prognosis.

Identification of the function and pathways closely related to CST2 expression

To investigate the function of CST2 in GC, GSEA was used to explore the functions and pathways related to CST2 expression. The information in Fig. 2 shows that CST2 was involved in the processes of cell migration (2A) and proliferation (2B). In addition, the expression of CST2 was closely associated with

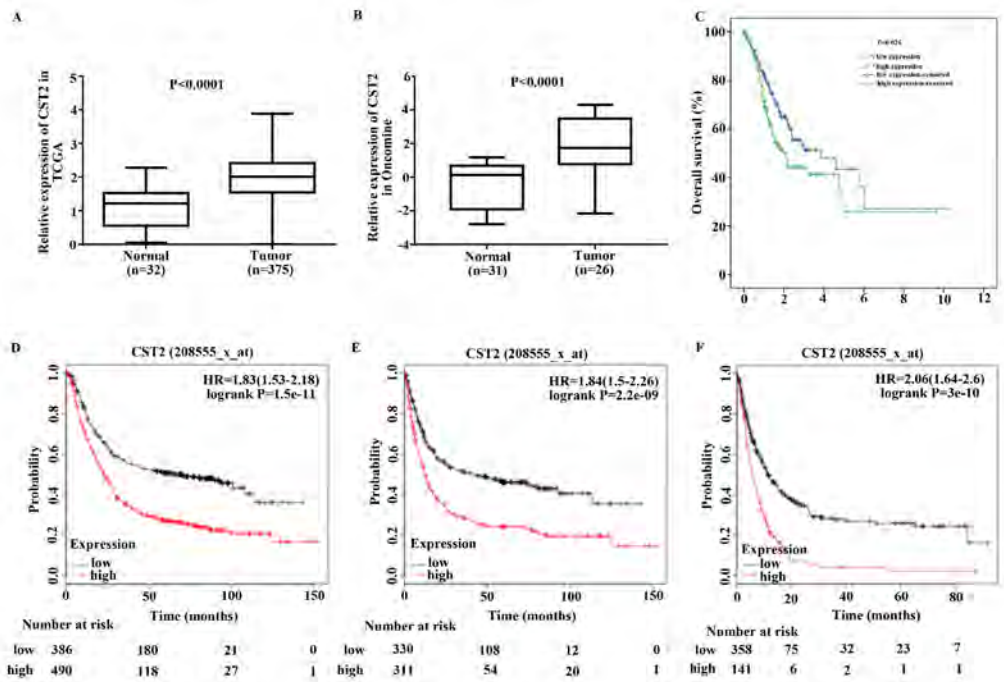


Fig. 1. *Overexpression of CST2 resulted in unfavorable prognosis in patients with GC.* ***A****) The data from TCGA revealed that CST2 was profoundly upregulated in GC tissues (P<0.0001).* ***B****) The result from the Oncoming exhibited that CST2 was overexpressed in GC tissues in contrast with normal tissues (P<0.0001).* ***C****) The survival of GC patients was analyzed by KM plotter with support of the TCGA dataset (P=0.026). The overall survival (****D****), first progression (****E****), and post-progression survival (****F****) of GC patients were analyzed by KM plotter with the help of the 208555_x_at database.*

cytokine receptor interaction (2C) and the TGF-β signaling pathway (2D). These findings provided direction for our following research.

CST2 expression correlated positively with the activity and aggressiveness of GC cells

Based on the analysis from GSEA and the literature review, we discovered that CST2 was closely related to cell proliferation and migration. We assessed the expression of CST2 in the GC cell lines. The PCR result presented that the expression of CST2 was elevated in the GC cell line compared with normal cell GSE-1 (Fig. 3A, P<0.01). To discover the function of CST2 in GC, we employed AGS and SGC-7901 cells for gain and loss-of-function assays due to their significant difference in the expression of CST2. Firstly, si-CST2 and pcDNA3.1-CST2 were employed to regulate CST2 expression in GC cells. As Fig. 3 B–C shows, both si-CST2#1 and si-CST2#2 were used to knock down CST2 expression in AGS cells; the interference with si-CST2#2 was the most effective. Therefore, in the subsequent experiments, si-CST2#2

Table I. *Relationship between CST2 expression and clinical pathological characteristics of patients with gastric cancer.*

Characteristics	Expression of CST2		P value
	Low	High	
Age			0.810
<60	49	51	
≥60	113	111	
Gender			0.300
female	64	55	
male	98	107	
Grade			
G1+G2	75	46	0.001*
G3	87	116	
Pathologic-Stage			0.315
I+II	78	69	
III+IV	84	93	
Pathologic-T			0.054
T1+T2	48	33	
T3+T4	114	129	
Pathologic-N			0.041*
N0	59	42	
N1+N2+N3	103	120	
Pathologic-M			1.000
M0	151	151	
M1	11	11	

**P<0.05; T: tumor; N: lymph nodes; M: metastasis. Data from the TCGA database.*

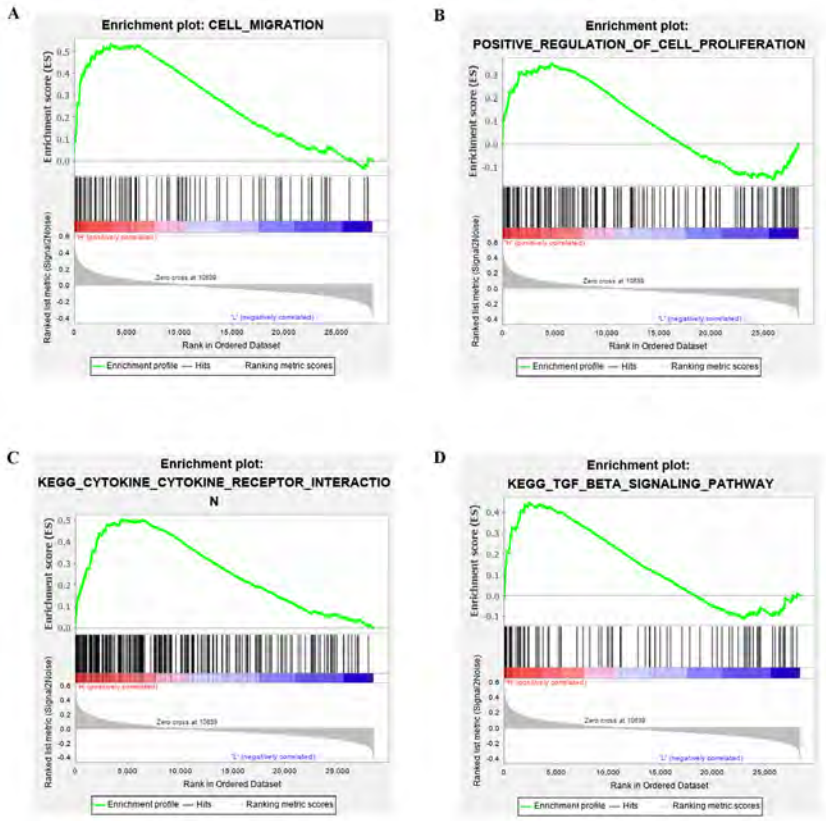


Fig. 2. *Functions and pathways related to CST2 were enriched.* ***A****) CST expression was related to cell migration.* ***B****) CST expression was connected with cell proliferation.* ***C****) CST expression was associated with cytokine-cytokine receptor interaction.* ***D****) CST expression was related to the TGF-β1 signaling pathway.*

was selected for interference-related experiments. In addition, the expression of CST2 in SGC-7901 cells was significantly upregulated after treatment with pcDNA3.1-CST2 (Fig. 4 A–B, P<0.01). Next, the data from the CCK-8 and Transwell assays revealed that depletion of CST2 reduced the activity of AGS cells, as well as the number of invaded and migrated AGS cells (Fig. 3 D–F, P<0.01). Upregulation of CST2 increased the activity of SGC-7901 cells, as well as the number of invaded and migrated SGC-7901 cells, compared with the control group (Fig. 3 C–E, P<0.01). These results suggested that the upregulation of CST2 enhanced the growth and metastasis of the GC cells.

CST2 expression regulated the biological behavior of the GC cells by affecting the proliferation/invasion/TGF-β signaling

According to the analysis from GSEA, we discovered that CST2 was not only related to proliferation and invasion but also closely connected with the TGF-β1 signaling pathway. Therefore, we detected the protein expression of cyclin D1, E-cadherin, N-cadherin, vimentin, TGF-β1, and Smad4 in GC cells with different CST2 treatments. After silencing CST2, the expression of cyclin D1, N-cadherin, vimentin, TGF-β1, and Smad4 were reduced, while E-cadherin expression was increased. These phenomena demonstrated that depletion of CST2 attenuated the growth, invasive, and migratory abilities of AGS cells via blocking the EMT/TGF-β1 signaling pathway. InSGC-7901 cells, after treatment with pcDNA3.1-CST2, the expression levels of cyclin D1, N-cadherin, vimentin, TGF-β1, and Smad4 were elevated, and E-cadherin expression was decreased. These data suggested that overexpression of CST2 strengthened the proliferative, invasive, and

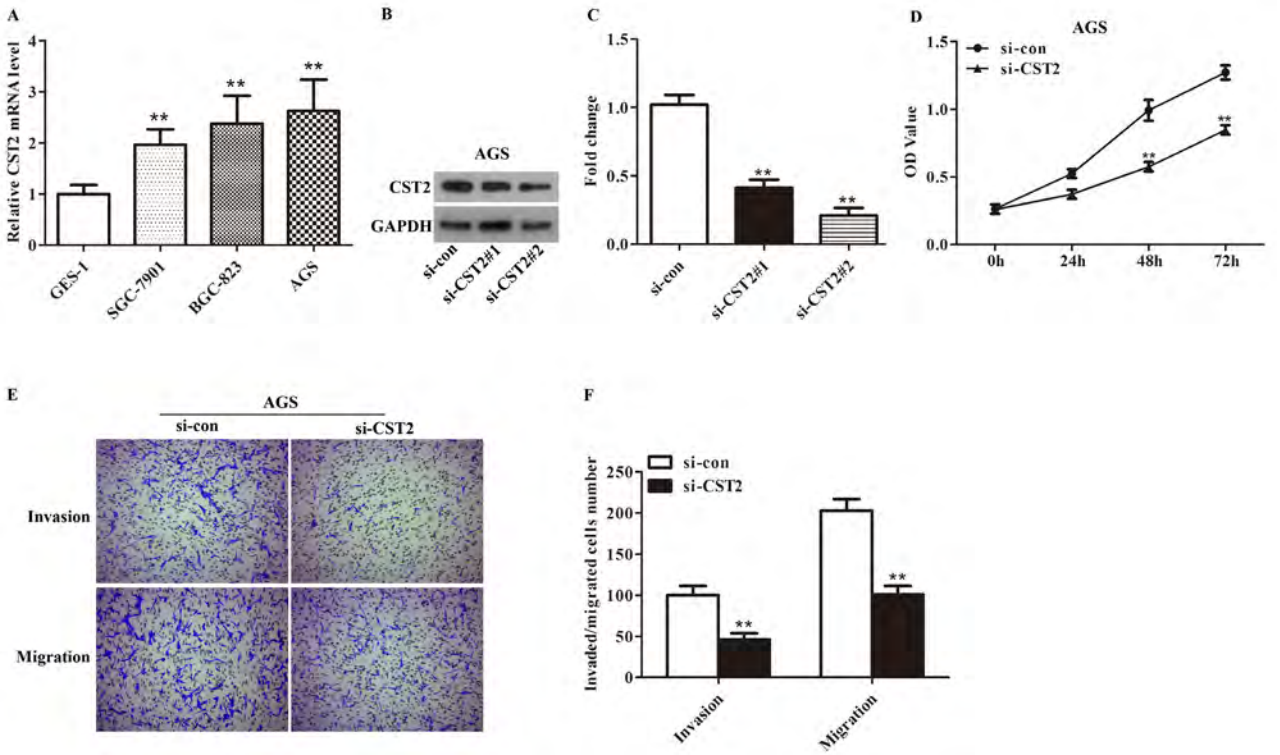


Fig. 3. *Depletion of CST2 limited the activity and aggressiveness of AGS cells.* ***A****) The expression of CST2 was obviously elevated in the GC cell lines in contrast with the normal cell GSE-1.* ***B–C****) The protein expression of CST2 was profoundly decreased after si-CST2 treatment.* ***D****) The activity of AGS cells was reduced with CST2 depletion.* ***E–F****) The invasion and migration number of AGS cells were lower with si-CST2 treatment.* $^{**}P<0.01$ *vs control.*

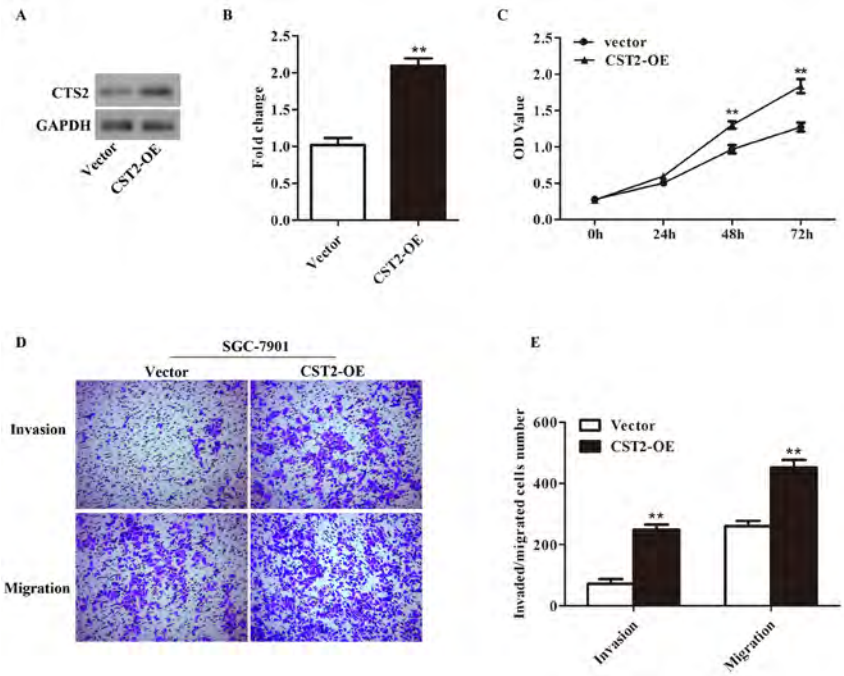


Fig. 4. *Upregulation of CST2 increased the growth and metastasis of SGC-7901 cells.* ***A–B****) The protein expression of CST2 was increased after pcDNA3.1-CST2 treatment.* ***C****) The activity of SGC-7901 cells was elevated with CST2 upregulation.* ***D–E****) The number of invaded and migrated SGC-7901 cells was increased with pcDNA3.1-CST2 treatment.* $^{**}P<0.01$ *vs control.*

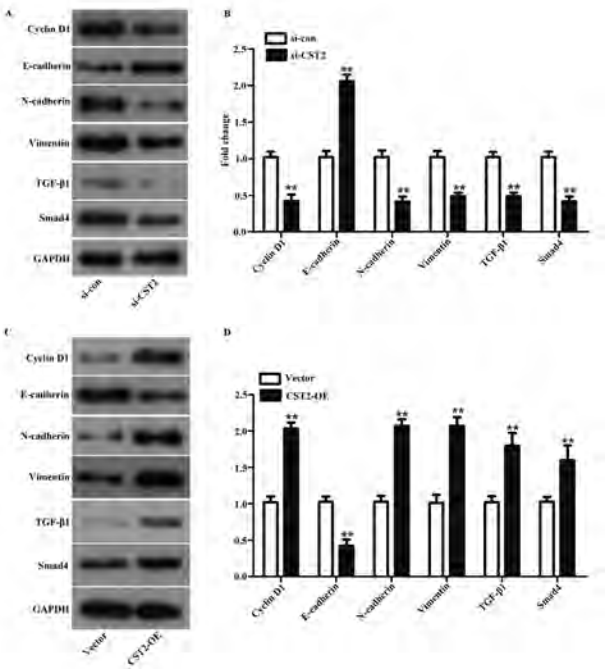


Fig. 5. *Key proteins involved in CST2 regulation in GC cells were evaluated by western blot.* ***A–B****) The expression of cyclin D1, E-cadherin, N-cadherin, vimentin, TGF-β1, and Smad4 were evaluated in AGS cells after knockdown of CST2.* ***C–D****) The expression of cyclin D1, E-cadherin, N-cadherin, vimentin, TGF-β1, and Smad4 were evaluated in SGC-7901 cells after the upregulation of CST2.* $^{**}P<0.01$ *vs control.*

migratory abilities of SGC-7901 cells via activating the EMT/TGF-β1 signaling pathway. The results suggest that CST2 affected GC cell proliferation, invasion, and migration by regulating the TGF-β1 signaling pathway.

DISCUSSION

In the present study, we provide evidence that CST2 is highly expressed in human GC cells. The bioinformatics analysis showed that CST2 expression is closely related to proliferation and migration, as well as a poor prognosis of GC patients. In addition, consistent with the results from the bioinformatics research, we also found that CST2 elevates the growth and metastasis capacities of GC cells partly through mediating the EMT and TGF-β1 signaling pathway.

The *CST2* gene, belonging to the CST family, has been reported as a specific allele, indicating that amino acid substitution in one of the most conserved domains is in charge of the cysteine proteinase inhibitory activity (11). Moreover, research has revealed that high expression of salivary cystatin CST2 promotes bone metastasis *in vivo* (12). To date, little research has concentrated on the function of CST2 in any type of tumor, apart from the discovery that CST2 responded to the anti-growth activity of triptolide in ovarian cancer cells (13), and that CST2 is involved in the development of breast cancer (14). In our study, by bioinformatics analysis, CST2 was observably upregulated in gastric cancer and associated with worse outcomes in GC patients. It was also related to cell proliferation, invasion, and the TGF-β1 pathway. Consistent with the bioinformatics analysis, experiments *in vitro* confirmed that GST2 was highly expressed in GC cell lines and accelerated the proliferation and metastasis of the GC cells.

EMT is regarded as one of the crucial processes in GC cell invasion and metastasis (15). During EMT, epithelial cells drop their characteristic marker E-cadherin and acquire mesenchymal markers, including N-cadherin and vimentin (16). To investigate whether the function of GST2 on GC is related to the EMT process, we detected EMT-related proteins after up- and down-regulation of CST2. The data showed that E-cadherin expression was elevated, and the expressions of N-cadherin and vimentin were reduced after CST2 depletion. Inversely, upregulation of CST2 attenuated E-cadherin expression and elevated the expression of N-cadherin and vimentin. These findings suggest that CST2 increases the biological characteristics of GC cells by promoting EMT.

Recent research on gastric cancer (17, 18) has generated interest in the function of TGF-β in GC biology. It was reported that the TGF-β family plays a critical role in modulating cancer cell behavior in the tumor microenvironment (19), including cell proliferation and metastasis. A study from Pak et al. stated that TGF-β signaling could elevate VEGF-C expression, resulting in lymphangiogenesis in GC (20). Moreover, a previous study disclosed that the TGF-β/Smad4 signaling pathway was activated in gastric cell lines after irradiation exposure (21). Considering these reports and the results from the GSEA analysis,

we examined the expression of TGF-β1 and Smad4 after CST2 aberrant expression. The findings suggest that the expression trends of TGF-β1 and Smad4 were consistent with that of CST2, speculating that CST2 has a positive regulatory effect on the TGF-β/Smad4 signaling pathway.

While our study has made some findings, the results are not yet applicable in clinical diagnosis. More animal studies are needed to confirm our conclusions.

In short, our outcomes state that high expression of CST2 was actively associated with a worse outcome in GC patients. Moreover, upregulation of CST2 promoted the proliferation, invasion, and migration abilities by activating EMT and the TGF-β1 signaling pathway.

ACKNOWLEDGEMENT

This work was supported by the grant from Shanghai Municipal Commission of Health and Family Planning (No. 2017-239).

REFERENCES

1. Jemal A, Bray F, Center MM, Ferlay J, Ward E, Forman D. Global cancer statistics. CA Cancer J Clin 2011; 61:69-90.
2. Bertuccio P, Chatenoud L, Levi F, et al. Recent patterns in gastric cancer: a global overview. Int J Cancer 2009; 125:666-73.
3. Hundahl SA, Phillips JL, Menck HR. The National Cancer Data Base Report on poor survival of U.S. gastric carcinoma patients treated with gastrectomy: Fifth Edition American Joint Committee on Cancer staging, proximal disease, and the "different disease" hypothesis. Cancer 2000; 88:921-32.
4. Shin VY, Chu KM. MiRNA as potential biomarkers and therapeutic targets for gastric cancer. World J Gastroenterol 2014; 20:10432-9.
5. Mueller SK, Wendler O, Nocera A, et al. Escalation in mucus cystatin 2, pappalysin-A, and periostin levels over time predict need for recurrent surgery in chronic rhinosinusitis with nasal polyps. Int Forum Allergy Rhinol 2019; 9:1212-19.
6. Kato Y, Takabayashi T, Sakashita M, et al. Expression and Functional Analysis of CST1 in Intractable Nasal Polyps. Am J Respir Cell Mol Biol 2018; 59:448-57.
7. Singhania A, Wallington JC, Smith CG, et al. Multitissue transcriptomics delineates the diversity of airway t cell functions in asthma. Am J Respir Cell Mol Biol 2018; 58:261-70.
8. Zhou X, Wang X, Huang K, et al. Investigation of the clinical significance and prospective molecular mechanisms of cystatin genes in patients with hepatitis B virusrelated hepatocellular carcinoma. Oncol Rep 2019; 42:189-201.
9. Wang Z, Chen G, Wang Q, Lu W, Xu M. Identification and validation of a prognostic 9-genes expression signature for gastric cancer. Oncotarget 2017; 8:73826-36.
10. Saitoh E, Kim HS, Smithies O,Maeda N. Human cysteine-proteinase inhibitors: nucleotide sequence analysis of three members of the cystatin gene family. Gene 1987; 61:329-38.
11. Haga T, Minaguchi K. Sequence variations of the CST2 gene related to the polymorphism of salivary cystatin SA. J Dent Res 1999; 78:835-39.
12. Blanco MA, LeRoy G, Khan Z, Aleckovic M, Zee BM, Garcia BA,Kang Y. Global secretome analysis identifies novel mediators of bone metastasis. Cell Res 2012; 22:1339-55.
13. Li H, Takai N, Yuge A, et al. Novel target genes responsive to the anti-growth activity of triptolide in endometrial and ovarian cancer cells. Cancer Lett 2010; 297:198-206.
14. Bao Y, Wang L, Shi L, et al. Transcriptome profiling revealed multiple genes and ECM-receptor interaction pathways that may be associated with breast cancer. Cell Mol Biol Lett 2019; 24:38.
15. Zong W, Yu C, Wang P,Dong L. Overexpression of SASH1 Inhibits TGF-beta1-Induced EMT in Gastric Cancer Cells. Oncol Res 2016; 24:17-23.
16. Hugo H, Ackland ML, Blick T, Lawrence MG, Clements JA, Williams ED,Thompson EW. Epithelial--mesenchymal and mesenchymal--epithelial transitions in carcinoma progression. J Cell Physiol 2007; 213:374-83.
17. Wu Y, Grabsch H, Ivanova T, et al. Comprehensive genomic meta-analysis identifies intra-tumoural stroma as a predictor of survival in patients with gastric cancer. Gut 2013; 62:1100-11.
18. Ren X, Chen Y, He L, et al. Prevalence of underweight,

overweight and obesity in university students from the region of Anhui (China). Nutr Hosp 2014; 31:1089-93.
19. Zhang F, Li F, Lu GH, et al. Engineering magnetosomes for ferroptosis/immunomodulation synergism in cancer. ACS Nano 2019; 13:5662-73.
20. Pak KH, Park KC,Cheong JH. VEGF-C induced by TGF- beta1 signaling in gastric cancer enhances tumor-induced lymphangiogenesis. BMC Cancer 2019; 19:799.
21. Yang T, Huang T, Zhang D, et al. TGF-beta receptor inhibitor LY2109761 enhances the radiosensitivity of gastric cancer by inactivating the TGF-beta/SMAD4 signaling pathway. Aging (Albany NY) 2019; 11:8892-910.

Serum metabolic markers and metabolic pathways in rats with metabolomic cecal ligation and puncture-induced sepsis

R. Liu[1], Y. Li[2], D-X. Yang[3], M. Xu[4], Y-X. Yan[5], F-G. Zhou[3], Y-M. Liu[6], C. Xu[1], K. Zhao[1], G-Y. Jiang[1] and M-W. Liu[7]

[1]ICU, The First Hospital Affiliated To Kunming Medical University, Kunming, Yunnan, P.R. China; [2]Oral Medicine Center, The First People's Hospital ofYunnan Province, Kunming, Yunnan, P.R. China; [3]Department of Emergency Medicine, The First People's Hospital ofYunnan Province, Kunming, Yunnan, P.R. China; [4]SICU, The Fuwai Cardiovascular Disease Hospital of Yunnan province, Kunming, Yunnan, P.R. China; [5]ICU, The Shenzhen Bao 'an Hospital Affiliated To Southern Medical University, Shenzhen, Guangdong, P.R. China; [6]Department of Gerontology, The People's Hospital of Chongqing, Chongqing, P.R. China; [7]Department of Emergency Medicine, The First Hospital Affiliated To Kunming Medical

Received August 17, 2020 – Accepted November 30, 2020

The aim of this study was to explore the dynamic changes in characteristic serum metabolic markers and pathways during early sepsis in rats. By using cecal ligation and puncture (CLP), we made rat models of sepsis, which were randomly divided into 5 groups with 10 rats in each group: group A, group B, group C, group D, and group E. We collected 2 mL of arterial blood at 0, 6, 12, 24, and 48 hours from rats in group A-E respectively and isolated serum via centrifugation. Next, adopting metabolomics analysis methods, we screened for metabolites from the animal serum with statistically and biologically significant abundance changes, and used the KEGG database to analyze the respective metabolic pathways. In all, our findings reveal that D-glucosamine 6-phosphate, D-glucosamine phosphate, α-D-glucosamine 1-phosphate, D-glucosamine 1-phosphate, and 5-hydroxy isocyanate decline continuously from 12 hours, while L-phenylalanine, (S) -α-amino-β-phenylpropionic acid, 5-methoxy indole acetic acid salt, 5-methoxy indole acetic acid, goose deoxyglycolic acid salt, goose deoxyglycolic acid, and Chen's deoxygenated sugar alcohol started to decrease from 6 hours. Additionally, 3.2,3-Bis-O-(geranyl geranyl)-sn-glycerol-1-phosphoric acid-L-serine levels rose continuously from 12 hours. We found 13 differentially regulated ions, primarily ones involved in pathways responsible for the metabolism of sugar, amino acids, and lipids, which are related to the disorder of energy metabolism. Our findings mark serum-derived D-glucosamine and its phosphorous derivatives as characteristic metabolic markers of sepsis in rats.

Currently, no reliable biomarkers have been found that allow for the early identification of sepsis in a clinical setting and discovering specific markers will have significant impact on sepsis treatment and modern medicine. Most studies focus on small metabolic molecules, such as sugars and amino acid intermediates, with a molecular mass of less than 1000, and computational analysis methods, such as advanced analysis and detection technology combined with pattern recognition and expert system, are at the core of metabolomics research. First proposed by Oliver et al. in 1998 (1) and named

Key words: sepsis; metabolomics; cecal ligation and puncture; liquid chromatography-mass spectrometry

Corresponding Author:
Dr Ming-wei Liu,
Department of Emergency Medicine,
The First Hospital Affiliated to Kunming Medical University,
295 Xichang Road, Wuhua District, Kunming,
Yunnan 650032, P.R. China
e-mail: lmw2004210@163.com

0393-974X (2020)
Copyright © by BIOLIFE, s.a.s.
This publication and/or article is for individual use only and may not be further reproduced without written permission from the copyright holder.
Unauthorized reproduction may result in financial and other penalties
DISCLOSURE: ALL AUTHORS REPORT NO CONFLICTS OF INTEREST RELEVANT TO THIS ARTICLE.

"metabolomics" by Nicholson et al in 1999(2), metabolomics aims to analyze the metabolites produced by an organism in response to external stimuli and to elucidate its metabolic regulation (2). When an organism is subjected to pathological or physiological perturbations, its metabolic flux will undergo dynamic and significant changes, continuously generating metabolites that regulate the biological mechanisms underlying cell functions. Therefore, using metabolomics to measure these metabolites can accurately reflect the state of the biological system (4). Similarly, these metabolites, such as glucose, cholesterol, lactic acid, and free fatty acids, are produced through multiple biochemical pathways in the pathophysiology of sepsis (5).

This study used the metabolomic technology based on liquid chromatography-mass spectrometry to analyze the changes in characteristics of serum metabolites in rats with sepsis in order to seek and identify potential biomarkers for sepsis.

MATERIALS AND METHODS

Fifty SD rats, male, age 6-8 weeks, weight 250-300 g, were provided by the Animal Experiment Center of Kunming Medical University under pathogen-free conditions in controlled (30–70%) humidity. Standard laboratory chow and water were provided ad libitum. In all experiments, 8-9-week-old rats were used. All experiments were approved by the Animal Care Committee of Kunming Medical University. The animals were treated humanely consistent with the relevant national, international, and/or institutional guide lines and legislations

Establishment of sepsis model

SD rats were divided randomly into five groups. According to previously described methods (6), after successful anesthesia using intravenous 2% sodium pentobarbital (40mg/kg) (Shanghai Jixing Biotechnology Co., Ltd. Shanghai, China), the rats were fixed on a splint, the abdomen was opened with a scalpel, and incisions were made on the middle and lower parts of the abdomen, about 1.5 cm long. The skin and muscles were separated and fixed with sterile tweezers. The abdominal and intestinal tubes were separated and protected with wet gauze. The cecum was found and placed on the wet gauze. Blunt forceps were used to isolate the cecum at the end of 1 cm mesentery. The distal part of the cecum was 1 cm long, or about $^{1}/_{2}$ of the cecum, and it was ligated using 5-0 silk thread. A 21G needle was used to puncture the intestinal wall twice with spacing of about 3 mm. Then, the cecum was replaced in the abdominal cavity *in situ* and the abdominal wall muscles and skin were sutured layer by layer. Sodium chloride (3ml/100g) was injected subcutaneously after abdominal closure to replace the loss of body fluid during the operation and the rats were placed in the same environment after the operation. The changes of anesthesia waking time, diet, fur, posture, and activity of rats were then observed.

Rat arterial blood collection

The rats were divided into groups A, B, C, D, and E, and 2 mL femoral artery blood was collected for each group at the respective time points: before surgery (0 h), 6 h, 12 h, 24 h, and 48 h after the cecal ligation and puncture (CLP) was performed. The blood was centrifuged at 3000 r/min for 3 min, and the supernatant was collected and stored at -80°C for later analysis. After blood collection, the rats were anesthetized with intravenous pentobarbital sodium (40mg/kg) (Shanghai Jixing Biotechnology Co., Ltd. Shanghai, China) and sacrificed via cervical dislocation, and the organs were collected for analysis.

Metabolite extraction

According to previously described (7), the serum samples stored at -80°C (including quality control, QC) were thawed by a 30-min incubation at -20°C first and then at 4°C until completely thawed. 40 μL of each sample (including QC) were put into a 96-well plate, and then 120 μL of methanol were added to each well, shaken for 1 min and then stored at -20C for 30 min, and then centrifuged for 20 min at 4,000 x g at 4°C. 20 μL of supernatant were then taken from each well and put into a new 96-well plate and 180 μL of 50% methanol were added to each well, mixed, and 80 μL of each sample were transferred into a new 96-well plate, and stored at -80°C.

Liquid-phase description

A C18 chromatographic column (100 mm×2.1 mm, 1.7 μm, Waters, USA) was used for separation of samples. The column temperature was set at 50°C and the flow rate was 0.4 mL/min. The elution solution A was water

containing 0.1% formic acid and the elution solution B was methanol containing 0.1% formic acid. The following gradient was used for the separation of metabolites: 100% phase A for the first 2 min, followed by a 9-min transition from 0 to 100% phase B, 2 min of 100% phase B, and finally 2 min of 100% phase A (Fig. 1).

Mass spectrum parameter description

According to previously described methods (8), the ingredients of samples were separated using chromatographic column and collected using SYNAPT G2-XS QTOF (Waters, USA) with positive and negative ion patterns. In both the positive and negative ion modes, the capillary and the cone voltages were set to 2 kV and 40 V, respectively. Using the MSE pattern to carry out the centroid data collection, the first level scan range was 50-1200 Da and the scan time was 0.2 s. All parent ions were fragmented at energies of 20 to 40 eV, and all fragment information was collected, and the scanning time was 0.2 s. In the process of data acquisition, the LE signal was corrected for real-time quality every 3 seconds. At the same time, the collection of mass control samples was carried out every 10 samples to evaluate the stability of the instrument state during sample processing (Fig. 1).

Data preprocessing

The original data of the quality of the material was uploaded into the commercial software Progenesis QI (version 2.2, hereinafter referred to as QI) for peak extraction, so as to obtain the relevant information of the mass-to-charge ratio, retention time and ion area of metabolites. After removing the low mass ions from the extracted data, the method was corrected by using the quality control-based robust LOESS signal correction (9). To filter the corrected data, namely the relative standard deviation (RSD) of all QC samples > 30% of ions was filtered off – the variation of RSD > 30% ion was larger in the experimental process and was not included in the downstream statistical analysis (Fig. 2) .

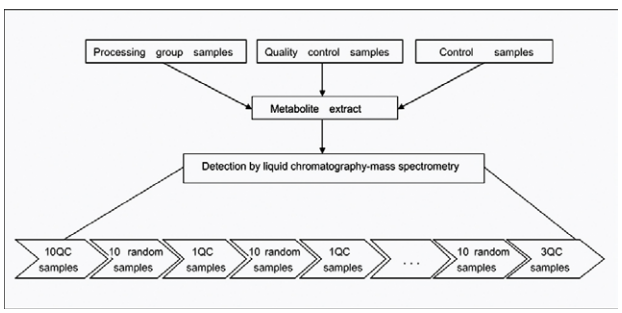


Fig. 1. *Experimental process*

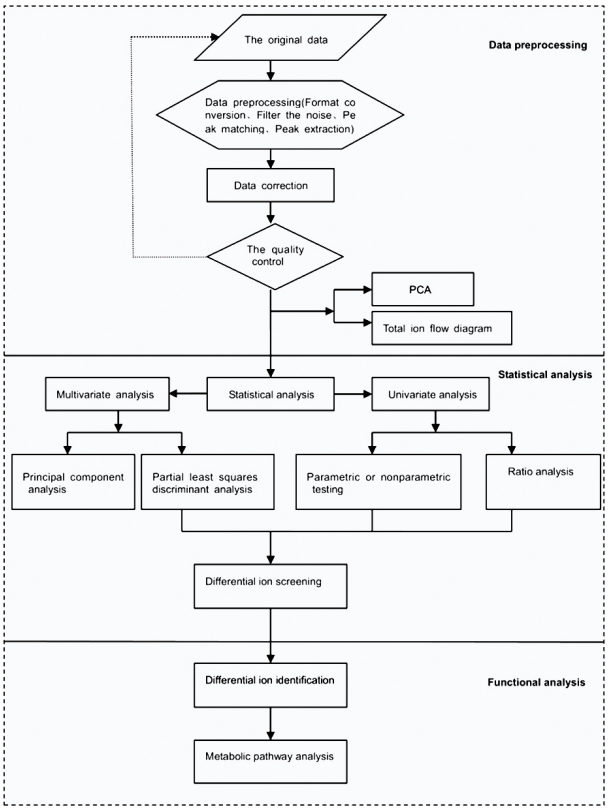


Fig. 2. *Flow chart of information analysis*

Statistical analysis

Because the metabolic group data have the characteristics of "high dimension and mass", it is necessary to analyze data with single-dimensional and multi-dimensional methods according to the data characteristics. In this study, the metabolomics data analysis process independently developed by BGI metabolomics research team was adopted: univariate and multivariate analyses were performed to obtain intergroup differential metabolites. The methods include both parametric and non-parametric tests, differential expression multiple analysis, principal component analysis (PCA), and partial least squares-discriminant analysis (PLS-DA).

The advanced mass spectrometer Xevo G2-XS QTOF (Waters, USA) was used for mass spectrometry data

collection. Progenesis QI (version 2.2) (Waters, USA) and metaX (metabolomics R software package) were used for in-depth analysis of mass spectrometry data, in which metabolite identification and metabolic pathway analysis were based on the KEGG. PCA and PLS-DA were used to retrieve potential biomarkers in the metabolomics of sepsis (Fig. 2).

In this project, the advanced mass spectrometer Xevo g2-xs QTOF (Waters, USA) was used for mass spectrum data collection. Progenesis QI (version 2.2) (Waters, USA) and metaX (metabolomics R software package) independently developed by BGI metabolomics research team, were used for in-depth analysis of mass spectrometry data, in which metabolite identification and metabolic pathway analysis were based on the KEGG database.

RESULTS

Sepsis model in rats

The general observation results showed that the anesthesia waking time of the rats was basically the same, about 60±30min. Postoperative diet and drinking water were significantly reduced in all groups of rats, with listless spirit, less movement, reduced activity and dull skin. After the blood collection at the preset time point, the abdomen of the rats was cut open with scissors to observe the changes of the abdomen of the rats. It was found that the longer the experiment lasted, the more obvious the abdominal ischemia and infection became (Fig. 3). According to the changes of general conditions and the changes of abdominal conditions in thr rats, the success of the rat CLP sepsis model replication can be determined.

Differential ion screening and identification

According to the above information analysis flow chart, the project adopted multivariate analysis of VIP values of the second principal component of the pls-da model, and univariate analysis of fold-change and q-value to screen the metabolites with differential expressions. Screening criteria: ii) VIP>

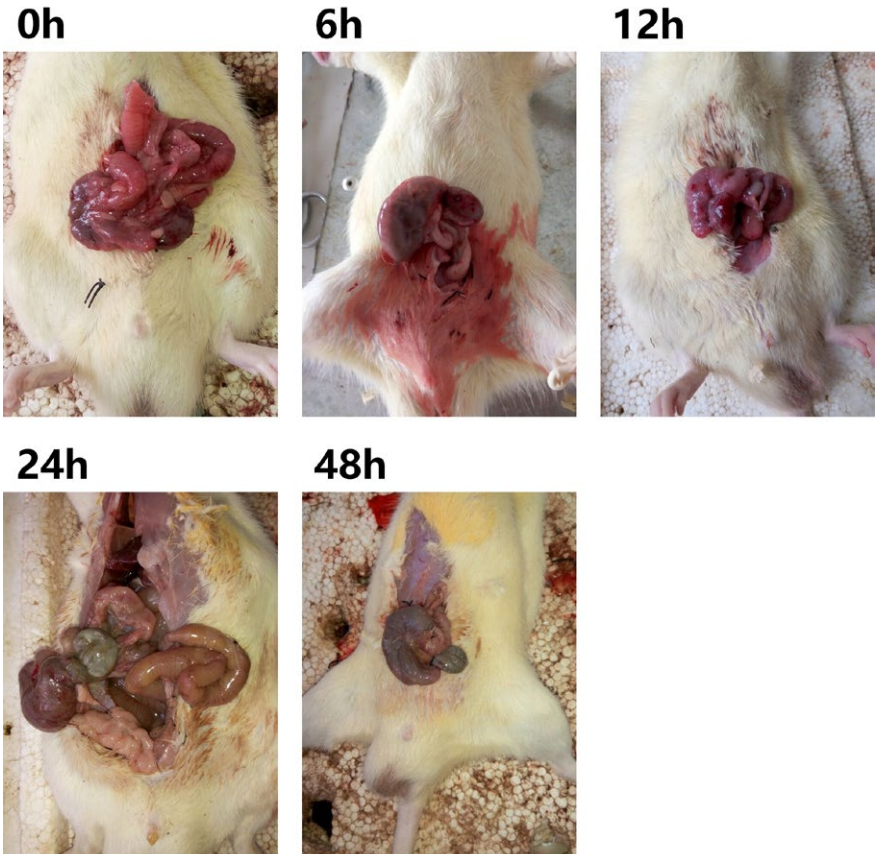


Fig. 3. *Sepsis model of rats in each group*

1; ii) fold change >1.2 or < 0.8333; iii) if the q-value is <0.05, the intersection of the three will be taken to obtain the common ions, namely the difference ions. The software used for differential ion identification was Progenesis Q (version 2.2). The results of ion difference (Table I) showed that Neg and Pos ion patterns were different between each group and the control group, and the differences were observed within 24 hours. The difference in ion number between the d-a group was the largest, and it was found that the changes in metabolites began within the first six hours in the animals of the sepsis model, namely the b-a group (or even earlier), and the biggest changes occurred around 24 hours, namely the d-a group.

Cluster analysis was performed according to the screened differential ions

According to the screened differential ions, clustering analysis was performed and presented in the form of heat map. The clustering analysis diagram of differential ions was compared between group A rats and other groups of rats. Each row represents a dif ion, each column represents a sample, and different colors represent different intensities, with green to red representing increasing intensities. Differential ions can be found in the serum of group B rats from 6 hours after surgery (or even earlier) (Fig. 4). By 24 hours, the difference and intensity of serum ions were the most obvious in groups D and A (Fig. 4).

Differential metabolite pathway analysis

According to the screened differential ions, metabolic pathways of metabolites were searched based on KEGG database. Metabolic pathway analysis can help understand the major biochemical metabolic pathways and signal transduction pathways involved by metabolites. Finally, 75 metabolic pathways were determined according to the Neg ion model, and 158 metabolic pathways were

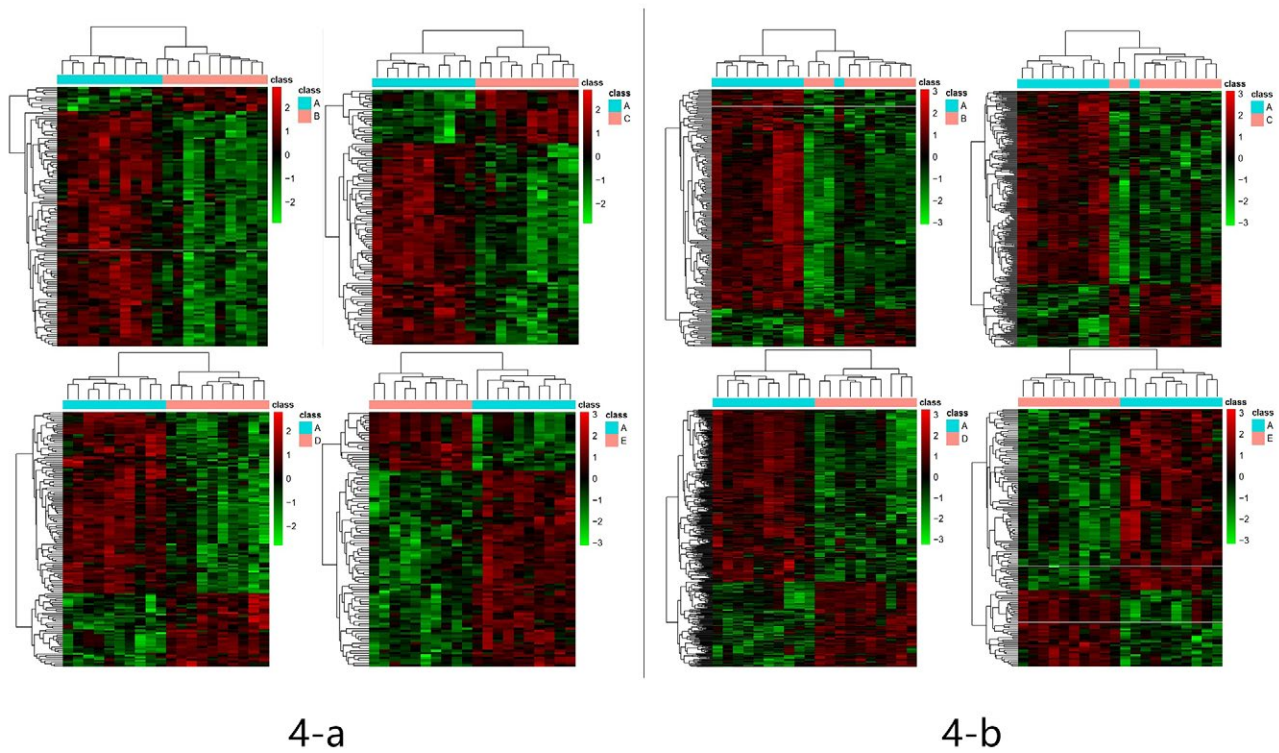


Fig. 4. *neg ion model and pos ion mode.* ***a****) neg ion model shows the clustering analysis diagram of differential ions. Each row represents a dif ion, each column represents a sample, different colors represent different intensities, and colors ranging from green to red indicate emphasis from low to high.* ***b****) Pos ion mode shows the clustering analysis diagram of differential ions. Each row represents a dif ion, each column represents a sample, different colors represent different intensities, and colors ranging from green to red indicate emphasis from low to high.*

determined according to the Pos ion model. These pathways mainly include carbohydrate, protein, amino acid, lipid, steroid, purine, bile acid and other metabolic pathways, and they are interrelated.

PCA was analyzed by principal component analysis between group A and other groups; PLS-DA was analyzed by partial least squares discriminant

PCA analysis of serum metabolites in groups A, B, C, D and E showed that the overall distribution of serum samples was stable and the model was stable and reliable (Fig. 5). PCA diagram showed that the aggregation degree in group A was higher than that in the other groups, indicating that the individual difference of serum metabolites in rats 0 hours after surgery was the smallest (Fig. 5). Further PLS-DA analysis showed that groups B, C, D and E had significantly different degrees of deviation from group A, among which group D had the largest degree of deviation, indicating that group D had the most drastic changes in serum metabolites (Fig. 6).

Biomarker screening

After differential ions were screened out, metabolic pathways of metabolites were searched according to the KEGG database. Metabolic pathway analysis can help understand the major biochemical metabolic pathways and signal transduction pathways involved by metabolites. Its pathways mainly include sugar, amino acids, lipids, steroids, purines and other metabolic pathways, and they are interrelated. From the analysis of these common differential metabolic pathways, we found the ions with a common change trend, and found their measured values from the heat map, calculated the ratio of groups B, C, D, E to group A, and made a line chart (Fig. 6). From Fig. 6-a, we can conclude that D-glucosamine 6-phosphate, D-glucosamine phosphate, α-D-glucosamine 1-phosphate, and D-glucosamine 1-phosphate gradually declined with the development of MODS, and it was found that they began to decline in group C (12 h); moreover, these four substances are involved in the insulin resistance

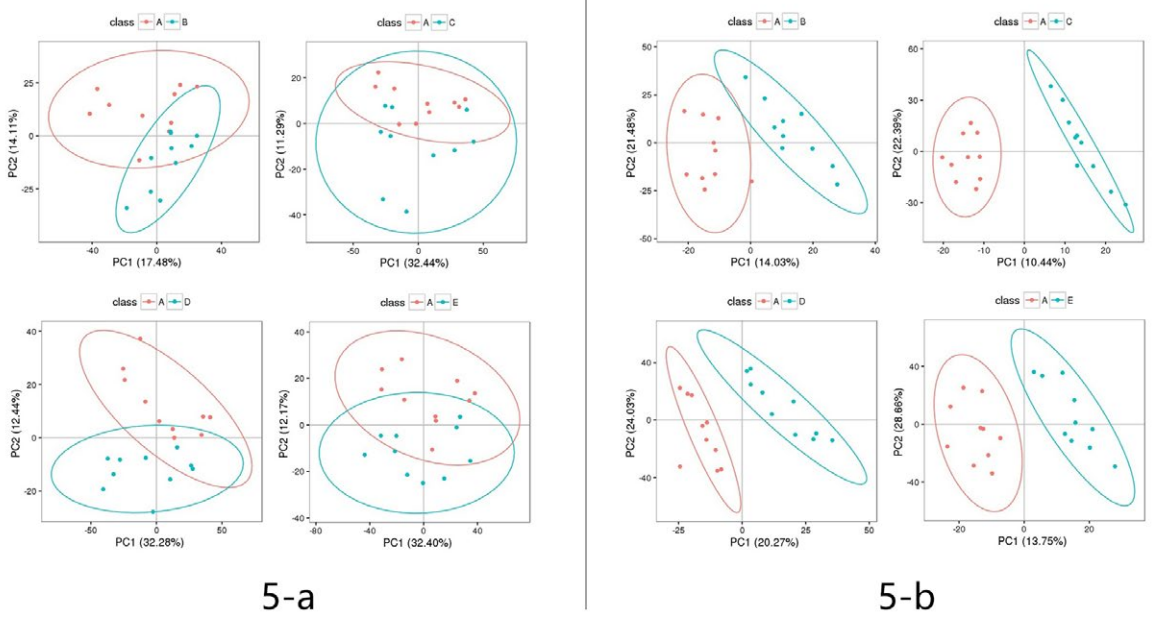


Fig. 5. *PCA and PLS-DA analysis of group A and each group.* ***a)*** *PCA analysis diagram of group A and each group;* ***b)*** *PLS-DA analysis of group A and each group.*

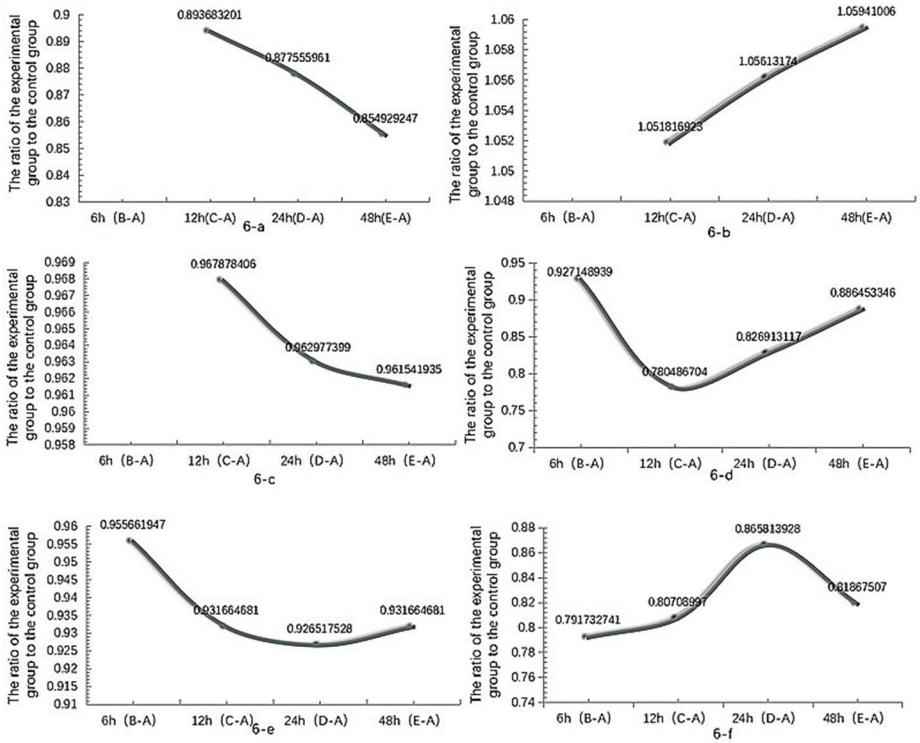


Fig. 6. *Biomarker screening of Metabolic pathway analysis. a) D-glucosamine 6-phosphate; D-glucosamine phosphate; α-D-glucosamine 1-phosphate; D-glucosamine 1-phosphate.* ***b)*** *2,3-Bis-O-(geranyl acyl geranyl acyl)-sn-glycerol-1-phosphate-L-serine.* ***c)*** *5-hydroxy isocyanate.* ***d)*** *(L-phenylalanine, (S) -α-amino-β-phenylpropionic acid); 5-(3-pyridine)-2-hydroxytetrahydrofuran; 4-hydroxyl-1- (3-pyridine)-1-butanone.* ***e)*** *5-methoxy indole acetic acid salt and 5-methoxy indole acetic acid.* ***f)*** *goose deoxyglycolic acid salt; goose deoxyglycolic acid; Chen's deoxygenated sugar alcohol.*

pathway. From Fig. 6-b, the trend of 2,3-Bis-O-(geranyl acyl geranyl acyl)-sn-glycerol-1-phosphate-L-serine with the development of pyrisis was increased. Also in group c (12h), 2,3-Bis-O-(geranyl acyl geranyl acyl)-sn-glycerol-1-phosphate-L-serine is involved in the metabolism of glycerin phospholipids. As shown in Fig. 6-c, the trend of 5-hydroxy isocyanate from 12h began to decline, and the 5-hydroxy isocyanate was involved in the metabolism of purine. It can be concluded from Fig. 6-d that L-phenylalanine, and (S)-α-amino-β-phenylpropionic acid 5-(3-pyridine)-2-hydroxytetrahydrofuran, and 4-hydroxyl-1-(3-pyridine)-1-butanone showed a downward trend within 6-12h and an upward trend within 12-48h. As shown in Fig. 6-e, 5-methoxy indole acetic acid decreased from 6h to 24h, and increased slightly from 2h to 48h. It can be seen from Fig. 6-f that goose deoxyglycolic acid salt, goose deoxyglycolic acid, and Chen's deoxygenated sugar alcohol show an upward trend from 6h to 24h, but generally lower than the normal level, and a downward trend from 24h to 48h.

DISCUSSION

In this study, the CLP model was used to generate septic rats, a clinically accurate method that is considered the gold standard for models of sepsis (10), and liquid chromatography-mass spectrometry-based metabolomics was applied to screen for sepsis biomarkers**.** We uncovered 13 differentially regulated ions, primarily those involved in pathways responsible for the metabolism of sugar, amino acids, and lipids, which are related to the disorder of energy metabolism. Our findings mark serum-derived D-glucosamine and its phosphorous derivatives as characteristic metabolic markers of sepsis in rats. We reveal new

Table I. *Differential ion identification table*

mode	Group	diff ion number	up MS	down MS	up MS2	down MS2
pos	B-A	183	18	55	9	39
pos	C-A	278	37	72	24	41
pos	D-A	388	63	88	29	50
pos	E-A	151	17	64	9	41
pos	E-B	297	52	46	42	25
pos	D-C	3	1	0	0	0
pos	C-B	6	2	3	1	2
pos	D-B	136	24	29	14	12
pos	E-D	204	46	21	31	8
neg	B-A	119	2	24	1	4
neg	C-A	110	7	21	5	4
neg	D-A	149	15	24	6	6
neg	E-A	104	8	29	3	3
neg	E-B	127	16	12	7	1
neg	D-C	2	0	0	0	0
neg	C-B	4	0	1	0	0
neg	D-B	37	7	6	2	2
neg	E-D	5	1	0	0	0

The table shows the differential ions between groups, at the same time presents the experimental group compared with control group the difference of general idea of the ion on the cut (such as category 1_2, 1 group compared with group 2). Pos: positive ion mode refers to the addition ion of a substance at the ion source is H+, NH4+, Na+, K+ and other positive ions. Neg: anion mode, refers to that the adduct ion of a substance at the ion source during ionization is -h, +Cl, +OAc plasma. Diff ion number: refers to the number of ion differences after screening. MS: primary identification number refers to the number of ions identified after searching the database with primary data; Primary data refers to the data on the mass spectra of metabolites after adding H+/NH4+/ COOH- to the ion source. MS2: secondary identification number refers to the number of theoretical secondary fragments searched in the database that have been identified; Secondary data refers to the primary data in the mass spectrometer after the fragmentation, with metabolite fragment ion data information. Note: primary identification number refers to the number of ions with identification results; Secondary identification results refer to the number of ions with both primary and secondary identification. The primary identification number includes the secondary identification.

biomarkers and metabolic perturbations at the core of sepsis disease progression. Our findings highlight the complexity of septic disease and underline that multiple metabolic disorders are involved in its pathology. By continuing to develop a comprehensive understanding of sepsis, and the endogenous metabolic changes of the small molecules involved in its pathogenesis, there will be significant biomedical advancements in rapid and effective diagnosis techniques, treatments, and patient care strategies at the clinical level. The potential biomarkers outlined in this study will allow for an early detection and prognosis of sepsis and its associated diseases, contributing to patient recovery and survival.

There are, however, some limitations to this study: the difference in the amount of overflow of the cecal content; the puncture hole is wrapped by the omentum and surrounding tissues, so that persistent abdominal infection cannot be formed; metabolomics is in the downstream of life activities

and suffers more interference factors, and individual differences are obvious. These are the main reasons for the differences in experimental results.

ACKNOWLEDGEMENTS

This research received funding via a grant provided by the National Natural Science Foundation (Grant No. 81960350) and Yunnan Applied Basic Research Project-Union Foundation of China (Grant No.2015FB022).

REFERENCES

1. Holstein EM, Ngo G, Lawless C, et al. Systematic analysis of the DNA damage response network in telomere defective budding yeast. G3 (Bethesda) 2017; 7(7):2375-89.
2. Nicholson JK. Lindon JC. Holmes E. Metabonomics: understanding the metabolic responses of living systems to pathophysiological stimuli via multivariate statistical analysis of biological NMR spectroscopic data. Xenobiotica 1999; 29(11):1181-89.
3. Pham-Tuan H, Kaskavelis L, Daykin CA, et al. Method development in high-performance liquid chromatography for high-throughput profiling and metabonomic studies of biofluid samples. J Chromatogr B Analyt Technol Biomed Life Sci 2003; 789(2):283-301.
4. Eckerle M, Ambroggio L, Puskarich MA, et al. Metabolomics as a driver in advancing precision medicine in sepsis. Pharmacotherapy 2017; 37(9):1023-32.
5. Gong W, Wen H. Sepsis induced by cecal ligation and puncture. Methods Mol Biol 2019; 1960:249-55.
6. Li H, Cai Y, Guo Y, Chen F, Zhu ZJ. MetDIA: Targeted metabolite extraction of multiplexed MS/MS spectra generated by data-independent acquisition. Anal Chem 2016; 88(17):8757-64.
7. Hou TY, Chiang-Ni C, Teng SH. Current status of MALDI-TOF mass spectrometry in clinical microbiology. J Food Drug Anal 2019; 27(2):404-14.
8. Dunn WB, Broadhurst D, Begley P, et al. Procedures for large-scale metabolic profiling of serum and plasma using gas chromatography and liquid chromatography coupled to mass spectrometry. Nat Protoc 2011; 6(7):1060-83.
9. Englert JA, Rogers AJ. Metabolism, metabolomics, and nutritional support of patients with sepsis. Clin Chest Med 2016; 37:321-31.
10. Deng W, Rao J, Chen X, et al. Metabolomics study of serum and urine samples reveals metabolic pathways and biomarkers associated with pelvic organ prolapse. J Chromatogr B Analyt Technol Biomed Life Sci 2020; 1136:121882.

LETTER TO THE EDITOR

Histological analysis of epidermal growth factor receptor gene mutation and clinical characteristics of advanced peripheral lung cancer

JJ. Jin, LX. Xu, D. Zhang, CX. Wang, Z. Fan, TT. Xu, S. Wang and Y. Huang

Department of Respiratory Medicine, North China University of Science and Technology Affiliated Hospital, Tangshan, Hebei, China

Received April 17, 2020 – Accepted October 13, 2020

To the Editor,

Lung cancer is one of the most common malignancies and has been reported to rank first in morbidity and mortality among all malignancies (1-4). The anatomy can be divided into peripheral lung cancer and central lung cancer, with peripheral lung cancer being the more common. The clinical symptoms of patients with advanced peripheral lung cancer are late and non-specific. By the time patients are diagnosed, the symptoms have already metastasized, they have lost the chance of radical operation, and most patients are older, in poor physical condition, and cannot tolerate the side effects of chemotherapy. Therefore, the exploration of targeted therapy is particularly important.

Recently, several lung cancer-driving genes have been identified, such as epidermal growth factor receptor (EGFR), which is the most common mutation in advanced peripheral lung cancer. For these patients, targeting EGFR-TKIS with tyrosine kinase inhibitors has become an important therapeutic tool. However, the clinical manifestations of patients are diverse. Whether it is related to EGFR gene mutation status or not, it is worth exploring (5). Therefore, we conducted this study to analyze the clinical characteristics of EGFR gene mutation in patients with advanced peripheral lung cancer to provide evidence for targeted therapy.

MATERIALS AND METHODS

Study subjects

From September 2017 to July 2019, 124 patients with advanced peripheral lung cancer diagnosed by histopathology were recruited for this study. EGFR gene expression was detected by amplification refractory mutation system (ARMS), droplet digital PCR (DDPCR), or next-generation sequencing (NGS) in all patients, and the clinical data were complete. The study was conducted in accordance with the Declaration of Helsinki and was approved by the ethics committee of our hospital. All participants provided signed informed consent.

The inclusion criteria were; patients with advanced peripheral lung cancer diagnosed by histopathology; patients who needed ARMS, DDPCR, or NGS methods to detect EGFR mutations; age ranging from 18 to 75 years; Eastern Cooperative Oncology Group (ECOG) scores of 0–2; patients whose CT imaging features advanced peripheral lung cancer; patients whose medical records were complete, including their general situation, medical history, physical examination, laboratory results, and imaging auxiliary examination; patients whose informed consent was signed.

Exclusion criteria were: patients who could not obtain a definite histopathological diagnosis; patients whose

Key words: advanced peripheral lung cancer; epidermal growth factor receptor (EGFR) gene mutation; Computerized tomography (CT) imaging; clinical features; pleural indentation

Corresponding Author:
Dr Yan Huang,
Department of Respiratory Medicine,
North China University of Science and Technology Affiliated Hospital,
No. 73 of Jianshe Road, Lubei District, Tangshan,
Hebei, 063000, China
Tel.: +86 18713877946
e-mail: huangy95201@163.com

0393-974X (2020)
Copyright © by BIOLIFE, s.a.s.
This publication and/or article is for individual use only and may not be further reproduced without written permission from the copyright holder.
Unauthorized reproduction may result in financial and other penalties
DISCLOSURE: ALL AUTHORS REPORT NO CONFLICTS OF INTEREST RELEVANT TO THIS ARTICLE.

chest CT was performed in other medical institutions and who could not obtain complete imaging data; patients with malignant tumors secondary to other organs or with other malignant tumors; patients who had severe liver or kidney dysfunctions; patients who had severe coagulation dysfunction, patients whose data were incomplete.

EGFR gene detection was performed by ARMS, DDPCR, or NGS. The results were classified as EGFR mutant and EGFR wild. Spiral CT was performed by a 256-slice Philips Brilliance ICT 126 from the lung apex to the lung base. All images were interpreted, analyzed, and summarized by two clinical directors and two radiologists with five or more years of experience in chest CT scanning.

Statistical analysis

The software program SPSS 20.0 (SPSS INC, Chicago, IL, USA) was used to conduct the statistical analysis. Continuous variables were expressed as mean ± SD. Discontinuous variables were expressed as a percentage (%). For two comparisons, each value was compared by a *t*-test when each datum conformed to a normal distribution, while the non-normally distributed continuous data were compared using non-parametric tests. The counting data were tested by the *Chi*-squared test. Logistic regression was used for multivariate analysis. Multiple logistic regression was used for EGFR gene mutation. A value of $P < 0.05$ was considered statistically significant.

RESULTS

Patient general characteristics

A total of 124 patients (64 males; 60 females) with peripheral lung cancer were included in this study, of whom 37 were EGFR gene mutation, 87 were wild EGFR gene mutation, 34 were <60 years, 90 were ≥60 years, 44 were smokers, 80 were non-smokers, 76 had adenocarcinoma of the lung, 16 had squamous cell carcinoma of the lung, and 32 had small-cell carcinomas.

Relationship between EGFR gene status and general clinical features in advanced peripheral lung cancer

In 124 patients with advanced peripheral lung cancer, 37 (37/124, 29.84%) had the gene mutation, including 12 males and 25 females, and 47.1% of the patients were under 60 years. EGFR gene mutation was correlated with gender, age, smoking history, and pathological type of patients. The difference was statistically significant ($P < 0.05$) (Table I).

Table I. *Relations hip between E GFR gene status and clinical features in advanced peripheral lung cancer (N%)*

Clinical features	Number of examples	EGFR positive group (n=37)	EGFR negative group (n=87)	$\chi 2$	P
Gender					
Male	64	12 (18.8)	52 (81.2)	7.768	<0.01
Female	60	25 (41.7)	35 (58.3)		
Age					
<60 years old	34	16 (47.1)	18 (52.9)	6.635	<0.05
≥60years old	90	21 (23.3)	69 (76.7)		
Smoking history					
Without	80	29 (36.3)	51 (63.7)	4.427	<0.05
With	44	8 (18.2)	36 (81.8)		
Pathologic types					
Adenocarcinoma	76	29 (38.2)	47 (61.8)	6.022	<0.05
Squamous cell carcinomas	15	2 (13.3)	13 (86.7)		
Small cell lung cancer	31	6 (19.4)	25 (80.6)		

Application of different test methods in EGFR gene detection

There are many methods to detect EGFR gene in clinical practice. The most commonly used are ARMS, DDPCR, and NGS. In 124 patients, the NGS method was the most commonly used method for EGFR gene testing, accounting for 43.5%. Choosing the appropriate test method could improve the diagnosis rate, guide the treatment plan, and improve patient satisfaction (Table II).

Relationship between EGFR gene mutation and CT findings in advanced peripheral lung cancer

Analysis of CT findings of EGFR gene mutation in the chest showed that there was a correlation between EGFR gene mutation and signs of pleural indentation. Patients with advanced peripheral lung cancer with signs of pleural indentation were more likely to have EGFR gene mutation. The difference was statistically significant ($P < 0.05$), but signs of burr, vessel convergence, cavities, vacuole, and ground-glass nodules were not related to EGFR gene mutation, and the difference was not statistically significant ($P > 0.05$). Therefore, CT findings can be used to predict EGFR gene mutation and to guide the diagnosis and treatment (Table III).

DISCUSSION

Patients with peripheral lung cancer who have atypical, non-specific symptoms, which are not easily found, lose the chance of radical surgery when their symptoms are more advanced, so chemotherapy is the basic treatment program.

Table II. *A pplication of different detection methods in Egfr gene detection in patients with advanced peripheral lung cancer (N ..%)*

Detection method	Number of examples	Percentage of total patients（%）
ARMS method	37	29.8
ddPCR method	33	26.7
NGS method	54	43.5
Total	124	100

Table III. *Correlation between EGFR gene m utation and CT findings in advanced peripheral lung cancer (N ..%)*

CT imaging signs		EGFR positive group (n=37)	EGFR negative group (n=87)	χ^2	*P*
Burr sign	without	18 (30.5)	41 (69.5)	0.024	>0.05
	with	19 (29.2)	46 (70.8)		
Vessel convergence sign	without	10 (24.3)	28 (75.7)	1.267	>0.05
	with	28 (32.6)	58 (67.4)		
Empty	without	22 (32.8)	45 (67.2)	0.625	>0.05
	with	15 (26.3)	42 (73.7)		
Vacuolar sign	without	30 (27.5)	79 (72.5)	2.308	>0.05
	with	7 (46.7)	8 (53.3)		
Lobulation sign	without	20 (30.8)	45 (69.2)	0.460	>0.05
	with	17 (29.3)	41 (70.7)		
Pleural indentation	without	12 (20.3)	47 (79.7)	6.447	<0.05
	with	27 (41.5)	38 (58.5)		
Amputated bronchus sign	without	26 (35.1)	48 (64.9)	1.155	>0.05
	with	13 (26.0)	37 (74.0)		
Ground-glass nodule	without	31 (34.8)	58 (65.2)	1.671	>0.05
	with	8 (22.9)	27 (77.1)		

However, some patients are too old to tolerate the adverse effects of chemotherapy, so it is imperative to find other treatments. In recent years, molecular targeted therapy has become a hot topic, and EGFR tyrosine kinase inhibitor (EGFR-TKI) has become an important treatment for advanced peripheral lung cancer with EGFR gene mutation. EGFR gene mutation was found to be an important factor in predicting therapeutic efficacy of EGFR-TKI (6,7). Therefore, it is necessary to detect EGFR gene mutation in peripheral lung cancer patients (8). Analysis of the relationship between EGFR gene mutation and clinical features and CT findings in advanced peripheral lung cancer is helpful in improving the diagnosis and treatment (9).

The chest CT imaging of lung tumors had certain characteristics. The main CT imaging signs of advanced peripheral lung cancer were of burr, vascular bundle, cavities, vacuole, lobulation, pleural indentation, bronchial truncation, and ground-glass nodules (10, 11). Through the analysis of these imaging findings and EGFR gene mutation status, we found that the presence of pleural indentations may be more prone to EGFR gene mutation. However, the tumor location and organ metastasis were not analyzed, as they will be further explored in future studies.

In conclusion, in advanced peripheral lung cancer, women who were non-smokers and younger than 60 years with adenocarcinoma of the lung were more likely to have EGFR mutations. Pleural indentation in imaging was associated with a higher mutation rate of the EGFR gene, which can be used to predict EGFR gene mutation and guide clinical treatment.

ACKNOWLEDGEMENTS

This study was supported by" Lung cancer with metabolic syndrome management - Excellent talents project of Hebei provincial health commission"and" Study on screening and intervention of drug-resistant genes in lung cancer (Item number: ZD20140302)"and " Detection of microscopic RNA in lung cancer under endoscopic thoracoscopy and study on targeted drug resistance (Item number: 20120151)".

REFERENCES

1. Thakur MK, Ruterbusch JJ, Schwartz AG, Gadgeel SM, Beebe-Dimmer JL, Wozniak AJ. Risk of Second Lung Cancer in Patients with Previously Treated Lung Cancer: Analysis of Surveillance, Epidemiology and End Results (SEER) Data. J Thorac Oncol 2018; 13:46-53.
2. Hannaway N , Gardiner J , Hughes A , Greystoke A. Lung cancer treatment and compliance with NICE Chemotherapy Guidelines in patients aged over 70 years. Lung Cancer 2018; 115:S10.
3. Pešek M, Mužík J. Small-cell lung cancer: epidemiology, diagnostics and therapy. Vnitr Lek. Winter 2018; 63:876-83.
4. Torre LA, Bray F, Siegel RL, Ferlay J, Lortet-Tieulent J, Jemal A. Global Cancer Statistics, 2012. CA Cancer J Clin 2015; 65:87-108.
5. Wang WQ, Liu HX, Shi DW, Li ZJ. Comparison of clinical features and prognosis between young and old non-small-cell Lung Carcinoma. J China Med Univ 2014; 43:661-63.
6. Thumallapally N, Yu H, Farhan M, Ibrahim U, Odiami M. Concomitant Presence of EGFR and ALK Fusion Gene Mutation in Adenocarcinoma of Lung: A Case Report and Review of the Literature. J Pharm Pract 2018; 31:244-48.
7. Nie Y, Gao W, Li N, et al. Relationship between EGFR gene mutation and local metastasis of resectable lung adenocarcinoma. World J Surg Oncol 2017; 15:55.
8. Cho A, Hur J, Moon YW, et al. Correlation between EGFR gene mutation, cytologic tumor markers, 18F-FDG uptake in non-small cell lung cancer. BMC Cancer 2016; 16:224.
9. Griffin CA, Lu C, Fishman EK, Khouri N, Markman M, Siegelman SS, Abeloff MD. The role of computed tomography of the chest in the management of small-cell lung cancer. J Clin Oncol 1984; 2:1359-65.
10. Yang X, Soimakallio S. Ural signs of small peripheral pulled masses: Pathologic correlation with chest radiographs and diagnostic value J. Eur J Radiol 1997; 25:146-51.
11. Hsu KH, Chen KC, Yang TY, et al. Epidermal growth factor receptor mutation status in stage I lung adenocarcinoma with different image patterns. J Thorac Oncol 2011; 6:1066-72.

LETTER TO THE EDITOR

Repairing effects of liraglutide on spinal cord injury in rats via PI3K/AKT/ENOS signaling pathway

T.-M. Qi[1*], F.-R. Wang[1*], C.-M. Fan[2], L.-M. Liu[1], J.-Y. Zhou[1], X.-C. Lin[1] and A.-X. Suonan[1]

[1]Department of Orthopaedics, Qinghai Provincial People's Hospital, Xining, China; [2]Department of Gastroenterology, The Fifth People's Hospital of Qinghai Province, Xining, China

Received May 9, 2020 – Accepted October 14, 2020

[*] These Authors contributed equally to this work

To the Editor,

Spinal cord injury (SCI) refers to the damage to the structure and function of the spinal cord caused by direct and indirect factors such as external impact, and its incidence rate is rising gradually with social development (1, 2). It is usually a complication induced by spinal injury, but the consequence is fairly severe, easily leading to paraplegia and serious dysfunction (3, 4). The severity of SCI mainly depends on the site and degree of injury, and a high-degree impact injury will cause irreversible pathological changes of the spinal cord (5, 6). General SCI may be restored to some extent by means of drug therapies (7), hence, finding drugs promoting repair of SCI is of great importance. As a glucagon-like peptide-1 analogue, liraglutide is primarily applied to treat type 2 diabetes mellitus (8). It works mainly by affecting cell function and stimulating hormone secretion as well as cell proliferation and differentiation (9, 10), however, the role and mechanism of this drug in SCI remain unknown. In this research, therefore, 18 adult Sprague-Dawley (SD) rats were divided into control group, SCI group and liraglutide group. The rat model of SCI was established and treated with liraglutide, and the changes in motor nerve function were evaluated. Moreover, the gene expression patterns in each group of rats were detected, enrichment analyses were conducted, and the repairing effect of liraglutide on SCI was explored combined with the expression of the phosphatidylinositol 3-kinase (PI3K)/protein kinase B (Akt)/endothelial nitric oxide synthase (eNOS) signaling pathway.

MATERIALS AND METHODS

Grouping of laboratory animals and modeling of SCI in rats

A total of 18 adult SD rats (250-280 g) were selected and randomly assigned into 3 groups (control group, SCI group and liraglutide group). Pentobarbital sodium at a dose of 40 mg/kg was intraperitoneally injected into the rats, and an incision was made on the median line of the back after disinfection with cotton balls soaked with 75% alcohol. The T_6-T_{10} vertebral laminae were merely resected without any treatment of the spinal cord in the control group. The SCI model was established using Allen's weight-dropping method, and the rats in liraglutide group were intraperitoneally injected with 50 μg/kg liraglutide based on the treatment in the SCI group. This study was approved by the Animal Ethics Committee of Qinghai Provincial People's Hospital Animal Center.

Key words: SCI; liraglutide; PI3K/Akt/eNOS signaling pathway

Corresponding Author:
Nanangxiu Suo, MM.
Department of Orthopaedics, Qinghai Provincial People's Hospital,
2nd Gonghelu Road, Chengdong District,
Xining, 810007Qinghai, China
Tel.: +86 013897582592
e-mail: suona19630312@163.com

0393-974X (2020)
Copyright © by BIOLIFE, s.a.s.
This publication and/or article is for individual use only and may not be further reproduced without written permission from the copyright holder.
Unauthorized reproduction may result in financial and other penalties
DISCLOSURE: ALL AUTHORS REPORT NO CONFLICTS OF INTEREST RELEVANT TO THIS ARTICLE.

Evaluation of motor nerve function

The motor nerve function of the rats in all 3 groups was evaluated using Basso, Beattie & Bresnahan (BBB) scoring system and slope test. Specifically, the hindlimb motor function was assessed before surgery and at 1, 3, 7, 21 and 28 d after operating through the BBB score, and the critical angle of inclined plane was measured at 1, 3, 7, 21 and 28 d after the operation via the Rivlin method of slope test.

Detection of gene expression patterns

Total ribonucleic acids (RNA) were extracted from the spinal cord tissues in the 3 groups using TRIzol method (Invitrogen, Carlsbad, CA, USA), and the expression profiles of messenger RNAs (mRNAs) in each group were analyzed by means of transcriptome sequencing. The FPKM value of mRNAs in each group of rats was obtained, normalized and visualized using R3.3.2 Package pheatmap to obtain the heat map.

Enrichment analyses of differential genes

Genome Ontology (GO) and Kyoto Encyclopedia of Genes and Genomes (KEGG) enrichment analyses were adopted for differential genes. The differentially expressed genes (FC>2 and P<0.05) in the 3 groups were screened, subjected to enrichment analyses and visualized via web page tool (http://enrich.shbio.com/index/ga.asp).

Detection of expression of molecules in the PI3K/Akt/eNOS signaling pathway via quantitative polymerase chain reaction (qPCR)

Real-time (RT)-qPCR was performed to determine the expression of molecules in the PI3K/Akt/eNOS signaling pathway, including Akt, eNOS and internal reference glyceraldehyde-3-phosphate dehydrogenase (GAPDH). Later, the total RNA extracted through TRIzol method in each group was reversely transcribed into complementary deoxyribose nucleic acid (cDNA), which was examined by RT-qPCR under the following conditions: 95°C for 5 min, (95°C for 35 s, 57°C for 45 s and 72°C for 40 s) ×45 cycles, and 72°C for 5 min. The primers are shown below: Akt: Forward: AGCGACGTGGCTATTGTGAAG, Reverse: GCCATCATTCTTGAGGAGGAAGT; eNOS: Forward: TCCTCCTCAAGAATGATGGCA, Reverse: GTGCGTTCGATGACAGTGGT; GAPDH: Forward: GTCATCGAACGCACCTTCCAT, Reverse: AGCTTCAGGTACTCAAACTCGT.

Detection of expressions of Akt, phosphorylated Akt (p-Akt), nitric oxide (NO) and Enos

The protein expressions of Akt and p-Akt in the 3 groups were measured through Western blotting assay, and the content of NO and eNOS was detected using enzyme-linked immunosorbent assay in strict accordance with the kit instructions. The spinal cord tissues in the three groups were lysed by protein lysate containing PMSF for 30 min and then centrifuged at 14,000 rpm for 15 min. Subsequently, the protein was subjected to electrophoresis, transferred onto membrane, incubated with primary antibodies and secondary antibodies and exposed. After that, the protein expression levels of Akt and p-Akt were detected by comparing with that of GAPDH.

Statistical analysis

Statistical Product and Service Solutions (SPSS) 22.0 software (IBM, Armonk, NY, USA) was utilized for statistical analysis. Differences between two groups were analyzed by using the Student's *t*-test. Comparison between multiple groups was made using One-way ANOVA test followed by Post Hoc Test (Least Significant Difference). P<0.05 suggested that the difference was statistically significant.

RESULTS

Changes of critical angle in slope test and BBB scores in control group, SCI group and liraglutide group

The BBB scores in three groups before operation and at 1, 3, 7, 21 and 28 d after operation are shown in Table I. There were significant differences in the BBB score of rats between the SCI group and control group at 7, 21 and 28 d after operation (P<0.05) and between the liraglutide group and SCI group at 21 and 28 d after operation (P<0.05). Based on the changes of critical angle in slope test before and after operation in the three groups (Table I), the changes of critical angle in the slope test were different between the SCI group and control group at 21 and 28 d after operation (P<0.05) and between the liraglutide group and SCI group at 7, 21 and 28 d after operation (P<0.05).

Gene expression profiles in control group, SCI group and liraglutide group

The gene expression profiles in the 3 groups are

displayed in Fig. 1. Prominent differences in the gene expression patterns in spinal cord tissues were observed among the three groups, and the difference in the expression of a part of genes was greater between the liraglutide group and control group as well as the SCI group. Those genes were clustered into one group, including the key genes of the PI3K/Akt/eNOS signaling pathway (Akt and eNOS).

Enrichment analysis results of differential genes in the 3 groups

According to the GO enrichment analysis (Fig. 2) and KEGG enrichment analysis (Fig. 3) of differential genes in the 3 groups, the differential genes in all three groups were mainly enriched in the PI3K-related signaling pathway, phosphorylated pathway, mammalian target of rapamycin (mTOR) signaling pathway, vascular endothelial growth factor (VEGF) signaling pathway, T-cell receptor signaling pathway and ErbB signaling pathway, suggesting that the critical molecules in these pathways may participate in the repair process of SCI stimulated by liraglutide.

Expressions of Akt, p-Akt, NO and eNOS in control group, SCI group and liraglutide group

mRNA expression levels of Akt and eNOS in the 3 groups (Fig. 4A) declined remarkably in the SCI group compared with those in the control group ($P<0.05$), while they rose notably in the liraglutide group in comparison with those in the SCI group ($P<0.05$). In terms of the changes in mRNA expression levels of Akt and p-Akt in the 3 groups (Fig. 4B), the protein expression of p-Akt was decreased obviously in the SCI group in contrast with that in the control group, but the protein expressions of Akt and p-Akt were increased markedly in the liraglutide group compared with those in the SCI

Table I. *Changes of critical angle (°) in slope test before and after operation in control group, spinal cord injury group and liraglutide group*

Index	Groups	Before	1 d	3 d	7 d	21 d	28 d
Critical angle (°)	Control	61.23±1.84	32.12±2.14	36.86±3.65	37.84±4.57	40.01±4.74	46.38±3.15
	SCI	61.08±1.29	33.84±3.14	36.46±3.92	37.32±4.17	38.54±4.02[a]	39.42±5.45[a]
	Liraglutide	60.94±1.33	32.74±3.15	36.35±4.14	40.24±4.21[b]	45.29±4.12[b]	54.22±4.98[b]
BBB scores	Control	21	2.14±0.34	3.25±0.67	5.21±1.35	8.74±2.14	10.25±2.41
	SCI	21	2.25±0.24	3.14±0.48	4.74±1.87[a]	6.64±2.28[a]	7.31±2.11[a]
	Liraglutide	21	2.13±0.27	3.15±0.98	4.98±1.74	7.01±1.74[b]	12.87±3.21[b]

[a]P<0.05 vs control group, and [b]P<0.05 vs spinal cord injury group, t-test.

Table II. *Changes in content of NO and eNOS in control group, SCI group and liraglutide group*

Group	NO	eNOS
Control group	87.23±11.24	3.21±0.74
SCI group	45.21±4.21[a]	1.18±0.79[a]
Liraglutide group	165.35±8.48[b]	11.47±1.24[b]

[a]P<0.05 vs control group, and [b]P<0.05 vs SCI group, t-test

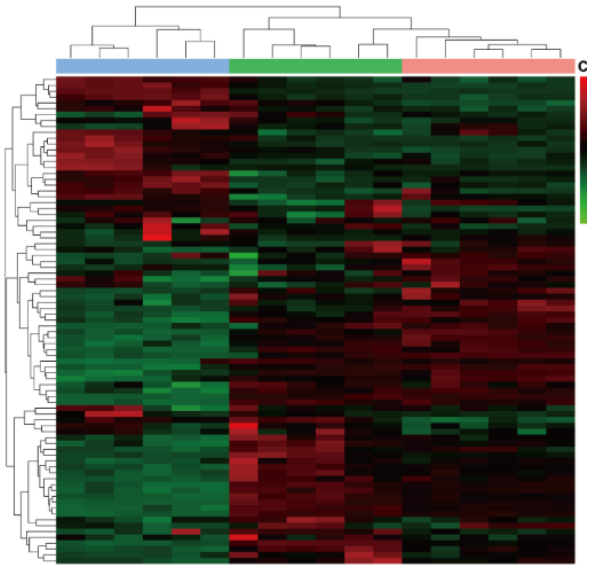


Fig. 1. *Gene expression profiles in spinal cord tissues in control group, SCI group and liraglutide group.*

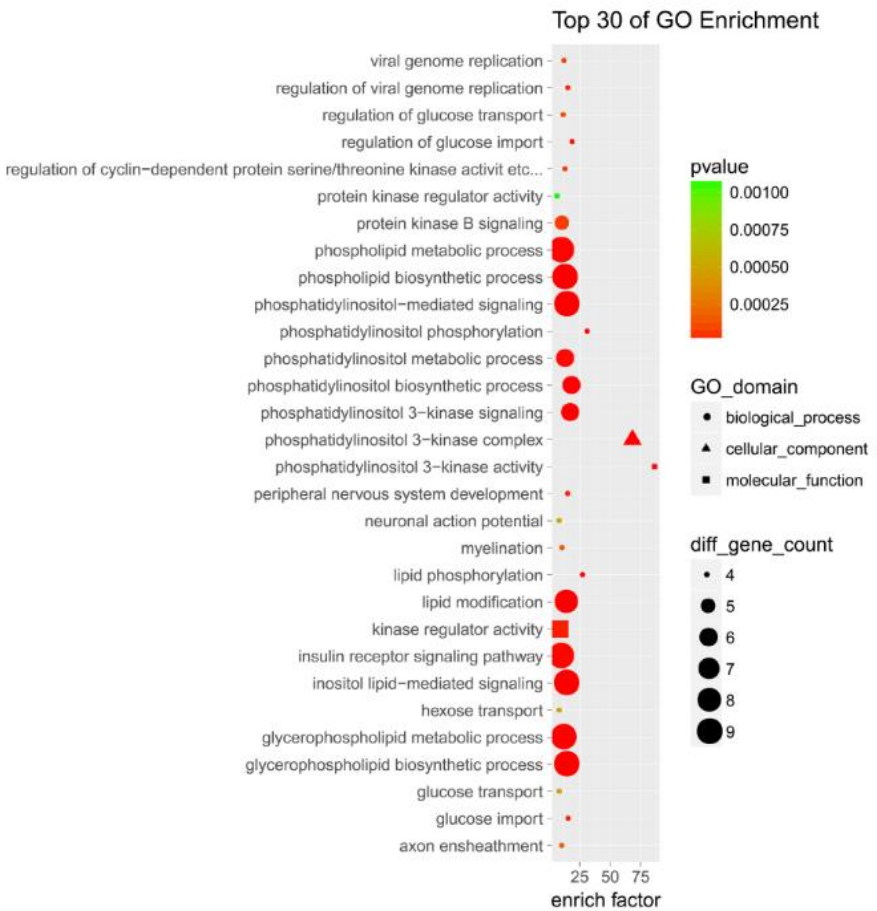


Fig. 2. *GO enrichment analysis of differential genes in control group, SCI group and liraglutide group*

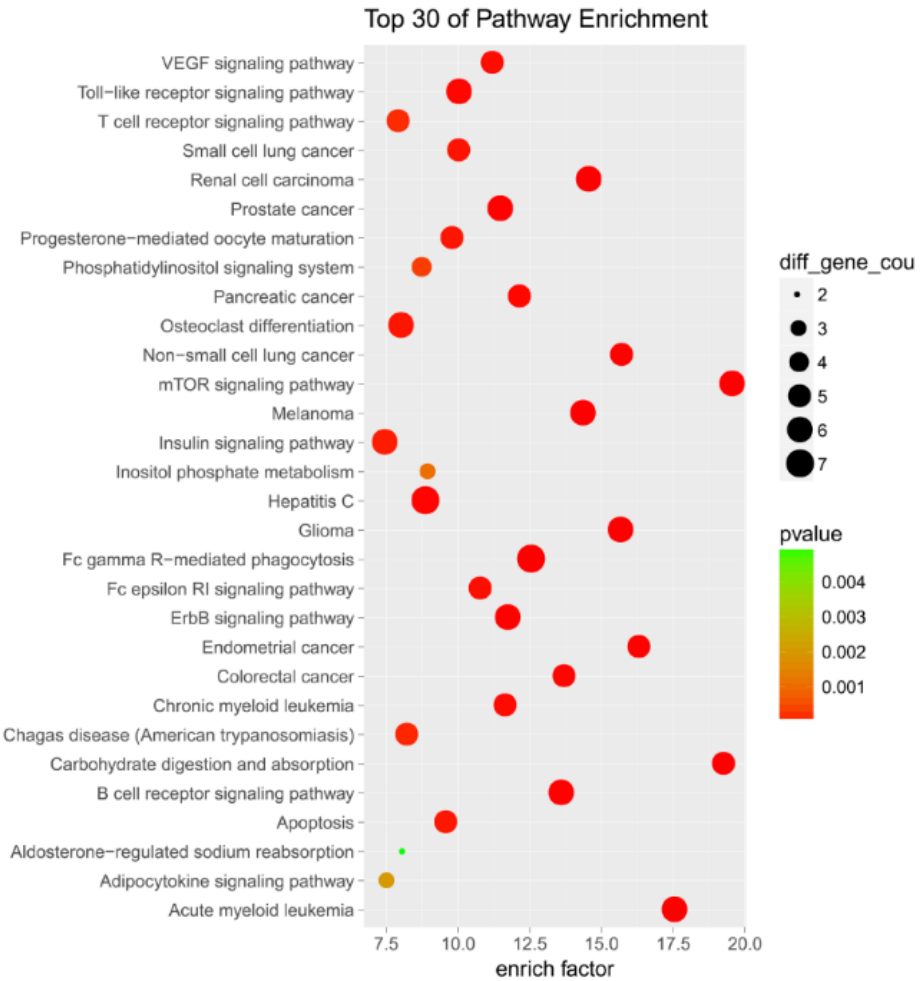


Fig. 3. *KEGG enrichment analysis of differential genes in control group, SCI group and liraglutide group.*

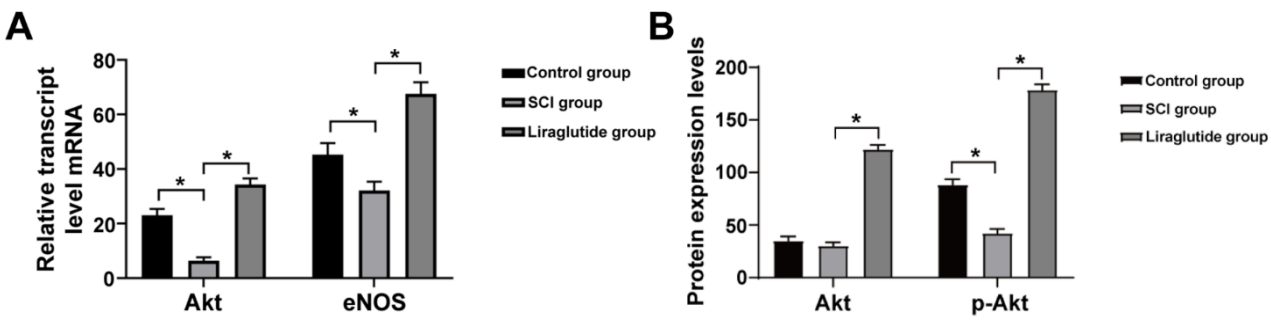


Fig. 4. *Akt and eNOS declined remarkably in SCI group. **A**) mRNA expression levels of Akt and eNOS in control group, SCI group and liraglutide group; **B**) Protein expression levels of Akt and p-Akt in control group, SCI group and liraglutide group (*P<0.05)*

group. The changes in the content of NO and eNOS in the control group, SCI group and liraglutide group are shown in Table II. The content of NO and eNOS was distinctly lower in the SCI group than that in the control group ($P<0.05$), while it was evidently higher in the liraglutide group than that in the SCI group ($P<0.05$).

DISCUSSION

Liraglutide is primarily utilized to treat diabetes mellitus, but it has been reported that liraglutide plays a role in the treatment of other diseases, including hepatitis C virus, osteoporosis and coronary microvascular dysfunction (11,12). In this research, 18 adult SD rats were divided into control group, SCI group and liraglutide group, the rat model of SCI was established and treated by liraglutide, and the changes in motor nerve function were assessed. It was found that the BBB score of rats was significantly different between the SCI group and control group at 7, 21 and 28 d after operation ($P<0.05$) and between the liraglutide group and SCI group at 21 and 28 d after operation ($P<0.05$). As for the changes of critical angle in the slope test, there were differences between the SCI group and control group at 21 and 28 d after operation ($P<0.05$) and between the liraglutide group and SCI group at 7, 21 and 28 d after operation ($P<0.05$). All these results suggest that liraglutide probably has crucial efficacy in repairing SCI, but its specific mechanism has not yet been clarified.

Furthermore, the mechanism of liraglutide in treating SCI was analyzed. The results manifested that the gene expression patterns in spinal cord tissues were prominently different among the control group, SCI group and liraglutide group, and there was a significant difference in the expression of some genes between the liraglutide group and control group as well as SCI group. Among them, the key genes of the PI3K/Akt/eNOS signaling pathway, such as Akt and eNOS, were clustered into one group. In addition, the differential genes in the three groups were mainly enriched in the PI3K-related signaling pathway, phosphorylated pathway, mTOR signaling pathway, VEGF signaling pathway, T-cell receptor signaling pathway and ErbB signaling pathway, implying that the critical molecules in these pathways are probably involved in repairing SCI by liraglutide. The above results illustrate that the treatment of SCI with liraglutide may be realized by influencing the conduction of some signaling pathways in cells, thereby intervening in the expression of critical genes, repressing cell apoptosis and reducing local immuno-inflammatory responses.

Finally, the expression changes in the PI3K/Akt/eNOS signaling pathway during the treatment of SCI with liraglutide were determined in this research to preliminarily explore the action mechanism of the drug. It was found that the mRNA expression levels of Akt and eNOS were clearly lower in the SCI group than those in the control group ($P<0.05$), while they were evidently higher in liraglutide group than those in SCI group ($P<0.05$). Moreover, the SCI group exhibited remarkably lower protein expression of p-Akt than the control group, but the liraglutide group had notably higher protein expressions of Akt and p-Akt than the SCI group. The content of NO and eNOS was distinctly lowered in the SCI group compared to the control group ($P<0.05$), while it was raised in the liraglutide group compared with that in the SCI group ($P<0.05$). In summary, all the above findings suggest that liraglutide has a repairing effect on SCI in rats by modulating intra-cellular signal transduction, which may be related to the PI3K/Akt/eNOS signaling pathway.

REFERENCES

1. Franz S, Kirshblum SC, Weidner N, Rupp R, Schuld C. Motor levels in high cervical spinal cord injuries: Implications for the International Standards for Neurological Classification of Spinal Cord Injury. J Spinal Cord Med 2016; 39:513-17.
2. Barbara-Bataller E, Mendez-Suarez JL, Aleman-Sanchez C, Sanchez-Enriquez J, Sosa-Henriquez M. Change in the profile of traumatic spinal cord injury over 15 years in Spain. Scand J Trauma Resusc Emerg Med 2018; 26:27.
3. Roach MJ, Chen Y, Kelly ML. Comparing blunt and penetrating trauma in spinal cord injury: analysis of long-term functional and neurological outcomes. Top Spinal Cord Inj Rehabil 2018; 24:121-32.

4. Ding H, Yu J, Chang W, Liu F, He Z. Searching for differentially expressed proteins in spinal cord injury based on the proteomics analysis. Life Sci 2020; 242:117235.
5. Chang FH, Liu CH, Hung HP. An in-depth understanding of the impact of the environment on participation among people with spinal cord injury. Disabil Rehabil 2018; 40:2192-99.
6. Yue JK, Hemmerle DD, Winkler EA, et al. Clinical implementation of novel spinal cord perfusion pressure protocol in acute traumatic spinal cord injury at U.S. level I trauma center: TRACK-SCI Study. World Neurosurg 2020; 133:e391-e396.
7. Halvorsen A, Pettersen AL, Nilsen SM, Halle KK, Schaanning EE, Rekand T. Epidemiology of traumatic spinal cord injury in Norway in 2012-2016: a registry-based cross-sectional study. Spinal Cord 2019; 57:331-38.
8. Zborowski J, Corazzi L, Arienti G. Regulation of liver base-exchange activity by acidic phospholipids. Biosci Rep 1991; 11:231-36.
9. Zhou JY, Poudel A, Welchko R, et al. Liraglutide improves insulin sensitivity in high fat diet induced diabetic mice through multiple pathways. Eur J Pharmacol 2019; 861:172594.
10. Tsai TH, Lee CH, Cheng CI, et al. Liraglutide inhibits endothelial-to-mesenchymal transition and attenuates neointima formation after endovascular injury in streptozotocin-induced diabetic mice. Cells-Basel 2019; 8
11. Yang L, Yang J, Pan T, Zhong X. Liraglutide increases bone formation and inhibits bone resorption in rats with glucocorticoid-induced osteoporosis. J Endocrinol Invest 2019; 42:1125-31.
12. Suhrs HE, Raft KF, Bove K, et al. Effect of liraglutide on body weight and microvascular function in non-diabetic overweight women with coronary microvascular dysfunction. Int J Cardiol 2019; 283:28-34.

LETTER TO THE EDITOR

Expression of ERR-α in ovarian cancer and endometrial carcinoma and its significance

Y. Tai, J. Li, XH. Zhang, JF. Fu and J. Wang

Department of Obstetrics and Gynecology, Xijing Hospital Affiliated to the Air Force Military Medical University, Xian City, Shaanxi, China

Received June 2, 2020 – Accepted October 16, 2020

To the Editor,

The incidence of gynecological cancer has significantly increased in recent years. The occurrence of endometrial cancer is closely associated with classical estrogen and its receptor (1). There are different causes of ovarian cancer, most of which are closely related to abnormal estrogen levels in the body (2). Estrogen exerts its biological activity through estrogen receptor (ER) (3). Estrogen binds to ER, ER responds to SRC proteins through allosteric effects, and the response of co-activating molecules to the receptor can be antagonized by anti-estrogen therapy (4). Therefore, anti-estrogen drugs play a significant role in the treatment of gynecological cancer.

Estrogen-related receptors (ERRs) are composed of ERR-α, ERR-β, and ERR-γ. ERR-β is expressed in cells forming chorionic villi at embryonic stage, and it can also be detected in the digestive, cardiovascular and urinary systems after birth (5). However, ERR-α shares high homology with ER in DNA binding regions, thus, it is feasible to regulate signaling pathways that overlap with ER and participate in the development of gynecological cancer (6). The present study aimed to analyze expression of ERR-α in ovarian cancer, and endometrial cancer tissues as well as the correlation between ERR-α and clinicopathological features, and provide a theoretical experimental basis for pathogenesis and early diagnosis of gynecological cancer.

MATERIALS AND METHODS

Patients

Thirty patients with endometrial cancer who were admitted to Xijing Hospital Affiliated to the Air Force Military Medical University from February 2018 to June 2019, 30 healthy controls underwent hysteroscopy and 30 patients with endometrial carcinoma were enrolled in the study. The patients had received no radiotherapy, chemotherapy, or hormone therapy preoperatively. The study was approved by the Ethics Committee of Xijing Hospital Affiliated to the Air Force Military Medical University, and all the subjects signed the written informed consent form prior to commencing the study.

Specimen collection

Thirty cases of endometrial cancer tissue specimens and thirty cases of normal endometrial tissues of healthy patients who underwent hysteroscopy were resected. Moreover, 30 specimens of ovarian cancer and adjacent tissues (more than 5 cm from the edge of cancer) confirmed by pathology were resected. Some of the fresh specimens were stored at -8°C for extraction of RNA and protein, and others were fixed in 4% paraformaldehyde (Shanghai Xinyu Biological Technology Co., Ltd., China).

Immunohistochemistry

Expression and distribution of ERR-α in human ovarian cancer, endometrial cancer tissues and corresponding

Key words: estrogen-related receptor-α; ovarian cancer; endometrial cancer; targeted therapy

Corresponding Author:
Jian Wang,
Department of Obstetrics and Gynecology, Xijing Hospital Affiliated to the Air Force Military Medical University,
No. 127 Changle Road,
New City Zone, Xian City, 710032, Shaanxi, China
e-mail: wangjianxijingmed@163.com

0393-974X (2020)
Copyright © by BIOLIFE, s.a.s.
This publication and/or article is for individual use only and may not be further reproduced without written permission from the copyright holder.
Unauthorized reproduction may result in financial and other penalties
DISCLOSURE: ALL AUTHORS REPORT NO CONFLICTS OF INTEREST RELEVANT TO THIS ARTICLE.

normal tissues were detected and localized. The collected specimens were partially fixed with 4% paraformaldehyde for 72 h, and they were embedded into paraffin and cut into slices with a thickness of about 8 μm. Immunohistochemistry (IHC) was carried out. The paraffin section was dewaxed and underwent gradient ethanol hydration, then was incubated with 3% hydrogen peroxide deionized water (Anhui Zhonghong Biological Engineering Co., Ltd., China) for 20 min at room temperature, and endogenous peroxidase activity was blocked, followed by phosphate-buffered saline (PBS) rinsing. The sections were immersed in citrate buffer (pH=6) and heated for 10 min in a microwave oven (Panasonic, Japan) and then cooled to room temperature. The sections were washed three times with PBS (each time for 3 min). Primary antibody (rabbit anti-human ERR-α monoclonal antibody; Abcam, Cambridge, UK) was diluted with PBS solution to 1:500, incubated at 4°C overnight, and washed three times with PBS (each time for 3 min). Secondary antibody (anti-rabbit IgG; Jackson ImmunoResearch Laboratories, Inc., West Grove, PA, USA) was added and incubated at room temperature for 30 min, and then was washed three times with PBS (each time for 3 min). The sections were stained with diaminobenzidine (DAB) Chromogenic Reagent kit (Shanghai Xinyu Biological Technology Co., Ltd., China) for 5 min and washed with distilled water; afterwards, hematoxylin (Shanghai Guchen Biological Co., Ltd., China) was used to re-dye, and the sections were dehydrated and sealed.

The cytoplasm, cell membrane, and nucleus were observed under a light microscope (Leica, Germany) to check whether there were clear orange or brown particles. The cells with particles were positive cells. Five typical fields were randomly selected under a low-power lens, and 100 cells were counted under a high-power lens (×400). The average percentage of positive cells in the five high-power fields was calculated. The percentage of positive cells was the average of the percentage of positive cells in five random fields under the high-power lens (×400).

Reverse transcription polymerase chain reaction (RT-PCR)

Total RNA was extracted from tissue samples, and tissues were maintained at -80°C. RT-PCR was carried out according to the manufacturer's instructions (Fermentas K1622; Thermo Fisher Scientific, USA); reverse transcription conditions were as follows: at 37°C for 15 min, and at 85°C for 5 s. Product of reverse transcription cDNA was stored at -80°C. Premier Primer5 software was used to design primers as shown Table I.

PCR reaction system: 10×buffer 2.5 uL, dNTP 2 uL, Taq 0.3 uL, MgCl 1.5 uL, primer 1uL, cDNA 2 uL, sterilized water 14.7 uL. PCR reaction conditions were as follows: pre-denaturation at 95°C for 4 min; denaturation at 95°C for 30; annealing at 53°C for 30 s; amplification with 35 cycles at 72°C for 7 min. Electrophoretic analysis of the PCR products 1 and 2 was performed at 100 V for 40 min.

Western blot assay

For Western blotting, 50 mg tissues were used to extract total protein by tissue lysate. Bicinchoninic acid (BCA) assay was utilized for determination of the protein concentration; 5% concentrated glue and 8% separation glue were prepared, and 200 ug protein sample buffer was added into 100°C boiling water for 5 min, and quickly put in ice to cool. Proteins were transferred onto polyvinylidene fluoride (PVDF) membranes after undergoing sodium dodecyl sulfate-polyacrylamide gel electrophoresis (SDS-PAGE), and the membranes were

Table I. *Primer sequence*

Primer		Sequence	Fragment size
ERRα	Upstream	5-TCGCTGTCTGACCAGATGTC-3	502bp
	Downstream	5-CCTCGAGCATCTCCAAGAAC-3	
β-actin	Upstream	5-ATGGATGATGATATCGCCGCG-3	249bp
	Downstream	5-CTCCATGTCGTCCCAGTTGGT-3	

added into an antibody (1:1000) and kept overnight at 4℃. The secondary antibody (1:2000) was added after washing the membranes with Tris-Buffered Saline +Tween (TBST).

Statistical analysis

SPSS 19.0 software (IBM, USA) was used for statistical analysis. The data were expressed as mean ± standard deviation ($\bar{x}\pm s$), and tested with Student's *t*-test. $P<0.05$ was considered statistically significant.

RESULTS

IHC

The expression level of ERR-α was detected by IHC. It was found that ERR-α was localized in the nucleus and cytoplasm of cells (Fig. 1), and the expression level of ERR-α protein in cancer tissues was significantly higher than that in corresponding normal tissues ($P<0.05$).

RT-PCR

RT-PCR results showed that the mRNA level of ERR-α in cancer tissues was significantly higher than that in corresponding normal tissues ($P<0.05$) (Fig. 2).

Western blot assay

Results of Western blotting revealed that the expression of ERRα protein in ovarian cancer and endometrial carcinoma was higher than that in the

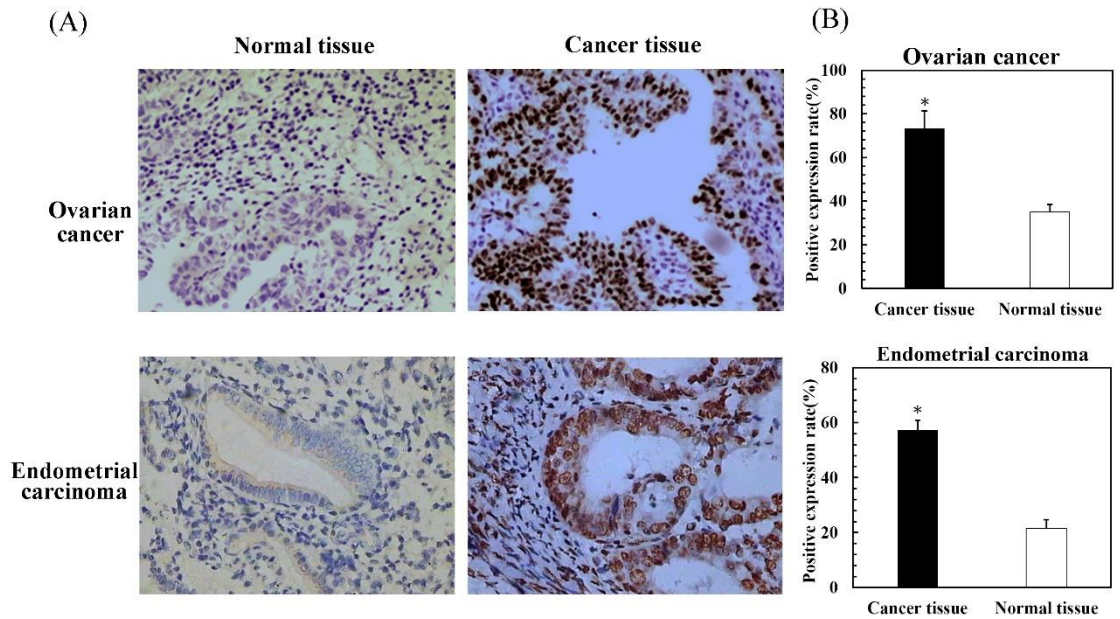


Fig. 1. *IHC for detecting ERR-α expression. **A)** IHC results, 400×; **B)** Positive expression rates in cancer tissues and normal tissues *P<0.05.*

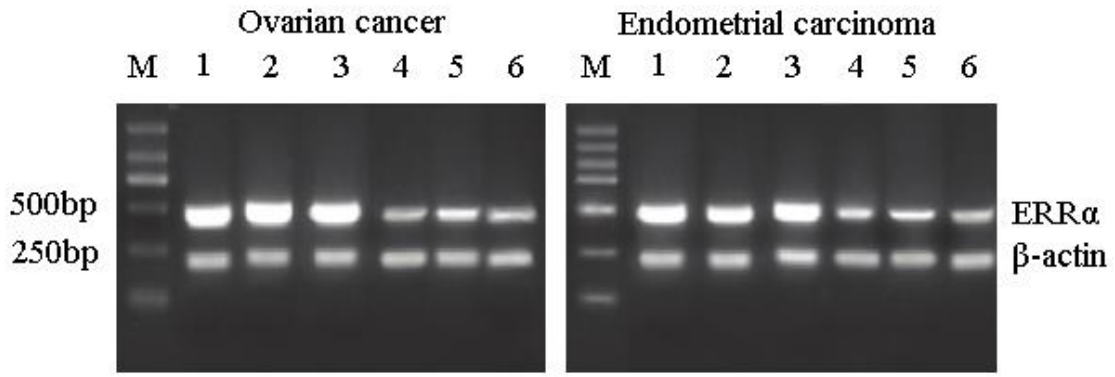


Fig. 2. *mRNA levels of ERR-α detected by RT-PCR; M: DNA marker-□; 1, 2, 3: cancer tissues; 4, 6, 6: normal tissues.*

Table II. *Expression of ERR-α protein in ovarian cancer tissues and its correlation with clinico-pathological features of patients with ovarian cancer.*

Clinical data		Endometrial cancer		Ovarian cancer	
		ERR-α protein expression	P	ERR-α protein expression	P
Age (year)	≤40	0.38±0.08	0.28	0.41±0.10	0.65
	>40	0.35±0.12		0.42±0.10	
Degree of differentiation	Medium and high differentiation	0.30±0.09	0.03	0.31±0.06	0.01
	Low differentiation	0.38±0.12		0.46±0.11	
Lymphatic metastasis	+	0.32±0.12	0.02	0.48±0.09	0.02
	-	0.33±0.10		0.39±0.11	
Clinical stages	I stage	0.22±0.13	0.02	0.34±0.09	0.01
	II ~ IV stages	0.39±0.16		0.45±0.11	
ER	+	0.21±0.04	0.01	0.30±0.07	0.01
	-	0.39±0.05		0.52±0.12	
PR	+	0.37±0.08	0.87	0.42±0.09	0.58
	-	0.39±0.09		0.43±0.11	
P53	+	0.30±0.12	0.38	0.46±0.09	0.18
	-	0.37±0.08		0.42±0.11	

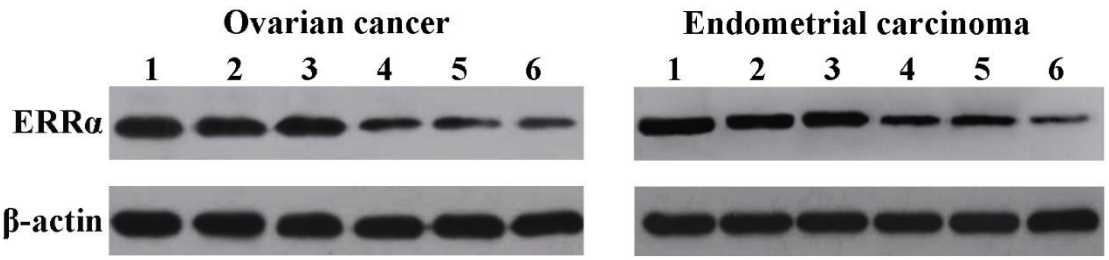


Fig. 3. *Expression of ERR-α protein detected by Western blotting. 1, 2, 3: cancer tissues; 4, 5, 6: normal tissues.*

corresponding normal tissues, and the difference was statistically significant (Fig. 3). It was also revealed that Western blotting results were compatible with those achieved by RT-PCR.

Relationship between ERR-α protein expression and clinico-pathological features

The expression of ERR-α protein in ovarian cancer tissues was negatively correlated with tumor differentiation, lymph node metastasis, clinical stage, and ER ($P<0.05$), while no significant relationship was found with age, PR, and P53 expression ($P>0.05$) (Table II).

DISCUSSION

Several studies have shown that the expression of ER-α can be used as an indicator to assess the prognosis of endometrial cancer(7, 8). The prognosis of ERR-α-positive patients is significantly better than that of ERR-α-negative patients (9). Gao et al. and Kokabu et al. also showed that ERR-α is an

effective predictor of gynecological cancer (10, 11).

It was disclosed that the expression of ERR-α was positively correlated with the tumor differentiation, clinical stage, and lymph node metastasis, and negatively correlated with ER, while no significant correlation was noted with the age, PR, and P53 expression. It is surmised that ERRα could promote the occurrence and development of tumors in various ways, therefore, may be an indicator of poor prognosis of ovarian cancer and endometrial cancer. If ERRα is combined with ER as an indicator to judge the prognosis of ovarian cancer and endometrial cancer, its predictive value will be significantly improved. Sun et al. detected the expression of ERR subtypes in ovarian cancer tissues and normal ovarian tissues and analyzed its relationship with prognosis (12). Their study showed that the expression of ERRα mRNA in ovarian cancer tissues was higher than that in normal ovarian tissues, and the high expression of ERRα was associated with poor prognosis of ovarian cancer, which was consistent with our results. However, ER has some limitations for assessment of the prognosis of patients with ovarian cancer and endometrial cancer.

REFERENCES

1. Pandey V, Zhang M, Chong QY, et al. Hypomethylation associated enhanced transcription of trefoil factor-3 mediates tamoxifen-stimulated oncogenicity of ER+ endometrial carcinoma cells. Oncotarget 2017; 8(44):77268-91.
2. Fujimoto J, Alam SM, Jahan I, Sato E, Sakaguchi H, Tamaya T. Clinical implication of estrogen-related receptor (ERR) expression in ovarian cancers. J Steroid Biochem Mol Biol 2007; 104(1):301-304.
3. Ranhotra HS. Estrogen-related receptor alpha and mitochondria: tale of the titans. J Recept Signal Transduct Res 2015; 35(5):386-90.
4. Wang CW, Hsu WH, Tai CJ. Antimetastatic effects of cordycepin mediated by the inhibition of mitochondrial activity and estrogen-related receptor α in human ovarian carcinoma cells. Oncotarget 2017; 8(2):3049-58.
5. Tanida T, Matsuda KI, Yamada S, Hashimoto T, Kawata M. Estrogen-related receptor β Reduces the subnuclear mobility of estrogen receptor α and suppresses estrogen-dependent cellular function. J Biol Chem 2015, 290(19):12332-45.
6. Yamamoto T, Mori T, Sawada M, et al. Estrogen-related receptor-γ regulates estrogen receptor-α responsiveness in uterine endometrial cancer. Int J Gynecol Cancer 2012; 22(9):1509-16.
7. Hou X, Zhao M, Wang T, Zhang G. Upregulation of estrogen receptor mediates migration, invasion and proliferation of endometrial carcinoma cells by regulating the PI3K/AKT/mTOR pathway. Oncol Rep 2014; 31(3):1175-82.
8. Cincin ZB, Kiran B, Baran Y, Cakmakoglu B. Hesperidin promotes programmed cell death by downregulation of nongenomic estrogen receptor signalling pathway in endometrial cancer cells. Biomed Pharmacother 2018; 103:336-45.
9. Vincent B, Douglas GA, Frances C, MacPherson S, Critchley HOD, Saunders PTK. A role for the orphan nuclear receptor estrogen-related receptor α in endometrial stromal cell decidualization and expression of genes implicated in energy metabolism. J Clin Endocrinol Metab 2010; 95(10):E224-28.
10. Gao M, Wei LH, Sun PM, Wang JL, Zhao D, Zhao C, Wang ZQ. Regulation of orphan receptor ERR alpha by estrogen and progesterone in endometrial carcinoma cell line. Beijing Da Xue Xue Bao Yi Xue Ban 2005; 37(3):281-83.
11. Kokabu T, Mori T, Matsushima H, Yoriki K, Kataoka H, Tarumi Y, Kitawaki J. Antitumor effect of XCT790, an ERRα inverse agonist, on ERα-negative endometrial cancer cells. Cell Oncol (Dordr) 2019; 42(2):223-35.
12. Sun P, Sehouli J, Denkert C, et al. Expression of estrogen receptor-related receptors, a subfamily of orphan nuclear receptors, as new tumor biomarkers in ovarian cancer cells. J Mol Med (Berl) 2005; 83(6):457-67.

LETTER TO THE EDITOR

Comparison of effects of chloroprocaine and lidocaine epidural block on emergency response of gynecologic patients after pelvic surgery

LL. Wang[1,2,3], X. Li[4], HT. Tian[1,2,3], Y. Sun[1,2,3] and C. Sun[5]

[1]Department of Anesthesiology, Jining No.1 People's Hospital, Jining, China; [2]Department of Anesthesiology, Affiliated Jining No.1 People's Hospital of Jining Medical University, Jining, China; [3]Jining Medical University, Jining, China; [4]Department of Obstetrics and Gynecology, Zhangqiu District Maternal and Child Health Care Hospital, Jinan, China; [5]Department of Anesthesiology, Maternity and Child Health Care of Zaozhuang, Zaozhuang, China

Received May 22, 2020 – Accepted October 19, 2020

To the Editor,

The increasing economic level in China, as well a good medical and health service system have raised the health awareness of women (1). However, gynecopathy is still a problem plaguing many women. A domestic study reported that among 511 female employees who received gynecological examination in Changchun, the prevalence rates of bacterial vaginosis and cervicitis were 5.3% and 22.1% respectively (2). In the United States, about 800,000 women are diagnosed with pelvic inflammation every year (3). One report pointed out that 7 years after the diagnosis of pelvic inflammatory disease, 21.3% of women relapsed, 19% suffered from infertility, and 42.7% reported chronic pelvic pain (4). Gynecological diseases still contribute to an unfavorable factor threatening women's health, and early diagnosis, prevention and treatment are essential.

Surgery is an effective method for clinical treatment of various pelvic diseases. Lidocaine is a commonly used local anesthetic clinically to relieve pain after surgery, trauma or treatment (5). Lidocaine brings new risks and potential hazards while the use of epidural anesthesia is increasing. Lidocaine toxic symptoms usually occur after excessive or unintentional intravascular injection, and the latter is more common in the case of local anesthesia toxicity (6). Chloroprocaine has been approved by the U.S. Food and Drug Administration (FDA) for peripheral nerve block and epidural anesthesia due to its fast onset and short duration (7). This study aimed to explore the effects of chloroprocaine and lidocaine on anesthetic effect and postoperative emergency response.

MATERIAL AND METHODS

Study subjects

A total of 120 gynecologic patients who underwent pelvic surgery in Jining No.1 People's Hospital between February 2016 and March 2018 were included in the study. The 120 patients were divided into a chloroprocaine group (CA group) (n=60) and a lidocaine group (LA group) (n=60). Epidural anesthesia was performed in both groups, and patients in the CA group were given chloroprocaine and those in the LA group were given lidocaine. This study was approved by the Medical Ethics Committee of Jining NO.1 People's Hospital. All patients enrolled in this study gave written informed consent after a detailed explanation.

Key words: anesthetic effect; chloroprocaine; emergency response; epidural block; lidocaine

Corresponding Author:
Dr Chao Sun,
Department of Anesthesiology,
Maternity and Child Health Care
of Zaozhuang, Xuecheng District,
Zaozhuang 277100, China
e-mail: bho6yo@126.com

0393-974X (2020)
Copyright © by BIOLIFE, s.a.s.
This publication and/or article is for individual use only and may not be further reproduced without written permission from the copyright holder.
Unauthorized reproduction may result in financial and other penalties
DISCLOSURE: ALL AUTHORS REPORT NO CONFLICTS OF INTEREST RELEVANT TO THIS ARTICLE.

Inclusion criteria were ASA classification ≤ grade II; no obvious cognitive dysfunction. Exclusion criteria were: age < 20 or > 55; insufficient heart, liver, or lung function; infection; insufficient blood coagulation function; those who cannot finish the test independently; those with poor compliance.

Anesthesia methods

Patients in the two groups were given intramuscular injection of 0.5 mL atropine (Suicheng Pharmaceutical Co., Ltd., H41021257) 30 min before entering the operating room to establish venous access. Multifunctional monitors (Beijing Haifuda Technology Co., Ltd., M312773) were used for heart rate, blood pressure and respiratory frequency. Epidural space puncture (lateral approach) was performed at the position of the 1st and 2nd lumbar vertebrae of the patients, followed by catheterization (length of 3-4cm). After catheterization, the CA group was given 3% chloroprocaine hydrochloride immediately (Jincheng Hayes Pharmaceutical Co., Ltd., SFDA Approval No. : H20020079), and the LA group was given 2% lidocaine hydrochloride (Shandong Hualu Pharmaceutical Co., Ltd, SFDA Approval No. : H37022147). The test dose of patients in the two groups was 5 mL, no adverse reactions or signs of spinal anesthesia were confirmed, and the additional dose of 10 mL was administered after 5 min.

Sample collection and detection

Thirty minutes after surgery, 3 ml of venous blood was drawn from patients in the two groups, heparin solution was added to prepare plasma, and then the contents of adrenaline and norepinephrine in plasma were determined by ELISA method (adrenaline/norepinephrine ELISA detection kit, IBL company of Germany, Art. No. : RE59242).

In brief, the 96-well plate coated with the corresponding antibodies was taken, added with the standard solution or sample solution, and affixed with the sealing membrane, followed by incubation at 37°C for 90 min. After the liquid in the plate was patted dry, the biotin-labeled antibody was added, and the plate was sealed with the sealing membrane, followed by incubation at 37°C for 60 min. After the plate was washed with washing solution for 4 times (3 min per time), ABC working solution was added, and the plate was sealed, followed by incubation at 37°C for 30 min. After the plate was washed again with washing solution for 4 times, TMB solution was added, and the plate was sealed, followed by incubation in a dark place at 37°C for 20 min. Then TMB stop buffer was added and mixed evenly. The absorbance (OD value) was measured by a microplate reader at 450 nm wavelength, and the corresponding concentration was converted from the standard curve.

Outcome measures

The changes of heart rate, respiratory frequency and arterial blood pressure of patients in the two groups 30 min before anesthesia, 30 min after anesthesia and at the end of surgery were observed and compared, and the contents of adrenaline and norepinephrine of patients in the two groups 30 min after operation were compared.

The anesthetic effect of patients in the two groups were compared. The cognitive function of patients in the two groups was compared by mini-mental state examination (MMSE) (11) score at 6 h, 12 h and 24 h after operation; patients with a score less than 27 showed cognitive dysfunction, and the lower the score was, the higher the degree of impairment was; the adverse reactions of both groups were compared.

Statistical analysis

In this study, data were processed using Statistical Product and Service Solutions (SPSS) 19.0 software (SPSS Inc., Chicago, IL, USA). Enumeration data were presented as mean ± standard deviation and *t*-test was used for comparison between two groups. *Chi*-squared test was used for the enumeration data. $p<0.05$ suggested that the difference was statistically significant.

RESULTS

There was no statistical difference in age, BMI, ASA classification, smoking history, exercise habits, place of residence, marital status and diet preference between the CA group and LA group ($P>0.05$, Table I).

Before anesthesia, 30 min after anesthesia and at the end of surgery, there was no significant difference in heart rate or respiratory frequency between the CA group and LA group ($P>0.05$, Table II). There was no difference in arterial blood pressure between the CA group and LA group before anesthesia and at the end of surgery ($P>0.05$). Arterial blood pressure in the LA group was lower than that in the CA group 30 min after anesthesia ($P<0.05$, Table II).

By detecting the plasma adrenaline and norepinephrine contents in the two groups 30 min before surgery, it was found that there was no statistical difference in the plasma adrenaline and norepinephrine

Table I. *Comparison of general clinical data of patients in the two groups*

Group	CA group (n=60)	LA group (n=60)	t/χ^2 value	P value
Age	36.6±7.2	37.1±6.8	0.391	0.697
BMI (kg/m^2)	21.8±1.6	22.1±1.2	1.162	0.248
ASA classification				
Grade I	38 (63.33)	41 (68.33)	0.333	0.564
Grade II	22 (36.67)	19 (31.67)		
Smoking history				
Yes	13 (21.67)	10 (16.67)	0.484	0.487
No	47 (78.33)	50 (83.33)		
Exercise habits				
Yes	28 (46.67)	31 (51.67)	0.300	0.584
No	32 (53.33)	29 (48.33)		
Place of residence				
Cities and towns	33 (55.00)	28 (46.67)	0.834	0.361
Countryside	27 (45.00)	32 (53.33)		
Marital status				
Married	44 (73.33)	47 (78.33)	0.409	0.522
Unmarried	16 (26.67)	13 (21.67)		
Diet preference				
Light	38 (63.33)	41 (68.33)	0.333	0.564
Spicy	22 (36.67)	19 (31.67)		

Table II. *Comparison of indicators between the two groups (times /min)*

	Group	Before anesthesia	30 min after anesthesia	At the end of the operation
heart rate (times/min)	CA group (n=60)	85.56±6.78	86.08±6.54	84.89±7.33
	LA group (n=60)	86.13±6.67	85.27±6.98	85.53±6.56
	t value	0.440	0.622	0.635
	p value	0.661	0.535	0.476
respiratory frequency (times/min)	CA group (n=60)	17.35±1.88	17.21±1.91	17.32±1.98
	LA group (n=60)	17.52±2.15	17.39±1.78	17.65±1.82
	t value	0.461	0.534	0.951
	p value	0.646	0.594	0.344
arterial blood pressure (KPa)	CA group (n=60)	124.3±10.7	116.5±11.4*	120.5±10.1
	LA group (n=60)	121.8±11.2	112.4±10.9*	118.6±11.5
	t value	1.250	2.014	0.962
	p value	0.214	0.046	0.338

Table III. *Comparison of MMSE scores of patients between the two groups*

Group	24 h before operation	6 h after operation	12 h after operation	24 h after operation
CA group (n=60)	29.48±0.46	24.34±1.33	28.21±2.12	29.35±1.03
LA group (n=60)	29.52±0.41	22.12±1.84	27.18±1.53	29.32±1.25
t value	0.503	7.574	3.052	0.144
p value	0.616	<0.001	0.003	0.886

Table IV. *Comparison of adverse reactions in perioperative period of patients between the two groups*

Group	Dizziness	Vomiting	Eclampsia	Tinnitus
CA group (n=60)	4 (6.67)	3 (5.00)	0 (0.00)	2 (3.33)
LA group (n=60)	5 (8.33)	5 (8.33)	1 (1.67)	11 (18.33)
t value	0.120	0.536	1.008	6.988
p value	0.729	0.464	0.315	0.008

contents of patients in the CA group [(86.25±14.55)μ/L] [(219.33±15.78)μ/L] and LA group [(89.54±13.86) μ/L] [(221.48±14.28)μ/L] (P>0.05), as shown in Fig. 1. The plasma adrenaline content in the CA group [(102.98±18.66)μ/L] 30 min after operation was lower than that in the LA group [(121.48±20.47)μ/L] ($p < 0.001$), and the plasma norepinephrine content in the CA group [(231.52±17.85)μ/L] was lower than that in the LA group [(265.28±19.62)μ/L] ($p < 0.001$), as shown in Fig. 2.

By comparing the anesthetic effects of patients in the two groups, it was found that the onset time of anesthesia (3.95±1.21 min), onset time of motor block (13.58±2.72 min) and duration time of motor block (77.58±13.42 min) in the CA group were shorter than those in the LA group (4.78±1.35 min, 18.24±3.59 min, 87.25±15.38 min, respectively) (P<0.001), and there was no statistical difference between the two groups (P>0.05).

By comparing the MMSE scores of patients in the two groups, it was found that there was no statistical difference between the MMSE scores of either group 24 h before surgery and 24 h post-surgery (P>0.05). The MMSE scores of patients in the CA group 6 h after the operation were higher than those in the LA group(P<0.001 and also 24 h post-surgery were higher (P=0.003, Table III).

By comparing the occurrence of adverse reactions between the two groups during the perioperative period, it was found that there was no statistical difference in the occurrence of dizziness, vomiting and eclampsia between the two groups (P>0.05), while the occurrence of tinnitus in the LA group was more than that in the CA group (P=0.008, Table IV).

DISCUSSION

Epidural anesthesia, which has been widely used in non-cardiac surgery, can improve analgesia and reduce the risk of complications, especially pulmonary

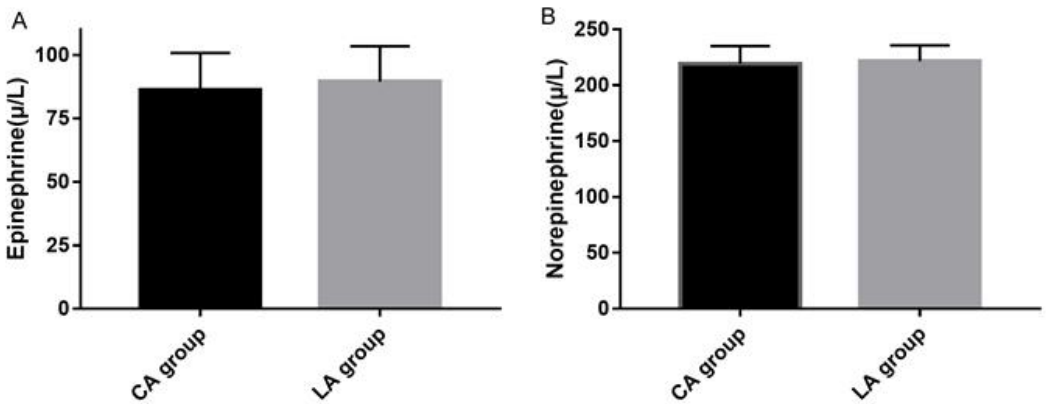


Fig. 1. *Comparison of plasma adrenaline and norepinephrine contents between the two groups 30 min before surgery.* ***A****) There was no statistical difference between the plasma adrenaline content in the CA group [(86.25±14.55)μ/L] and LA group [(89.54±13.86)μ/L].* ***B****) There was no statistical difference between the plasma norepinephrine content in the CA group [(219.33±15.78)μ/L] and LA group [(221.48±14.28)μ/L].*

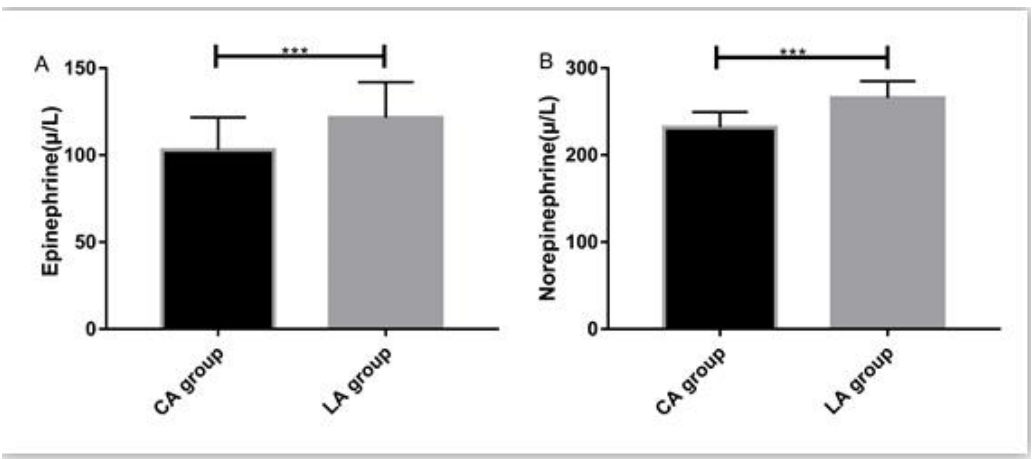


Fig. 2. *Comparison of plasma adrenaline and norepinephrine contents between the two groups 30 min after surgery.* ***A****) The plasma adrenaline content in the CA group [(102.98±18.66)μ/L] was lower than that in the LA group [(121.48±20.47) μ/L], and *** indicates p < 0.001.* ***B****) The plasma norepinephrine content in the CA group [(231.52±17.85)μ/L] was lower than that in the LA group [(265.28±19.62)μ/L]. *** indicates p < 0.001.*

(8). Studies have reported that epidural anesthesia is best for gynecological laparoscopic surgery patients to reduce stress response, improve coagulation function and hemorheology indexes, and maintain normal blood glucose levels (9, 10). This study applied chloroprocaine and lidocaine, respectively, to epidural anesthesia for gynecologic patients undergoing pelvic surgery, and compared the effects. The plasma levels of adrenaline and norepinephrine in the CA group were significantly lower than those in the LA group 30 min after surgery. Previous studies have shown that endogenous catecholamine is released in chronic stress: adrenal medulla and sympathetic nerve release norepinephrine, and adrenal medulla releases adrenaline (11). However, our research results also revealed that the plasma levels of adrenaline and norepinephrine increased after surgery, indicating that the body had been stimulated to a certain extent.

Lidocaine can reduce surgical pressure, postoperative pain and adverse cardiovascular reactions (12). By comparing the MMSE scores of patients in the two groups, we found that there was

no statistical difference between the MMSE scores 24 h before and 24 h after surgery, and the MMSE scores of the CA group were significantly higher than those of the LA group 6 h and 24 h post-surgery. The results showed that chloroprocaine had a lower effect on postoperative cognitive function and higher patient satisfaction. Our data found that there was no statistical difference in the incidence of dizziness, vomiting and eclampsia between the two groups by comparing the incidence of adverse reactions during the perioperative period, while the incidence of tinnitus in the LA group was significantly higher than that in the CA group. The results revealed that chloroprocaine and lidocaine had fewer adverse reactions and higher safety under the premise of the same anesthesia duration.

In summary, chloroprocaine epidural block has less influence on the emergency response of gynecologic patients after pelvic surgery, with fewer adverse reactions, and its anesthetic effect is generally better than lidocaine.

REFERENCES

1. Kilfoyle KA, Vitko M, O'Conor R, Bailey SC. Health literacy and Women's reproductive health: a systematic review. J Womens Health (Larchmt) 2016; 25:1237-55.
2. Puglia C, Sarpietro MG, Bonina F, Castelli F, Zammataro M, Chiechio S. Development, characterization, and in vitro and in vivo evaluation of benzocaine and lidocaine-loaded nanostructrured lipid carriers. J Pharm Sci 2011; 100:1892-99.
3. Naguib M, Magboul MM, Samarkandi AH, Attia M. Adverse effects and drug interactions associated with local and regional anaesthesia. Drug Saf 1998; 18:221-50.
4. Arevalo-Rodriguez I, Smailagic N, Roqué I Figuls M, et al. Mini-Mental State Examination (MMSE) for the detection of Alzheimer's disease and other dementias in people with mild cognitive impairment (MCI). Cochrane Database Syst Rev 2015; CD010783.
5. Vasconcelos A, Mathias LA. Effects of pudendal nerve, epidural and subarachnoid block on coagulation of pregnant women. Rev Bras Anestesiol 2008; 58:95-105.
6. Carli F. Physiologic considerations of Enhanced Recovery After Surgery (ERAS) programs: implications of the stress response. Can J Anaesth 2015; 62:110-19.
7. Walker AK, Martelli D, Ziegler AI, et al. Circulating epinephrine is not required for chronic stress to enhance metastasis. Psychoneuroendocrinology 2019; 99:191-95.
8. Veneziano G, Tobias JD. Chloroprocaine for epidural anesthesia in infants and children. Paediatr Anaesth 2017; 27:581-90.
9. Estebe J. Intravenous lidocaine. Best Pract Res Clin Anaesthesiol 2017; 31:513-21.
10. Vatter H, Konczalla J, Seifert V. Endothelin related pathophysiology in cerebral vasospasm: what happens to the cerebral vessels? Acta Neurochir 2011; 1l0:177-80.
11. Fathy W, Hussein M, Khalil H. Effect of local anesthesia (with lidocaine vs bupivacaine) on cognitive function in patients undergoing elective cataract surgery. Local Reg Anesth 2019; 12:1.
12. Hensley M, Singer BH. Alternative topical anesthesia for bronchoscopy in a case of severe lidocaine allergy. Respir Med Case Rep 2018; 23:90-92.

LETTER TO THE EDITOR

Efficacy and safety analysis of dopamine combined with creatine phosphate sodium in the treatment of infantile pneumonia combined with heart failure

J. Zhang[1], CH. Wang[2], XJ. Liu[3], SF. Cheng[4], LH. Han[5] and CL. Lv[6]

[1]Department of Pharmacy, Maternal and Child Health Care Hospital of Zhangqiu District, Jinan, China; [2]Department of Pediatrics, the People's Hospital of Zhangqiu Area, Jinan, China; [3]Department of Nursing, the People's Hospital of Zhangqiu Area, Jinan, China; [4]Department of Nephrology, the People's Hospital of Zhangqiu Area, Jinan, China; [5]Department of Health Examination, the People's Hospital of Zhangqiu Area, Jinan, China; [6]Disinfection Supply Room, Weifang Traditional Chinese Hospital, Weifang, China

Received May 22, 2020 – Accepted October 19, 2020

To the Editor,

Pneumonia, mostly caused by virus infection, is the main cause of death among children in the world (1). Mycoplasma pneumoniae is one of the most common pathogens causing children's acquired pneumonia, which can result in various pulmonary and extrapulmonary complications, and may endanger the life of children in serious cases (2). Heart failure is a complex disease process, which may be secondary to various causes, such as cardiomyopathy, coronary heart disease and acquired diseases, with extremely high morbidity and mortality (3).

Dopamine is an endogenous catecholamine, which can enhance alveolar tension, stimulate the respiratory center, inhibit cortical network structure, and improve the body's anoxia state (4). Dopamine plays an important role in swallowing and cough reflex in senile pneumonia. Dopamine agonists that enhance dopamine neurons can prevent aspiration pneumonia. Intravenous injection of creatine phosphate sodium can quickly provide energy to compensate for trauma caused by surgery, improve energy metabolism of cells under ischemia and hypoxia environment, increase utilization of glucose, enhance contractility of myocardium, and improve tolerance of myocardium and tissues to hypoxia. Previous study showed creatine phosphate sodium plays a protective role in liver transplantation for patients with myocardial injury (5). The present study detected the improvement in clinical symptoms of pneumonia combined with heart failure in children by using dopamine and creatine phosphate sodium, aimed to provide a reference basis for the treatment, and discussed the therapeutic value of the combination of the two drugs.

MATERIALS AND METHODS

Study subjects

From March 2014 to June 2015, 76 children with pneumonia combined with heart failure in the Maternal and Child Health Care Hospital of Zhangqiu District were selected and divided into an observation group (40 cases) and a control group (36 cases). In the observation group, there were 21 males

Key words: creatine phosphate sodium; dopamine; efficacy; infantile pneumonia combined with heart failure; safety

Corresponding Author:
Dr Chunling Lv,
Disinfection Supply Room,
Weifang Traditional Chinese Hospital,
1055 Weizhou Road,
Kuiwen District, Weifang 261041, China
e-mail: exf3ht@126.com

0393-974X (2020)
Copyright © by BIOLIFE, s.a.s.
This publication and/or article is for individual use only and may not be further reproduced without written permission from the copyright holder.
Unauthorized reproduction may result in financial and other penalties
DISCLOSURE: ALL AUTHORS REPORT NO CONFLICTS OF INTEREST RELEVANT TO THIS ARTICLE.

and 19 females aged 2-7 years, with an average age of (3.6±0.5) years and an average weight of (12.3±2.4) kg. The course of disease was 2-13 days, with an average course of disease (5.48±1.25) days. There were 12 cases of lobar pneumonia, 15 cases of bronchopneumonia, and 13 cases of interstitial pneumonia. The control group consisted of 16 males and 20 females aged 1-6 years, with an average age of (3.5±0.6) years and an average weight of (12.1±2.1) kg. The course of disease was 2-15 days, with an average course of disease (5.55±1.29) d, there were 9 cases of lobar pneumonia, 13 cases of bronchopneumonia, and 14 cases of interstitial pneumonia.

Inclusion criteria were: children suffering from sudden aggravation of dyspnea, accelerated breathing with > 40 times/min, sudden acceleration of heart rate with >140 times/min, progressive enlargement of liver ≥ 2.0 cm, edema in both lower limbs, oliguria or anuria, and sudden extreme irritability, which was clinically diagnosed as pneumonia combined with heart failure; age between 1 and 7 years; complete general clinical data; no contraindications for surgical treatment; and no measles, whooping cough and other respiratory diseases. Exclusion criteria were: severe physical diseases; other infectious diseases; children with cognitive impairment. The guardians of children from the two groups participating in the study were informed and signed an informed consent. The study was approved by the Medical Ethics Committee of Maternal and Child Health Care Hospital of Zhangqiu District.

Treatment methods

Children from the two groups were given effective antibiotic resistance [azithromycin (2 ml:0.1 g, H20051466 Yabao Pharmaceutical Group Co., LTD.) was added to 5% glucose injection for intravenous injection], oxygen inhalation, sedation and other treatments. On this basis, the observation group was given dopamine (Chongqing Polyco Biotechnology Co., Ltd., item number: 656382) intravenous drip, 0.5 mg/kg, at an infusion speed of 3 ~ 5 ug/(kg min), and creatine phosphate sodium was given by injection (Haikou Qili Pharmaceutical Co., Ltd., item number: H20053430), 0.5g/time intravenous drip for children under 5 years old, and 1g/time intravenous drip for children over 5 years old, once/d. The control group was given creatine phosphate sodium for injection, children under 5 years old were given 0.5g/time intravenous drip, children over 5 years old were given 1g/time intravenous drip, once/d. Both groups were treated for 7 days. Treatment was stopped when it was ineffective.

Observation indicators

The Efficacy Evaluation Criteria were as follows: Excellent: Dyspnea and cough of children disappeared; respiratory frequency, blood oxygen saturation degree and myocardial enzyme level returned to normal. Effective: Children's dyspnea and cough were relieved, and the heart rate did not exceed 120 beats/min. Respiration frequency did not exceed 40 times/min; the saturation of blood sample exceeded 95%; the level of myocardial enzyme was gradually normal after detection. Ineffective: There was no obvious improvement in clinical symptoms orvarious body indexes. Total effective rate = (number of excellent cases+number of effective cases)/total number of cases in the group ×100%.

Determination of myocardial enzyme level was as follows: The levels of myocardial enzyme (AST, LDH, CK-MB) before and after treatment in children from the two groups were determined. One day before treatment and one week after treatment, 5 mL of fasting venous blood of children from the two groups was taken in the morning, placed in a centrifuge tube, centrifuged at 5000 r/min for 15 min, and the serum was separated. UniCel DxC 800 Synchron automatic biochemical analysis system (Beckman Coulter Commercial Enterprise (China) Co., Ltd., item number: N/A), AST (Beijing Zhongxi Yuanda Technology Co., Ltd., item number: M357749), LDH (Shanghai Xinfan Biotechnology Co., Ltd., item number: XF018-a), and CK-MB (Chongqing Dingrun Medical Devices Co., Ltd., item number: Chongqing Machinery Note 20182400102) were used for tests.

Statistical analysis

SPSS version 21.0 statistical software (from EASYBIO, China) was used for analysis. The data

in the group were expressed by the number of cases/percentage [n (%)]<, *chi*-squared test was used for comparison of the data among groups; when the theoretical frequency in the *chi*-squared test was less than 5, the continuity correction *chi*-squared test was adopted; the measuring data were expressed by mean±standard deviation (x±sd), the comparison of the measuring data among the groups adopted independent-samples T test, and the comparison of the counting data among the groups successively adopted paired *t*-test. Two-tailed P-values <0.05 were considered statistically significant.

RESULTS

There were no significant differences between children from the two groups regarding their general data, as shown in Table I ($p>0.05$). The disappearance time of bilateral lung rales, control time of heart failure, disappearance time of wheezing symptoms, and hospital stays in the observation group were significantly shorter than those in the control group ($p<0.05$, Table I).

There were no significant differences in heart rate, respiratory frequency or blood oxygen saturation degree between the observation group and the control group before treatment ($p>0.05$). After treatment, the heart rate and respiratory rate in the observation group were lower than those in the control group ($p<0.05$). Moreover, the blood oxygen saturation degree of the observation group was significantly higher than that of the control group ($p<0.05$, Fig. 1).

There were no significant differences in AST, LDH, and CK-MB between the observation group and the control group before treatment ($p>0.05$). AST, LDH, and CK-MB in the observation group and the control group decreased significantly after treatment ($p < 0.05$). And AST, LDH, and CK-MB in the observation group were significantly lower than those in the control group after treatment ($p<0.05$, Fig. 2).

There were 35 excellent cases (87.5%), 4 effective cases (10%), and 1 ineffective case (2.5%) in the observation group after treatment; the total effective rate was 87.5%. There were 11 excellent cases (66.67%), 24 effective cases (22.22%), and

Table I. *General data of children from the two groups [n (%)] (x±s)*

Classification	Observation group (n=40)	Control group (n=36)	t/χ^2 value	*p* value
Gender			0.492	0.483
Male	21(52.50)	16(44.44)		
Female	19(47.50)	20(55.56)		
Age (years)			0.792	0.431
	3.6±0.5	3.5±0.6		
Weight (kg)			0.385	0.702
	12.3±2.4	12.1±2.1		
Place of residence			0.005	0.941
City	23(57.50)	21(58.33)		
Countryside	17(42.50)	15(41.67)		
Ethnicity			0.338	0.561
Han	27(67.50)	22(61.11)		
Minority	13(32.50)	14(38.89)		
Pathological type			0.399	0.819
Lobar pneumonia	12(30.00)	9(25.00)		
Bronchopneumonia	15(37.50)	13(36.11)		
Interstitial pneumonia	13(32.50)	14(38.89)		
Mode of birth			0.038	0.846
Eutocia	22(55.00)	19(52.78)		
Cesarean	18(45.00)	17(47.22)		
Course of disease (d)			0.240	0.811
	5.48±1.25	5.55±1.29		
Gestational age (weeks)			0.425	0.672
	37.5±2.0	37.7±2.1		
Asphyxia			0.338	0.561
Mild asphyxia	27(67.50)	22(61.11)		
Moderate asphyxia	13(32.50)	14(38.89)		
Clinical symptoms			0.306	0.858
Fever	17(42.50)	14(38.89)		
Cyanopathy	12(30.00)	10(27.78)		
Twitch	11(27.50)	12(33.33)		
Smoking history of parents			0.620	0.431
Yes	18(45.00)	13(36.11)		
No	22(55.00)	23(63.89)		
Alcoholism history of parents			0.010	0.920
Yes	26(65.00)	23(63.89)		
No	14(35.00)	13(36.11)		
Disappearance time of bilateral lung rales (h)	54.17±10.45	101.45±12.34	18.08	<0.001
Control time of heart failure (h)	30.71±8.44	41.67±9.45	5.341	<0.001
Disappearance time of wheezing symptoms (h)	87.42±12.99	112.26±19.77	6.535	<0.001
Hospital stays (d)	7.88±1.81	12.76±3.21	8.268	<0.001

p<0.05 was considered statistically significant

Table II. *Comparison of efficacy of treatment in children from the two groups [n(%)]*

Efficacy	Observation group (n=40)	Control group (n=36)	χ^2 value	*p* value
Excellent	35(87.5)	24(66.67)	-	-
Effective	4(10)	8(22.22)	-	-
Ineffective	1(2.5)	4(11.11)	-	-
Total effective rate	35(87.5)	24(66.67)	4.736	0.029

p<0.05 was considered statistically significant

Table III. *Comparison of adverse reaction rates of children from the two groups after treatment [n(%)]*

Category	Observation group (n=40)	Control group (n=36)	χ^2 value	*p* value
Cough	3(7.50)	2(5.00)	0.213	0.644
Vomiting	2(5.00)	3(7.50)	0.213	0.644
Shortness of breath	1(2.50)	2(5.56)	0.467	0.495
Dyspnea	0(0.00)	1(2.78)	1.126	0.287
Total incidence rate of adverse reactions	6(15.00)	8(20.00)	0.346	0.556

p<0.05 was considered statistically significant

4 ineffective cases (11.11%), the total effective rate was 66.67%. The total effective rate of the observation group was higher than that of the control group ($p<0.05$, Table II).

There were 3 cases of cough (7.5%), 2 cases of vomiting (5%), 1 case shortness of breath (2.5%), and no cases of dyspnea in the observation group; the total incidence rate of adverse reactions (any unexpected or dangerous reaction to the drug) was 15%. There were 2 cases of cough (5%), 3 cases of vomiting (7.5%), 2 cases of shortness of breath (5.56%), 1 case of dyspnea (2.78%) in the control group, with a total incidence rate of 20%. There were no significant differences in the total adverse reaction rate between children from the two groups ($p > 0.05$, Table III).

DISCUSSION

Pneumonia is the main cause of morbidity and mortality among children under the age of 5 years (6). Due to the severity and rapidity of childhood diseases, they often suffer from acute heart failure, respiratory failure and toxic encephalopathy at the same time. Dopamine has been used in patients with

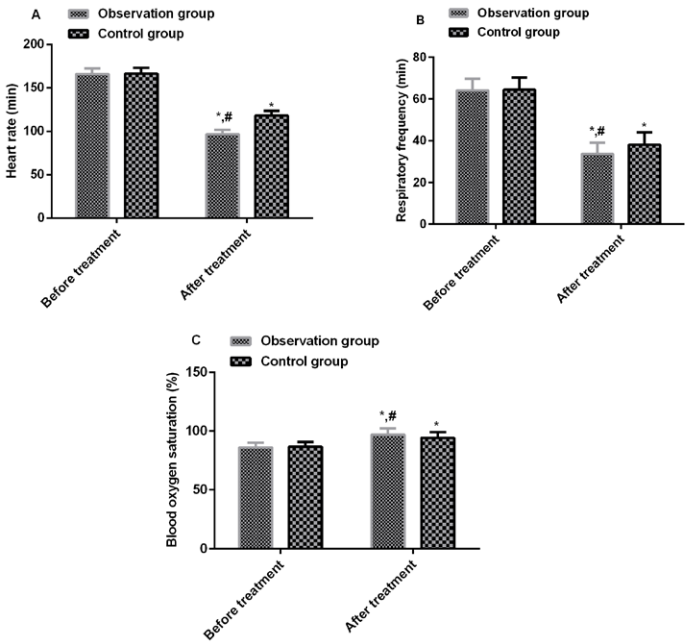


Fig. 1. *Comparison of heart rate, respiratory frequency and blood oxygen saturation degree before and after treatment between observation group and control group. There were no significant differences in heart rate, respiratory frequency and blood oxygen saturation degree between the observation group and the control group before treatment (p>0.05). After treatment, the heart rate (**A**) and respiratory rate (**B**) in the observation group were lower than those in the control group (p<0.05). Blood oxygen saturation degree (**C**) was higher than that of the control group (p<0.05). * compared with the control group, p<0.05. # compared with the control group after treatment, p<0.05. was considered statistically significant.*

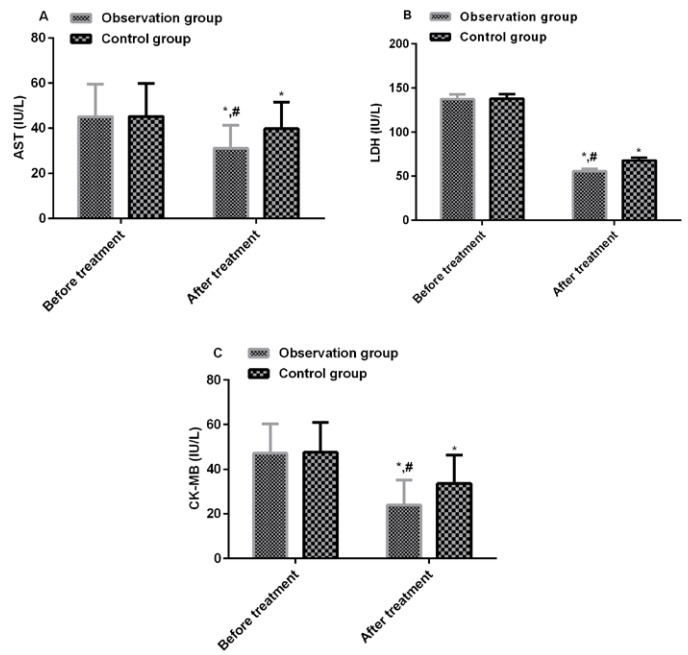


Fig. 2 *Comparison of myocardial enzyme indexes between observation group and control group before and after treatment. There were no significant differences in AST, LDH, and CK-MB between the observation group and the control group before treatment (p>0.05). After treatment, AST (**A**), LDH (**B**), and CK-MB (**C**) in the observation group were lower than those in the control group (p<0.05). * compared with the control group, p<0.05. # compared with the control group after treatment. p<0.05 was considered statistically significant.*

cardiac insufficiency for more than 50 years. It can show neuroprotective effect by reducing cell death, maintaining blood-brain barrier and improving interstitial cerebral edema (7). AST, LDH, and CK-MB are detection indexes with high specificity and sensitivity in the process of heart failure. Changes in serum levels of myocardial enzymes have high clinical diagnostic value in the diagnosis of severity of myocardial injury (8). The results of this study show that the remission time of the clinical symptoms of children from the observation group, such as the disappearance of bilateral lung rales, the control of heart failure and the disappearance time of wheezing symptoms, are all lower than those of the control group, and the hospital stays were also significantly lower than that of the control group. The detection of myocardial enzyme index showed that AST, LDH, and CK-MB of children from the observation group were significantly reduced compared to those from the control group, which provided evidence for the effective treatment of infantile pneumonia combined with heart failure by dopamine combined with creatine phosphate sodium. It has been indicated that in pediatric heart transplantation, treatment with low dose of dopamine can reduce the risk of right heart failure of the recipient, and reduce myocardial cell injury during cold ischemia (9).

To sum up, compared with creatine phosphate sodium alone, dopamine combined with creatine phosphate sodium has better efficacy and fewer adverse reactions in the treatment of infantile pneumonia combined with heart failure, which may be due to the synergistic effect of dopamine and creatine phosphate sodium, and is worthy of clinical promotion.

REFERENCES

1. Rhedin S, Lindstrand A, Hjelmgren A, et al. Respiratory viruses associated with community-acquired pneumonia in children: matched case-control study. Thorax 2015; 70:847-53.
2. Zhang Y, Zhou Y, Li S, Yang D, Wu X, Chen Z. The clinical characteristics and predictors of refractory mycoplasma pneumoniae pneumonia in children. PLoS One 2016; 11:e0156465.
3. Xu YD, Li YM, Xiao ZL, Liu XQ, He WQ, Zhong NS. Study of continuous blood purification in severe pneumonia patients with multiple organ failure. Zhongguo Wei Zhong Bing Ji Jiu Yi Xue 2005; 17:747-51.
4. Matsui T, Ebihara T, Ohrui T, Yamaya M, Arai H, Sasaki H: Cerebrovascular disease and pneumonia in the elderly. Nihon Ronen Igakkai Zasshi 2003; 40:325-28.
5. Sun Z, Lan X, Ahsan A, et al. Phosphocreatine protects against LPS-induced human umbilical vein endothelial cell apoptosis by regulating mitochondrial oxidative phosphorylation. Apoptosis 2016; 21:283-97.
6. Lassi ZS, Haider BA, Bhutta ZA. Zinc supplementation for the prevention of pneumonia in children aged 2 months to 59 months. Cochrane Database Syst Rev 2010; 12:CD005978.
7. Li W, An X, Fu M, Li C. Emergency treatment and nursing of children with severe pneumonia complicated by heart failure and respiratory failure: 10 case reports. Exp Ther Med 2016; 12:2145-49.
8. Wang Z, Chen R, Zhu Z, Zhang X, Wang S. Effects of insulin combined with ethyl pyruvate on inflammatory response and oxidative stress in multiple-organ dysfunction syndrome rats with severe burns. Am J Emerg Med 2016; 34:2154-58.
9. Richmond ME, Easterwood R, Singh RK, et al. Low-dose donor dopamine is associated with a decreased risk of right heart failure in pediatric heart transplant recipients. Transplantation 2016; 100:2729-34.

LETTER TO THE EDITOR

Gene expression of *RAGE, HMGB1* and *BAX* as Genetic markers of diabetic myocardial infarction in population of Pakistan

W. Hameed[1], N. Sheikh[1], I. Liaqat[2], M. Mukhtar[1], A. Tayyab[3], F. Azam[1] and R. Mehmood[1]

[1]Cell and Molecular Biology Laboratory, Department of Zoology, University of Punjab Quaid-i-Azam Campus, Lahore, Pakistan; [2]Department of Zoology, Government College University, Lahore, Pakistan; [3]School of Biological Sciences, University of Punjab Quaid-i-Azam Campus, Lahore, Pakistan

Received June 9, 2020 – Accepted October 19, 2020

To the Editor,

Myocardial infarction (MI) is systemically defined as myocardial cell death due to sustained anoxia or ischemia and it is a severe demonstration of coronary heart disease (CHD) (1). Such cardiovascular diseases (CVD) are the sole basis of disease and death burden globally (2). Diabetes and Ischemia/Reperfusion (I/R) injuries are major factors that increase oxidative stress, leading to the oxidation of biological macromolecules that results in impaired cell function (3). High-mobility-group box-1 (*HMGB1)* stimulation to toll like receptors and receptors for advanced glycation end products (*RAGE*) create a functional tripod that helps to increase the level of proinflammatory mediators and endure the chronic inflammatory state due to diabetes. The interaction between TLR2, TLR and host-derived ligands resulting in activation of *RAGE* triggers a series of metabolic processes including the synthesis and release of pro-inflammatory cytokines (4).

Hyperglycemia plays its part in vascular injury via formation of advanced glycation end products (AGEs). AGEs are found to be involved (directly or receptor-mediated) in atherosclerosis. A deleterious link between AGEs and diabetic vascular complications has been reported previously (5). *HMGB1* is an effective inflammatory cytokine and a DNA-binding protein that decreases contractility and induces hypertrophy and apoptosis in cardiomyocytes and promotes cardiac stem cell proliferation and differentiation. The innate immune system uses extracellular *HMGB1* as necrotic marker to identify tissue damage and initiate repair (6).

BAX is member of the *Bcl-2* family that is essential for apoptosis in normal cells. The ratio of *Bcl-2* to *BAX* determines survival or death after an apoptotic stimulus. Overexpressed *BAX* accelerates apoptotic death. However, overexpression of *Bcl-2* increases cell survival by apoptosis suppression in cells exposed to apoptosis-inducing stimuli (7**).** Oxidative stress induced by glucose deprivation triggers *BAX*-associated events comprised of subsequent caspase activation along with the progression of apoptotic cell death.

The current study evaluates the changes in the expression of these genes in diabetes myocardial infarction subjects.

MATERIALS AND METHODS

This study was approved by the research ethics committee of Punjab Institute of Cardiology vide letter Number (RTPGME-Research-071) and Advanced Studies and Research Board, University

Key words: Advanced glycation end-products (AGE); coronary heart disease (CHD); ischemia/reperfusion; oxidative stress; reactive oxygen species (ROS)

Corresponding Author:
Prof. Dr. Nadeem Sheikh,
Department of Zoology,
University of Punjab,
Quaid-i-Azam campus,
Lahore, 54590, Pakistan
e-mail: s_nadeem77@yahoo.com

0393-974X (2020)
Copyright © by BIOLIFE, s.a.s.
This publication and/or article is for individual use only and may not be further reproduced without written permission from the copyright holder.
Unauthorized reproduction may result in financial and other penalties
DISCLOSURE: ALL AUTHORS REPORT NO CONFLICTS OF INTEREST RELEVANT TO THIS ARTICLE.

of the Punjab Lahore. All subjects were informed and signed the consent form to participate in the study. The subjects of two categories, having myocardial infarction and diabetic myocardial infarction were diagnosed clinically. Subjects were referred from all over the Punjab Province to hospitals in Lahore. Samples of four categories i.e. myocardial infarction (MI), diabetes mellitus (DM), diabetes myocardial infarction (DMI) and control (c) patients were collected. Each category had 80 patients. The patients aged 20-80 years were included while pregnant females or feeding mothers were excluded. Hospital-admitted MI patients with any two of these components i.e., MI history, ECG, angiography and enzymes were considered as inclusion criteria. For DM, DMI groups random and fasting blood glucose levels were measured for inclusion of the subjects.

Blood samples were taken from the selected patients and 250 µl were transferred immediately to Eppendorf tubes containing 750 µl TRIzol® Reagent. RNA was extracted from the blood samples by Trizol method. cDNA was prepared using total RNA with Revert Aid First Strand cDNA kit # K 1621 20 Rxns (µl) #K 1622 100 Rxns (µl). The primers earlier reported (8, 9) for *HMGB1*, *BAX* and *RAGE* were used to study the gene expression (Table I). The primers were optimized to find the optimum annealing temperature through gradient PCR. The annealing temperatures were 59.5°C, 59°C and 57°C for *HMGB1*, *RAGE* and *BAX,* respectively. The amplified PCR products were checked through agarose gel electrophoresis. Real time PCR was used to study the changes in the gene expression by Ct method with the thermal profile as shown in Fig. 1. The samples were run in triplicates along with non-template controls (reaction mixture minus template) and the expression levels were normalized to the *GAPDH* (housekeeping) gene expression.

The specificity of the amplified products was determined by melt curve analysis using PikoReal™ Software 2.2. For data analysis arithmetic formula was used. To determine the quantitative values of gene expression, comparative Ct method i.e., $2^{-\Delta\Delta Ct}$ proposed by Schmittgen and Livak_(10) was used to compare the expression of target gene in a treatment group to that of an untreated control. From all the replicates, average of means and standard deviations were calculated and then used to calculate ΔCt values.

RESULTS

The melt curve analysis showing a single sharp peak indicates single specific gene amplification. The gene expression of *HMGB1, RAGE* and *BAX* were analyzed in all groups and presented in Table II. Gene expression analysis of *RAGE* through one-way ANOVA, showed (P = 0.0002) a significant decrease in MI, DMI and D groups (0.84-, 0.56- and 0.49-fold, respectively) as compared to controls. Intergroup comparison showed that *RAGE* expression was not significantly different among the experimental groups when compared using one-way ANOVA (Fig. 2).

Gene expression analysis of *HMGB1* through one-way ANOVA, showed significant variation in *HMGB1* expression (P< 0.0001) when compared with the control group (Fig. 3). *HMGB1* expression was increased in the MI, DMI and DM groups compared to the control group. The upregulation of *HMGB1* expression in the MI group was statistically significant (7.05-fold) when compared with control. However, in DMI and D groups the increase in *HMGB1* expression as compared with control was not statistically significant (1.50- and 1.48-fold respectively). The intergroup comparison showed a significant increase of *HMGB1* expression in MI in comparison with DMI (5.55-fold) and DM (5.57-fold) groups.

BAX expression showed significant variations (P< 0.0001) in different experimental groups as compared to the control group (Fig. 4). There was a significant decrease in *BAX* expression in MI (0.45-fold) and DMI (0.28-fold) groups, whereas a significant (1.24-fold) increase in the DM group was found in comparison to control.

DISCUSSION

Cardiovascular complications, such as long QT syndrome, restenosis and arhythmogenic right ventricular dysplasia, are a leading cause of mortality and morbidity among diabetics (11**) t**herefore, the

Table I. *List of primers used for Real time PCR.*

GENE	PRIMERS
RAGE	Forward 5′-CACTTGTGCTAAGCTGTAAGGG-3′
	Reverse 5′-CATCGACAATTCCAGTGGCTG -3′
HMGB1	Forward 5′-GCTCAGAGAGGTGGAGACCA-3′
	Reverse 5′-GGTGCATTGGGATCCTTGAA-3′
BAX	Forward 5′-TCTGACGGCAACTTCAACTG-3
	Reverse 5′- CAGCCCATGATGGTTCTGA-3′
GAPDH	Forward 5′-CTCTGATTTGGTCGTATTG-3′R
	Reverse 5′-TGTAAACCATGTAGTTGAGG-3′

Table II. *Fold change of gene expression (Mean ± Standard error of Mean) in different groups.*

GENE	GROUPS			
	Control	MI	DMI	D
RAGE	1.00 ± 0.00	0.16 ± 0.02	0.44 ± 0.17	0.51 ± 0.03
HMGB1	1.00 ± 0.00	7.05 ± 0.50	1.50 ± 0.28	1.48 ± 0.32
BAX	1.00 ± 0.00	0.55 ± 0.01	0.72 ± 0.04	1.24 ± 0.01

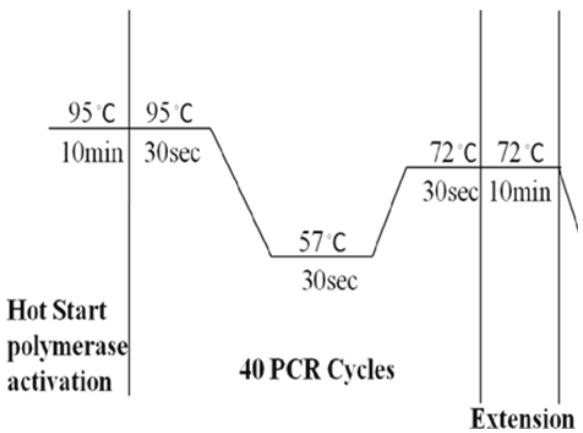


Fig. 1. *PCR temperature cycling profile of Real-Time PCR used for amplification.*

current investigation was aimed at finding alterations of *RAGE, HMGB1* and *BAX* gene expression in diabetic myocardial infarction patients. The present study revealed a significant downregulation of *RAGE* in all the groups studied, i.e. MI, DMI and D, as compared to the control group. Our findings are concordant with a previous study where *sRAGE* levels were also found to be reduced in non-STEMI patients ,and in 2018, similar results were recorded for a study on 1,201 patients with follow-up of 18 years. It was found that as s*RAGE* level decreased, the risk of CAD, DM and all-cause mortality was increased, therefore there is a direct association between s*RAGE* and presence of CAD (12**).** Park described that *RAGE* has elevated levels in acute coronary syndrome patients (ACS) (13).

HMGB1 plays an important role in transcription regulation, nucleosome assembly and DNA repair and replication (6). A markedly significant up-regulation of *HMGB1* was found in MI subjects in comparison with the control and remaining study groups. A study on MI patients revealed a significant increase in serum *HMGB1* level that can ultimately lead to pump failure, cardiac rupture and ultimately cardiac death. Similarly, research on animal models also depicts that in infarcted area the expression of myocardial *HMGB1* was increased. Inhibition of *RAGE* and *HMGB1* expression by metformin

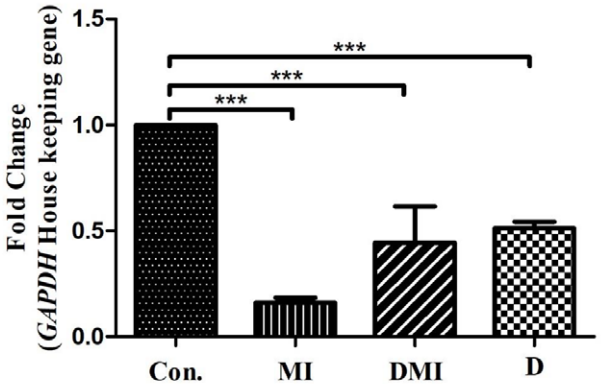


Fig. 2. *mRNA expression of RAGE through quantification. Data from q RT PCR is described as fold change in mRNA expression of normalized housekeeping gene GAPDH. Values represent mean ± S.E.M.sstatistical analysis was performed through one way ANOVA, *** = P ≤ 0.001.*

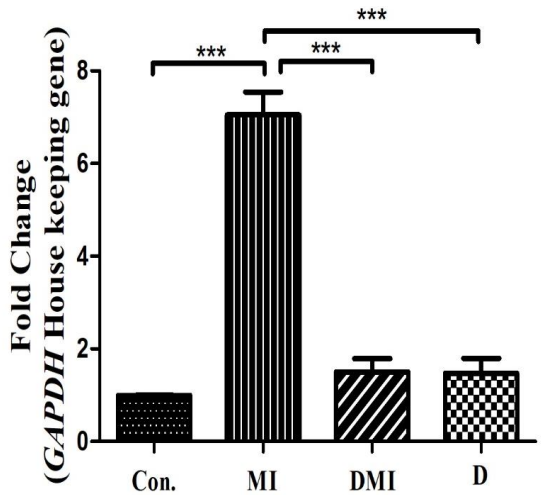


Fig. 3. *mRNA expression of HMGB1 through quantification. Data from qRT PCR is described as fold change in mRNA expression of normalized housekeeping gene GAPDH. ValueS represent mean ± S.E.M analysis through one way ANOVA, *** = P ≤ 0.001.*

was found to be protective against hyperglycemia-induced cardiomyocyte injury **(**14**).** In follow-up studies of MI patients, *HMGB1* described the decrease in apoptosis of cardiomyocytes. During acute MI, induction of autophagy is protective and ultimately improves the cardiac function (6).

Bcl2 and *BAX* are involved in regulation of apoptosis, and support or suppress cell death. Activation of these proteins through various cellular actions, such as DNA damage, loss of growth signaling and energy stress, can initiate apoptosis. *BAX* overexpression promotes cell death while overexpression of *Bcl-2* increases cell survival by suppressing apoptosis (15). Bcl-2-associated X apoptosis regulator (*BAX*) acts as pro-apoptotic marker.

In the present study, *BAX* expression in diabetic subjects (D) was significantly increased, whereas a significant downregulation of *BAX* was observed in MI and DMI subjects as compared to controls. *BAX* increased in blood vessels of diabetic patients in comparison to the normal subjects, and its overexpression promotes cell death (16). Overexpression of *BAX* in diabetics point outs endothelial cell dysfunction that resultantly triggers endothelial cell death. It was demonstrated that in response to normal glucose levels, hypoxia stimulates apoptosis and inhibits proliferation. Whereas, hyper glycaemia significantly attenuates the hypoxic-induced growth response. Hence, high glucose levels could lead to endothelial dysfunction by activating the expression of *BAX* and down regulating *Bc1-2* in diabetic patients (16). *BAX* expression level is important, as overexpression was found to accelerate myocyte apoptosis during ischemia and reperfusion (17).

From these findings, it can be concluded that the significant changes in *RAGE, HMGB1* and *BAX* expression in the experimental groups were associated with the progression of myocardial infarction, diabetic myocardial infarction and

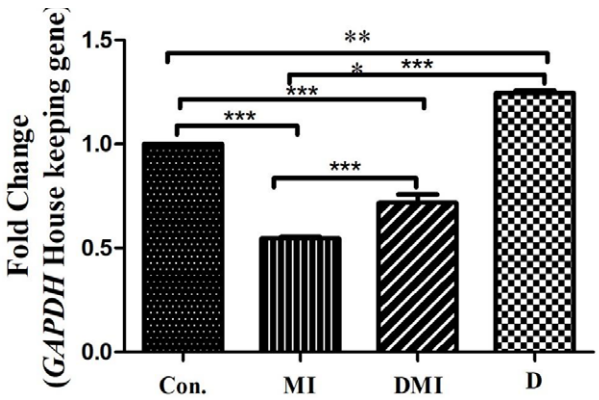


Fig. 4. *mRNA expression of BAX through Quantification. Data from qRT PCR is described as fold change in mRNA expression of normalized housekeeping gene GAPDH. Value represent mean ± S.E.M analysis through one way ANOVA, *** = P ≤ 0.001.*

diabetes, which makes these genes candidates to be considered as a marker to predict early onset of these health issues.

REFERENCES

1. Sun T, Dong YH, Du W, et al. The role of microRNAs in myocardial infarction: From molecular mechanism to clinical application. Int J Mol Sci 2017; 18:745.
2. Lara MJ, Nitze I, Grosse G, Martin P, McGuire AD. Reduced arctic tundra productivity linked with landform and climate change interactions. Sci Rep 2018; 8:2345. _
3. Ji L, Fu F, Zhang L, et al. Insulin attenuates myocardial ischemia/reperfusion injury via reducing oxidative/nitrative stress. Am J Physiol Endocrinol Metab 2010; 298:E871–E80.
4. Nogueira-Machado JA, Volpe CMO, Veloso CA, Chaves MM. HMGB1, TLR and RAGE: a functional tripod that leads to diabetic inflammation. Expert Opin Ther Targets 2011; 15:1023-35.
5. Barlovic DP, Soro-Paavonen A, Jandeleit-Dahm KAM. *RAGE* biology, atherosclerosis and diabetes. Clin Sci (Lond) 2011; 121:43-55.
6. Raucci A, Maggio SD, Scavello F, D'Ambrosio A, Bianchi ME, Capogrossi MC. The Janus face of *HMGB1* in heart disease: a necessary update. Cell Mol Life Sci 2019; 76:211-29.
7. Hasnan J1, Yusof MI, Damitri TD, Faridah AR, Adenan AS, Norbaini TH. Relationship between apoptotic markers (*BAX* and Bcl-2) and biochemical markers in type 2 diabetes mellitus. Singapore Med J 2010; 51:50-55.
8. Hiwatashi K, Ueno S, Abeyama K. A novel function of the Receptor for Advanced Glycation End-Products (*RAGE*) in association with tumorigenesis and tumor differentiation of HCC Ann Surg Oncol 2008; 15(3):923-33.
9. Dolca T, Hua Y, Daniel B, et al. Proapoptotic *BAX* is hyperexpressed in isolated human islets compared with antiapoptotic bcl-21. Transplantation 2002; 74 (11):1489-96.
10. Schmittgen TD, Livak KJ. Analyzing real-time PCR data by the comparative C (T) method. Nat Protoc 2008; 3:1101-8.
11. Nolan CJ, Damm P, Prentki M. Type 2 diabetes across generations: from pathophysiology to prevention and management. Lancet 2011; 378:169-81.
12. Fishman SL, Sonmez H, Basman C, Singh V, Poretsky L. The role of advanced glycation end-products in the development of coronary artery disease in patients with and without diabetes mellitus. Mol Med 2018; 24(1):59. doi: 10.1186/s10020-018-0060-3.
13. Park HJ, Baek JY, Shin WS, et al. Soluble receptor of advanced glycated endproducts is associated with plaque vulnerability in patients with acute myocardial infarction. Circ J 2011; 75:1685-90.
14. Wang Y, Zhong Y, Zhang X, Liu Z, Yuan Yang Y, Gong Q, Ren B. The Role of *HMGB1* in the Pathogenesis of Type 2 Diabetes. J Diabetes Res 2016; 2016:2543268. doi: 10.1155/2016/2543268.
15. Gokalp-Ozkorkmaz E, Kirman G, Pekkolay Z, Asir F, Deveci E. Expression of apoptotic proteins *BAX* and Bcl-2 in blood cells of type 2 diabetic patients. 2nd International Cell Death Research Congress, Izmir, Turkey 2018; 1-4.
16. Liu T, Zhou Y, Wang JY, Su Q, Tang ZL, Liu YC, Li L. Coronary microembolization induces cardiomyocyte apoptosis in swine by activating the LOX-1-dependent mitochondrial pathway and Caspase-8-dependent pathway. J Cardiovasc Pharmacol Ther 2016; 21(2):209-18.

LETTER TO THE EDITOR

Neoadjuvant chemotherapy combined with concurrent chemoradiotherapy *versus* concurrent chemoradiotherapy alone on locally advanced nasopharyngeal carcinoma

H. Liu[1*], XR. Ding[1*], YQ. Song[2], C. Jiang[1], XM. Zhong[1] and HX. Hui[1]

[1]Department of Oncology, The Affiliated Huai'an No.1 People's Hospital of Nanjing Medical University, Huai'an, China; [2]Department of Radiation Oncology, The Affiliated Huai'an No.1 People's Hospital of Nanjing Medical University, Huai'an, China

Received May 19, 2020 – Accepted October 26, 2020

[*]These Authors contributed equally to this work

To the Editor,

Nasopharyngeal carcinoma (NPC) is one of the most common malignant cancers in south China (1, 2). Due to its insidious onset, most NPCs are already in the advanced stage. At present, concurrent chemoradiotherapy (CRT) is the standard treatment for locally advanced nasopharyngeal carcinoma (LANPC) (1, 3). Neoadjuvant concurrent chemoradiotherapy (NCCRT) has frequently been rejected in the past, due to its intolerable adverse effects and/or little benefit to survival (4). However, with the development of radiation techniques and the decrease in radiation-related adverse reactions, patient tolerance to neoadjuvant chemotherapy has significantly improved. As a result, the efficacy of NCCRT for LANPC has become a focal point (5). This study is a retrospective study of the role of NCCRT in the treatment of 60 LANPC patients.

MATERIALS AND METHODS

Patients

The present study selected 60 LANPC patients (T3-4N1M0 or TanyN2M0, III-IVa, 2010 7th AJCC staging), who were admitted to The Affiliated Huai'an No.1 People's Hospital of Nanjing Medical University between August 2010 and June 2016. The inclusion criteria were as: patients with a biopsy that had been pathologically confirmed to be a poorly differentiated squamous cell carcinoma; patients with initial treatment; patients with a Karnofsky performance scale (6) of ≥70; patients with magnetic resonance imaging (MRI) and computed tomography (CT) results confirming stage III-IVa cancer.

The 60 patients were equally divided into two groups: an NCCRT group and a CRT group. The baseline characteristics of these two groups showed no significant differences (Table I). The Institutional Review Board for human studies of the Affiliated Huai'an No.1 People's Hospital of Nanjing Medical University approved the study protocol, and all subjects gave informed, signed consent to participate in the study.

Treatment

Neoadjuvant chemotherapy regimen: the chemotherapy with Cisplatin (DDP) combined with 5-fluorouracil (5-Fu) regimen (DDP 80 mg/m^2 d1 + 5-Fu 800 mg/m^2 d1-5, *q28d*) was based on the study conducted by Lee (7). It was performed two or three times, and finished two weeks before the concurrent chemoradiotherapy. Only the NCCRT group received this regimen.

Radiotherapy regimen: Patients took a supine position,

Key words: locoregionally advanced nasopharyngeal carcinoma; neoadjuvant chemotherapy; concurrent chemoradiotherapy; locoregional failure rate

Corresponding Author:
Dr Hong-Xia Hui,
Department of Oncology, The Affiliated Huai'an No.1 People's Hospital of Nanjing Medical University, 6 Beijing Road West, Huai'an, Jiangsu 223300, China
Tel: +86 13852498556 - Fax.: +86 0517 80872938
e-mail: hl_dr999@163.com

0393-974X (2020)
Copyright © by BIOLIFE, s.a.s.
This publication and/or article is for individual use only and may not be further reproduced without written permission from the copyright holder.
Unauthorized reproduction may result in financial and other penalties
DISCLOSURE: ALL AUTHORS REPORT NO CONFLICTS OF INTEREST RELEVANT TO THIS ARTICLE.

with the head and neck held by an immobilization device. A CT simulation scan was performed from the top of the head to the carina using a 3 mm thickness, in order to guide the gross tumor volume (GTV) target. Image registration and fusion applications with MRI and/or PET-CT scans were used to help the delineation of target volumes. The target volume delineation and treatment planning were based on the guidelines from the Radiation Therapy Oncology Group (RTOG) Nasopharyngeal Cancer Trials 0225 (8). The intensity modulated radiotherapy (IMRT) dose fractionation schemes used for the present study were as follows: the gross disease region (PTV_{70}) received 70 Gy/2.12 Gy/33 F, the high-risk region ($PTV_{59.4}$) received 59.4 Gy/1.8 Gy/33 F, and the low-risk region ($PTV_{50.4}$) received 50.4 Gy/1.8 Gy /28 F.

Concurrent chemotherapy regimen: The DDP concurrent chemotherapy regimen (DDP 100 mg/m^2 d1, 22, 43) was based on the RTOG Nasopharyngeal Cancer Trials 0225 (8). This commenced on the first day of radiotherapy. Both groups received the concurrent chemoradiotherapy regimen.

Outcome measures

Short-term efficacy was classified as either complete remission (CR), partial remission (PR), stable (SD), or progress (PD) using the Response Evaluation Criteria in Solid Tumors (RECIST) V1.1 (9), and a head and neck scan and enhanced MRI and/or CT were performed four weeks after the treatment was finished.

Long-term efficacy: All patients were followed up until December 2018, or when they died. The follow-up intervals were: three months in the first two years after treatment; six months between the third and fifth years; and twelve months after five years. There were no missing cases. The three-year incidence, overall survival (OS), progression free survival (PFS) rate, locoregional failure rate (LFR), and distant metastasis rate (DMR) were recorded and analyzed.

Toxicity and side effects: Acute toxicity responses, such as oral mucosa, skin, blood and gastrointestinal toxicity, were recorded and analyzed according to the RTOG criteria of acute radiation injury (oral mucosa, and skin) (10) and the drug toxicity standard CTC 3.0 (blood and gastrointestinal) (11).

Statistical analysis

A *t*-test and *Chi*-squared test were used to analyze the differences in quantitative data and enumeration data, respectively. Univariate analysis with a log-rank test was used to filter the possible related factors of OS, PFS, LFR and DMR, with a statistically significant difference at a value of $P<0.1$. Univariate and multivariate analysis was performed using the Cox proportional hazards regression model to explore the independent prognosis factor of the DMR. The univariate analyses had a statistically significant difference at a *P*-value of <0.10. Except for the univariate analyses, all the analyses had a statistically significant difference at a *P*-value of <0.05. All the analyses were performed using Stata/SE 11.2 for Windows.

RESULTS

All the patients were followed up until December 2018 or when they died, with a median follow-up time of 45 months and a follow-up rate of 100%. The follow-up range was from 18 to 58 months.

The primary cancer (PC) and positive lymph node (PLN) response rate of the two groups were compared. There were 26 CR cases and 4 PR cases of PC in the CRT group, 28 CR cases and 2 PR cases of PC in the NCCRT group, 22 CR cases and 8 PR cases of PLN in the CRT group, and 27 CR cases and 3 PR cases of PLN in the NCCRT group. None of the patients were SD or PD. Furthermore, there was no significant difference between these two groups (Table II).

The analysis of the three-year incidence of OS, PFS, LFR and DMR is presented in Table III. The univariate analysis with a log-rank test was performed to analyze the OS, PFS, LFR and DMR, and the Kaplan-Meier method was used for the survival curves. The results showed that only DMR revealed a significant statistical difference between the two groups (Table III, Fig. I). The DMR was significantly lower in the NCCRT group, when compared to the CRT group ($P<0.05$).

The univariate analysis of DMR revealed that treatment and staging were the only two possible independent prognostic factors of DMR ($P<0.10$). The further multivariate survival analysis of DMR with treatment and staging revealed that the clinical stage and neoadjuvant chemotherapy were independent prognostic factors for the DMR ($P<0.05$), and that

Table I. *Baseline characteristics of two the groups*

Group(N)	Gender		Age		KPS		Staging	
	male	female	≤40	40-70	70-80	≥90	III	IVa
CRT(30)	22	8	4	26	17	13	20	10
NCCRT(30)	23	7	5	25	18	12	20	10
χ^2	0.089		0.131		0.069		0.000	
P[a]	0.766		0.612		0.793		1.000	

Table II. *Side effects in the two groups*

Group (N)	Oral mucositis			Skin			Gastrointestinal			blood			PC		PLN	
	0-1	2	3	0-1	2	3	0-1	2	3	0-1	2	3-4	CR	PR	CR	PR
CRT(30)	5	19	6	6	21	3	5	23	2	5	20	5	26	4	22	8
NCCRT(30)	2	20	8	5	22	3	1	21	8	1	15	14	28	2	27	3
χ^2	1.641			0.114			6.857			8.067			0.185		1.781	
P	0.440			0.944			0.032*			0.018*			0.667		0.182	

**Chi-squared test, P<0.05*

Table III. *Three year incidence of OS, PFS, LFR and DMR in the two groups*

Group(N)	OS	PFS	LFR	DMR
CRT(30)	24/30	23/30	5/30	6/30
NCCRT(30)	26/30	24/30	6/30	0/30
χ^2	0.480	0.098	0.111	4.435
P	0.488	0.754	0.739	0.035*

**Chi-squared test, P<0.05*

neoadjuvant chemotherapy was negatively associated with distant metastasis (Table IV).

The side effects in these two groups consisted of acute oral mucositis, skin reaction, gastrointestinal reaction, and blood reaction. The oral mucositis and skin reactions, both of which disappeared within three months of treatment, were not significantly different between the two groups, but the gastrointestinal and blood reactions were significantly higher in the NCCRT group when compared to the CRT group (P<0.05). The gastrointestinal reaction in both groups and the blood reaction in the CRT group all disappeared within three months of treatment. However, the blood reaction of eight patients in the NCCRT group continued for more than six months, during which time one patient continued to have a grade 1 blood reaction up to the cut-off date (Table II).

DISCUSSION

Currently, neoadjuvant chemotherapy is under the spotlight due to its unique advantages. However, neoadjuvant chemotherapy may also bring more toxic side effects and interfere with subsequent treatments.

Table IV. *Univariate analysis of DMR of the two groups*

	Factors	H.R	95% CI		P
Univariate analysis	Treatment (NCCRT *vs* CRT)	0.227	0.048	1.069	0.061*
	Staging (IVa *vs* III)	4.654	1.247	17.000	0.02*
	KPS (≥90 *vs* 70-80)	0.624	0.180	2.165	0.457
	Age (≤40 *vs* 40-70)	1.544	0.195	12.200	0.681
	Gender (Male *vs* Female)	0.591	0.075	4.675	0.618
Multivariate analysis	Treatment (NCCRT *vs* CRT)	0.178	0.037	0.862	0.032#
	Staging (IVa Vs. III)	6.109	1.550	24.069	0.009#

** Cox Proportional Hazard Model test, P<0.10; # Cox Proportional Hazard Model test, P<0.05.*

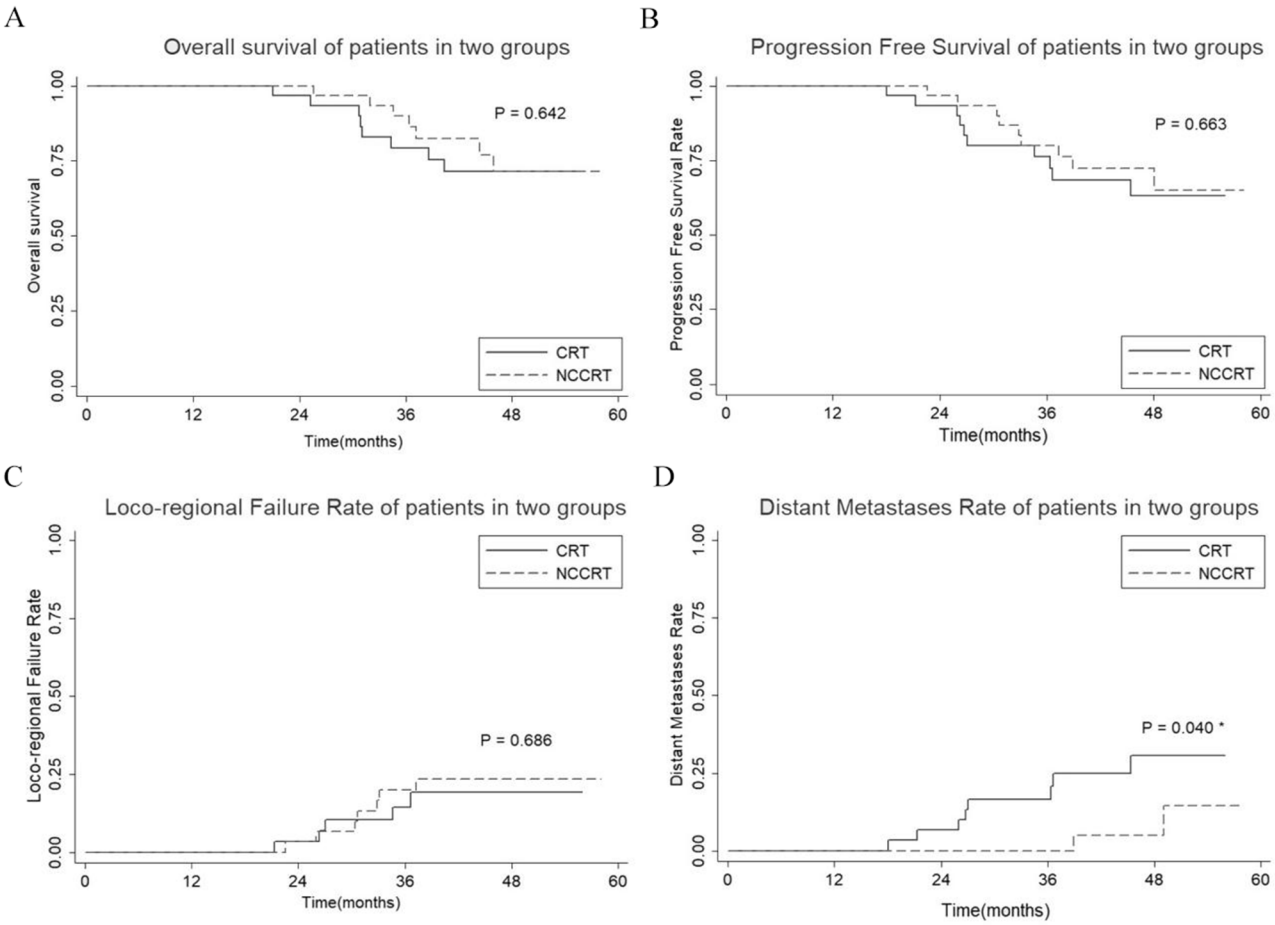


Fig. 1. *Survival analysis of the OS (**A**), PFS (**B**), LFR (**C**) and DMR (**D**) of patients between the two groups*

The study conducted by Ribassin-Majed et al. (12) proved that neoadjuvant chemotherapy could only reduce distant metastasis of LANPC. However, the study conducted by Wang et al. (5) concluded that NCCRT did not improve the 5-year LFFS rate, DFS rate, OS rate, or cause-specific survival (CSS) rate of LANPC, and had more side effects, when compared to CRT. Therefore, the present study was designed to compare the efficacy and adverse effects of NCCRT and CRT in the treatment of LANPC.

The results revealed the following: (i) The primary lesions and metastatic lymph node complete remission rates of CRT *vs* NCCRT were 26/30 *vs* 28/30 and 22/30 *vs* 27/30, respectively. Neither of these showed significant differences between the two groups. (ii) The 3-year incidence of OS, PFS, LFR and DMR exhibited a significant reduction in the 3-year DMR in the NCCRT group. The univariate analyses for OS (P=0.642), PFS (P=0.663) and LFR (P=0.686) suggest that NCCRT brings no benefit to OS, PFS, or LFR, while the NCCRT group had a low DMR (P=0.040). This was consistent with the conclusion of the studies conducted by Ribassin-Majed et al. (12). The further univariate and multivariate analysis on the DMR suggested that NCCRT can reduce the DMR of LANPC patients. (iii) The oral mucositis and skin reactions were similar in the two groups (P>0.05), while the high-grade gastrointestinal and blood reactions were significantly higher in the NCCRT group, when compared to the CRT group (P<0.05), but most of these were bearable and reversible.

In summary, the present study revealed that compared with CRT, NCCRT could significantly reduce the DMR of LANPC patients, but it offered no significant benefit to short-time efficacy, OS, PFS, or LFR. In addition, NCCRT led to higher gastrointestinal and hematological toxicity, but it was mostly tolerable.

REFERENCES

1. Lang J, Gao L, Guo Y, Zhao C, Zhang C. Comprehensive treatment of squamous cell cancer of head and neck: Chinese expert consensus 2013. Future Oncol 2014; 10(9):1635-48.
2. Chen W, Zheng R, Baade PD, et al. Cancer Statistics in China, 2015. CA Cancer J Clin 2016; 66(2):115-32.
3. National Comprehensive Cancer Network. Head and Neck Cancers. Cancer 2018. doi:10.1007/978-3-642-31292-2.
4. Lee AWM, Ngan RKC, Tung SY, et al. Preliminary results of trial NPC-0501 evaluating the therapeutic gain by changing from concurrent-adjuvant to induction-concurrent chemoradiotherapy, changing from fluorouracil to capecitabine, and changing from conventional to accelerated radiotherapy fractionation in patients with locoregionally advanced nasopharyngeal carcinoma. Cancer 2015; 121(8):1328-38.
5. Wang C, Tang X, Wang J, Song J, Xu Y. Induction chemotherapy plus concurrent chemoradiotherapy vs concurrent chemoradiotherapy in elderly patients with advanced nasopharyngeal carcinoma. Otolaryngol Head Neck Surg 2017; 157(2):233-38.
6. Schag CC, Heinrich RL, Ganz PA. Karnofsky performance status revisited: reliability, validity, and guidelines. J Clin Oncol 1984; 2(3):187-93.
7. Wakamatsu T, Kakunaga S, Takenaka S, et al. Prognostic implication of adjuvant/neoadjuvant chemotherapy consisting of doxorubicin and ifosfamide in patients with extraskeletal osteosarcoma. Int J Clin Oncol. 2019; 24;1311-19.
8. Lee N, Garden A, Kramer A, et al. Phase II multi-institutional study of IMRT ± chemotherapy for nasopharyngeal carcinoma (RTOG 0225): preliminary results. Int Radiat Oncol 2007; 69(3):S13-4.
9. Eisenhauer EA, Therasse P, Bogaerts J, et al. New response evaluation criteria in solid tumours: Revised RECIST guideline (version 1.1). Eur J Cancer 2009; 45(2):228-47.
10. Cooperative group common toxicity criteria. Int J Radiat Oncol 1995; 31:1361-64. doi:10.1016/0360-3016(95)90160-4.
11. Savarese DM. Common terminology criteria for adverse events. NCI 2006; 1:1–72. http://www.uptodate.com/contents/common-terminology-criteria-for-adverse-events.
12. Ribassin-Majed L, Marguet S, Lee AWM, et al. What is the best treatment of locally advanced nasopharyngeal carcinoma? An individual patient data network meta-analysis. J Clin Oncol 2017; 35(5):498-505.

LETTER TO THE EDITOR

Effects of butylphthalide on cognitive dysfunction and expression of superoxide dismutase and Smac in cortex of rats with chronic cerebral ischemia

WH. Song[1], A. Liu[2], YF. Zhu[3], SY. Wang[4], XH. Yang[5] and LN. Ma[6]

[1]Department of Psychiatry, Ji'nan City Yingcheng Rongjun Hospital, Jinan, China; [2]Department of Pharmacy, Zhangqiu Maternity and Child Care Hospital, Jinan, China; [3]Department of Anesthesiology, Qingdao Central Hospital, Qingdao University, Qingdao, China; [4]Emergency Ward, the People's Hospital of Zhangqiu Area, Jinan, China; [5]Department of Pharmacy, the People's Hospital of Zhangqiu Area, Jinan, China; [6]Department of Internal Medicine, Community Health Service Centers of Grand View Garden, Blood Station of Jinan, Jinan, China

Received March 22, 2020 – Accepted October 26, 2020

To the Editor,

Recent clinical studies have found that chronic cerebral ischemia is a common pathological manifestation of all kinds of dementia including Binswager and vascular dementia (1). It is of great significance to find prevention and treatment methods of chronic cerebral ischemia (2). Butylphthalide (3-n-butylphthalide) is a new type of anti-ischemia medicine which has been shown to reduce the area of cerebral infarction after middle cerebral artery occlusion in rats, reduce cerebral edema, maintain the integrity of blood-brain barrier, and increase local cerebral blood flow in ischemic areas (3). Superoxide dismutase (SOD) is a specific enzyme for scavenging superoxide anion *in vivo*, which can protect cells from oxidative damage and plays a vital role in the balance between oxidation and oxidation resistance of the body (4). During chronic cerebral ischemia, intracellular calcium overload leads to excessive proliferation of free radicals and consumption of a large number of antioxidants, which results in decompensation of SOD activity and further damages the structure and function of nerve cells. The changes indirectly reflect the alternations in free radical scavenging ability *in vivo* (5). The second mitochondrial-derived cysteine protease activator (Smac) is one of the mitochondrial proteins discovered in recent years, and is one of the pro-apoptotic proteins that can induce cascade reactions by activating various levels and promote apoptosis (6). This study aims to prove the value of butylphthalide in treating chronic cerebral ischemia by establishing a rat model of chronic cerebral ischemia and exploring the changes of SOD and Smac during the treatment of butylphthalide to provide reference and guidance for clinical practice.

MATERIALS AND METHODS

Experimental animals

Forty-five clean Wistar rats, weighing 280-320 g, aged 3-7 weeks, were purchased from Nanjing Better Biotechnology Co., Ltd., and were maintained in cages with good ventilation, indoor humidity of 50± 5% and temperature of 24±2°C. After screening by the Morris water maze test, they were randomly divided into a normal control group, an ischemia model group, and a butylphthalide group. Each group was further randomly

Key words: Butylphthalide; chronic cerebral ischemia; Smac; SOD

Corresponding Author:
Lining Ma,
Department of Internal Medicine,
Community Health Service Centers of Grand View Garden,
Blood Station of Jinan,
No. 86 Weisan Road, Daguanyuan Street, Jinan, China
e-mail: ok541n@126.com

0393-974X (2020)
Copyright © by BIOLIFE, s.a.s.
This publication and/or article is for individual use only and may not be further reproduced without written permission from the copyright holder.
Unauthorized reproduction may result in financial and other penalties
DISCLOSURE: ALL AUTHORS REPORT NO CONFLICTS OF INTEREST RELEVANT TO THIS ARTICLE.

divided into 3 groups of 1-, 3- and 5-day groups according to ischemia time, with 5 rats in each group. This study was approved by the Ethics Committee of Ji'nan City Yingcheng Rongjun Hospital, and the experimental process followed the Guidelines for the Protection and Use of Laboratory Animals.

Animal model

Bilateral common carotid arteries were permanently blocked. The rats were anesthetized by intraperitoneal injection of 300mg/kg of 10% chloral hydrate. A median incision in the anterior part of the neck was made and the bilateral common carotid arteries (CCA) were bluntly separated. The rats were double ligated with No.1 surgical line and sutured layer by layer. During the operation, breathing changes were closely observed to ensure spontaneous breathing. In the normal control group the rats underwent only separated and exposed bilateral CCA without ligation. The butylphthalide group (Butylphthalide, CSPC NBP Pharmaceutical Co., Ltd., SFDA Approval No. H20100041) was given intraperitoneal injection of 80mg/kg of Butylphthalide within 48 h after the operation. The model group received intraperitoneal injection of the same amount of sodium chloride solution at the same time. The rats in each group were anesthetized with 10% chloral hydrate (0.4 g/kg) 3, 6 and 9 days after permanent occlusion of the common carotid artery. The rats were sacrificed by cervical dislocation, and the cortex was separated and preserved in liquid nitrogen.

Morris water maze

Morris water maze test was used to measure the spatial learning and memory ability of rats in each group. Morris water maze consists of a circular pool, an automatic camera and a computer analysis system. Before the test, water was injected into the pool to a depth of 30 cm (i.e. the water surface was 1 cm higher than the platform surface, so the rats could not see the platform). Powdered milk was added to make the water milk-white and the water temperature was controlled at 26±1°C. The experiment was conducted in a soundproof and dark room, and all experimental conditions remained unchanged. One day before the experiment, each rat's head was stained with picric acid to facilitate timely capture by the camera. The experiment lasted for 7 days and the rats were trained once a day. The selected positions for entering the pool were the opposite to the platform and the adjacent quadrants. The rats were put into the pool with their heads at 1/2 radian of the edge of the quadrants. At the same time, the camera began to record. The time when the rats found the platform (escape latency) and memory ability time were recorded.

Detection of SOD activity and Smac level in rats

Rats in each group were sacrificed by decapitation at different time points, cortex was separated, 10% tissue homogenate was prepared, and mitochondria were extracted. SOD activity and Smac level of chemical colorimetry were measured on a fully automatic biochemical instrument according to the instructions of the SOD kit (Nanjing Jiancheng Biotechnology Co., Ltd.). Western blot was used to detect Smac level in tissues. Coomassie brilliant blue colorimetric method was used to detect protein concentration, and SDS-PAGE electrophoresis separation was performed, after which the tissues were rinsed with deionized water. The protein was transferred to nitrocellulose membrane, then placed in 5% of skimmed milk powder, and sealed overnight at 4°C. The blocking solution was discarded. The sample was then rinsed with TBST for 2-3 times. The primary antibody diluted by 1:500 (Shanghai Hengfei Biotechnology Co., Ltd., bs-1298R-1) was added and incubated on shaking table for 2 h at room temperature. The horseradish peroxidase (HRP)-labeled sheep anti-mouse secondary antibody was added after TBST rinsing, and incubated at 37°C for 1 h. The diaminobenzidine (DAB) color development was performed after TBST rinsing, and the gray values were analyzed in Quantity One (Molecular Devices Corp, The Bay Area, CA, USA).

Statistical analysis

SPSS22.0 (IBMCorp, Armonk, NY, USA) was used for statistical analysis. The measurement data were expressed in the form of mean standard deviation ($\bar{x}\pm s$), and independent sample *t*-test was used for comparison. The comparison among multiple time points used the variance analysis of repeated measurement. The counting data between groups were expressed by the number of cases/percentage [n (%)], and *chi*-squared test was used to compare the counting data. The P value less than 0.05 was regarded as statistical significance.

RESULTS

There was no difference between the experimental group and the control group in sex, week age, length, blood sugar (Glu), body mass, indoor temperature and indoor humidity of the rats (P> 0.05, Table I).

The Morris water maze test was used to compare the escape latency of the three groups in the positioning navigation test and the target quadrant residence time in the space exploration test. It was found that the escape latency of the butylphthalide group was significantly lower than that of the model control group (P<0.05), but higher than that of the normal control group (P<0.05) within 5 days. The target quadrant residence time of the butylphthalide group (26.51±4.31 s) was significantly lower than that of the model control group (21.37±6.19 s) (P<0.05) but higher than that of the normal control group (35.26±5.75 s) (P<0.05, Table II, Fig. 1).

By measuring the changes of SOD activity in cerebral cortex at different time points in each group, it was found that the normal control group had no significant changes within 5 days (P>0.05). SOD activity and Smac level in the model group and butylphthalide group on the 3rd day were significantly lower than that on the 1st day and higher than that on the 5th day. SOD activity and Smac level in the model group had a more obvious decrease than that in the model group on the 5th day, compared with that on the 3rd day (Table II, Figs. 2 and 3).

Table I. *General conditions of rats [n(%)]/($\bar{x}$±s)*

Category	Normal control group (n=15)	Model group (n=15)	Butylphthalide group (n=15)	F/χ2 value	P
Gender				0.536	0.765
Male	6(40.00)	7(46.67)	8(53.33)		
Female	9(60.00)	8(53.33)	7(46.67)		
Body mass before modeling (g)	224.78±15.29	226.61±14.56	225.13±15.18	0.063	0.939
Body mass after modeling (g)	211.26±8.12	208.57±10.16	209.15±9.23	0.355	0.704
Length (cm)	18.57±1.16	18.84±0.93	18.73±1.19	0.229	0.797
Week age (week)	8.28±0.37	8.31±0.25	8.34±0.56	0.789	0.924
Glu (mmol/L)	71.27±3.68	72.31±4.23	71.67±4.17	0.254	0.777
Indoor temperature (°C)	26.27±2.61	26.87±2.13	25.18±3.13	1.562	0.222
Indoor humidity (%)	50.18±2.43	51.27±1.87	51.54±2.16	1.658	0.203

Table II. *Escape latency period, changes of SOD activity and Smac level (nU/mg) in rats at different ischemia time points*

	Group	n	1st day	3rd day	5th day	F	P
Escape latency period	Butylphthalide group	15	45.74±4.14	36.08±3.63*	31.15±3.23*,#	60.83	<0.001
	Model group	15	55.29±7.27	51.31±4.25*	42.21±6.17*,#	18.56	<0.001
	Normal control group	15	34.27±4.21	25.13±2.69*	18.16±2.61*,#	92.45	<0.001
	F	-	66.97	98.121	0.696	-	-
	P	-	<0.001	<0.001	<0.001	-	-
SOD activity	Normal control group	15	282.25±14.59	276.46±11.43	279.17±12.88	-	-
	Model group	15	182.32±24.39	145.62±31.37*	126.26±35.47*,#	-	-
	Butylphthalide group	15	237.18±26.33	193.08±14.63*	150.39±29.15*,#	-	-
	t	-	75.08	148.6	35.07	-	-
	P	-	<0.001	<0.001	<0.001	-	-
Smac level	Normal control group	15	6.61 ±0.81	6.32 ±0.42	6.29 ±0.24	1.579	0.218
	Model group	15	4.17 ±0.16 *,#	3.50 ±0.12 *,#	3.06 ±0.20	175.7	<0.01
	Butylphthalide group	15	4.92 ±0.13	4. 43±0.89	3.27±0.21	37.88	<0.01
	F	-	100.6	94.54	172.2	-	-
	P	-	<0.01	<0.01	<0.01	-	-

**indicates that compared with the first day, P< 0.05. # indicates that compared with the 3rd day, P< 0.05.*

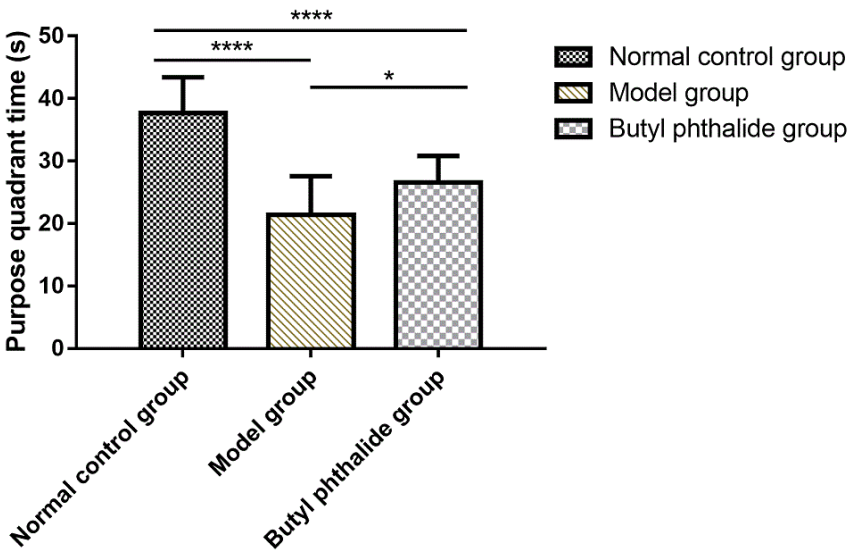


Fig. 1. *Changes of residence time in different target quadrants of rats. The residence time in the target quadrant of the butylphthalide group was significantly lower than that of the model control group, but higher than that of the normal control group.*

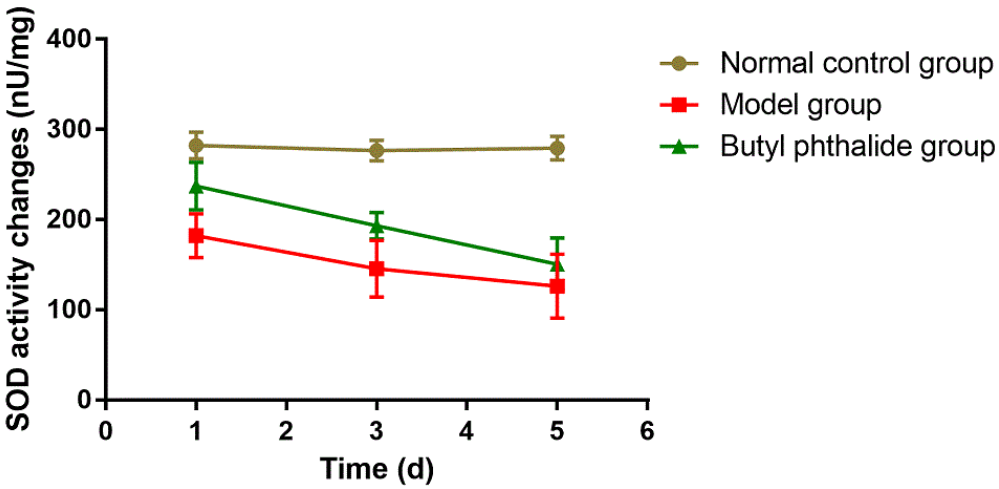


Fig. 2. *Changes of SOD activity in rats at different time points. SOD activity in cerebral cortex of normal control group did not change significantly within 5 days (P>0.05). SOD activity in cerebral cortex of model group and butylphthalide group on the 3rd day was significantly lower than that on the 1st day and higher than that on the 5th day. SOD activity level in the model group had a more obvious decrease than that in the butylphthalide group on the 3rd day.*

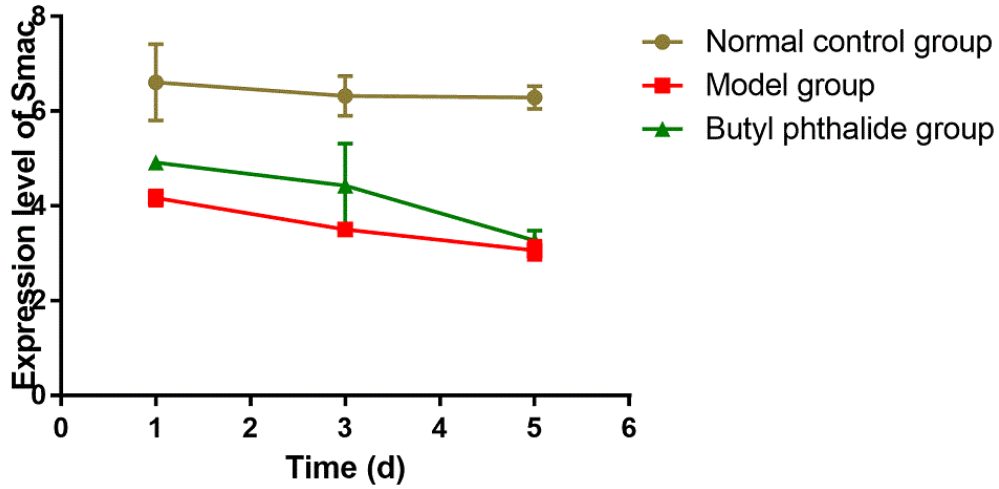


Fig. 3. *Changes of Smac level at different time points in rats. The Smac level in cerebral cortex of normal control group did not change significantly within 5 days (P>0.05). The Smac level in cerebral cortex of model group and butylphthalide group on the 3rd day was significantly lower than that on the 1st day and higher than that on the 5th day. Smac level in the model group had a more obvious decrease than that in the butylphthalide group on the 3rd day.*

DISCUSSION

Chronic cerebral ischemia is one of the common brain injuries in clinical practice, and is a common pathological process in the development of many diseases such as Alzheimer's disease, vascular dementia and Binswanger's disease. Its injury mechanism is not fully clarified, and often leads to neuropathological changes such as degeneration and necrosis of neurons (7). Butylphthalide can improve microcirculation, inhibit oxygen free radicals, increase antioxidant enzyme activity, inhibit platelet aggregation, improve brain perfusion, increase ATP and phosphocreatine levels in rat brain, improve

brain energy metabolism, mitochondrial function, and promote neurological function (8). In the present study, we compared the escape latency of the three groups in the location navigation test and the residence time in the target quadrant of the space exploration test through Morris water maze test. We found that chronic ischemia can significantly prolong the escape latency and the residence time in the target quadrant of the rat. The learning and memory function of the rat changed and gradually increased with the passage of time, indicating that the cognitive dysfunction caused by chronic cerebral ischemia in the rat had been successfully established. However, the escape latency and target quadrant residence time of rats in the butylphthalide group were significantly lower than those in the model group but higher than those in the normal control group, which suggested that butylphthalide can improve the learning and memory ability of rats with chronic cerebral ischemia. It was found that butylphthalide was an effective method to treat white matter injury and cognitive impairment caused by chronic cerebral hypoperfusion, which is similar to our results (9).

SOD blocks the free radical toxic reaction, eliminates superoxide anion free radical, and protects cells from damage by catalyzing superoxide anion free radical to generate disproportionation reaction (10). We measured the changes of SOD activity and Smac level in the cerebral cortex of the three groups of rats at different time points. The results showed that the SOD activity and Smac level in the cerebral cortex of the normal control group had no significant changes within 5 days. The SOD activity and Smac level in the cerebral cortex of the model group and butylphthalide group on the 3rd day were significantly lower than that on the 1st day and higher than that on the 5th day. This result indicates that SOD and Smac may participate in the occurrence and development of cerebral ischemic injury and have the potential to become markers for judging the severity of brain injury. To sum up, butylphthalide can effectively improve the learning and memory ability of rats with chronic cerebral ischemia. The expression of SOD and Smac in cerebral cortex of rats with chronic cerebral ischemia is significantly lower than that of normal rats. Butylphthalide can increase the SOD activity and Smac level in cerebral cortex of rats with chronic cerebral ischemia.

REFERENCES

1. Edrissi H, Schock SC, Hakim AM, Thompson CS. Microparticles generated during chronic cerebral ischemia increase the permeability of microvascular endothelial barriers in vitro. Brain Res 2016; 1634:83-93.
2. Zhao Y, Gong CX. From chronic cerebral hypoperfusion to Alzheimer-like brain pathology and neurodegeneration. Cell Mol Neurobiol 2015; 35:101-10.
3. Xu HL, Feng YP. Inhibitory effects of chiral 3-n-butylphthalide on inflammation following focal ischemic brain injury in rats. Acta Pharmacol Sin 2000; 21:433-38.
4. Ilhan M, Turgut S, Turan S, et al. The assessment of total antioxidant capacity and superoxide dismutase levels, and the possible role of manganese superoxide dismutase polymorphism in acromegaly. Endocr J 2017; 65:91-99.
5. Chen L, Zhao Y, Zhang T, et al. Protective effect of Sheng-Nao-Kang decoction on focal cerebral ischemia-reperfusion injury in rats. J Ethnopharmacol 2014; 151:228-36.
6. Cao Y, Gou Z, Du Y, et al. Glutamatergic and central cholinergic dysfunction in the CA1, CA2 and CA3 fields on spatial learning and memory in chronic cerebral ischemia-induced vascular dementia of rats. Neurosci Lett 2016; 620:169-76.
7. Akpinar M B, Sahin V, Sahin N, et al. Previous chronic cerebral infarction is predictive for new cerebral ischemia after carotid endarterectomy. J Cardiothorac Surg 2015; 10:141.
8. Xu J, Huai Y, Meng N, et al. L-3-n-butylphthalide activates Akt/mTOR signaling, inhibits neuronal apoptosis and autophagy and improves cognitive impairment in mice with repeated cerebral ischemia-reperfusion injury. Neurochem Res 2017; 42:1-14.
9. Wang Y, Yuan L, Liu P and Zhao M: Delayed hyperoxic ventilation attenuates oxygen-induced free radical accumulation during early reperfusion after global brain ischemia. Neuroreport 2015; 26:131-38.
10. Wu F, Liu R, Shen X, Xu H and Sheng L: Study on the interaction and antioxidant activity of theophylline and theobromine with SOD by spectra and calculation. Spectrochim Acta A Mol Biomol Spectrosc 2019; 215:354-62.

LETTER TO THE EDITOR

Protective effect of sufentanil on skeletal muscle wasting in patients with sepsis

H-X. Li[1*], J-L. Zhao[2*], L. Liu[3], Y. Li[4], L-Z. Yin[5], P. Fu[6] and H-F. Li[7]

[1]Department of Anesthesiology, The People's Hospital of Zhangqiu, Jinan, China; [2]Department of Anesthesiology, Zhangqiu Maternity and Child Care Hospital, Jinan, China; [3]EEG Room, The People's Hospital of Zhangqiu, Jinan, China; [4]Interventional Vascular Department, The People's Hospital of Zhangqiu, Jinan, China; [5]Health Management Center, The People's Hospital of Zhangqiu, Jinan, China; [6]Department of Anesthesiology, Qingdao Fuwai Cardiovascular Hospital, Qingdao, China; [7]Department of Anesthesiology, The Third People's Hospital of Qingdao, Qingdao, China

Received June 8, 2020 – Accepted October 27, 2020

[*]These Authors contributed equally to this work

To the Editor,

Sepsis and septic shock are common diseases in intensive care units (ICU), and are often accompanied by multiple organ dysfunction, which leads to high mortality (1). At the same time, complex metabolic disorders are frequently observed, such as decreased appetite, decreased anabolism, and increased catabolism of protein and fat. In patients with sepsis, the abnormally high catabolism of body protein may lead to muscle atrophy and exhaustion, as well as being seriously life-threatening (2). It is therefore of great significance in clinical practice to protect skeletal muscle in sepsis patients, rather than to offer nutritional support to improve the condition of skeletal muscle after skeletal muscle wasting.

Sufentanil mainly acts on μ opioid receptors and is more selective to μ1-R (analgesia) than μ2-R (respiratory inhibition). It presents characteristics of long analgesia time and weak respiratory inhibition (3, 4). Currently, sufentanil is gradually applied in sepsis patients. Combined with sedative drugs such as dexmedetomidine, sufentanil can play a sedative and analgesic effect with good safety and few adverse reactions (5, 6). However, whether sufentanil can improve muscle catabolism in sepsis patients remains to be determined, therefore, this study investigated the muscle protective effect of sufentanil on sepsis patients.

MATERIALS AND METHODS

Study subjects

A total of 110 patients admitted to the Third People's Hospital of Zhangqiu from August 2016 to August 2018 who met the criteria of sepsis were selected as research subjects. Inclusion criteria were: age18-75 years; diagnosis of SIRS or sepsis; complete case data. Exclusion criteria were: age <18 years or >75 years; unclear diagnosis of sepsis; patients whose cachexia occurred on admission, i.e., a 5% weight loss or body mass index (BMI) < 20 kg/m^2, or limb skeletal muscle index consistent with sarcopenia (male <7.26 kg/m^2, female <5.45 kg/m^2); serious heart and kidney diseases; allergy to opioids or with previous long-term use of opioids. This study was approved by the Medical Ethics Committee of the People's Hospital of Zhangqiu. All patients enrolled in this study gave written informed consent after a detailed explanation.

Key words: sedation; sepsis; skeletal muscle wasting; sufentanil

Corresponding Author:
Dr Haifang Li,
Department of Anesthesiology,
the Third People's Hospital of Qingdao,
29 Yongping Road, Licang District,
Qingdao266041, China
e-mail: zrs4o4@163.com

0393-974X (2020)
Copyright © by BIOLIFE, s.a.s.
This publication and/or article is for individual use only and may not be further reproduced without written permission from the copyright holder.
Unauthorized reproduction may result in financial and other penalties
DISCLOSURE: ALL AUTHORS REPORT NO CONFLICTS OF INTEREST RELEVANT TO THIS ARTICLE.

Sedative and analgesic methods

Patients were randomly divided into a Sufentanil group and a Non-sufentanil group. In the Sufentanil group, sufentanil was intravenously infused at a dosage of 2 μg/kg/d by continuous infusion according to the body weight of patients. Meanwhile, patients in both groups were sedated with dexmedetomidine intravenously at a rate of 0.2-0.7 mg/kg/h. The sedative target was set at -1 to 0 point according to the Richmond Agitation Sedation Scale.

The patients were routinely evaluated by acute physiology and chronic health evaluation system (APACHE) scores after admission to the ICU, and blood routine examination, biochemistry, blood gas analysis and other hematological indicators were routinely monitored. Meanwhile, serum interleukin-6 (IL-6) and C-reactive protein (CRP) levels were measured by enzyme linked immunosorbent assay (ELISA).

After patients were admitted to the ICU, their height and weight were measured. Body composition tests were also performed on all enrollees using Bioelectrical impedance analysis (BIA), including body mass index, fat free mass, lean body mass, limb muscles, fat percentage indices and trunk muscle. At the same time, the thickness of tricep skin fold and middle arm circumference of patients were measured three times with a tape, and the average value was calculated. The measurements were repeated after 10 days.

Statistical analysis

SPSS 21.0 software was used to analyze the data. Measurement data were expressed as mean ± standard deviation or ($\bar{x}$±s), and *t*-test was used for inter-group comparison. Enumeration data were qualified by *chi*-squared test, and $P<0.05$ was considered statistically significant.

RESULTS

There was no significant difference in age, gender, height, weight and complications between the two groups ($P>0.05$, Table I).

After 10 days of treatment, CRP levels in both groups were relatively reduced. Of note, the levels of IL-6 and LAC were significantly lower than those before treatment ($P<0.05$). After treatment, the levels of IL-6 and LAC in the Sufentanil group were significantly lower than those in the Non-sufentanil group ($P<0.05$, Table I).

The mass of trunk muscle in the Sufentanil group after treatment was statistically lower than that before treatment ($P<0.05$). Fat tissue, lean tissue and limb muscle tissue were also reduced. In the Non-sufentanil group, the lean tissue, limb muscle tissue and trunk muscle tissue were significantly decreased compared with those before treatment ($P<0.05$, Table II). Moreover, the lean tissue, limb muscles tissue and trunk muscles tissue of the Non-sufentanil group after treatment were significantly decreased compared to those of the Sufentanil group after treatment ($P<0.05$, Table II).

DISCUSSION

Clinically, patients with sepsis are often complicated with significant metabolic disorders,

Table I. *Comparison of CRP, IL-6 and LAC between the two groups before and after treatment (x±s)*

Groups		CRP (mg/L)	IL-6(pg/mL)	LAC (mmol/L)
Sufentanil group	Before treatment	21.7±3.9	117.4±22.6	6.8±1.3
	After treatment	18.5±4.2	68.8±16.4*△	1.9±0.7*△
Non-sufentanil group	Before treatment	23.2±5.0	109.9±19.5	6.5±1.1
	After treatment	20.8±7.7	78.6±14.1*	2.6±0.5*

** compared with the same group before treatment, $P<0.05$. △compared with the control group during the same period, $P<0.05$.*

Table II. *Comparison of body composition between the two groups before and after treatment (x±sd)*

Groups		Adipose tissue (%)	Lean tissue （kg）	Limb muscles tissue (kg)	Trunk muscles tissue (kg)
Sufentanil group	Before treatment	23.5±4.1	46.8±5.2	20.4±3.3	25.7±3.6
	After treatment	22.7±3.9	44.9±3.8△	19.5±2.6△	22.9±4.1*△
Non-sufentanil group	Before treatment	24.1±4.6	47.1±4.9	21.0±2.9	24.8±3.5
	After treatment	21.4±3.3	41.7±5.5*	17.7±2.1*	20.4±3.7*

**compared with the same group before treatment, P<0.05. △compared with the control group during the same period, P<0.05.*

characterized by progressive skeletal muscle wasting, weight loss, and decreased protein reserves (1, 7). The mechanism involves functional anorexia, anemia, insulin resistance of fat cells and peripheral skeletal muscle cells, etc., which further results in nitrogen imbalance in the body and poor prognosis. Skeletal muscle protein accounts for about 50% of the total weight of cells in the body, and its excessive consumption undoubtedly gives rise to a profound impact on sepsis patients (8).

At present, sedation and analgesia are commonly used in critical care medicine, while midazolam and fentanyl are widely accepted as sedative and analgesic agents. It has been revealed that midazolam combined with dexmedetomidine can significantly improve the prognosis of septic rats (9). As a sedative medicine, propofol can activate GABA receptor-chloride ion complex to increase chloride ion conduction, thereby inhibiting the central nervous system through desensitizing GABA receptor (10). Meanwhile, propofol has significant antioxidant properties and exerts a protective function on acute lung injury. In the current study, we found that sufentanil combined with dexmedetomidine can play a good anti-inflammatory and organ protection role. Compared with the Non-sufentanil group, the serum levels of IL-6, CRP and LAC in the Sufentanil group were markedly lower after 10 days of treatment. We used BIA to detect changes of body composition, especially changes in skeletal muscle content of patients, as previously described (11). The result indicated that after treatment the lean body mass, limb muscle tissue and trunk muscle tissue of the Sufentanil group were significantly higher than that of the Non-sufentanil group, suggesting that it is effective to use sufentanil for sedation and analgesia to reduce the wasting of skeletal muscle.

In conclusions, for sepsis patients, sufentanil combined with dexmedetomidine can effectively reduce the skeletal muscle wasting of patients, which provides insights for the improvement of body stress and the reduction of systemic inflammatory response in patients with sepsis.

ACKNOWLEDGEMENTS

This study was funded by Qingdao Medical Scientific Research Guidance Plan (2017-WJZD068, 2017-WJZD140, 2018-WJZD136); supported by Qingdao Outstanding Health Professional Development Fund; Shandong Medical and Health Science and Technology Development Plan Project (2015WS0316).

REFERENCES

1. Dellinger RP, Levy MM, Rhodes A, et al. Surviving sepsis campaign: international guidelines for management of severe sepsis and septic shock: 2012. Crit Care Med 2013; 41:580-637.
2. Bear DE, Puthucheary ZA, Hart N. Early feeding during critical illness. Lancet Respir Med 2014; 2:15-17.

3. Meijer F, Cornelissen P, Sie C, et al. Sublingual sufentanil for postoperative pain relief: first clinical experiences. J Pain Res 2018; 11:987-92.
4. Flint RB, Bahmany S, van der Nagel B, Koch B. Simultaneous quantification of fentanyl, sufentanil, cefazolin, doxapram and keto-doxapram in plasma using liquid chromatography-tandem mass spectrometry. Biomed Chromatogr 2018; 32:e4290.
5. Kweon DE, Koo Y, Lee S, Chung K, Ahn S, Park C. Postoperative infusion of a low dose of dexmedetomidine reduces intravenous consumption of sufentanil in patient-controlled analgesia. Korean J Anesthesiol 2018; 71:226-31.
6. Nie Y, Tu W, Shen X, et al. Dexmedetomidine added to sufentanil patient-controlled intravenous analgesia relieves the postoperative pain after cesarean delivery: a prospective randomized controlled multicenter study. Sci Rep 2018; 8:9952.
7. Alverdy JC. Hypermetabolism and nutritional support in sepsis. Surg Infect (Larchmt) 2018; 19:163-67.
8. Borges RC, Soriano FG. Association between muscle wasting and muscle strength in patients who developed severe sepsis and septic shock. Shock 2019; 51:312-20.
9. Qiu R, Yao W, Ji H, et al. Dexmedetomidine restores septic renal function via promoting inflammation resolution in a rat sepsis model. Life Sci 2018; 204:1-8.
10. Bao HG, Li S. Effects of propofol on the outcomes of rats with sepsis. J Surg Res 2011; 168:e111-e115.
11. Player EL, Morris P, Thomas T, et al. Bioelectrical impedance analysis (BIA)-derived phase angle (PA) is a practical aid to nutritional assessment in hospital in-patients. Clin Nutr 2019; 38:1700-706.

LETTER TO THE EDITOR

Changes of related hormone levels in patients with acute coronary syndrome and their clinical significance

Q. Wu, ZP. He, TQ. Chen, XB. Shen and PJ. Shi

Department of Internal Medicine Cardiovascular, Beilun District People's Hospital, Ningbo, Zhejiang, China

Received June 12, 2020 – Accepted October 28, 2020

To the Editor,

Heart failure is often a common result of cardiovascular disease, which has become a worldwide public health problem. (1). Acute coronary syndrome (ACS) is an acute or subacute myocardial ischemia syndrome caused by coronary plaque rupture, vasospasm or thrombosis, and is the main cause of clinical heart failure (2). Acute myocardial infarction can cause acute myocardial necrosis, reduce cardiac systolic function, cause hemodynamic disorder, activate the renin angiotensin aldosterone system (RAAS) and sympathetic nervous system, and promote the aggravation and deterioration of heart failure. The pathophysiological processes mentioned above can take place on the basis of basic pathological changes, or acute heart failure can occur under the rapid stimulation of various trigger factors. The clinical manifestations are extreme fidgety, shortness of breath, phlegm white foam or pink foam, double lungs dry wet rales, sitting breathing (3). However, there are few reports on the related influencing factors of the severity of coronary heart disease.

In this study, 223 patients with ACS were selected for medical records analysis, and the correlation between the levels of estrogen, high sensitivity C-reactive protein (hs-CRP), matrix metalloproteinase-9 (MMP-9), epinephrine (EPI), norepinephrine (N), renin (REN), angiotensin (ANG), aldosterone (Aldo) levels and the severity of coronary heart disease were explored, and their clinical significance was analyzed.

MATERIALS AND METHODS

Patients and grouping

This is an observational cross-sectional study. This study registered 223 ACS patients diagnosed in Beilun District People's Hospital from January 2015 to January 2020. The patients were classified according to the diagnosis and treatment of unstable angina pectoris and the guidelines for diagnosis and treatment of acute myocardial infarction (AMI) by the cardiovascular branch of Chinese Medical Association. Exclusion criteria were: thyroid-related diseases, acute cerebrovascular accident, acute pancreatitis, chronic cholecystitis, uremia, severe obstructive emphysema, liver cirrhosis. The participants did not take iodine-containing drugs for 2 weeks prior to blood collection. The patients signed informed consent, and the research plan was approved by the ethics committee of Beilun District People's hospital.

The 223 cases were divided into two groups: 105 cases of acute myocardial infarction (AMI group), 118 cases of unstable angina pectoris (UAP group. Moreover, a control

Key words: acute coronary syndrome; estrogen; coronary artery disease; related hormone levels

Corresponding author:
Dr Peijian Shi,
Department of Internal Medicine Cardiovascular,
Beilun District People's Hospital,
Beilun District, Ningbo,
315800, Zhejiang, China.
e-mail: shipeijianblyy@163.com

0393-974X (2020)
Copyright © by BIOLIFE, s.a.s.
This publication and/or article is for individual use only and may not be further reproduced without written permission from the copyright holder.
Unauthorized reproduction may result in financial and other penalties
DISCLOSURE: ALL AUTHORS REPORT NO CONFLICTS OF INTEREST RELEVANT TO THIS ARTICLE.

group was included of 55 patients with stable angina pectoris (SAP group) and 45 patients with coronary angiography (CAG) excluding coronary heart disease.

Methods

The patients' demographic and clinical data included gender, age, height, weight, ACS-associated risk factors (hypertension, dyslipidemia, diabetes, history of smoking), heart function classified by Killip classification system, and the levels of estrogen, hs-CRP, MMP-9, EPI, N, REN, ANG-II, and Aldo.

Echocardiography was performed on all the patients before treatment and one month after discharge, and left ventricular end diastolic volume (LVEDV) was recorded in the two groups before treatment and one month after discharge. Left ventricular end systolic volume (LVESV) and left ventricular ejection fraction (LVEF) were measured during hospitalization, and 6-min walk test (6MWT) was carried out one month after drug withdrawal. Acute heart failure (AHF) was defined as < 150 m for the outcome of 6MWT; moderate heart failure was defined as 150-450 m for the outcome of 6MWT; and mild heart failure was defined as 450 m for the outcome of 6MWT. The incidence of major adverse cardiac events (MACEs) (e.g., cardiac death, AHF, malignant arrhythmia) in the two groups within 6 months after discharge was recorded.

Statistical analysis

Data were statistically analyzed by using SPSS 19.0 software (IBM, Armonk, NY, USA). Descriptive statistics were performed by calculating mean ± standard deviation (SD) for numerical data and frequency/percentages for categorical data. The *t*-test was used for comparing differences in the patients' demographic characteristics and clinical data between the two groups. One-way analysis of variance (ANOVA) test was employed for comparing differences in the patients' demographic characteristics and clinical data among multiple groups. The Cochran's Q test was utilized to compare the distributions of the two qualitative variables. Pearson's correlation test was used to assess the strength of association between two variables. $P<0.05$ was considered statistically significant.

Table I. *Characteristics of Patients with ACS and SAP*

Variable	Characteristic
Gender	
Male	85 (30.6)
Female	193 (69.4)
Age	59.9±37.2
Previous disease	
Arterial hypertension	158 (56.8)
Diabetes mellitus	182 (65.5)
Coronary heart disease	250 (89.9)
Coronary heart disease	
AMI	105 (37.8)
UAP	118 (42.4)
SAP	55 (19.8)

Note: Data are presented as No.(%) or Mean±SD.

RESULTS

General characteristics of samples

Baseline characteristics of 223 patients with ACS, 55 patients with SAP, and 45 patients without CHD who were tested by CAG are presented in Table I.

Comparison of hormone levels in each group

The estrogen levels in AMI, UAP and SAP groups were significantly lower than those in the control group ($P < 0.05$). There were statistically significant differences in estrogen levels among AMI, UAP and SAP groups ($P<0.05$), and the concentration level gradually increased. The levels of hs-CRP, MMP-9, EPI, N, REN, ANG II and Aldo in AMI, UAP and SAP groups were significantly higher than those in the control group ($P<0.05$), and the differences among the three groups were statistically significant ($P<0.05$) (Table II).

Correlation between numbers of coronary stenosis lesions and related hormone levels

In Fig. 1, the number of coronary stenosis lesions was negatively correlated with Estrogen levels ($r= -0.635$, $P<0.05$), and hs-CRP ($r=0.537$), MMP-9 ($r=0.475$), EPI ($r=0.553$), N ($r=0.631$), REN ($r=0.531$), and Aldo ($r=0.637$) ($P<0.05$). In addition, the incidence of MACE events in AMI, UAP and SAP group was higher than that in the control group ($P<0.05$).

DISCUSSION

AHF is defined as a life threatening clinical syndrome with rapidly developing or worsening

Table II. *Determination results of related hormones in each group*

Groups	Number of cases	Estrogen (ng/L)	Hs-CRP (mg/L)	MMP-9 (ng/mL)	EPI (ng/mL)	N (ng/mL)	REN (ng/mL·h)	ANG II (pg/mL)	Aldo (pg/mL)
AMI	105	51.16±6.15	8.19±2.59	361.17±23.18	1105±251.13	15.09±3.17	8.05±2.43	88.72±18.19	180.47±35.18
UAP	118	60.23±9.17	6.81±2.23	291.55±18.72	885±178.15	11.85±2.86	6.45±1.99	67.16±12.17	138.46±27.35
SAP	55	68.47±7.19	4.21±1.58	199.53±19.32	645±99.17	7.68±2.14	4.58±1.76	43.28±9.04	93.16±19.24
Control	45	85.13±9.12	2.67±1.04	119±20.13	418±28.76	3.89±1.45	2.05±0.98	27.29±5.17	53.78±10.19
P value		0.0024	0.0031	0.0027	0.0025	0.0030	0.0033	0.0045	0.0019

(Mean±SD)

typical heart failure symptoms and signs requiring urgent treatment. The main cause of acute heart failure is acute myocardial ischemia, myocardial necrosis or deterioration of original ischemia, and the rupture of unstable coronary artery plaque, vasospasm or thrombosis are the main causes of acute myocardial ischemia. Active sympathetic nervous system, renin angiotensin aldosterone system, increase of vasopressin and endothelin, and activation of inflammatory proteins form a positive feedback loop (4, 5). In recent years, studies have shown that for some primary diseases that can be cured, the degree of decline in related hormones often reflects the severity of the disease (6). For incurable primary diseases, the prognosis can be judged according to the decreasing degree of related hormones (7). Studies have confirmed that the decrease of estrogen level can be used as a sensitive index to judge the severity of acute myocardial infarction (8). Recent studies have shown that the activation of inflammatory response may be an important factor leading to plaque instability, and inflammation plays an important role in the occurrence and development of coronary heart disease (9, 10). This study found that hs-CRP level in the ACS group was higher than that in the control group, suggesting that inflammation plays an important role in the pathogenesis of ACS. Estrogen, MMP-9, EPI, N, Ren, ang II, and Aldo were positively correlated with the severity of CAG. The above hormone levels can be used as indicators to evaluate the severity of CAG and the stability of plaque.

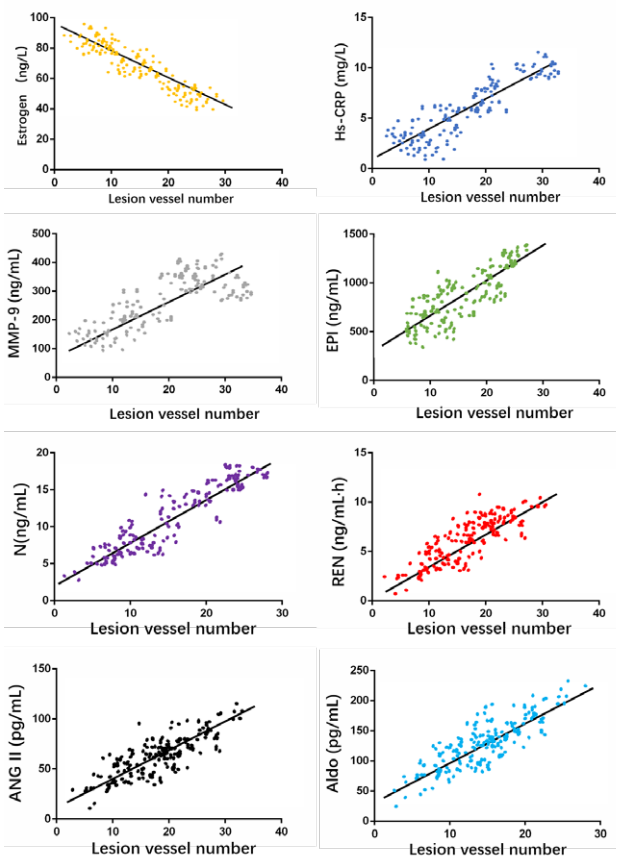


Fig. 1. *Correlation between numbers of coronary stenosis lesions and related hormone levels.*

ACKNOWLEDGEMENT

This work was supported by Zhejiang medical and health science and technology plan project in 2018 (2018KY746).

REFERENCES

1. Klein I, Danzi S. Thyroid Disease and the Heart. Circulation 2016; 41(2):65-92.
2. Tanai E, Frantz S. Pathophysiology of heart failure.

Compr Physiol 2015; 6(1):187-214.
3. Danzi S, Klein I. Thyroid hormone-regulated cardiac gene expression and cardiovascular disease. Thyroid 2002; 12(6):467-72.
4. Falkenham A, Saraswat MK, Wong C, et al. Recovery free of heart failure after acute coronary syndrome and coronary revascularization. ESC Heart Fail 2018; 5(1):107-14.
5. Cini G, Carpi A, Mechanick J, et al. Thyroid hormones and the cardiovascular system: pathophysiology and interventions. Biomed Pharmacother 2009; 63(10):742-53.
6. Yang L, Zou J, Zhang M, Xu H, Qi W, Gao L, Zhao J. The relationship between thyroid stimulating hormone within the reference range and coronary artery disease: impact of age. Endocr J 2013; 60(6):773-9.
7. Iervasi G, Pingitore A, Landi P, et al. Low-T3 Syndrome: A Strong Prognostic Predictor of Death in Patients With Heart Disease. Circulation 2003; 107(5):708-13.
8. Mulvihill NT, Foley JB, Murphy R, Crean P, Walsh M. Evidence of prolonged inflammation in unstable angina and non-Q wave myocardial infarction. J Am Coll Cardiol 2000; 36(4):1210-16.
9. Chew DP, Bhatt DL, Robbins MA, et al. Incremental prognostic value of elevated baseline C-reactive protein among established markers of risk in percutaneous coronary intervention. Circulation 2001; 104(9):992-7.
10. Khafaji HA, Bener A, Osman M, Al Merri A, Al Suwaidi J. The impact of diurnal fasting during Ramadan on the lipid profile, hs-CRP, and serum leptin in stable cardiac patients. Vasc Health Risk Manag 2012; 8:7-14.

LETTER TO THE EDITOR

A comparative study of dexmedetomidine in combination with midazolam and dexmedetomidine alone for sedation during spinal anesthesia

XL. Sun, L. Sun, WX. Sun, XL. Zong

Department of Anesthesia, Zibo Central Hospital, Zibo, Shandong Province, China

Received June 12, 2020 - Accepted October 29, 2020

To the Editor,

Patients with spinal anesthesia usually need to be adequately sedated in order to reduce the stress response induced by noxious stimuli of surgery (1, 2). Midazolam is a commonly used sedative drug in clinical practice, but it may inhibit respiratory and circulatory functions of patients. In addition, it has an accumulative effect inducing delirium and leading to prolonged awakening time.

Dexmedetomidine is a highly selective α2-adrenoceptor agonist with both sedative and analgesic effects. Previous studies have shown that dexmedetomidine has no respiratory depression effects and reduced incidence of delirium (3, 4). In addition, intravenous (i.v.) administration of dexmedetomidine prolongs the duration of spinal anesthesia (5), therefore, it has been widely used for the sedation of patients during surgery. A variety of studies have demonstrated that dexmedetomidine provides effective sedation during endoscopy (6, 7), colonoscopy (8) and gastric endoscopic submucosal dissection (ESD) (9). However, operations requiring spinal anesthesia need deeper sedation compared to the above procedure. In addition, several studies have reported that dexmedetomidine induces severe bradycardia, which is usually related to the infusion of a large-dose (10).

The present study was therefore conducted to investigate whether Midazolam bolus loading of 0.05mg/kg followed by dexmedetomidine continuous infusion of 0.5μg/kg/h could achieve better sedative effects compared to the traditional dexmedetomidine alone method.

MATERIALS AND METHODS

Study design

The present study was performed in accordance with the Declaration of Helsinki. The study protocol was reviewed and approved by the Medical Ethics Committee of Zibo Central Hospital. The patients signed written informed consent to participate in the present study, and a total of 60 patients scheduled to undergo surgery under spinal anesthesia between March 2019 and December 2019 were enrolled. The inclusion criteria included: age 20 ~ 60 years; body mass index (BMI) 21 ~ 25 kg/m^2; Acute Physiology and Chronic Health Evaluation (APACHE) II score 10 ~ 25. Exclusion criteria included: renal insufficiency; bradycardia; central nervous system diseases. The patients were randomly divided into two groups: a dexmedetomidine combined with midazolam group (Group DM, n=30) and a dexmedetomidine alone group (Group D, n=30).

Anesthesia methods

On arrival at the operating room, routine monitoring with an electrocardiogram, a pulse oximeter, and a non-invasive blood pressure cuff was performed. Patients' initial

Key words: dexmedetomidine; midazolam; sedation; spinal anesthesia

Corresponding Author:
Xiaoling Zong,
Department of Anesthesia, Zibo Central Hospital,
54 Gongqingtuan West Road,
Zhangdian District, Zibo City 255000,
Shandong Province, China
e-mail: qiaodunlin51234@163.com

0393-974X (2020)
Copyright © by BIOLIFE, s.a.s.
This publication and/or article is for individual use only and may not be further reproduced without written permission from the copyright holder.
Unauthorized reproduction may result in financial and other penalties
DISCLOSURE: ALL AUTHORS REPORT NO CONFLICTS OF INTEREST RELEVANT TO THIS ARTICLE.

vital signs and Ramsay Sedation Scale (RASS) scores were recorded. Spinal anesthesia was performed in the lateral decubitus position with a 25-gauge Quincke needle by using a midline approach at the L2–3 or L3–4 interspace; 0.5% bupivacaine was infused intrathecally, the amount of which was determined according to the patient's age and height to reach a target sensory level.

For the patients in Group MD, 10 min after receiving a bolus dose of 0.05mg/kg of midazolam (T2), the i.v. infusion of dexmedetomidine (Precedex ; Hospira, Rocky Mount, NC, USA, 200 μg/2 ml) at 0.5 μg/kg/h as a maintenance dose was initiated. For the patients in Group D, 1μg/kg of dexmedetomidine was i.v.-loaded via an infusion pump for 10 min, and then the i.v. infusion of dexmedetomidine at 0.5μg/kg/h as a maintenance dose was initiated. The vital signs, RASS scores, bradycardia, and hypotension were monitored and recorded at 30-min intervals. Hypotension was defined as a mean blood pressure (MBP) of less than 60 mmHg, and 4 mg of ephedrine was IV-infused upon detection of hypotension. Bradycardia was defined as a heart rate (HR) of less than 45 beats/min, and 0.5 mg of atropine was i.v.-infused upon incidence of bradycardia.

Evaluation indicators

After the surgery, the surgeons' satisfaction with sedation was evaluated using a self-report questionnaire comprising three options including very satisfied, satisfied, and not satisfied. In addition, the awakening time and incidences of delirium and re-sleeping within 2 hours after the end of sedation were also recorded. The postoperative pain was evaluated using modified objective pain score (MOPS): 0 point=painless, 1-3 points=mild pain, 4-6 points=moderate pain, and 7-10 points=severe

Table I. *Characteristics of study subjects*

	Group MD (n=30)	**Group D (n=30)**	***p* value**
Gender (n, %)			0.09
Male	16 (53.3%)	13 (43.3%)	
Female	14 (46.7%)	17 (56.7%)	
Age (years), mean±SD	45.7±12.7	46.5±11.7	0.29
Weight (kg), mean±SD	63.8±9.7	62.5±10.5	0.54
Height (cm), mean±SD	165.5±9.5	169.3±8.8	0.96
BMI(kg/m^2), mean±SD	23.5±2.5	22.7±3.7	0.35
APECHE II score, mean±SD	18.4±1.9	18.7±2.5	0.12
Level of sensory block (T10=10, L1=12+1)	9.28±2.15	8.75±2.27	0.13
Comorbidities (n, %)			0.17
Pneumonia	8 (26.7%)	9 (30.0%)	
COPD	11 (36.7%)	10 (33.3%)	
CHD	9 (30.0%)	8 (26.7%)	
Multiple fractures	2 (6.6%)	3 (10.0%)	

BMI: Body mass index; APACHE: Acute Physiology and Chronic Health Evaluation; Levels of sensory block are presented as T10=10, L1=12+1, L2=12+2; COPD: chronic obstructive pulmonary diseases; CHD: coronary heart disease

Table II. *Comparison of satisfaction rate of the two groups*

	Group MD (n=30)	Group D (n=30)	*p* value
Very satisfied (n, %)	21 (70.0%)	12 (40.0%)	
Satisfied (n, %)	6 (20.0%)	8 (26.7%)	
Not satisfied (n, %)	3 (10.0%)	10 (33.3%)	
Satisfaction rate (n, %)	27 (90.0%)	20 (66.7%)	0.006

pain at the time of postoperative awakening (T1), 30 min after awakening (T2), 1 h after awakening (T3), and 3 h after awakening (T4).

Statistical analysis

Statistical analysis was performed by the SPSS for Windows version 17.0 (SPSS, Chicago, IL). Data were presented as number (percentage), mean (SD), depending on the types of the data. Differences between groups were tested using one-way ANOVA for continuous variables, and Fisher's exact test or *Chi*-squared test for categorical variables. A two-sided p-value <0.05 was considered statistically significant.

RESULTS

As shown in Table I, a total of 60 patients scheduled to undergo surgery under spinal anesthesia between March 2019 and December 2019 were enrolled in the present study. No significant differences were found between the patients' age, gender, height, weight, BMI, APACHE II score, level of sensory block, and comorbidities.

As shown in Tables II, III and IV, compared with Group D, more surgeons in Group MD were very satisfied with the sedative effects. In addition, the awakening time was significantly shortened, and the incidences of delirium and re-sleeping within 2 hours after the end of sedation were significantly decreased in Group MD (all $p<0.05$). The incidences of bradycardia and hypotension did not differ statistically between the two groups (both $p>0.05$). A total of 8 patients in group MD and 9 patients in group D had bradycardia, which was resolved after the i.v. administration of 0.5 mg atropine (Table III). A total of 8 patients in group MD and 4 patients in group D had hypotension, which was corrected after the i.v. administration of 4 mg ephedrine (Table III).

There were significant differences in MOPS between the two groups at T1-T4 after surgery (all

Table III. *Sedation-related side-effects during surgery and after surgery*

	Group MD (n=30)	Group D (n=30)	*p* value
Bradycardia (HR<45)	8 (26.7%)	9 (30.0%)	0.714
Hypotension (MBP<60)	8 (26.7%)	4 (13.3%)	0.089
Delirium	0 (0.0)	10 (33.3)	<0.001
Nausea	2 (6.7%)	3 (10.0%)	1.000
Vomiting	0 (0.0)	0 (0.0)	-
Paradoxical behavior	0 (0.0)	0 (0.0)	-

Table IV. *The awakening time and re-sleeping rate within 2 hours after the end of sedation*

	Group MD (n=30)	Group D (n=30)	*p* value
Awakening time (min), mean±SD	28.3±4.5	81.9±9.3	0.014
Re-sleeping (n, %)	0 (0.0)	10 (33.3%)	<0.001

Table V. *The comparison of MOPS between the two groups at each time point after surgeries.*

	Group MD (n=30)	Group D (n=30)	*p* value
T1	$1.13\pm0.25^{\#\Delta\dagger}$	$1.35\pm0.27^{\#\Delta\dagger}$	<0.001
T2	$1.69\pm0.21^{\#\Delta}$	$1.98\pm0.32^{\#\Delta}$	<0.001
T3	$2.58\pm0.27^{\#}$	$2.75\pm0.36^{\#}$	0.025
T4	3.03±0.15	3.65±0.17	<0.001

 # p< 0.05, compared to T4; ∆ p< 0.05, compared to T3; † p< 0.05, compared to T2

$p < 0.05$). The MOPS at T1-T3 were significantly lower than that at T4 (all $p< 0.05$). The MOPS at T1 and T2 were significantly lower than that at T3 (all $p< 0.05$). The MOPS at T1 was significantly lower than that at T2 ($p< 0.05$). The MOPS of Group MD were significantly lower than those in Group D at each time point after surgeries (all $p< 0.05$) (Table V and Fig, 1).

DISCUSSION

We found that for patients with spinal anesthesia, midazolam bolus followed by dexmedetomidine continuous infusion demonstrated better sedative effects than dexmedetomidine only. Compared with dexmedetomidine only, a higher percentage of surgeons were satisfied with the sedative effects induced by dexmedetomidine combined with midazolam.

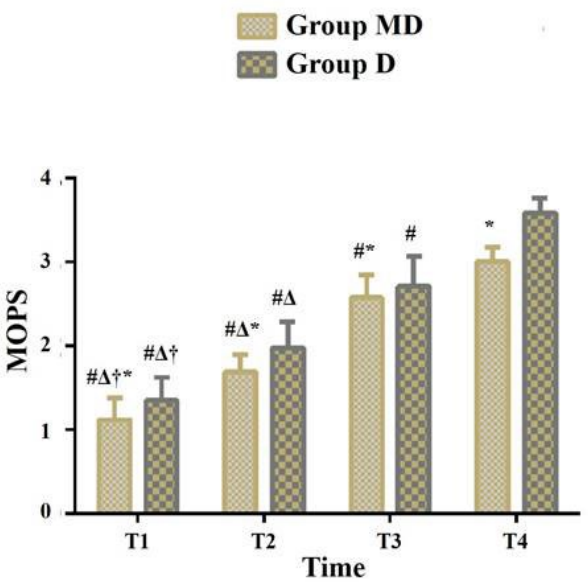


Fig. 1. *The comparison of MOPS between the two groups at each time point after surgery. The MOPSs at T1-T3 were significantly lower than that at T4 (all p < 0.05). The MOPSs at T1 and T2 were significantly lower than that at T3 (all p < 0.05). The MOPS at T1 was significantly lower than that at T2 (p < 0.05). The MOPSs of Group MD were significantly lower than those in Group D at each time point after surgeries (all p < 0.05). # p< 0.05, compared to T4; Δ p< 0.05, compared to T3; † p< 0.05, compared to T2; * p< 0.05, compared to Group D.*

Because dexmedetomidine can induce side effects such as hypotension and bradycardia, we did not include patients with preexisting bradycardia in the present study. In addition, the t study was aimed to evaluate and compare the sedative effects of dexmedetomidine combined with midazolam, and dexmedetomidine only, therefore patients with preexisting central nervous system diseases were also excluded. In China, due to its short latency to sedation and effectiveness in maintaining sedation, midazolam remains one of the major sedative choices during surgery (11). However, in many cases, especially those with heavy alcohol-drinking habits, midazolam usually cannot achieve sufficient sedation. The underlying mechanism could be that the activity of cytochrome P450 enzyme is usually increased in the population with heavy alcohol-drinking habits. Therefore, as a member of benzodiazepines, midazolam is hyper-metabolized, thus becomes ineffective for those patients. A combination of dexmedetomidine with midazolam was therefore chosen, the latter providing a hypnotic effect during sedation. This combination of drugs provided the desired sedative effect to ease patients' anxiety and discomfort.

In conclusion, we demonstrated in the present study that for patients with spinal anesthesia, midazolam bolus followed by dexmedetomidine continuous infusion demonstrated better sedative effects than dexmedetomidine only. The combination successfully provided satisfactory results for the majority of surgeons.

REFERENCES

1. Prabhakar H, Mahajan C, Kapoor I. Anesthesia for minimally invasive neurosurgery. Curr Opin Anaesthesiol 2017; 30(5):546-50.
2. Kokki H. Spinal blocks. Paediatr Anaesth. 2012; 22(1):56-64.
3. Gerlach AT, Dasta JF. Dexmedetomidine: an updated review. Ann Pharmacother 2007; 41(2):245-54.
4. Chiu TH, Chen MJ, Yang YR, Yang JJ, Tang FI. Action of dexmedetomidine on rat locus coeruleus neurones: intracellular recording in vitro. Eur J Pharmacol 1995; 285(5):261-68.

5. Elcicek K, Tekin M, Kati I. The effects of intravenous dexmedetomidine on spinal hyperbaric ropivacaine anesthesia. J Anesth 2010; 24(4):544-48.
6. Hashiguchi K, Matsunaga H, Higuchi H, et al. Dexmedetomidine for sedation during upper gastrointestinal endoscopy. Dig Endosc. 2008; 20:178-83.
7. Demiraran Y, Korkut E, Tamer A, Yorulmaz I, Kocaman B, Sezen G, Akcan Y. The comparison of dexmedetomidine and midazolam used for sedation of patients during upper endoscopy: a prospective, randomized study. Can J Gastroenterol 2007; 21(1):25-29.
8. Jalowiecki P, Rudner R, Gonciarz M, Kawecki P, Petelenz M, Dziurdzik P. Sole use of dexmedetomidine has limited utility for conscious sedation during outpatient colonoscopy. Anesthesiology 2005; 103(2):269-73.
9. Takimoto K, Ueda T, Shimamoto F, et al. Sedation with dexmedetomidine hydrochloride during endoscopic submucosal dissection of gastric cancer. Dig Endosc 2011; 23(2):176-81.
10. Vuyk J, Sitsen E, Reekers M. Intravenous anesthetics. In: Miller's Anesthesia. 8th ed. Edited by Miller RD: Philadelphia, Churchill Livingstone/Elsevier. 2015, pp 854-58.
11. Kato M, Nishida T, Yamamoto K, et al. Scheduled endoscopic surveillance controls secondary cancer after curative endoscopic resection for early gastric cancer: a multicentre retrospective cohort study by Osaka University ESD study group. Gut. 2013; 62(10):1425-32.

LETTER TO THE EDITOR

Effect of general anesthesia combined with epidural anesthesia on cognitive function, stress response and NLR after radical mastectomy

HL. Xue[1], ZK. Liu[2], LL. Wang[3], Z. Meng[4], JX. Du[5] and YL. Li[1]

[1]Medical Examination Center, Qingdao West Coast New Area Central Hospital, Qingdao, China; [2]Department of Pain Clinic, People's Hospital of Chiping, Chiping, China; [3]Department of Critical Care Medicine, Qingdao Central Hospital, Qingdao University, Qingdao, China; [4]Department of Ultrasound, The People's Hospital of Zhangqiu Area, Jinan, China; [5]Department of Neurology, The People's Hospital of Zhangqiu Area, Jinan, China

Received May 22, 2020 – Accepted October 29, 2020

To the Editor,

Breast cancer is a common malignant tumor which threatens women's health, with considerably high morbidity (1). At present, the clinical treatments of breast cancer mainly include surgery and chemoradiotherapy as well as other comprehensive treatments (2). However, it has been reported that anesthesia in trauma surgery could affect the postoperative recovery of patients (3). The activation of inflammatory response in patients contributes to a positive effect on growth, metastasis and infiltration of breast cancer, as well as some other biological processes. Neutrophil-to-lymphocyte ratio (NLR) in peripheral blood functions as a non-specific systemic inflammatory indicator, which is of importance to estimate inflammatory responses in patients. High levels of NLR indicate poor prognosis of patients with breast cancer (4). Anesthesia methods may have certain effects on levels of leukocytes, neutrophils and lymphocytes in peripheral blood (5).

In order to identify an ideal anesthesia method for patients who received radical mastectomy, this study determined the effects of general intravenous anesthesia and intravenous-inhalational anesthesia on cognitive function, stress response and NLR levels of patients who received radical mastectomy.

MATERIALS AND METHODS

Study subjects

In this study, 126 patients, who received radical mastectomy in Qingdao West Coast New Area Central Hospital, were enrolled. All the patients were female, and the average age was (45.19±7.36) years, with BMI index less than 25. Patients were randomly divided into 2 groups according to different anesthesia methods. Sixty-five patients who received general anesthesia combined with epidural anesthesia were in group A. Sixty-one patients who received general anesthesia were in group B. All the patients received laparoscopic radical mastectomy. There was no significant difference in age, BMI, tumor staging and other aspects of patients between the two groups (p>0.05) (Table I).

Inclusion criteria: Patients were diagnosed with breast cancer by pathology and planned to receive radical mastectomy; the age of patient was from 35 to 55 years; BMI index was less than 25. Exclusion criteria: Patients with severe liver dysfunction and kidney dysfunction; patients with severe immune diseases; patients with

Key words: cognitive function; general anesthesia combined with epidural anesthesia; neutrophil to lymphocyte ratio; radical mastectomy; stress response

Corresponding Author:
Dr Yanli Li,
Medical Examination Center,
Qingdao West Coast New Area Central Hospital,
9 Huangpujiang Road, Qingdao 266555, China
Tel.: +86 053286895767
e-mail: af19bf@163.com

0393-974X (2020)
Copyright © by BIOLIFE, s.a.s.
This publication and/or article is for individual use only and may not be further reproduced without written permission from the copyright holder.
Unauthorized reproduction may result in financial and other penalties
DISCLOSURE: ALL AUTHORS REPORT NO CONFLICTS OF INTEREST RELEVANT TO THIS ARTICLE.

coagulopathy; patients who were allergic to anesthetic medicines; patients who took hormonal medicines during the 24 h prior to surgery; patients who did not cooperate with the examination; patients with communication disorder and cognitive disorder. All the subjects and their family members agreed to participate in the study, and signed the informed consent form. This study was approved by the ethics committee of the hospital.

Anesthesia methods

The patients were not allowed food or drink for 8 h before surgery. The patients in group A were anesthetized by general anesthesia combined with epidural anesthesia. After the patients entered the operating room, they received routine examinations, including blood pressure and ECG monitoring. Then the position between the third thoracic vertebra and the fourth thoracic vertebra was punctured, and 6~7 ml of 1% lidocaine (Xi'an Tecenet Biological Pharmaceutical Co., Ltd., SFDA approval number: H61020713) was injected before general anesthesia induction. Next, the patients were anesthetized by general anesthesia. Intravenous infusion of Ringer's solution

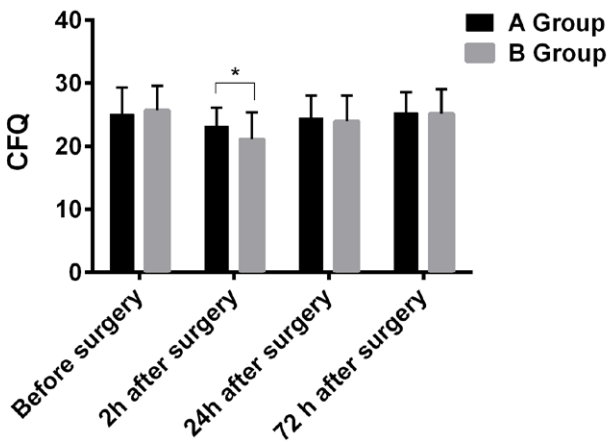


Fig. 1. *Comparison of CFQ scores of the patients in two groups before and after the operation. There was no significant difference in CFQ scores of the patients in the two groups before surgery (p>0.05). Although CFQ scores of the patients in both groups 2 h after surgery were lower than those before the operation, the decrease of CFQ scores of the patients in group B was greater than that in group A. CFQ scores of the patients in both groups increased gradually 24 h and 72 h after surgery compared to those in 2 h after the operation, then the CFQ scores returned to the preoperative level 72 h after the operation. * p<0.05.*

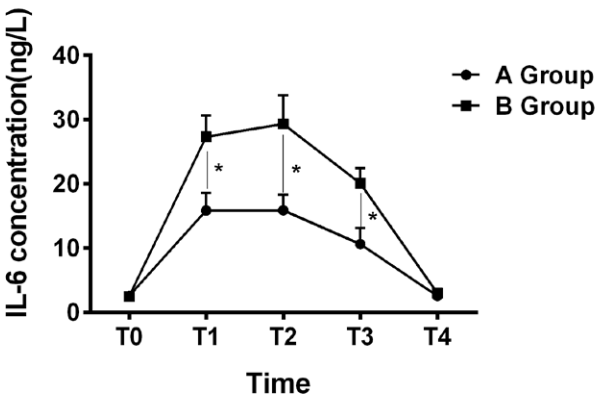


Fig. 2. *Comparison of the levels of IL-6 of the patients in the two groups at different time points. ELISA showed that there was no significant difference in the level of IL-6 of the patients in either group at T0 (p>0.05), but the levels of IL-6 at T1, T2 and T3 were significantly higher than those at T0 (p<0.05). The levels of IL-6 of the patients in group A at T1, T2, and T3 were significantly lower than those of the patients in group B. The differences were statistically significant (p<0.05). The level of IL-6 of the patients in both groups returned to the preoperative level at T4. * p<0.05.*

was performed. The medication of anesthesia induction contained midazolam (Jiangsu Enhwa Pharmaceutical Group Co., Ltd., SFDA approval number: H10980025) 0.05 mg/kg, propofol (Beijing Feisen Yousikabi Pharmaceutical Co., Ltd., approval number: J20040122) 2 mg/kg, vecuronium (Yichang Humanwell Pharmaceutical Co., Ltd., SFDA approval number: H20133079) 0.15 mg/kg, and fentanyl (Yichang Humanwell Pharmaceutical Co., Ltd., SFDA approval number: H20054172) 3 μg/kg. After the anesthesia, induction was continued for 3 min, a cannula was inserted into the patient's trachea, and mechanical ventilation was carried out. Oxygen flow was 1.5 L/min, and tidal volume was 8 ml~10 ml/kg. Maintenance stage: micro pump was filled with propofol [1 mg~2 mg/(kg·min)] and fentanyl [0.5 μg~1 μg/(kg·mg)]. The dosage of the medicines was monitored and adjusted according to the vital signs of the patients during the operation. Approximately 20-30 min before the end of surgery, the medication of anesthesia was suspended. Patients in group B were treated with general intravenous anesthesia, and the procedure was similar to that used for group A.

Biomarker assessments

Cognitive function of the patients was assessed by a

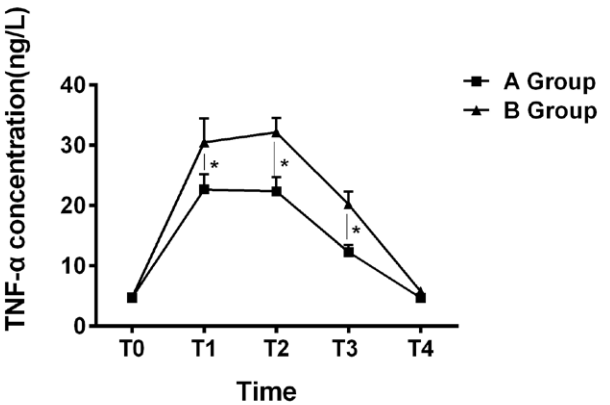


Fig. 3. *Comparison of the levels of TNF-α of the patients in two groups at different time points. ELISA showed that there was no significant difference in the level of TNF-α of the patients in the two groups at T0 ($p>0.05$), but at T1, T2 and T3 the levels were significantly higher than those at T0 ($p<0.05$). The levels of TNF-α of the patients in group A at T1, T2, and T3 were significantly lower than those of the patients in group B. The differences were statistically significant ($p<0.05$). The level of TNF-α of the patients in the two groups returned to the preoperative level at T4. * $p<0.05$.*

questionnaire (CFQ) before the operation, and 2 h, 24 h, 72 h after the operation. When the patients' postoperative CFQ evaluation results no more than 2, their cognitive ability was considered to be recuperative. (2) Venous blood of patients in the two groups was collected before the patients were anesthetized (T0), 2 h after skin incision (T1), and 12 h (T2), 24 h (T3), and 72 h (T4)after surgery. The concentrations of IL-6 and TNF-α were detected by ELISA in strict accordance with the manufacturer's instructions (Shanghai Hengyuan Biotechnology Development Co., Ltd.). NLR: 3 ml of venous blood of the patients was collected 3 days before and 24 h after surgery. The number of neutrophils and lymphocytes was measured by Mindray BC-5000 automatic blood cell analyzer. The operations were carried out in strict accordance with the instructions of the analyzer. The levels of neutrophils, lymphocytes and NLR in peripheral blood of patients in the two groups were observed and compared. The adverse reactions, including back pain, nausea, vomiting and dizziness, within 3 days after surgery were recorded and compared. The total dose of fentanyl and postoperative extubation time were recorded and compared between the two groups.

Statistical analysis

SPSS18.0 software was used to carry out statistical analysis. The measurement data were expressed in the form of mean value ± standard deviation. *t*-test was used for comparison between the two groups. Repeated measurement analysis of variance was used in the comparison among different time points. Paired *t*-test was used in the comparison before and after the operation. The count data were analyzed by *chi*-squared test. $p<0.05$ was considered to be statistically significant.

RESULTS

There was no significant difference in CFQ scores between the two groups of patients before surgery ($p>0.05$). Although CFQ scores of the patients in the two groups at 2 h after the operation were lower than those before surgery, the scores of the patients in group B was significantly lower than that in group A ($p<0.05$). CFQ scores of the patients in the two groups were increased gradually at 24 h and 72 h after the operation compared to those at 2 h after surgery. Additionally, the CFQ scores returned to the preoperative level at 72 h after the operation (Table II and Fig. 1).

There was no significant difference in levels of IL-6 and TNF-α between the patients of the two groups at T0 ($p>0.05$), but levels of IL-6 and TNF-α in both groups at T1, T2 and T3 were significantly elevated compared to those at T0 ($p<0.05$). Levels of IL-6 and TNF-α of group A at T1, T2 and T3 were significantly lower than those of group B at T1, T2 and T3 ($p<0.05$). Levels of IL-6 and TNF-α in both groups returned to the preoperative level at T4 (Figs. 2 and 3).

There was no significant difference in levels of neutrophils, lymphocytes and NLR in eithergroups. The number of neutrophils in the two groups at 24 h after surgery was significantly higher than that before surgery ($p<0.05$), but the increase in group B was more evident than in group A ($p<0.05$). There was no significant difference of lymphocytes between group A after the operation and that before surgery ($p>0.05$), but the level of lymphocytes of group B at 24 h after the operation was significantly lower than that before surgery ($p<0.05$). NLR in both groups after surgery was significantly higher than that before the operation, but the NLR of group B was significantly increased

Table I. *General data of the patients in the two groups [(n), %]*

Factors	Group A (n=65)	Group B (n=61)	t/χ^2	*p*
Age(year old)			0.066	0.797
≤45	27(41.54)	25(40.98)		
>45	38(58.46)	36(59.02)		
BMI(kg/m^2)			0.005	0.996
≤ 21	32(49.23)	30(49.18)		
>21	33(50.77)	31(50.82)		
Pathological types			0.020	0.990
Carcinoma in situ	21(32.31)	20(32.79)		
Invasive lobular carcinoma	21(32.31)	19(31.15)		
Invasive ductal carcinoma	23(35.38)	22(36.07)		
Pathological grading			0.014	0.993
Grading I	31(47.69)	29(47.54)		
Grading II	24(36.92)	23(37.70)		
Grading III	10(15.38)	9(14.75)		
Staging [n(%)]			0.010	0.920
Staging I ~ II	41(63.08)	39(63.93)		
Staging III	24(36.92)	22(36.07)		
Liver function indicators				
Serum total protein (g/L)	72.56±2.31	72.32±2.50	0.560	0.576
glutamic-pyruvic transaminase(μmol/L)	28.20±4.46	28.34±4.56	0.174	0.862
Total bilirubin (μmol/L)	11.42±2.10	11.44±2.13	0.053	0.958
Renal function indicators				
Creatinine(μmol/L)	67.89±4.46	68.20±4.43	0.391	0.696
Serum urea(μmol/L)	5.24±0.72	5.26±0.74	0.154	0.878
Uric acid (μmol/L)	280.12±10.93	282.52±12.12	1.169	0.245

compared to that of group A ($p<0.05$, Table II). In group A, there were 2 patients with nausea, 2 with vomiting, 1 with dizziness, and 2 with back pain, and the overall incidence of adverse reactions was 10.77%. In group B, there were 4 patients with nausea, 3 with vomiting, 4 with dizziness, and 4 with back pain, and the general incidence of adverse reactions was 24.59%. The incidence of adverse reactions in group A was significantly lower than that in group B ($p<0.05$, Table II). The dose of fentanyl and the time of extubation were significantly lower in group A than those in group B ($p<0.05$, Table II).

Table II. *The CFQ scores, levels of neutrophils, lymphocytes, NLR, postoperative adverse reactions, fentanyl dose and postoperative extubation time of the patients in two groups before and after the operation*

	Time	Group A (n=65)	Group B (n=61)	t	*p*
CFQ scores	Before the operation	25.11±4.23	25.71±3.91	0.825	0.412
	2 hours after the operation	23.19±2.91	21.12 ±4.31	3.178	<0.05
	24 hours after the operation	24.56±3.51	23.98±4.12	0.852	0.396
	72 hours after the operation	25.31±3.32	25.17±3.87	0.218	0.828
	F	4.779	15.56	-	-
	p	<0.05	<0.05	-	-
Neutrophils ($\times 10^3$ /mL)	In 3 days before the operation	3.39±0.31	3.41±0.34	0.345	0.730
	In 24 hours after the operation	7.74±0.59	9.21±0.41	16.14	<0.05
	t	2.62	5.05		
	p	<0.001	<0.001		
Lymphocytes ($\times 10^3$ /mL)	In 3 days before the operation	1.98±0.29	1.97±0.26	0.203	0.839
	In 24 hours after the operation	2.01±0.43	0.96±0.23	16.93	<0.05
	t	0.466	2.72		
	p	0.642	<0.001		
NLR	In 3 days before the operation	1.71±0.11	1.73±0.14	0.895	0.373
	In 24 hours after the operation	3.85±0.28	9.59±0.21	129.5	<0.001
	t	7.35	3.21		
	p	<0.001	<0.001		
postoperative adverse reactions	Nausea	2(3.08)	4(6.56)	-	-
	Vomiting	2(3.08)	3(4.92)	-	-
	Dizziness	1(1.54)	4(6.56)	-	-
	Back pain	2(3.08)	4(6.56)	-	-
	Adverse reaction rate	7(10.77)	15(24.59)	4.171	0.041
fentanyl dose and postoperative extubation time	fentanyl dose (ug/kg)	10.56±3.16	19.22±4.26	13.01	<0.001
	postoperative extubation time(min)	35.91±8.42	96.32±13.28	30.72	<0.001

DISCUSSION

Breast cancer represents as one of the most common life-threatening malignant tumors for women (6). Radical mastectomy is considered to be an effective treatment, and can obviously improve the clinical efficacy and prognosis of patients (7). Different methods of anesthesia have different impacts on the patient's cognitive function, which could increase medical costs, delay recovery, and even severely affect the life quality of the patient after surgery (8). The results of the present study suggest that epidural anesthesia combined with general anesthesia has little effect on stress response of patients compared to general anesthesia. Previous studies have shown that epidural anesthesia combined with general anesthesia can block the patient's sympathetic excitability and reduce the patient's stress response during surgery (9), which is in line with the conclusion of the present study. General anesthesia is able to transmit and inhibit the stimulation from the operative site to the central nervous system, but it cannot effectively control the intraoperative stress response (10).

It has been shown that NLR is one of the risk factors for poor prognosis of the patient with breast cancer (11). The increase of NLR often indicates the increase of neutrophils or the decrease of lymphocytes. Our results revealed that NLR of the patients in both groups after surgery was significantly higher than before the operation, but NLR in group B was significantly lower than that of group A, suggesting that epidural anesthesia combined with general anesthesia has little effect on inflammatory response of patients compared to general anesthesia. Consistently, anesthesia cannot effectively reduce the intraoperative stress response, and can even lead to immunosuppression with different degrees.

REFERENCES

1. Conant EF, Beaber EF, Sprague BL, et al. Breast cancer screening using tomosynthesis in combination with digital mammography compared to digital mammography alone: A cohort study within the PROSPR consortium. Breast Cancer Res Treat 2016; 156:109-16.
2. Plesca M, Bordea C, El Houcheimi B, Ichim E, Blidaru A. Evolution of radical mastectomy for breast cancer. J Med Life 2016; 9:183-86.
3. Berkowitz AC, Ginsburg AM, Pesso RM, Angus GL, Kang A, Ginsburg DB. Comparison of intraoperative ketamine vs. fentanyl use decreases postoperative opioid requirements in trauma patients undergoing cervical spine surgery. Middle East J Anaesthesiol 2016; 23:415-20.
4. Murugappan K, Saboo A, Kuo L, Ung O. Paradigm shift in the local treatment of breast cancer: mastectomy to breast conservation surgery. Gland Surg 2018; 7:506-19.
5. Jones C, Lancaster R. Evolution of operative technique for mastectomy. Surg Clin North Am 2018; 98:835-44.
6. De Paula JJ, Costa DS, Miranda DM. Brazilian version of the Cognitive Failures Questionnaire (CFQ): cross-cultural adaptation and evidence of validity and reliability. Braz J Psychiatry 2017; 40:312-15.
7. Jin G, Mao X, Qiao Z, Chen B, Jin F. RAP80 expression in breast cancer and its relationship with apoptosis in breast cancer cells. Onco Targets Ther 2019; 12:625-34.
8. El Mourad MB, Amer AF. Effects of adding dexamethasone or ketamine to bupivacaine for ultrasound-guided thoracic paravertebral block in patients undergoing modified radical mastectomy: a prospective randomized controlled study. Indian J Anaesth 2018; 62:285-91.
9. Hadimioglu N, Ulugol H, Akbas H, Coskunfirat N, Ertug Z, Dinckan A. Combination of epidural anesthesia and general anesthesia attenuates stress response to renal transplantation surgery. Transplant Proc 2012; 44:2949-54.
10. Li Y, Wang B, Zhang LL, He SF, Hu XW, Wong GT, Zhang Y. Dexmedetomidine combined with general anesthesia provides similar intraoperative stress response reduction when compared with a combined general and epidural anesthetic technique. Anesth Analg 2016; 122:1202-10.
11. Li Y, Shao Y, Bai L, Zhou X. Increased derived neutrophil-to-lymphocyte ratio and Breast Imaging-Reporting and Data System classification predict poor survival in patients with non-distant metastatic HER2+ breast cancer treated with neoadjuvant chemotherapy. Cancer Manag Res 2018; 10:3841-47.

LETTER TO THE EDITOR

Effects of ulinastatin combined with octreotide on blood coagulation function, inflammatory factors and amylase in patients with severe acute pancreatitis

Z-F. Li[1], M-Y. Xu[2], D-H. Zhang[3], T-T. Gao[4], Z. Gao[5] and H. Li[6]

[1]Emergency Department, Weifang People's Hospital, Weifang, China; [2]Clinical Laboratory, People's Hospital of Rizhao, Rizhao, China; [3]Chemotherapy Department, the People's Hospital of Zhangqiu Area, Jinan, China; [4]Department of Nephrology, The People's Hospital of Zhangqiu Area, Jinan, China; [5]Department of Rehabilitation, the People's Hospital of Zhangqiu Area, Jinan, China; [6]No 2 Department of Gynaecology, Weifang People's Hospital, Weifang, China

Received June 11, 2020 – Accepted October 30, 2020

To the Editor,

Acute pancreatitis (AP) is one of the common acute abdomen diseases in the digestive system (1). There are multiple factors for the abnormal activation of pancreatic enzymes in the pancreas which result in self-digestion, edema, bleeding, and even necrosis in pancreatic tissues (2). Clinically, AP is divided into mild AP (MAP) and severe AP (SAP) (3). SAP is characterized as a disease with rapid progression and high mortality and mainly manifests as multiple organ failure. Clinically, the effect of single drug therapy is unsatisfactory compared to combined therapy (4). Octreotide is a synthetic somatostatin analogue that resembles the native polypeptide, which has the pharmacological function of natural somatostatin (5). Octreotide reduces secretion of pancreatic digestive enzymes and pancreatic juice by inhibiting the secretion of gastrin, cholecystokinin, glucagon, secretin and pancreatin. In addition, octreotide also facilitates intestinal peristalsis, relieves abdominal pain, and regulates hemodynamic abnormalities to a certain extent (6). Ulinastatin is a polypeptide glycoprotein isolated and purified from human urine (7). Ulinastatin has a broad-spectrum enzyme inhibitory effect and anti-inflammatory effects, so it is used to treat AP. Ulinastatin can effectively inhibit cytokines such as interleukin (IL)-8 and tumor necrosis factor alpha (TNF-α), and can also inhibit the release of inflammatory mediators by blocking the fluidity of biological lipid membranes (8, 9). In this study, 60 SAP patients admitted to Weifang People's Hospital were selected as the research subjects, in order to explore the clinical effect of SAP combined with ulinastatin and octreotide.

MATERIALS AND METHODS

Study subjects

Sixty patients who met the SAP diagnostic criteria from March 2016 to October 2018 in Weifang People's Hospital were selected as the research subjects, and were randomly divided into an observation group and a control group (n=30 in each). In the observation group, there were 18 males and 12 females, with an average age of 41.2 years. In the control group, there were 17 males and 13 females, with an average age of 42.9 years. This study was reviewed and approved by the Medical Ethics

Key words: acute pancreatitis; amylase; blood coagulation function; inflammatory factor; octreotide; ulinastatin

Corresponding Author:
Dr Hong Li,
No 2 Department of Gynaecology,
Weifang People's Hospital,
151 Guangwen Street,
Kuiwen District, Weifang 261041, China
e-mail: weifanglh2019@126.com

0393-974X (2020)
Copyright © by BIOLIFE, s.a.s.
This publication and/or article is for individual use only and may not be further reproduced without written permission from the copyright holder.
Unauthorized reproduction may result in financial and other penalties
DISCLOSURE: ALL AUTHORS REPORT NO CONFLICTS OF INTEREST RELEVANT TO THIS ARTICLE.

Committee of Weifang People's Hospital. All patients and their families understood the contents of this study and signed an informed consent.

Each enrolled patient was evaluated according to the Acute Physiology and Chronic Health Evaluation (APACHE-II scores) and the Ranson scores. The inclusion criteria were patients who met the relevant standards in the "AP Diagnosis and Treatment Guidelines (2014)"; one of the following complications occurred within 7 hours after onset: shock, renal failure, respiratory failure, coagulopathy, sepsis, pancreatic abscess, pancreas and fat necrosis; patients who still had symptoms of systemic inflammatory response syndrome 24 hours after admission to the hospital; APACHEE II score reached 8 points on admission. The exclusion criteria were: allergy to the drugs used; diabetes, severe hypertension or blood diseases; AP caused by trauma or surgery; obstructive biliary, autoimmune, and pregnancy pancreatitis; severe liver and kidney dysfunction and combined with immune system diseases, infectious diseases, and digestive system diseases; pregnancy or lactation; intellectual disability; history of mental illness; and pancreatic tumor.

Therapy

Patients in the control group were given routine treatment after admission, including fasting, gastrointestinal decompression, suppression of pancreatic secretion, acid suppression, correction of water electrolytes and acid-base balance. Patients were given blood transfusion, organ system support, pain relief, and prophylactic antibiotics (ciprofloxacin and metronidazole or imipenem/cilastatin). At the same time, mechanical ventilation was conducted to treat respiratory distress syndrome. Patients with concomitant shock were treated with anti-shock therapy. Cardiotonic therapy was used on patients with concurrent heart failure.

Patients in the observation group were treated with octreotide (Hainan Zhonghe Pharmaceutical Co., Ltd., National Pharmaceutical Standard H20103210), ulinastatin (Guangdong Tianpu Biochemical Pharmaceutical Co., Ltd., National Pharmaceutical Standard H19990134) in combination with pantoprazole sodium (North China Pharmaceutical Co., Ltd., National Pharmaceutical Standard H20066495), on the basis of the control group. The specific usage was as follows, 0.3 mg octreotide was added to 50 ml of normal saline, and the micro-pump was pumped for 5 days at a speed of 4.2 ml/h. After that, the pumping was stopped, and subcutaneous injection was performed with 0.1 mg every 12 h, until the patient's indicators returned to normal. Ulinastatin was adopted at a dose of 100,000 units + 5% glucose, 250 ml intravenous infusion, 2 times/d. Once the patient improved significantly, the dose was adjusted to 50,000 units/time intravenous infusion, continuous treatment for 2 weeks. Pantoprazole sodium was administered intravenously, 40 mg each time, 2 times/d, and continued treatment for 1 week.

Detection of indicators

The blood coagulation function index, serum inflammatory factor index, amylase recovery time, APACHE domain score and treatment effect were measured before and after treatment. The level of immune index indicated the level of whole blood T-cell subsets, including CD4+, CD8+, CD4+/CD8+. The index of serum inflammatory factors reflects the inflammatory state, including TNF-α, interleukin (IL)-6, and IL-8, IL-10. The levels of CD4+, CD8+, CD4+/CD8+ of lymphocyte subsets were detected by flow cytometry, and the levels of TNF-α, IL-6, IL-8, and IL-10 were detected by ELISA. The APACHE domain score was used to assess the severity of systemic disease. The APACHE domain score system was composed of three parts: acute physiology score (APS), age score, and chronic health status score. The final score was the sum of the three, the highest theoretical score was 71 points. The score revealed the severity of the disease.

The evaluation criteria of treatment effects included significant effectiveness, effectiveness and ineffectiveness. Significantly effective: the patient's clinical symptoms and signs all disappeared; abdominal CT showed that the pancreatic inflammatory exudation was completely absorbed, the shape of the pancreas improved significantly, and the blood routine and blood and urine amylase returned to normal. Effective: the patient's clinical symptoms and signs were significantly improved; abdominal CT showed that the pancreatic inflammatory exudation was significantly reduced compared with before treatment; the shape of the pancreas improved, mild edema, and serum amylase was about 500 U /L. Ineffective: the status of the patient did not meet the above standards after treatment or the condition deteriorated or the patient died. The total clinical effective rate = (significant effect + effective) number of cases/total number of cases.

Statistical analysis

SPSS 20.0 statistical software was used to analyze the data of this study. The measurement data was expressed as the mean according to the standard deviation, using *t*-test. *Chi*-squared test was used for enumeration data. P-values <0.05 were considered statistically significant.

RESULTS

The total clinical effective rate of the observation group was significantly higher than that of the control group (P <0.05) (Table I). Before treatment, there was no significant difference in the levels of CD4+, CD8+, CD4+/CD8+ between the two groups of patients (P> 0.05). After treatment, the CD4+ and CD4+/CD8+ levels of the two groups were higher than those before treatment, along with reduction of CD8+ level. Furthermore, the levels of CD4+ and CD4+/CD8+ in the observation group after treatment were statistically higher than those in the control group, along with significant decrease of CD8+ level (Table II).

Before treatment, no significant difference was found in the levels of TNF-α, IL-6, IL-8 and IL-10 between the two groups (P> 0.05). After treatment, the levels of TNF-α, IL-6, IL-8, and IL-10 in the two groups were significantly lower than before treatment, and the levels in the observation group were significantly reduced compared to those in the control group (P <0.05) (Table III).

After treatment, the levels of urinary amylase and blood amylase were significantly lower than before treatment (P <0.05). However, the urine amylase and blood amylase levels of the observation group were significantly lower than those of the control group (P <0.05) (Table IV). There was no statistically significant difference in APACHE II score between the two groups before treatment (P>

Table I. *Comparison of the total effective rate of treatment between the two groups of patients*

Groups	Cases	Significantly effective	Effective	Invalid	Treatment is always effective
Control group	30	14 (46.7)	8 (26.7)	8 (26.7)	22 (73.3)
Observation group	30	19 (63.3)	7 (23.3)	2 (6.7)	28 (93.3) *

*Compared with the control group, * P <0.05*

Table II. *Comparison of immune index levels between the two groups of patients before and after treatment*

Groups	Cases	CD4+(%)		CD8+(%)		CD4+(%)/ CD8+(%)	
		Before treatment	After treatment	Before treatment	After treatment	Before treatment	After treatment
Control group	30	41.2	47.6*	33.3	28.4*	1.3	1.8*
Observation group	30	40.8	53.5*#	32.8	22.6*#	1.3	2.4*#

*Compared with the same group before treatment, * P <0.05; compared with the control group after treatment, #P <0.05*

Table III. *Comparison of serum inflammatory factor indexes between two groups of patients before and after treatment*

Groups	Cases	TNF-α		IL-6		IL-8		IL-10	
		Before treatment	After treatment	Before treatment	After treatment	Before treatment	After treatment	Before treatment	After treatment
Control group	30	89.2	72.5*	77.1	41.5*	18.3	11.2*	40.1	18.1*
Observation group	30	88.9	61.3*#	76.8	27.6*#	18.6	6.6*#	39.8	12.4*#

*Compared with the same group before treatment, * P <0.05; compared with the control group after treatment, #P <0.05.*

Table IV. *Comparison of amylase level and APACHE II score before and after treatment*

Groups	Cases	TNF-α		IL-6		IL-8		IL-10	
		Before treatment	After treatment	Before treatment	After treatment	Before treatment	After treatment	Before treatment	After treatment
Control group	30	89.2	72.5*	77.1	41.5*	18.3	11.2*	40.1	18.1*
Observation group	30	88.9	61.3*#	76.8	27.6*#	18.6	6.6*#	39.8	12.4*#

*Compared with the same group before treatment, * P <0.05; compared with the control group after treatment, #P <0.05.*

0.05). The APACHE II score of the two groups of patients after treatment was markedly lower than that before treatment. The APACHE II score of the observation group after treatment was significantly reduced compared to that of the control group (P <0.05) (Table IV).

DISCUSSION

SAP accounts for 15-20% of the incidence of AP, and the mortality rate is as high as 30-40%. Multiple organ failure is the main cause of death (10). When SAP occurs, a large number of inflammatory factors can be produced, which leads to systemic proinflammation and dysfunction. In this scenario, inflammatory factors, reperfusion injury, pancreatic self-digestion and other factors can destroy the intestinal mucosal barrier function, and cause secondary infection and even sepsis (11).

Octreotide is a synthetic natural somatostatin, the pharmacological effect of which is similar to somatostatin. Ulinastatin can effectively improve tissue perfusion and microcirculation, thereby protecting the function of organs, and plays an important role in the treatment of SAP (12). The results of this study suggest that the total clinical effectiveness of the observation group was higher than that of the control group. The levels of CD4+ and CD4+/CD8+ in the observation group after treatment were apparently elevated compared to

those in the control group. The levels of TNF-α, IL-6, IL-8 and IL-10 in the observation group after treatment were significantly inhibited compared to those in the control group. The levels of urinary amylase and blood amylase, along with the APACHE domain score in the observation group after treatment was obviously lower than that of the control group, suggesting that the clinical effect of octreotide combined with ulinastatin in SAP patients was significantly improved compared to patients in the control group, which provides new leads for further therapy against SAP in clinical practice.

REFERENCES

1. Lankisch P, Apte M, Banks P. Acute pancreatitis. Lancet 2015; 386:85-96.
2. Liu HS, Pan CE, Liu QG, Yang W, Liu XM. Effect of NF-kappaB and p38 MAPK in activated monocytes/macrophages on pro-inflammatory cytokines of rats with acute pancreatitis. World J Gastroenterol 2003; 9:2513-18.
3. He F, Zhu HM, Li BY, Li XC, Yang S, Wang Z, Zhang M. Factors predicting the severity of acute pancreatitis in elderly patients. Aging Clin Exp Res 2020; [Online ahead of print]
4. Zhou X, Wang W, Wang C, et al. DPP4 Inhibitor attenuates severe acute pancreatitis-associated intestinal inflammation via Nrf2 signaling. Oxid Med Cell Longev 2019; 2019:6181754.
5. Mezazadeh O, Sadeghzadeh C. Effect of conformation on the photodegradation of Trp- and cystine-containing cyclic peptides: octreotide and somatostatin. Mol Pharm 2014; 11:3537-46.
6. Rezazadeh F, Sadeghzadeh N. Tumor targeting with Tc radiolabeled peptides: Clinical application and recent development. Chem Biol Drug Des 2019; 93:205-221.
7. Liu B, Huang W, Xiao X, Xu Y, Ma S, Xia Z. Neuroprotective effect of ulinastatin on spinal cord ischemia-reperfusion injury in rabbits. Oxid Med Cell Longev 2015; 2015:624819.
8. Shu H, Liu K, He Q, et al. Ulinastatin, a protease inhibitor, may inhibit allogeneic blood transfusion-associated pro-inflammatory cytokines and systemic inflammatory response syndrome and improve postoperative recovery. Blood Transfus 2014; s109-18.
9. Wang G, Li JY, Weng YQ, et al. Protective effect of ulinastatin combined with dexmedetomidine on lung injury after cold ischemia-reperfusion in rats. Eur Rev Med Pharmacol Sci 2018; 22:5712-18.
10. Yao WY, Zhou YF, Qian AH, et al. Emodin has a protective effect in cases of severe acute pancreatitis via inhibition of nuclear factor-κB activation resulting in antioxidation. Mol Med Rep 2015; 11:1416-20.
11. Ho J, Chan H, Liang Y, et al. Cathelicidin preserves intestinal barrier function in polymicrobial sepsis. Crit Care (London, England) 2020; 24:47.
12. Takada K, Komori M, Notoya A, Tomizawa Y, Ozaki M. Effect of ulinastatin on microcirculation during excessive hemorrhage using fluid therapy. In Vivo (Athens, Greece) 2003; 17:129-35.

LETTER TO THE EDITOR

Serum anti-Mullerian hormone level and its predictive value for pregnancy outcomes in women of late reproductive age

YJ. He[1*], DN. Yi[1*], CF. Cai[1], CY. Zhu[1], WT. Zhan[1] and L. Chen[2]

[1]Gynecologic Outpatient Department, Guangzhou Women and Children's Medical Center, Guangzhou, Guangdong Province, China; [2]Adult Chinese Traditional Medical Outpatient Dept, Guangzhou Women and Children's Medical Center, Guangzhou, Guangdong Province, China

Received June 11, 2020 – Accepted October 30, 2020

[*]These Authors contributed equally to this work

To the Editor,

It has been widely accepted that the ovarian follicular reserve and oocyte quality determine female fecundability. The biomarkers of ovarian follicular reserve are very important in terms of reproductive matters. Anti-Müllerian hormone (AMH) is a member of the transforming growth factor beta (TGF-β) superfamily. Previous studies demonstrated that AMH plays an important role in gender differentiation of the fetus. However, more recent studies have found that AMH is produced by the granulosa cells of pre-antral and small antral follicles, and its role is to regulate the recruitment and selective growth of follicles (1-2). In addition, its level can indirectly reflect the ovarian follicular reserve (3). In clinical practice, serum AMH level is used to assess ovarian follicular reserve and predict the ovarian response to hyperstimulation methods (4). Most studies regarding AMH are focused on its relationship with the primordial follicle pool (5). There is a lack of literature regarding the association between AMH and pregnancy outcomes in females of late reproductive age. The present study was designed to investigate the association between AMH and pregnancy outcome in a total of 431 women of late reproductive age.

MATERIALS AND METHODS

Study design

The present study was a cross-sectional study which comprised women who were aged ≥35 and were preparing for pregnancy in the clinic of reproductive medicine during December 2012 – December 2018. Inclusion criteria included: age 35-45 years; pregnancy conceived naturally; the couple gave consent to participate. Exclusion criteria included: no AMH measurement; pregnancy conceived using assisted reproductive technology (ART).

Anti-Müllerian hormone

Blood samples were taken on the day of the visit to the clinic. Serum was conserved at -24°C before being analysed at the Clinical Laboratory using the Bechman Coulter ELISA AMH-assay (Immunotech, Beckman Coulter).

All participants filled in an *ad hoc* questionnaire on the

Key words: anti-Müllerian hormone (AMH); pregnancy outcome; infertility; ovarian follicular reserve

Corresponding Author:
Dr Yaojuan He,
Gynecologic Outpatient Dept,
Guangzhou Women and Children's Medical Center,
9 Jinsui Road, Tianhe District, Guangzhou 510000,
Guangdong Province, China
Tel.: +86 13501541112
e-mail: he259778@163.com

0393-974X (2020)
Copyright © by BIOLIFE, s.a.s.
This publication and/or article is for individual use only and may not be further reproduced without written permission from the copyright holder.
Unauthorized reproduction may result in financial and other penalties
DISCLOSURE: ALL AUTHORS REPORT NO CONFLICTS OF INTEREST RELEVANT TO THIS ARTICLE.

day of the visit. The questionnaire regarded socio-demography, lifestyle factors, medical and reproductive history.

Statistical analysis

Statistical analysis was performed by the SPSS for Windows version 17.0 (SPSS, Chicago, IL, USA). Data was presented as number (percentage), mean (SD), depending on the types of the data. Differences between groups were tested using one-way ANOVA for continuous variables, and Fisher's exact test or *Chi*-squared test for categorical variables. The logistic regression method and partial correlation analysis were used to judge the main factors which determined pregnancy outcome by controlling the confounding factors. The receiver operating characteristic curve (ROC) was used to evaluate the predictive sensitivity and specificity of AMH. A two-sided p-value <0.05 was considered statistically significant.

RESULTS

The basic characteristics of the subjects are shown in Table I. The subjects were categorized as low (<1.5 ng/mL), intermediate (1.5-4.5 ng/mL), or high (>4.5 ng/mL) based on their levels of serum AMH. A total of 431 women with a mean age of 40.9 years, serum AMH levels ranging from undetectable (<0.5 ng/mL) to 5.5 ng/mL with a median serum concentration of 2.0 ng/mL) participated in the study. A total of 57 women aged 38–45 years had an AMH-level <1.0 ng/mL; in 12 cases AMH was undetectable.

Correlation between serum AMH levels and clinical characteristics

As shown in Table II, in women of late reproductive age, serum AMH levels were negatively correlated with age and preconception BMI (both p<0.05). There was no statistically significant correlation between serum AMH levels and the other clinical characteristics including cycle length, irregular menstrual cycle, previous conception, and nulliparity.

Factors determining pregnancy outcome

As shown in Table III, pregnancy outcome was independent of age. Moreover, it was unrelated to preconception BMI, cycle length, irregular menstrual cycle, previous conception, and nulliparity. Pregnancy outcome was related to serum AMH level when modelled as a continuous covariate and remained so after multiple adjustments (aOR 2.05, 95% CI: 1.23; 3.24, p=0.006).

Predictive value of AMH for pregnancy outcome

The receiver operating characteristic curve (ROC) was conducted to assess the predictive value of AMH for pregnancy outcome in women of late reproductive age. As shown in Fig. 1, the area under curve (AUC) of ROC was 0.535 (0.419~0.652). The results showed that AMH has no independent predictive value for pregnancy outcome in women of late reproductive age (p= 0.560).

DISCUSSION

It is widely accepted that the ovarian follicular reserve is decreases with increasing female age (11). The present study showed that Serum AMH was negatively correlated with age (r=-0.367, p<0.01). A large number of studies have demonstrated that obesity can lead to metabolic disorders such as impaired glucose tolerance and insulin resistance which will hinder the growth of follicles and cause stagnant follicular development, clinically demonstrated as oligomenorrhea or amenorrhea. The present study showed that Serum AMH was negatively correlated with preconception BMI (r=-0.332, p<0.01), which is in line with previous studies.

In this cohort of women of late reproductive age, serum AMH level had no predictive value for pregnancy outcome. However, the high AMH level group had the highest planned pregnancy rate. In addition, the logistic regression model showed that pregnancy outcome was related to serum AMH level when modelled as a continuous covariate even after adjustment for multiple female confounding factors. This is consistent with previous studies conducted on women with infertility who received ART treatment. The results demonstrated that low serum AMH levels were associated with a reduced pregnancy rate in patients receiving ART treatment. The underlying mechanism could be that the low serum AMH levels were associated with poor ovarian response to

Table I. *Basic characteristics of 431 women of late reproductive age.*

	Total	Low AMH	Intermediate AMH	High AMH	p value
n (%)	431 (100%)	166 (39.4%)	145 (34.4%)	120 (26.2%)	
Age (years), mean±SD	40.9±3.6	42.4±3.6	40.8±3.6	38.3±3.1	<0.001
AMH (ng/mL), mean±SD	2.0±0.7	1.0±0.25	2.5±1.5	5.0±0.5	<0.001
Preconception BMI (kg/m^2), n (%)					0.20
<18.5	27 (6.3%)	11 (6.5%)	7 (4.8%)	9 (%)	
18.5-24.9	344 (79.8%)	116 (70.0%)	121 (83.4%)	107 (80.0%)	
25.0-29.9	46 (10.7%)	30 (9.0%)	14 (9.7%)	2(9.2%)	
≥30	14 (3.2%)	9 (14.5%)	3 (2.1%)	2 (1.6%)	
Cycle length (days), mean±SD	28.0±3.5	28.0±6.0	29.0±4.5	30.0±3.0	<0.001
Irregular menstrual cycle, n (%)					0.29
Yes	31 (7.2%)	5 (3.0%)	11 (7.6%)	15 (12.5%)	
No	400 (92.8%)	161 (97.0%)	134 (92.4%)	105 (87.5%)	
Previous conception, n (%)					0.04
Yes	221 (51.3%)	100 (60.2%)	74 (51.0%)	47 (39.2%)	
No	210 (48.7%)	66 (39.8%)	71 (49.0%)	73 (60.8%)	
Parity, n (%)					0.08
Parous	142 (32.9%)	72 (43.4%)	47 (32.4%)	23 (19.2%)	
Nulliparous	289 (67.1%)	94 (56.6%)	98 (67.6%)	97 (80.8%)	
Planned pregnancy, n (%)					<0.001
Yes	394 (91.4%)	144 (86.7%)	131 (90.3%)	112 (93.3%)	
No	37 (8.6%)	22 (13.3%)	14 (9.7%)	8 (6.7%)	

Serum AMH levels were categorised in low (<1.5 ng/mL), intermediate (1.5-4.5 ng/mL), and high (>4.5 ng/mL). Data are presented for the total cohort and for the three AMH groups. Differences between the three AMH groups were tested.

Table II. *Correlation between serum AMH levels in women of late reproductive age and clinical characteristics.*

Clinical characteristics	r value	p value
Age	-0.367	<0.01
Preconception BMI	-0.332	<0.01
Cycle length	-0.051	0.596
Irregular menstrual cycle	-0.082	0.392
Previous conception	-0.017	0.861
Nulliparity	0.080	0.408

Spearman correlation method was used.

Table III. *The logistic regression method was used to determine the main factors which affect pregnancy outcome by controlled the confounding factors.*

Covariates	Unadjusted OR (95% CI)	p-value	Adjusted OR (95% CI)	p-value
Age (years)	0.98 (0.94;1.02)	0.53	0.95 (0.89;1.01)	0.34
AMH (pmol/L)	1.96 (1.18; 3.27)	0.008	2.05 (1.23;3.24)	0.006
AMH category				
Low	1.55 (1.08;2.28)	0.17	1.75 (1.10;2.75)	0.18
Intermediate	1		1	
High	1.17 (0.82; 1.72)	0.39	0.99 (0.65;1.55)	0.95
Preconception BMI (kg/m^2)				
<18.5	0.85 (0.45;1.55)	0.55	0.57 (0.26;1.35)	0.15
18.5-24.9	1		1	
25.0-29.9	0.82 (0.55;1.27)	0.34	0.82 (0.45;1.40)	0.45
≥30	0.61 (0.24; 1.15)	0.25	0.55 (0.15;1.45)	0.34
Irregular menstrual cycle	1.27 (0.28; 2.17)	0.37	1.45 (0.75; 2.15)	0.29
Previous conception	1.22 (0.92; 1.65)	0.15	1.35 (0.99; 1.86)	0.07
Nulliparity	0.70 (0.51; 0.95)	0.025	0.63 (0.45; 0.89)	0.15

Results are presented as odds ratios (OR) and 95% confidence interval (CI).

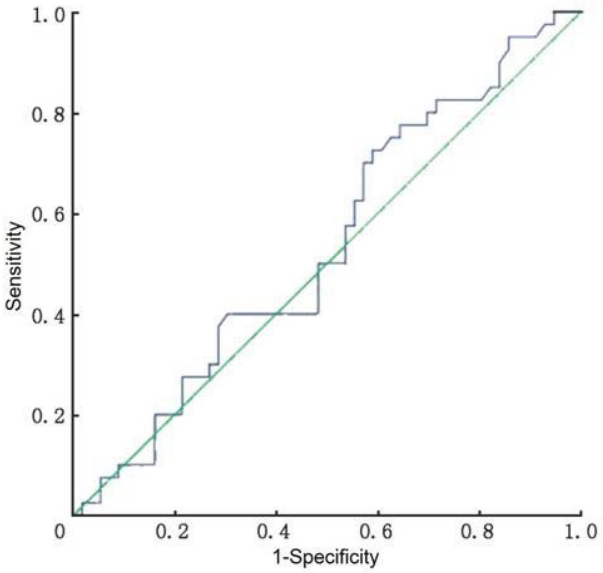


Fig. 1. *The receiver operating characteristic curve (ROC) evaluating the predictive values of serum AMH levels for pregnancy outcomes in women of late reproductive age.*

hyperstimulation, therefore low pregnancy rate.

In conclusion, our results suggest that serum AMH level has no predictive value for the pregnancy outcomes in women of late reproductive age. However, the planned pregnancy rate of women with high AMH level is statistically higher than women with low AMH level, which may be related to the better ovarian follicular reserve of the high AMH level group. In order to determine the correlation between serum AMH level and natural fecundability, large prospective studies are needed to ensure the longitudinal follow-up on the pregnancy outcome in a cohort of women with a wide age range.

REFERENCES

1. Weenen C, Laven JS, Von Bergh AR et al. Anti-Müllerian hormone expression pattern in the human ovary: potential implications for initial and cyclic follicle recruitment. Mol Hum Reprod 2004; 10(2):77-88.
2. Hansen KR, Hodnett GM, Knowlton N, Craig LB. Correlation of ovarian reserve tests with histologically determined primordial follicle number. Fertil Steril 2011; 95(1):170-75.
3. La Marca A, Volpe A. Anti-Müllerian hormone (AMH) in female reproduction: is measurement of circulating AMH a useful tool? Clinical Endocrinol 2006; 64(6):603-20.
4. La Marca A, Sunkara SK. Individualization of controlled ovarian stimulation in IVF using ovarian reserve markers: from theory to practice. Hum Reprod Update 2014; 20(1):124-40.
5. te Velde ER, Pearson PL. The variability of female reproductive ageing, Hum Reprod Update 2002; 8(2):141-54.
6. Steiner AZ, Jukic AM. Impact of female age and nulligravidity on fecundity in an older reproductive age cohort. Fertil Steril 2016; 105(6):1584-88.
7. Seif MW, Diamond K, Nickkho-Amiry M. Obesity and menstrual disorders. Best Pract Res Clin Obstet Gynaecol. 2015; 29(4):516-27.
8. Moy V, Jindal S, Lieman H, Buyuk E. Obesity adversely affects serum anti-müllerian hormone (AMH) levels in Caucasian women. J Assist Reprod Genet. 2015; 32(9):1305-11.
9. Goswami M, Nikolaou D. Is AMH level, independent of age, a predictor of live birth in IVF? J Hum Reprod Sci 2017; 10(1):24-30.
10. Iliodromiti S, Kelsey TW, Wu O, et al. The predictive accuracy of anti-Müllerian hormone for live birth after assisted conception: a systematic review and meta-analysis of the literature. Hum Reprod Update 2014; 20:560-70.
11. Lee TH, Liu CH, Huang CC, et al. Serum antiMüllerian hormone and estradiol levels as predictors of ovarian hyperstimulation syndrome in assisted reproduction technology cycles. Hum Reprod 2008; 23:160-67.

LETTER TO THE EDITOR

Clostridium novyi exhibits antitumor effect in mice transplanted with H22 hepatocarcinoma by down-regulation of hypoxia-inducible factor-1α

XJ. Huang[1,2#], Y. Yang[2#], ZM. Deng[2,3], Y. Kuang[2], H. Shi[4], WY. Li[2*] and MY. Li[2,4*]

[1]Department of pathogen biology, Medical school,Hubei Minzu University, Ensi, China; [2]Department of Microbiology, West China School of Basic Medical Sciences & Forensic Medicine, Sichuan University, Chengdu, China; [3]Hospital of Chengdu Office of People's Government of Tibetan Autonomous Region, Chengdu, China; [4]Department of Laboratory Medicine, West China Second University Hospital, Sichuan University, Chengdu, China

Received April 10, 2020 – Accepted November 2, 2020

[#]Contributed equally as co-first authors

[*]contributed equally as co-last authors

To the Editor,

In 2018, there were 18.1 million new cancer cases and 9.6 million cancer deaths (1). Hepatocarcinoma is one of the most common malignant tumors and the fourth leading cause of cancer mortality worldwide (1), and the five-year survival rate is only 18% (2). While multiple factors may contribute to the low survival rate, one of the main reasons is that hepatocarcinoma contains large and poorly vascularized areas (hypoxic areas) which greatly limit the efficacy of therapies. The study of tumor biology showed that hypoxia promotes not only the basis of proliferation, invasion and metastasis of tumor cells, but also chemoresistance and radioresistance in cancer. Therefore, novel approaches are urgently needed to overcome the hypoxic microenvironmental barrier.

Previous research has shown that tumors, treated with nontoxigenic *Clostridium novyi (C.novyi-NT)*, shrank and went into complete remission. The treatment significantly enhanced the survival rate of experimental animals with melanoma, colorectal tumor, pancreatic carcinoma, renal tumor, brain tumor, soft tissue sarcomas or glioblastoma (3). The vast majority of findings came from athymic nude mice model. To date, there are no studies regarding the antitumor effects of *C.novyi* against hepatocarcinoma in mice with normal immunity. In the presentstudy, *C. novyi-NT* was generated in our laboratory and the safety and efficacy of *C.novyi-NT* were assessed for treatment of BALB/c mice bearing implanted H22 hepatocarcinoma. Furthermore, the optimum dose and possible mechanisms were also explored initially from hypoxic tumor environment.

MATERIALS AND METHODS

Animals

Six-week-old male BALB/c mice (weight, 18-20 g) were purchased from the Experimental Animal Center of Sichuan University. All mice were fed in a standard experimental environment and given sterile water.

Key words: bacteriolytic therapy; C.novyi-NT; hepatocarcinoma; hypoxia-inducible factor-1α

Corresponding Author:
Prof. Mingyuan Li,
Department of Microbiology,
West China School of Basic Medical Sciences & Forensic Medicine,
Sichuan University. 17#,
Section 3rd, Renmin Road, South, Chengdu,
Sichuan, 610041, China
e-mail: lmy3985@sina.com

0393-974X (2020)
Copyright © by BIOLIFE, s.a.s.
This publication and/or article is for individual use only and may not be further reproduced without written permission from the copyright holder.
Unauthorized reproduction may result in financial and other penalties
DISCLOSURE: ALL AUTHORS REPORT NO CONFLICTS OF INTEREST RELEVANT TO THIS ARTICLE.

Padding materials and fodder were sterilized by radiation. All mouse experiments were approved by the Animal Welfare Committee of Sichuan University and were in accordance with university standards.

Cell lines

H22 hepatocarcinoma cell was kindly provided by the Department of Pharmacology, West China School of Basic Medical Sciences & Forensic Medicine, Sichuan University. H22 cell was grown in RPMI 1640 medium (Hyclone, USA) supplemented with 10% feta bovine serum (Tbdscience, China) and 1% penicillin/streptomycin (Hyclone, USA) at 37°C in the presence of 5% carbon dioxide.

Bacteria

C.novyi was purchased from the American Type Culture Collection (ATCC 19402, Lot: 60629031). *C.novyi* was cultivated in Columbia Blood Agar Base Medium (OXOID, England) with 10% fresh rabbit blood cultures anaerobically at 37°C. About three days after cultivation in obligate anaerobic environment, colonies of vegetative bacteria were transferred into sporulation medium. After ten days in the medium, abundant spores settled in the cooked meat particle layer. Spores were further purified from contaminating vegetative forms on the discontinuous Percoll gradient (GE healthcare, Sweden). To inactivate the phage carrying the toxin of *C.novyi*, purified spores were heated at 70°C for 15 min. The spores then were plated on Columbia Blood Agar Medium and cultivated anaerobically at 37°C for 72 h. Isolated colonies were tested for the presence of the lethal toxin gene by PCR. The colonies devoid of the lethal toxin were plated on Columbia Blood Agar Medium and cultivated. A *C.novyi*-NT clone was obtained and used in the animal studies as described below.

Tumor model and treatment

H22 cells (1.0×10^7, 200 μl) were injected subcutaneously into the left forelimb of the animals. Tumor growth was routinely monitored twice a week. After ten days, all of the mice had visible implanted tumors. Tumor diameter was measured by electronic digital vernier caliper and its volume was calculated according to the formula: $V = \text{width}^2 \times \text{length} \times 0.5$. Tumor-bearing mice were randomly divided into four groups by tumor volume with eight mice in each group. The experimental group mice were intratumorally injected with *C.novyi*-NT (low-dose group 1.0×10^7/ml, 500 μl; medium-dose group, 1.0×10^8/ml, 500 μl; high-dose group, 1.0×10^9/ml, 500 μl). The control group mice were injected with 500 μl physiological saline. During the experiment, general conditions of the mice were observed and recorded every day. The animals were weighed three times a week, and tumor diameter was measured twice a week. Mice were euthanized at day 12 post-treatment or when they became moribund. Subsequently, complete tumor, liver, spleen, lung, kidney, brain, thymus were stripped for further analysis and detection of *C.novyi-NT* by staining and culturing .

Real-time quantitative PCR

Tumor tissues (30 mg) were homogenized and total RNA was extracted according to kit protocol (OMEGA, USA). RNA was reversed transcribed to cDNA using a PrimeScript RT Reagent Kit (TaKaRa, Japan). Takara Bio.Inc. synthesised the primers. The reactions were carried out with an initial denaturation at 95°C for 5 min, followed by 40 cycles of 95°C for 10 s, 58°C for 30 s. The products were detected with 1% agarose gel electrophoresis. Gene expression data were analyzed using Real time PCR detection system (Bio-Rad, CFX96, USA) and $2^{-\triangle\triangle CT}$ method.

Immunohistochemistry

The expression levels of HIF-1α, VEGF and bFGF in tumor tissues were assessed by immunohistochemical SABC method. Immunohistochemistry staining was conducted with the instruction of test kits. The primary antibodies were rabbit polyclonal anti-HIF-1α (1:50, 20960-1-AP, Proteintech), mouse monoclonal anti-VEGF (1:100, sc-7289, Santacruz), and mouse monoclonal anti-bFGF (1:50, ab24826, Abcam). Adequate biotin-labeled secondary antibodies were added at 37°C for 30 min. After dropping SABC, the section was stained with DAB solution and counterstained with hematoxylin, and then dehydrated, transparentized, and sealed. The cellular distributions and HIF-1α, VEGF, bFGF expression in tumors were observed by two independent blinded investigators using a light microscope (Leica DM 750, Germany). For each slide, three fields were counted to access the frequency of HIF-1α-positive nucleus, VEGF-positive cytoplasm and bFGF-positive cytoplasm. The positive expression was determined by the means of

percentage of immunoreactive cells. No evaluation of colour intensity was used in the study. Hematoxylin-eosin was used to stain tumor tissues.

Statistical analysis

All data were expressed as mean±standard deviation ($\bar{x}$±s). Differences among groups were compared with analysis of variance (ANOVA). LSD was used to check the differences between means. Significant differences were defined as $p<0.05$.

RESULTS

Bacteria selective colonization and tumor inhibitory effects

The subcutaneously implanted tumor models were successful in all the mice. In the control group the tumor color looked bright, bled easily and adhered to the adjacent tissues. Substantial fluid had accumulated within the tumor (Fig. 1A). When stripped tumors of the experiment groups were observed, massive shoddy tissues filled the tumor, the tumor color was whitish and the capsule was complete. HE staining of tumor tissues showed that no obvious necrosis tissue was observed in the control group. In the low-dose group, granular focal necrosis with irregular boundaries were found. In the high-dose group, a small amount of necrosis with bleeding was seen. In the medium-dose group, however, multiple focal necrosis tissue was observed. The necrotic tissue was powdery, granular, and irregularly bound with chronic inflammatory cell infiltration at the margins (Fig. 1B). Tumor weights were different after administering *C.novyi*-NT (Table I). Tumor inhibitory rates of the low-dose group, medium-dose group, and high-dose group were 8.48%, 44.59% and 14.84%, respectively (Table I). Tumor necrosis tissue, liver, spleen, lung, kidney, and brain were stained and cultured, and it was found *C.novyi*-NT selectively populated hypoxic regions and the bacteria did not invade into other organs except liver in the high dose group.

Coefficient of spleen and thymus

The quality and coefficient of immune organs can be used as indicators to judge the effect of the intervention on the immune system. Spleen and thymus were weighed after being harvested completely. Spleen was greatly enlarged to the naked eye, but the thymus weight decreased in all three groups. The spleen coefficient of the medium-dose group and high-dose group were bigger than that of the control group and the difference

Table I. *Tumor inhibitory rates of different groups ($\bar{x}$±s) (n=8)*

Group	Tumor weight (g)	Tumor inhibitory rates（%）
Control group	5.788±2.185	
Low-dose group	5.297±1.467	8.48
Medium-dose group	3.207±1.486	44.59
High-dose group	4.929±1.334	14.84

Tumor inhibitory rates = (control group tumor weight-experiment group tumor weight)/ (control group tumor weight)

Table II. *Coefficient of spleen and thymus in different groups ($\bar{x}$±s) (n=8)*

Group	Spleen		Thymus	
	Spleen weight (g)	Coefficient of spleen	Thymus weight (g)	Coefficient of thymus
Control group	0.284±0.075	0.954±0.266	0.167±0.028	0.566±0.092
Low-dose group	0.383±0.108	1.23±0.359	0.162±0.034	0.52±0.118
Medium-dose group	0.441±0.177	1.463±0.596*	0.147±0.019	0.5±0.101
High-dose group	0.612±0.127	2.183±0.405* #	0.118±0.017	0.422±0.078*

*Significant differences (P<0.05) compared with the control groups and medium dose group are denoted by * and #, respectively.*

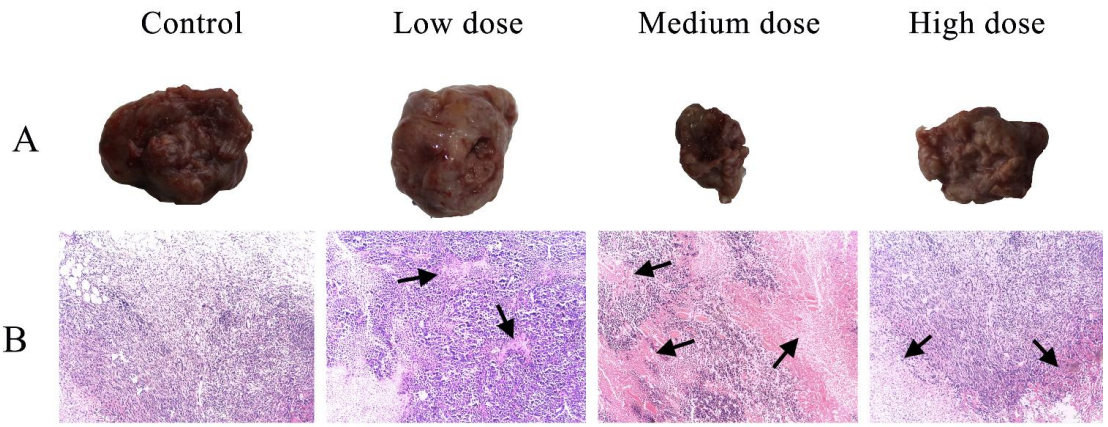


Fig. 1. *Photographs of tumor (**A**) and H&E staining (**B**) (×100).*

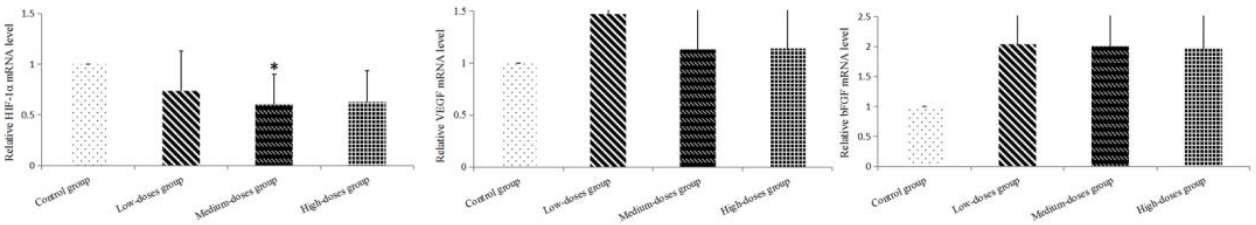


Fig. 2. *Real-time PCR quantitative analysis. Significant differences (P<0.05) compared with the control groups is denoted by *.*

was statistically significant (P=0.026, P <0.01, respectively). The thymus coefficient of the high-dose group was smaller than that of the control group and the difference was statistically significant (P=0.008). It was not significantly different in the coefficient of thymus in other groups (P > 0.05) (Table II).

Decreased expression of HIF-1α mRNA in tumors by real-time quantitative PCR in medium-dose mice

Real-time PCR showed amplified fragments of *HIF-1α*, *VEGF*, *bFGF* and internal reference *β-Actin* with expected sizes of 163 bp, 118 bp, 141 bp and147 bp, respectively, which was verified by DNA sequencing. The average relative expression levels of *HIF-1α* mRNA were 0.738±0.392, 0.601±0.301, 0.627±0.310 in the low-dose group, medium-dose group and high-dose group, respectively. The average relative expression levels of *VEGF* mRNA were 1.474±0.581, 1.130±0.583 and 1.114±0.598 in the same groups, respectively, and the *bFGF* mRNA expression levels were 2.036±0.813, 2.008±0.985, 1.962±0.948, respectively. The expression levels of HIF-1α mRNA in the medium-dose group were significantly lower than those in the control group (P=0.038). The mRNA expression levels of *VEGF*, *bFGF* in the experimental groups were higher than those in the control group, but they were not statistically significant (P>0.05) (Fig. 2).

Decreased expression of HIF-1α in tumor by immunohistochemistry in medium-dose mice

Immunoreactivity for the VEGF, bFGF and HIF-1α positive expression were defined by the presence of cytoplasm stained yellow or brown. Few HIF-1α were detected in nucleus. Fig. 3A shows the expression of HIF-1α, VEGF and bFGF on immunohistochemistry. The average HIF-1α-positive staining in the low-dose group, medium-dose group, high-dose group and control group were 55.2±8.59, 49.5±5.93, 57.8±8.61 and 59.1±7.96, respectively. The average VEGF-

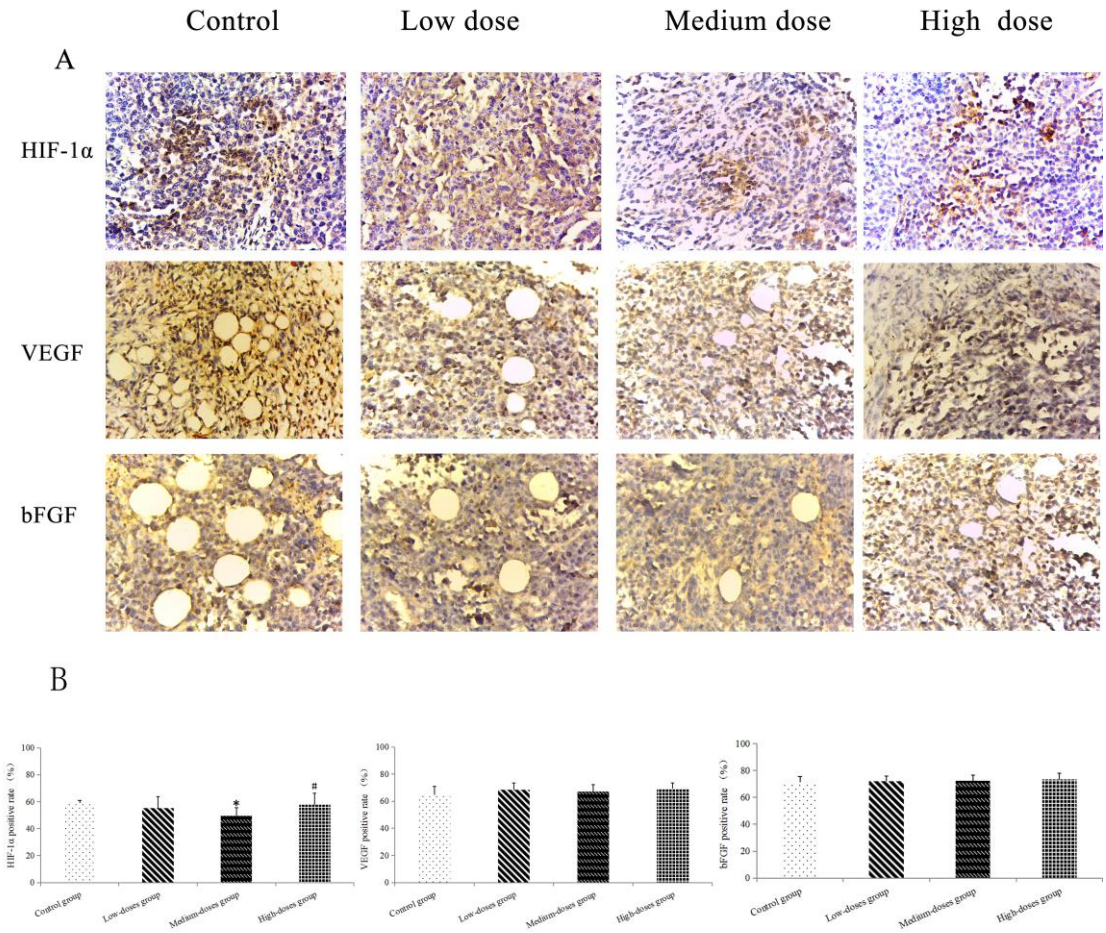


Fig. 3. *Immunohistochemical analysis (×100). Significant differences (P<0.05) compared with the control groups and medium dose group are denoted by * and #, respectively.*

positive staining for the same groups were 68.4±5.15, 67.1±5.28, 69.3±4.11 and 64.8±6.03, respectively, and the average bFGF-positive staining were 72.1±3.75, 72.5±4.06, 73.5±4.60 and 71.4±4.17, respectively. Medium-dose group HIF-1α expression significantly reduced (P=0.009 , compared with the control group). The expression of VEGF, bFGF were higher in the experimental group than the control group, but the difference was not statistically significant (P>0.05) (Fig. 3B).

DISCUSSION

In conclusion, *C.novyi-NT* selectively populated and caused oncolysis in hypoxic regions of hepatocarcinoma. The normal immunity mice with implanted H22 hepatocarcinoma were intratumorally injected with *C.novyi-NT* which was safe and effective. The effect of medium dose was optimum. Tumor inhibitory rate was more than 40%. Spleen enlarged significantly in the experiment groups. HIF-1a mRNA/HIF-1a protein decreased significantly in cancer tissues. The expression changes of VEGF, bFGF were not statistically significant. The antitumor effects of *C. novyi-NT* related to down-regulation HIF-1α and spleen enlargement.

Hypoxia promotes tumor progression such as proliferation, neoangiogenesis and metastasis (4). Under normoxic conditions HIF-1α is constantly synthesized but rapidly degraded, whereas HIF-1α

stabilizes in hypoxic condition (5, 6). HIF-1α proved as a positive factor regulating plant in VEGF (5, 7). HIF-1α increased, instead, VEGF decreased in the research. Presumably, because the tumor volume was too large before treatment, severe oxygen deficiency led HIF-1 expression to increase heavily. Under hypoxic conditions, HIF-1 up-regulates VEGF transcription and stabilizes *VEGF* mRNA (7). On the contrary, after *C.novyi*-NT was administered, HIF-1α expression decreased, which caused VEGF down-regulation, but the total of VEGF had not reduced in a short period of time. These observations may lead to the change of bFGF. In this model, tumor volume and termination time of the experiment could have affected therapeutic effectiveness. If *C.novyi-NT* is injected in advance, or when the tumor is medium-size, or the observation time is prolonged, perhaps the expression of VEGF/ bFGF will decrease, the tumor inhibitory rate will be much higher and mice with tumor will be completely cured.

Administration of *C.novyi*-NT could also cause the change of cytokines (such as TNF, IL-6, MIP-2, G-CSF and TIMP-1), immune cells (such as T cell, B cell, NK cell, neutrophil, monocyte) (8). However these parameters were not evaluated in this study. *C.novyi-NT* combination with chemotherapeutics/ radiotherapy/radiofrequency ablation, carrier prodrug activation enzyme gene/cytokine gene will give a huge boost to *C.novyi-NT* against tumors. Further studies with optimal treatment window, alternative administration routes, combination therapy, and gene-modified bacteria will be needed to further evaluate the anti-tumor effect of *C.novyi-NT* as well as the mechanism.

ACKNOWLEDGEMENTS

The study was financially supported by the key project of science and technology research plan of education department of Hubei province grant (no. D20181903), and the doctors start fund project of Hubei Minzu University grant (no.MY2017B031)

REFERENCES

1. Bray F, Ferlay J, Soerjomataram I, Siegel RL, Torre LA, Jemal A. Global Cancer Statistics 2018: GLOBOCAN Estimates of Incidence and Mortality Worldwide for 36 Cancers in 185 Countries. CA Cancer J Clin 2018; 68:394-424.
2. Asrani SK, Devarbhavi H, Eaton J, Kamath PS. Burden of liver diseases in the world. J Hepatol 2019; 70:151-71.
3. Staedtke V, Bai RY, Sun W, et al. Clostridium novyi-NT can cause regression of orthotopically implanted glioblastomas in rats. Oncotarget 2015; 6:5536-46.
4. Song M, Liu T, Shi C, Zhang X, Chen X. Bioconjugated manganese dioxide nanoparticles enhance chemotherapy response by priming tumor-associated macrophages toward M1-like phenotype and attenuating tumor hypoxia. ACS Nano 2016; 10:633-47.
5. Semenza GL. The hypoxic tumor microenvironment: A driving force for breast cancer progression. Biochim Biophys Acta 2016; 1863:382-91.
6. Nagaraju GP, Bramhachari PV, Raghu G, El-Rayes BF. Hypoxia inducible factor-1α: Its role in colorectal carcinogenesis and metastasis. Cancer Lett 2015; 366:11-18.
7. Rankin EB, Nam JM, Giaccia AJ. Hypoxia: Signaling the metastatic cascade. Trends Cancer 2016; 2:295-304.
8. Binnewies M, Roberts EW, Kersten K, et al. Understanding the tumor immune microenvironment (TIME) for effective therapy. Nat Med 2018; 24: 541-50.

LETTER TO THE EDITOR

Effects of prophylactic injection of methoxamine on pregnant women undergoing cesarean delivery using spinal anesthesia

HJ. He[1], DB. Xu[1], XY. Zheng[2], YQ. Yang[1], WP. Zheng[1] and XL. Tao[3]

[1]Department of Anesthesiology, Taizhou Hospital of Zhejiang Province affiliated to Wenzhou Medical University, Linhai, Zhejiang, China; [2]Department of Anesthesiology, Fujian Medical University Union Hospital, Fuzhou, Fujian, China; [3]Department of Obstetrics and Gynecology, Taizhou Hospital of Zhejiang Province affiliated to Wenzhou Medical University, Linhai, Zhejiang, China

Received June 2, 2020 – Accepted October 12, 2020

To the Editor,

In recent years, due to various factors, such as improved living standards and gradually changing fertility concepts, cesarean section has been increasingly used to replace natural childbirth (1). Therefore, ensuring the safety of both mother and infant during cesarean section has significantly attracted anesthetists' attention. Spinal anesthesia is the first choice for cesarean section (2). A number of studies pointed out that prophylactic injection of methoxamine for cesarean delivery using spinal anesthesia can effectively reduce the incidence of intraoperative hypotension (3). Methoxamine hydrochloride is a highly selective α1 receptor agonist (4), and it has almost no agonistic effect on α2 and β receptors, while it can increase arterial blood pressure, decrease heart rate (HR), and reduce cardiac output and myocardial oxygen consumption (5). It also has been extensively used to prevent and treat maternal hypotension. Due to the limitations of the current clinical use of a cuff to measure blood pressure, which can only measure the blood pressure changes of the parturient intermittently, and cannot obtain continuous real-time blood pressure, it is impossible to judge the best timing of methoxamine. Non-invasive hemodynamic monitoring methods can be applied to assess differences in the effects of methoxamine on mothers and infants, exploring the best timing of medication. Our findings may provide a reliable basis for prevention and treatment of hypotension in cesarean section using spinal anesthesia.

MATERIALS AND METHODS

Patients

From February 2019 to December 2019, 75 patients with fetal head engagement underwent elective cesarean section using spinal anesthesia. No significant abnormality in HR and lung function was noted, and patients had no diabetes, gestational diabetes or heart disease. The subjects were divided into two groups: a control group (n = 15) and an experimental group (n = 60). The subjects in the experimental group were randomly divided into three subgroups (n = 20 for each subgroup): Group A, Group B, and Group C. The study protocol was approved by the Ethics Committee of Taizhou Hospital of Zhejiang Province affiliated to Wenzhou Medical University, and the patient or his family members signed the written informed consent form.

Exclusion criteria were as follows: i) allergy to methoxamine; ii) severe cardiovascular disease or

Key words: subarachnoid block anesthesia; cesarean section; methoxamine; hemorheology; fetal umbilical arterial blood gas

Corresponding Author:
Dr Xiaoling Tao,
Department of Obstetrics and Gynecology,
Taizhou Hospital of Zhejiang Province
affiliated to Wenzhou Medical University,
Linhai, 317000, Zhejiang, China
e-mail: taoxiaolinxl_enze@163.com

0393-974X (2020)
Copyright © by BIOLIFE, s.a.s.
This publication and/or article is for individual use only and may not be further reproduced without written permission from the copyright holder.
Unauthorized reproduction may result in financial and other penalties
DISCLOSURE: ALL AUTHORS REPORT NO CONFLICTS OF INTEREST RELEVANT TO THIS ARTICLE.

hypertensive complications of pregnancy [systolic blood pressure (SBP) ≥ 180 mmHg (1 mmHg = 0.133kPa), diastolic blood pressure ≥ 110 mmHg], chronic kidney disease, hyperthyroidism, or bradycardia.

Anesthesia method

Patients in both groups were given spinal anesthesia for caesarean section, and were deprived of food and water for 8 h and over 6 h before operation, respectively. After entering into the operating room, routine monitoring of pulse, blood oxygen saturation, electrocardiogram, and blood pressure was carried out. Spinal anesthesia was given at an inter-vertebral space between the third and fourth cervical vertebrae. After successful puncture, spinal 2.0-2.5 mL hyperbaric 0.5% bupivacaine was given, and the injection was completed after about 25 s; patients in Group A were given 0.02 mg/kg methoxamine (Yuanda Pharmaceutical Chemical Co., Ltd., China) immediately after injecting local anesthetic into the subarachnoid space; those in Group B were given methoxamine (0.02 mg/kg) 1 min after prophylactic injection of local anesthetic into the subarachnoid space; in Group C, when the SBP decreased to 10% of the basal value after injecting local anesthetic into the subarachnoid space, methoxamine (0.02 mg/kg) was given immediately. Those whose blood pressure dropped by more than 10% were excluded. After the puncture was successful, the prophylactic injection rate was maintained at 0.1 mg/min; If the HR was below 60 beats/min due to bradycardia during the operation, 0.25 mg atropine (Shanghai Hefeng Pharmaceutical Co, Ltd., China) was injected or prophylactic injection of methoxamine was stopped. If the patient had hypotension [SBP < 90 mmHg], 25-60 μg phenylephrine was given in a single injection. In case of SBP > 140 mmHg during injection when methoxamine was pumped, methoxamine was stopped immediately.

Continuous monitoring of arterial blood pressure

The T-Line TL-300 (Tensys Medical, USA), a non-invasive arterial blood pressure monitoring system, was used. The left side of the maternal radial artery pulsation was fully exposed with a fixed plate. The HR and real-time arterial blood pressure readings were displayed.

Observational indicators

The patient's general condition was recorded, including height, weight, age, gestational age, blood loss, urine output, operation time, and total infusion volume. The HR before anesthesia (T0), at 1 min after anesthesia (T1), 2 min after anesthesia (T2), delivery of the fetus (T3), 1 min after delivery of the fetus (T4), 3 min after delivery of the fetus (T5), and after surgery (T6) was separately recorded in addition to changes in blood pressure levels. Blood passage time (BPT), as an index of blood rheology, was recorded via collecting blood samples at T0, T1, T4, and T6.

For assessment of the neonatal situation, 3 mL neonatal umbilical arterial blood was drawn. Blood gas indicators in the control group and experimental group, such as pH, base excess (BE), partial pressure of oxygen in the arterial blood (PaO2), and partial pressure of carbon dioxide in the arterial blood (PaCO2), were measured using a blood gas analyzer. The newborn's physical condition after birth was evaluated by Apgar scores, with a total of 10 points, in which the higher the score, the better the newborn's physical condition.

Adverse reactions were assessed via recording the following items: hypotension, hypertension, bradycardia (HR < 60 beats/min), nausea, and vomiting.

Statistical analysis

The relevant data were extracted, sorted and summarized into Excel, followed by standardized preprocessing. Then, Excel was used to build the database. Next, SPSS 19.0 software (IBM, USA) was used to perform statistical analysis. Measured data were expressed as mean ± standard deviation ($\bar{x}\pm s$). Pairwise comparison was conducted using least significant difference (LSD) test. Other indicators were analyzed using one-way analysis of variance (ANOVA); count data were presented as incidence rate, and comparison between the groups was made using *Chi*-squared test. $P < 0.05$ was considered statistically significant.

RESULTS

There were no statistically significant differences in total intraoperative fluid infusion, blood loss, and urine volume among the four subgroups ($P > 0.05$) (Table I).

Hemodynamic changes

The three groups A, B and C all received the

Table I. *Comparison of indicators for maternal health among the four groups*

Indicator	Control group	Group A	Group B	Group C
Age (years old)	26.41±7.43	25.78±8.02	26.57±7.37	26.12±6.16
Height (cm)	162.27±2.83	162.35±2.24	163.35±3.47	162.14±2.49
Weight (kg)	69.31±4.15	70.32±3.05	71.54±4.53	70.25±3.33
Gestational age (week)	39.8±1.4	39.4±1.4	40.2±1.0	39.6±1.6
Intraoperative total infusion (mL)	1195±44.0	1150±50.2	1130±51.6	1160±35.2
Bleeding volume (mL)	225±17.3	221±18.2	212±20.5	220±14.6
Urine output (mL)	205.6±22.6	195.2±20.5	203.8±18.6	198.7±19.3

Note: The difference between the groups was not significant, P>0.05.

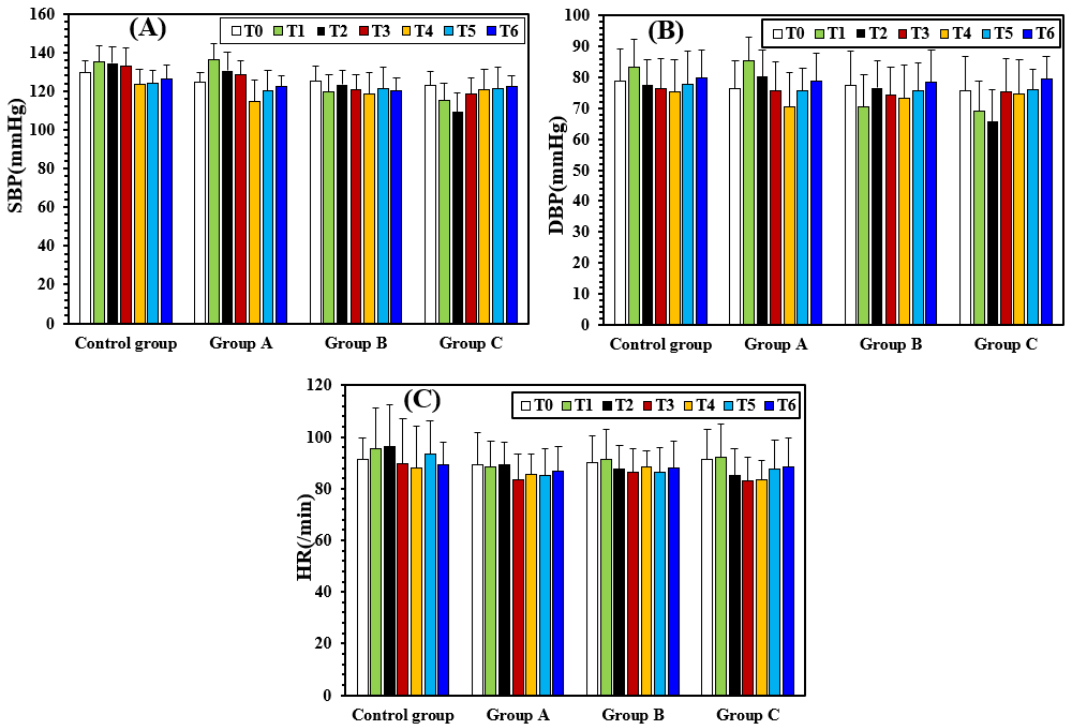


Fig. 1. *Comparison of hemodynamic changes in each group at T0-T6. **A**) SBP index; **B**) DBP index; **C**) HR index.*

same dose of methoxamine (0.02 mg/kg). The HR slightly decreased in those three groups compared with that in the control group, while there was no bradycardia. In Group B, the prophylactic injection of methoxamine 0.02 mg/kg was carried out at 1 min after anesthesia, and the maternal hemodynamic fluctuations were insignificant. It was found that the mentioned injection method is the most appropriate strategy for preventing and treating maternal hypotension (Fig.1).

Changes in hemorheological indexes related to pregnancy

No significant difference was found in plasma viscosity, nor in high-, medium, and low-whole blood viscosity between the control group and the experimental group ($P > 0.05$). Compared with the control group, the blood rheological indices in the experimental group at T1, T4, and T6 were significantly lower ($P < 0.05$) (Fig.2).

Apgar scores and results of umbilical cord blood gas analysis

The 1-min and 5-min Apgar scores and results of umbilical cord blood gas analysis (pH, BE, PaO_2, and $PaCO_2$ values) in each group were within the normal range, and their differences were not statistically significant ($P > 0.05$) (Table II).

Adverse reactions

The incidence of nausea, vomiting, and hypotension in Group A and Group B was significantly lower than that in the control group ($P<0.05$). Although the incidence in Group C was lower than that in the control group, the difference was not significant ($P> 0.05$). The incidence of hypertension in Group A and Group B was significantly lower than that in the control group. The incidence in Group B was the lowest. The use of atropine in Group C was higher than that in Group A and Group B ($P<0.05$), while lower than that in control group ($P< 0.05$). Taken together, the adverse reactions of Group B were less than those of Group A and Group C, indicating that prophylactic injection of methoxamine 1 min after anesthesia can effectively reduce the adverse reactions of patients (Table III).

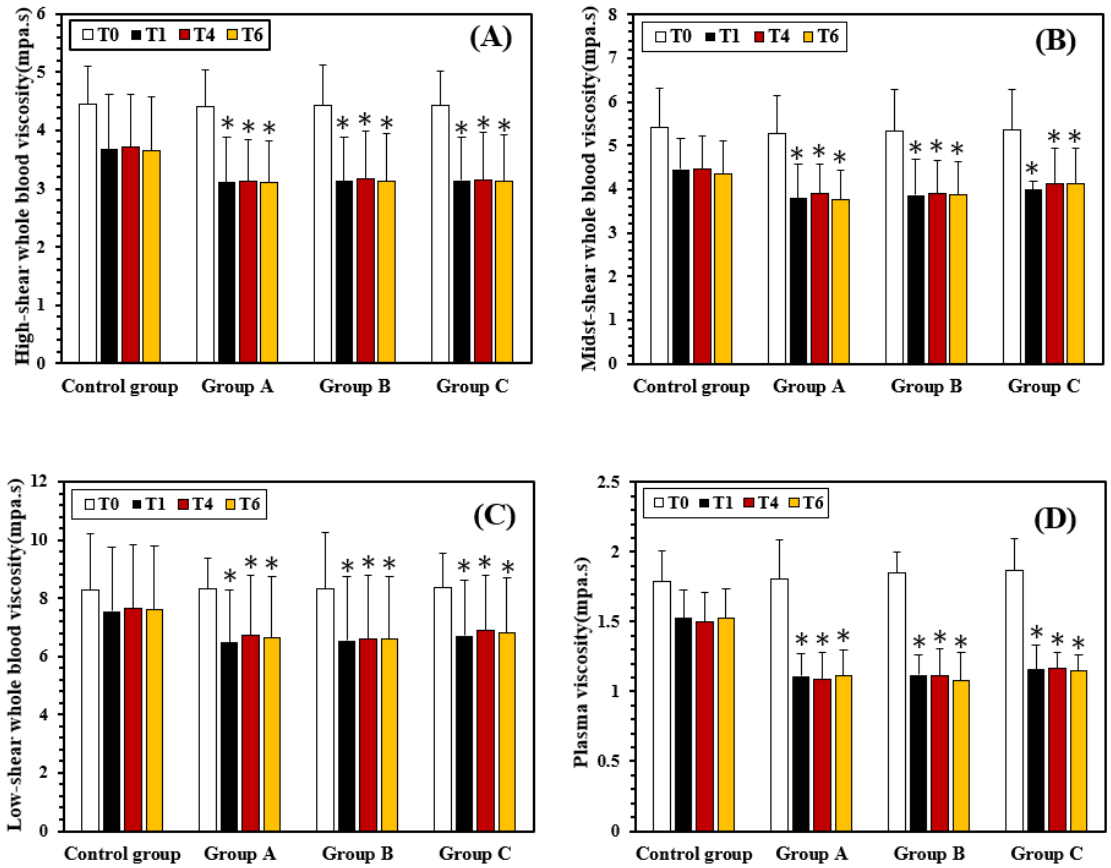


Fig. 2. *Changes in blood rheological indices at different time points. **A**) High whole blood viscosity; **B**) Medium whole blood viscosity; **C**) Low whole blood viscosity; **D**) Plasma viscosity. Compared with the control group at the same time point, *P<0.05.*

Table II. *Comparison of Apgar scores and results of umbilical cord blood gas analysis*

Indicator	Control group	Group A	Group B	Group C
1-min Apgar's score	9.39±0.42	9.54±0.53	9.41±0.61	9.65±0.42
5-min Apgar's score	10	10	10	10
Umbilical artery pH	7.33±0.04	7.34±0.03	7.33±0.04	7.36±0.02
BE (mmol/L)	-2.4±1.3	-2.6±1.9	-2.3±1.8	-2.5±1.7
PaO_2 (mmHg)	26.67±2.91	25.56±0.65	24.86±1.35	22.02±0.86
$PaCO_2$ (mmHg)	42.18±3.83	43.63±3.14	44.56±3.18	46.09±3.08

Note: The difference between the groups was not significant, P>0.05.

Table III. *Comparison of the incidence of maternal adverse reactions*

Control Group	5(33.33)	2(13.33)	5(33.33)	2(13.33)	6(40.00)	5
Group A	2(10.00) *	0(0) *	3(15.00)	1(5.00)	5(25.00) *	1*
Group B	1(5.00) *	0(0) *	2(10.00) *	0(0) *	4(20.00) *	1*
Group C	4(20.00)&	1(5.00)	4(20.00)	1(5.00)	3(15.00) *	3#&

*Note: Compared with the control group, *P<0.05; compared with Group A, #P<0.05; compared with Group B, #P<0.05.*

DISCUSSION

In recent years, numerous studies (6-8) pointed out the following outcomes: the use of α1 receptor stimulants, such as phenylephrine and anesthesia, during spinal anesthesia can be targeted to reduce the risk of intraoperative hypotension through simple vasoconstrictor effects. Methoxamine is similar to phenylephrine, which is a selective α1-adrenergic receptor activator and conducive to myocardial protection (9, 10). The three groups A, B and C all received the same dose of methoxamine (0.02 mg/kg), and their HR decreased, while there was no bradycardia. In Group B, with prophylactic injection of methoxamine (0.02 mg/kg) 1 min after anesthesia, the maternal hemodynamic fluctuations were limited. Also, it can effectively reduce maternal plasma viscosity, as well as high-, medium-, and low-whole blood viscosity. It is believed that prophylactic injection of methoxamine 1 min after anesthesia is the best plan in preventing and treating maternal hypotension under spinal anesthesia. The umbilical cord blood gas analysis was conducted to predict the adverse consequences on newborns. Two of the important indicators are pH value (< 7.2) and BE (< 12 mmol/L) (11, 12). Prophylactic injection of methoxamine for cesarean delivery could not affect the result of arterial blood gas analysis nor newborn's physical status. Moreover, prophylactic injection of methoxamine can reduce the incidence of intraoperative hypotension, while it does not increase the incidence of bradycardia and nausea and vomiting.

In summary, prophylactic injection of methoxamine for cesarean delivery using spinal anesthesia can markedly reduce the incidence of intraoperative hypotension. Prophylactic injection of methoxamine (0.02 mg/kg) at 1 min after anesthesia has limited negative consequences on both mothers and infants, indicating its safety in clinical application.

REFERENCES

1. Tian F, Wang K, Hu J, Xie Y, Sun S, Zou Z, Huang S. Continuous spinal anesthesia with sufentanil in labor analgesia can induce maternal febrile responses in puerperas. Int J Clin Exp Med 2013; 6(5):334-41.
2. Veeser M, Hofmann T, Roth R, Klöhr S, Rossaint R, Heesen M. Vasopressors for the management of hypotension after spinal anesthesia for elective cesarean section. systematic review and cumulative meta-analysis. Acta Anaesthesiol Scand 2012; 56(7):810-6.
3. Luo XJ, Zheng M, Tian G, Zhong HY, Zou XJ, Jian DL. Comparison of the treatment effects of methoxamine and combining methoxamine with atropine infusion to maintain blood pressure during spinal anesthesia for cesarean delivery: a double blind randomized trial. Eur Rev Med Pharmacol Sci 2016; 20(3):561-7.
4. Sun D, Wu Y, Yang L, Han J, Liu R, Wang L. Effects of continuous intravenous infusion of methoxamine on the intraoperative hemodynamics of elderly patients undergoing total hip arthroplasty. Med Sci Monit 2014; 20:1969-76.
5. Bell D, Duffin A, Gruss HJ, Pediconi C, Jacobs A. A randomised, controlled, crossover study to investigate the pharmacodynamics, pharmacokinetics and safety of 1R,2S-methoxamine hydrochloride (NRL001) in healthy elderly subjects. Colorectal Dis 2014; 16 Suppl 1:27-35.
6. George RB, Mckeen D, Columb MO, Habib AS. Up-down determination of the 90% effective dose of phenylephrine for the treatment of spinal anesthesia-induced hypotension in parturients undergoing cesarean delivery. Anesth Analg 2010; 110(1):154-8.
7. Doherty A, Ohashi Y, Downey K, Carvalho JCA. Phenylephrine infusion versus bolus regimens during cesarean delivery under spinal anesthesia:, a double-blind randomized clinical trial to assess hemodynamic changes. Anesth Analg 2012; 115(6):1343-50.
8. Ferré F, Marty P, Bruneteau L, et al. Prophylactic phenylephrine infusion for the prevention of hypotension after spinal anesthesia in the elderly: a randomized controlled clinical trial. J Clin Anesth 2016; 35:99-106.
9. Sun S, Sun D, Yang L, Han J, Liu R, Wang L. Dose-dependent effects of intravenous methoxamine infusion during hip-joint replacement surgery on postoperative cognitive dysfunction and blood TNF-α level in elderly patients: a randomized controlled trial. BMC Anesthesiol 2017; 17(1):75.
10. Luo XJ, Zheng M, Tian G, Zhong HY, Zou XJ, Jian DL. Comparison of the treatment effects of methoxamine and combining methoxamine with atropine infusion to maintain blood pressure during spinal anesthesia for cesarean delivery: a double blind randomized trial. Eur Rev Med Pharmacol Sci 2016; 20(3):561-7.
11. Varkilova L, Slancheva B, Emilova Z, Nikolov A, Metodieva V, Hitrova S, Boicheva E. [Blood lactate measurments as a diagnostic and prognostic tool after birth asphyxia in newborn infants with gestational age > or = 34 gestational weeks]. Akush Ginekol (Sogiia) 2013; 52(3):36-43.
12. Inês N, Ayres-De-Campos D, Ugwumadu A, et al. Central fetal monitoring with and without computer analysis: a randomized controlled trial. Obstet Gynecol 2017; 129(1):83-90.

LETTER TO THE EDITOR

Effects of dexmedetomidine combined with propofol on peri-anesthesia hemodynamics and postoperative sedation and analgesia in patients undergoing radical esophagectomy

HY. Gong[1], ZY. Wang[2], YZ. Sui[3], JJ. Zhao[4], YY. Jing[5] and M. Wang[6]

[1]Department of Anesthesiology, Zhangqiu District Maternal and Child Health Care Hospital, Jinan, Shandong, China; [2]Department of Anesthesiology, People's Hospital of Rizhao, Rizhao, Shandong, China; [3]Department of Thoracic Surgery, Qingdao Central hospital, Qingdao University, Qingdao, China; [4]Department of Surgery, The People's Hospital of Zhangqiu Area, Jinan, Shandong, China; [5]Department of Obstetrics, The People's Hospital of Zhangqiu Area, Jinan, Shandong, China; [6]Department of Anesthesiology, Maternity and Child Health Care of Zaozhuang, Zaozhuang, Shandong, China

Received July 1, 2020 – Accepted October 8, 2020

To the Editor,

Esophageal cancer (EC) ranks as the sixth leading cause of cancer death, and its 5-year survival rate is about 15-25% (1). and over the past few decades, its incidence in the Western world has risen sharply (2). Despite improvements in management and treatment, the results of the overall 5-year survival rate and 5-year esophagectomy postoperative survival rate remain unsatisfactory (3). In order to improve the prognosis of patients after surgery, neoadjuvant concurrent radiotherapy and chemotherapy (CCRT) are adopted to reduce the size of the tumor (4).

Traditionally, the method of deepening anesthesia is used to relieve stress response, but it still leads to complications such as respiratory circulation inhibition and delayed postoperative recovery. In addition, general anesthesia cannot completely eliminate the stress response (5). Dexmedetomidine via intravenous injection can exert antisympathetic, analgesic and sedative effects on the body (6). The half-life of dexmedetomidine is 6 minutes, so dexmedetomidine hydrochloride injection should be continued during the operation until surgery is finished (7). The purpose of this study was to investigate the effect of dexmedetomidine combined with propofol on patients who received radical resection of esophageal cancer, and peripheral anesthesia hemodynamics, postoperative sedation and analgesia were evaluated (8).

MATERIALS AND METHODS

Patients

From April 2017 to April 2018, 40 patients with esophageal cancer admitted to Zhangqiu District Maternal and Child Health Care Hospital were randomly divided into 2 groups, with 20 cases in each group. All patients presented normal liver and kidney functions, and had no history of hypertension, diabetes, coronary heart disease, or arrhythmia. In the control group there were 12 males and 8 females, with an average age of (40.50±8.95) years. The research group included 11 males and 9 females, with an average age of (40.25±9.10) years.

Key words: dexmedetomidine; propofol; esophageal cancer; hemodynamics; sedative pain

Corresponding Author:
Dr Min Wang,
Department of Anesthesiology,
Maternity and Child Health Care of Zaozhuang,
25 Wenhua East Road,
Zaozhuang 277100, China
e-mail: yqy22e@163.com

0393-974X (2020)
Copyright © by BIOLIFE, s.a.s.
This publication and/or article is for individual use only and may not be further reproduced without written permission from the copyright holder.
Unauthorized reproduction may result in financial and other penalties
DISCLOSURE: ALL AUTHORS REPORT NO CONFLICTS OF INTEREST RELEVANT TO THIS ARTICLE.

Anesthesia method

The research group received dexmedetomidine combined with propofol, and the control group was treated with only propofol. The two groups of patients were intravenously infused with longtonin 0.01 mg/kg 30 min before anesthesia. Routine vital signs were monitored, and then anesthesia depth monitor was used to determine the anesthesia depth index. The control group was given intravenous injection of propofol 1.5 mg/kg, midazolam 0.06 mg/kg, sufentanil 0.3 μg/kg, and cis-atracurium 0.15mg/kg. The research group was given dexmedetomidine 0.5μg/kg/h intravenously during induction, and 10 min later, propofol was switched to 1mg/kg intravenously. The doses of other induction medicines were the same as those of the control group. After induction, the two groups of patients were observed with anesthesia depth index below 50 for tracheal intubation. Before skin incision 0.2-0.3μg/kg sufentanil was added according to the operation time. The control group was maintained with propofol and cis-tracurium micropumps during operation. The research group was given dexmedetomidine, propofol, and cis-tracurium pumps for maintenance, and dexmedetomidine continued until 40 min before the end of the operation. The micropump travel speed of dexmedetomidine and propofol were adjusted according to the depth of anesthesia index (40-60). After the operation, 1 mg of atropine and 2 mg of neostigmine were used to antagonize the muscle. The tidal volume and respiratory rate were normal. When the eyes of the patient opened, the tracheal tube was removed. Further monitoring continued until fully awake and returned to the ward.

Observation indicators

The heart rate, mean arterial pressure, and EEG dual frequency index were recorded at the time points of skin incision, drug injection, tracheal intubation, anesthesia and apology, anesthesia, as well as at 1 min, 1 h and 4 h after surgery.

Visual analogue scoring standard: the painless state was 0 points, the score increased with the aggravation of pain. Ten points was the top score, indicating the pain was serious and unbearable. Postoperative sedation scoring criteria: 6 points represent deep sleep, no response to external call stimuli; shallow sleep was 5 points, and it meant the rapid response to external call stimuli; drowsiness was 3 points and meant response to instructions; the awake state was 2 points; and the state of irritability was 1 point.

Statistical analysis

The statistical software SPSS 22.0 was used to perform statistical analysis on the two sets of data. The data obtained in the experiment was expressed in the form of mean ± standard deviation, and the *t*-test was used for component comparison. P-values<0.05 were considered statistically significant.

RESULTS

Comparing the general data of the two groups of patients, no statistical difference was observed in age, sex, anesthesia time and surgery (P>0.05, Table I).

Before anesthesia induction, the EEG dual frequency index of the experimental group was significantly lower than that of the control group (P<0.05). At other time points, there was no statistically significant difference in the EEG dual frequency index between the 2 groups (P>0.05). Compared with before the injection of drugs, EEG dual-frequency index in the experimental group

Table I. *Comparison of general information between the two groups*

Groups	Cases	Age(years)	Male(cases)	Female(cases)	Anesthesia time (min)	Operation time(min)
Research group	20	40.25	11	9	226.2	254.5
Control group	20	40.50	12	8	231.3	259.6

Table II. *Comparison of EEG dual-frequency index changes at different time points between two groups of patients*

Groups	Before injection	Before induction of anesthesia	Immediately before tracheal intubation	1 min after intubation	When cutting skin	When probing	Immediately after extubation
Research group	94.52	71.52*#	50.32*	49.22*	48.63*	52.15*	97.56
Control group	95.15	94.92	50.95*	53.45*	49.11*	51.65*	97.94

*Compared with before injection, * P <0.05; compared with control group, # P <0.05.*

Table III. *Comparison of changes in mean arterial blood pressure and heart rate at different time points*

Times	Research group		Control group	
	HR/(Times/min)	MAP/kPa	HR	MAP
Before injection	77.15	12.06	78.12	12.36
Before induction of anesthesia	64.15*#	11.52*	80.64	12.95
Immediately before tracheal intubation	67.94#	10.74#	70.13#	10.84#
1min after intubation	71.66*#	11.08*#	85.21#&	12.04&
When cutting skin	70.24*#	11.13*#	80.05&	12.25&
When probing	83.06*&	13.21*&	97.13#&	14.02#&
Immediately after extubation	75.41*&	13.54*&	89.24#&	13.84#&

*Compared with before injection, * P <0.05; compared with control group, #P<0.05; Compared with the same group immediately before intubation, & P<0.05.*

before induction of anesthesia, immediately before tracheal intubation, 1 min after intubation, skin incision, and exploration, and the control group immediately before trachea tea house, 1 min after intubation, skin incision, and EEG dual frequency index were decreased significantly (P<0.05). At the time of induction of anesthesia, 1 min after intubation, skin incision, exploration, and immediately after extubation, the average arterial blood pressure of the experimental group was significantly reduced (P<0.05), and the heart rate was statistically significantly slowed (P<0.05, Table II).

Compared with before drug injection, the average arterial blood pressure and heart rate of the research group immediately before tracheal intubation, 1 min after intubation, and skin incision were significantly downregulated compared to those in the control group (P<0.05, Table III).

The sedation score of the research group after 15 min was significantly higher than that of the

Table IV. *Visual simulation and sedation score at different time points*

Score	Groups	1h after operation	4h after operation
Sedation score	Research group	3.22*	2.35*
	Control group	1.76	1.82
Visual simulation score	Research group	1.20*	1.56*
	Control group	2.53	2.04

*Compared with the control group, *P< 0.05*

control group, whereas the visual simulation score was significantly lower than that of the control group (P<0.05, Table IV).

DISCUSSION

Dexmedetomidine is a new type of highly selective α2 receptor agonist, which can act on the adrenergic α2 receptor of the central nervous system blue spot nucleus, thus exerting the roles of sedation and analgesia (9). At the same time, dexmedetomidine can also act on the peripheral nervous system, inhibit C fiber and Aα fiber, and have an analgesic effect (10). When the brainstem blue lobe nucleus α2 receptor is activated, dexmedetomidine can cause the body to produce anti-anxiety, hypnosis, and sedative effects (11).

The results of this study showed that 15 min after infusion of dexmedetomidine before anesthesia induction, the heart rate and mean arterial blood pressure in the research group were decreased significantly compared to those in the control group, indicating that dexmedetomidine can effectively maintain the stability of hemodynamic changes during intubation. As an important indicator to evaluate the depth of anesthesia sedation, the results showed that the EEG dual frequency index of the experimental group was significantly lower than that of the control group after the injection of the drug and before the induction of anesthesia. After injection of dexmedetomidine hydrochloride in the experimental group, the EEG dual-frequency index before the induction of anesthesia, immediately before tracheal intubation, 1 min after intubation, skin incision, and exploration were significantly lower than that of the control group, indicating that dexmedetomidine can produce an effective sedative effect on the body.

In summary, dexmedetomidine combined with propofol for general anesthesia can effectively maintain hemodynamic stability, which can help to improve the surgical efficacy and postoperative recovery of patients.

REFERENCES

1. Huang FL, Yu SJ. Esophageal cancer: Risk factors, genetic association, and treatment. Asian J Surg 2018; 41:210-15.
2. Domper Arnal MJ, Ferrández Arenas Á, Lanas Arbeloa Á. Esophageal cancer: Risk factors, screening and endoscopic treatment in Western and Eastern countries. World J Gastroenterol 2015; 21:7933-43.
3. Watanabe M, Otake R, Kozuki R, Toihata T, Takahashi K, Okamura A, Imamura Y. Recent progress in multidisciplinary treatment for patients with esophageal cancer. Surg Today 2020; 50:12-20.
4. Kato H, Nakajima M. Treatments for esophageal cancer: a review. Gen Thorac Cardiovasc Surg 2013; 61:330-5.
5. Devroe S, Van de Velde M, Rex S. General anesthesia for caesarean section. Curr Opin Anaesthesiol 2015; 28:240-6.

6. Kim BS, Choi JH, Baek SH, Lee DH. Effects of intraneural injection of dexmedetomidine in combination with ropivacaine in rat sciatic nerve block. Reg Anesth Pain Med 2018; 43:378-84.
7. Cho HK, Yoon HY, Jin HJ, Hwang SH. Efficacy of dexmedetomidine for perioperative morbidities in pediatric tonsillectomy: A metaanalysis. 2018; 128:E184-e93.
8. Wang X, Shan Y, Tang Z, Gao L, Liu H. Neuroprotective effects of dexmedetomidine against isoflurane-induced neuronal injury via glutamate regulation in neonatal rats. Drug Des Devel Ther 2019; 13:153-60.
9. Gao J, Sun Z, Xiao Z, et al. Dexmedetomidine modulates neuroinflammation and improves outcome via alpha2-adrenergic receptor signaling after rat spinal cord injury. Br J Anaesth 2019; 123:827-38.
10. Schnabel A, Reichl SU, Weibel S, Kranke P, Zahn PK, Pogatzki-Zahn EM, Meyer-Frießem CH. Efficacy and safety of dexmedetomidine in peripheral nerve blocks: A meta-analysis and trial sequential analysis. Eur J Anaesthesiol 2018; 35:745-58.
11. Milanick WJ, Polo-Parada L, Dantzler HA, Kline DD. Activation of alpha-1 adrenergic receptors increases cytosolic calcium in neurones of the paraventricular nucleus of the hypothalamus. J Neuroendocrinol 2019; 31:e12791.

LETTER TO THE EDITOR

Yifei Xuanfei Jiangzhuo Chinese bioformulation improves cognitive function in a murine model of vascular dementia – the implication of PI3K/AKT and Erk signalling pathway

W. Chen[1,2#], L. Wu[2,3#], LF. Jiang[4], YQ. Hu[1,2], Y. Zhai[2,5], JH. Li[1,2], Y. Wu[4] and N. Tang[1,2]

[1]Department of Neurology, The First Affiliated Hospital of Guangxi University of Chinese Medicine, Nanning, Guangxi, China; [2]Guangxi Key Laboratory of Chinese Medicine Foundation Research, Guangxi University of Chinese Medicine, Nanning, Guangxi, China; [3]Scientific Laboratorial Centre, Guangxi University of Chinese Medicine, Nanning, Guangxi, China; [4]Graduate College, Guangxi University of Chinese Medicine, Nanning, Guangxi, China; [5]Guangxi International Zhuang Medicine Hospital, Nanning, Guangxi, China

Received May 22, 2020 – Accepted September 22, 2020

[#]These authors contributed equally to this work

To the Editor,

Vascular dementia (VD) is a syndrome of acquired and sustained intellectual impairment caused by various cerebrovascular diseases (1). A recent global epidemiological study of cognitive impairment shows that, based on current trends, the incidence of the Alzheimer's disease and VD will reach 42.3% globally by 2020, with 11.7% in developing countries including China (2). The increase in the incidence of VD brings a heavy burden to the society and family, mainly due to the lack of specificity of treatment. In recent years, Traditional Chinese Medicine (TCM) has made remarkable progress in treating VD (3). Cerebral ischemia leads to nerve injury, limited nerve repair, cognitive dysfunction and development of VD. Even three months after cerebrovascular injury, neural stem cells could migrate from the neural stem cell pool to the ischemic injury area and differentiate into neurons (4). However, the ability of neural stem cells to differentiate into neurons is limited. Neurogenesis is regulated by intracellular signalling pathways and extracellular microenvironment. PI3K/AKT and Erk signalling pathways play essential biological roles in regulating learning and memory (5).

Studies have shown that Yifei xuanfei jiangturbid (YXJF), a Chinese traditional drug improves memory impairment in cerebral ischemia/reperfusion rats, inhibits hippocampal apoptosis in a dose-dependent manner, and attenuates B-cell lymphoma 2 (Bcl-2)-related X protein and c-Jun and reduces the expression of Bcl-2 protein in the hippocampus (6). YXJF is made from 9 traditional Chinese medicines, including Campanulaceae, Mountain Apricot, Ginseng, Ophiopogon japonicus, Astragalus, Panax notoginseng, Perilla, Shichangpu, Rhubarb, and is used as a water decoction (7).

This study aimed to evaluate *in vivo* on a rat model of vascular dementia the beneficial effect of Yifei Xuanfei Jiangzhuo formula (YFXFJZ-P) on learning and memory and the underlying mechanism associated with PI3K, AKT and Erk signalling pathway. An *in vitro* study on the third generation rat brain microvascular endothelial cells (BMECS)

Key words: Yifei Xuanfei Jiangzhuo prescription; vascular dementia; PI3K-AKT pathway; Erk pathway; BMECS

Corresponding Author:
Dr Nong Tang,
Department of Neurology,
The First Affiliated Hospital
of Guangxi University of Chinese Medicine,
Nanning, 530023, Guangxi, China
e-mail: tangnongtn000@163.com

0393-974X (2020)
Copyright © by BIOLIFE, s.a.s.
This publication and/or article is for individual use only and may not be further reproduced without written permission from the copyright holder.
Unauthorized reproduction may result in financial and other penalties
DISCLOSURE: ALL AUTHORS REPORT NO CONFLICTS OF INTEREST RELEVANT TO THIS ARTICLE.

was used to evaluate the effect of YFXFJZ-P on the proliferation and apoptosis of cerebrovascular cells.

MATERIALS AND METHODS

Drug

YFXFJZ-P (made up of 10 g of platycodon grandiflorum, 10 g of almond, 15 g of ginseng, 15 g of radix ophiopogonis, 10 g of aconite, 15 g of astragalus, 15 g of tianqi, 15 g of suzi, 15 g of acus tatarinus, 6 g of rhubarb) was purchased by the pharmacy of The First Affiliated Hospital of Guangxi University of Chinese Medicine, Nanning,, Guangxi, China for standby use (every single herb requires the same origin, the same quality level and the same batch). This formula was divided into two, and each quantity was used for water decoction and then concentrated to 1 g/mL and maintained at 4°C for later use. High-performance liquid chromatography (HPLC; Milford, MA, USA) was used to analyze the concentration of the decoction. A standard curve was first drawn using a standard concentration of reference compound, and then a 20 µl reagent sample diluted with water was tested. The chemical structure was compared with the reference compound to determine the concentration of each component.

Animals

Male Wistar rats (n=80; age, 8-weeks old; weight, 200-230 g) were used in the experiment. The animals were kept in standard laboratory conditions with controlled temperature, humidity and a 12-hour dark/light cycle and adapted for one week before the starting of the experiment. The animals received free access to standard animal feed and filtered water. The animal experiment was approved by the Ethics Committee of The First Affiliated Hospital of Guangxi University of Chinese Medicine, China.

In Vivo Animal Study

VD animal model

After the adaptability period, the rats from the VD model group underwent 8-12 h of fasting with free access to drinking water before surgery. The animals were anaesthetized with 10% chloral hydrate in doses of 3 mL/kg injected intraperitoneally, the hair on the neck areas was removed, the animal was fixed in a prone position, and a midline incision was performed on the neck, and the carotid artery was ligatured with a silk thread for blocking the blood flow for 20 min. At the same time, from the tail of the rats, 3 mL of blood was left to flow. After 20 min of ischemia, the silk thread was released and the blood flow was left to restore for 10 min. This period of 20 min ischemia/10 min of reperfusion was repeated for 3 successive times until the VD model was obtained.

After the third blood reperfusion, respiratory and cardiac beats were observed to be stable. After the incision was closed, each rat received cephalosporin (25 mg/kg bw, Guangzhou Baiyun pharmaceutical, China) and was put back into the cage for normal feeding.

The rats were divided into 4 groups, 20 per group as follows:

- Normal group: 20 rats, without surgery that received 10mL/kg/day normal saline solution for 8 weeks from the third day after modelling.
- Sham-operated group: 20 rats were incised locally on the neck, and after the common carotid artery was isolated, the skin was neither ligated nor cut, and the skin was directly stitched after exposure for 5 min. Starting from the third day after modelling, the rats received 10mL/kg/day normal saline solution for 8 weeks.
- VD model group: 20 rats in which the VD model was obtained as previously described. Starting from the third day after modelling, the rats received 10mL/kg/day normal saline solution for 8 weeks.
- Treatment group: 20 rats in which the VD model was obtained as previously described. Starting from the third day after modelling, the rats received 3 mL YFXFJZ-P decoction for 8 weeks.

Behavioural tests

Morris water maze automatic control instrument (Type: SMG - 2) was used to evaluate learning and memory of rats in the four groups. The rats were placed in a large circular pool with the head up to prevent drowning and the time till the animal found a hidden platform was registered as escape latency. The time for the rats to find the platform was 120 s. The rats were numbered in sequence and put into the water according to the order of four quadrants. The time was recorded from the start till the rat found and climbed onto the platform. If the rat could not find the platform within 120 s, it was artificially guided to the platform and left to stay for 30 s before being removed and dried, and the incubation period was

recorded as 120 s (2 min). The test was repeated four times per day of evaluation and the arithmetic mean of four trials was taken as the result of the day. The test was carried out after 7 days, 4 weeks and 8 weeks of treatment.

After 8 weeks of treatment, the rats were sacrificed by exsanguinations after anaesthesia with chloral hydrate (300 mg/kg, i.p) (Beyotime Institute of Biotechnology Co., Ltd., Shanghai, China) and the brain was isolated, the hippocampus was separated and divided into 2 parts, one used to detect the apoptosis rate of nerve cells and the other used to evaluate the expression of PI3K, AKT and Erk proteins.

Flow cytometry

Flow cytometry (FCM) was used to detect the apoptosis rate of hippocampal nerve cells in rats after treatment. The hippocampus was separated and cleaned with phosphate buffer saline (PBS, 0.01 mol/L, pH 7.4, Sigma-Aldrich, USA). The hippocampal envelope and blood vessels were removed under a surgical microscope. The hippocampus was cut into pieces of 1 mm × 1 mm × 1 mm and digested with 25% trypsin solution in PBS at 37°C. After digestion, Dulbecco's Modified Eagle's Medium DMEM (Thermo Fisher Scientific, USA) containing 10% calf serum was added and centrifuged at 1000 r/min for 5 min and the cell precipitate was washed with PBS and then the cells were suspended in PBS. The cells were fixed for 1 h at 4°C in 70% ethanol, then washed with PBS and stained with propidium iodide (PI) (Thermo Fisher Scientific, USA) at 4°C for 30 min in the dark. Finally, the percentage of apoptotic cells was evaluated using a flow cytometry instrument (Type: MoFlo Astrios EQ, Beckman Coulter, USA).

Western blot

The other part of the hippocampus collected from the rats was used to detect the level of PI3K, AKT and Erk proteins. The hippocampus was homogenized and centrifuged. Proteins were extracted with RIPA Lysis Buffer (Thermo Fisher Scientific, USA) and then 10% sodium lauryl sulfate-polyacrylamide gel electrophoresis was used for denaturation and separation of protein samples. The separated proteins were transferred to the polyvinylidene fluoride membrane (Shanghai Yuanye Biotechnology Co., Ltd., China). These membranes were incubated overnight with primary antibodies-beta Actin Monoclonal Antibody (Item No: MA1-140, Thermo Fisher Scientific, USA) (dilution: 1:5000) at 4°C and then incubated with the corresponding secondary antibodies-Goat anti-Mouse IgG (H+L) (Item No: A32723TR, Thermo Fisher Scientific, USA) (dilution: 0.3 μg/mL) at room temperature for 1 hour. Finally, the concentration of myosin was determined by chemiluminescence to detect the ability of antibody binding.

In Vitro Study

Primary culture of brain microvascular proliferation cells

At the end of the experiment *in vivo*, the rats in the normal group were sacrificed as previously described and the brain from 1 rat was quickly removed with as much integrity as possible. The brain was placed in a precooled Dulbecco's Modified Eagle Medium/Nutrient Mixture F-12 (DMEM/F12) (Thermo Fisher Scientific, USA). The outer blood scab, meninges, and outer blood vessels were removed and then the white matter, and the grey matter was retained (shell-like left and right sides of the brain). The grey matter was washed several times with a precooling medium at 4°C. The brain was cut into 1 mm3 block and transferred to a sterile 50 mL centrifuge tube. The brain block was cut into pieces and blown by the pipette and centrifuged at 900 r/min at room temperature for 4 min, and then the supernatant was discarded and 5 mL DMEM/F12 serum-free medium was added. Then 10 mL medium plus 100 μL collagenase II (Gibco, USA) was added and left to digest at 37°C for 30-45 min. After digestion, the DMEM/F12 serum-free medium was added for neutralization and centrifuged at 900 r/min at room temperature for 10 min. 15 mL 25% Biotin-Avidin System (BAS) (Thermo Fisher Scientific, USA) was added directly and centrifuged at 2,000 r/min for 20 min. After centrifugation, the centrifuge tube was stratified, and the lower layer was dark red (a small amount) for brain microvascular cells. The excess poly-lysine in the 6-well plate was gently rinsed with normal saline twice. The sub-brain microvasculature was precipitated, mixed with normal saline, and centrifuged at 900 r/min at room temperature for 5 min. The cells were re-suspended with fresh DMEM/F12 complete medium and then transferred to a 6-well plate for culture.

Cells groups after modelling

The third generation of BMECS cells was taken, digested and densified to 1.5 × 105 /mL, and inoculated into 6-well plate. After the fusion state was presented, the cells were

divided into 3 groups (control group, model group and treatment group) and each group was worked in 6 replicates.

Corresponding concentration of drug-containing serum was added to the treatment group to a final concentration of 10% and incubated for 12 h. The model group and the treatment group were exposed to hypoxia and sugar deprivation to simulate ischemia and hypoxia. The cells were incubated at 37°C for 6 h in an incubator with an airlock and continuously gassed with 93% N2/ 5% CO2/ 2% O2. Hank's balanced salt solution lacking glucose was used as an incubation medium and was treated for 30 min, with 93%N_2/5%CO2/2%O2 before culture.

Cell counting kit-8 assay

Cells were seeded onto a 96-well plastic plate at a density of 5×104/mL. 10 mL Cell Counting Kit (CCK-8) (WST-8/CCK8) (ab228554, Abcam, UK) was added at 0, 12, 24, 48, 60, 72 and 84 h after incubation, respectively. The plates were then incubated at 37°C for 4 h. The optical density (OD) was measured at 450 nm by Fluorescence Spectrophotometer (Thermo Fisher Lumina, USA).

Apoptosis assay

Hoechst staining was used to analyze apoptosis in the cell groups. In a cell culture plate (Nunc 6-well plate, round, Thermo Fisher, USA), the cells were immobilized and stained with 10g/mL fluorescent dye (Hoechst 33342, Sigma-Aldrich, USA) in the dark for 10 min. The samples were observed under an inverted fluorescence microscope (EVOS XL Core, Thermo Fisher, USA) and washed with PBS. Apoptotic cells have obvious morphological changes in the nucleus, which can be identified by densification of the nucleus or densification of stained fragments. The apoptosis was determined at 84 h after incubation.

Statistical analysis

SPSS 18.0 statistical software (IBM, USA) was used for analysis. The results were expressed as mean ± standard

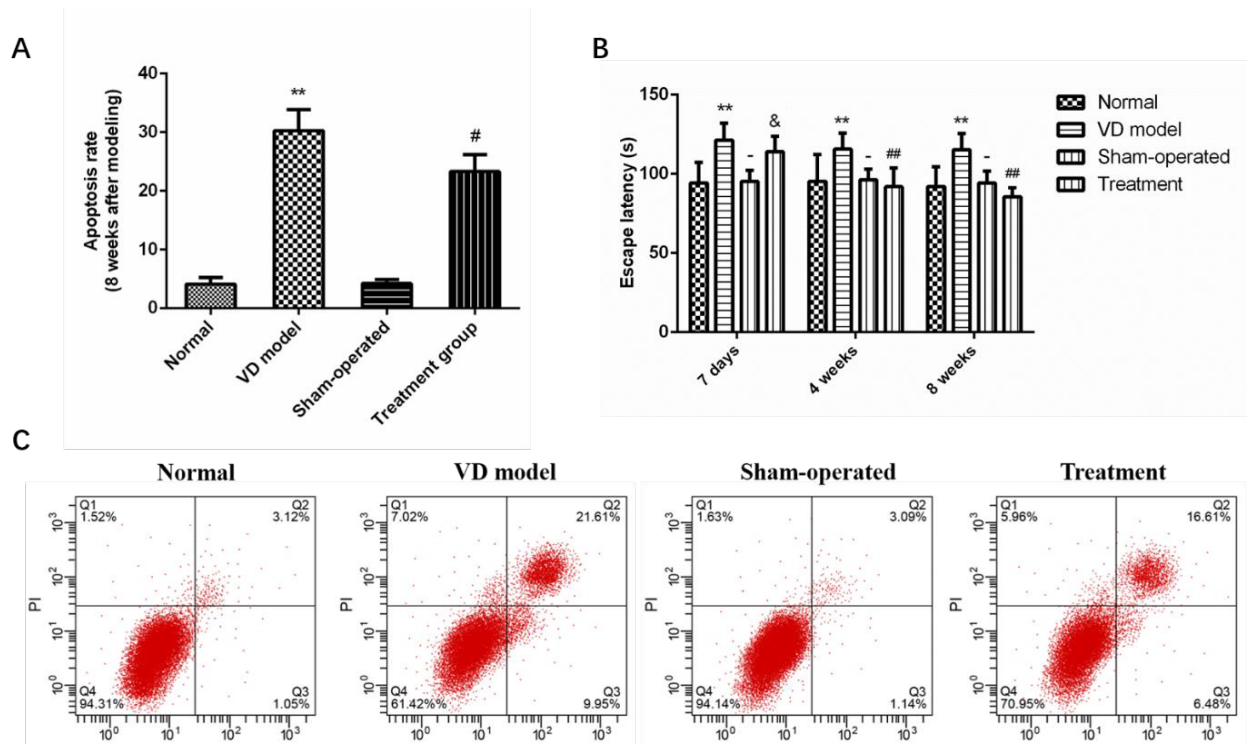


Fig. 1. *Results of apoptosis rate, evasive latency and apoptosis ability in each group.* ***A)*** *Comparison of apoptosis rate of hippocampal nerve cells in each group (%);* ***B)*** *Comparison of evasive latency at each time node in four groups;* ***C)*** *Apoptotic cells in each group at 8 weeks after modelling.* ** *Comparison between VD model group and sham-operated group (P<0.01);* # *Comparison between treatment group and model group (P < 0.05);* ## *Comparison between treatment group and model group (P < 0.01);* & *Comparison between normal group and treatment group (P < 0.05); Comparison between normal group and sham-operated group (P > 0.05).*

deviation (x ± s). All statistical tests were conducted by *t*-test. P <0.05 was considered statistically significant.

RESULTS

In Vivo Animal Study

Effect of YFXFJZ-P on the rat behaviour

Seven days after the modelling, the escape latency in the VD model group (116.47±6.99) and the treatment group (116.89±5.44) was higher than that of the sham group (94.85±13.47), showing that the model was successful obtained (Fig. 1). Four weeks after modelling, the escape latency in the treatment group (89.92±3.20) decreased significantly compared to the VD model group (117.00±5.64) (Fig. 1B). After 8 weeks of modelling, the escape latency in the treatment group (87.15±12.74) decreased significantly compared to the model group (117.54±5.05) (P < 0.05), reaching the same level as the normal and sham-operated group (Fig. 1B).

Effect of YFXFJZ-P on the apoptosis rate of rat hippocampal nerve cells

After 8 weeks of modelling, the apoptosis rate of hippocampal nerve cells was significantly increased in the VD model group compared to the sham-operated group (P<0.01). In the treatment group, the apoptosis rate significantly decreased compared to the VD model group (P<0.05) (Fig. 1A, C).

Effect of YFXFJZ-P on PI3K, AKT and Erk protein expression in the hippocampus of rats

Western blot analysis showed that the expression of PI3K, AKT, and Erk proteins in the VD model group was significantly decreased compared to the sham-operated group (P < 0.05). In the treatment group, the expression of PI3K, AKT, and Erk proteins were significantly decreased compared with the sham-operated group but significantly increased compared to the VD model group (P < 0.01) (Fig. 2 A, B).

In vitro study

Effect of YFXFJZ-P on cell proliferation after the primary culture of rat brain microvascular endothelial cells

The results of CCK-8 assay showed that compared with the control group, YFXFJZ-P could restore the proliferation of BMECS, while the model group could inhibit the proliferation of BMECS (Fig.3A).

Effect of YFXFJZ-P on apoptosis rate of cerebrovascular cells

The apoptosis rate of the model group and the treatment group was significantly increased compared with the control group (P<0.05). In the treatment group, the apoptosis rate significantly decreased compared with the model group (P<0.05), indicating that YFXFJZ-P had a significant protective effect against ischemia and hypoxia injury (Fig. 3 B, C).

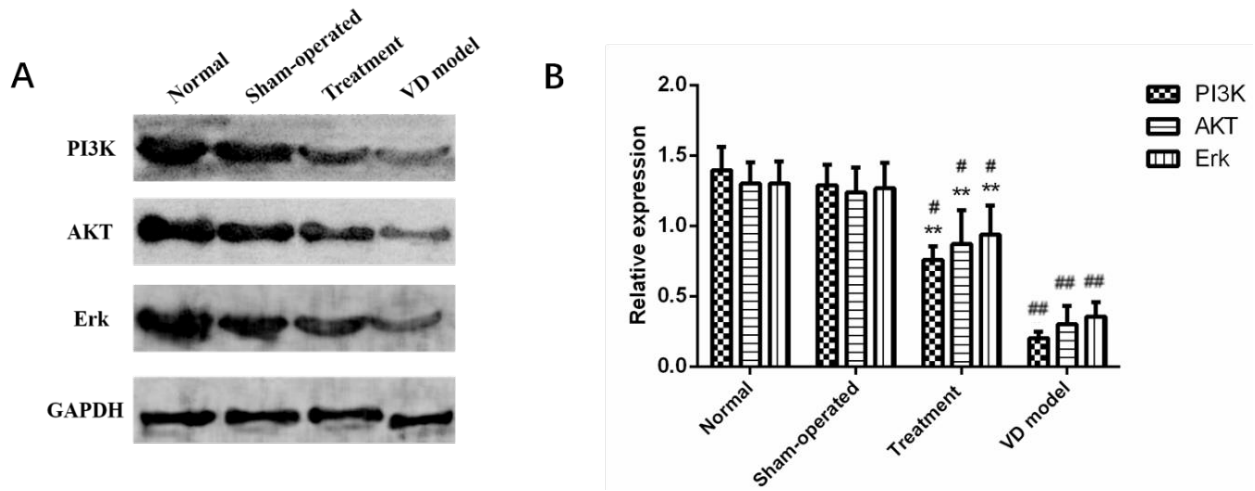


Fig. 2. *PI3K, AKT and Erk protein expression in the normal group, Sham-operated group, VD model group and Treatment group. **A)** Western blotting; **B)** Relative expression of the proteins. ** Compared with the VD model group (P<0.01); # compared with the sham-operated group (P<0.05), ## Compared with sham-operated group (P < 0.01).*

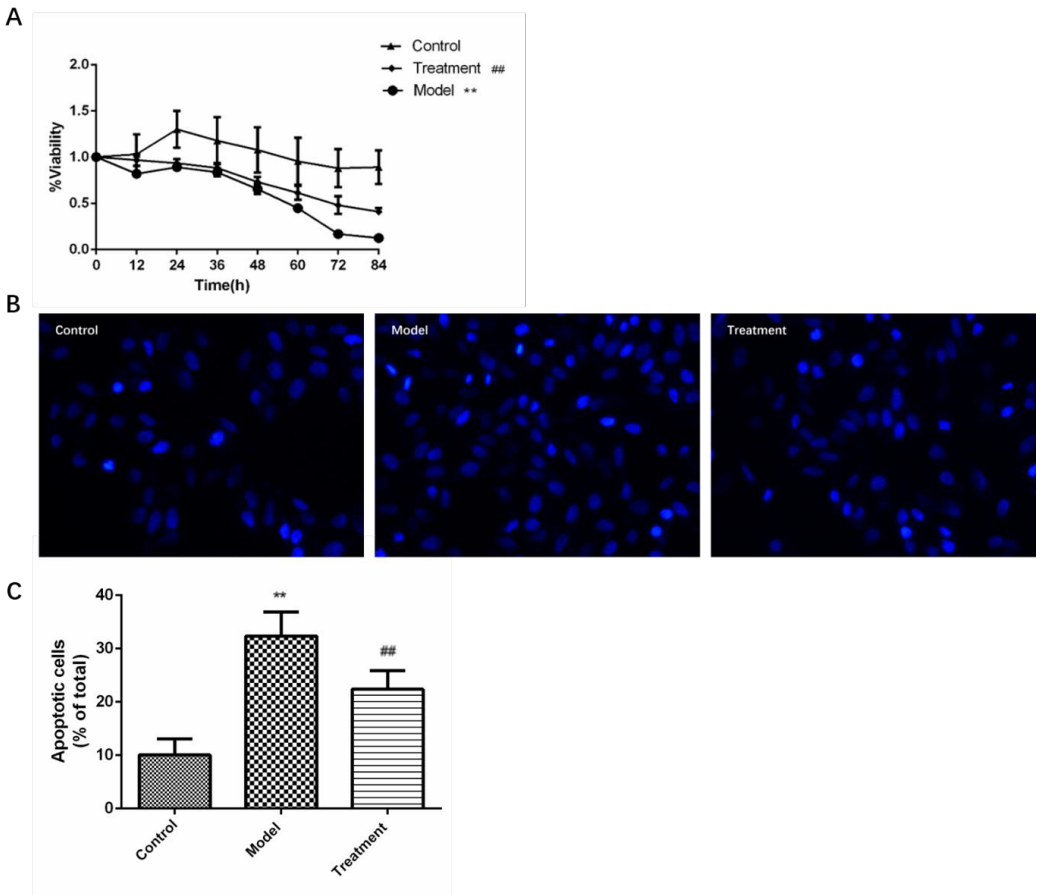


Fig. 3. *Results of cell proliferation assay and apoptosis assay in each group.* ***A****) Results of cell proliferation assay in Control group, Model group and Treatment groups;* ***B, C****) Results of apoptosis assay in Control group, Model group and Treatment group. ** Comparison between model group and control group (P<0.01); ## Comparison between treatment group and model group (P < 0.01).*

DISCUSSION

VD is a cognitive dysfunction syndrome caused by a reduced circulation of the blood in the brain, that deprives the brain of nutrients and oxygen. Several pathological conditions such as stroke, atherosclerosis, diabetes and brain haemorrhage can lead or increase the risk for vascular dementia (8, 9).

In this study, we used a murine model of VD successfully obtained by inducing ischemia-reperfusion by ligature of the carotid artery of rats that showed significant impairment of the memory and learning functions, which was in accordance with previous studies that used the same model of VD (10). The treatment with YFXFJZ-P formula showed beneficial effects in cognitive impairment after 4 and 8 weeks of treatment.

Apoptosis of delayed nerve cells after cerebral ischemia is one of the main mechanisms of VD. In our VD murine model, the apoptosis rate significantly increased in the model group compared to the normal and sham-operated group. The treatment with YFXFJZ-P formula reversed these effects after 8 weeks of treatment. The PI3K/AKT signalling pathway exists in various types of nerve cells. It acts in maintaining cerebral blood flow and regulating learning and memory capacity (11). ERK (including ERK1 and ERK2), also known as p44MAPK and p42MAPK, is an important intracellular serine/threonine-protein kinase, and pERK is its active form. The substrates of ERK include other important kinases, transcription factors, histones and K+

channels in cells, which are important components in cells and are essential in the formation of learning and memory (12). The present study shows that the expression of PI3K, AKT and Erk proteins levels in the hippocampus significantly decreased in the VD model group compared with the sham-operated group. The treatment with YFXFJZ-P formula for 8 weeks succeeded in significantly reversing these effects. In the second part of our study, we use an *in-vitro* model of VD using brain microvascular endothelial cells exposed to ischemia and hypoxia. The survival rate and apoptosis rate of endothelial cells after hypoxia and hypoglycemia injury were significantly increased compared to the control group, while the treatment with YFXFJZ-P formula significantly decreased the apoptosis rate and increased the viability of the BMECS cells compared with the model group.

In summary, this study showed that YFXFJZ-P formula could significantly improve the learning and memory function of VD rats by regulating PI3K/AKT and Erk signalling pathways in the hippocampus and promoting the growth of rat brain microvascular endothelial cells and inhibiting their apoptosis.

ACKNOWLEDGMENTS

This work was supported by The Project of National Natural Science Foundation of China (No.81760847), The Key research and development Program of Science and Technology Plan Project of Guangxi (No. Guike AB16380324), The Key Project of National Natural Science Foundation of China (No. 2018GXNSFDA050018), The Project of Guangxi Key Laboratory of Chinese Medicine Foundation Research (No. 16-380-58-04) and The High-level Talent Team Cultivation Project of Qihuang Project of Guangxi University of Traditional Chinese Medicine (No.2018003).

REFERENCES

1. Azarpazhooh MR, Hachinski V. Vascular cognitive impairment: A preventable component of dementia. Handb Clin Neurol 2019; 167:377-91.
2. Ortega RL, Dakterzada F, Arias A, Blasco E, Naudi A, Garcia FP, Piñol-Ripoll G. Usefulness of CSF biomarkers in predicting the progression of amnesic and nonamnesic mild cognitive impairment to Alzheimer's disease. Curr Aging Sci 2019; 12(1):35-42.
3. Zhang YY, Zhang XJ, Yang J, Fan YQ, Cui JC, Wang P, Zhang QP. [Effects of huayu tongluo moxibustion on learning and memory ability and the hippocampal BDNF/TrkB expressions in the rats of vascular dementia]. Zhongguo Zhen Jiu 2019; 39(1):65-71.
4. Sun L, Li M, Sun X, Li X. Zerumbone promotes proliferation of endogenous neural stem cells in vascular dementia by regulating Notch signalling. Folia Neuropathol 2019; 57(3):277-84.
5. Shu Y, Zhang H, Kang T, Zhang JJ, Yang Y, Liu H, Zhang L. PI3K/Akt signal pathway involved in the cognitive impairment caused by chronic cerebral hypoperfusion in rats. PloS One 2013; 8(12):e81901.
6. Wu L, Zhao QS, Li TW, et al. Yifei Xuanfei Jiangzhuo formula, a Chinese herbal decoction, improves memory impairment through inhibiting apoptosis and enhancing PKA/CREB signal transduction in rats with cerebral ischemia/reperfusion. Mol Med Rep 2015; 12(3):4273-83.
7. Li TW, Tang N, Zhao QS. Clinical observation of Yifei Xuanfei Jiangzhuo Formula treated vascular dementia. Guangxi J Trad Chin Med 2014; 37:105-7.
8. Tsatsakis A, Docea AO, Calina D, et al. A Mechanistic and Pathophysiological Approach for Stroke Associated with Drugs of Abuse. J Clin Med 2019; 8(9):1295.
9. Buga AM, Docea AO, Albu C, et al. Molecular and cellular stratagem of brain metastases associated with melanoma. Oncol Lett 2019; 17(5):4170-75.
10. Wu L, Feng XT, Hu YQ, et al. Global gene expression profile of the hippocampus in a rat model of vascular dementia. Tohoku J Exp Med 2015; 237(1):57-67.
11. Qi YY, Feng XF, Qiu L, Yang F. 3-n-butylphthalide inhibits the apoptosis of nerve cells in rats with cerebral small vessel disease via the PI3K/Akt pathway. Eur Rev Med Pharmacol Sci 2019; 23(10):4474-80.
12. Lai HC, Chang QY, Hsieh CL. Signal Transduction Pathways of Acupuncture for Treating Some Nervous System Diseases. Evid Based Complement Alternat Med 2019; 2019:2909632.

LETTER TO THE EDITOR

Investigating the relationship between peripheral blood eosinophils and myocardial infarction complicated by *Helicobacter pylori* infection

J. Han, M. Jiu and W-D. Fan

Department of Cardiovascular Medicine, Henan Provincial Chest Hospital, Zhengzhou, Henan, China

Received July 16, 2020 – Accepted November 4, 2020

To the Editor,

Acute myocardial infarction (AMI) is a common coronary heart disease, mainly occurring in patients suffering from coronary atherosclerosis with vulnerable plaque (1, 2). In coronary atherosclerotic stenosis, it is generally considered that the vulnerable coronary atherosclerotic plaque rupture, and platelets then accumulate on the surface of this ruptured plaque to form a thrombus, which suddenly blocks the coronary artery lumen and causes myocardium ischemic necrosis (1, 2). Some studies suggest that coronary atherosclerosis results from lipid accumulation in the blood vessel wall (3, 4); whereas, recently, other studies have argued that inflammation was the root cause of atherosclerosis in patients, with inflammation being closely related to the formation of atherosclerotic plaques (5, 6). Peripheral blood eosinophils (EOS) are a subpopulation of cells involved in the body's inflammatory response, with some studies indicating that immune cells could speed up atherosclerosis and cause inflammation, and may be associated with coronary artery disease (7, 8). Chen LL. et al. suggested that *Helicobacter pylori* (*H.pylori*) might affect the EOS level in the peripheral blood by aggravating the inflammatory response of AMI (9). Therefore, this paper aims to further explore the relationship between EOS count and AMI patients infected by *H.pylori*.

MATERIALS AND METHODS

Two hundred and twenty-four patients with coronary heart disease who were treated in our hospital from March 2, 2016 to March 2, 2018 were enrolled in this study. AMI patients were selected as the AMI group, and stable angina pectoris (SAP) patients were selected as the SAP group. The AMI group had 106 subjects, of whom 67 were male and 39 were female. The group had an age range from 35 to 68 years (average age: 46.97±12.34 years) and had coronary heart disease duration from 3 to 38 days (average duration: 13.74±3.55 days). The SAP group had 118 cases that consisted of 52 males and 66 females. Their ages ranged from 32 to 67 years (average age: 45.29±13.50 years), with coronary heart disease duration range from 4 to 36 days (average duration: 12.65±3.12 days). There were no statistically significant differences in age, gender, or disease duration between the two groups ($P>0.05$).

Inclusion criteria: patients diagnosed with coronary heart disease by coronary angiography, and among the anterior branch, circumflex branch, left main trunk, and right coronary artery, at least one of them had a stenosis exceeding 50%; age between 18 and 75 years; patients had stayed in hospital for more than 3 days; patients and their families signed the informed consent form.

Key words: peripheral blood eosinophils; concurrent Helicobacter pylori infection; myocardial infarction; correlation

Corresponding Author:
Wei-Dong Fan,
Department of Cardiovascular Medicine,
Henan Provincial Chest Hospital,
No. 1 Weiwu Road, Jinshui District
Zhengzhou 450000, China
Tel.: +86 0371 65662413- Fax: +86 0371 65662413
e-mail: fanwd93725@163.com

0393-974X (2020)
Copyright © by BIOLIFE, s.a.s.
This publication and/or article is for individual use only and may not be further reproduced without written permission from the copyright holder.
Unauthorized reproduction may result in financial and other penalties
DISCLOSURE: ALL AUTHORS REPORT NO CONFLICTS OF INTEREST RELEVANT TO THIS ARTICLE.

Exclusion criteria: malignant tumors; other infections; severe damage to liver or kidney function; blood system diseases; pregnancy; patients taking drugs, such as hormones and antibiotics, one week prior to the study.

Drug sensitivity test

At the time of admission, 5 mL of fasting venous blood was collected for routine centrifugation at the speed of 1500 r/min for 20 min. When the centrifugation was completed, the supernatant was collected for testing. Automatic biochemical analyzer (Hitachi, Japan) was used to detect the level of serum high-sensitivity C-reactive protein (hs-CRP), and the reference range was 0–3.0mg/L. The automatic blood cell analyzer (Sysmex medical electronics) Co., Ltd.) was used to test the absolute value of serum EOS, and the reference range was $0–0.8\times10^9$/L.

The ^{14}C-UBT test kit (Shanghai Puke Biotechnology Co., Ltd.) was used to test patients with *H.pylori* infection, in strict accordance with the test kit operating instructions. YH2000 *H.pylori* detection analyzer was used to analyze the results from the ^{14}C-UBT test kit. When "+" appeared on the test, patients were diagnosed with *H.pylori* infection and were recorded as "*H.pylori* (+)". When "-" appeared on the test, patients were not infected by *H.pylori* and were recorded as "*H.pylori* (-)".

Observation indicators

The patients' clinical data were collected on the day of admission, including gender, age, heart rate, height, systolic blood pressure, diastolic blood pressure, diabetes history, hypertension history, hyperlipidemia history, smoking history, white blood cell count, EOS count, hs-CRP levels, and fibrinogen levels, as well as the total number of cases that were *H.pylori* (+). The general data was compared between the AMI and SAP groups. Moreover, the clinical data from the AMI and the SAP patients in the *H.pylori* (+) and (-) groups was also compared.

Statistical analysis

SPSS 23.0 statistical software was used for data analysis. The normal measurement data was expressed as "Mean±SD" and comparison between the two groups was performed by the *t*-test. Non-normal data was expressed by "Median (IQR)" and enumeration data was calculated by a percentage. Comparison among groups was performed by the *Chi*-squared test or Fisher's exact probability method. Multivariate analysis was performed by the logistic regression model, and $P<0.05$ was considered statistically significant.

RESULTS

There were no statistically significant differences in age, heart rate, diabetes history, and fibrinogen levels between the AMI and SAP groups ($P>0.05$). For males with a long-term smoking history, their white blood cell count, *H.pylori* (+), and hs-CRP levels were higher in the AMI group than those in the SAP group. The AMI group had significantly lower systolic blood pressure, diastolic blood pressure, history of hypertension, history of hyperlipidemia, and EOS than those in the SAP group ($P<0.05$) (Table I).

In the *H.pylori* (+) group, there was no statistically significant difference between AMI and SAP patients in gender, age, heart rate, diabetes history, hypertension history, and long-term smoking history ($P>0.05$). The AMI patients had significantly lower EOS counts and higher hs-CRP levels than those in the SAP patients ($P<0.05$). In the *H.pylori* (-) group, there was no statistically significant difference between AMI and SAP patients in relation to their heart rate, history of diabetes, and EOS count ($P>0.05$). However, the hs-CRP levels of AMI patients were significantly higher than those of the SAP patients ($P<0.05$) (Table II). Logistic multivariate regression analysis showed that gender, hypertension history, EOS counts, and hs-CRP levels were independent risk factors for AMI patients with *H.pylori* infection ($P<0.05$) (Table III). The analysis revealed that the EOS count had a negative correlation with hs-CRP levels of AMI patients in the *H.pylori* (+) group ($r=-0.312$, $P=0.021$).

DISCUSSION

In this study, the percentage of male patients, long-term smoking history, white blood cell count, hs-CRP levels, and presence of *H.pylori* infection

Table I. *Comparison of clinical data between the AMI group and the SAP group*

Items	The AMI group (n=106)	The SAP group (n=118)	χ^2	*P*
Male [n(%)]	67(63.21)	52(44.07)	8.954	0.004
Age (years)	46.97±12.34	45.29±13.50	1.147*	0.213
Heart rate (times/min)	74.32±26.54	73.94±25.41	1.217*	0.131
Systolic blood pressure (mmHg)	121.62±35.94	132.54±30.11	2.419*	0.014
Diastolic blood pressure (mmHg)	70.65±15.30	79.55±19.38	2.476*	0.012
Diabetes history [n(%)]	39(36.79)	43(36.44)	1.524	0.239
Hypertension history [n(%)]	59(55.66)	78(66.10)	9.012	0.003
Hyperlipidemia history [n(%)]	27(25.47)	83(70.34)	9.234	0.002
Long-term smoking history [n(%)]	73(68.87)	60(50.85)	4.368	0.041
White blood cell count ($\times10^9$/L)	10.31±2.47	6.35±1.67	2.283*	0.032
Hp(+) [n(%)]	54(50.94)	38(32.20)	5.169*	0.024
EOS count ($\times10^9$/L)	0.11±0.07	0.20±0.09	2.687*	0.005
hs-CRP (mmol/L)	6.98±1.20	2.13±0.24	2.531*	0.006
Fibrinogen (g/L)	4.12±0.23	4.36±0.34	1.013*	0.329

**t value*

Table II. *Comparison of clinical data between AMI patients and SAP patients in the Hp (+) group and the Hp ((--) group*

Items	The Hp (+) group (n=92)				The Hp (-) group (n=132)			
	AMI patients (n=54)	SAP patients (n=38)	χ^2/t	*P*	AMI patients (n=52)	SAP patients (n=80)	χ^2/t	*P*
Male [n(%)]	43(79.63)	26(68.42)	1.359	0.234	24(46.15)	26(32.50)	4.628	0.036
Age (years old)	44.89±11.39	46.76±13.66	1.159	0.268	45.12±12.58	46.32±12.87	1.196	0.219
Heart rate (times/ min)	76.19±20.47	70.54±18.32	1.398	0.096	73.69±21.64	74.25±22.69	0.963	0.339
Systolic blood pressure (mmHg)	123.07±30.84	134.92±32.65	2.467	0.016	121.04±33.69	130.47±30.21	2.691	0.005
Diastolic blood pressure (mmHg)	71.03±17.35	79.62±18.22	2.315	0.020	72.51±21.65	78.96±22.06	2.637	0.006
Diabetes history [n(%)]	21(38.89)	16(42.11)	2.549	0.117	16(30.77)	23(28.75)	1.309	0.247
Hypertension history [n(%)]	33(61.11)	27(71.05)	3.058	0.069	25(48.08)	55(68.75)	7.824	0.006
Hyperlipemia history [n(%)]	21(38.89)	24(63.16)	6.562	0.013	10(19.23)	41(51.25)	7.810	0.007
Long-term smoking history [n(%)]	34(62.96)	24(63.16)	0.836	0.359	36(69.23)	39(48.75)	6.412	0.018
EOS count ($\times10^9$/L)	0.01±0.02	0.21±0.05	2.849	0.000	0.16±0.03	0.19±0.05	1.410	0.089
hs-CRP level (mmol/L)	6.38±1.20	2.13±0.06	2.932	0.000	6.59±1.26	2.24±0.23	2.714	0.001

Table III. *Logistic regression analysis of independent risk factors for AMI patients with Hp infection*

Items	*β*	*SE（β）*	*Wald-χ^2*	*P* value	*OR*	*95%CI*	
Male [n(%)]	0.366	0.127	8.233	0.005	1.442	1.123	1.851
Systolic blood pressure (mmHg)	0.640	0.047	185.451	0.285	1.897	1.730	2.08
Diastolic blood pressure (mmHg)	0.687	0.066	106.046	0.326	1.989	1.745	2.267
Hypertension history [n(%)]	1.102	0.468	5.544	0.032	3.012	1.203	7.541
Hyperlipemia history [n(%)]	0.764	0.606	1.587	0.119	2.147	0.654	7.048
Long-term smoking history [n(%)]	1.376	0.317	18.847	0.231	3.962	2.128	7.376
White blood cells count ($\times10^9$/L)	0.747	1.342	0.309	0.220	2.111	0.152	29.317
EOS count ($\times10^9$/L)	0.858	-0.523	2.693	0.024	2.361	6.581	0.846
hs-CRP (mmol/L)	0.048	0.019	6.062	0.015	1.050	1.010	1.091

(+) in the AMI group were significantly higher than those in the SAP group (P<0.05). But the systolic blood pressure, diastolic blood pressure, hypertension history, hyperlipemia history, and EOS counts in the AMI group were significantly lower than those in the SAP group (P<0.05), possibly because EOS were involved in the inflammatory reaction, to a certain extent. The single pathogenesis was not completely clear, and we hypothesize that EOS releases the main eosinophilic cationic and basic proteins in the body. The eosinophilic cationic and basic proteins would adjust the anion in the protein via binding to it, which would cause greater damage to the anticoagulant activity and largely contribute to thrombosis (10). The EOS counts of AMI patients were significantly lower than those of the SAP patients in the *H.pylori* (+) group. For both *H.pylori* (+) and (-) groups, the hs-CRP levels of AMI patients were significantly higher than those of the SAP patients (P<0.05). Possibly, the presence of the *H.pylori* infection strengthened the patients' inflammatory response, affecting the hs-CRP and EOS levels and promoting thrombosis (11). Logistic multivariate regression analysis showed that being male, having a history of hypertension, EOS count, and hs-CRP levels were the independent risk factors for AMI patients with *H.pylori* infection (P<0.05). The correlation analysis suggested that the EOS count had a negative correlation with hs-CRP levels for AMI patients in the *H.pylori* (+) group (r=-0.312, P=0.021). A possible reason was that EOSs may be involved in the inflammatory reaction. As hs-CRP was not specific in the body, trauma and acute infections (such as systemic inflammatory diseases, and *H.pylori* infection) will cause hs-CRP levels to rise significantly. However, EOS count not only had large cyclical fluctuations during the day and night, but it was also susceptible to glucocorticoids, which may have caused variations in the results of this study.

In summary, *H.pylori* infection can enhance the inflammatory response of myocardial infarction patients and affect their EOS count, and EOS may play an important role in patients with thrombosis, which is consistent with the previous studies.

REFERENCES

1. Boateng S, Sanborn T. Acute myocardial infarction. Dis Mon 2013; 59(3):83-96. doi: 10.1016/j.disamonth.2012.12.004. PMID: 23410669.
2. Alpert JS, Thygesen K, Antman E, Bassand JP.

Myocardial infarction redefined--a consensus document of The Joint European Society of Cardiology/American College of Cardiology Committee for the redefinition of myocardial infarction. J Am Coll Cardiol 2000; 36(3):959-69. doi: 10.1016/s0735-1097(00)00804-4. Erratum in: J Am Coll Cardiol 2001; 37(3):973. PMID: 10987628.

3. López-Sendón J, Gurfinkel EP, Lopez de Sa E, et al. Factors related to heart rupture in acute coronary syndromes in the Global Registry of Acute Coronary Events. Eur Heart J 2010; 31:1449-56. doi: 10.1093/eurheartj/ehq061.
4. Boudoulas KD, Triposciadis F, Geleris P, Boudoulas H. Coronary atherosclerosis: pathophysiologic basis for diagnosis and management. Prog Cardiovasc Dis 2016; 58(6):676-92. doi: 10.1016/j.pcad.2016.04.003.
5. Delaney JA, Nance RM, Whitney BM, et al. Cumulative human immunodeficiency viremia, antiretroviral therapy, and incident myocardial infarction. Epidemiology 2019; 30(1):69-74. doi: 10.1097/EDE.0000000000000930.
6. Davenport ED, Gray G, Rienks R, et al. Management of established coronary artery disease in aircrew without myocardial infarction or revascularisation. Heart 2019; 105(Suppl 1):s25-s30. doi: 10.1136/heartjnl-2018-313054.
7. Davenport ED, Syburra T, Gray G, et al. Management of established coronary artery disease in aircrew with previous myocardial infarction or revascularisation. Heart 2019; 105(Suppl 1):s31-s37. doi: 10.1136/heartjnl-2018-313055.
8. Rios-Navarro C, Gavara J, Vidal V, et al. Characterization and implications of the dynamics of eosinophils in blood and in the infarcted myocardium after coronary reperfusion. PLoS One 2018; 13:e0206344. doi: 10.1371/journal.pone.0206344.
9. Chen LL, Wang ZD. Relationship between peripheral blood eosinophil level and acute myocardial infarction combining helicobacter pylori infection. Chin Circ J 2017; 32(12):1185-89.
10. Lee CH, Fang CC, Tsai LM, Gan ST, Lin SH, Li YH. Patterns of acute myocardial infarction in Taiwan from 2009 to 2015. Am J Cardiol 2018; 122(12):1996-2004. doi: 10.1016/j.amjcard.2018.08.047.
11. Kimura T, Roger VL, Watanabe N, et al. The unique mechanism of functional mitral regurgitation in acute myocardial infarction: a prospective dynamic 4D quantitative echocardiographic study. Eur Heart J Cardiovasc Imaging 2019; 20(4):396-406. doi: 10.1093/ehjci/jey177. Erratum in: Eur Heart J Cardiovasc Imaging. 2019; 20(4):406. PMID: 30517693; PMCID: PMC6429236.

LETTER TO THE EDITOR

Exploring the role of serum fibroblast growth factor 21 in thyroid papillary carcinoma cells and its molecular mechanism

Y. Li[1], JJ. Fu[2], YY. Sun[3], XD. Zhang[1] and X. Geng[1]

[1]General Surgery, the Affiliated Changzhou No.2 People's Hospital of Nanjing Medical University, Changzhou, China; [2]Department of Gastrointestinal, the Affiliated Changzhou No.2 People's Hospital of Nanjing Medical University, Changzhou, China; [3]Pathology Department, the Affiliated Changzhou No.2 People's Hospital of Nanjing Medical University, Changzhou, China

Received June 8, 2020 – Accepted November 4, 2020

To the Editor,

Thyroid carcinomas (TC) are common endocrine malignant tumors, among which papillary thyroid carcinoma (PTC) is the most common, followed by follicular carcinoma. The incidence of PTC accounts for 70% of TC, which has been increasing year by year, especially in regions with high iodine intake, such as coastal areas (1, 2). PTC, if timely treated, has a good prognosis, with a 5-year survival rate of up to 90% (3). However, cervical lymph node metastasis may occur in the early stage of cancer, and the existing imaging examinations are not sensitive enough to detect early metastasis, so the lymph node capsule is often broken through before diagnosis, affecting the treatment outcome and prognosis of patients (4).

Fibroblast growth factor 21 (FGF21), a member of the fibroblast blast factor family, plays a crucial role in the regulation of various cellular processes, such as glucose, lipids and vitamin D. Previous studies have shown that the expression level of FGF21 in the serum of PTC patients is significantly higher than that of healthy patients, and it can be used as an effective biomarker for PTC (5). However, the mechanism of FGF21 has not yet been studied. Previous studies have shown that epithelial-mesenchymal transitions (EMT) signal pathways play an important role in tumor progression (invasion and metastasis) in a variety of cancers (6). Fibroblast growth factor (FGF) receptor (FGFR) signaling pathway disorders may be related with the MAPK signaling pathway or phosphatidyl inositol 3 kinase (PI3K) pathways. The selection of key targets on the signaling pathway can promote targeted therapy in clinical settings. This study analyzed the FGFR expression in PTC cells, and preliminarily explored the mechanism of FGF21 in the progress of PTC.

MATERIALS AND METHODS

Normal thyroid cell line (nthy-ori3-1 and 8505c) and PTC cell line (BCPAP and TPC-1) were purchased from the American Type Culture Collection (ATCC). BCPAP and TPC-1 cell lines were cultured in DMEM medium containing 100mg/L penicillin, 100mg/L streptomycin and 10% FBS. Nthy-ori3-1 and 8505c cell line was cultured in RPMI 1640 medium containing 100mg/L penicillin, 100mg/L streptomycin and 10% FBS in a 5% CO_2 incubator at 37°C.

After starvation in sterile PBS containing 0.1% BSA for 24 h, the cells were treated with rFGF21, and then diluted to adjust the concentration of rFGF21. The diluted rFGF21 was added to the medium containing PTC and

Key words: fibroblast cytokines; thyroid cancer; attacks; transfer; signaling pathways

Corresponding Author:
Dr Xiang Geng,
General Surgery,
the Affiliated Changzhou No.2 People's Hospital of Nanjing Medical University, Yanghu District, Changzhou 213000, China
e-mail: puyekangyong7723@163.com

0393-974X (2020)
Copyright © by BIOLIFE, s.a.s.
This publication and/or article is for individual use only and may not be further reproduced without written permission from the copyright holder.
Unauthorized reproduction may result in financial and other penalties
DISCLOSURE: ALL AUTHORS REPORT NO CONFLICTS OF INTEREST RELEVANT TO THIS ARTICLE.

nthy-ori3-1 cells to continue the culture. After culturing for 48 h, the medium was discarded and washed once with sterile PBS, and the cells were collected after digestion with 0.25% trypsin.

Western blotting to determine protein expression

Nthy-ori3-1, BCPAP, 8505c and TPC-1 cells were washed with PBS, added with RIPA lysate buffer, and allowed to stand for 30 min at 4°C. After centrifugation, the supernatant was extracted. The protein content was measured by using protein determination kit (BCA). Equal amounts (40 μg) of extracted proteins were separated by 10% SDS-PAGE and then transferred to PVDF membranes. Then, the PVDF membranes were blocked with 5% non-fat milk for 1 h at room temperature. Subsequently the primary antibodies including: anti-glyceraldehyde phosphate dehydrogenase (1:2000 dilution), β-actin (1:2000 dilution), KLB (1:1000 dilution), FGFR1 (1:1000 dilution), FGFR2 (1:1000 dilution), FGFR3 (1:1000 dilution), FGFR4 (1:1000 dilution), AKT (1:1000 dilution), p-AKT (1:1000 dilution), ERK (1:1000 dilution), p-ERK (1:1000 dilution), Vimentin (1:1000 dilution), E-cadherin (1:1000 dilution) and p-FGFR (1:1000 dilution). Then, the membrane was washed with TBST, and incubated with secondary antibody (1:2000 dilution) at room temperature for 2 h. Finally, the enhanced chemiluminescence (ECL) was applied for detecting the immune complexes. β-actin was used as the internal control. The optical density values were normalized, and Image J software was used to analyze the results after scanning.

Determination of cell viability

Nthy-ori3-1, BCPAP, 8505c and TPC-1 cells were taken in the logarithmic growth phase into the culture plate and treated with 0.1% BSA (control group) or rFGF21 (200 ng/ mL) at concentration to 5×10^3. After incubating at 5% CO_2, 37°C for 12 h, the cell viability was determined using WST-1 cell viability reagent.

Detection of cell invasion ability

Cells were inoculated in the prepared Transwell chamber (8-μm pore size; Corning Inc., NY, USA) with Matrigel (BD Biosciences), and each group was adjusted with serum-free RPMI-1640 culture medium. Briefly, 5×10^8 cells were added to the upper chamber and RPMI-1640 culture medium containing 20% FBS was added to the lower chamber. After incubation for 24 h at 37°C, 5% CO_2, observed the numbers of cell invasion under the microscope. After the cells were fixed with 4% paraformaldehyde and stained with 0.5% crystal violet (Sigma-Aldrich; Merck KGaA) for 15 min at room temperature. The number of transmembrane cells from 5 random different fields were selected under the microscope (magnification, x 100; Olympus, Tokyo, Japan).

Detection of cell migration

Cells were seeded in 24-well plates at a density of 5×10^3/well. Cells were converted into slices and streaked, and the corresponding cell culture medium containing FBS was added and cultured at 5% CO_2 and 37°C for 24 h. The width of the scratches were observed under the microscope and the cell frontal migration distance (the difference between the scratch widths after 0h to 24h of culture) was calculated

Statistical analysis

SPSS 22.0 software was used for statistical analysis. The results are presented as the mean ± standard deviation (SD). The differences between the three groups were analyzed using single-factor analysis of variance. $P<0.05$ was considered to be a significant difference. GraphPad Prism 5 was used for drawing.

RESULTS

The expression of FGFRs in PTC cells

The expressions of FGFRs (including FGFR1, FGFR2, FGFR3, FGFR4, FGFR21, KLB and p-FGFR) were abnormally expressed in PTC cells (BCPAP and TPC-1) compared to Nthy-ori3-1, and the expression levels of FGFR1, FGFR4 and p-FGFR in BCPAP and TPC-1 cells were significantly higher than those in normal thyroid Nthy-ori3-1 cells. There was no significant difference of FGFR2, FGFR3, FGFR21 and KLB expressions between PTC cells and Nthy-ori3-1 cells, as shown in Table I.

Effect of FGF21 on cell activity, cell invasion and migration ability

Compared with the control group (0.1% BSA treatment), there were no significant differences in cell activity after treatment with rFGF21 between PTC cells (BCPAP and TPC-1) and Nthy-ori3-1

cells, as shown in Table II. There was no significant difference in the invasion and migration of normal thyroid cells between treatment with rFGF21 and 0.1% BSA. Compared with the control group, treatment with rFGF21 could significantly promote the invasion and migration of PTC cells (BCPAP and TPC-1) (Tables III and IV).

FGF21 activates the EMT pathway and up-regulates the FGFR pathway

In the PTC cells treated with rFGF21, the expression level of EMT marker vimentin was significantly higher than that of the control group, and the expression level of E-cadherin was significantly lower than that of the control group, as shown in Fig. 1. In PTC cells treated with rFGF21, the expression levels of p-ERK, p-AKT and p-FGFR were significantly higher than those of the control group, but there was no significant difference between total ERK and AKT (Fig. 2).

DISCUSSION

Previously performed studies indicated that

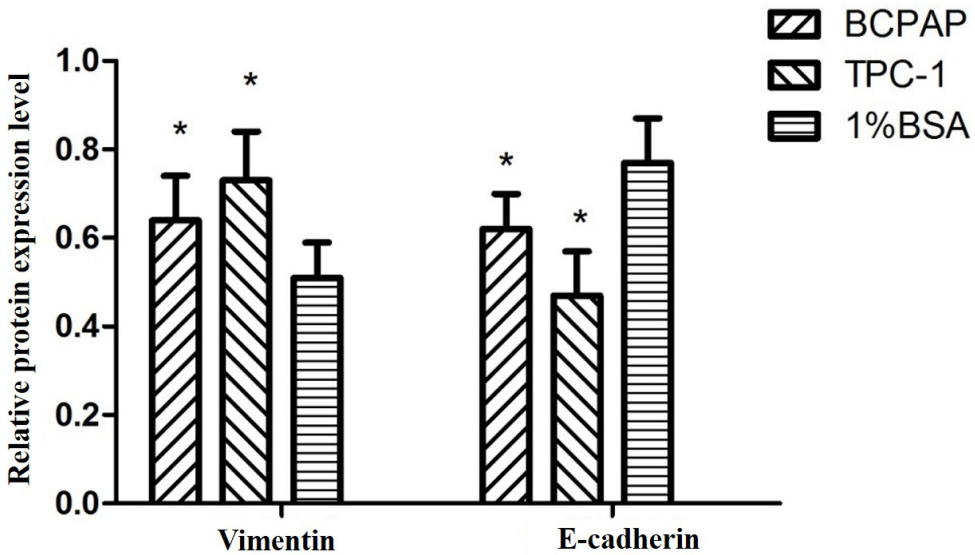


Fig. 1. *Comparison of expression levels of EMT markers*

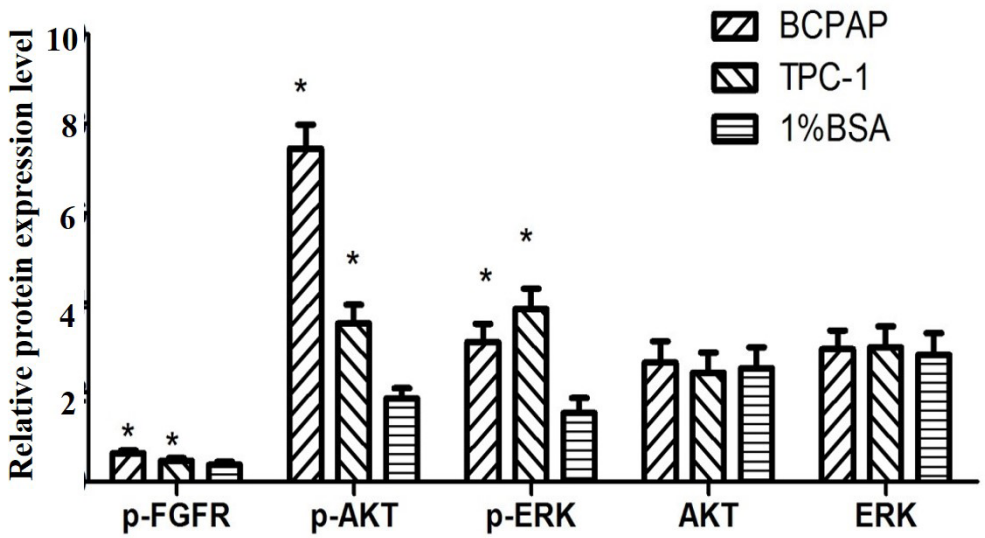


Fig. 2. *Comparison of FGFR pathology-related protein expression levels. *significant difference between the 1%BSA group*

FGFs play an important biological role in regulating cell growth and differentiation. Studies reported that the FGF21 levels in serum of patients with various tumors were significantly increased (7-9), but its specific mechanism is currently lacking research-based proof. This study analyzed the expression of FGFRs in normal thyroid cells and PTC cells. The results show that the expression of FGFRs between PTC cells (BCPAP and TPC-1) and normal thyroid cells were different. Among them, the expression levels of FGFR1 and FGFR4 in PTC cells were significantly higher than in normal thyroid Nthy-ori3-1 cells. However, the expression level of FGFR21 was not different from normal cells, which may be related to the low expression level detected. In order to explore the mechanism of FGF21, rFGF21 were used to treat PTC cells to detect the levels of proteins related to the pathway. The results showed that rFGF21 can significantly increase the invasion and migration ability of PTC cells, and the level of E-cadherin in PTC cells with rFGF21 was decreased significantly, while the level of Vimentin was increased significantly, indicating that rFGF21 activates EMT signaling pathway and participates in tumor progression. Phosphorylated ERK and AKT were used as downstream targets of FGFR signaling pathway. The levels of p-AKT and p-ERK in PTC cells with rFGF21 were significantly increased, and FGFR pathway was up-regulated. The results showed that FGF21 played a regulatory role in the progression of cancer, which can promote the clinical selection of FGF21 as an effective target. Further investigation is necessary through population cohort experiments in order to establish effective clinical selection of diagnostic indicators.

REFERENCES

1. Zhang X, Wang Z, Tian L, Xie J and Jiang F. Increased expression of FGF19 contributes to tumor progression and cell motility of human thyroid cancer. Otolaryngol Head Neck Surg 2015; 154:52-58.
2. Jin J, Ren Y and Haiyang L. The effect and mechanism of up-regulating the expression of miR-124 on thyroid cancer cells. J Gerontol 2018; v.38:190-93.
3. Gou J, Cheng W, Lei J, et al. Health-related quality-of-life assessment in surgical patients with papillary thyroid carcinoma: A single-center analysis from Mainland China. Medicine 2017; 96:e8070.
4. Cabanillas ME, Habra MA. Lenvatinib: Role in thyroid cancer and other solid tumors. Cancer Treat Rev 2016; 42:47-55.
5. Kang YE, Kim JT, Lim MA, et al. Association between circulating fibroblast growth factor 21 and aggressiveness in thyroid cancer. Cancers (Basel) 2019; 11(8):1154.
6. Tan Y, Peng Z. Progress of epithelial-mesenchymal transition and mucin in tumor research. Gastroenterology 2019; 024:243-46.
7. Gustafson MP, Lin Y, Bleeker JS, et al. Intratumoral CD14+ cells and circulating CD14+HLA-DRlo/neg monocytes correlate with decreased survival in patients with clear cell renal cell carcinoma. Clin Cancer Res 2015; 21:4224-33.
8. Akyol M, Alacacioglu A, Demir L, et al. The alterations of serum FGF-21 levels, metabolic and body composition in early breast cancer patients receiving adjuvant endocrine therapy. Cancer Biomark 2017; 18:441-49.
9. Tahara M, Schlumberger M, Elisei R, et al. Exploratory analysis of biomarkers associated with clinical outcomes from the study of lenvatinib in differentiated cancer of the thyroid. Eur J Cancer 2017; 75:213-21.

LETTER TO THE EDITOR

LncRNA LINC00847 contributes to hepatocellular carcinoma progression by acting as a sponge of miR-99a to induce E2F2 expression

LR. Tu[1*], W. Li[2*], J. Liu[1], XG. Song[1] and HW. Xu[3]

[1]Department of Infectious Diseases, Jinan Infectious Diseases Hospital affiliated to Shandong University, Jinan, Shandong, China; [2]The First College of Clinical Medical Science, China Three Gorges University/ Yichang Central People's Hospital, Yichang, Hubei, China; [3]Department of Gastroenterology, Shandong Provincial Hospital affiliated to Shandong University, Jinan, Shandong, China

Received July 6, 2020 – Accepted November 4, 2020

[*] These Authors contributed equally to this work

To the Editor,

Hepatocellular carcinoma (HCC) is a common malignant tumor and accounts for a large proportion of tumor-related deaths worldwide, which is increasing yearly (1). At present, the surgical treatment for early-stage HCC is limited, and most patients are already in advanced stages when they are diagnosed, at which time the efficacy of chemotherapy and radiotherapy is limited. It is difficult for traditional therapies to completely inhibit HCC progression.

Accumulating studies have shown that abnormal regulation of tumor suppressor genes or oncogenes is implicated in HCC tumorigenesis. Non-coding RNAs (ncRNAs) have no protein-coding capacities (2). Long non-coding RNA (lncRNA, >200nt in length) has been found to regulate gene transcription through epigenetic regulation (3). Dysregulation of lncRNA has been frequently identified in human tumors (4), exerting regulatory functions in malignant behaviors of tumor cells (5). Although numerous lncRNAs have been identified in HCC progression, the expressions and roles of LINC00847 in HCC are still unclear.

MicroRNAs (miRNAs) have key functions in modulating protein expressions at post-transcriptional level. According to previous studies, dysregulation of miR-99a has been confirmed in various cancers, including HCC (6), regulating tumor progression (7) . Moreover, studies have demonstrated that lncRNA can serve as competing endogenous RNAs (ceRNAs) through sponging miRNAs in cancers (8). However, the interaction between LINC00847 and miR-99a in HCC has never been revealed.

MATERIALS AND METHODS

Tissue samples

Forty-six human HCC specimens were collected from patients who were undergoing surgery at the Jinan Infectious Diseases Hospital affiliated to Shandong University. In addition, corresponding adjacent normal tissue samples were obtained from each patient and regarded as controls. All included patients provided written informed consent and had not received any preoperative chemotherapy or radiotherapy. The fresh tissue samples were immediately frozen in liquid nitrogen for further assays. The present study was approved by the Ethics committee of Jinan Infectious Diseases Hospital affiliated

Key words: hepatocellular carcinoma; LINC00847; miR-99a; E2F2

Corresponding Author:
Dr Hongwei Xu,
Department of Gastroenterology,
Shandong Provincial Hospital
affiliated to Shandong University,
No. 324, Jingwuweiqi Road, Jinan, Shandong, China
e-mail: raodtgsppi750461@163.com

0393-974X (2020)
Copyright © by BIOLIFE, s.a.s.
This publication and/or article is for individual use only and may not be further reproduced without written permission from the copyright holder.
Unauthorized reproduction may result in financial and other penalties
DISCLOSURE: ALL AUTHORS REPORT NO CONFLICTS OF INTEREST RELEVANT TO THIS ARTICLE.

PROOF

to Shandong University and conducted in accordance with the Declaration of Helsinki.

Cell lines and cell culture

Human HCC cells (Huh7 and HCCLM3) and normal liver cells LO2 were procured from American Type Culture Collection (ATCC, Manassas, VA, USA). Dulbecco's Modified Eagle Medium (DMEM) containing 10% fetal bovine serum (FBS) was utilized to culture the above cells. All cell cultures were kept at 37°C in a humidified incubator with 5% CO_2.

Cell transfection

The specific LINC00847 siRNA was synthesized by Gene Pharma (Shanghai, China) to knockdown LINC00847. The whole sequences of LINC00847 or E2F2 were cloned into pcDNA3.1 vector to overexpress LINC00847/E2F2. At the same time, miR-99a inhibitor or mimic was also designed by Gene Pharma. The transfections of the above plasmids were implemented as demanded by Lipofectamine 2000 (Invitrogen).

Quantitative real-time polymerase chain reaction

The total RNAs were isolated from the cells or tissues by TRIzol® reagent (Invitrogen). The synthesis of cDNA from total RNA was implemented via a reverse transcription kit (Takara, Dalian, China). Thereafter, the synthesized cDNA was subjected to Real-time polymerase chain reaction (RT-qPCR) analysis with SYBR Premix Ex Taq (Takara) on an Applied Biosystems 7500 sequence detection System. Glyceraldehyde 3-phosphate dehydrogenase (GAPDH) and U6 were internal controls. The relative expression was calculated using the $2^{-\Delta\Delta Ct}$ method.

Cell Counting Kit-8 assay

Cell Counting Kit-8 (CCK-8) assays were performed to investigate cell viability. In brief, transfected HCC cells were plated into a 96-well plate and subjected to a 4-day culturing. Then, CCK-8 solution was added into the wells every day at indicated time points (24, 48, 72, 96 h); 2 h after incubation at 37°C, a microplate reader (Olympus, Japan) was used to determine OD values at 450 nm.

Transwell assay

Transwell assays were implemented to estimate HCC cell invasion and migration capacities. For invasion assays, the upper Transwell chamber (Corning Costar, Cambridge, Massachusetts, USA) was enveloped with Matrigel, while for migration assays, it was not. Thereafter, cell suspension was pipetted into the apical chambers with serum-free medium, and the bottom chambers were added with DMEM containing 10% FBS. After incubating for 48 h, cells in the top chamber were eliminated and the migrated or invaded cells in the lower chambers were fixed and stained. Finally, the cells were quantified under a microscope (Olympus, Japan).

Luciferase reporter assay

The wildtype or mutant plasmids [WT/MUT-LINC00847/E2F transcription factor 2 (E2F2)] with binding sites of miR-99a were integrated into pGL3 promoter vectors (GenePharma). After seeding HCC cells into a 24-well plate, the above recombinant plasmids were cotransfected into the cells with miR-99a mimics using Lipofectamine 2000 reagents. Luciferase activities were determined by a dual-luciferase reporter assay kit (Promega, Madison, WI. USA).

Statistical analysis

All the above experiments were performed in triplicate. The SPSS 17.0 version (SPSS Inc. Chicago, IL, USA) was used to perform the statistical analysis. The overall survival of HCC patients was determined with Kaplan-Meier curve together with log-rank test. Data was tested using Student's *t*-test or one-way ANOVA analysis with Tukey's post hoc test. $P<0.05$ was considered to be statistically significant difference.

RESULTS

Overexpression of LINC00847 in HCC indicated poor prognosis and exhibited oncogenic roles

Firstly, to note the effects of LINC00847 in HCC, LINC00847 expressions in HCC tissues and cells were detected. RT-qPCR analysis demonstrated that LINC00847 levels were remarkably increased in HCC tissues when compared to the adjacent para-carcinoma tissues (Fig. 1A). Similarly, the elevated LINC00847 expressions in HCC cells were also observed (Fig. 1B). Moreover, we explored the prognostic value of LINC00847 in HCC patients by Kaplan-Meier curve analysis and it turned out

that high LINC00847 level was associated with a shorter survival rate (Fig. 1C). To identify the specific roles of LINC00847 in HCC progression, LINC00847 was overexpressed or silenced in Huh7 and HCCLM3 cells, which presented the originally lower or higher LINC00847 expressions. The successful upregulation of LINC00847 in Huh7 cells and downregulation in HCCLM3 cells were confirmed by RT-qPCR analysis (Fig. 1D). Then, as demonstrated by CCK-8 assays, pcDNA-

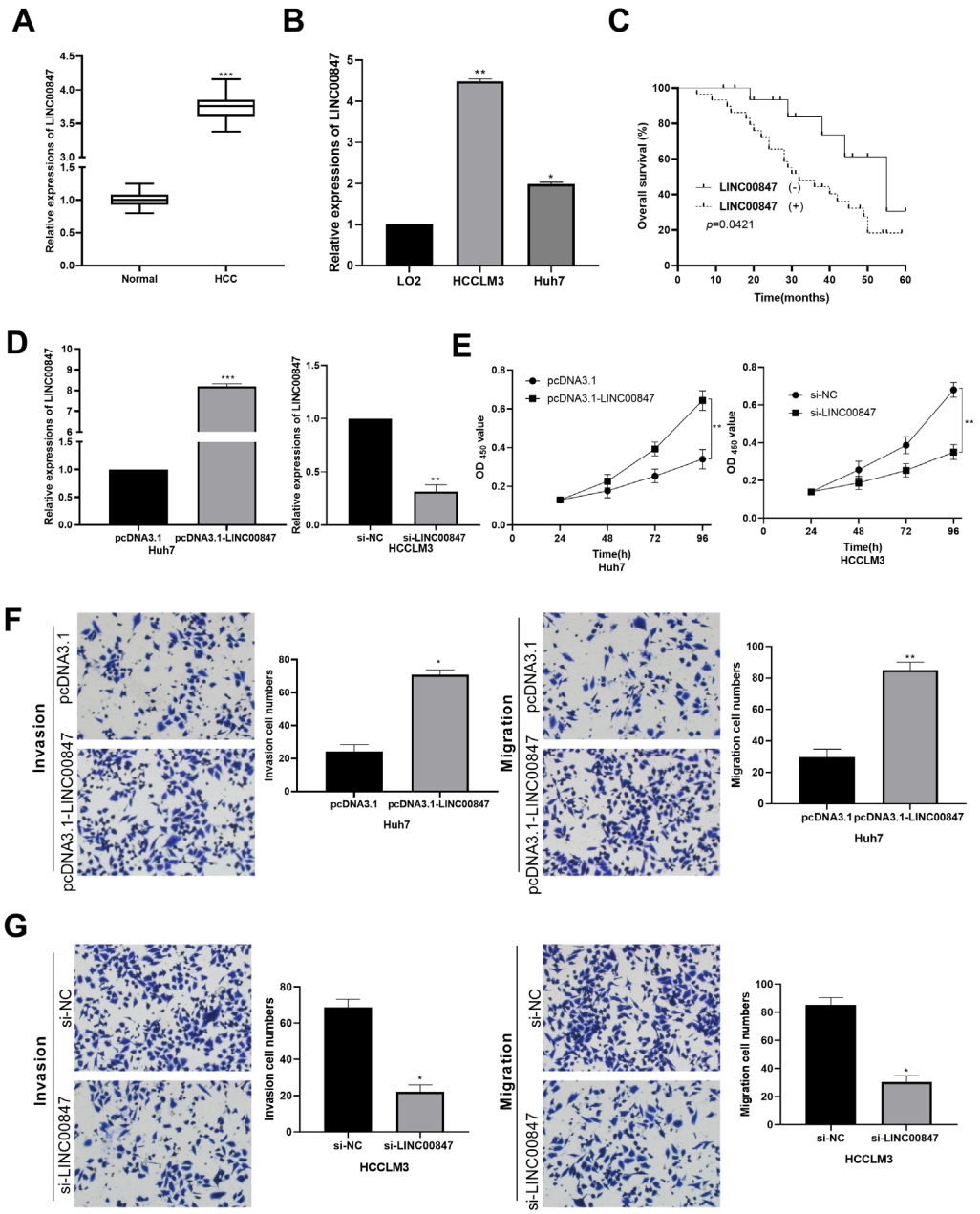


Fig. 1. *Overexpression of LINC00847 in HCC indicated shorter overall survival and promoted HCC progression.* ***A, B****) RT-qPCR analysis demonstrated the overexpression of LINC00847 in HCC tissues and cells.* ***C****) Shorter overall survival of HCC patients was associated with high LINC00847 expression.* ***D****) Successful upregulation or downregulation of LINC00847 in HCC cells was confirmed by RT-qPCR.* ***E****) LINC00847 upregulation facilitated HCC cell viability as demonstrated by CCK-8 assays.* ***F, G****) Transwell assays indicated that LINC00847 upregulation contributed to HCC cell invasion and migration.*

LINC00847 obviously enhanced the proliferative capacity of Huh7 cells whereas si-LINC00847 transfection dramatically suppressed HCCLM3 cell growth (Fig. 1E). Transwell assays were conducted to investigate whether LINC00847 influenced HCC cell invasion and migration. As expected, the

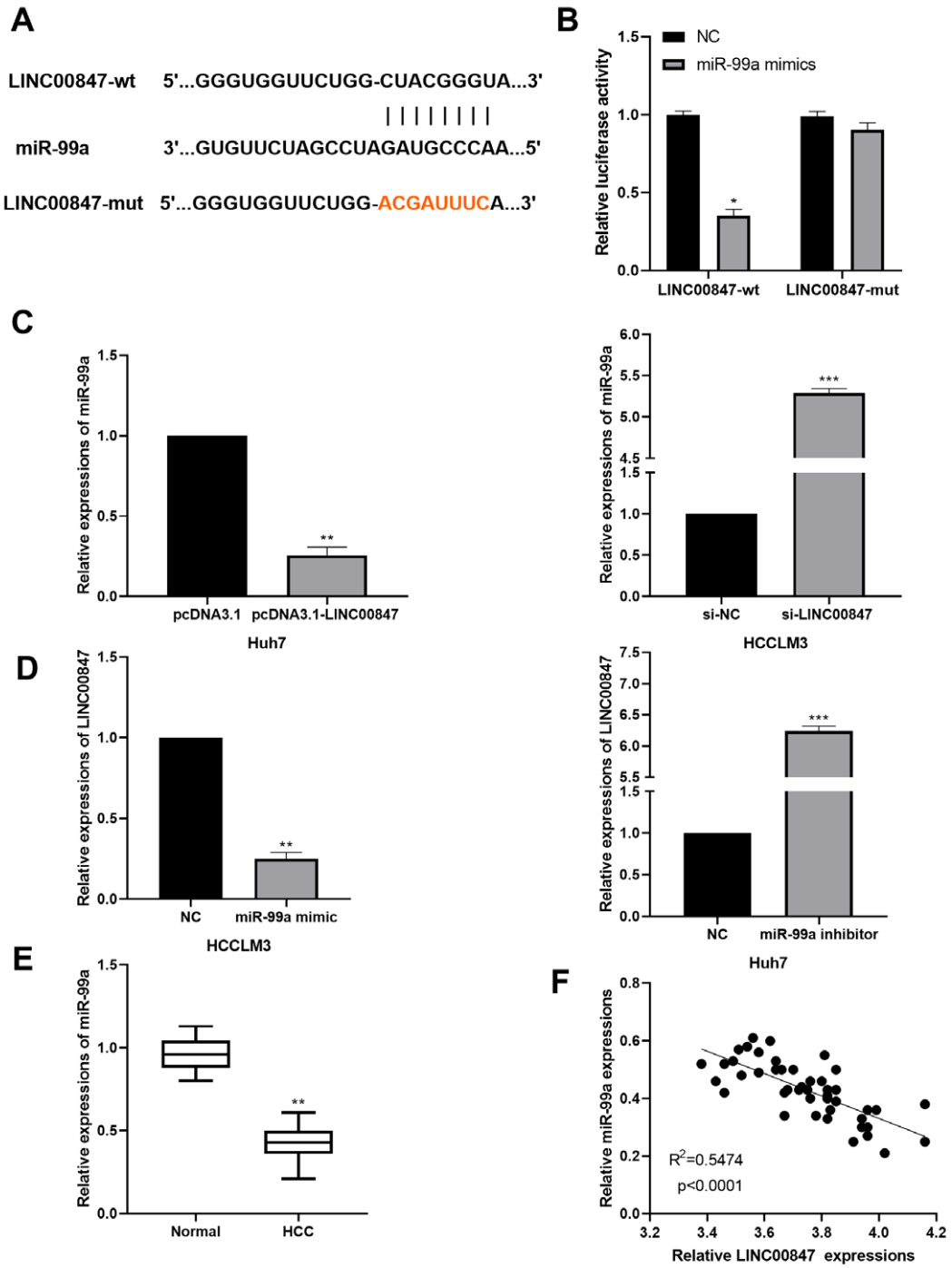


Fig. 2. *LINC00847 acted as a sponge of miR-99a in HCC cells.* ***A)*** *Putative binding sites of miR-99a in 3'-UTR of LINC00847 were obtained from Starbase. (B)Relative luciferase activities of HCC cells with transfection of LINC00847 -wt/mut reporter plasmid and miR-99a mimic.* ***C, D)*** *The regulatory functions of LINC00847 and miR-99a in each other were confirmed by RT-qPCR analysis.* ***E)*** *Downregulated miR-99a expressions were identified in HCC tissues.* ***F)*** *A negative correlation between LINC00847 and miR-99a expressions in HCC tissues was confirmed.*

invasion and migration abilities of Huh7 cells were conspicuously promoted by pcDNA-LINC00847 and HCCLM3 cell invasion and migration abilities were significantly inhibited by LINC00847 silence (Fig. 1 F, G). In general, LINC00847 promoted the malignant characteristics of HCC cells.

LINC00847 bound to miR-99a and negatively regulated its expression in HCC

Since lncRNAs played crucial roles in various tumors via binding to miRNAs, herein, the candidate miRNAs which might be inactivated by LINC00847 were explored by StarBase. The results showed that LINC00847 contained conserved binding sites of miR-99a (Fig. 2A). Then, luciferase reporter assay was further performed to verify the relationship between LINC00847 and miR-99a in HCC cells. As evidenced by the results of luciferase reporter assay, miR-99a mimic notably decreased the luciferase activity of LINC00847-wt vector, while the luciferase activity of LINC00847-mut vector was not significantly influenced (Fig. 2B). Additionally, the relationship between LINC00847 and miR-99a were confirmed by RT-qPCR. LINC00847 upregulation dramatically reduced miR-99a levels in Huh7 cells and LINC00847 knockdown obviously increased miR-99a expressions in HCCLM3 cells (Fig. 2C). Similarly, the influence of miR-99a on LINC00847 expressions was also confirmed (Fig. 2D). Thereafter, the miR-99a expressions in HCC tissues were also measured and results exhibited a notable decrease of miR-99a expressions in HCC tissues than that

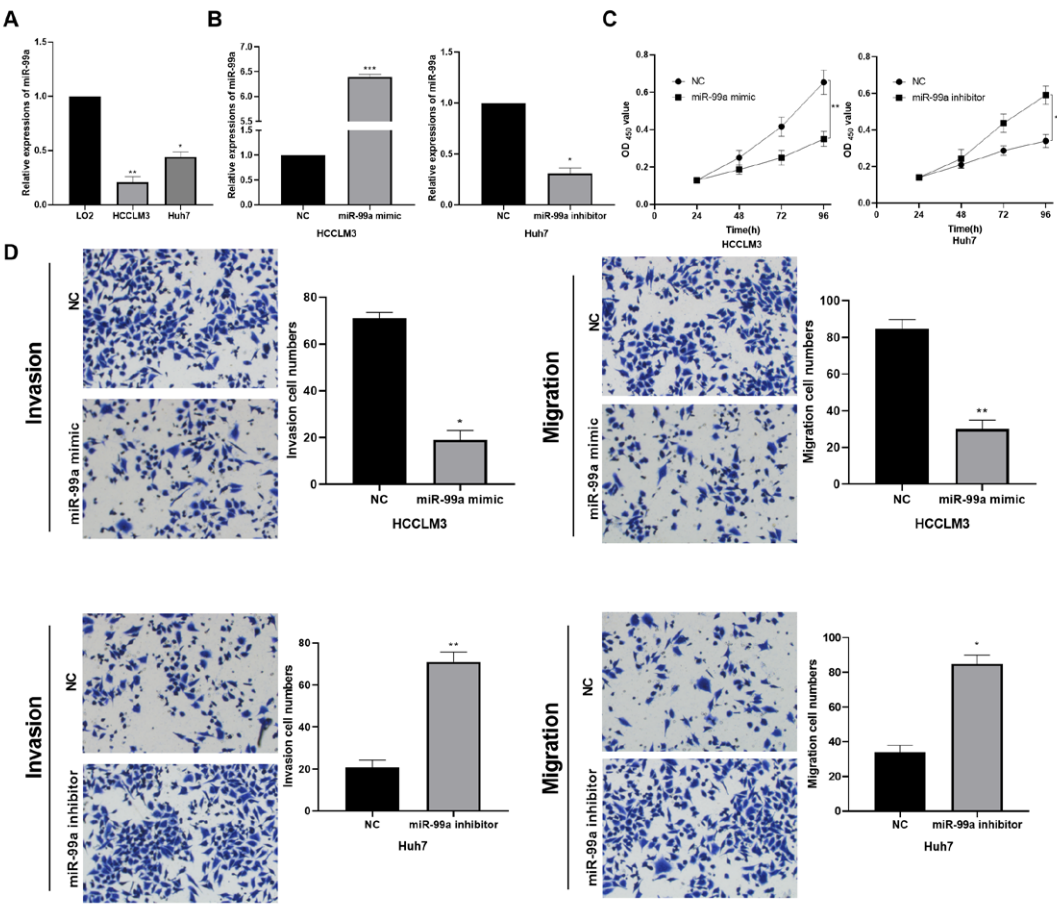


Fig. 3. *miR-99a inhibited proliferation, invasion and migration in HCC cells.* ***A)*** *miR-99a was downregulated in HCC cells.* ***B)*** *miR-99a expression was efficiently overexpressed and silenced by miR-99a mimics and inhibitor.* ***C, D)*** *miR-99a inhibited proliferation, invasion and migration in HCC cells.*

in surrounding healthy tissues (Fig. 2E). A reverse correlation between miR-99a and LINC00847 in HCC tissues was also observed (Fig. 2F). All these results suggested that LINC00847 and miR-99a may be composed of competing endogenous RNA (ceRNA) regulatory system where LINC00847 were treated as rivals to mRNAs to bind with miR-99a so that those mRNAs lost their ability to translate into protein.

Elevating miR-99a inhibited HCC cell proliferation, invasion and migration

MiR-99a expressions in HCC cells were also measured and results indicated that miR-99a was downregulated in HCC cells. (Fig. 3A). Subsequently, HCCLM3 and Huh7 cells were transfected with either miR-99a mimic or inhibitor and subjected to functional assays. According to CCK-8 assays,

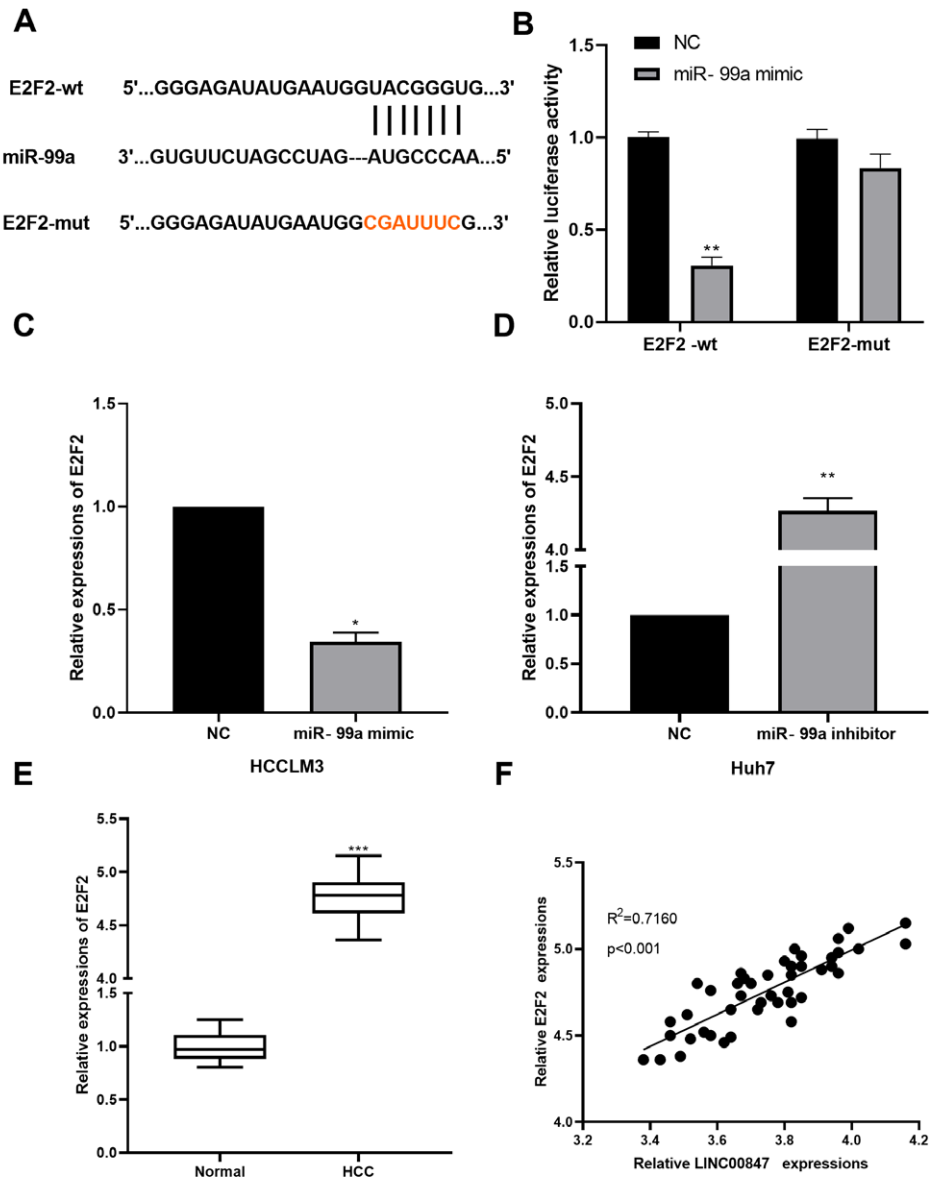


Fig. 4. *E2F2 served as a target of miR-99a in HCC cells.* ***A)*** *Putative binding sites of miR-99a in E2F2 3'-UTR were predicted by Targetscan.* ***B)*** *miR-99a mimic significantly decreased relative luciferase activities of E2F2-wt reporter plasmid.* ***C, D)*** *The E2F2 expressions were regulated by miR-99a in HCC cells.* ***E, F)*** *High E2F2 expressions were identified in HCC tissues, which was positively correlated with LINC00847 expressions.*

miR-99a mimic appreciably impeded HCCLM3 cell proliferation and miR-99a inhibitor promoted Huh7 cell viability (Fig. 3B). Correspondingly, as revealed by Transwell assays, when miR-99a was overexpressed, the invasion and migration capacities of HCCLM3 cells were weaker than cells transfected with controls (Fig. 3C). On the contrary, miR-99a silence exerted conducive functions in Huh7 cell invasion and migration (Fig. 3D).

E2F2 served as a target of miR-99a in HCC cells

E2F2 was predicted as a candidate target for miR-

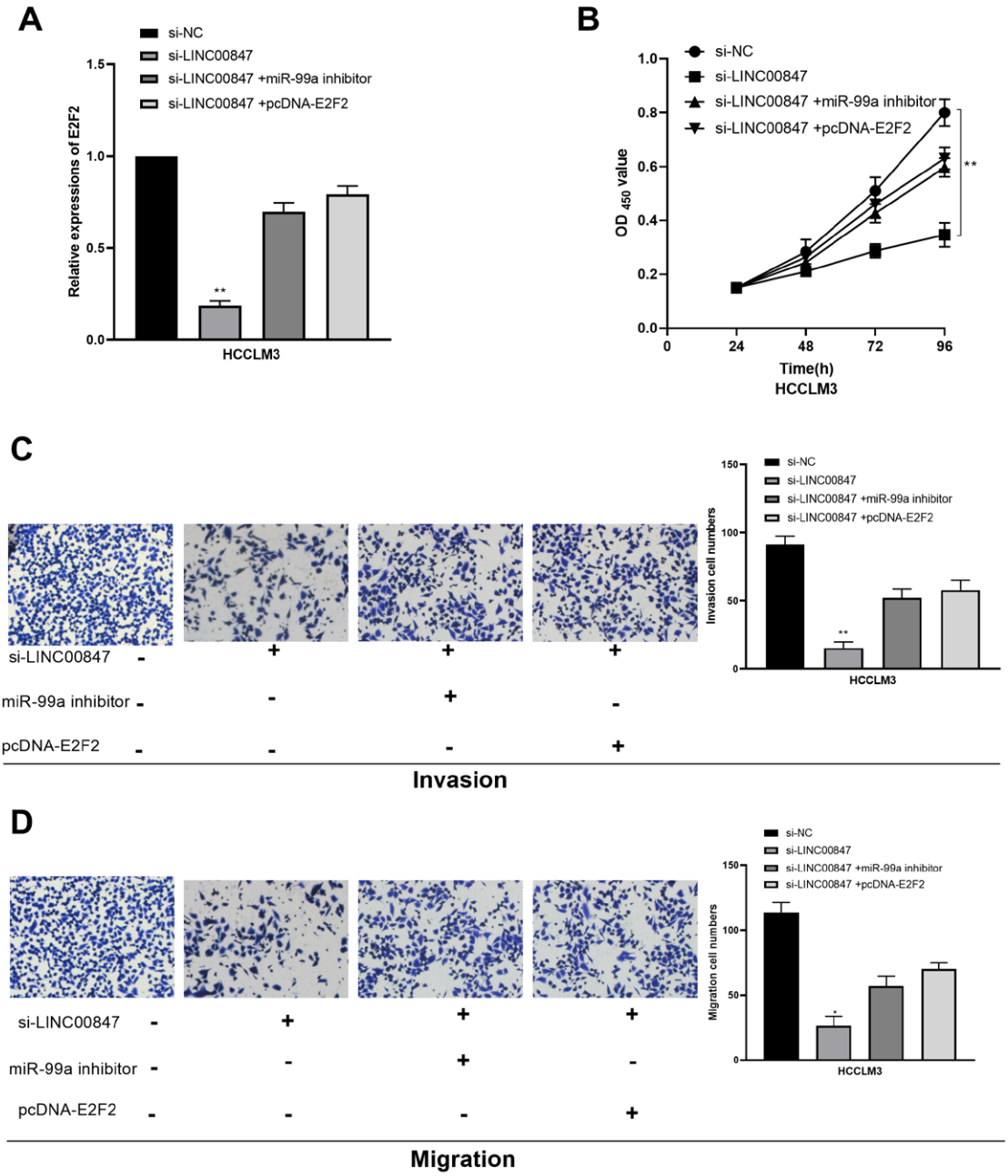


Fig. 5. *LINC00847 promoted HCC tumorigenesis by sponging miR-99a to upregulate E2F2.* ***A)*** *E2F2 expressions were silenced by si-LINC00847, and this reduction could be partially reversed by miR-99a inhibitor or pcDNA-E2F2.* ***B-D)*** *miR-99a inhibitor or pcDNA-E2F2 could reverse the inhibitory functions of si-LINC00847 in HCC cell proliferation, invasion and migration.*

99a by TargetScan, the binding sites of miR-99a on E2F2 3'UTR were displayed in Fig. 4A. Luciferase reporter assays were conducted to confirm this prediction. When co-transfected with miR-99a mimic, the luciferase activity of E2F2-wt vector was remarkably reduced and E2F2-mut vector abrogated this decrease (Fig. 4B). Then, E2F2 expressions in miR-99a mimic- or inhibitor-transfected cells were measured to determine whether miR-99a could regulate E2F2 expressions in HCC cells. Results indicated that E2F2 expressions were decreased by miR-99a mimic while increased by miR-99a inhibitor (Fig.4 C, D). In addition, E2F2 expressions were also quantified in HCC tissues and RT-qPCR analysis demonstrated significant increase in E2F2 expressions (Fig. 4E). Furthermore, E2F2 was positively correlated with LINC00847 among these HCC samples (Fig. 4F).

LINC00847 promoted HCC tumorigenesis by sponging miR-99a to upregulate E2F2

To validate the involvement of miR-99a/E2F2 axis in the oncogenic roles of LINC00847 in HCC, rescue assays were further performed by cotransfecting with si-LINC00847 and miR-99a inhibitor/pcDNA-E2F2 into HCC cells. As presented in Fig. 5A, the decrease of E2F2 expressions caused by si-LINC00847 could be partially recovered by miR-99a inhibitor or pcDNA-E2F2. Moreover, miR-99a silence or E2F2 recovery counteracted the impact of LINC00847 on HCC cell proliferation, invasion and migration (Fig. 5 B-D). These findings demonstrated that LINC00847 promoted the malignant characteristics of HCC cells by sponging of miR-99a and, thereby, increasing E2F2 expressions.

DISCUSSION

The high recurrence rate and poor prognosis of HCC patients are largely due to the high rate of extrahepatic and intrahepatic metastasis (9). Metastasis is a complex process, and the metastatic potential of HCC cells were affected by cell-intrinsic identities and multiple extrinsic microenvironment factors (10). However, the potential mechanism underlying the metastasis is still largely unclear. In recent years, growing evidence have greatly promoted our understanding of the critical roles of lncRNAs in HCC pathogenesis. In this paper, we found that LINC00847 was at high levels in HCC tissues and cells. Moreover, we confirmed that LINC00847 downregulation could inhibit HCC cell proliferation, invasion and migration. These results demonstrated the tumor-suppressive functions of LINC00847 downregulation in HCC. Our study also presented evidence that LINC00847 regulated HCC progression via binding to miR-99a.

E2F2 could regulate cell proliferation and growth by regulating the cell cycle-related genes (11). Previous findings showed that E2F2 exhibited oncogenic functions in multiple cancers (12). In the present study, E2F2 was also found to be obviously upregulated in HCC. Most importantly, LINC00847 upregulated E2F2 expression via inhibiting miR-99a in HCC. In conclusion, the current study uncovered that LINC00847 was highly expressed in HCC, promoting HCC progression via acting as a sponge for miR-99a and up-regulating E2F2 expression. Taken together, LINC00847/miR-99a/E2F2 axis may be promising therapeutic targets for HCC patients. However, these data should be further validated in independent cohorts and prospective trials, such as EMT and *in vivo* study.

REFERENCES

1. Ruohoniemi DM, Taslakian B, Aaltonen EA, et al. Comparative analysis of safety and efficacy of transarterial chemoembolization for the treatment of hepatocellular carcinoma in patients with and without pre-existing transjugular intrahepatic portosystemic shunts. J Vasc Interv Radiol 2020; 31:409-15.
2. Yan X, Hu Z, Feng Y, et al. Comprehensive genomic characterization of long non-coding RNAs across human cancers. Cancer Cell 2015; 28:529-40.
3. Shields EJ, Petracovici AF, Bonasio R. lncRedibly versatile: biochemical and biological functions of long noncoding RNAs. Biochem J 2019; 476:1083-104.
4. Guzel E, Okyay TM, Yalcinkaya B, Karacaoglu S, Gocmen M, Akcakuyu MH. Tumor suppressor and oncogenic role of long non-coding RNAs in cancer.

North Clin Istanb 2020; 7:81-86.

5. Fatma H, Siddique HR. Role of long non-coding RNAs and MYC interaction in cancer metastasis: A possible target for therapeutic intervention. Toxicol Appl Pharmacol 2020; 399:115056.
6. Ning S, Liu H, Gao B, Wei W, Yang A, Li J, Zhang L. miR-155, miR-96 and miR-99a as potential diagnostic and prognostic tools for the clinical management of hepatocellular carcinoma. Oncol Lett 2019; 18:3381-87.
7. Xia M, Li H, Wang JJ, Zeng HJ, Wang SH. MiR-99a suppress proliferation, migration and invasion through regulating insulin-like growth factor 1 receptor in breast cancer. Eur Rev Med Pharmacol Sci 2016; 20:1755-63.
8. Ni Y, Li C, Bo C, et al. LncRNA EGOT regulates the proliferation and apoptosis of colorectal cancer by miR-33b-5p/CROT axis. Biosci Rep 2020; doi: 10.1042/BSR20193893. Online ahead of print.
9. Budhu A, Forgues M, Ye QH, et al. Prediction of venous metastases, recurrence, and prognosis in hepatocellular carcinoma based on a unique immune response signature of the liver microenvironment. Cancer Cell 2006; 10:99-111.
10. Wang QY, Zhou CX, Zhan MN, et al. MiR-133b targets Sox9 to control pathogenesis and metastasis of breast cancer. Cell Death Dis 2018; 9:752.
11. Stevaux O, Dyson NJ. A revised picture of the E2F transcriptional network and RB function. Curr Opin Cell Biol 2002; 14:684-91.
12. Fang ZQ, Li MC, Zhang YQ, Liu XG. MiR-490-5p inhibits the metastasis of hepatocellular carcinoma by down-regulating E2F2 and ECT2. J Cell Biochem 2018; 119:8317-24.

JOURNAL OF BIOLOGICAL REGULATORS & HOMEOSTATIC AGENTS Vol. 34, no. 6, 2205-2207 (2020)

LETTER TO THE EDITOR

Criolaser-assisted drug delivery in the treatment of refractory keloids

S. Zafiropoulou[1], M. Tirant[2], N. Van Thuong[3], A. Salimi[1], R. Sadoughifar[1] and T. Lotti[1,3]

[1]Department of Dermatology, University of Rome G. Marconi, Rome, Italy; [2]Hanoi Medical University, Department of Dermatology, Hanoi, Vietnam; [3]Department of Dermatology and Venereology, I.M. Sechenov First Moscow State Medical University, Moscow, Russia

Received July 13, 2020 – Accepted November 5, 2020

To the Editor,

Keloids are common lymphoproliferative lesions of the skin related to benign hyper proliferative growth induced by relatively unknown abnormal reaction to skin injuries (1-5). Quality of life of patients with keloids is often impaired due to its high recurrence rate, itch, disfiguration and functional impairing. Treatment of keloids is still suboptimal even after the introduction of intralesional corticosteroid and verapamil, 5 fluorouracil, bleomycin and interferon α2b injections, sophisticated compression therapies, different laser treatments and radiotherapy. Criolaser-assisted drug delivery is a new treatment modality recently introduced by C.I.R.C.E. Srl (Fig. 1).

We present here the perception amongst 10 patients affected by disfiguring and functionally impairing refractory keloids before and after treatment with criolaser-assisted drug delivery. We used a retrospective chart review to record patient-recorded scores of "discomforts" after the use of criolaser-assisted drug delivery. Thirty random cases were evaluated in the winter season 2017-2018 after informed consent (Fig. 2). All subjects showed refractory keloids at least two times after the treatment with intralesional corticosteroids and verapamil. Discomfort reported by the subjects included itch, pain, functional impairing and disfiguring perception. Discomfort scores were recorded on a scale 0-5 where 0 represented no discomfort and 5 the highest level of discomfort, and a visual analogue scale was used (Table I).

Treatment with criolaser-assisted drug delivery was performed weekly for 10 consecutive weeks. Each treatment was carried out with 1 ml Kenacort A Retard (Triamcinolone Acetonide) diluted by 50% with 1 ml hyaluronic acid [Hyaluronic acid 200mg (Acef Spa)] per 3 cm² of keloid.

Each treatment lasted 30-60 min according to the size of the keloid. Patients were aged 39-60 years, 15 men and 15 women. In this retrospective review all subjects reported improved scores on keloid discomfort after 5 and 10 treatments with criolaser-assisted drug delivery (Fig. 3). No side effects were reported by any patients. Interestingly, the 20 patients with "average discomfort 3" at time 0 reported the best subjective improvement rate (88% overall improvement) after 10 weeks of treatment. The 7 patients with the highest discomfort 5 reported a relevant overall subjective improvement by 75%. Surprisingly, the 3 subjects with modest discomfort at time 0 (3 patients), showed a modest overall improvement after 10 weeks of treatment with criolaser-assisted drug delivery (6-13).

Key words: criolaser; keloid

Corresponding Author:
Dr Roxanna Sadoughifar,
Department of Dermatology,
University of Rome,
Via Pilinio, 44, 00193 Roma RM, Italy
Fax: +39 0637725647
e-mail: bidarskincenter@gmail.com

0393-974X (2020)
Copyright © by BIOLIFE, s.a.s.
This publication and/or article is for individual use only and may not be further reproduced without written permission from the copyright holder.
Unauthorized reproduction may result in financial and other penalties
DISCLOSURE: ALL AUTHORS REPORT NO CONFLICTS OF INTEREST RELEVANT TO THIS ARTICLE.

Table I. *Visual analogue scale of 30 patients regarding discomfort before and after 10 consecutive criolaser-assisted treatment of refractory keloids.*

Discomfort at time 0	Discomfort after 5 weeks treatment	Discomfort after 10 weeks treatment
Discomfort 5 (7 patients)	30% overall improvement	75% overall improvement
Discomfort 3 (20 patients)	35% overall improvement	88% overall improvement
Discomfort 1 (3 patients)	10% overall improvement	30% overall improvement



Fig. 1. *Medical Device – Lasericemed*



Fig. 2. *First step application Lasericemed laser handpiece transfer of drug molecules under the dermis.*

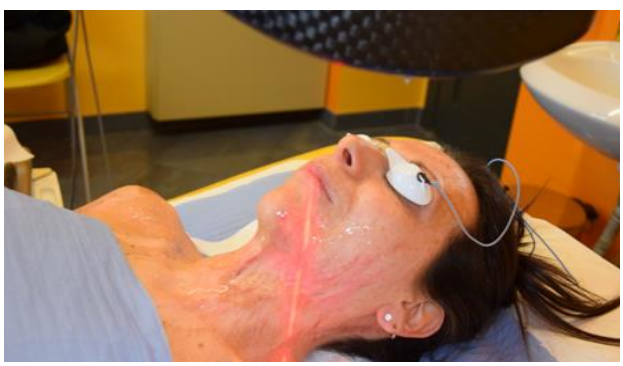


Fig. 3. *Second step application Lasericemed laser scanner transfer of drug molecules to the target site.*

In consideration of the good overall results reported by all subjects and by the complete lack of side effects we recommend the use of criolaser-assisted drug delivery in refractory keloids instead of injecting corticosteroids inside the keloidal lesions.

ACKNOWLEDGEMENTS

The Authors wish to thank Dr. M. Goldust for his help in revision of the paper.

REFERENCES

1. Cicchi R, Kapsokalyvas D, De Giorgi V, et al. Scoring of collagen organization in healthy and diseased human dermis by multiphoton microscopy. J Biophotonics 2010; 3:34-43.
2. de Giorgi V, Sestini S, Mannone F, Papi F, Alfaioli B, Gori A, Lotti T. The use of silicone gel in the treatment of fresh surgical scars: a randomized study. Clin Exp Dermatol 2009; 34:688-93.
3. Cicchi R, Sestini S, De Giorgi V, Massi D, Lotti T, Pavone FS. Nonlinear laser imaging of skin lesions. J Biophotonics 2008; 1:62-73.
4. Lotti T, Teofoli P, Bianchi B, Mauviel A. POMC and fibroblast biology. Ann N Y Acad Sci 1999; 885:262-67.
5. Teofoli P, Motoki K, Lotti TM, Uitto J, Mauviel A. Propiomelanocortin (POMC) gene expression by normal skin and keloid fibroblasts in culture: modulation by cytokines. Exp Dermatol 1997; 6:111-15.
6. Huu ND, Huu SN, Thi XL, et al. Successful treatment of intralesional bleomycin in keloids of Vietnamese population. Open Access Maced J Med Sci 2019; 7:298-99.
7. Huu ND, Huu SN, Thi XL, et al. Successful treatment

of intralesional triamcilonon acetonide injection in keloid patients. Open Access Maced J Med Sci 2019; 7:275-78.

8. Rasaii S, Sohrabian N, Gianfaldoni S, et al. Intralesional triamcinolone alone or in combination with botulinum toxin A is ineffective for the treatment of formed keloid scar: A double blind controlled pilot study. Dermatol Ther 2019; 32:e12781.
9. Fama F, Sindoni A, Tchernev G, et al. Uncommon clinical presentation of Kimura's disease as bilateral retroauricular masses in a young Malian male: successful surgical approach. J Biol Regul Homeost Agents 2016; 30:35-38.
10. Campolmi P, Bonan P, Cannarozzo G, et al. Highlights of thirty-year experience of CO2 laser use at the Florence (Italy) department of dermatology. ScientificWorldJournal 2012; 2012:546528.
11. Kraeva E, Ho D, Jagdeo J. Successful Treatment of keloid with fractionated carbon dioxide (CO2) laser and laser-assisted drug delivery of triamcinolone acetonide ointment in an African-American man. J Drugs Dermatol 2017; 16:925-27.
12. Waibel JS, Wulkan AJ, Shumaker PR. Treatment of hypertrophic scars using laser and laser assisted corticosteroid delivery. Lasers Surg Med 2013; 45:135-40.
13. Park JH, Chun JY, Lee JH. Laser-assisted topical corticosteroid delivery for the treatment of keloids. Lasers Med Sci 2017; 32:601-608.

LETTER TO THE EDITOR

Long noncoding RNA HOTAIR sponging miR-211 regulates cerebral ischemia-reperfusion injury

NH. Ma[1], MH. Zhang[2], JX. Yang[3], ZJ. Sun[4], F. Yuan[1] and XL. Qiu[5]

[1]Department of Neurology, the Fourth People's Hospital of Zibo, Zibo, Shandong, China; [2]Department of Cardiology, the Fourth People's Hospital of Zibo, Zibo, Shandong, China; [3]Comprehensive treatment department of the Fourth People's Hospital of Zibo, Zibo, Shandong, China; [4]Department of critical medicine, the Fourth People's Hospital of Zibo, Zibo, Shandong, China; [5]Department of Neurology, Zibo Central Hospital, Zibo, Shandong, China

Received Arrived May 18, 2020 – Accepted October 15, 2020

To the Editor,

Ischemic stroke is caused by local cerebral blood supply disorders, and is affected by a variety of pathological factors (1). Early reperfusion after cerebral ischemia is important to restore the functions of the ischemic area and reduce the incidence of disease. However, blood oxygen reaching the ischemic tissue can cause ischemia/reperfusion (I/R) injury (2). Therefore, it is necessary to develop potential neuroprotective or therapeutic agents to effectively improve the sequelae of stroke.

Long non-coding RNAs (lncRNAs) are considered to be critical non-coding RNAs with more than 200 nucleotides (3). In recent years, it has been shown that long non-coding RNAs are involved in several processes (4). For example, it is reported that HOX antisense intergenic RNA (HOTAIR) acted as a suppressor by inhibiting cell proliferation and promoting cell apoptosis of glioblastoma (5). Knocking down of HOTAIR can inhibit cell proliferation, invasion and migration, whilst increasing cell apoptosis in colorectal cancer (6). However, the functions of HOTAIR in cerebral ischemia/reperfusion injury remain unclear.

The molecules regulated by lncRNA are involved in a variety of mechanisms. MiRNAs negatively regulate gene expression by directly binding to the 3'-untranslated regions (3'-UTR) of the mRNA of a target gene (7). MiR-155 accelerates cerebral ischemia-reperfusion injury via targeting DUSP14 (8). After 24 h of reperfusion, overexpression of miR-211 reduced the apoptosis of PC12 cells subject to OGD/R and MCAO rat brain (9).

In the present study, an *in vitro* OGD/R cell model was established to explore the effect of HOTAIR on cerebral I/R injury and the underlying mechanisms. Our results suggest that HOTAIR can be used for the diagnosis, prognosis and therapeutic intervention of ischemic stroke.

MATERIALS AND METHODS

Cell culture

HCN-2 cells were purchased from American Type Culture Collection (ATCC, USA). The cells were incubated in Dulbecco's modified Eagle medium (DMEM; Sigma-Aldrich, Grand Island, NY, USA) supplemented with 10% fetal bovine serum (FBS; Scientific, Waltham, MA, USA) at 37°C in a humidified atmosphere comprising 5% CO_2.

OGD/R Model

An oxygen glucose deprivation/reoxygenation (OGD/R) was established to simulate I/R model *in vitro*.

Key words: HOTAIR; miR-211; cerebral ischemia-reperfusion injury; glucose deprivation/reoxygenation

Corresponding Author:
Dr Xueliang Qiu,
Department of Neurology, Zibo Central Hospital,
No.54 Gongqingtuan West Road,
Zhangdian District, Zibo 255200, Shandong, China
Tel./Fax: +86 0533-2881510
e-mail: renjiyun40546862@163.com

0393-974X (2020)
Copyright © by BIOLIFE, s.a.s.
This publication and/or article is for individual use only and may not be further reproduced without written permission from the copyright holder.
Unauthorized reproduction may result in financial and other penalties
DISCLOSURE: ALL AUTHORS REPORT NO CONFLICTS OF INTEREST RELEVANT TO THIS ARTICLE.

The cells were treated with OGD when the density of HCN-2 cells was approximately 80%. At first, HCN-2 cells were cultured with deoxygenated glucose-free Hanks' Balanced Salt Solution (Invitrogen), and cultured in an anaerobic chamber including 5% CO_2 at 37°C for 6 h. After that, the medium was replaced with a standard DMEM medium containing 10% FBS, and reoygenation at 37°C for 24 h under a normoxic environment containing 5% CO2 oxygen for reoxygenation. Cells incubated in normal medium and normal environment were used as controls.

Cell viability assay

HCN-2 cells were cultured in a 96-well microtiter plate at a density of 1×10^4 cells for 24 h, and then treated with OGD for 6 h and re-oxygenated for 24 h. Subsequently, the treated cells were stained with 10 µl MTT (mg/ml) (Sigma, Glpbio, CA, USA), and incubated at 37°C for another 4 h. Next, the violet formazan crystals were completely dissolved with 150 µl of dimethyl sulfoxide (DMSO), and then shaken for 10 min. Finally, the absorbance was measured at 490 nm on a microplate reader (Multiskan, FC, USA).

RNA isolation and real-time quantitative polymerase chain reaction (RT-qPCR)

The TRIzol reagent (Qiagen, Valencia, CA, USA) was used to extract total RNA. Then, reverse transcription was performed by using a SuperScript II First-Strand cDNA Synthesis Kit (Thermo Fisher Scientific, San Jose, CA, USA) to synthesize cDNA. qPCR was performed using the Express SYBR GreenER miRNA RT-qPCR kit (Invitrogen, Rainbio, MA, USA) on an ABI Prism 7900 detection system (Thermo Fisher Scientific). By using the formula $2^{-\Delta\Delta Ct}$ to compare with an internal reference, the relevant quantitative analysis of the target gene can be detected. The primers were: HOTAIR F: 5'-CAGTGGGGAACTCTGACTCG-3', R: 5'-GTGCCTGGTGCTCTCTTACC-3'; GAPDH F: 5'-TGTTCGTCATGGGTGTGAAC-3', R: 5'-ATGGCATGGACTGTGGTCAT-3'; miR-211 F: 5'-TTGTGGGCTTCCCTTTGTCATCCT-3', R: 5'-TGCTGTGGGAAGTGACAACTGA-3'; U6 F: 5'-CTCGCTTCGGCAGCACA-3', R: 5'-AACGCTTCACGAATTTGCGT-3'.

Dual-luciferase reporter assay

The wild-type and mutant HOTAIR were introduced into pmiR-GLO dual luciferase reporter gene vector to build pmiR-GLO-HOTAIR-3'UTR and pmiR-GLO-HOTAIR-3'UTR luciferase reporter systems. HCN-2 cells were incubated in 24-well plates, and Lipofectamine 2000 was used to co-transfect the miR-211 mimic and pmiR-GLO-HOTAIR-3'UTR in HCN-2 cells. The cells were collected after 48 h of cultivation. The dual luciferase reporter gene assay system was used to detect the luciferase activity, which was evaluated by the ratio of firefly luminescence to Renilla luminescence.

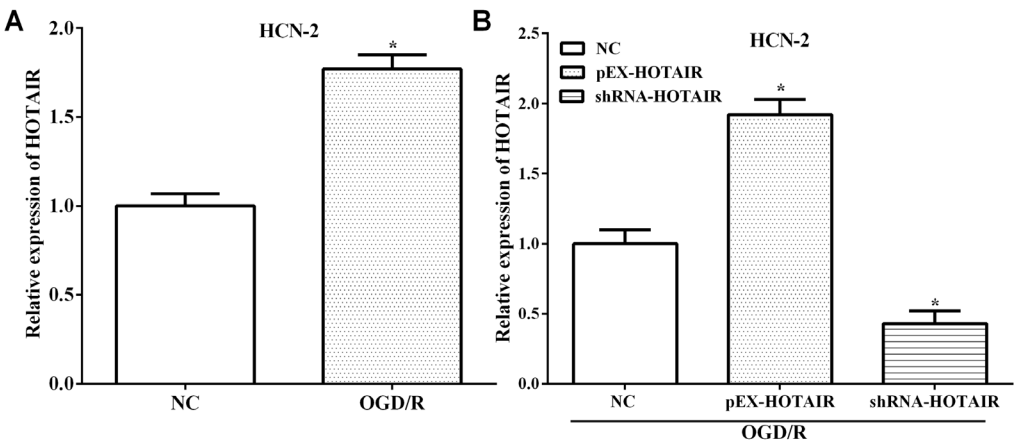


Fig. 1. *The expression of HOTAIR is elevated in OGD/R models.* ***A)*** *The expression of HOTAIR was increased in OGD/R-treated cells versus normal cells.* ***B)*** *The expression of HOTAIR was overexpressed by pEX-HOTAIR, while shRNA-HOTAIR was utilized to knockdown HOTAIR in HCN-2 cells.*

Statistical analysis

The data was demonstrated as the mean± standard deviation (SD) from at least three independent experiments. Statistical analysis was performed using Statistical Program for Social Sciences (SPSS) 21.0 and GraphPad Prism 5.0 software. Student's *t*-test and one-way ANOVA were employed to compare the differences between the two and multiple groups. Differences are considered significant if the probability of the difference occurring by chance is less than 0.05.

RESULTS

Expression of HOTAIR was elevated in OGD/R models

Firstly, the expression of HOTAIR was measured in OGD/R treated and normal HCN-2 cells. The results showed that the expression of HOTAIR was increased in cells treated with OGD/R compared with normal HCN-2 cells ($P<0.05$) (Fig. 1A). Subsequently, in order to investigate the functions of HOTAIR in cerebral ischemia-reperfusion injury, HOTAIR was overexpressed by pEX-HOTAIR ($P<0.05$), while shRNA-HOTAIR was utilized to knockdown HOTAIR in HCN-2 cells ($P<0.05$) (Fig. 1B).

HOTAIR promotes the viability and inhibits the apoptosis of HCN-2 cells

Cell viability was evaluated using MTT assay. As expected, OGD/R reduced the viability of HCN-2 cells compared with normal cells ($P<0.05$) (Fig. 2A). On the other hand, upregulation of HOTAIR enhanced cell viability, and it was inhibited by knocking down HOTAIR ($P<0.05$) (Fig. 2B). The mRNA level of cell apoptosis associated genes (Bax and Bcl-2) were

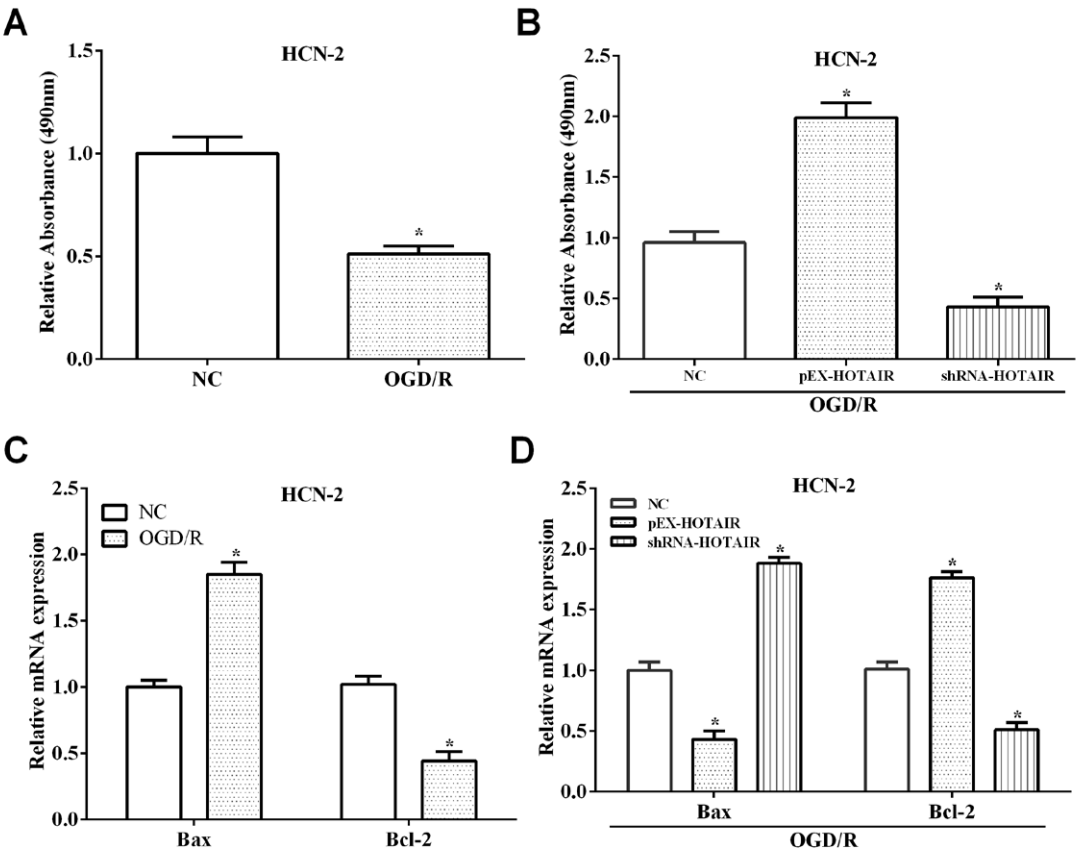


Fig. 2. *HOTAIR promotes the viability and inhibits the apoptosis of HCN-2 cells.* ***A****) OGD/R reduced the viability of HCN-2 cells compared to normal cells.* ***B****) Upregulation of HOTAIR enhanced and cell viability was inhibited by knocking down HOTAIR.* ***C****) After treating with OGD/R, the level of Bax was enhanced while Bcl-2 mRNA level was reduced.* ***D****) The mRNA levels of Bax and Bcl-2 were calculated when altering HOTAIR.*

measured using RT-qPCR. The expression of Bax was enhanced (P<0.05), while Bcl-2 was reduced after being treated with OGD/R (P<0.05) (Fig. 2C). In addition, the mRNA level of Bax was inhibited by overexpressing HOTAIR (P<0.05), and it was increased after silencing HOTAIR (P<0.05). On the contrary, the expression of Bcl-2 was enhanced after upregulating HOTAIR (P<0.05), while Bcl-2 was downregulated when HOTAIR when HOTAIR was knocked down (P<0.05) (Fig. 2D).

HOTAIR directly targets miR-211

The binding area between HOTAIR and miR-211 is shown in Fig. 3A. Moreover, the mutation was made in HOTAIR sequence. Next, co-transfection of wild type HOTAIR and the miR-211 mimic significantly reduced the reporter activity of HCN-2 cells (P<0.05). Meanwhile, miR-211 mimic had no significant effect on the luciferase activity of mutant HOTAIR (P>0.05) (Fig. 3B).

The expression of miR-211 was assessed when treated with OGD/R, miR-211 was found to be downregulated after treating with OGD/R compared to the normal HCN-2 cells (P<0.05) (Fig. 3C). In addition, the expression of miR-211 was reduced when upregulating HOTAIR (P<0.05), whereas it was increased when downregulating HOTAIR in OGD/R-treated HCN-2 cells (P<0.05) (Fig. 3D).

miR-211 partially restores the viability and apoptosis of HOTAIR on OGD/R-treated HCN-2 cells

In order to confirm the biological functions of HOTAIR and miR-211 in OGD/R-treated HCN-2 cells, miR-211 inhibitor was transfected in HOTAIR knockout cells (P<0.05) (Fig. 4A). The results of MTT analysis showed that inhibition of miR-211

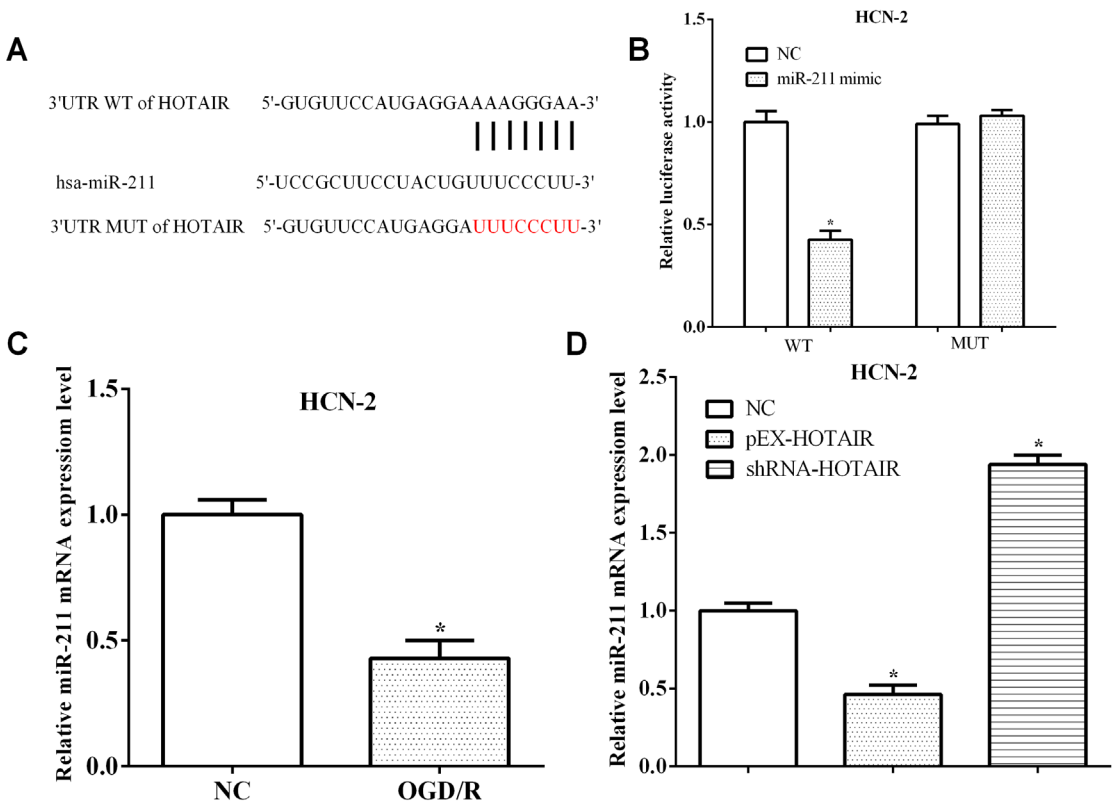


Fig. 3. *HOTAIR directly targets miR-211. **A**) The binding area between HOTAIR and miR-211. **B**) Co-transfection of wild type HOTAIR with miR-211 mimic significantly reduced the reporter activity of HCN-2 cells. **C**) miR-211 was downregulated after treated with OGD/R compared to the normal HCN-2 cells. **D**) The expression of miR-211 was reduced when altering HOTAIR in OGD/R treated HCN-2 cells.*

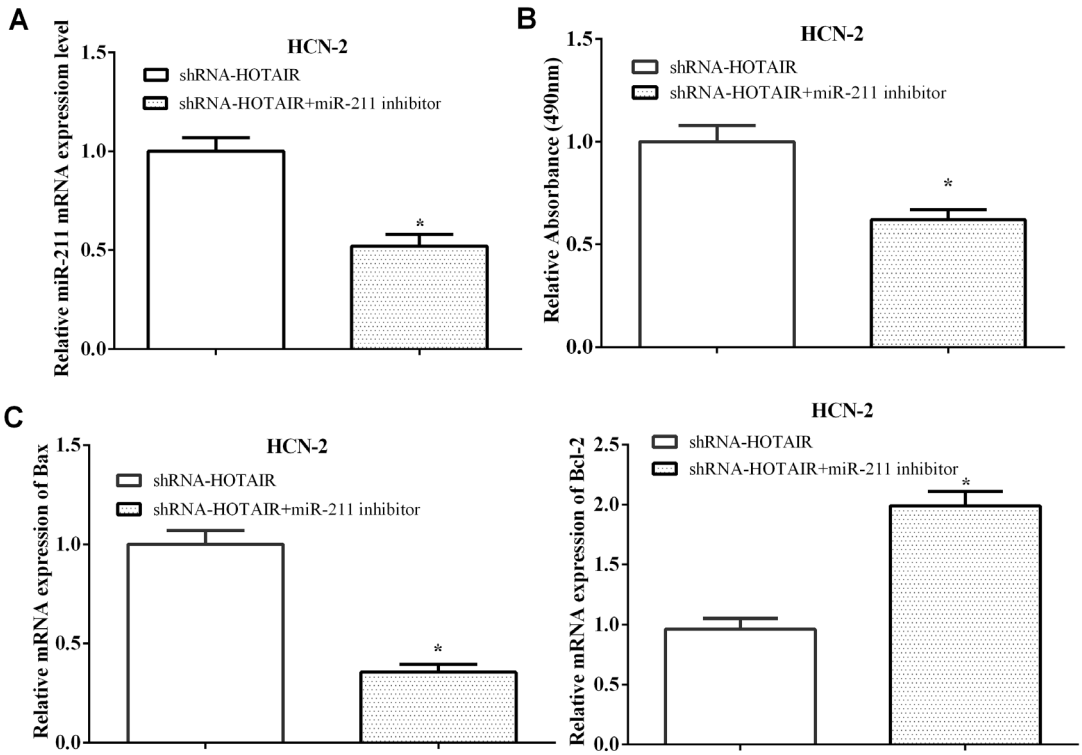


Fig. 4. *miR-211 partially restores the viability and apoptosis of HOTAIR on OGD/R-treated HCN-2 cells.* ***A****) The expression of miR-211 in HOTAIR knockout cells.* ***B****) MTT analysis showed that inhibition of miR-211 significantly reversed the promotion of HOTAIR on cell activity in OGD/R-treated HCN-2 cells.* ***C****) Inhibition of the expression of miR-211 partially reversed the effects on OGD/R-induced apoptosis of HOTAIR.*

significantly reversed the promotion of HOTAIR on the viability of OGD/R-treated HCN-2 cells compared to the control group ($P<0.05$) (Fig. 4B). In addition, inhibition of the expression of miR-211 partially reversed the effects on OGD/R-induced apoptosis of HOTAIR ($P<0.05$) (Fig. 4C). All the findings indicated that miR-211 partially restored the functions of HOTAIR on cell viability and cell apoptosis.

DISCUSSION

Although great progress has been made in the treatment of ischemia-reperfusion brain injury, the molecular biology of ischemia-reperfusion brain injury remains unclear. Identification of new biomarkers is essential for accurate diagnosis of ischemia-reperfusion brain injury.

In this study, HCN-2 cells were selected to establish the OGD/R model. Current research showed that the expression of HOTAIR was increased in OGD/R HCN-2 cells. HOTAIR functions as a competitive endogenous RNA to regulate the expression of PRAF2 by sponging miR-326 in cutaneous squamous cell carcinoma (10). We found that overexpression of HOTAIR promoted cell viability and inhibited cell apoptosis. In contrast, silencing of HOTAIR inhibited the viability and promoted the apoptosis in HCN-2 cells.

Previous studies revealed that HOTAIR played important roles by sponging miRNAs (11). Through dual luciferase activity reporter assay, we confirmed that HOTAIR directly binds to miR-211. In this study, we found that miR-211 was low expressed after treating with OGD/R, and that HOTAIR promoted cell viability and inhibited cell apoptosis via sponging miR-211, which was consistent with the results in breast cancer (12). In addition, rescue experiments were performed to verify that HOTAIR

regulates cell viability and apoptosis via directly binding to miR-211.

In conclusion, the results showed that HOTAIR accelerates the growth of OGD/R cells and inhibits cell apoptosis. Study of the mechanism demonstrated that HOTAIR affects ischemia-reperfusion injury through sponge miR-211. This study may provide new potential therapeutic targets for ischemia-reperfusion injury.

REFERENCES

1. Rana AK, Singh D. Targeting glycogen synthase kinase-3 for oxidative stress and neuroinflammation: Opportunities, challenges and future directions for cerebral stroke management. Neuropharm 2018; 139:124-36.
2. Gourdin M, Bree B, De Kock M. The impact of ischaemia-reperfusion on the blood vessel. Eur J Anaesthesiol 2009; 26:537.
3. Choudhari R, Sedano MJ, Harrison AL, et al. Long noncoding RNAs in cancer: from discovery to therapeutic targets. Adv Clin Chem 2020; 95:105-47.
4. Luo G, Wang M, Wu X, et al. Long non-coding RNA MEG3 inhibits cell proliferation and induces apoptosis in prostate cancer. Cell Physiol. Biochem 37:2209-20.
5. Li H, Guan C. HOTAIR inhibits the proliferation of glioblastoma cells by targeting miR-219. Cancer Biomark 2020.
6. Lin K, Jiang H, Zhang LL, et al. Down-Regulated LncRNA-HOTAIR Suppressed Colorectal Cancer Cell Proliferation, Invasion, and Migration by Mediating p21. Dig Dis Sci 2018; 63:2320-31.
7. Tafrihi M, Hasheminasab E. MiRNAs: Biology, biogenesis, their web-based tools, and databases. Microrna 2019; 8:4-27.
8. Shi Y, Li K, Xu K, Liu QH. MiR-155-5p accelerates cerebral ischemia-reperfusion injury via targeting DUSP14 by regulating NF-κB and MAPKs signaling pathways. Eur Rev Med Pharmacol Sci 2020; 24:1408-19.
9. Liu W, Miao Y, Zhang L, Xu X, Luan Q. MiR-211 protects cerebral ischemia/reperfusion injury by inhibiting cell apoptosis. Bioengineered 2020; 11:189-200.
10. Yu GJ, Sun Y, Zhang DW, Zhang P. Long non-coding RNA HOTAIR functions as a competitive endogenous RNA to regulate PRAF2 expression by sponging miR-326 in cutaneous squamous cell carcinoma. Cancer Cell Int 2019; 19:270.
11. McCool MA, Bryant CJ, Baserga SJ. MicroRNAs and long non-coding RNAs as novel regulators of ribosome biogenesis. Biochem Soc Trans 2020; 48:595-612.
12. Li X, Wang S, Li Z, Long X, Wen L. The lncRNA NEAT1 facilitates cell growth and invasion via the miR-211/HMGA2 axis in breast cancer. Int J Biol Macromol 2017; 105:346.

JOURNAL OF BIOLOGICAL REGULATORS & HOMEOSTATIC AGENTS Vol. 34, no. 6, 2215-2220 (2020)

LETTER TO THE EDITOR

Effects of combined therapy of valsartan and rosuvastatin on patients with atrial fibrillation

WM. Hu*, ZH. Shi*, DY. Wu*, SY. Ye, YJ. Xiang, C. Liu, JC. Chen and CL. Zeng

Department of Cardiology, Lishui Municipal Central Hospital, Lishui, Zhejiang, China

Received June 2, 2020 – Accepted September 28, 2020

*These authors contributed equally to this work

To the Editor,

Atrial fibrillation (AF) refers to an abnormal heart rhythm (arrhythmia) characterized by the rapid and irregular beating of the atrial chambers of the heart. It causes several complications, such as thrombosis, heart failure, and moderate stroke (1). Nowadays, the treatment regimens for AF include drug therapy and surgery (2). The effective therapeutic strategies alleviate symptoms, such as palpitations, chest tightness, shortness of breath, and fatigue, as well as significant reduction in complications and mortality (3).

Studies have pointed out that the occurrence of AF was found to be associated with inflammatory response, electrical remodeling, and tissue reconstruction (4, 5). Statins inhibit important intracellular pathways activated by Ang II, such as Rho-kinase and MAPK pathways, suppressing connective tissue growth factor expression in vascular smooth muscle cells (VSMCs), a mediator of vascular fibrosis (6). Valsartan was reported as an Ang II receptor antagonist (7) that could inhibit the activity of renin-angiotensin system (RAS), and reduce myocardial fibrosis and ventricular diastolic dysfunction (8). Therefore, in the present study, the changes of left anterior descending (LAD), brain natriuretic peptide (BNP), and levels of inflammatory factors in AF patients were assessed before and after combined treatment of valsartan and rosuvastatin, and the effects were explored.

MATERIALS AND METHODS

Patients

From January 2018 to November 2019, 67 AF patients, who were treated in Lishui Municipal Central Hospital, were divided into four groups: control group (15 cases), valsartan group (18 cases), rosuvastatin group (16 cases), and combination therapy group (18 cases). The protocol was approved by the Ethics Committee of Lishui Municipal Central Hospital, and all eligible subjects signed the written informed consent form prior to commencing the study.

Inclusion criteria were: AF patients diagnosed through 12-lead electrocardiogram (ECG) or 24-h dynamic ECG; patients who underwent 2 or more anti-arrhythmia medications, which were ineffective, not effective enough, or could not be tolerated; age <75 years.

Exclusion criteria were: valvular AF; AF combined with severely infected or non-infectious inflammatory diseases; severe renal insufficiency, tumors, blood or immune system diseases; thyroid, lung, and liver diseases; low blood pressure, hyperkalemia and other electrolyte disorders; patients who cannot tolerate combination treatment with valsartan and rosuvastatin or drug-induced diseases.

Key words: valsartan; rosuvastatin; atrial fibrillation; anti-inflammatory effects

Corresponding Author:
Dr Chunlai Zeng,
Department of Cardiology,
Lishui Municipal Central Hospital,
289 Kuocang Road, Liandu District,
Lishui, 323000, Zhejiang Province, China
e-mail: huwm5580@163.com

0393-974X (2020)
Copyright © by BIOLIFE, s.a.s.
This publication and/or article is for individual use only and may not be further reproduced without written permission from the copyright holder.
Unauthorized reproduction may result in financial and other penalties
DISCLOSURE: ALL AUTHORS REPORT NO CONFLICTS OF INTEREST RELEVANT TO THIS ARTICLE.

PROOF

Therapies

All four groups of patients received amine-iodine (Sanofi (Hangzhou) Pharmaceutical Co., Ltd., China), as well as rosuvastatin and warfarin (Shanghai Fuda Pharmaceutical Co., Ltd., China) therapies. The rosuvastatin and warfarin therapies were discontinued after 3 months. The dosage of amine-iodine was reduced once a week, from 600 mg/day in the first week to 200 mg/day orally. Warfarin recipients should undergo international normalized ratio (INR) testing to control the INR at the range of 2.0-3.0. Patients in the control group only received original drugs for the underlying diseases. Based on the conventional treatment (control group), patients in the valsartan group were given valsartan (80 mg; 1 time/day; Beijing Novartis Pharma Co. Ltd., Beijing, China); those in the rosuvastatin group received rosuvastatin calcium (20 mg; 1 time/night; AstraZeneca Pharmaceutical Co., Ltd., Wuxi, China); those in the combination therapy group received valsartan (80 mg; 1 time/d), and rosuvastatin calcium (20 mg; 1 time/night).

Sample collection

Blood samples were collected before and after treatment. For this purpose, 3-4 mL of venous blood (EDTA [Shandong Feier New Material Co., Ltd., China] anticoagulation) was extracted in the morning and centrifuged at 3000 r/min for 15 min. Then, the supernatant was taken from micropipettes (BIOBASE, China) and stored at -80°C until further analysis.

Detection of indicators

All the patients were re-examined at the time of admission and at 1, 3, 6, and 9 months after treatment for detection of indicators. Moreover, the levels of C-reactive protein (CRP), BNP, tumor necrosis factor-α (TNF-α), and interleukin-6 (IL-6) were measured by a commercially used enzyme-linked immunosorbent assay (ELISA) kit.

Statistical analysis

Data were statistically analyzed using SPSS 22.0 software (IBM, USA). The least significant difference (LSD) test was used to compare two datasets. The measured data were expressed as mean ± standard deviation (SD). The enumeration data were compared by *chi*-squared test. $P<0.05$ was considered statistically significant.

RESULTS

Demographic and clinical data

As shown in Table I, there were no significant differences in age, gender, type of AF, combination of diabetes mellitus and hypertension, and different levels of LAD, BNP, CRP, TNF-α, and IL-6 at pre-treatment ($P>0.05$).

LAD Examination

There was no significant difference in LAD among the four groups before treatment ($P>0.05$).

Table I. *Patients' demographic and clinical data.*

Index	Control group	Valsartan group	Rosuvastatin group	Combination therapy group	P
Sex (man/woman)	8/7	10/8	9/7	9/9	0.528
Age (years)	56.28±19.11	59.28±15.24	56.38±20.17	58.27±20.04	0.883
Hypertension (case)	9	8	8	7	0.782
Diabetes (case)	2	3	2	3	0.618
Burst atrial fibrillation (case)	8	10	9	10	0.316
Persistent atrial fibrillation (case)	5	5	6	6	0.836
Permanent atrial fibrillation (case)	2	3	1	2	0.407
LAD (mm)	119.87±3.19	119.91±3.28	119.98±3.07	119.89±3.11	0.592
BNP (pg/mL)	113.43±27.17	110.45±27.17	114.53±27.17	112.17±27.17	0.981
CRP (mg/L)	12.16±1.89	12.27±1.72	11.98±1.29	12.03±1.37	0.594
TNF-α (mg/L)	72.39±6.87	73.30±6.59	72.50±8.16	73.41±7.41	0.639
IL-6 (ng/L)	158.45±26.58	159.43±21.44	158.10±29.54	160.82±25.57	0.703

One month after the treatment, less LAD was found in the four groups compared with pre-treatment. At 3 months after treatment, a significant difference was noted between the groups (P<0.05). The above-mentioned results suggested that the LAD in patients with AF who received rosuvastatin therapy was lower than that before treatment, indicating that the prescribed drug could effectively reduce the LAD. However, valsartan significantly reduced the LAD, while rosuvastatin exhibited no similar effect (Fig.1).

Comparison of BNP levels among the groups

Fig. 2 shows that BNP levels gradually decreased compared with those before the treatment, while the

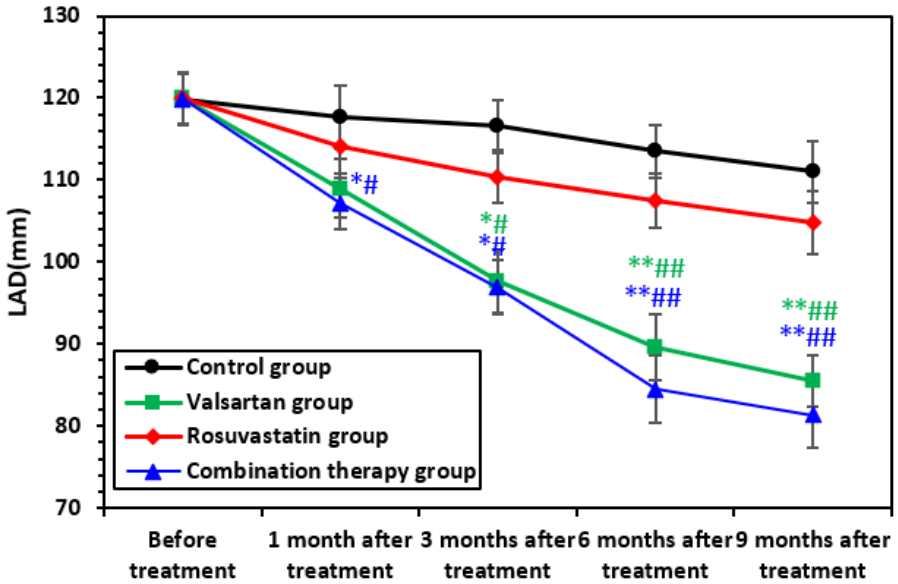


Fig. 1. *Comparison of patients' LAD. Compared with the control group, *P<0.05, **P<0.01; compared with before treatment, #P<0.05, ##P<0.01.*

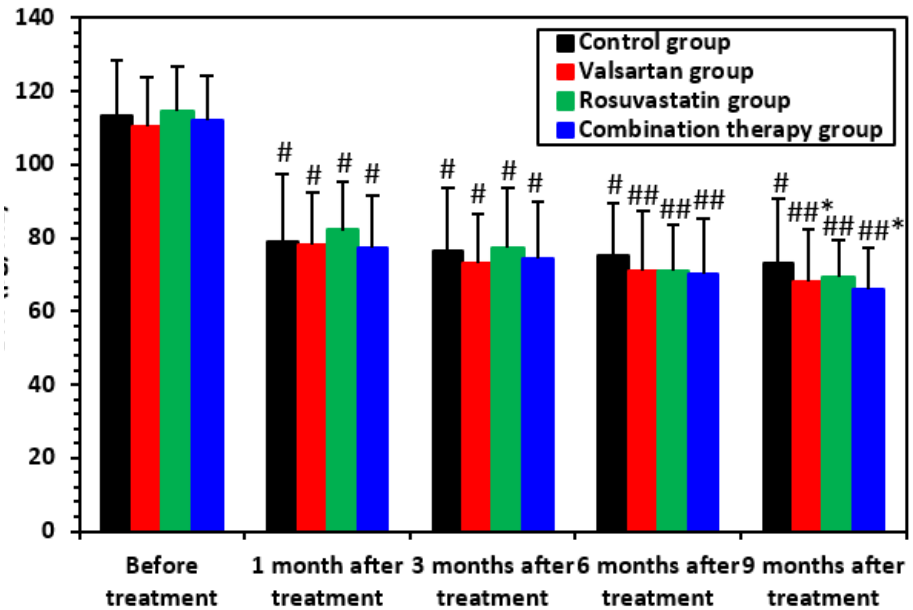


Fig. 2. *Comparison of BNP concentration. Compared with the control group, *P<0.05; compared with before treatment, #P<0.05, ##P<0.01.*

difference between 1 month and 6 months after the treatment was not statistically significant (P>0.05). The BNP level was significantly different among the four groups at 9 months after medication (P<0.05), indicating that BNP levels decreased in AF patients who underwent rosuvastatin therapy. After drug treatment, the BNP level was markedly reduced, and reduction of BNP levels in the combination therapy group was greater than other groups.

Levels of inflammatory factors

There was no significant difference in levels of CRP, TNF-α, and IL-6 in the control group before or after treatment (P>0.05). The levels of CRP, TNF-α, and IL-6 were gradually decreased after treatment among the three groups, and reduction of levels was more remarkable in the combination therapy group compared with other groups. The levels of CRP, TNF-α, and IL-6 were decreased in both the rosuvastatin group and the combination therapy group compared with those in the control group at 9 months after treatment (P<0.05) (Table II).

AF recurrence

As shown in Table III, there was no significant difference in the AF recurrence rate among the four

Table II. *Comparison of the concentrations of various inflammatory factors.*

Indicator	Point in time	Control group	Valsartan group	Rosuvastatin group	Combination therapy group	P
CRP(mg/L)	Before treatment	12.16±1.89	12.27±1.72	11.98±1.29	12.03±1.37	0.594
	1 month after treatment	10.96±1.28	10.78±1.79	10.12±1.88#	10.08±1.87#	0.413
	3 months after treatment	8.81±1.12#	8.51±1.67#	7.34±1.23*#	7.18±1.02*#	0.205
	6 months after treatment	7.03±1.08#	7.16±1.36#	5.88±1.32*#	5.31±1.28*#	0.092
	9 months after treatment	5.89±1.18#	5.86±1.10#	4.12±1.29*#	3.89±0.93*##	0.041
TNF-α(mg/L)	Before treatment	72.39±6.87	73.30±6.59	72.50±8.16	73.41±7.41	0.639
	1 month after treatment	70.33±6.61	69.35±5.47	68.05±6.37	66.16±9.59#	0.520
	3 months after treatment	70.08±7.07	68.28±6.52	65.38±7.53	63.36±7.46#	0.212
	6 months after treatment	69.27±6.36	66.17±7.27#	63.31±5.81#	60.81±6.83*##	0.083
	9 months after treatment	68.97±8.34	65.57±7.25#	61.91±8.36*##	58.59±8.87*##	0.039
IL-6(ng/L)	Before treatment	158.45±26.58	159.43±21.44	158.10±29.54	160.82±25.57	0.703
	1 month after treatment	150.71±26.34	148.46±23.39	148.23±26.68	149.02±24.46	0.501
	3 months after treatment	146.43±26.66	143.71±26.07	140.16±25.74	140.03±28.53	0.338
	6 months after treatment	143.82±26.57	139.86±27.13	135.93±27.59	134.18±23.64#	0.118
	9 months after treatment	140.16±24.67	136.13±24.47#	131.06±24.63#	129.11±25.62#	0.083

*Note: Compared with the control group, *P<0.05; compared with before treatment, #P<0.05, ##P<0.01.*

Table III. *Comparison of AF recurrence rates among the 4 groups.*

	Control group	Valsartan group	Rosuvastatin group	Combination therapy group	P
1 month after treatment	0	0	0	0	-
3 months after treatment	3	1	2	1*	0.182
6 months after treatment	3	2	2	1*	0.382
9 months after treatment	7	4	5	2*	0.093

*Note: Compared with the control group, *P<0.05.*

groups (P>0.05). However, a significant difference (P<0.05) was noted between the combination therapy group and the control group, indicating that the combination therapy could reduce the rate of AF recurrence.

DISCUSSION

SR can be maintained in the left atrium with normal inner diameter. However, with the continuous increase of LAD (9), the more obvious pulling stimulation of the atrium wall leads to increased secretion of BNP in the atrium, making AF more likely to occur (10, 11). The results revealed that LAD was lower after treatment compared with before treatment. However, valsartan could significantly reduce the LAD. Valsartan was noted more effective in reducing blood Ang II concentrations, inhibiting AF, thereby inhibiting atrial arrhythmogenic remodeling, which might be related to the above-mentioned results. Although rosuvastatin could inhibit left atrial remodeling through anti-inflammatory and antioxidant effects, it exerted less effect on myocardial remodeling than valsartan. In addition, the present experiment also revealed that the effect of the single application of rosuvastatin and valsartan to reduce serum levels was notably negligible, whereas the combination of the two could reduce BNP concentrations by regulating the activity of the neuroendocrine system as well as significantly decreasing the levels of inflammatory factors (CRP, TNF-α, and IL-6) and left atrium remodeling in AF patients.

In summary, the application of valsartan may improve the microstructure of atrium in AF patients and reduce the concentration of BNP, thereby preventing the recurrence of AF after surgery. Rosuvastatin could inhibit the reconstruction of the left atrium via anti-inflammatory effects. Combination therapy could reduce BNP levels, reduce the rate of AF recurrence, and prevent thrombosis by regulating the activity of the neuroendocrine system, such as sympathetic nerve stimulation, RAS activation, and other common pathways.

ACKNOWLEDGEMENT

This study was financially supported by the Medical Health Science and Technology Project of Zhejiang Provincial Health Commission (Grant No. 2020ZH015).

REFERENCES

1. Zimetbaum P. Atrial fibrillation. Ann Intern Med 2017; 166(5):ITC33-ITC48.
2. Lip GY, Lane DA. Stroke prevention in atrial fibrillation: a systematic review. JAMA 2015; 313(19):1950-62.
3. Latchamsetty R, Morady F. Atrial fibrillation ablation. Annu Rev Med 2018; 69:53-63.
4. Xiang L, You T, Chen J, Xu W, Jiao Y. Serum Soluble

Semaphorin 4D is associated with left atrial diameter in patients with atrial fibrillation. Med Sci Monit 2015; 21:2912-17.

5. Efremidis M, Letsas K, Giannopoulos G, et al. Early pulmonary vein reconnection as a predictor of left atrial ablation outcomes for paroxysmal atrial fibrillation. Europace 2015; 17(5):741-46.
6. van der Harst P, Groenewegen HC, Roks AJ, Buikema H, Zijlstra F, van Gilst WH, de Smet BJ. Rosuvastatin attenuates angiotensin II-induced neointimal formation after stent implantation in the rat. Coron Artery Dis 2008; 19(1):47-53.
7. Merlanti B, De Chiara B, Maggioni AP, et al. Rationale and design of the GISSI-Atrial Fibrillation trial: a randomized, prospective, multicentre study on the use of valsartan, an angiotensin II AT1-receptor blocker, in the prevention of atrial fibrillation recurrence. Int J Cardiol 2015; 199:180-85.
8. Li C, Lin Y, Luo R, et al. Intrarenal renin-angiotensin system mediates fatty acid-induced ER stress in the kidney. Am J Physiol Renal Physiol 2016; 310(5):F351-63.
9. Han M, Zhang Y, Sun S, et al. Renin-angiotensin system inhibitors prevent the recurrence of atrial fibrillation: a meta-analysis of randomized controlled trials. J Cardiovasc Pharmacol 2013; 62(4):405-15.
10. Abid L, Charfeddine S, Kammoun S, Turki M, Ayedi F. Cystatin C: A prognostic marker after myocardial infarction in patients without chronic kidney disease. J Saudi Heart Assoc 2016; 28(3):144-51.
11. Therkelsen SK, Groenning BA, Kjaer A, Svendsen JH, Boje Jensen G. ANP and BNP in atrial fibrillation before and after cardioversion--and their relationship to cardiac volume and function. Int J Cardiol 2008;127(3):396-99.

LETTER TO THE EDITOR

Inhibitory effect of synthetic prostacyclin stimulants on liver fibrosis and related mechanisms

JL. Wang[1], YX. Yang[2], G. Xu[3] and Q. Xu[4]

[1]Department of Pharmacy, Mudanjiang Medical University, Affiliated Hongqi Hospital, Mudanjiang, China; [2]Department of Neurosurgery, The Second Affiliated Hospital of Mudanjiang Medical University, Mudanjiang, China; [3]Department of Orthopaedic Surgery, Mudanjiang Medical University, Affiliated Hongqi Hospital, Mudanjiang, China; [4]Department of Neurology, Mudanjiang Medical University, Affiliated Hongqi Hospital, Mudanjiang, China

Received July 21, 2020 – Accepted November 6, 2020

To the Editor,

Hepatic fibrosis (HF) is a stage that occurs in the development of cirrhosis in the context of chronic liver disease. It is a compensatory reaction in the process of liver inflammation as well as tissue repair caused by various pathogenic factors (1). It arises when extracellular matrix synthesis is greater than the degradation caused by excessive deposition. Indeed, the essence of liver fibrosis is excessive deposition of extracellular matrix (ECM) (4). The activation of hepatic stellate cells (HSC) is the central link in the formation of hepatic fibrosis.

The transforming growth factor beta (TGF-β) family comprises a class of peptide growth factor subfamilies related to structure and function, including TGF-β, activin, bone morphogenetic protein (BMP), growth differentiation factor (GDF). TGF-β not only affects cell proliferation and differentiation, but also plays an important role in embryonic development, extracellular matrix formation, bone formation and reconstruction. TGF-β family members exist widely in various tissues, and have significant effects on normal cells and cancerous cells. It has been found that the TGF-β signaling pathway plays an important role in regulating stem cell activity and organogenesis. With regards to the stimulation of HSC activation and the secretion of ECM, TGF-β1 is the strongest cytokine (5). The TGF-β1/Smad signaling pathway is a common signaling pathway. Anti-heart failure therapy targeting the TGF-β1/Smad pathway has become a new hotspot in drug development (6). The aim of this study was to investigate the effect of prostacyclin on the expression of TGF-β1 and its downstream signal transduction Smad molecules, and to explore its anti-HF mechanism.

MATERIALS AND METHODS

Animals and grouping

Sixty male specific pathogen free (SPF) Wistar rats (six months old, weight 300±20g) were purchased from Nanjing Junke Bioengineering Co., Ltd., China. The rats were reared in a 40% humidity atmosphere. Drinking water was changed 3-4 times a week and the environment was disinfected. The rats were randomly divided into 6 groups (10 rats in each group): normal group, model group, PGI2 (prostacyclin) high dose group, medium dose group, low dose group and PGI2 prevention group. The animal experiment procedures were conducted in accordance with the International Regulations on Animal Protection and Management and was

Key words: prostacyclin; liver fibrosis; TGF-β1; Smad protein

Corresponding Author:
Dr Qing Xu,
Department of Neurology,
Mudanjiang Medical University,
Affiliated Hongqi Hospital, 5 Tongxiang Road,
Aimin District, Mudanjiang, 157011, China
e-mail: xuqingpharmacy@163.com

0393-974X (2020)
Copyright © by BIOLIFE, s.a.s.
This publication and/or article is for individual use only and may not be further reproduced without written permission from the copyright holder.
Unauthorized reproduction may result in financial and other penalties
DISCLOSURE: ALL AUTHORS REPORT NO CONFLICTS OF INTEREST RELEVANT TO THIS ARTICLE.

approved by the ethics committee of Hongqi Hospital Affiliated to Mudanjiang Medical University.

Animal model

Aside from the normal group, pig serum was used in all other groups to replicate a model of liver fibrosis. Intraabdominal injections were carried out using 0.5ml/animal, twice a week, for 10 weeks, and liver fibrosis developed 5 weeks later. The CHSGS prevention group was treated with PGI2 (30ug/kg) at 6:00 p.m. every day for 10 weeks. Each treatment group was given PGI2 at 60/30/10 UG/kg at 6:00 p.m. every day, and the model group was given an identical amount of normal saline until the end of the 10th week.

Histopathology

The left lobe fresh liver tissue was fixed with formalin and embedded in sections. Fresh liver tissues were fixed with formalin and embedded in sections. After fixation, the tissues were dehydrated and embedded with water-insoluble paraffin. The tissue was immersed in a gradually increasing concentration of dehydrating agents (such as alcohol) and dehydrated slowly. The gradual change in hydrophobicity could minimize cell damage. Before paraffin embedding, tissues were incubated in xylene to remove the dehydrating agent. Paraffin wax was typically heated to 60°C and allowed to harden overnight. Finally, the tissue was sliced with a slicer. It was possible for the tissue sections to be dried on microscope slides and stored at room temperature. The tissue sections were then hydrated before starting the immunostaining protocol. Liver fibrosis was divided into 0-4 stages by HE staining and collagen fiber staining. Stage 0: no fibrosis; stage 1: fibrosis; Stage 2: fibrosis from portal area to hepatic lobule 2/3; stage 3: bridging fibrosis with structural distortion, but without obvious sclerosis; stage 4: pseudolobule formation, cirrhosis.

Immunohistochemistry

The expression of TGF-β1, Smad 7, phosphorylated Smad 2/3 (p-Smad 2/3) was detected. All sections were positive for brown granules and negative for non-staining. 10 high power fields (× 400) were randomly selected for each section, and the positive staining

Table I. *Primer sequences used for RT-qPCR*

	Upstream primer (5'-3')	Downstream primer (5'-3')
β-actin	GTGACGAGGCCCAGAGCAAGAG	AGGGGCCGGACTCATCGTA
TGF-β1	CGCAACAACGCAATCTATG	ACCAAGGT AACGCCAGGA
Smad 2	GGAAAGGGTTGCCACATGTT	AGAATCTCCGTGTGCCGAGG
Smad 3	AATGACAGCAGCAGGGACAC	GAGGTAGGACCCACAGTAGAGC
Smad 4	ACGGCCATCTTCAGCACCAC	AGAATGCACAATCGCCGGAG
Smad 7	TGGTGCGTGGTGGCATACT	CAGCCGATCTTGCTCCTCA

Table II. *Effect of PGI2 on liver fibrosis stage in rats with liver fibrosis*

Groups	n	Hepatic fibrosis stage				
		0	1	2	3	4
Normal group	10	10	0	0	0	0
Model group	10	0	2	3	4	1
PGI2 high dose group	10	5	4	1	0	0
PGI2 prevention group	10	6	3	1	0	0

absorbance was detected by the automatic image analysis system, with the average value taken for statistical analysis.

RT-qPCR

The mRNA levels of Smad2, Smad3, Smad4 and Smad7 were detected by RT-qPCR. Total RNA was provided by Trizol (Invitrogen) according to the instructions. Using an ultraviolet spectrophotometer (BD, Franklin Lakes, NJ, NJ) to measure the concentration and purity of RNA, RNA with an A260/A280 ratio of 1.8-2.0 was considered high-quality RNA without protein and DNA contamination. High-quality RNA was reversely transcribed into complementary DNA using a reverse transcription kit (TaKaRa, Dalian, China). PCR amplification was performed using SYBR premix Ex Taq™ II (Takara). Primer sequences are shown in Table I. The PCR procedures were 95°C for 3 min, 40 cycles; 95°C for 10 s, 59°C for 20 s, with the ABI Stepone plus Real-time PCR system (Applied Biosystems, Foster City, CA, USA). Glyceraldehyde-3-phosphate dehydrogenase (GAPDH) and U6 were used as internal controls to determine the level of related mRNA, using data analysis and the 2-ΔΔCt method.

Statistical analysis

All data were processed with SPSS 23.0 (IBM, USA). The measured data were expressed in the form of mean ± standard deviation. When the variance was homogeneous, an independent sample *t*-test was used to compare the two groups. In the case of uneven variance, the corrected *t*-test was used. Comparative analysis involving three or more groups was implemented via ANOVA. $P < 0.05$ was considered to be statistically significant.

RESULTS

Effect on the tissue structure of the liver

Pathological changes associated with liver tissues have been reported. Compared with the model group, the damage observed in the liver lobule structure in the PGI2 prevention group and the PGI2 high dose group was mild. The stages of liver fibrosis are shown in Table II. Pathological sections of liver fibrosis in each group are shown in Fig.1.

Effect on the mRNA level of TGF-β1, Smad2, 3, 4, 7 in the liver tissue of each group

Compared with the normal group, the mRNA

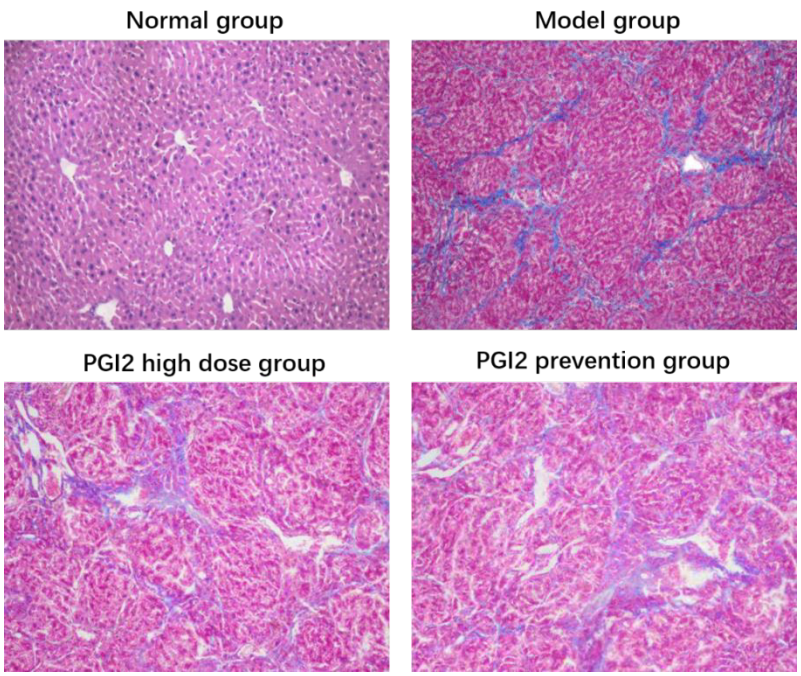


Fig. 1. *Pathological diagrams of liver fibrosis in each group*

Table III. *Effect of PGI2 on liver fibrosis stage in rats with liver fibrosis*

Groups	n	TGF-β1/β-actin	Smad 2/β-actin	Smad 3/β-actin	Smad 4/β-actin	Smad 7/β-actin
Normal group	10	0.86±0.23	0.04±0.13	0.13±0.14	0.87±0.25	0.66±0.32
Model group	10	9.56±2.46	0.46±0.25	0.83±0.26	1.34±0.46	0.16±0.57
PGI2 high dose group	10	5.35±1.35	0.56±0.27	0.71±0.09	1.31±0.25	0.66±0.45
PGI2 prevention group	10	4.34±0.33	0.57±0.48	0.67±0.08	1.34±0.37	0.64±0.26

Table IV. *Effect of PGI2 on TGF-β, p-SMad 2/3 and Smad 7 protein expression in rat liver*

Groups	n	TGF-β1/A	p-Smad 2/3 /A	Smad 7/A
Normal group	10	0.77±0.24	8.45±4.15	34.51±6.45
Model group	10	8.23±0.89	28.31±5.35	7.35±1.35
PGI2 high dose group	10	5.14±2.35	14.64±5.76	30.15±3.56
PGI2 prevention group	10	4.68±0.36	13.57±6.47	33.56±3.46

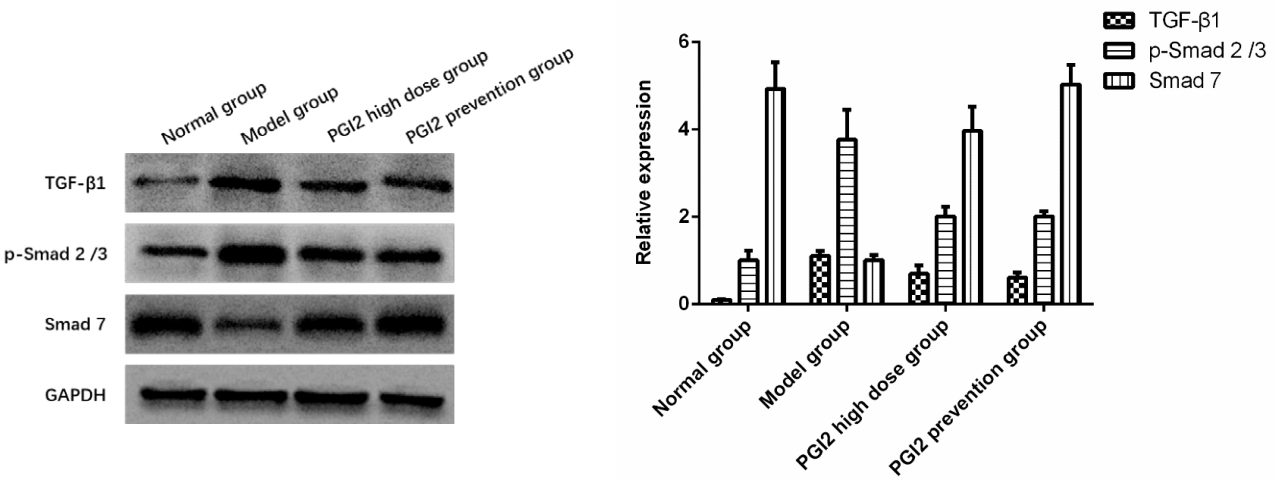


Fig. 2. *Relative expression of TGF-β, p-SMad 2/3 and Smad 7 protein in each group.*

expression of TGF-β1, Smad 2 and Smad 3 in the model group increased significantly (all $P < 0.01$), and the mRNA expression of smad7 mRNA decreased significantly ($P < 0.01$); compared with the model group, the mRNA expression of TGF-β1 and Smad 3 in the PGI2 middle dose group decreased significantly, and the mRNA expression of smad 7 mRNA increased significantly ($P<0.01$), as shown in Table III.

Effect on the expression of TGFβ1, p-Smad2/3 and Smad7 protein in the liver tissue of each group

Compared with the normal group, the positive expression of p-Smad 2/3 and TGF-β1 protein in the model group was significantly increased ($P<0.01$), and the positive expression of Smad 7 was significantly decreased ($P<0.01$); compared with the model group, the expression of p-Smad 2/3 and TGF-β1 protein in the PGI2 high and medium

dose groups and the PGI2 prevention group was significantly decreased ($P<0.05$, $P<0.01$), while the expression of Smad 7 protein was significantly increased ($P<0.01$), as shown in Fig.2 and Table IV.

DISCUSSION

TGF-β1 is one of the most significant fibroblast factors, which combines with downstream Smad Protein to form the TGF-β1/Smad signaling pathway, an important target for investigations into the mechanisms of drugs in liver fibrosis (9). Phosphorylation of Smad 2 and Smad 3 induces the formation of the TGF-β1/Smad complex, which leads to the activation of HSC into fibroblasts (10), increasing the synthesis of type I collagen, proteoglycan and fibronectin. Smad 7 is an inhibitory negative regulator (11) which can inhibit HSC transformation by inhibiting the phosphorylation of Smad2 and Smad3. The TGF-β1/Smad signaling pathway plays an important role in HSC activation (12). Drug intervention may provide a new method for the prevention and treatment of liver fibrosis. The purpose of this study was to investigate the effect of PGI2 on TGF-β1 and downstream signal transduction molecules.

In this study, the mRNA expressions of TGF-β1, Smad 2, Smad 3, p-Smad 2/3 and Smad 7 in the model group were significantly lower than those in the normal group. Compared with the model group, the mRNA expression of TGF-β1 and Smad 3 in the PGI2 medium dose group was significantly lower than that in the model group, suggesting that PGI2 has obvious preventive and therapeutic effects with regards to heart failure, and its mechanism may be associated with the promotion of the expression of Smad 7. Prostacyclin has obvious anti-heart failure effects, and its mechanism may be related to the inhibition of the TGF-β1/Smad signaling pathway. PGI2 inhibited TGF-β1 and Smad 3, while upregulating the expression of Smad 7. However, whether PGI2 affects the binding of the TGF-β1 ligand receptor, phosphorylation and nuclear translocation of Smads represents the next step in this field of research.

ACKNOWLEDGEMENT

This work was supported by the Fund of Science Research, Education of Department Heilongjiang Province (Grant/Award Number:1254HQ010).

REFERENCES

1. Ma C, Liu A, Wang Y, et al. The hepatocyte phase of Gd-EOB-DTPA-enhanced MRI in the evaluation of hepatic fibrosis and early liver cirrhosis in a rat model: an experimental study. Life Sci 2014; 108(2):104-8.
2. Elsharkawy A, Alboraie M, Fouad R, et al. Establishing ultrasound based transient elastography cutoffs for different stages of hepatic fibrosis and cirrhosis in Egyptian chronic hepatitis C patients. Arab J Gastroenterol 2017; 18(4):210-15.
3. Pavlov CS, Casazza G, Nikolova D, Tsochatzis E, Burroughs AK, Ivashkin VT, Gluud C. Transient elastography for diagnosis of stages of hepatic fibrosis and cirrhosis in people with alcoholic liver disease. Cochrane Database Syst Rev 2015; 1(1):CD010542.
4. Zhang HC, Hu RF, Zhu T, Tong L, Zhang QQ. Primary biliary cirrhosis degree assessment by acoustic radiation force impulse imaging and hepatic fibrosis indicators. World J Gastroenterol 2016; 22(22):5276-84.
5. Ozaki K, Matsui O, Gabata T, Kobayashi S, Koda W, Minami T. Confluent hepatic fibrosis in liver cirrhosis: possible relation with middle hepatic venous drainage. Jpn J Radiol 2013; 31(8):530-37.
6. Rahman MS. Prostacyclin: A major prostaglandin in the regulation of adipose tissue development. J Cell Physiol 2019; 234(4):3254-62.
7. Gybel-Brask M, Rasmussen R, Stensballe J, Johansson PI, Ostrowski SR. Effect of delayed onset prostacyclin on markers of endothelial function and damage after subarachnoid hemorrhage. Acta Neurochir (Wien) 2017; 159(6):1073-78.
8. Akagi S, Oto T, Kobayashi M, et al. High frequency of acute adverse cardiovascular events after lung transplantation in patients with pulmonary arterial hypertension receiving preoperative long-term intravenous prostacyclin. Int Heart J 2017;

58(4):557-61.
9. Yafawi RE, Wirth JA. What is the role of oral prostacyclin pathway medications in pulmonary arterial hypertension management? Curr Hypertens Rep 2017; 19(12):97.
10. Wang Q, Gu X, Wang J. Transforming growth factor-β1 (TGF-β1) induces mouse precartilaginous stem cell differentiation through TGFRII-CK1ε-β-catenin signalling. Int J Exp Pathol 2018; 99(3):113-20.
11. Zhu D, Zhao J, Lou A, et al. Transforming growth factor β1 promotes fibroblast-like synoviocytes migration and invasion via TGF-β1/Smad signaling in rheumatoid arthritis. Mol Cell Biochem 2019; 459(1-2):141-50.
12. Wang S, Zhang Q, Wang Y, You B, Meng Q, Zhang S, Li X, Ge Z. Transforming Growth Factor β1 (TGF-β1) appears to promote coronary artery disease by upregulating sphingosine kinase 1 (SPHK1) and further upregulating its downstream TIMP-1. Med Sci Monit 2018; 24:7322-28.

JOURNAL OF BIOLOGICAL REGULATORS & HOMEOSTATIC AGENTS Vol. 34, no. 6, 2227-2231 (2020)

LETTER TO THE EDITOR

Tamoxifen combined with sumer extract in the treatment of endometriosis in rats

ZY. Fang*, HY. Yang*, YQ. Ma, W. Wei and WY. Wu

Department of Obstetrics and Gynecology, Liuzhou Workers' Hospital, Liuzhou, China

Received July 21, 2020 – Accepted November 6, 2020

* These authors contributed equally to this article

To the Editor,

Endometriosis (EMS) is a benign disease caused by the combination of genetic susceptibility, hormonal imbalance and immune susceptibility of endometrial tissues with hormone activity, but EMS also has the characteristics of growth, invasion and implantation similar to those of malignant tumors (1). EMs is regarded as a chronic disease that needs lifelong treatment. The goal of EMS treatment is to use drugs with as few side effects as possible and to avoid invasive treatment such as surgery (2). However, due to delayed diagnosis, perioperative complications, adverse drug reactions and other related factors, the recurrence rate of EMS stays at a high level, and EMS patients need multiple assisted laparoscopic surgeries (3). Therefore, the development of new drugs has become the focus of EMS research.

Vascular endothelial growth factor (VEGF) can promote the formation and diffusion of new blood vessels (4). VEGF is highly expressed in the lesion tissues and has the function of regulating cell proliferation, migration and apoptosis, therefore may be an effective target for the treatment of EMS (5, 6). In recent years, many studies have found that phenolic compounds, such as medicinal plants, plant chemicals and multi-component herbal preparations, have anti-proliferation, apoptosis promotion, anti-angiogenesis and immune regulation functions, and can reverse the abnormal epigenetic changes of EMS by affecting the genome.

Therefore, this study innovatively explored the therapeutic effect of tamoxifen (TAM) combined with hematoxylin extract on rats with EMS, so as to provide a new idea for the combined treatment of EMS.

MATERIALS AND METHODS

Examination of estrous cycle by vaginal smear and hematoxylin eosin staining in rats

Sixty healthy female rats weighing 200-250g (Beijing Vital River Laboratory Animal Technology Co., Ltd., China) were selected. During the study, a sterilized cotton swab was inserted into the vagina of each rat and gently rotated twice before the swab was taken out for smear test. After sample fixation, ethanol and water were added onto the samples in turn, and then a hematoxylin dye solution was added onto the samples for 10-15 min of incubation. After 7-10 min of water washing, differentiation with hydrochloric acid ethanol and more water washing, an eosin dye solution was added onto the samples for 3-5 minutes of incubation. After water washing and dehydration with ethanol, ethanol, anhydrous ethanol and xylene, the samples were mounted in neutral gum and observed under a microscope. Sixty female rats within one day of estrous cycle were selected. The model was established when the vaginal smear showed keratinocytes.

Key words: tamoxifen; sumeria; endometriosis; vascular endothelial growth factor; ezrin

Corresponding Author:
Dr Weiying Wu,
Department of Obstetrics and Gynecology,
Liuzhou Workers' Hospital,
Liuzhou, 545005, Guangxi, China
e-mail: wuweiyingworksyy@126.com

0393-974X (2020)
Copyright © by BIOLIFE, s.a.s.
This publication and/or article is for individual use only and may not be further reproduced without written permission from the copyright holder.
Unauthorized reproduction may result in financial and other penalties
DISCLOSURE: ALL AUTHORS REPORT NO CONFLICTS OF INTEREST RELEVANT TO THIS ARTICLE.

The animal experiment procedures were in accordance with the International Regulations on Animal Protection and Management and were approved by the ethics committee of Liuzhou Workers' Hospital.

Animal models and grouping

The rats were anesthetized by intraperitoneal injection of 5% Pentobarbital Sodium (40mg/kg). Then, the rats were fixed on the operating plate, and the abdominal hair was cut and the skin was sterilized. A skin sample was cut out about 3 cm from the middle point of the upper end of the urethra. Ligation of uterine blood vessels, incision of the left uterine horn and end-to-end anastomosis were performed. Submerged in a luo-nutrition solution, the angle of the uterus was cut longitudinally to separate endometrium from myometrium, and 5 x 5mm endometrial tissue segments were obtained. After the operation, the surface epithelium of the incision was ligated to the right abdominal wall in the abdominal cavity. The remaining endometrial tissues were examined histologically to confirm that the graft was endometrium, and penicillin was placed in the abdominal cavity (200000 U/piece) and then the rats were given penicillin for 3 days to prevent infection.

In the week after modeling, the second laparotomy was performed to examine the growth of ectopic endometrium, which showed that the volume of transplanted focus was increased, and the focus had a transparent nodular and saccular shape, with light yellow transparent fluid accumulated in the tissue. The rats were randomly divided into 5 groups, with 12 rats in each group. Model group: the rats were given bacteria-free saline twice a day; TAM group: 5mg/kg prepared with 0.3 ml sterile saline and given to the rats twice a day; Sumeria extract group: 30ug/kg, prepared with 0.3ml sterile saline and given to the rats twice a day; TAM+Sumeria extract group: 5mg/kg TAM + 30ug/kg Sumeria extract, prepared with 0.3ml sterile saline and given to the rats twice a day.

Tissue collection and immunohistochemical analysis

After 4 weeks, the treatment was finished, and the vaginal cytology smear was examined continuously for 6 days. Then, the rats were sacrificed in estrus. The rats in the control group and the remaining rats in the treatment group were sacrificed 6 days later by decapitation. The growth of ectopic endometrium was observed by the third laparotomy, and the eutopic uterus and ectopic endometrium were collected. If the inner membrane was not easy to peel off, it could be collected together with some muscle layers. The tissue samples were fixed in 10% formaldehyde solution and embedded in paraffin to make 4 um continuous sections. The sections were then dewaxed in water and mounted in 3% dioxygen water for 15 min. After phosphate buffer saline (PBS) rinsing, a rabbit anti-mouse monoclonal antibody (1:100) was added onto tissue samples after an appropriate dilution and incubated at 37°C for 1 h. The secondary antibody labeled with biotin was added dropwise onto tissue samples, which were then placed into a wet box and incubated at 37°C for 30 min. Finally, the tissue samples were colorized using diaminobenzidine (DAB), rinsed with tap water to fully stop reaction, re-stained, dehydrated, made transparent, and mounted.

Western blot

Using a 12.5% SDS-PAGE gel and a half dry sucking instrument (Bio-Rad, USA), the proteins were transferred to a nitrocellulose membrane (Millipore, Eschborn, Germany) by electricity and incubated overnight at 4°C with the primary antibody. The secondary antibody conjugated to horseradish peroxidase (HRP) was added for 2 h of incubation, and the samples were washed for 3 times. Amersham enhanced chemiluminescence (ECL) was used to detect the reaction bands. An Amersham scanning imprinted image 600 scanner (GE Healthcare Life Sciences, USA) was used to quantify protein band density.

Statistical analysis

All data were processed by SPSS 23.0 (IBM, USA). The measured data were expressed in the form of mean ± standard deviation. The *t*-test was used for comparison between two groups, and analysis of variance was used for comparison among three or more groups. $P < 0.05$ was considered statistically significant.

RESULTS

Ectopic endometrial volume and VEGF expression

As shown in Fig. 1 and Table I, the post-treatment volume of ectopic endometrium in each treatment group was smaller than its corresponding pre-treatment value and the post-treatment value in

the model group ($P < 0.05$). There was a significant difference in VEGF expression between TAM and model groups, as well as between the TAM and TAM+ Sumeria extract groups ($P < 0.05$), as shown in Fig. 2 and Table II.

Expression of prohibitin, hnRNPA2/B1 and ezrin

Western blot results are shown in Fig. 3, which suggested that the expression intensity of prohibitin and hnRNPA2/B1 in the model group was lower than that of the normal group, and there was no significant difference in the expression of these two proteins among the TAM group, Sumeria extract group and TAM + Sumeria extract group. The expression of ezrin in the model group was significantly higher than that in the normal group, and the expression of ezrin in the TAM + Sumeria extract group was significantly lower than that in the TAM group and Sumeria extract group.

DISCUSSION

Tamoxifen is a type of estrogen antagonist and estrogen agonist, and its estrogen antagonistic activity serves as the pharmacological basis for its efficacy in endocrine therapy (7). The ectopic lesions in ectopic endometrium not only react to estrogen in the systemic circulation, but also produce estrogen themselves, rendering local tissues estrogen enriched and promoting the implantation and growth of ectopic endometrium. As the basic reason for endometrium growth and development, there are always dominant subtypes in the *in situ* or ectopic endometrium. Studies have shown that apoptosis is a key factor in maintaining the stability of cell cycle, structure and function of endometrial cells (8). Ectopic endometrial cells can survive outside the uterine cavity due to their enhanced anti-apoptotic ability (9).

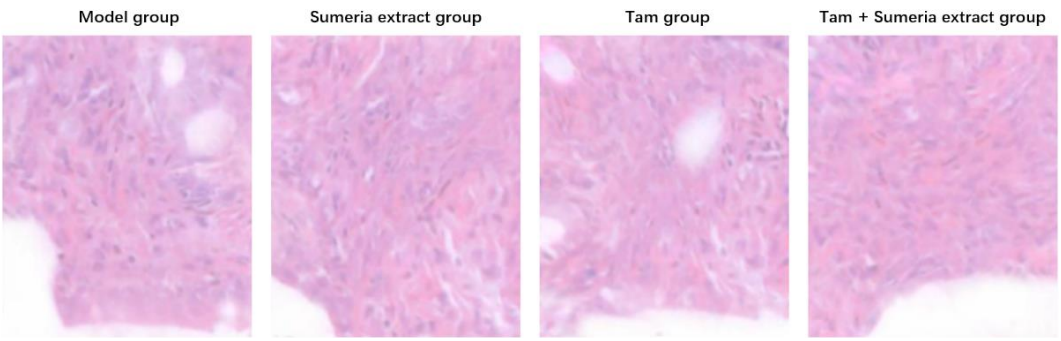


Fig. 1. *Post-treatment ectopic endometrium in each group (HE × 200).*

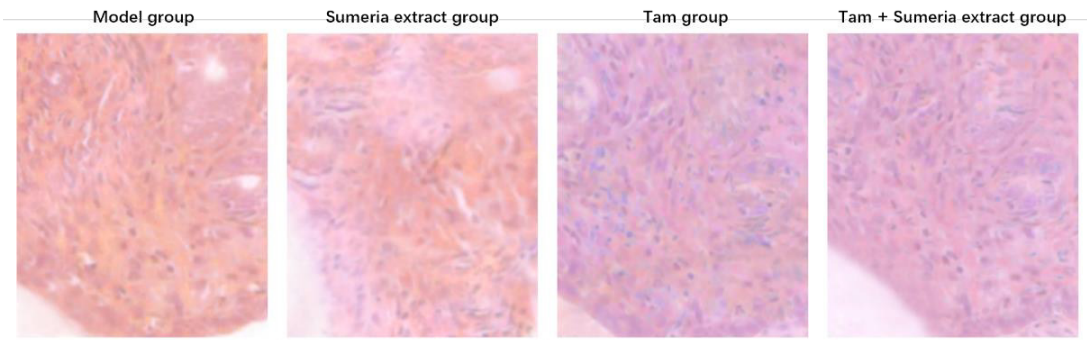


Fig. 2. *Expression of VEGF in each group (SP × 200).*

Table I. *Changes of endometrial volume in each group before and after treatment* ($\bar{x}\pm s$)

Group	Volume (mm^3) before treatment (n=12)	Volume (mm3) after treatment (n=12)
Model group	36.3±1.6	37.2±1.7
Sumeria extract group	36.8±0.6	15.3±1.2
TAM group	35.6±1.3	12.3±0.6
TAM+ Sumeria extract group	34.9±1.2	8.6±0.8

Table II. *Histological scores of VEGF in each group before and after treatment* ($\bar{x}\pm s$)

Group	Histological scores of VEGF before treatment (n=12)	Histological scores of VEGF after treatment (n=12)
Model group	4.6±1.3	4.5±1.7
Sumeria extract group	4.5±0.7	3.3±0.9
TAM group	4.5±1.5	2.9±0.8
TAM + Sumeria extract group	4.3±1.4	2.3±1.2

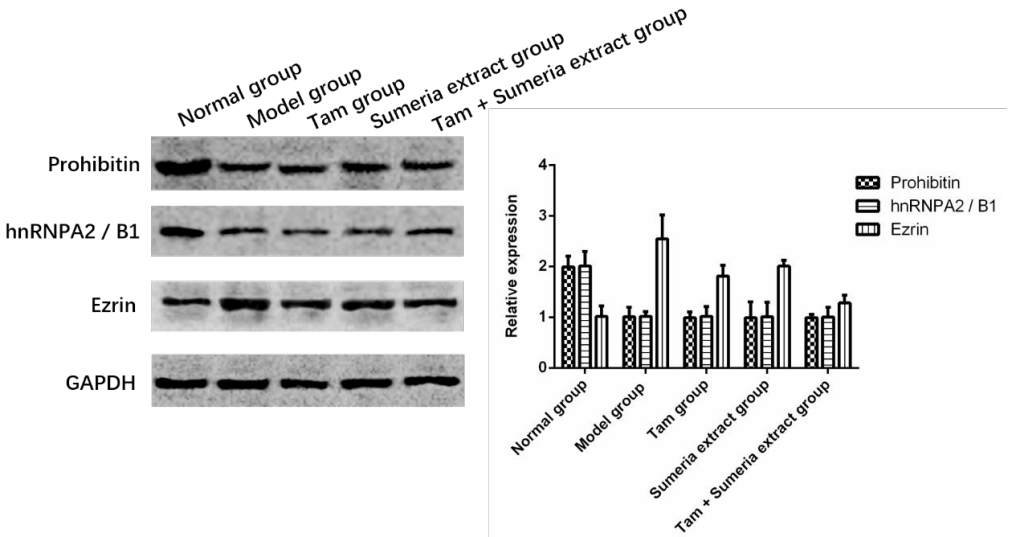


Fig. 3. *Expression of prohibitin, hnRNPA2/B1 and ezrin in in different groups.*

In the treatment of endometriosis, traditional Chinese medicines can effectively inhibit the metabolic activity and secretion of ectopic endometrial epithelial cells, and result in atrophy of these ectopic endometrial epithelial cells (10), thus promoting the proliferation, maturation, release and activation of lymphocytes, and enhancing cellular immune function (11, 12).

In this study, selective estrogen receptor modulators were used to inhibit the growth of ectopic lesions. The results showed that TAM combined with hematoxylin extract can reduce the size of ectopic endometrium and the expression of VEGF. Inhibin and hnRNP A2/B1 may participate in the formation of ectopic endometrium in a way independent of the hematoxylin extract. Ezrin may be one of the molecules involved in the mechanism to promote EMS.

REFERENCES

1. Paulino E, de Melo AC, da Silva VF. Endometrioid carcinoma arising from an endometriosis-associated abdominal wall scar. Am J Case Rep 2020; 21:e922973.
2. Egekvist AG, Marinovskij E, Forman A, Kesmodel US, Graumann O, Seyer-Hansen M. Conservative treatment of rectosigmoid endometriosis: A prospective study. Acta Obstet Gynecol Scand 2019; 98(9):1139-47.
3. Gadducci A, Zannoni GF. Endometriosis-associated extraovarian malignancies: a challenging question for the clinician and the pathologist. Anticancer Res 2020; 40(5):2429-38.
4. Berendsen AD, Olsen BR. How vascular endothelial growth factor-A (VEGF) regulates differentiation of mesenchymal stem cells. J Histochem Cytochem 2014; 62(2):103-8.
5. Stathopoulou MG, Xie T, Ruggiero D, et al. A transnational collaborative network dedicated to the study and applications of the vascular endothelial growth factor-A in medical practice: the VEGF Consortium. Clin Chem Lab Med 2018; 56(4):83-86.
6. Danastas K, Miller EJ, Hey-Cunningham AJ, Murphy CR, Lindsay LA. Expression of vascular endothelial growth factor A isoforms is dysregulated in women with endometriosis. Reprod Fertil Dev. 2018 Mar;30(4):651-57.
7. Emons G, Mustea A, Tempfer C. Tamoxifen and endometrial cancer: a janus-headed drug. Cancers (Basel) 2020; 12(9):E2535.
8. Stevens M, Star E, Lee M, et al. The VEGF-A exon 8 splicing-sensitive fluorescent reporter mouse is a novel tool to assess the effects of splicing regulatory compounds. RNA Biol 2019; 16(12):1672-81.
9. Fonseca BM, Correia-da-Silva G, Teixeira NA. Cannabinoid-induced cell death in endometrial cancer cells: involvement of TRPV1 receptors in apoptosis. J Physiol Biochem 2018; 74(2):261-72.
10. Shan J, Cheng W, Zhai DX, et al. Meta-analysis of Chinese traditional medicine Bushen Huoxue prescription for endometriosis treatment. Evid Based Complement Alternat Med 2017; 2017:5416423.
11. Jiang H, Shen Y, Wang XG. Current progress of Chinese medicinal treatment of endometriosis. Chin J Integr Med 2010; 16(3):283-88.
12. Ma K, Chen YX, Li M. [Clinical experience of Bushen Huoxue therapy in treatment of infertility due to endometriosis]. Zhongguo Zhong Yao Za Zhi 2019; 44(6):1094-98.

LETTER TO THE EDITOR

Diagnostic analysis of three-dimensional reconstruction of multi-slice spiral CT in the localization of ocular foreign bodies

X.X. Gao[1], J.S. Bai[1] and J.G. Qi[2]

[1]Department of Ophthalmology, Dongying Second People's Hospital, Dongying, Shandong Province, China; [2]Department of Imaging, Dongying Second People's Hospital, Dongying, Shandong Province, China

Received July 1, 2020 – Accepted November 9, 2020

To the Editor,

Recently, with the development of medical computed tomography imaging technology (CT), it was found that CT has many advantages in clinical diagnosis, such as diagnosis sensitivity, scanning speed and imaging clarity, and it has been widely applied in some medical domains (1). Multi-slice spiral CT (MSCT), which evolved from single slice spiral CT, has a better advantage in three-dimensional reconstruction, and has many functions in clinical interventions, such as 3D imaging of the body, cardiac imaging, angiographic imaging, which could effectively diagnose many diseases (2). The invasion of foreign matter is a common reasons for eyes diseases, which may cause mechanical damage to ocular tissue to impair the sight of patients, and even lead to blindness (3,4). Therefore, timely diagnosis of this disease is important for subsequent treatment**.**

MATERIALS AND METHODS

Patients

The clinical data of 88 patients with suspected ocular foreign bodies treated in Dongying Second People's Hospital from March 2016 to March 2018 were retrospectively analyzed. They were randomly divided into a test group and a control group, with 44 cases in each group. Patients in the control group received digital radiography examination, and patients in the test group underwent MSCT 3D reconstruction localization examination to analyze and compare the diagnostic value of the two positioning methods for ocular foreign bodies. There were 23 males (23 eyes) and 21 females (21 eyes) in the test group with an average age of (46.25±3.76) years. There were 24 males (24 eyes) and 20 females (20 eyes) in the control group with an average age of (46.31±3.46) years. There was no significant difference in general clinical indicators such as sex ratio and age between the two groups of patients ($p>0.05$). The study was approved by the hospital ethics committee, and the patients knew the purpose and process of the experimental study and signed the informed consent.

Digital radiography examination

This method included orthogonal projection, lateral projection and vertical projection. In the orthogonal projection, the patient took the supine position with the table at 90° right angle to the head sagittal plane and 45° between the table and the orbitomeatal line (CML). The patient gazed vertically at the table. During the operation, we should always pay attention to the appropriate placement of the patient's orbital center, i.e. the locating

Key words: multi-slice spiral CT (MSCT); three-dimensional reconstruction (3D reconstruction); ocular foreign body localization; diagnostic analysis

Corresponding Author:
Dr Jianguo Qi,
Department of Imaging, Dongying Second People's Hospital,
No.28 ChangChun Road, Guangrao, Dongying 257335,
Shandong Province, China
Tel.: +860546-6881821
e-mail: qbog98@163.com

0393-974X (2020)
Copyright © by BIOLIFE, s.a.s.
This publication and/or article is for individual use only and may not be further reproduced without written permission from the copyright holder.
Unauthorized reproduction may result in financial and other penalties
DISCLOSURE: ALL AUTHORS REPORT NO CONFLICTS OF INTEREST RELEVANT TO THIS ARTICLE.

ring (about 11.5 mm in diameter). Finally, the vertical distance between the ocular foreign body and the sagittal plane, and the vertical distance between the foreign body and the horizontal plane were accurately measured. In the lateral projection, the patient took the lateral position, making the foreign body eyeball of the patient close to the table and the head sagittal plane parallel to the table. The patient was told to gaze at the object horizontally, making the limbal plane of corneosclera at 90° right angle to the table surface, and the distance between them was measured. In the vertical projection, the patient took the supine position with head raised. The chin was close to the table, and the CML was at a 30° angle to the table. The patient was told to gaze horizontally at the object, and a straight line (about 11.5 mm in length) was taken as the locating ring for projection. The distance between the CML and the table was measured.

MSCT 3D reconstruction localization method

The patient took the supine position with head in the orthogonal position. The auditory nasal line was used as the scanning baseline to continue scanning toward the head end with a layer thickness of 1 mm and the layer number as 50 layers. When 3D reconstruction was performed in the coronal plane, the plane was at a 90° right angle to the sagittal axis of the eyeball, and the foreign body locating ruler was used to locate and calculate the patient's ocular foreign bodies. When reconstructing the sagittal plane, the plane should be kept parallel to the sagittal axis, and the two planes should be superimposed to measure the distance from the corneoscleral limbus on both sides and the foreign body in the eye to the horizontal plane. When reconstructing the horizontal plane, the vertical axis of the eyeball was at a right angle of 90° to the plane. The distance from the ocular foreign body to the sagittal plane was measured, and then the position and size of the foreign body in the eye were measured and recorded.

RESULTS

As shown in Fig. 1, the number of foreign bodies detected in the test group was significantly higher than that in the control group, with a statistically significant difference ($p < 0.05$). The diagnostic positive rate, sensitivity and correct index in the test group were significantly higher than those in the control group, with statistically significant difference ($p<0.05$) (Table I).

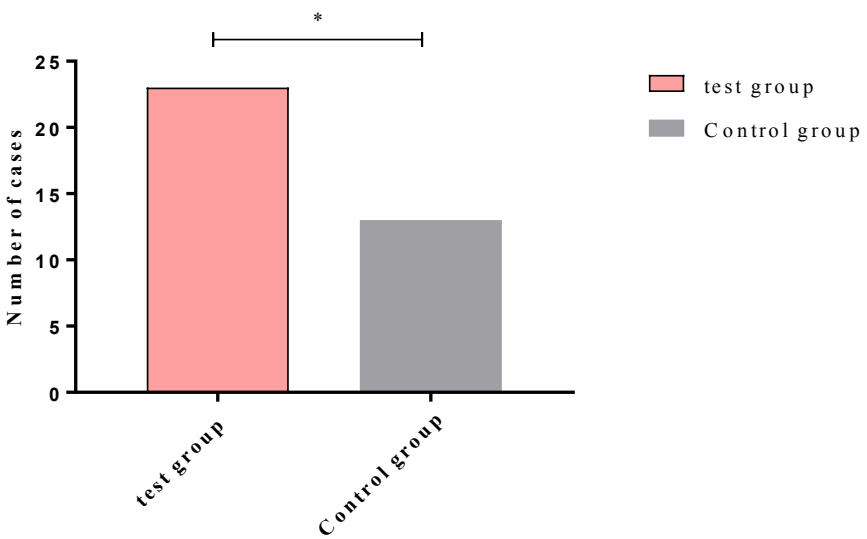


Fig. 1. *Comparison of foreign body detection cases between the two groups of patients. The abscissa represents groups, and the ordinate represents number of cases. In the test group, 24 patients showed ocular foreign bodies, accounting for 43.2% of the total cases while 13 patients in the control group showed ocular foreign bodies, accounting for 29.5% of the total cases. *significant difference in the number of cases of foreign bodies detected between the two groups of patients ($c^2=4.701$, $p=0.030$).*

Table I. *Comparison of diagnostic positive rate, sensitivity and correct index between the two groups of patients*

Group	Positive Rate	Sensitivity	Correct Index
Test group	43.2%	93.4%	93.4
Control group	29.5%	74.3%	74.3
χ^2	4.056	13.470	13.470
p	0.044	0.000	0.000

DISCUSSION

Compared with digital radiography positioning, MSCT 3D reconstruction localization has a higher resolution and its scanning layer thickness can reach 1 mm. The thinner the layer thickness, the less tissue overlap, the higher the resolution of fine structure, and the clearer the foreign body display (5). It also has an amplification effect, which can magnify a high-density foreign body 5-10 times. In this study, 44 patients with suspected ocular foreign body were diagnosed by MSCT 3D reconstruction localization, and 24 patients showed ocular foreign body, accounting for 43.2% of the total cases, which was significantly better than that by digital radiography. MSCT 3D reconstruction localization technology can clearly display foreign bodies in the lens, ciliary body, eyeball wall and optic nerve, making the image more intuitive and vivid to define the position, size and number of ocular foreign bodies (6). In this study, the positive rate, sensitivity and correct index of diagnosis in the test group were 43.2%, 93.4% and 93.4 respectively, which were significantly better than 29.5%, 74.3% and 74.3 in the control group, indicating that MSCT 3D reconstruction localization had a significant effect in clinical diagnosis of patients with suspected ocular foreign body.

In conclusion, MSCT 3D reconstruction localization technology has a high detection rate of foreign bodies and accurate localization, which can be used for the clinical diagnosis of ocular foreign bodies.

REFERENCES

1. Diaz JD, Arroyo JG. Modern Clinical Applications of Endoscopic Pars Plana Vitrectomy in Vitreoretinal Surgery. Int Ophthalmol Clin 2020; 60:25-33.
2. Short Orals. FPMRS 2019; 25:S26-S79.
3. Jain S, Madani K, Swaroop M. Inaugural women in medicine summit: an evolution of empowerment in Chicago, Illinois, September 20 and 21, 2019: event highlights, scientific abstracts, and dancing with markers. Int J Acad Med 2019; 5:240-301.
4. Poster Abstract. Journal of Datta Meghe Institute of Medical Sciences University 2019; 14:54-74.
5. Turel MK, Tripathi M, Aggarwal A, et al. A summary of some of the recently published, seminal papers in neuroscience. Neurol India 2019; 67:242-58.
6. Dandpat SK, Tripathi M, Varshney N, Batish A, Mohindra S. Not a refugee, nasogastric tube in the brain: Modes of prevention and controversies in management. Neurol India 2018; 66:523-24.

LETTER TO THE EDITOR

Potential role of lnc-PTGS2 in fibrosis progression after laminectomy via targeting EGR1

J. Tang[1,2#], X.-Y. Xu[3#], B.-L. Luo[1#], L. Yang[4], X.-L. Zhang[1], Y.-D. Sun[1], Z.-Q. Hou[1#] and G. Yao[1]

[1]Department of Plastic and Burn Surgery, The First Affiliated Hospital with Nanjing Medical University, Nanjing, China; [2]Nanjing Shuangjian Medical Technology Co., Ltd., Nanjing, China; [3]Department of Ophthalmology, Affiliated Hospital with Nanjing University of Chinese Medicine, Nanjing, China: [4]Department of Orthopedics, Nanjing First Hospital, Nanjing Medical University, Nanjing, Jiangsu, China

Received May 17, 2020 – Accepted September 21, 2020

# These Authors contributed equally to this work

To the Editor,

Failed back surgery syndrome (FBSS) results from postoperative scar connecting with dura and nerve root and elicits deteriorating neurogenic pain and disorder (1, 2). Following laminectomy, local excessive deposits and aberrant proliferation and differentiation of fibroblasts in the surgery site contribute to scar conglutination in epidural space, which increases risk of iatrogenic nerve root injury and dural slit and endangered secondary surgical repair (3). However, epidural fibrosis (EF) still lacks specific available therapy. During the process of epithelial tissue injury and surgical incision repair, transforming growth factor-beta (TGF-β) acts as a crucial cytokine concerning wound repair and scarification, which stimulates fibroblasts to secrete collagen, promotes fibroblast differentiation to myofibroblasts that produce α-Smooth muscle actin (α-SMA), and accelerates ECM deposition (4-6). Early growth response gene1 (EGR1) has been shown to regulate the fibrosis process in EF and is responsible for significant difference between fetal and adult fibroblasts in mice, indicating EGR1 is involved in TGF-β induced scar tissue and fibroblast development (7). EGR1, as an immediate transcriptional factor, plays a critical role in proliferation and differentiation, apoptosis, and a series of physiological events (8-10). However, few studies have reported the specific regulated mechanism of EGR1 upstream gene. Long non-coding RNAs (lncRNAs) consist of more than 200 nucleotides and present an important effect on dosage compensation, epigenetic regulation, cell cycle, and cell differentiation (11, 12). However, very little has been reported on lnc-PTGS2 to regulate fibrosis progress. The purpose of the study was to seek a potential upstream factor of EGR1 in fibrogenesis during EF. It was verified that EGR1 suppression elevated α-SMA and collagen I expressions, mitigated fibroblast activation and ECM deposition, and alleviated accumulation of fibers. Moreover, the results showed that the high level of lnc-PTGS2 in fetal cells and decreased expression in adult fibroblasts after TGF-β treatment, which may relate to the increase of EGR1 in TGF-β-activated adult fibroblasts. Therefore, lnc-PTGS2 may become an upstream and specific target for EGR1 and lnc-PTGS2 regulation may mitigate fibrotic degree in EF.

Key words: lnc-PTGS2; EGR1; epidural fibrosis; fibroblast; TGF-β

Corresponding Author:
Gang Yao, MM
300 Guangzhou Road,
Nanjing, Jiangsu,
210029, China
e-mail: yaogang19680119@163.com

0393-974X (2020)
Copyright © by BIOLIFE, s.a.s.
This publication and/or article is for individual use only and may not be further reproduced without written permission from the copyright holder. Unauthorized reproduction may result in financial and other penalties
DISCLOSURE: ALL AUTHORS REPORT NO CONFLICTS OF INTEREST RELEVANT TO THIS ARTICLE.

MATERIALS AND METHODS

Cell culture

Fetal and adult human fibroblasts were purchased from American Type Culture Collection (ATCC) (Manassas, VA, USA) and seeded into 75 cm^2 flasks supplemented Dulbecco's modified eagle medium (DMEM) (Gibco, Rockville, MD, USA) and 10% fetal bovine serum (FBS) (Gibco, Rockville, MD, USA) as well as 1% penicillin-streptomycin. When growing to 95% density, cells were inoculated into 6-well plates and continued to culture until they were acceptable for subsequent treatment.

Mice

Male C57BL/6J mice (eight weeks old, weighing 18-20g) were purchased from Nanjing Medical University Animal Center and housed at the Medical University Animal Center under the conditions of 22±2°C and humidity of 55-65%. Animals were provided with available food and tap water and 12 h/12 h cycle. This study was approved by the Animal Ethics Committee of Nanjing Medical University Animal Center.

Vector construction and transfection

EGR1 cDNA,siRNA-EGR1, lnc-PTGS2 and sh-RNA-PTGS2 were obtained from GenePharma (Shanghai, China) and transfected into human fibroblasts using Lipofectamine 3000 (Invitrogen, Carlsbad, CA, USA). Lentivirus loading siRNA-EGR1 were synthesized using Lentivirus Generation Kit (TaKaRa, Dalian, China) according to the manufacturer's instructions. The empty lentivirus vectors served as negative control. Cell transfection was allowed for 3 days prior to TGF-β stimuli (2 ng/mL). Seven days prior to laminectomy, lentivirus was injected into the mice via tail vein.

EF model establishment

Mice were anesthetized using ketamine (280mg/kg). After skin antisepsis, the skin was cut and the muscles were separated, then laminectomy at the level of T9-11 was performed. After washing with normal saline, the incision was sutured and disinfected using iodophor. All the mice received the treatment with cephalosporin for 3 days.

Reverse transcription-polymerase chain reaction (RT-PCR)

Total RNA of cells was isolated using TRIzol reagent (YiFeiXue, Nanjing, China) following the manufacturer's protocol. Total mRNA was administrated reverse transcription using cDNA Synthesis Kits (Beyotime, Shanghai, China). Then, RT-PCR was conducted using SuperScript™ III One-Step RT-PCR System with Platinum™ Taq DNA Polymerase (Thermo Fisher Scientific, Waltham, MA, USA) in a Quantstudio 6 Flex Real-Time Fluorescence Quantitative PCR System (Thermo Fisher Scientific, Waltham, MA, USA). Normalization for each RNA sample was evaluated using 18S RNA. Relative mRNA expression levels were quantified with the $2^{-\Delta\Delta Ct}$ method. Primer sequences are listed at Table I.

Western blot analysis

Scar tissues were dissected, and cells and tissue fragments were harvested using lysis buffer in Total Protein Extraction Kit (KeyGen, Nanjing, China) according to the manufacturer's instructions. After being lysed for 10 min, the extracted protein mix was centrifuged at 12000 rpm for 15 min at 4°C. Then the supernatant protein was collected again and the concentration in each tube was measured using bicinchoninic acid (BCA) Protein Assay Kit (Beyotime, Shanghai, China). Equivalent proteins in each group were separated using sodium dodecyl sulfate polyacrylamide gel electrophoresis (SDS-PAGE). The proteins were transferred into polyvinylidene fluoride (PVDF) membrane(Millipore, Billerica, MA, USA) and the membrane blocked with 5% skim milk, membrane loading proteins was incubated overnight with anti-Collagen I (Abcam, Cambridge, MA, USA, 1:1000), anti-Collagen III (Abcam, Cambridge, MA, USA, 1:1000),anti-α-SMA (Abcam, Cambridge, MA, USA, 1:1000), anti-EGR1 (Abcam, Cambridge, MA, USA, 1:1000), anti-TGF-β (Abcam, Cambridge, MA, USA, 1:1000), anti-TGF-β RI (Abcam, Cambridge, MA, USA, 1:1000), anti-TGF-β RII (Abcam, Cambridge, MA, USA, 1:1000), anti-p-Smad 2/3 (Abcam, Cambridge, MA, USA, 1:1000), anti-Smad 2/3 (Abcam, Cambridge, MA, USA, 1:1000), anti-Smad 7 (all from Abcam, Cambridge, MA, USA, 1:1000) and anti-GAPDH (Proteintech, Wuhan, China, 1:10000). After being washed with Tris-Buffered Saline with 0.01% Tween-20 (TBST), the membrane was incubated with HRP-secondary antibody (YiFeiXue, Nanjing, China, 1:10000) for 1 h at room temperature. Membrane was processed with an enhanced chemiluminescence (ECL)

reagent (Tanon, Shanghai, China) to visualize protein bands. Glyceraldehyde-3-phosphate dehydrogenase (GAPDH) was exhibited as standardization.

Immumohistochemical staining (IHC) and histologic staining

Mouse spines were fixated with 4% paraformaldehyde (PFA) for 24 h and decalcified for 1 month. Then the spines were dehydrated *via* different alcoholic gradients and embedded into paraffin and dissected into sections (5 μm) using a rotary microtome. Sections were deparaffinized and rehydrated in xylene and alcohol in sequence. The antigen was recovered in sodium citrate buffer at 95°C for 7 min. After blocking with goat serum, sections were incubated with Collagen I (Abcam, Cambridge, MA, USA, 1:200). Sections were subsequently reacted with secondary antibody for 1 h and colored using a DAB Substrate Kit (ServiceBio, Wuhan, China). Nucleus was counterstained with hematoxylin. Then, images were visualized using a microscope. Masson's trichrome staining was performed according to manufacturer's protocol (Servicebio, Wuhan, China). The images were captured with a microscope.

Kyoto Encyclopedia of Genes and Genomes (KEGG) enrichment analysis and Lnc-RNA microarray

RNA was extracted from fetal and adult fibroblasts following 2ng/mL TGF-β treatment, respectively. Then the gene expression profile (Agilent, Santa Clara, CA, USA) and lnc-RNA microarray (Agilent, Santa Clara, CA, USA) were used respectively to detect and analyze the related pathways and lnc-RNA level changes concerning fibrogenesis. All the above biological operations were carried out 3 times.

Statistical analysis

Data were defined as the means ± SD (standard deviation). Differences between two groups were analyzed by using the Student's *t*-test. Comparison between multiple groups was made using One-way ANOVA test followed by Post Hoc Test (Least Significant Difference). Post hoc comparisons were analyzed using Tukey's test. Data were gathered and evaluated using Statistical Product and Service Solutions (SPSS) 21.0 (IBM, Armonk, NY, USA). P-value of <0.05 was taken for statistical significance.

RESULTS

EGR1 expression with fibroblast biomarkers change in different periods

It was firstl explored whether EGR1 expression changes in fetal and adult human fibroblast after TGF-β stimuli or not. Cells were extracted into RNA to measure EGR1 expression after TGF-β treatment for 24 h. RT-PCR result exhibited that EGR1 level was increased in adult human fibroblasts following TGF-β administration, however, fetal fibroblasts

Table I. *Primer sequences of reverse transcription-polymerase chain reaction.*

Oligo Name		Sequence (5' --------> 3')
EGR1	Forward	GGTCAGTGGCCTAGTGAGC
(Human)	Reverse	GTGCCGCTGAGTAAATGGGA
18 S	Forward	GTAACCCGTTGAACCCCATT
(Human)	Reverse	CCATCCAATCGGTAGTAGCG

were not affected by TGF-β (Fig. 1A). The protein level of collagen III, myofibroblast marker α-SMA as well as EGR1 in fibroblasts were also detected, and it was found that collagen III, α-SMA and EGR1protein were increased markedly in adult fibroblasts treated with TGF-β, while they were only slightly elevated in fetal cells (Fig. 1B), suggesting that EGR1 differential expression may influence fibroblasts response to TGF-β.

Differences of signaling pathway and lncRNA expression in fibroblasts at different stages

The results showed that primary signaling pathway changes and lncRNAs expression in both fetal and adult fibroblasts after TGF-β treatment. KEGG enrichment analysis exhibited that there were 20 related signaling pathways in adult fibroblasts showing remarkable expression difference compared with that in fetal **fibroblast** cells, in which TGF-β signaling pathway displayed the most significant difference (Fig. 2A). Moreover, the related lncRNAs expression changes were assessed *via* gene microarray technique, presenting that there were 7 up-regulated lncRNAs and 15 down-regulated lncRNAs including the most significant down-regulation of lnc-PTGS2 (Fig. 2B). Therefore, lnc-PTGS2 decrease may be involved in the initiation of TGF-β signaling pathway after TGF-β stimuli in adult fibroblasts.

TGF-β/Smad signaling pathway was not involved in EGR1-mediating fibrosis

To explore whether EGR1 level plays a crucial role in fibrogenesis, the level of EGR1 after overexpression (OE) and knockdown (KO) in adult fibroblasts was detected. Western blotting showed a prominent increase of EGR1 expression following OE treatment, however, the KO treatment silenced EGR1 in adult fibroblasts. Consistently, the expression of collagen I was increased after EGR1 OE and decreased after EGR1 KO (Fig. 3A). Furthermore, the effect of EGR1 KO on EF model was evaluated in mice. Masson staining showed that the amount of fibers in EGR1 KO mice decreased,

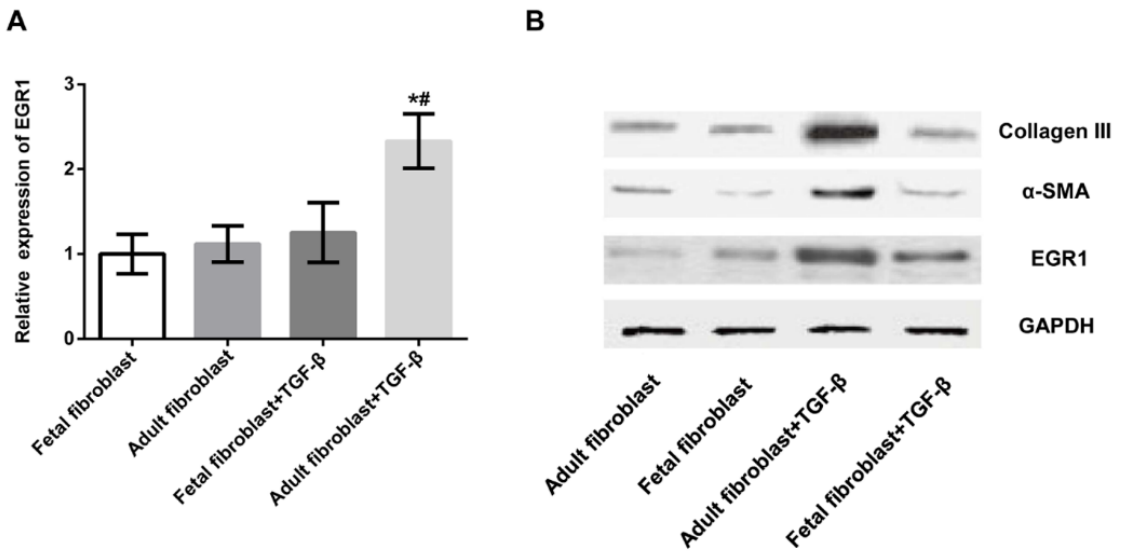


Fig. 1. *EGR1 expression with fibroblast biomarkers change in different periods. **A**) Representative EGR1 RNA level in fetal fibroblast, adult fibroblast, fetal fibroblast+TGF-β, and adult fibroblast+TGF-β group. **B**) Representative Western blotting of Collagen I, α-SMA, EGR1 in fetal fibroblast, adult fibroblast, fetal fibroblast+TGF-β, and adult fibroblast+TGF-β group. "*" means vs adult fibroblast group with statistical significance, "#" means vs fetal fibroblast+TGF-β group with statistical significance.*

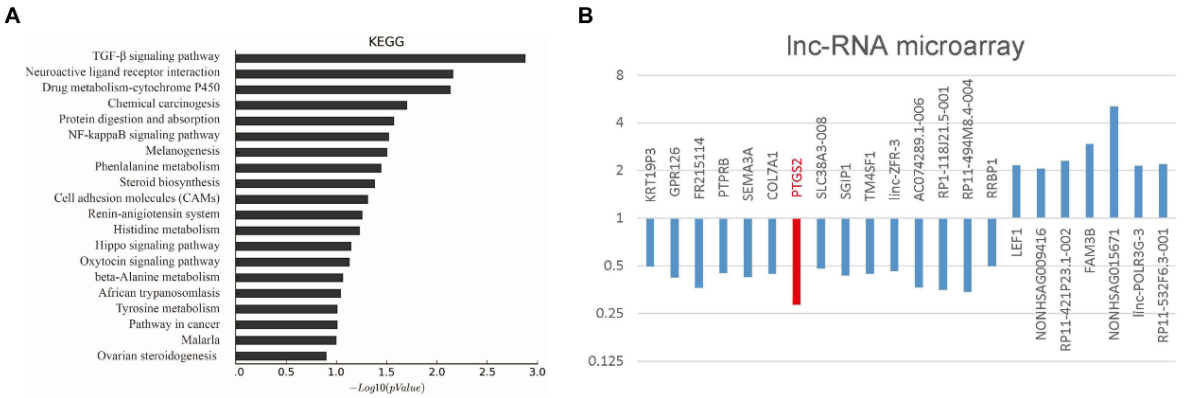


Fig. 2. *The differences of signaling pathway and lncRNA expression in fibroblasts at different stages.* ***A)*** *KEGG analysis of fibrosis-related pathways change in adult fibroblasts compared with those in fetal fibroblasts after TGF-β stimuli.* ***B)*** *Representative microarray of lnc-RNA level in adult fibroblast and fetal fibroblast.*

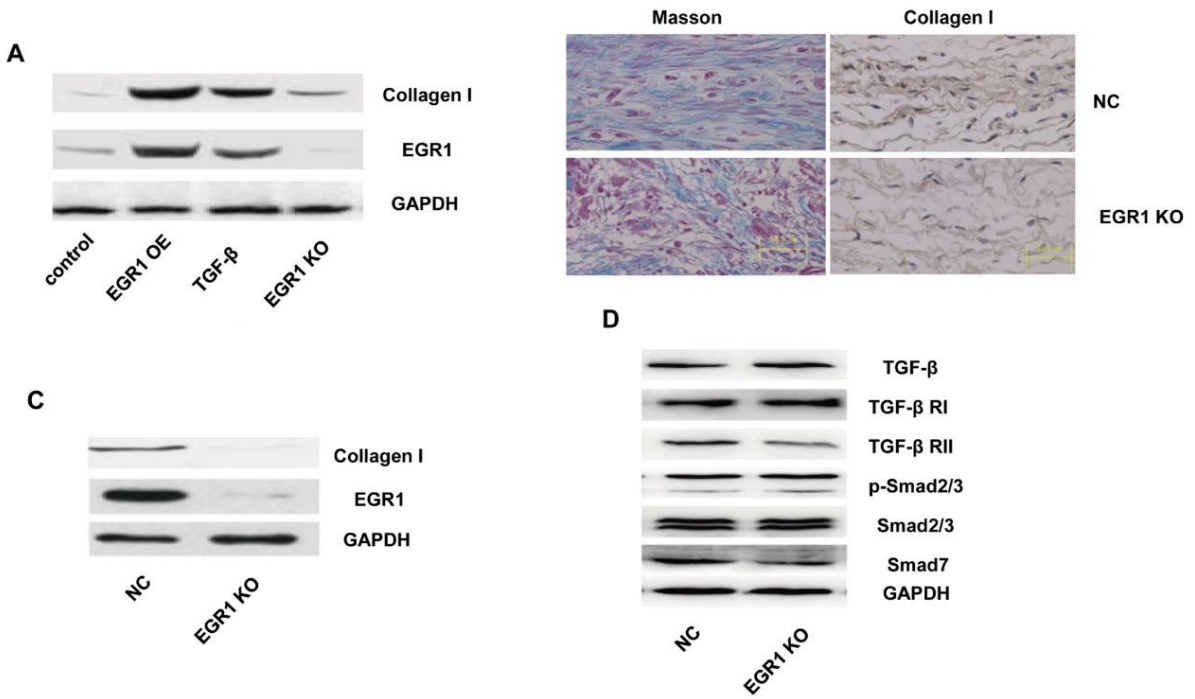


Fig. 3. *TGF-β/Smad signaling pathway was not involved in EGR1 mediating fibrosis.* ***A)*** *Representative protein level of Collagen I, EGR1 in control, EGR1 OE, TGF-β, TGF-β+EGR1 KO group.* ***B)*** *Representative Masson staining and IHC of Collagen I in NC and EGR1 KO group at 7 days post-injury, (magnification: 400×).* ***C)*** *Representative protein level of Collagen I, EGR1 in NC and EGR1 KO group at 7 days post-injury.* ***D)*** *Representative Western blotting of TGF-β, TGF-β RI, TGF-β RII, p-Smad2/3, Smad2/3, and Smad7 in NC and EGR1 KO group at 7 days post injury.*

however the results were inconsistent with the expression change of collagen I in IHC staining compared with that in empty vector (NC) group (Fig. 3B). Moreover, Western blotting exhibited that both collagen I and EGR1 levels were reduced in the EGR1 KO group (Fig. 3C). In addition, the TGF-β signaling pathway-related protein was detected using Western blotting, showing that the levels of TGF-β,TGF-β receptor I (TGF-β RI), TGF-β receptor II (TGF-β RII), phosphorylated Smad2/3 (p-Smad2/3), Smad2/3, and Smad7 did not change after EGR1 KO (Fig. 3D). This indicated that TGF-β promoting

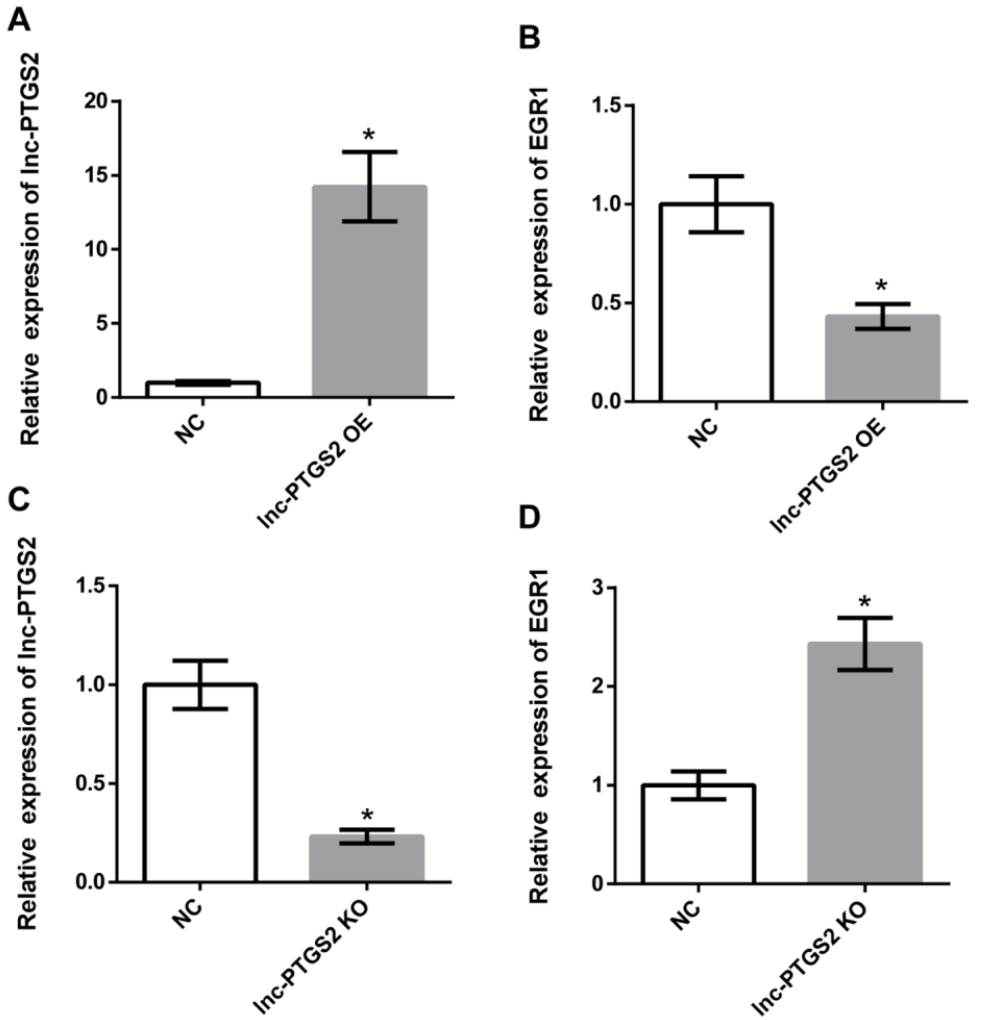


Fig. 4. *Negative role of lnc-PTGS2 in regulating EGR1 expression in fibroblasts.* ***A****) Representative lnc-PTGS2 level in NC and lnc-PTGS2 OE group.* ***B****) Representative EGR1 level in NC and lnc-PTGS2 OE group.* ***C****) Representative lnc-PTGS2 level in NC and lnc-PTGS2 KO group.* ***D****) Representative EGR1 level in NC and lnc-PTGS2 KO group. "*" means vs NC group with statistical significance.*

collagen generation through EGR1 did not depend on Smad pathway. Therefore, the above results verified that EGR1 KO decreased fibrosis degree in EF but did not affect Smad pathway.

Negative role of lnc-PTGS2 in regulating EGR1 expression in fibroblasts

Given the KO of EGR1 repressing tissue fibrosis after laminectomy, the level changes of lnc-PTGS2 and EGR1 level changes after TGF-β treatment were examined in adult fibroblast with lnc-PTGS2 OE. To reflect the level of lnc-PTGS2 in fetal and adult fibroblasts, RT-PCR was conducted to reveal lnc-PTGS2 and EGR1 expressions (Fig. 4 A, B), exhibiting that increased lnc-PTGS2 treatment reduced the level of EGR1 compared to the NC group. Furthermore, the lnc-PTGS2 level was inhibited in fibroblasts, and it was found that lnc-PTGS2 decrease induced the increased expression of EGR1 (Fig. 4 C, D). These results indicated that lnc-PTGS2 negatively regulated EGR1 expression in adult fibroblasts after TGF-β treatment and might act as a potential up-stream target of EGR1 to modulate fibrogenesis in EF.

DISCUSSION

Our findings showed that EGR1 was excessively expressed accompanied with collagen, and α-SMA increase accounted for the significance of EGR1 in the modulation of fibrogenesis owing to TGF-β stimuli. Hence, it was feasible that controlling EGR1 up-stream factor inhibits the process of fibrosis *via* decrease of cell response to TGF-β. It was also displayed that EGR1KO, both *in vitro* and *in vivo*, dramatically decreased EGR1 expression, which caused less fibers and collagen I. Further KEGG analysis revealed significant difference in expression of TGF-β signaling pathway in fetal and adult fibroblasts post-TGF-β treatment. However, this study demonstrated that the reduction of fibrosis caused by EGR1 KO did not involve in TGF-β/Smad pathway. In this study, it was noted that lnc-PTGS2 expression decreased significantly in adult fibroblasts compared with fetal fibroblasts *via* microarray and dCHIP algorithm. It was speculated that lnc-PTGS2 may affect fibrogenesis and scarring after TGF-β stimuli *via* targeting EGR-1. Hence, lnc-PTGS2 was overexpressed or knocked down in TGF-β induced fibroblasts. Consistently, the result showed that lnc-PTGS2 OE reduced EGR1 expression, while lnc-PTGS2 KO enhanced EGR1 level in adult fibroblast following TGF-β treatment. These results showed that lnc-PTGS2 down-regulation after fibroblast activation may lead to increased expression of EGR1 and eventually elicit abundant fibroblast accumulation and overwhelming ECM deposition. Therefore, reversing lnc-PTGS2 expression in fibroblast potentially played a novel effective role in negative regulation of fibrogenesis. The present evidence indicated that TGF-β induced different expression of EGR1 in fetal and adult fibroblasts. However, It was verified that the repression of EGR1 prominently inhibited collagen production and fiber amount in EF model, and lnc-PTGS2 negatively mediated EGR1 expression in fibroblasts. Therefore, it was a feasible regulated target of EGR1 up-stream factor to alleviate fibrogenesis. In this study, it was proved that an association existed of lnc-PTGS2 with EGR1 in fibroblasts following TGF-β treatment, but the regulatory mechanism and effect of lnc-PTGS2 on fibrosis and other diseases still needs to be further studied.

In conclusion, our study certified EGR1 as a critical factor of fibrogenesis in TGF-β-induced fibroblasts and EF model. The results showed that the negative modulation of lnc-PTGS2 to EGR1 in fibroblasts after TGF-β treatment may be a promising target for EF amelioration and other fibrotic researches.

ACKNOWLEDGEMENTS

This study was funded by Natural Science Foundation of Jiangsu Province (Grant No. BK20171089) and National Natural Science Foundation of China (Grant No. 81802149)

REFERENCES

1. Kapural L, Peterson E, Provenzano DA, Staats P. Clinical evidence for spinal cord stimulation for Failed Back Surgery Syndrome (FBSS): systematic review. Spine (Phila Pa 1976) 2017; 42 Suppl 14:S61-S66.
2. Amirdelfan K, Webster L, Poree L, Sukul V, McRoberts P. Treatment options for failed back surgery syndrome patients with refractory chronic pain: an evidence based approach. Spine (Phila Pa 1976) 2017; 42 Suppl 14:S41-S52.
3. Sun Y, Zhao S, Li X, et al. Local application of rapamycin reduces epidural fibrosis after laminectomy via inhibiting fibroblast proliferation and prompting apoptosis. J Orthop Surg Res 2016; 11:58.
4. Yang L, Qiu CX, Ludlow A, Ferguson MW, Brunner G. Active transforming growth factor-beta in wound repair: determination using a new assay. Am J Pathol 1999; 154:105-111.
5. Lichtman MK, Otero-Vinas M, Falanga V. Transforming growth factor beta (TGF-beta) isoforms in wound healing and fibrosis. Wound Repair Regen 2016; 24:215-222.
6. Lorenz HP, Adzick NS. Scarless skin wound repair in the fetus. West J Med 1993; 159:350-355.
7. Yang L, Tang J, Chen H, et al. Taurine reduced epidural fibrosis in rat models after laminectomy via downregulating EGR1. Cell Physiol Biochem 2016; 38:2261-2271.

8. Wang S, Liang C, Ai H, et al. Hepatic miR-181b-5p Contributes to glycogen synthesis through targeting EGR1. Dig Dis Sci 2019; 64:1548-59.
9. Ao H, Liu B, Li H, Lu L. Egr1 mediates retinal vascular dysfunction in diabetes mellitus via promoting p53 transcription. J Cell Mol Med 2019; 23:3345-3356.
10. Li J, Xu C, Liu Y, et al. Fibroblast growth factor 21 inhibited ischemic arrhythmias via targeting miR-143/EGR1 axis. Basic Res Cardiol 2020; 115:9.
11. Ponting CP, Oliver PL, Reik W. Evolution and functions of long noncoding RNAs. Cell 2009; 136:629-41.
12. Mercer TR, Dinger ME, Mattick JS. Long non-coding RNAs: insights into functions. Nat Rev Genet 2009; 10:155-59.

LETTER TO THE EDITOR

Velocity vector imaging for assessing the heart function in pregnant women with gestational diabetes mellitus

Z-S. Gao[1], Y-C. Yuan[2], Q-M. Niu[1], J-J. Zhang[3], J. Zhao[4] and L-P. Guo[1]

[1]Department of Ultrasound, Weifang People's Hospital, Weifang, China; [2]Department of Obstetrics and Gynecology, The People's Hospital of Zhangqiu Area, Jinan, China; [3]Ionizing Radiation Room, Weifang Metrology and Testing Institute, Weifang, China; [4]Department of Surgery, The People's Hospital of Zhangqiu Area, Jinan, China

Received July 1, 2020 – Accepted November 10, 2020

To the Editor,

Gestational diabetes mellitus (GDM) is a gestational disease (1) which can lead to overweight, or obesity, affecting the patient's quality of life. GDM particularly occurs in older women (2, 3). Moreover, the disease can lead to neonatal hyperbilirubinemia, premature delivery, preeclampsia, congenital malformation, and intrauterine growth retardation (4). The specific pathogenesis of GDM remains to be further identified. It is believed that the key factors leading to GDM are islet β cell secretory decompensation and insulin resistance (5). Currently, velocity vector imaging (VVI) technology is applied to evaluate GDM. It is a new non-invasive imaging diagnostic technique for quantitative assessment of regional and global myocardial systolic and diastolic function. The improved version of strain rate imaging (SRI) and speckle tracking technology (STT) specifically analyzes the spatial motion of myocardial tissue from the long axis, short axis and circumferential directions. VVI enables accurate analysis of changes in the regional myocardial function and reduces the limitations such as overall heart motion, cardiac rotation, adjacent myocardial segmental motion, and restriction effect (6). This study aims to investigate the role of VVI technology on the prenatal left ventricular function of pregnant women with GDM, seeking to provide new leads for the diagnosis and treatment of GDM.

MATERIALS AND METHODS

Study subjects

Forty-five GDM patients in late pregnancy admitted to Weifang People's Hospital from June 2014 to December 2017 were enrolled as the observation group, and 40 healthy women in late pregnancy were enrolled as the control group. All research subjects had an average age of (24.32±6.12) years and an average gestation of 37 weeks (ranging from 36 to 39 weeks). No statistical difference in age, height, or gestation was found ($p>0.05$), but there was statistical difference in heart rate, body mass, systolic blood pressure, and diastolic blood pressure ($p<0.05$, Table I)

Inclusion criteria: GDM diagnosed by a urine test, B-ultrasound in accordance with the IADPSG criteria (7). Exclusion criteria: diabetes prior to pregnancy; substantial lesions in other organs; liver and kidney dysfunction; cognitive impairment or communication disorders; patients with poor compliance. The study was approved by the Ethics Committee of Weifang People's Hospital.

Key words: GDM; heart function; VVI

Corresponding Author:
Dr Liping Guo,
Department of Ultrasound,
Weifang People's Hospital,
No. 151 Guangwen Street,
Weifang261041, China
e-mail: xuefucang29378@163.com

0393-974X (2020)
Copyright © by BIOLIFE, s.a.s.
This publication and/or article is for individual use only and may not be further reproduced without written permission from the copyright holder.
Unauthorized reproduction may result in financial and other penalties
DISCLOSURE: ALL AUTHORS REPORT NO CONFLICTS OF INTEREST RELEVANT TO THIS ARTICLE.

Table I. *General information of the study subjects (x ± s)*

Parameter	Observation group (n=45)	Control group (n=40)	t	*p*
Age	24.21±6.43	23.74±5.91	0.349	0.728
Height (cm)	162.49±7.61	162.39±7.12	0.062	0.950
Gestation (week)	37.2±1.4	37.1±1.1	0.363	0.718
Heart rate (/min^{-1})	83.13±4.45	72.43±4.54	10.960	<0.001
Body mass (kg)	79.34±8.94	67.20±8.71	6.325	<0.001
Systolic blood pressure (mmHg)	146.74±14.42	114.76±10.42	11.590	<0.001
Diastolic blood pressure (mmHg)	89.53±8.53	72.77±7.89	8.148	<0.001
Blood sugar 2 hours after meals (mmol/L)	10.78±0.93	8.42±0.64	13.460	<0.001
HbA1c (%)	8.11±0.76	5.42±0.56	18.380	<0.001

All patients enrolled in this study gave written informed consent after a detailed explanation.

Color Doppler echocardiography

Left lateral position or supine position was taken, and all pregnant women received two-dimensional dynamic gray-scale imaging from conventional apical four-chamber view, apical two-chamber view, and left ventricle view, as well as color Doppler ultrasound scanning. The A-wave and E/A ratio were calculated in the standard section of two-dimensional echocardiography. The size of the interventricular septum of the heart, the diameter of the aorta, and the presence of abnormal shunt were also measured.

The C2000 ultrasonic diagnostic instrument, with 4V1c probe, at a frequency of 4.25 MHz., was purchased from Shanghai Hanfei Medical Instrument Co., Ltd., China.

VVI detection

All pregnant women were placed in the left lateral position. The left ventricular long-axis views of each segment, as well as the 3 consecutive cardiac cycle loops were recorded. Then an automated analysis was conducted at the VVI mode. The long-axis of the left ventricular artery was semi-automatically recorded. The velocity, strain, and strain rate of long-axis in the systolic and diastolic phase at each segment of the left ventricular wall was measured.

The A-wave and E/A ratios were compared between the observation group and the control group. Vsmax, Ssmax, SRsmax at each segment of the left ventricle in the systolic phase were compared between the observation group and the control group. Vdmax, Sdmax, SRdmax at each segment of the left ventricle in the diastolic phase were detected.

Statistical analysis

The experimental data were statistically analyzed by the SPSS19.0 software package (Bizinsight (Beijing) Information Technology Co., Ltd.). The measurement data were expressed with mean ± standard deviation. The independent *t*-test was used for analysis between the two groups. Repeated Measures ANOVA was used for analyzing the two groups at different time points. All figures of this experiment were finished using GraphPad Prism 8 software (GraphPad Software Inc). A statistical difference was recognized when $p<0.05$.

RESULTS

Our results showed that the A-wave value in the observation group was statistically higher than that in the control group ($p<0.05$). The E/A ratio in the observation group was statistically lower than that in the control group ($p<0.05$, Fig. 1). No significant difference of Vsmax, Ssmax, SRsmax at each segment of the left ventricle in the systolic phase of the observation group was found compared to those of the control group ($p>0.05$, Table II). Of note, the values of Vdmax, Sdmax, SRdmax at each segment of the left ventricle of the observation group in the diastolic phase were statistically lower than those of the control group ($p<0.05$, Table II)

DISCUSSION

In older pregnant women, a comparatively high incidence of GDM contributes to a serious threat to maternal and newborn health. Therefore, strict monitoring during pregnancy are of great importance

Table II. *Comparison of Vsmax, Ssmax, SRsmax, Vdmax, Sdmax and SRdmax at each segment of the left ventricular in the systolic phase between the observation group and the control group*

	Vsmax (cm/s)		Ssmax (%)		SRsmax (s^{-1})		Vdmax (cm/s)		Sdmax (%)		SRdmax (s^{-1})	
Group	observation group	control group	observation group	control group	observation group	control group	observation group	control group	observation group	control group	observation group	control group
Left ventricular lateral wall the basal segment	5.25±1.79	5.24±1.75	25.26±8.12	25.24±8.10	1.44±0.61	1.50±0.63	4.13±1.42*	5.27±1.73	6.14±2.13*	7.26±2.72	1.24±0.42*	1.58±0.64
Left ventricular lateral wall the middle segment	4.53±1.49	4.51±1.46	24.15±7.83	24.13±7.82	1.36±0.59	1.48±0.57	3.54±1.53*	4.64±1.83	5.25±2.11*	7.13±2.64	1.04±0.63*	1.43±0.84
Left ventricular lateral wall the apical segment	1.39±0.36	1.36±0.34	24.27±7.72	24.24±7.79	1.22±0.71	1.31±0.72	1.03±0.53*	1.37±0.73	5.14±2.03*	6.62±2.37	1.26±0.53*	1.55±0.72
Inferoseptal basal segment	5.20±2.14	5.17±2.13	21.26±7.63	21.27±7.62	1.37±0.68	1.43±0.62	4.01±1.53*	4.83±1.84	4.73±1.46*	5.67±1.73	1.14±0.52*	1.45±0.73
Inferoseptal middle segment	4.26 ± 1* 27	4.24±1.24	19.84±9.25	19.89±9.23	1.34±0.62	1.41±0.63	3.57±1.14*	4.42±1.25	4.64±1.32*	5.86±1.53	1.19±0.52*	1.45±0.63
Inferoseptal apical segment	1.27±0.32	1.29±0.34	20.15±8.81	20.12±8.83	1.26±0.53	1.37±0.52	0.74±0.45*	1.16±0.84	4.57±1.14*	5.43±1.36	1.08±0.71*	1.46±0.82
Left ventricular anterior wall the basal segment	6.76±1.83	6.79±1.84	23.23±8.77	23.26±8.79	1.20±0.45	1.26±0.46	5.35±1.74*	6.35±2.13	5.54±1.53*	6.34±1.96	1.31±0.53*	1.53±0.76
Left ventricular anterior wall the middle segment	4.93±1.54	4.97±1.53	21.15±7.37	21.17±7.39	1.21±0.35	1.27±0.36	3.82±1.13*	4.48±1.52	5.25±1.49*	6.16±1.74	1.18±0.24*	1.42±0.67
Left ventricular anterior wall the apical segment	2.33±0.82	2.34±0.85	22.84±6.76	22.89±6.77	1.22±0.46	1.28±0.47	1.84±0.24*	2.24±0.36	5.26±1.42*	6.15±1.57	1.03±0.46*	1.44±0.73
Left ventricular inferior wall the basal segment	7.33±2.11	7.36±2.10	23.17±8.53	23.16±8.54	1.32±0.43	1.38±0.42	5.14±1.53*	6.71±1.79	5.36±1.74*	6.33±1.88	1.04±0.57*	1.44±0.85
Left ventricular inferior wall the middle segment	5.52±1.56	5.56±1.58	21.26±6.72	21.25±6.71	1.31±0.54	1.35±0.52	4.14±0.75*	4.89±1.08	5.74±1.35*	6.11±1.64	1.09±0.57*	1.42±0.76
Left ventricular inferior wall the apical segment	2.64±0.77	2.65±0.79	22.24±7.16	22.23±7.17	1.23±0.37	1.27±0.36	1.84±0.25*	2.38±0.39	4.96±1.02*	5.64±1.14	1.03±0.39*	1.43±0.67

**,p<0.05 compared to control group.*

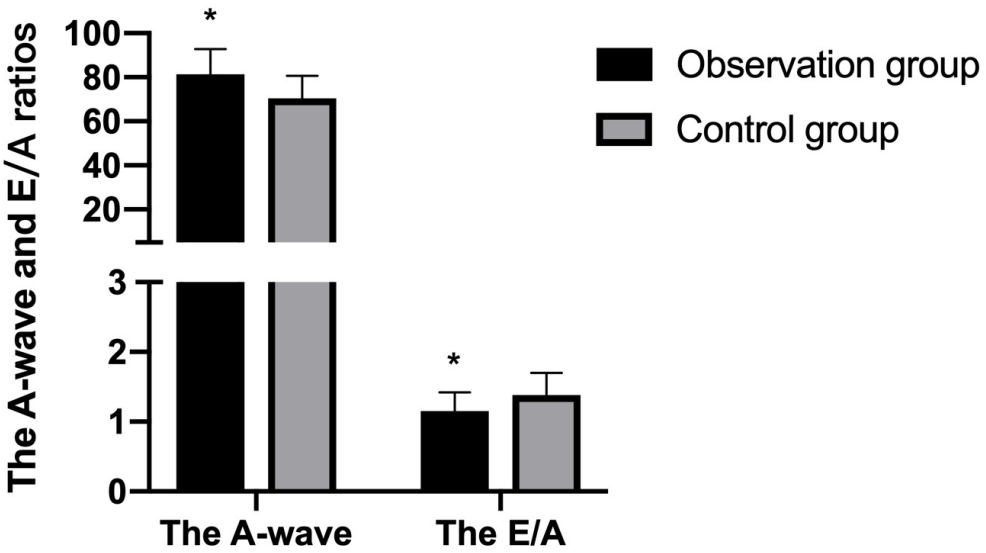


Fig. 1. *The A-wave and E/A ratios. The A-wave in the diastolic phase in the observation group was statistically higher than that in the control group ($p<0.05$). The E/A ratio in the observation group was statistically lower than that in the control group ($p<0.05$).*

(7). Color Doppler echocardiography has been proved as an essential non-invasive imaging method for prenatal assessment of cardiac function in pregnant women with GDM (8). VVI technology, based on the two-dimensional dynamic gray-scale image of color Doppler echocardiography, can track the direction of motion of each echogenic spot of the endocardium, measure the myocardial motion velocity, and present variation curves of motion strain and strain rate. It has been confirmed that VVI technology can be applied to evaluate left ventricular global systolic function and local myocardial motion (9). Therefore, this study explored the VVI technique in evaluating the cardiac function of pregnant women with GDM.

According to our results, the A-wave in the observation group was much higher than that in the control group, the E/A ratio in the observation group was somehow markedly lower than that in the control group. The color Doppler echocardiography displayed that the blood flow velocity of the left ventricular mitral valve in pregnant women with GDM was significantly altered compared to that in healthy pregnant women, suggesting a potential left ventricular diastolic dysfunction in patients in the observation group. In this study, the Vdmax, Sdmax, SRdmax at each segment of the left ventricle in the diastolic phase of the observation group were statistically lower than those of the control group. Previous evidence revealed that strain rate imaging technology directly displayed the deformation of different phases of myocardium through early diastolic strain rate (SRe) and late diastolic strain rate (SRa) (10). This study adopted the VVI technology to analyze the left ventricular long-axis movement in pregnant women before pregnancy from the perspective of myocardial mechanics. Our data demonstrate VVI technology serves as an accurate parameter in assessing myocardial function of pregnant women with GDM. It therefore provides a potential way to evaluate the local myocardial function in early GDM, and also offers a reliable basis for early clinical diagnosis and treatment.

REFERENCES

1. Salama AY, Arisha MJ, Nanda NC, Klas B, Ibeche B, Wei B. Incremental value of three-dimensional transthoracic echocardiography over the two-dimensional modality in the assessment of right heart compression and dysfunction produced by pectus excavatum. Echocardiography 2018; 36:150-63.
2. Huda SS, Brodie LE, Sattar N. Obesity in pregnancy:

prevalence and metabolic consequences. Semin Fetal Neonatal Med 2010; 15:70-76.
3. Kalçık M, Güner A, Özkan M. Incremental value of transesophageal echocardio-graphy in the evaluation of patients before percutaneous closure of atrial septal defects. Anatol J Cardiol 2019; 21:176-77.
4. Damm P, Houshmand-Oeregaard A, Kelstrup L, Lauenborg J, Mathiesen ER, Clausen TD. Gestational diabetes mellitus and long-term consequences for mother and offspring: a view from Denmark. Diabetologia 2016; 59:1396-99.
5. Burri MV, Nanda NC, Lloyd SG, et al. Assessment of systolic and diastolic left ventricular and left atrial function using vector velocity imaging in Takotsubo cardiomyopathy. Echocardiography 2008; 25:1138-44.
6. Schoenaker DA, Mishra GD, Callaway LK, Soedamah-Muthu SS. The role of energy, nutrients, foods, and dietary patterns in the development of gestational diabetes mellitus: a systematic review of observational studies. Diabetes Care 2016; 39: 16-23.
7. Elsayed M, Hsiung MC, Nanda NC, Alratroot A, Turaga NSS. Three-dimensional transthoracic echocardiographic identification of individual cusps of the pulmonary valve: Potential misidentification by the two-dimensional technique. Echocardiography 2018; 35:855-59.
8. Manning WJ, Silverman DI, Katz SE, Douglas PS. Atrial ejection force:a noninvasive assessment of atrial systolic function. Am Coll Cardiol 1993; 22:221-25.
9. Avdal J, Lovstakken L, Torp H, Ekroll IK. Combined 2-D vector velocity imaging and tracking doppler for improved vascular blood velocity quantification. IEEE Trans Ultrason Ferroelectr Freq Control 2017; 64:1795-804.
10. Alsharqi M, Woodward WJ, Mumith JA, Markham DC, Upton R, Leeson P. Artificial intelligence and echocardiography. Echo Res Pract 2018; 5:R115-R125.

LETTER TO THE EDITOR

Risk of acute kidney injury in myocardial infarction: New updates

B. Meng, B. Li, YH. Zhao, JT. Wang and H. Zhang

Department of Cardiology, Zibo Central Hospital, Zibo, P.R. China

Received March 10, 2020 – Accepted November 11, 2020

To the Editor,

Acute kidney injury (AKI), formerly known as acute renal failure, is a heterogeneous multiple disease, which can be due to various reasons, and is characterized by a rapid decrease in glomerular filtration rate, with an increase in serum creatinine or oliguria (1). This complication can occur in hospitalized patients and can be linked to other pathological disorders. In AKI there is a reduction or loss of excretory function of the kidneys characterized by the presence of the final products of nitrogen metabolism, such as urea and creatinine. In addition, AKI patients are more likely to suffer from chronic kidney disease (2). Furthermore, there may be other clinical manifestations such as the occasional decrease in urine, and increased concentrations of potassium and phosphorus. The likelihood of mortality increases with increasing creatinine concentration (3). This disease involves the inflammatory process of the renal parenchyma such as vasculitis and glomerulonephritis with the involvement of both innate and acquired immunity. Studies on animal models of acute ischemia have shown renal damage with the implication and impairment of the endothelium, infiltration of immune cells and activation of coagulation (4). Immune cells activated in kidney damage can release adhesion molecules and pro-inflammatory cytokines (IL-1 and IL-6) that can participate in kidney injury and apoptosis (5). There are many drugs that can contribute to AKI, such as beta-lactamases, methotrexate, cyclosporine, angiotensin-converting-enzyme inhibitors, radiocontrast agents, angiotensin-receptor blockers, non-steroidal anti-inflammatory drugs (NSAIDs) (6).

The therapy includes targeted treatments that also take into account the cause and it must be carried out in order to exclude complications (7). However, treatment must also consider the parameters mentioned above that mediate this important pathology. AKI generally occurs in patients with acute and chronic diseases with an incidence rate of approximately 20% including acute myocardial infarction (AMI).

Acute myocardial infarction

Myocardial infarction can lead to AKI which is a frequent complication with adverse outcomes (8). The worsening of the clinical course of patients is due to the conditions of nephropathy and other factors such as inflammatory markers, time of coronary reperfusion, cardiac pump and metabolic status. AKI is known to have a pathogenesis that presents various aspects with consequent reduction of renal function (9). There are various factors associated with AKI, and a detailed classification of them can help improve better understanding of complications and prevent unwanted effects. Prognosis in these patients presents a high mortality that can exceed 50%, with a very high social cost. These factors, that

Key words: acute myocardial infarction; acute kidney injury; risk factors

Corresponding Author:
Dr. Hui Zhang,
Department of Cardiology, Zibo Central Hospital,
No.54 Gongqingtuan West Road,
Zibo 255000, P.R. China
Tel.: +86 13953373558
e-mail: 13953373558@163.com

0393-974X (2020)
Copyright © by BIOLIFE, s.a.s.
This publication and/or article is for individual use only and may not be further reproduced without written permission from the copyright holder.
Unauthorized reproduction may result in financial and other penalties
DISCLOSURE: ALL AUTHORS REPORT NO CONFLICTS OF INTEREST RELEVANT TO THIS ARTICLE.

can lead to a decrease in glomerular filtration rate (GFR) and thereby increase mortality, are listed in Table II.

Among the inflammatory factors that play an important role in the development of AKI in patients with myocardial infarction, there is the C-reactive protein (CRP) which is very sensitive. CRP can be a powerful predictor of heart failure and patient mortality. However, this inflammatory marker, in some cases, can also be associated with an increased risk of AKI, as it could activate the coagulation system with the involvement of adhesion molecules and reduced nitric oxide and endothelial dysfunction. Damaged endothelium can lead to the release of pro-inflammatory cytokines, such as IL-1 and IL-6, with an increase in inflammation and worsening of the patient's condition.

Interleukin-1

Interleukin (IL)-1 is the main cytokine of innate immunity and it is the most studied of the IL-1 family involved in the inflammatory process that manifests itself in a myriad of diseases and intervenes mainly as a means of defense, but when it increases excessively can be harmful to the point of death. IL-1 is involved in cardiovascular disease and in particular in acute myocardial infarction and myocarditis, leading to heart failure (10) The precursor caspase-1 and IL-1 induce hypotension in several diseases including acute kidney injury in myocardial infarction causing a lowering of the glomerular filtration rate in mice. This effect is confirmed in animals with caspase deficiency. Indeed, the administration of IL-1 receptor antagonist (IL-1RA) protects against hypotension which, in severe cases, can lead to death (11). Furthermore, IL-1Ra protects against renal cell apoptosis, neutrophil infiltration and their activity (12). It can therefore be concluded that by blocking IL-1 in this disease, an improvement in the pathological course and relief for the patient could be obtained.

However, extensive studies still need to be carried out to improve the pathological status in this serious disease.

Table I. *Acute kidney injury: risk factors*

Chronic heart diseases
Liver Diseases
Lung Diseases
Diabete Mellitus
Cancer
Older Age
Anemia

Table II. *Factors that can lead to a decrease in glomerular filtration rate (GFR)*

Intratubular pressure
Increased urinary viscosity
Increased oxygen consumption
Increased vasoconstriction
Increased renal adenosine concentration
Increased blood viscosity
Increased formation of ROS (reactive oxygen species)
Elevated uric acid levels
Thrombosis
Inflammation
Anemia

REFERENCES

1. Pakula AM, Skinner RA. Acute kidney injury in the critically ill patient: A current review of the literature. J Intensive Care Med 2016; 31(5):319-24.
2. Shacham Y, Leshem-Rubinow E, Steinvil A, Assa EB, Keren G, Roth A, Arbel. Renal impairment according to acute kidney injury network criteria among ST elevation myocardial infarction patients undergoing primary percutaneous intervention: a retrospective observational study. Clin Res Cardiol 2014; 103:525-32.
3. Marenzi G, Cosentino N, Guastoni C (2015) How to balance risks and benefits in the management of

CKD patients with coronary artery disease. J Nephrol 28:403-13.

4. Lelubre C, Vincent JL. Mechanisms and treatment of organ failure in sepsis. Nat Rev Nephrol 2018;14(7):417-27.
5. Neveu H, Kleinknecht D, Brivet F, Loirat P, and Landais P. Prognostic factors in acute renal failure due to sepsis. Results of a prospective multicentre study. Nephrol Dial Transplant 1996; 11:293-99.
6. Levey AS, James MT. Acute kidney injury. Ann Intern Med 2017; 167(9):ITC66-ITC80.
7. Reis T. Acute kidney injury. Rev Assoc Med Bras (1992) 2020; 66(S1):s68-s74.
8. Eltzschig HK, Eckle T. Ischemia and reperfusion--from mechanism to translation. Nat Med 2011; 17(11):1391-401.
9. Bateman RM, Sharpe MD, Jagger JE, 36th International Symposium on Intensive Care and Emergency Medicine : Brussels, Belgium. 15-18 March 2016. Crit Care 2016; 20(S2):94.
10. Abbate A, Toldo S, Marchetti C, Kron J, Van Tassell BW, Dinarello CA. Interleukin-1 and the inflammasome as therapeutic targets in cardiovascular disease. Circ Res 2020; 126(9):1260-80.
11. Aiura K, Gelfand JA, Burke JF, Thompson RC, Dinarello CA. Interleukin-1 (IL-1) receptor antagonist prevents Staphylococcus epidermidis-induced hypotension and reduces circulating levels of tumor necrosis factor and IL-1 beta in rabbits. Infect Immun 1993; 61(8):3342-50.
12. Fantuzzi G, Zheng H, Faggioni R, Benigni F, Ghezzi P, Sipe JD, Shaw AR, and Dinarello CA. Effect of endotoxin in IL-1-deficient mice. J Immunol 1996: 157:29196.

LETTER TO THE EDITOR

LncRNA BC200 regulates neuron apoptosis and neuroinflammation via PI3K/AKT pathway in Alzheimer's disease

NX. Liu and QH. Li

Emergency Department, Zibo Central Hospital, Shandong Province, China

Received August 6, 2020 – Accepted November 11, 2020

To the Editor,

Alzheimer's disease (AD) is a frequent neurodegenerative disease characterized by progressive cognitive decline with loss of memory. The β-Amyloid (Aβ) has been shown to have a toxic effect on neurons, which results in facilitated neuronal death. However, the molecular mechanism of neuronal cell apoptosis is still unknown. As an important regulator of the central nervous system, lncRNAs are widely involved in the regulation of neuronal differentiation, synaptic plasticity and behavior (1). Moreover, the abnormal expression of lncRNAs has been proved to underlie the pathophysiological basis of AD pathophysiology, and thus can be used as a promising biomarker and a potential therapeutic target. Long noncoding RNA Brain Cytoplasmic RNA 1 (BCYRN1, BC200) has been found to play an important role in the pathophysiology of brain development, functional diversification and neurodegenerative diseases (2). To the best of our knowledge, the role of BC200 in the pathophysiology of AD has not yet been determined.

In the present study, the expression levels of lncRNA BC200 in cerebrospinal fluid (CSF) and serum of patients with AD were determined. In addition, PC12 cells were incubated with $A\beta_{25-35}$ to induce cell injury, and the effects of lncRNA BC200 suppression on $A\beta_{25-35}$-induced PC12 cell injury were investigated by assessing cell viability, apoptosis, inflammation, cytotoxicity, and oxidative stress. The regulatory mechanism of lncRNA BC200 was also explored in PC12 cells. Our data will provide a theoretical basis for better elucidation of the role and regulatory mechanism of lncRNA BC200 in AD.

MATERIALS AND METHODS

Patient samples

Fourteen AD patients (6 males and 8 females) and fifteen healthy individuals (7 males and 8 females) were enrolled in this study. According to the National Institute of Neurological and Communication Disorders and Stroke and the standards of the Alzheimer's Disease and Related Diseases Association (NINCDS/ADRDA), the diagnosis of AD is determined through clinical evaluation, neuropsychological testing and magnetic resonance imaging (3). The CSF samples of AD patients and healthy individuals were collected and then stored at −80°C. CSF samples with <4 leukocytes/μl and <200 erythrocytes/μl were selected. Meanwhile, the serum were harvested from all participants and stored at -80°C. This study was approved by the ethics committee of Zibo Central Hospital and all the patients enrolled in this study signed the informed consent.

Aβ preparation and treatment

$A\beta_{25-35}$ was dissolved in dimethyl sulfoxide (DMSO) at

Key words: LncRNA BC200; apoptosis; inflammation; Alzheimer's disease; PI3K/AKT

Corresponding Author:
Dr Qinghua Li,
Zibo Central Hospital, Department of Emergency,
No. 54, Gongqingtuan West Road, Zhangdian District, Zibo 255020,
Shandong Province, China
Tel./Fax: +86 0533 2881510
e-mail: huijialue598581298@163.com

0393-974X (2020)
Copyright © by BIOLIFE, s.a.s.
This publication and/or article is for individual use only and may not be further reproduced without written permission from the copyright holder.
Unauthorized reproduction may result in financial and other penalties
DISCLOSURE: ALL AUTHORS REPORT NO CONFLICTS OF INTEREST RELEVANT TO THIS ARTICLE.

10 mM and stored at −20°C until use. The original solution was diluted with deionized distilled water to the appropriate concentration and incubated at 37°C for 4 days for aggregation before use. The final concentration of DMSO was less than 0.01%, which did not affect cell viability.

Cell culture and transfection

The neuronal PC12 cells were purchased from the Cell Bank, Chinese Academy of Sciences (Shanghai, China), and cultured in Roswell Park Memorial Institute (RPMI) 1640 Medium (Gibco, USA) supplemented with 10% horse serum, 1% Pen-Strep (Gibco, USA) and 5% fetal bovine serum (FBS) (Gibco, USA) under 5% CO2 and 95% air at 37°C. PC12 cells were seeded in a 96-well plate and cultured for 24 h. Then, the cells were treated with 40 μM $A\beta_{25\text{-}35}$ (Sigma, MO, USA) for 24 h to establish AD model *in vitro*. Lnc-BC200 overexpression plasmids (OE-BC200), overexpression control plasmids (OE-NC), or lnc-BC200 shRNA (sh-BC200) and control shRNA (sh-NC) were purchased from GenePharma (Shanghai, China). Lipo-fectamine 2000 Reagent (Invitrogen, USA) was used to conduct the transfections according to the manufacturer's instructions.

MTT assay

Cell viability was measured by MTT cell proliferation assay kit (Sigma-Aldrich, MO, USA). 5×10^3/well PC12 cells were seeded in a 96-well plate. PC12 cells were then incubated with 15 μL MTT (0.5 mg/mL) for 4 h at 37°C with 5% CO2 after different treatment. Afterwards, the supernatant was removed by 100 μL DMSO. The absorbance at 490 nm was finally measured by a microplate reader (Becton Dickinson, CA, USA).

Real-time quantitative reverse transcriptase PCR (qRT-PCR)

TRIzol Reagent (Invitrogen, USA) was used to extract total RNA according to the manufacturer's instructions. cDNA was synthesized by using PrimeScript™ RT reagent Kit (Takara, Japan). PCR amplification was performed as follows: 95°C for 5 min, followed by 40 cycles of 95°C for 5 s, 61°C for 30 s. The RT-qPCR were calculated with the $2^{-\Delta\Delta Ct}$ method. The primers used were presented: BC200 forward, 5'-AGACCTGCCTGGGCAATATAGC-3' and reverse, 5'-GTTGTTGCTTTGAGGGAA GTTACG-3'. GAPDH forward, 5'-CATGAGAAGTATGACAACAGCCT-3' and reverse, 5'-AGTCCTTCCACGATACCAAAGT-3'). GAPDH was used as a reference gene.

Western blot assay

The total protein was extracted from tissues and cells using RIPA buffer (Thermo Fisher Scientific, USA). The measurement of protein concentration was used by the BCA kit. 50 μg protein samples were subjected to SDS-PAGE and then transfected onto polyvinylidene fluoride membranes (PVDF, Millipore, USA). After blocking with 5% skim milk for 2 h, the membranes were immunolabeled with the primary antibodies to Bcl-2 (1:2000, ab182858, Abcam), Bax (1:1000, ab32503, Abcam), Cyt C (1:1000, ab133504, Abcam), pro-caspase-3 (1:500, ab32150, Abcam), cleaved-caspase-3 (1:1000, ab214430, Abcam) and GAPDH (1:2000, ab9485, Abcam) at 4°C overnight. Afterwards, the membranes were incubated with the corresponding secondary antibodies for 1 h at 37°C. Immunoreactive bands were exposed by enhanced chemiluminescence method (ECL) and the gray values of the target protein bands were analyzed by Image J software (National Institutes of Health).

Enzyme-linked Immunosorbent assay (ELISA)

The productions of interleukin (IL)-6 (IL-6), IL-10 and tumor necrosis factor-α (TNF-α) in cell supernatant were measured by the corresponding ELISA kits according to the manufacturer instructions. The ELISA kits were as follows: IL-6 Rat ELISA Kit (Invitrogen, USA), IL-10 Rat ELISA Kit (Invitrogen, USA), TNF alpha Rat ELISA Kit (Invitrogen, USA).

LDH assay

The cytotoxicity was evaluated by measuring the LDH level using Cytoscan-LDH cytotoxicity assay kit (G-Biosciences Inc., St Louis, USA) according to the manufacturer's instructions. After adding 50 μL reconstituted Substrate Mix to PC12 cells and incubating at 37°C in the dark for 30 min, 50 μL Stop Solution was added to terminate the reaction. The absorbance at 490 nm was recorded by a microplate reader.

Measurement of Ca2+ and reactive oxygen species (ROS).

The Fluo-3 AM (fluorescence Ca2+ indicator) and ROS kits were used to measure the intracellular concentrations of Ca2+ and ROS in PC12 cells, respectively. For detecting

Ca2+ levels, PC12 cells were stained with Fura-3 AM (5 μg/ml) for 60 min and then incubated at 37°C for 30 min. Subsequently, a flow cytometer was applied to detect the fluorescence-intensity. The levels of Ca2+ in PC12 cells were expressed as intensity of the recorded fluorescence (NRFU) (U/cell). For detecting intracellular ROS levels, PC12 cells were incubated with the cell permeable DCFH-DA (10 μM) at 37°C for 20 min. Afterwards, a flow cytometer was used to detect the fluorescence, and the data were presented as an average of the NRFU (U/cell).

Measurement of mitochondrial membrane potential

JC-1 mitochondrial membrane potential assay kit (Cayman Chemical Co., MI, USA) was used to determine the mitochondrial membrane potential of PC12 cells following the manufacturer's instructions. A density of 5×10^5 cells were incubated with 500 μL JC-1 Staining Solution, and maintained at 37°C for 25 min. Fluorescence microscopy was then used to detect cells. The presence of green fluorescence indicated that the mitochondrial membrane potential has decreased, and the cells are likely to be in the early stage of apoptosis. The red fluorescence showed that the membrane potential is relatively normal and the state of the cells is relatively normal.

Statistical analysis

SPSS 22.0 software (IBM, NY, USA) was applied to perform statistical analysis. The quantitative data were represented as Mean±Standard Deviation (Mean±SD) from three independently repeated experiments. Student's *t*-test was used to compare the differences between two groups. Differences among groups were compared with one-way ANOVA, followed by Turkey's post hoc test. $P<0.05$ was considered statistically significant.

RESULTS

LncRNA-BC200 was up-regulated in patients with AD

The expressions of lncRNA-BC200 in CSF and serum of AD patients were measured by qRT-PCR. The results showed that lncRNA-BC200 was significantly increased in CSF of AD patients compared with that in CSF of healthy controls (Fig. 1A). Moreover, lncRNA-BC200 expression was also up-regulated in serum of AD patients in comparison with control (Fig. 1B).

$A\beta_{25-35}$ induced PC12 cell injury and increased the expression of lncRNA-BC200

The effects of $A\beta_{25-35}$ on PC12 cell viability, apoptosis, inflammation and oxidative stress were evaluated to detect whether $A\beta_{25-35}$ induced PC12 cell injury. The findings demonstrated that $A\beta_{25-35}$ treatment significantly inhibited PC12 cell viability

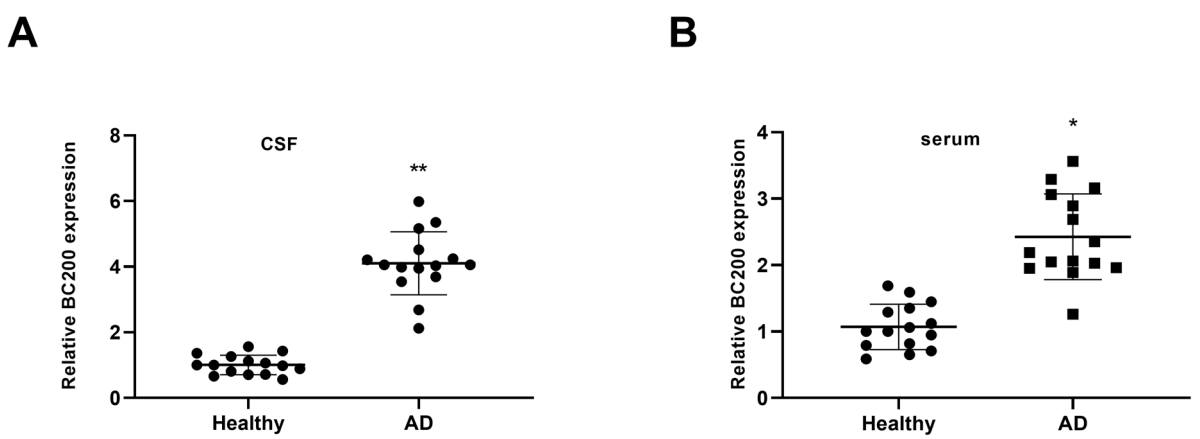


Fig. 1. *Up-regulated of lncRNA-BC200 in patients with AD. **A)** LncRNA-BC200 was increased in the CFS and serum (**B**) of patients with Alzheimer's disease (AD). The results are expressed as Mean ± SD of three independently repeated experiments. *P < 0.05 and **P < 0.01 compared with control.*

(Fig. 2A) and promoted cell apoptosis compared with control groups, $A\beta_{25-35}$ treatment significantly decreased Bcl-2 expression and increased the expressions of Bax, cleaved caspase-3 and cyt-c (Fig. 2B). Moreover, $A\beta_{25-35}$ treatment significantly promoted the production of inflammatory cytokines (IL-6, IL-1β, and TNF-α) (Fig. 2C), and cytotoxicity relative to controls (Fig. 2D). Furthermore, $A\beta_{25-35}$

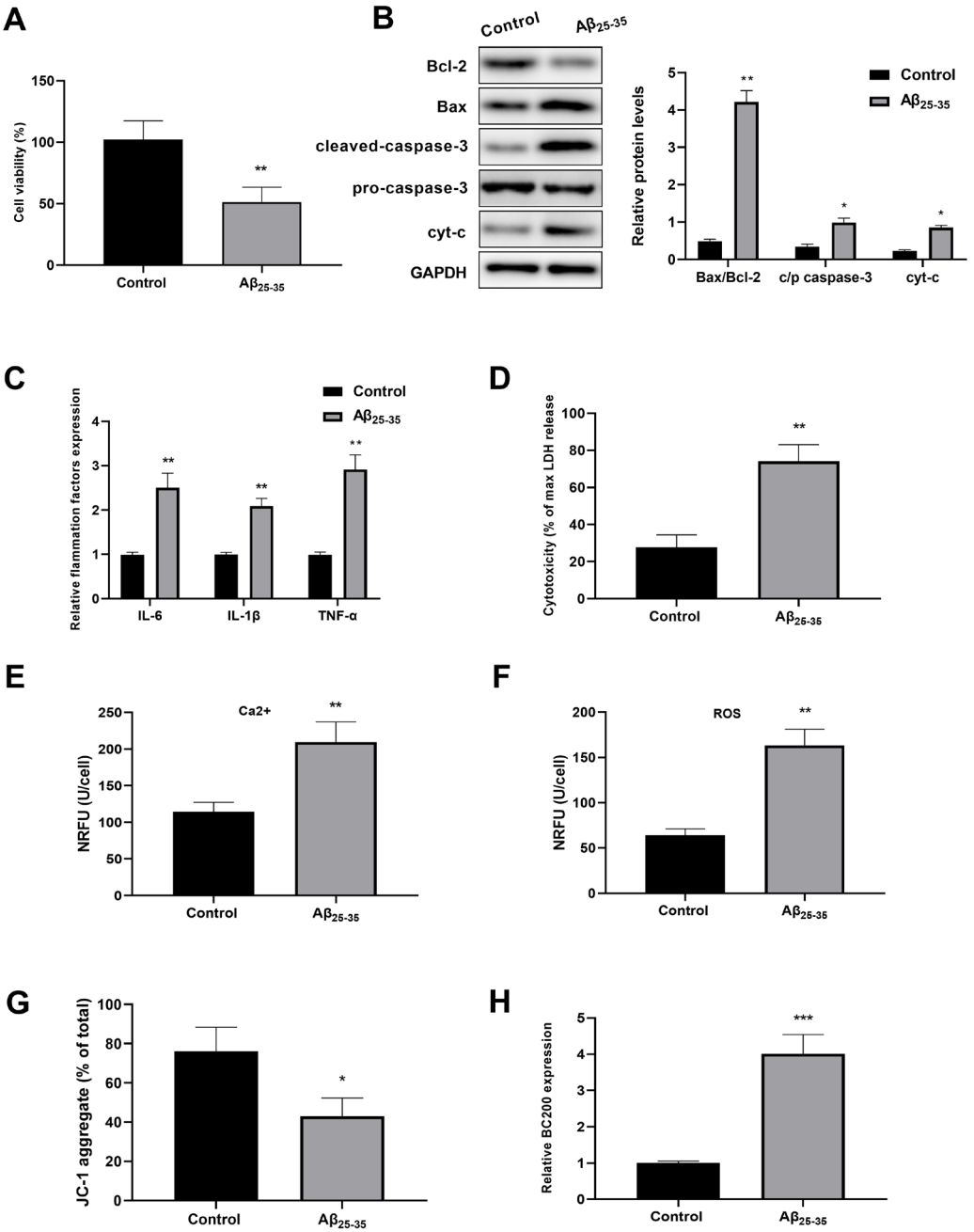


Fig. 2. *$A\beta_{25-35}$ induced PC12 cell injury and increased the expression of lncRNA-BC200.* ***A)*** *Decreased cell viability of PC12 cells after $A\beta_{25-35}$ treatment.* ***B)*** *Increased cell apoptosis, inflammation (**C**), cytotoxicity (**D**), Ca2+ (**E**), and ROS (**F**) in PC12 cells after $A\beta_{25-35}$ treatment.* ***G)*** *JC-1 aggregate was decreased in PC12 cells after $A\beta_{25-35}$ treatment.* ***H)*** *LncRNA-BC200 was increased in PC12 cells after $A\beta_{25-35}$ treatment.*

treatment remarkably increased oxidative stress to PC12 cells by increasing intracellular concentrations of Ca2+ (Fig. 2E) and ROS (Fig. 2F), and decreasing JC-1 mitochondrial membrane potential (Fig. 2G). Furthermore, the expression of lncRNA-BC200 was investigated in PC12 cells after $A\beta_{25-35}$ treatment.

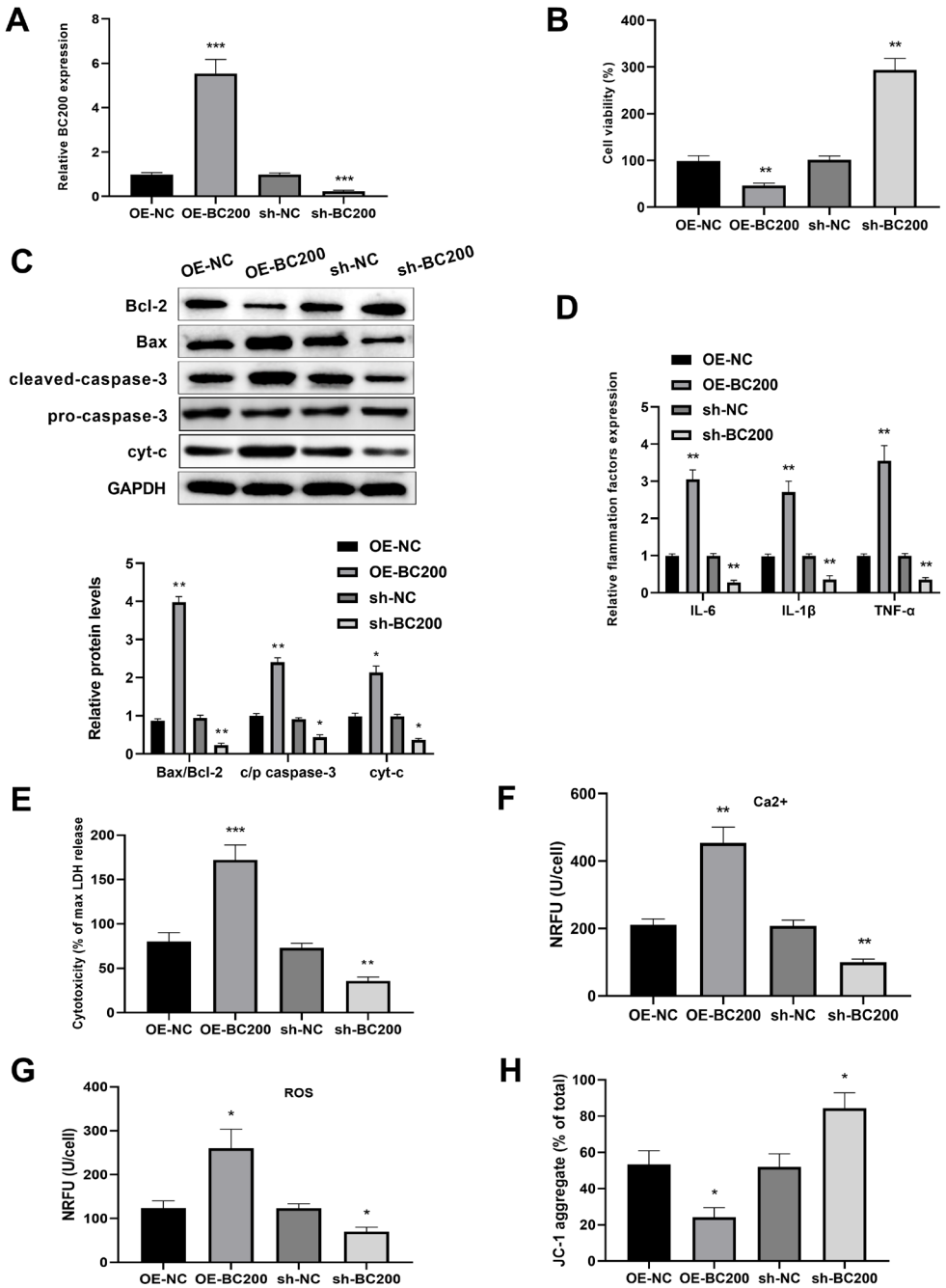


Fig. 3. *LncRNA-BC200 promoted $A\beta_{25-35}$-induced PC12 cell injury. **A**) LncRNA-BC200 was increased or decreased in PC12 cells after treatment with OE-BC200 or sh-BC200. **B**) Cell viability was inhibited by OE-BC200 or promoted by sh-BC200. **C**) Cell apoptosis, (**D**) inflammation, (**E**) cytotoxicity, (**F**) Ca2+, and (**G**) ROS were increased or decreased in PC12 cells after treatment with OE-BC200 or sh-BC200. **H**) JC-1 aggregate was decreased or increased in PC12 cells after treatment with OE-BC200 or sh-BC200.*

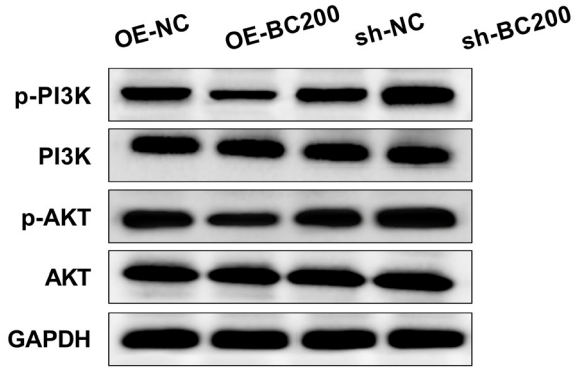


Fig. 4. *LncRNA-BC200 inactivated PI3K/AKT pathway in PC12 cells. Western blot results displayed that protein expressions of p-PI3K and p-AKT were down-regulated after lnc-BC200 over-expression, while up-regulated after knockdown of lnc-BC200.*

The results demonstrated that $A\beta_{25-35}$ significantly increased the expression of lncRNA-BC200 in PC12 cells (Fig. 2H).

LncRNA-BC200 regulated $A\beta_{25-35}$-induced PC12 cell injury

To investigate the functional role of lncRNA-BC200 in AD, the expression of lncRNA-BC200 was increased or decreased in PC12 cells after $A\beta_{25-35}$ treatment by transfection with OE-BC-200 or sh-BC200. As shown in Fig. 3A, the expression of lncRNA-BC200 was significantly increased in the OE-BC200 group, while decreased in the sh-BC200 group relative to the corresponding normal control group, confirming the successful efficiency of BC200. Increasing lncRNA-BC200 significantly elevated $A\beta_{25-35}$-induced PC12 cell injury by inhibiting cell viability (Fig. 3B), promoting apoptosis (Fig. 3C), increasing inflammation (Fig. 3D), cytotoxicity (Fig. 3E) and intracellular concentrations of Ca2+ (Fig. 3F) and ROS (Fig. 3G), and inhibiting JC-1 mitochondrial membrane potential (Fig. 3H). However, inhibition of BC200 showed the opposite effect on PC12 cell injury.

LncRNA-BC200 activated PI3K/AKT pathway in PC12 cells

PI3K/AKT pathway has been confirmed to regulate cellular functions, including cell survival and apoptosis. Hence, whether lncRNA-BC200 regulated AD development via PI3K/AKT pathway was speculated. Western blot results displayed that protein expressions of p-PI3K and p-AKT were down-regulated after lnc-BC200 over-expression in PC12 cells, while were up-regulated after knockdown of lnc-BC200. Moreover, the expressions of PI3K and AKT in PC12 cells were not significantly different (Fig. 4).

DISCUSSION

Increasing evidence indicated that apoptosis is related to the pathological changes of AD, and inhibiting nerve cell apoptosis may be one of the methods of treatment (4). Here, we found that treatment with $A\beta_{25-35}$ significantly reduced the expression of Bcl-2 and increased the expression of Bax, cleaved-caspase-3 and cyt-c, but these expressions were significantly reversed after the suppression of lncRNA-BC200. These results indicated that the inhibition of lncRNA-BC200 might inhibit the apoptosis of PC12 cells induced by $A\beta_{25-35}$, which were in agreement with previous findings regarding the role of $A\beta_{25-35}$ in causing mitochondrial dysfunction (5). Oxidative stress is considered to be the initial factor affecting the pathogenesis of neurodegenerative diseases including AD (4). Increased ROS production under stress conditions can lead to cellular oxidative stress damage (6). Similarly, our study found that ROS production was significantly enhanced in PC12 cells induced by $A\beta_{25-35}$, and inhibition of lncRNA-BC200 reduced the activity of ROS, suggesting that lncRNA-BC200 could reduce oxidative stress damage of PC12 cells induced by $A\beta_{25-35}$. Therefore, lncRNA-BC200 may be involved in the development of AD. PI3K/AKT pathway is an important signaling pathway involved in AD (7). In the present study, the results showed that BC200 promotes neuron apoptosis and neuroinflammation via PI3K/AKT pathway in AD.

In conclusion, our results indicated that lncRNA-BC200 is highly expressed in patients with AD, and suppression of lncRNA-BC200 might protect PC12 cells against amyloid-β-induced neurotoxicity via regulating PI3K/AKT pathway, providing a new insight for preventing AD.

REFERENCES

1. Qureshi IA, Mattick JS, Mehler MF. Long non-coding RNAs in nervous system function and disease. Brain Res 2010; 1338:20-35.
2. Wu P, Zuo X, Deng H, Liu X, Liu L, Ji A. Roles of long noncoding RNAs in brain development, functional diversification and neurodegenerative diseases. Brain Res Bull 2013; 97:69-80.
3. McKhann G, Drachman D, Folstein M, Katzman R, Price D, Stadlan EM. Clinical diagnosis of Alzheimer's disease: report of the NINCDS-ADRDA Work Group under the auspices of Department of Health and Human Services Task Force on Alzheimer's Disease. Neurology 1984; 34:939-44.
4. Borgman MP, Coleman T, Kolhatkar RB, Geyser-Stoops S, Line BR, Ghandehari H. Tumor-targeted HPMA copolymer-(RGDfK)-(CHX-A''-DTPA) conjugates show increased kidney accumulation. J Control Release 2008; 132:193-99.
5. Wang K, Zhu L, Zhu X, et al. Protective effect of paeoniflorin on Abeta25-35-induced SH-SY5Y cell injury by preventing mitochondrial dysfunction. Cell Mol Neurobiol 2014; 34:227-34.
6. Gomes P, Simao S, Silva E, et al. Aging increases oxidative stress and renal expression of oxidant and antioxidant enzymes that are associated with an increased trend in systolic blood pressure. Oxid Med Cell Longev 2009; 2:138-45.
7. Kamel AS, Abdelkader NF, Abd El-Rahman SS, Emara M, Zaki HF, Khattab MM. Stimulation of ACE2/ANG(1-7)/Mas Axis by Diminazene Ameliorates Alzheimer's Disease in the D-Galactose-Ovariectomized Rat Model: Role of PI3K/Akt Pathway. Mol Neurobiol 2018; 55:8188-202.

LETTER TO THE EDITOR

Knockdown of MMP16 inhibits cell proliferation and invasion in chordoma *in vitro*

DM. Xu[1], PH. Han[2], L. Chen[3], TT. Li[3], XH. Yang[4] and R. Guo[5]

[1]Department of General Surgery, Weifang People's Hospital, Weifang, China; [2]Department of Encephalopathy, Traditional Chinese Medical Hospital of Huangdao District, Qingdao, China; [3]Operation Room, The People's Hospital of Zhangqiu Area, Jinan, China; [4]Department of Pharmacy, The People's Hospital of Zhangqiu Area, Jinan, China; [5]Outpatient Department, The People's Hospital of Zhangqiu Area, Jinan, China

Received September 15, 2020 – Accepted November 11, 2020

To the Editor,

Chordoma belongs to a rare form of malignant tumor developed from benign notochordal tissues (1). This tumor often typically occurs in the midline skeleton, mainly concentrating on the skull base and spine (2). Chordomas are often clinically diagnosed at the advanced stages of disease which have destroyed the surrounding bone and invaded adjacent soft tissue. Except for the surgical resection and radiotherapy, there is no efficient treatment against chordoma at present. It is also essential to develop new biomarkers to apply for early diagnosis of chordoma. Matrix metalloproteinase (MMP) 16 is a membrane type metalloproteinase whose function is to activate proMMP2 (gelatinase A) into an active form as the zymogen is excreted from the cell. MMP2 has certain effects on the collagen IV of the basement membrane and is related to cancer metastasis (3). In addition, high MMP16 expression has been found to be associated with increasing invasiveness in gastric cancer (4), and hepatocellular carcinoma (5), as well as melanoma (6). Moreover, MMP16 has been reported to regulate tumorigenesis of human cancers by interacting with microRNAs (miRNAs). For example, miR-132 can inhibit glioma cell invasion and migration by target MMP16 *in vitro* (7). The present study aimed to determine the regulatory mechanism of miR-31/MMP16 axis for proliferation and invasion of chordoma cell.

MATERIALS AND METHODS

Human chordoma cell lines, UCH1 and UCH2 were obtained from the Chordoma Foundation. These cell lines were cultured in the RPMI1640 medium (Invitrogen, CA, USA) supplemented with 10% fetal bovine serum (FBS) and 1% penicillin/streptomycin. Then the cells were cultured at 37°C with an atmosphere of 5% CO_2.

Tissue samples

Surgical chordoma specimens and adjacent normal tissue samples from 33 patients were obtained from The People's Hospital of Zhangqiu Area with approval from the responsible Ethics Committee of The People's Hospital of Zhangqiu Area. All tissue samples were frozen in liquid nitrogen immediately, and then stored at -80°C. Written informed consent was obtained before the experiment was started. The patients had not undergone any radiotherapy or chemotherapy prior to surgery.

Transfection assay

Key words: chordoma; MMP16; invasion; proliferation; miR-31-5p

Corresponding Author:
Dr Rui Guo,
Outpatient Department, The People's Hospital of Zhangqiu Area,
No. 1920 Huiquan Road, Jinan, 250200,
Shandong Province, China
Tel.: +86 0531 83251203
e-mail: liuyihe0765@163.com

0393-974X (2020)
Copyright © by BIOLIFE, s.a.s.
This publication and/or article is for individual use only and may not be further reproduced without written permission from the copyright holder.
Unauthorized reproduction may result in financial and other penalties
DISCLOSURE: ALL AUTHORS REPORT NO CONFLICTS OF INTEREST RELEVANT TO THIS ARTICLE.

UCH1 cells were cultured in the RPMI1640 medium (Invitrogen, CA, USA) supplemented with 10% fetal bovine serum (FBS) and 1% penicillin/streptomycin at 37°C, 5% CO_2. Cells were passaged once every 2-3 days and cells at logarithmic growth were used in the experiment. The cells were seeded in 6-well plates at 1×10^5 cells/well followed by culturing for 24 h and then transfected with 30 nM of the MMP16 siRNA, miR-31 mimic or vector at (Ruibio, China) using Lipofectamine RNAiMAX (Invitrogen, USA) in serum-free RPMI1640 medium. Medium was replaced with fresh medium after transfection for 6 h, and the cells were cultured for another 48 h before further analysis.

RNA isolation and quantitative real-time PCR

Total RNA was isolated from chordoma cell lines and tissues using TRIzol® (Invitrogen, Carlsbad, CA, USA) according to the manufacturer's instructions, then reverse transcribed into cDNA using a TaqMan MicroRNA Reverse Transcription kit (Applied Biosystems, Foster City, CA, USA). Small RNA U6 was used as an internal control for quantification of miR-31-5p expression and MMP16 mRNA was normalized to GAPDH. MMP16 forward primer, 5'-GATTCAGCCATTTGGTGGGAGG-3', reverse primer 5'-CCCTTTCCAGACTGTGATTGGC-3'. GAPDH forward primer, 5'-GTCTCCTCTGACTTCAACAGCG-3', reverse primer 5'- ACCACCCTGTTGCTGTAGCCAA-3'. miR-31 forward primer, 5'- GCAAGATGCTGGCATAG-3', reverse primer 5'-GAACATGTCTGCGTATCTC-3'. The qRT-PCR was performed using SYBR Green PCR Kit (Takara, Japan) and ABI 7500 Fast Real-Time PCR system (ABI, USA) according to the manufacturer's instructions. The relative expression of genes was calculated using the $2^{-\Delta\Delta Ct}$ method.

Western blot analysis

Transfected UCH1 cells were lysed in RIPA lysis buffer. Equal amounts of protein were separated through 10% sodium dodecyl sulfate polyacrylamide gel electrophoresis (SDS-PAGE) for electrophoresis and then transferred onto a PVDF membrane (Millipore, Billerica, MA, USA). The membrane was blocked with 5% skimmed milk for 1 h, and then incubated with primary antibodies for 24 h at 4°C using anti-MMP16 (#TA347433, 1:1000, Origene) and anti-GAPDH antibody (#TA890003, 1:1000, Origene). After incubation with horseradish peroxidase-conjugated mouse anti-rabbit secondary antibody (#sc-2357, 1:5000, Santa Cruz Biotechnology) for 2 h, the proteins were detected by enhanced chemiluminescent using the ECL Plus Kit (Amersham, Buckinghamshire, UK).

MTT cell proliferation assay

The MTT (3-(4, 5-dimethyl-2-thiazolyl)-2, 5-diphenyl-2H-tetrazolium bromide) assay was applied to measure cell proliferation. Cells (2×10^3) were plated onto 96-well plates in medium containing with 10% FBS. The cells transfected with miR-31 mimics or miR-31 inhibitor were incubated for 24–96 h. After incubation, the cells were added with 50 mg/well of MTT (Sigma, MO, USA) and incubated for 4 h at 37°C. The MTT formazan was dissolved in acid-isopropanol. In turn, the absorbance was measured at 490 nm on a SPECTRAmax Microplate Spectrophotometer (Sunnyvale, CA, USA).

Cell invasion assay

Cell invasion was evaluated by Transwell assay. 5×10^4 cells were seeded into the upper chambers (8 μm pore size; Corning Incorporated, Corning, NY, USA), and medium with 10% FBS was added into the lower chamber. The invasion assay was performed for 24 h at 37°C in 5% CO_2. Then the invasive cells were on the lower surface were fixed in 70% ethanol and stained with crystal violet stain. Cells were counted by a light microscope. All experiments were repeated three times independently.

Luciferase reporter assay

A luciferase reporter assay was performed on HEK293T cells to confirm the relationship between miR-31-5p and MMP16. The cells were grown in 24-well plates with luciferase reporter plasmids containing wild-type MMP16 3'-UTR, mutant MMP16 3'-UTR, or a 3'-UTR negative control and hsa-miR-31-5p mimics. After 48 h transfection, cells were collected and analyzed using the Luciferase Assay System, according to the manufacturer's instructions (Promega Corporation, Madison, Wisconsin, USA).

Statistical analysis

All statistical analyses were performed using SPSS17.0. Continuous data are presented as means ±

standard deviation (SD). The comparison of miRNA expression level between chordoma and controls was performed using Student's *t*-test. *Chi*-squared test was used for enumeration data. Continuous data from multiple groups were analyzed by using one-way ANOVA, with the Tukey's post hoc test. Pearson's correlation analysis was used to assess the relations of MMP16 and miR-31 expressions. All experiments were repeated for three times. $P<0.05$ was considered statistically significant.

RESULTS

The level of MMP16 was detected in chordoma tissues and normal tissues. RT-qPCR showed that MMP16 expression was significantly increased in chordoma tissues compared to corresponding adjacent normal tissues ($P<0.05$, Fig. 1A). The relationship between the clinicopathologic characteristics in chordoma patients and the expression of MMP16 was then analyzed. We found that the abnormal expression of MMP16 was related to the tumor stage in chordoma patients ($P<0.05$, Table I). In addition, significant upregulation of MMP16 was found in UCH1 and UCH2 cell lines compared with immortal normal cell line Fibro ($P<0.05$, Fig. 1B).

In order to explore the effect of MMP16 on cell proliferation and invasion in chordoma, MMP16 siRNA was transfected into UCH1 cells. RT-qPCR showed that MMP16 siRNA significantly reduced MMP16 expression in UCH1 cells ($P<0.05$, Fig. 2A). Functionally, MTT assay indicated that downregulation of MMP16 significantly inhibited cell proliferation in chordoma compared to negative control ($P<0.05$, Fig. 2B). Similarly, Transwell assay revealed that knockdown of MMP16 statistically inhibited chordoma cell invasion (Fig. 2C). The number of invasive cells among the transfected chordoma cells was decreased to less than 36.7% of that in the control chordoma cells (Fig. 2D).

TargetScanHuman database (http://www.targetscan.org/vert_71/) predicted a binding site of MMP16 with miR-31-5p (site 6637-6644, Fig. 3A). Moreover, a dual luciferase reporter assay was performed to confirm the above prediction. The result showed that luciferase activity of MMP16 containing a wild-type 3'-UTR (WT) was significantly reduced by the miR-31-5p mimics in HEK293T cells ($P<0.05$, Fig. 3B). Therefore, we speculated that MMP16 may regulate miR-31-5p expression in chordoma by binding to miR-31-5p. Compared to normal tissues, significant downregulation of miR-31-5p was detected in chordoma tissues compared

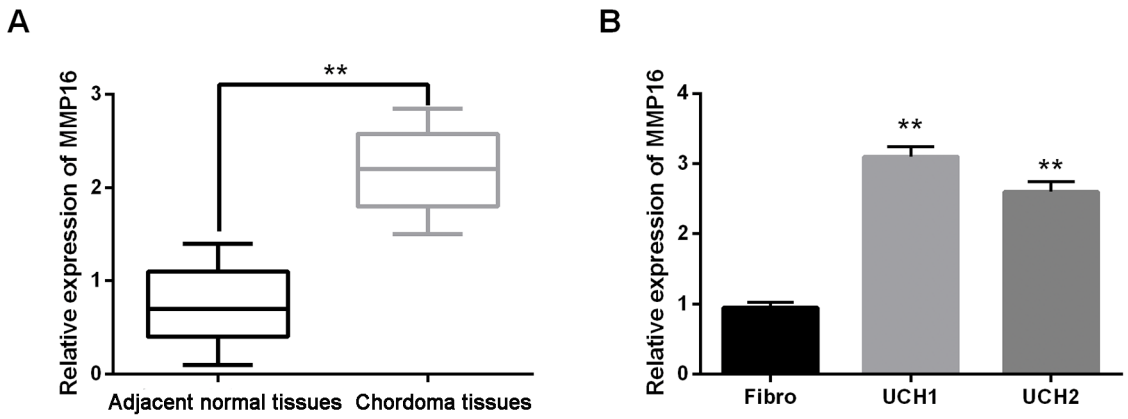


Fig. 1. *MMP16 is upregulated in chordoma tissues and cell lines.* ***A****) The expression of MMP16 in 33 pairs of chordoma tissues and adjacent normal tissues were examined by RT-qPCR. The level of MMP16 in chordoma tissues was significantly higher than that in adjacent normal tissues.* ***B****) The expression of MMP16 in chordoma cell lines (UCH1 and UCH2) was significantly increased compared to that in normal cell line Fibro. ** $P < 0.01$.*

to adjacent tissues (P<0.05, Fig. 3C). MMP16 was negatively correlated with miR-31-5p expression in chordoma tissues (P<0.05, Fig. 3D). It was also found that MMP16 mRNA and protein expression was significantly suppressed by miR-31-5p mimics and promoted by miR-31-5p inhibitor in UCH1 cells (Fig. 3E). These results indicate that MMP16 is a direct target of miR-31-5p and negatively regulates miR-31-5p expression in chordoma.

To verify the interaction between MMP16 and miR-31-5p in chordoma, MMP16 vector and miR-31-5p mimics were transfected into UCH1 cells. RT-qPCR showed that the expression of MMP16 was significantly increased by MMP16 vector (P<0.05). But miR-31-5p mimics reduced the upregulation of MMP16 induced by its vector (Fig. 4A). Functionally, upregulation of MMP16 promoted cell proliferation in chordoma. And overexpression of miR-31-5p weakened the promoting effect of MMP16 on cell proliferation (Fig. 4B). Similarly, MMP16 overexpression also promoted chordoma cell invasion. And the promoting effect of MMP16 on cell invasion was impaired by miR-31-5p mimics in UCH1 cells (Fig. 4 C, D).

DISCUSSION

Due to the complex anatomical location, tumor size and large amount of hemorrhage during operation, it is very difficult to completely remove chordoma through surgery. Efforts have been made to clarify the mechanisms underlying the regulation

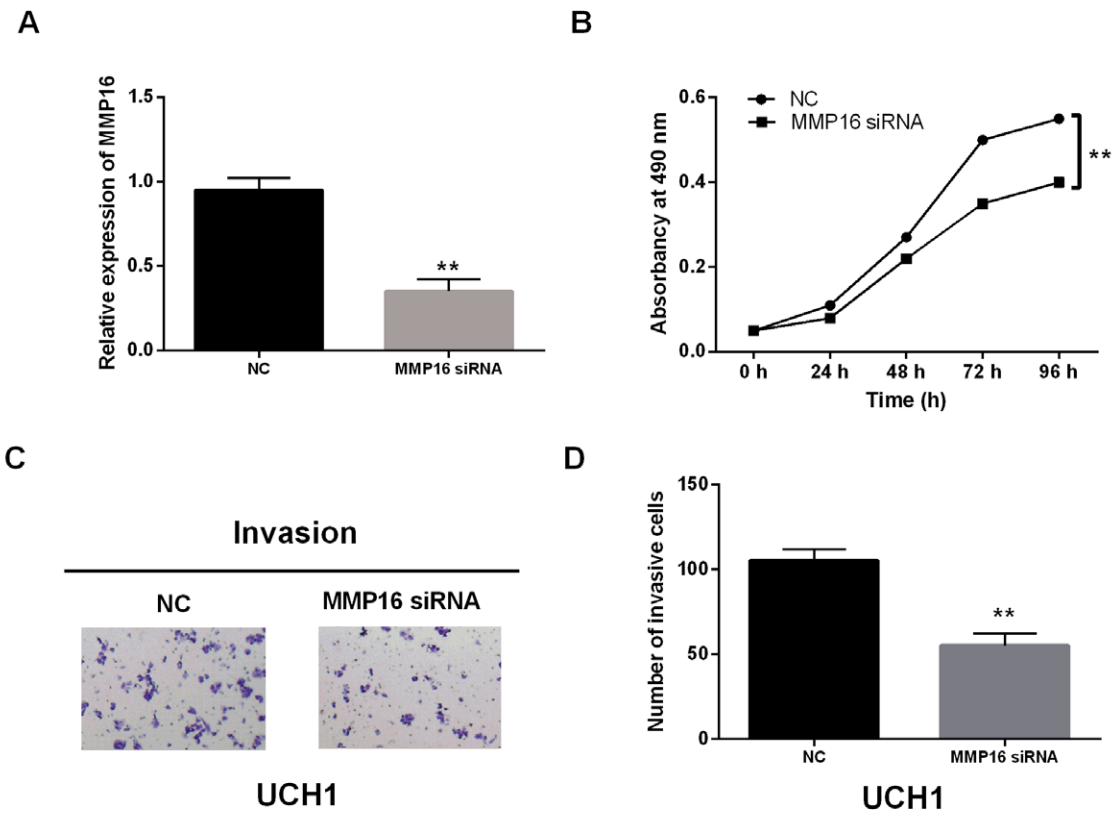


Fig. 2. Knockdown of MMP16 inhibits chordoma cell proliferation and invasion. **A**) Relative expression of MMP16 in UCH1 cells after transfection with MMP16 siRNA was significantly reduced compared to normal control. **B**) Cell proliferation in UCH1 cells with MMP16 siRNA was significantly decreased compared to normal control. **C, D**) *Cell invasion in UCH1 cells with MMP16 siRNA was significantly inhibited compared to normal control. ** P <0.01*

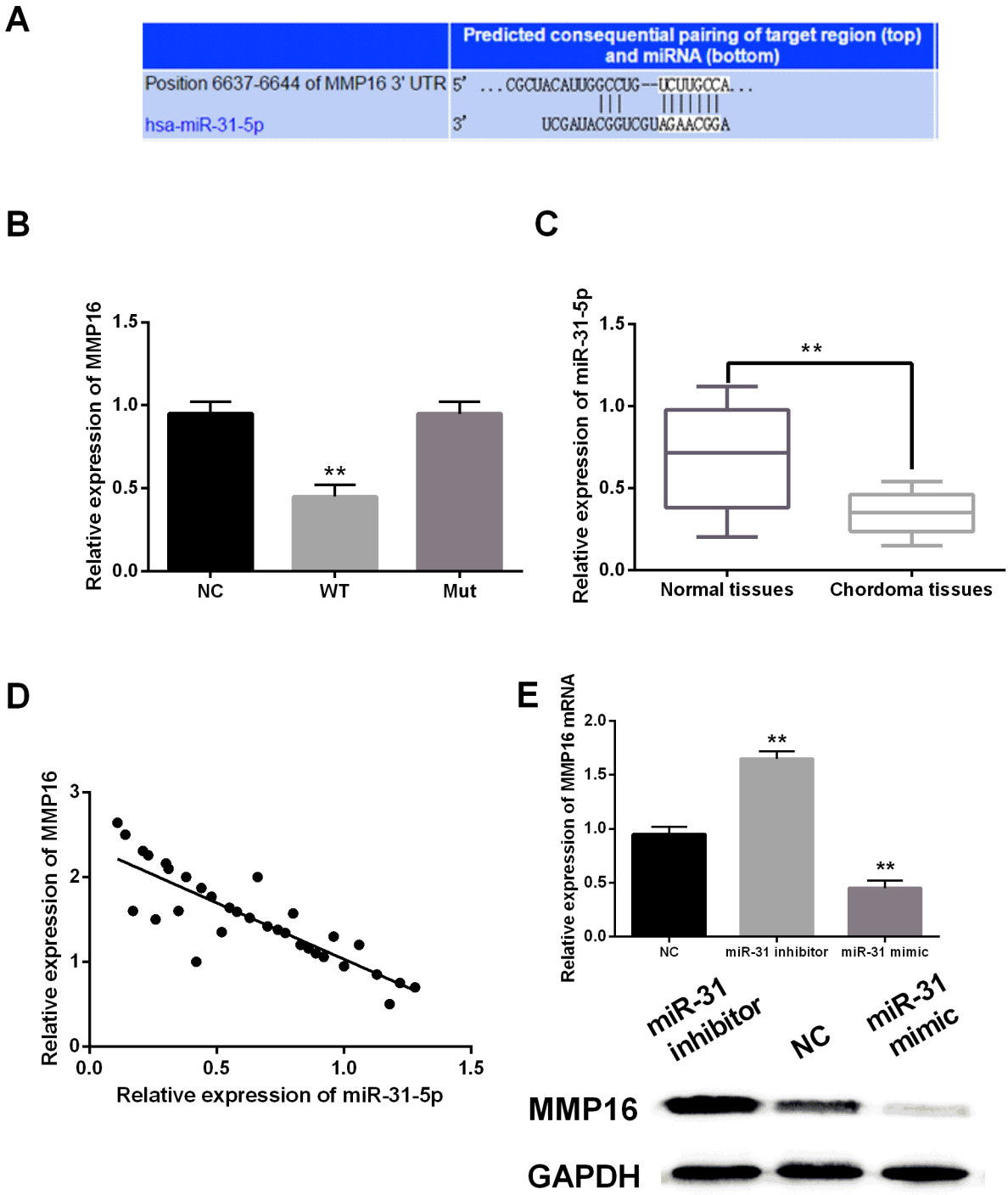


Fig. 3. *MMP16 negatively regulates miR-31-5p expression in chordoma.* ***A****) The binding sites between miR-31-5p and MMP16.* ***B****) Luciferase assay showed inhibitory role of miR-31-5p on MMP16 expression.* ***C****) The level of miR-31-5p in 33 pairs of chordoma tissues was significantly reduced compared to adjacent normal tissues examined by RT-qPCR.* ***D****) MMP16 negatively regulates miR-31-5p expression in chordoma tissues.* ***E****) The expression of MMP16 in UCH1 cells transfected with miR-31-5p mimics or inhibitor was measured. The level of MMP was upregulated as the expression of miR-31-5p was inhibited but suppressed as miR-31-5p was overexpressed. ** $P < 0.01$.*

Table I. *Correlation between MMP16 and clinic pathological characteristics expression in chordoma*

Characteristics	Total (n)	MMP16 expression		P-value
		Low(n=11)	High(n=22)	
Age				0.1814
≥ 50	19	7	12	
<50	14	4	10	
Tumor size (cm)				0.8026
≥ 5	17	6	11	
<5	16	5	11	
Gender				0.0522
Male	21	7	13	
Female	13	4	9	
stage				0.0009[a]
1A + 1B	22	5	17	
2A + 2B + 3	11	6	5	
Tumor location				0.1814
Sacral vertebra	19	5	14	
Cervical or thoracic vertebra	14	6	8	

Statistical analyses were performed by the χ2 test.
[a]*Indicates statistical significance. Statistical significance was defined as a P < 0.05.*

of MMP16 in chordoma in this study. MMP16 is a member of matrix metalloproteinases (MMPs), which is closely associated with the proliferation, invasion and metastasis in tumors (8). MMP16 downregulation also significantly suppressed cell proliferation and invasion in gastric cancer (9). The frequent upregulation of MMP16 expression in all kinds of human cancers emphasizes its potential as a novel therapeutic target for chordoma. In this study, MMP16 was found to regulate the progression of chordoma by binding to miR-31-5p, and MMP16 was negatively correlated with miR-31-5p expression in chordoma tissues. Previous studies have shown that miR-31-5p was downregulated in gastric cancer (10) and colorectal cancer (11). We also found that overexpression of miR-31-5p weakened the promoting effect of MMP16 on cell proliferation and invasion in chordoma which indicates that overexpression of miR-31-5p may inhibit cell proliferation and invasion in chordoma,

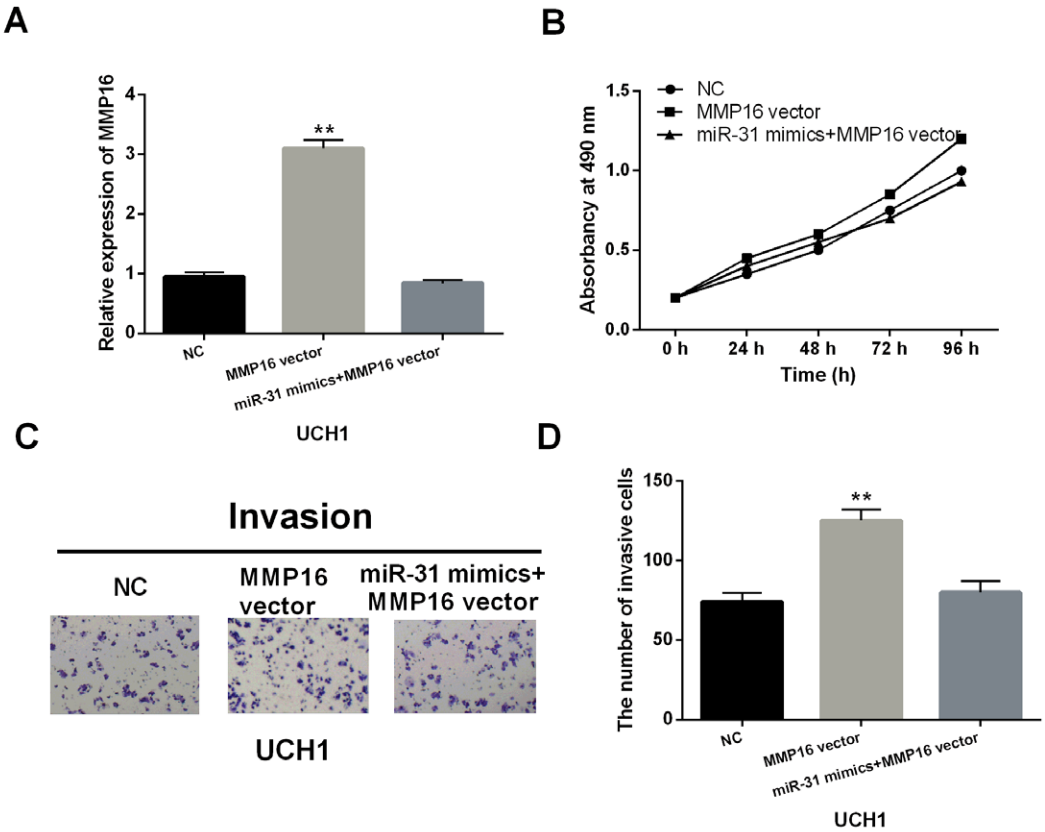


Fig. 4. *MMP16 regulates cell proliferation and invasion in chordoma by interacting with miR-31-5p.* ***A****) Expression levels of MMP16 were examined by qRT-PCR in UCH1 cells with miR-31-5p mimics+MMP16 vector.* ***B****) Cell proliferation in UCH1 cells with miR-31-5p mimics+MMP16 vector.* ***C, D****) Cell invasion in UCH1 cells with miR-31-5p mimics+MMP16 vector. The overexpression of miR-31-5p mimics retarded the expression of MMP16 as well as the promoting role of MMP16 on chordoma cell proliferation and invasion. ** P<0.01.*

which is in line with previous finding that miR-31 has been reported to inhibit cell migration and invasion in triple negative breast cancer and hepatocellular carcinoma (12). The novelties of this study is that miR-31/MMP16 axis can suppress the development of chordoma, however, the limitation still exists that the clinical function requires further validation by using an animal model.

In conclusion, this study demonstrates that MMP16 is upregulated in chordoma tissues and cells. Moreover, MMP16 promotes cell proliferation and invasion in chordoma by downregulating miR-31-5p. Therefore, the miR-31/MMP16 axis may provide new diagnostic and therapeutic targets for the treatment of chordoma in the future.

REFERENCES

1. Salisbury JR. Embryology and pathology of the human notochord. Ann Pathol 2001; 21:479-88.
2. Bettegowda C, Yip S, Lo SL, et al. Spinal column chordoma: prognostic significance of clinical variables and T (brachyury) gene SNP rs2305089 for local recurrence and overall survival. Neuro Oncol 2017; 19:405-13.
3. Nakada M, Nakamura H, Ikeda E, et al. Expression and tissue localization of membrane-type 1, 2, and 3 matrix metalloproteinases in human astrocytic tumors. Am J Pathol 1999; 154:417-28.
4. Lowy AM, Clements WM, Bishop J, et al. beta-Catenin/Wnt signaling regulates expression of the

membrane type 3 matrix metalloproteinase in gastric cancer. Cancer Res 2006; 66:4734-41.
5. Arai I, Nagano H, Kondo M, et al. Overexpression of MT3-MMP in hepatocellular carcinoma correlates with capsular invasion. Hepatogastroenterology 2007; 54:167-71.
6. Ohnishi Y, Tajima S, Ishibashi A. Coordinate expression of membrane type-matrix metalloproteinases-2 and 3 (MT2-MMP and MT3-MMP) and matrix metalloproteinase-2 (MMP-2) in primary and metastatic melanoma cells. Eur J Dermatol 2001; 11:420-23.
7. Wang H, Li XT, Wu C, et al. miR-132 can inhibit glioma cells invasion and migration by target MMP16 in vitro. Onco Targets Ther 2015; 8:3211-18.
8. Stippler M, Gardner PA, Snyderman CH, Carrau RL, Prevedello DM, Kassam AB. Endoscopic endonasal approach for clival chordomas. Neurosurgery 2009; 64:268-77; discussion 77-78.
9. Cao L, Chen C, Zhu H, et al. MMP16 is a marker of poor prognosis in gastric cancer promoting proliferation and invasion. Oncotarget 2016; 7:51865-74.
10. Ruoming W, Zhen Y, Tengteng Z, Jisheng H. Tumor suppressor microRNA-31 inhibits gastric carcinogenesis by targeting Smad4 and SGPP2. Cancer Gene Ther 2015; 22:564-72.
11. Schee K, Boye K, Abrahamsen TW, Fodstad O, Flatmark K. Clinical relevance of microRNA miR-21, miR-31, miR-92a, miR-101, miR-106a and miR-145 in colorectal cancer. BMC Cancer 2012; 12:505.
12. Luo LJ, Yang F, Ding JJ, et al. MiR-31 inhibits migration and invasion by targeting SATB2 in triple negative breast cancer. Gene 2016; 594:47-58.

LETTER TO THE EDITOR

Flavonoid extract of hawthorn (*Crataegus oxyacantha* L.) fruit alleviates oxidative stress, inflammation and vascular dysfunction in L-NAME-induced hypertensive rats

Z-P. Qiu[1], L. Lin[2], N. Dai[3], J-J. Li[4], Q. Chi[4], Q-H. Liu[4], J. Zhu[4] and H-H. Zhang[1]

[1]Department of Emergency, Affiliated Qingdao Hiser Hospital of Qingdao University, Qingdao, China; [2]Department of Health Examination, Affiliated Qingdao Hiser Hospital of Qingdao University, Qingdao, China; [3]Department of General Medicine, Affiliated Qingdao Hiser Hospital of Qingdao University, Qingdao, China; [4]Department of Urology, Affiliated Qingdao Hiser Hospital of Qingdao University, Qingdao, China

Received February 23, 2020 - Accepted August 4, 29020

To the Editor,

Hypertension is a principal risk factor for cerebral stroke, cardiovascular diseases, heart disease, and arteriosclerosis (1). A recent survey has indicated that approximately one billion of the population is affected by hypertension worldwide (2). Additionally, inadequate control of hypertension greatly increases the burden of cardiovascular diseases. It is widely considered that excessive production of reactive oxygen species-induced oxidative stress plays an important role in the etiopathogenesis of hypertension (3). Excessive reactive oxygen species production is causally related to the decline of nitric oxide (NO) bioavailability. Ultimately, the endothelial function is damaged and subsequently increases blood pressure (4). Therefore, natural substances with antioxidant activity that could improve endothelial function, inhibit inflammatory cytokines, and assuage oxidative stress may be an alternative therapy for the prevention and treatment of hypertension.

Crataegus oxyacantha L. also known as "hawthorn" and its fruit are used for the treatment of blood stasis, dyspepsia, and cardiovascular diseases in China (5). Although a previous study has shown that hawthorn extract prevents high salt-induced hypertension (6), the scientific proof of antihypertensive activities of hawthorn fruit still needs to be further investigated, including the underlying molecular mechanisms and identification of its representative active ingredient having antihypertensive effects. Therefore, we investigated the effects of flavonoid extract of hawthorn (EH) on vascular dysfunction, blood pressure, and oxidative stress, as well as the potential mechanisms involved in L-NAME-evoked hypertensive rats.

Preparation and HPLC analysis of EH

The fruits of hawthorn were obtained from Xi'an (Shanxi Province, China) in October 2019. The dried fruit of hawthorn was powdered and sieved through a 100-mesh sieve. The extraction process was performed using the reflux extraction method and EH was prepared by a professional following a standard protocol. Briefly, 500 g of hawthorn powder was extracted with 5 L of 70% ethanol under reflux for 1 h. After the extract was filtered, it was concentrated under vacuum conditions at 40ºC. The concentrate was dispersed with distilled water and subsequently extracted with petroleum ether. Then, the water layer was collected and purified by the

Key words: anti-hypertensive; flavonoid; angiotensin-converting enzyme; vascular dysfunction

Corresponding Author:
Dr Huanhua Zhang,
Department of Emergency,
Affiliated Qingdao Hiser Hospital,
of Qingdao University, Qingdao,
Shandong 266000, P.R. China
e-mail: zhanghh0215@163.com

0393-974X (2020)
Copyright © by BIOLIFE, s.a.s.
This publication and/or article is for individual use only and may not be further reproduced without written permission from the copyright holder.
Unauthorized reproduction may result in financial and other penalties
DISCLOSURE: ALL AUTHORS REPORT NO CONFLICTS OF INTEREST RELEVANT TO THIS ARTICLE.

D101 macroporous resin column. After the water layer was added to the column for 12 h, the column was eluted with distilled water and 95% ethanol sequentially. The ethanol elution was collected and concentrated under vacuum condition.

Then, the EH was obtained by the freeze-dried method. The flavonoids constituent of EH was quantified by high-performance liquid chromatography (HPLC) using a Shimadzu LC-20AT system (Tokyo, Japan). Flavonoid constituents were separated by the Agilent ZORBAX SB-C18 column (150 mm × 4.6 mm, 5 μm). Gradient elution was performed by a mixture of acetonitrile (A) and 0.1% phosphoric acid (B). The flow rate was 0.8 mL/min and the detection wavelength was set at 280 nm. The mobile phase was set by a linear gradient from 5 to 35% A between 0 and 20 min and subsequently kept at 35% A between 20 and 30 min.

Animals and experimental protocol

Forty 6-8-week-old Male Wistar rats (weighing 180-210 g) were obtained from the Experimental Animal Center of Guangdong province. Animals were housed in a temperature- and humidity-controlled animal laboratory under the conditions of 12 h dark-light cycle. All rats had free access to tap water and standard chow diet. Animal experiment protocols were approved by the Ethics Committee for Laboratory Animals Care and Use of Qingdao University.

Before the start of the experiments, all animals were adapted to the environment for seven days. The rats were divided into five groups (n=8 per group) as follow: normotensive control group (NT) that received deionized water; L-NAME treated group (LN) that received L-NAME (50 mg/kg/day) in deionized water for three weeks to establish hypertension model; LN + LEH (100 mg/kg); LN + HEH (200 mg/kg); LN + Captopril (5 mg/kg). All the treatments were intragastrically administered daily for 3 weeks. The dose of EH was based on a previous study (7), as well as results from our preliminary research which indicated that EH (100 and 200 mg/kg) caused a decline in systolic blood pressure (SBP).

Determination of blood pressure and heart rate

Systolic blood pressure (SBP) was assayed weekly by ALC-NIBP noninvasive caudal arterial blood pressure system (Columbus instrument, Model NIBP-8) in conscious rats. At least 8-10 cycles of inflation and deflation were performed, and values of SBP, mean arterial blood pressure (MAP), diastolic blood pressure (DBP), and heart rate were recorded. At the end of the experiment, the rats were anesthetized with pentobarbital sodium (60 mg/kg) by intraperitoneal injection.

Blood and aortic tissue collection

After the last blood pressure measurement, animals were sacrificed. Blood samples were collected from the inferior vena cava of the heart and centrifuged at 4000 g for 10 min. The supernatant was collected for assays of enzyme activities and other biochemical markers. Immediately afterward, the aortic tissues were collected and washed with ice-cold normal saline for assays of protein expression.

Measurement of Ang II, NO, cGMP, ACE, oxidative stress and inflammatory markers

Serum levels of Ang II, NO, and cGMP and ACE activity were measured by commercial ELISA Kits (Jiancheng Institute of Biotechnology, Nanjing, China) according to the manufacturer's protocol. Serum levels of MDA, IL-6, and TNF-α and the activities of antioxidant enzymes (SOD, CAT, and GSH-Px) were also measured by ELISA (Kangyuanruide Biotechnology Co. Ltd. Beijing, China) according to the manufacturer's protocol.

Western blot analysis

The aortic tissue was carefully homogenized in RIPA lysis buffer and centrifuged at 8.000 × g for 10 min at 4°C, and the supernatant was collected. The protein level of supernatant was assayed by a BCA method. Then, 40 μg of protein was loaded and separated by 12% SDS-PAGE and transferred onto a PVDF membrane (Millipore, MA, USA). After the membrane was blocked with TBS containing 5% non-fat milk at room temperature for 1 h, it was incubated overnight with the following primary antibodies: anti-eNOS (Abcam, USA, 1:1.000), anti-VCAM-1 (Abcam, USA, 1:1.000), anti-NF-κB (Abcam, USA, 1:1.000) and anti-β-actin (Abcam, USA, 1:1.000). Then, the membrane was washed with TBST and

incubated with HRP-conjugated secondary antibody for 1 h. Protein signals were detected using enhanced chemiluminescence reagents (Thermo Fisher, USA).

Statistical analysis

Data statistics processing was carried out using statistical software (GraphPad Software, Inc. La Jolla, CA, USA). All data were expressed as means ± SEM. The difference among experimental groups was evaluated using one-way ANOVA followed by Tukey's multiple comparison test. A value of $P < 0.05$ was defined as statistical significance.

RESULTS

Chemical characteristics of active compounds in EH

The content of total flavonoids was quantified to standardize the EH, and our results indicated the total flavonoid content of EH was 76.88%. Moreover, five constituents were also quantified by HPLC assay and the results are presented in Table I.

Effects of EH on blood pressure during L-NAME administration

As shown in Fig. 1A, there was no obvious

Table I. *Determination of representative flavonoid compounds and total flavonoid content in the flavonoid extracts of hawthorn (EH).*

Component	Content (%)
Chlorogenic acid	10.12 ± 1.67
Epicatechin	13.68 ± 1.04
Hyperoside	3.61 ± 0.91
Procyanidin B2	13.99 ± 0.51
Isoquercitrin	4.6 ± 0.87
Total flavonoids	76.88 ± 1.5

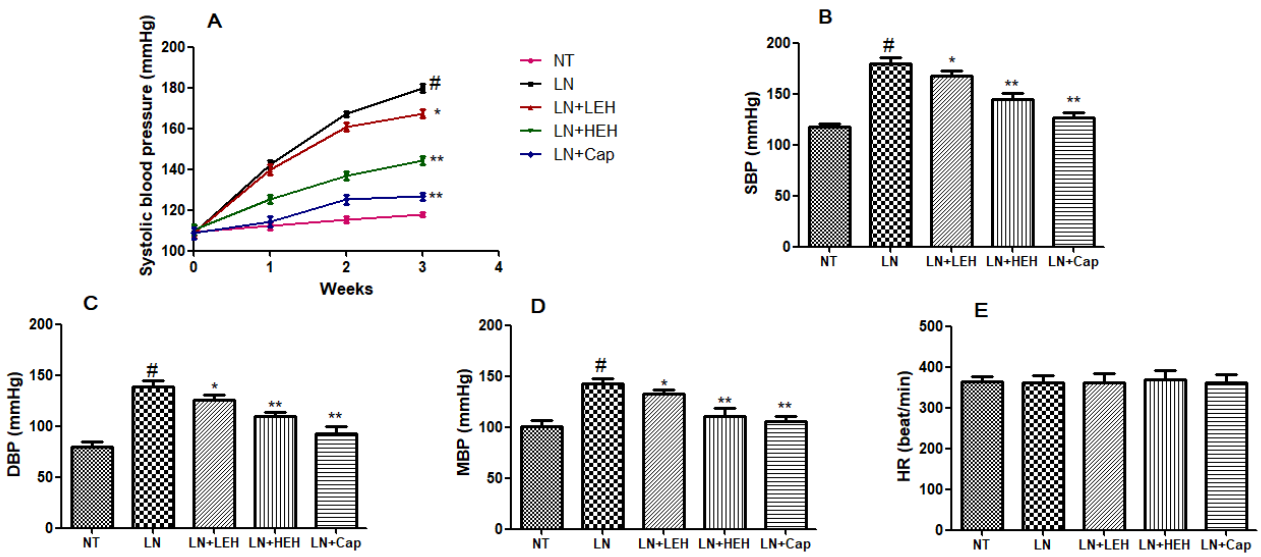


Fig. 1. *Effect of EH on blood pressure SBP (**A** and **B**); DBP (**C**); MBP (**D**); HR (**E**); in conscious rats of the experimental groups. Results are presented as mean ± SEM, n = 8 rats in each group. # P <0.01 compared with NT group; * P <0.05 compared with LN group; ** P <0.01 compared with LN group.*

difference in SBP among experimental groups at baseline (week 0). However, the daily administration of L-NAME for three weeks resulted in an obvious increase in SBP compared with that in the NT group (P <0.01). Interestingly, daily treatment with LEH or HEH for three weeks decreased SBP in L-NAME-induced hypertensive rats. Furthermore, the daily administration of L-NAME evoked hemodynamic dysfunctions, including an obvious increase in SBP, DBP, and MBP (Fig. 1 B-D). Daily treatment with LEH or HEH for three weeks decreased SBP, DBP, and MBP in L-NAME-induced hypertension rats (P < 0.01 or P < 0.05). However, there was no obvious difference in heart rate among the experimental groups (Fig. 1E).

Effects of EH on serum Ang II, ACE, NO, cGMP, and oxidative stress

As shown in Fig. 2 A-D, the serum Ang IIconcentration and ACE activity were increased in the LN group as compared to those in the NT group (P < 0.01). However, treatment with LEH or HEH for three weeks decreased Ang II concentration and ACE activity in L-NAME-induced hypertensive rats (P < 0.01). The levels of NO and cGMP were reduced in the LN group as compared to those in the NT group (P < 0.01).

However, treatment with LEH or HEH for three weeks increased NO and cGMP concentrations in L-NAME-induced hypertensive rats (P < 0.01). As shown in Fig. 2E-H, the activities of SOD, CAT, and GSH-Px decreased in the serum of rats which were administered L-NAME compared with those in the NT group (P <0.01). However, daily treatment with LEH or HEH for three weeks increased the activities of antioxidant enzymes in L-NAME-induced hypertensive rats (P <0.01 or P <0.05). Moreover, the level of MDA increased in the serum of rats which were administered L-NAME compared with those in the NT group (P < 0.01). However, daily treatment with LEH or HEH for three weeks decreased the level of MDA in L-NAME-induced hypertensive rats (P <0.01 or P <0.05).

Effects of EH on inflammatory markers, eNOS, VCAM-1 and NF-κB protein expressions

As shown in Fig. 3A-B, the increases of serum TNF-α and IL-6 were observed in the LN group compared to those in the NT group (P <0.01). However, treatment with LEH or HEH for three weeks decreased these high levels of pro-inflammatory cytokines in L-NAME-induced hypertensive rats (P <0.01 or P <0.05). The administration of L-NAME induced vascular dysfunction, as evidenced by the down-regulation of eNOS protein expression in the aorta (Fig. 3D).

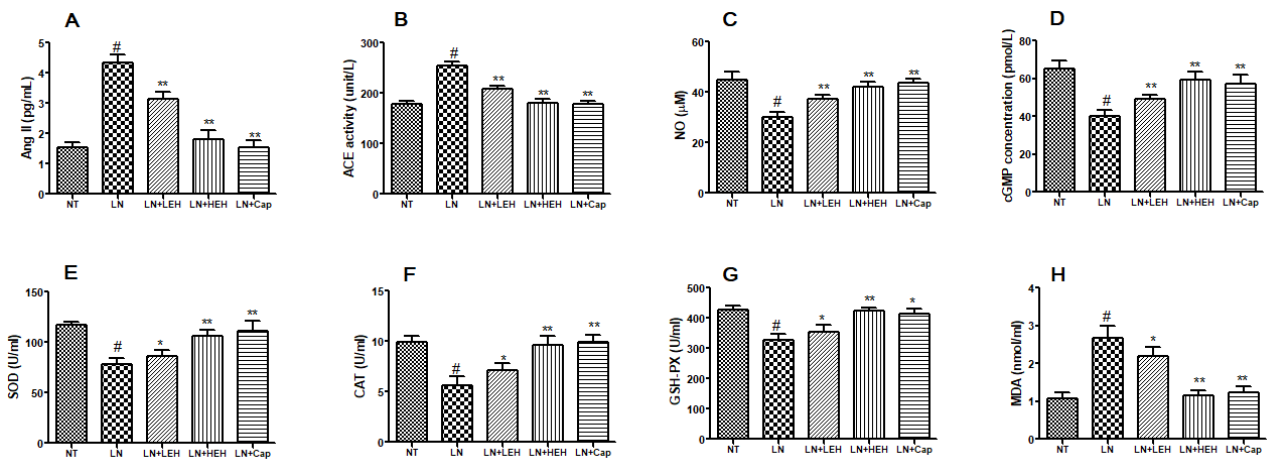


Fig. 2. *Effect of EH on Ang II concentration (**A**); ACE activity (**B**); NO concentration (**C**); cGMP concentration (**D**); SOD activity (**E**); CAT activity (**F**); GSH-PX activity (**G**); MDA concentration (**H**); in all experimental groups. Results are presented as mean ± SEM, n = 8 rats in each group. # P <0.01 compared with NT group; ** P <0.01 compared with LN group.*

Treatment with EH for three weeks increased the eNOS protein expression in L-NAME-induced hypertensive rats (P <0.01), and the administration of L-NAME also induced vascular damage and inflammation, as evidenced by the up-regulation of VCAM-1 and NF-κB protein expressions in the aorta (Fig. 3 E-F). However, the treatment decreased the VCAM-1 and NF-κB protein expression (P < 0.01).

DISCUSSION

In the present study, the HPLC analysis of EH indicated the presence of flavonoids, including chlorogenic acid, epicatechin, procyanidin B2, hyperoside, isoquercitrin, which possessed various biological activities such as anti-hypertension, anti-inflammatory, vascular protection and antioxidant. Previous reports have revealed that flavonoids are responsible for antihypertensive activities (8), which is consistent with our findings. We revealed that flavonoids are involved in the antihypertensive activities of EH.

Previous reports indicated that L-NAME evoked high blood pressure in rats involved in the suppression of eNOS protein expression, resulting in inhibition of aortic cyclic guanosine monophosphate (cGMP) content and NO formation, which in turn led to the increase of arterial blood pressure (9). In the renin-angiotensin-aldosterone system, ACE is an important protease involved in the transition of a non-vasoconstrictor Ang I to Ang □. Ang □ could regulate the secretion of aldosterone and remodel vessels, which results in cardiac dysfunction and hypertension (10). Consistent with these studies, the present findings indicated that EH increased the level of NO, and cGMP and decreased the plasma Ang □ concentration, and ACE activity in L-NAME-induced hypertensive rats. Therefore, EH, which contains a high content of flavonoid compound, might be able to inhibit the activated renin-angiotensin system.

Inflammation is implicated in the pathophysiology and progression of high blood pressure (11). Consistent with these studies, we found the increases in the serum level of TNF-α and IL-6, the overexpression of VCAM-1, and NF-κB in L-NAME-induced hypertensive rats. Moreover, these changes were restored by EH treatment for three weeks. This finding implies that EH could offer a defense against inflammation in high blood pressure.

The present findings demonstrated that EH against

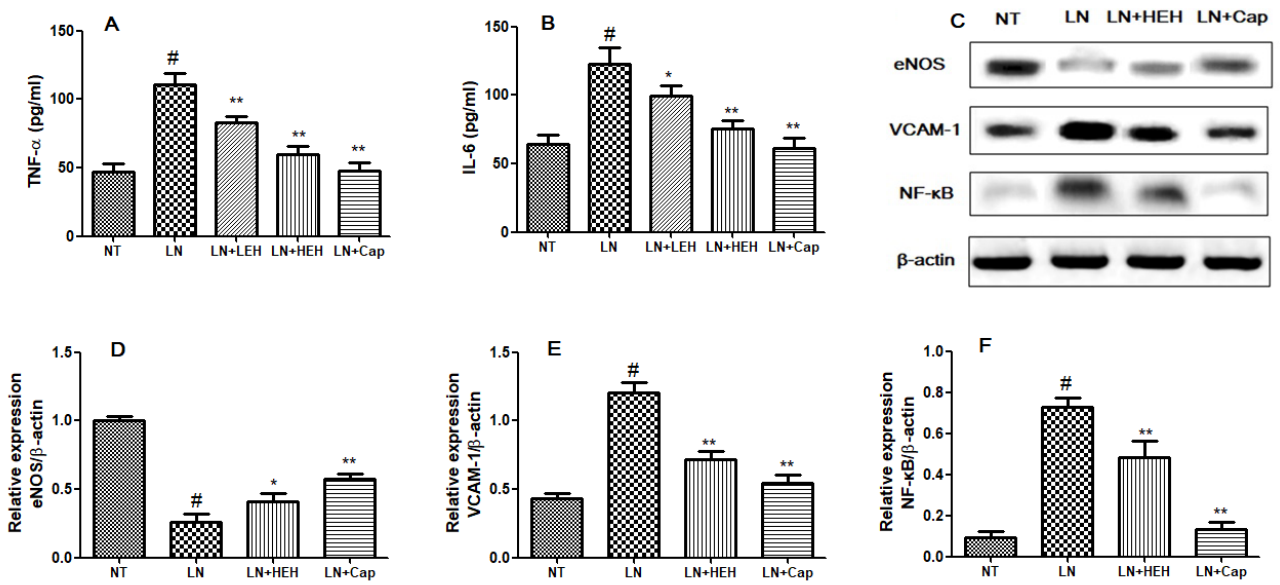


Fig. 3. *Effect of EH on TNF-α level (**A**); IL-6 level (**B**); eNOS protein expression (**D**); VCAM-1 protein expression (**E**); NF-κB protein expression (**F**); in all experimental groups. Results are presented as mean ± SEM, n = 8 rats in each group. # P <0.01 compared with NT group. * P <0.05 compared with LN group. ** P <0.01 compared with LN group.*

inflammation and oxidative stress in L-NAME evoked hypertensive rats. These activities might be associated with its high flavonoid content. Moreover, the lower blood pressure activity of EH might be related to the inhibition of VCAM-1 and NF-κB protein expression, and the activation of eNOS expression. These results imply that EH is a potential therapeutic agent for the prevention and treatment of hypertension.

REFERENCES

1. Kjeldsen SE. Hypertension and cardiovascular risk: General aspects. Pharmacol Res 2018; 129:95-9.
2. Guilbert JJ. The world health report 2002 - reducing risks, promoting healthy life. Educ Health (Abingdon) 2003; 16:230.
3. Touyz RM, Briones AM. Reactive oxygen species and vascular biology: implications in human hypertension. Hypertens Res 2011; 34:5-14.
4. Montezano AC, Dulak-Lis M, Tsiropoulou S, Harvey A, Briones AM, Touyz RM. Oxidative stress and human hypertension: vascular mechanisms, biomarkers, and novel therapies. Can J Cardiol 2015; 31:631-41.
5. Wu J, Peng W, Qin R, Zhou H. Crataegus pinnatifida: chemical constituents, pharmacology, and potential applications. Molecules 2014; 19:1685-712.
6. Zheng X, Li X, Chen M, et al. The protective role of hawthorn fruit extract against high salt-induced hypertension in Dahl salt-sensitive rats: impact on oxidative stress and metabolic patterns. Food Funct 2019; 10:849-58.
7. Rezaei-Golmisheh A, Malekinejad H, Asri-Rezaei S, Farshid AA, Akbari P. Hawthorn ethanolic extracts with triterpenoids and flavonoids exert hepatoprotective effects and suppress the hypercholesterolemia-induced oxidative stress in rats. Iran J Basic Med Sci 2015; 18:691-9.
8. Hanif K, Snehlata, Pavar MC, et al. Effect of 3-thienylalanine-ornithine-proline, new sulfur-containing angiotensin-converting enzyme inhibitor on blood pressure and oxidative stress in spontaneously hypertensive rats. J Cardiovasc Pharmacol 2009; 53:145-50.
9. Agunloye OM, Oboh G, Ademiluyi AO, et al. Cardio-protective and antioxidant properties of caffeic acid and chlorogenic acid: Mechanistic role of angiotensin converting enzyme, cholinesterase and arginase activities in cyclosporine induced hypertensive rats. Biomed Pharmacother 2019; 109:450-8.
10. Arnal JF, Warin L, Michel JB. Determinants of aortic cyclic guanosine monophosphate in hypertension induced by chronic inhibition of nitric oxide synthase. J Clin Invest 1992; 90:647-52.
11. Tong RC, Qi M, Yang QM, et al. Extract of Plantago asiatica L. Seeds ameliorates hypertension in spontaneously hypertensive rats by inhibition of angiotensin converting enzyme. Front Pharmacol 2019; 30(10):403.
12. Li JJ, Chen JL. Inflammation may be a bridge connecting hypertension and atherosclerosis. Med Hypotheses 2005; 64:925-9.

LETTER TO THE EDITOR

Clinical analysis of percutaneous vertebroplasty in the treatment of osteoporotic vertebral compression fractures

Q. Shang, S. Zhang and Y.D. Tang

Department of Orthopaedics, ShanXian Hygeia Hospital, HeZe, Shandong Province, China

Received July 23, 2020 – Accepted November 16, 2020

To the Editor,

Osteoporotic vertebral compression fracture (OVCF) is one of the common multiple diseases in orthopaedics, and the majority of the patients are elderly (1, 2). The clinical manifestation of OVCF is severe low back pain, which seriously affects the daily life of patients. In recent years, with the acceleration of population aging and the increasing incidence of OVCF, it has become one of the major diseases threatening the health of the elderly in China (3). Current treatment includes conservative and surgical treatment, however surgical treatment causes great damage to patients and leads to a slower recovery At present, most OVCF patients are treated conservatively, but as patients need to stay in bed for prolonged period with a long treatment time, they are prone to complications. Percutaneous vertebroplasty (PVP) is a minimally invasive technique in the treatment of OVCF which has many advantages, such as high safety, small trauma, rapid recovery and is a simple operation (4, 5). In order to explore the effect of PVP in OVCF patients, the clinical data of 50 OVCF patients treated with PVP in the orthopedics department of our hospital from March 2019 to January 2020 were selected for this study.

MATERIALS AND METHODS

General information

The clinical data of 50 OVCF patients treated with PVP in the orthopedics department of our hospital from March 2019 to January 2020 were selected. All the patients were examined by MRI, CT and X-ray after admission, and the specific location of vertebral compression fracture was accurately identified.

Inclusion and exclusion criteria

Inclusion criteria: patients clinically diagnosed as vertebral compression fracture without nerve compression; back and waist movement with severe pain; diagnosed as osteoporosis patients through detection by X-ray and other imaging on the bone mineral density; 59 years of age or over; injured vertebral compression degree was 25-75%.

Exclusion criteria: under 59 years of age; nerve compression; patients with pathological fractures such as infection; neurological and coagulation disorders; poor treatment compliance.

This study was approved by the ethics committee of our hospital and the consent form was signed after the patients and their families were informed of the study.

After admission, each patient's medical history was statistically analyzed, and MRI, CT and X-ray imaging were used to detect the position and layout of the vertebral arch and to judge whether the posterior wall of the vertebral body was intact. Relief was implemented according to clinical symptoms of patients such as pain. First, the patient was monitored by ECG. The patient took the lateral decubitus position, and C-arm X-ray was used to detect the pedicle and vertebral body of the patient

Key words: osteoporotic vertebral compression fracture (OVCF); application; percutaneous vertebroplasty (PVP); clinical efficacy

Corresponding Author:
Dr Y. D. Tang,
Department of Orthopaedics,
Shan Xian Hygeia Hospital,
NO.168, Southwest Hu Road, ShanXian,
HeZe, 274300, Shandong Province, China
e-mail: yundeqiang123@163.com

0393-974X (2020)
Copyright © by BIOLIFE, s.a.s.
This publication and/or article is for individual use only and may not be further reproduced without written permission from the copyright holder.
Unauthorized reproduction may result in financial and other penalties
DISCLOSURE: ALL AUTHORS REPORT NO CONFLICTS OF INTEREST RELEVANT TO THIS ARTICLE.

after anesthesia. After the puncture needle was placed in the anterior 1/3 position of the patient's vertebral body according to the direction of the pedicle, the contrast agent Omnipaque (approval number: H201600025, manufacturer: GE Healthcare Ireland Limited) was injected to complete the venography. The patients were observed for leakage of contrast media or not and no development of drainage veins. The bone cement was injected into the vertebral body. After the cement reached the posterior vertebral border of the patient, the injection was completed and then the needle was removed. The bone cement condition in the vertebral body should be monitored all the time during the injection, which should be stopped immediately if there are any adverse conditions such as bone cement leakage.

The patient's condition was observed for 3 days after surgery, and antibiotics were used to prevent infection. After 3 days, the patient was instructed to get out of bed for simple exercise. After 90 days, the patient's condition was again observed.

Evaluation indexes

The surgical success rate and the amount of bone cement injection were analyzed. Before, 3 days and 90 days after surgery, CT was used to detect the vertebral midline height, anterior vertebral height, Cobb angle of kyphosis and adverse reactions including infection, cement leakage, other vertebral fractures. The pain level and motor function were assessed by visual analogue scale (VAS) and Oswestry Disability Index (ODI) scores, respectively.

Statistical processing

In this study, the research data were processed and analyzed by the data software SPSS20.0. The measurement data were measured by *t*-test, expressed by ($\bar{x}\pm s$) and the count data were tested by χ^2, expressed by n (%). The difference was statistically significant when $p < 0.05$.

RESULTS

General clinical data of patients

Among the 50 patients, there were 28 females and 22 males, aged 59-85 years (average 72.45±4.48 years). The medical history was 7-13 weeks with an average history of (9.33±2.56) weeks. The injured vertebral segments of the patients were divided into 11 cases of L1, 5 cases of L2, 5 cases of L3, 3 cases of L4, 1 case of T5, 1 case of T6, 1 case of T8, 1 case of T10, 10 cases of T11 and 12 cases of T12 (Table I and Fig. 1).

Surgical success rate and amount of bone cement injection

The surgical success rate was 100% in 50 patients. The amount of bone cement injected into the patients was 4.21-7.63 ml with an average amount of (4.52±0.87) ml. The bone cement was found to be evenly distributed in the vertebral body of all patients through X-ray examination. Cement leakage occurred in 7 out of 50 patients during the operation with a cement leakage rate of 14%, including 4 cases of intervertebral space leakage, 2 cases of prevertebral soft tissue leakage, and 1 case of paravertebral vein leakage. No patients had complications such as infection, spinal cord nerve compression, pulmonary infarction and cardio-cerebrovascular diseases (Table II).

In all patients, there were significant differences in injured vertebral midline height, anterior vertebral height and Cobb angle after surgery compared to before surgery ($P<0.05$; Fig. 2.).

Table I. G*eneral clinical data of patients*

Number of patients	Gender ratio	Age	Average medical history (weeks)
50	Male (22), Female (28)	72.45±4.48	9.33±2.56

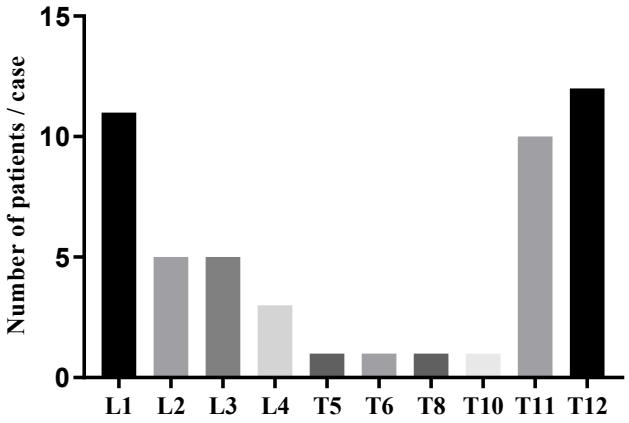


Fig. 1. *Distribution of injured vertebral segments. The ordinate represents the number of patient/cases, and the abscissa represents distribution of injured vertebral segments. The majority of the patients were at L1, T11 and T12 (unit: case).*

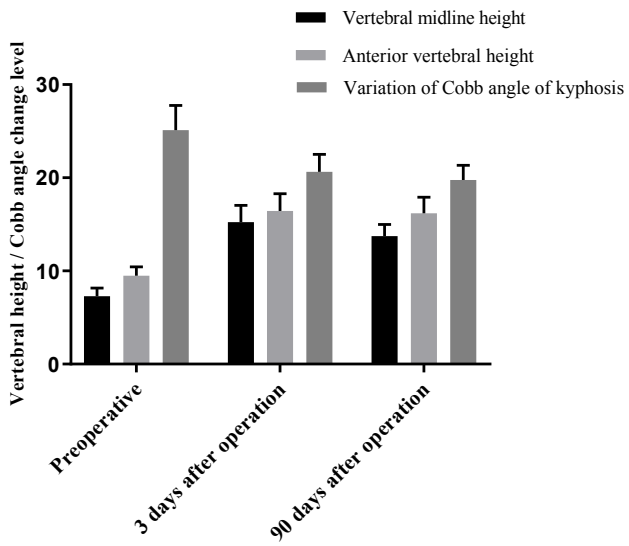


Fig. 2. *Comparison of changes in vertebral body height/ Cobb angle before and after operation. The ordinate represents the vertebral height/Cobb angle change level. and the abscissa represents preoperative, 3 days after surgery and 90 days after surgery. The black column chart shows the vertebral midline height, the gray-white column chart shows the anterior vertebral height, and the gray column chart shows the variation of Cobb angle of kyphosis. There were significant differences in the injured vertebral midline height, anterior vertebral height and the variation of Cobb angle of kyphosis before surgery compared to after surgery (3 days and 90 days after surgery). (Unit: mm and °)*

In all patients, there were significant changes in the VAS and ODI scores after surgery compared to before surgery ($P<0.05$; Fig. 3).

DISCUSSION

The causes of osteoporotic fracture are diverse, and the spine is the site of OVCF (6). OVCF has become one of the second largest diseases affecting the health of the elderly only after cardio-cerebrovascular diseases (7, 8). There are two treatment methods for OVCF nowadays. One is conservative treatment, which is mainly to improve the quality of life, while some patients who need to stay in bed for a long time are prone to complications such as lower limb venous thrombosis and bedsores (9). The second is surgical treatment where percutaneous vertebroplasty (PVP) is the current standard surgical method (10).

PVP has many advantages in operation time, rapid recovery, prognosis and analgesic effect (11). This study aimed to explore the clinical effect of PVP in OVCF. The results showed that the surgical success rate was 100% in 50 patients, and cement leakage

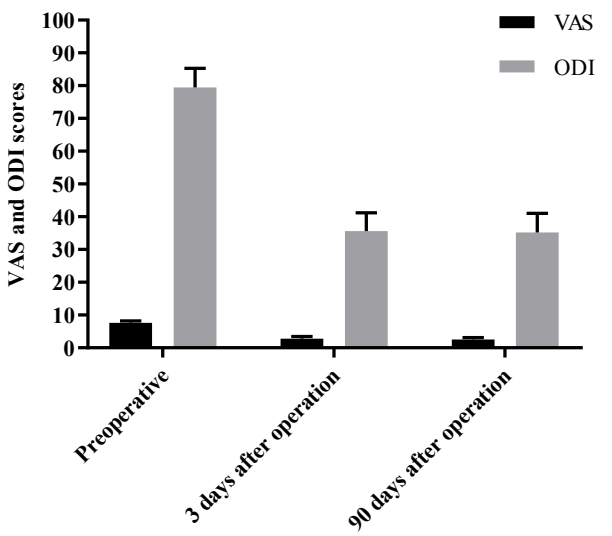


Fig. 3. *Changes in VAS and ODI scores before and after surgery. The ordinate represents VAS and ODI scores, and the abscissa represents preoperative, 3 days, and 90 days after surgery. The black column chart shows VAS scores and the gray column chart shows the ODI scores. There were significant differences in the VAS and ODI scores after surgery (3 days and 90 days after) compared to before surgery. (Unit: point)*

Table II. *Surgical success rate and amount of bone cement injection*

Bone cement injection (mL)	Intervertebral space leakage	Prevertebral soft tissue leakage	Paravertebral vein leakage	Cement leakage rate	Success ratio
4.52±0.87	4	2	1	14%	100%

occurred in 7 out of 50 patients during surgery with a cement leakage rate of 14%, including 4 cases of intervertebral space leakage, 2 cases of prevertebral soft tissue leakage, and 1 case of paravertebral vein leakage. None of the patients had complications. In all patients, there were significant differences after surgery in injured vertebral midline height, anterior vertebral height, Cobb angle of kyphosis, VAS and ODI scores compared to before surgery ($P<0.05$). This study fully demonstrated the role of PVP in reducing pain, improving motor function, correcting vertebral deformity and restoring the vertebral height in OVCF treatment, which is similar to the results of Xue et al. (12).

In summary, the application of PVP in OVCF patients can not only reduce pain and improve motor function, but also play a positive role in restoring the vertebral height and correcting deformity of the patients.

REFERENCES

1. Zhang H, Xuan J, Chen TH, et al. Projection of the most anterior line of the spinal canal on lateral radiograph: an anatomic study for percutaneous kyphoplasty and percutaneous vertebroplasty. J Invest Surg 2020; 33(2):134-40.
2. Cheng Y, Liu Y. Percutaneous curved vertebroplasty in the treatment of thoracolumbar osteoporotic vertebral compression fractures. J Int Med Res 2019; 47(6):2424-33.
3. Gao JC, Mi SJ, Liu CL. Percutaneous vertebroplasty for the treatment of acute burst thoracolumbar fractures. Zhongguo Gu Shang 2008; 21(1):7-9.
4. Li J, Lin J, Yang Y, Xu J, Fei Q. 3-Dimensional printing guide template assisted percutaneous vertebroplasty: Technical note. J Clin Neurosci 2018; 52:159-64.
5. Li YX, Guo DQ, Zhang SC, et al. Risk factor analysis for re-collapse of cemented vertebrae after percutaneous vertebroplasty (PVP) or percutaneous kyphoplasty (PKP). Int Orthop 2018; 42(9):2131-39.
6. Stella PYW, Chi CM. Update on symptomatic treatment of acute vertebral compression fracture. JCRI 2019; 19(02):47-52.
7. Zhou T, Lin H, Wang H, Chen X, He F. Comparative study on the biomechanics between improved PVP and traditional PKP in the treatment of vertebral peripheral wall damage-type OVCF. Exp Ther Med 2017; 14(1):575-80.
8. Xu K, Li YL, Song F, Liu HW, Yang HD, Xiao SH. Influence of the distribution of bone cement along the fracture line on the curative effect of vertebral augmentation. J Int Med Res. 2019; 47(9):4505-13.
9. Alpantaki K, Dohm M, Korovessis P, Hadjipavlou AG. Surgical options for osteoporotic vertebral compression fractures complicated with spinal deformity and neurologic deficit. Injury 2018; 49(2):261-71.
10. Ahn TK, Kim JO, Kim HW, et al. 3'-UTR Polymorphisms of MTHFR and TS associated with osteoporotic vertebral compression fracture susceptibility in postmenopausal women. Int J Mol Sci 2018; 19(3):824.
11. Lee CK, Choi SK, Shin DA, et al. Parkinson's disease and the risk of osteoporotic vertebral compression fracture: a nationwide population-based study. Osteoporos Int 2018; 29(5):1117-24.
12. Xu J, Lin J, Li J, Yang Y, Fei Q. "targeted percutaneous vertebroplasty" versus traditional percutaneous vertebroplasty for osteoporotic vertebral compression fracture. Surg Innov 2019; 26(5):551-59.

LETTER TO THE EDITOR

Terminal differentiation-inducing non-protein coding RNA acted as a competitive endogenous RNA by sponging miR-31 and promoted nasopharyngeal carcinoma cell proliferation and invasion

Y-F. He[1], N. Zhao[1], M-Y. Chen[2] and L. Wei[3]

[1]Department of Otolaryngology, Weifang Yidu Central Hospital, Weifang, Shandong, China;
[2]Department of General Surgery, Weifang Yidu Central Hospital, Weifang, Shandong, China;
[3]Department of Respiratory Medicine, Zibo Central Hospital, Zibo, Shandong, China

Received August 6, 2020 – Accepted November 17, 2020

To the Editor,

Nasopharyngeal carcinoma (NPC) is a cancer that is easy to metastasize, and is one of the most common head and neck epithelial cancers in South China and Southeast Asia (1). With the progress of intensity-modulated radiotherapy, and combined radiotherapy and chemotherapy, the prognosis of patients with NPC has been significantly improved (2), however, the metastasis rate is still high. Therefore, it is crucial to assess the metastatic potential of NPC for determining prognosis and treatment.

Long non-coding RNAs (lncRNAs) are a subset of ncRNAs, over 200 nt in length and involved in a large number of normal physiological and pathological processes (3). For example, knocking down of terminal differentiation-inducing non-protein coding RNA (TINCR) suppresses the proliferation and invasion in hepatocellular carcinoma via the miR-218-5p/DEAD-box helicase 5 (DDX5) axis (4). TINCR sponges miR-302 to upregulate cyclin D1 in cervical squamous cell carcinoma (CSCC) (5).

LncRNA is involved in certain processes, which may communicate and regulate with protein-coding genes through competing binding to miRNA, thus becoming competitive endogenous RNA (ceRNA) (6). For instance, lncRNA-TINCR acts as a competitive endogenous RNA (ceRNA) and regulates the migration of rat mesenchymal stem cells (rMSCs) by sponging miR-761, thereby modulating the role of Wnt2 (7).

MATERIALS AND METHODS

Tissue specimens

From February 2016 to December 2018, 50 patients with NPC underwent surgery at Weifang Yidu Central Hospital, and pairs of NPC tissues and adjacent non-tumor tissues were obtained. The tissue samples were removed surgically, immediately frozen in liquid nitrogen at -196°C, and preserved at -80°C. The study was approved by the Ethics Committee of Weifang Yidu Central Hospital, and all participants provided written informed consents.

Cell lines and culture

Human NPC cell line 5-8F and an immortalized normal nasopharyngeal epithelial cell line NP69 were purchased from the Institute of Biochemistry and Cell Biology of the Chinese Academy of Sciences (Shanghai, China). Cells were cultured in Dulbecco's Modified Eagle Medium (DMEM; HyClone, South Logan, UT, USA) supplemented with 10% fetal bovine serum (FBS; Gibco, Rockville, MD, USA) at 37°C in a humidified atmosphere with 5% CO2.

Key words: TINCR; miR-31; nasopharyngeal carcinoma; ceRNA; invasion

Corresponding Author:
Dr Lei Wei,
Department of Respiratory Medicine,
Zibo Central Hospital, No.54, Gongqingtuan West Road,
Zhangdian District, Zibo City, Shandong, China
Tel.: +86 13953373558
e-mail: xurtife1426@163.com

0393-974X (2020)
Copyright © by BIOLIFE, s.a.s.
This publication and/or article is for individual use only and may not be further reproduced without written permission from the copyright holder.
Unauthorized reproduction may result in financial and other penalties
DISCLOSURE: ALL AUTHORS REPORT NO CONFLICTS OF INTEREST RELEVANT TO THIS ARTICLE.

Cell transfection

Small interfering RNA directed against TINCR (siRNA-TINCR) was provided by GenePharma (Shanghai, China). The cells were seeded into 6-well plates with 4×105 cells per well, so that the cells were confluent to 70%. The transfection reagent was diluted to 3 μL/L using the serum-free medium and incubated at 37°C for 20 min. Cell transfection was performed with Lipofectamine 2000 (Invitrogen, Carlsbad, CA, USA).

RNA extraction and RT-qPCR

Total RNAs were extracted from tissues and cell lines using TRIzol reagent (Invitrogen, Carlsbad, CA, USA). The total RNAs were reverse transcribed to complementary deoxyribose nucleic acids (cDNAs) through reverse Transcription Kit (TaKaRa Biotechnology, Dalian, China). RT-qPCR was performed on an ABI 7300 machine (Applied Biosystems, Foster City, California, USA) using the SYBR Green PCR Master mix (Thermo Fisher Scientific, Beijing, China). Thermocycling conditions were as follows: 40 cycles of 30 s at 95°C, 5 s at 95°C and 35 s at 60°C. The relative expression of TINCR and miR-31 was calculated using the $2^{-\Delta\Delta Ct}$ method. The primer sequences for PCR of TINcR cDNA were as follows: TINCR Forward 5'-CCCAAGCTTGGTCTGGGCTCCCAGGTGGACC-3' and Reverse 5'-AGCGATATC CTATAGTTGTTT CAAACATGTAATCTT-3'; GAPDH Forward 5'-TTCACCACCATGGAGAAGGC-3' and Reverse 5'-GGCATGGACTGTGGTCATGA-3'; miR-31 Forward 5'-CAGCTATGCCAGCATCTTGCCT-3' and Reverse 5'-ATATGGAACGCTTCACGAATT-3; U6 Forward, 5'-CTCGCTTCGGCAGCACA-3' and Reverse 5'-AACGCTTCACGAATTTGCGT-3'.

Cell proliferation assay

Cell proliferation was calculated by using the Cell Counting Kit-8 (CCK-8; Beyotime, Beijing, China) assay every 24 h. The 5-8F cells (3000 cells per well) were cultured in 96-well plates for 1, 2, 3 and 4 days, respectively. Subsequently, 10 μl of CCK-8 reagent was added to each well, and the cells were incubated in the 96-well plate at 37°C for 1 h, and then the absorbance at 450 nm was measured using the Spectrophotometer (Thermo Scientific, Waltham, MA, USA).

Transwell assay

2 × 105 cells from each group were suspended in 100 μL of serum-free DMEM medium, and then placed in the upper chamber of an 8-μm culture insert (Corning, NY, USA) pre-coated with 50 μg Matrigel (BD Biosciences, Franklin Lakes, NJ, USA). The medium containing 10% FBS was then added to the lower chamber. After 24 h of incubation at 37°C, non-invaded cells were removed from the membranes. Subsequently, the invaded cells were fixed with 4% paraformaldehyde for 10 min, and then stained with 0.5% crystal violet for 30 min. After rinsing with tap water, the cells were counted under an inverted microscope (Olympus Corporation, Japan).

Dual luciferase reporter gene detection

The target fragments of wild type and mutant TINCR were integrated into pGL3 vector (Promega, Madison, Wisconsin, USA) to construct pGL3-TINCR-wild-type and pGL3-TINCR-mutant reporter vectors. The wild type TINCR or the mutant TINCR and the miR-31 mimetics or negative controls were co-transfected into 5-8F cells. After transfecting for 48 h, the luciferase activity of the cells was measured using a dual luciferase reporter gene analysis system (Promega, Madison, Wisconsin, USA). The relative luciferase activity was presented as the Firefly luciferase activity normalized to that of Renilla.

Statistical analysis

The data are expressed as mean ±standard deviation (SD). The statistical analysis was performed by the Statistical Product and Service Solutions 18.0 (SPSS, Chicago, IL, USA). *Chi*-squared test, Student's *t*-test and Kaplan-Meier method were selected to perform the statistical analyses. It was considered statistically significant when $P<0.05$.

RESULTS

Expressions of TINCR and miR-31 were detected in NPC tissues and cell lines

The expression of TINCR and miR-31 in 43 pairs of NPC tissues and adjacent tissues were detected by using RT-qPCR. It was found that TINCR was overexpressed in NPC tissues compared with normal tissues ($P<0.05$) (Fig. 1A). Similarly, the expression of TINCR was also up-regulated in NPC cell line 5-8F in comparison with normal nasopharyngeal epithelial cell line NP69 ($P<0.05$) (Fig. 1B).

Overexpression of TINCR could promote the proliferation and invasion of NPC cells

Since TINCR was highly expressed in 5-8F cells, 5-8F cell was selected for the TINCR knock-down assay ($P<0.05$) (Fig. 2A). The results of CCK-8 assay indicated that knocking down of TINCR could significantly suppress the proliferation of 5-8F cells ($P<0.05$) (Fig. 2B). Transwell assay indicated that knocking down of TINCR could significantly inhibit the migration of 5-8F cells compared with the negative control ($P<0.05$) (Fig. 2C). Taken together, it could be concluded that TINCR promoted the growth and metastasis of NPC cells.

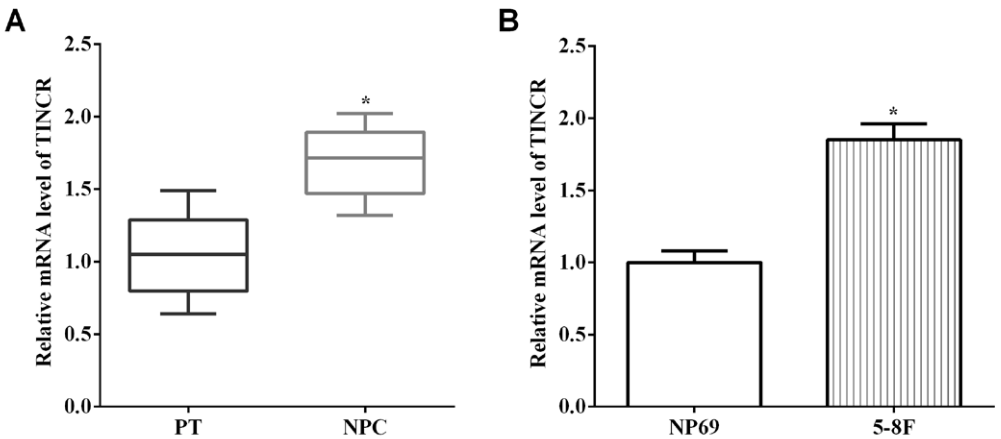


Fig. 1. *The expression of TINCR and miR-31 is observed in NPC tissues and cells.* ***A****) Compared with normal tissues, TINCR is overexpressed in NPC tissues.* ***B****) The expression of TINCR was also up-regulated in NPC cells. PT, paracancerous tissues; NPC, nasopharyngeal carcinoma.*

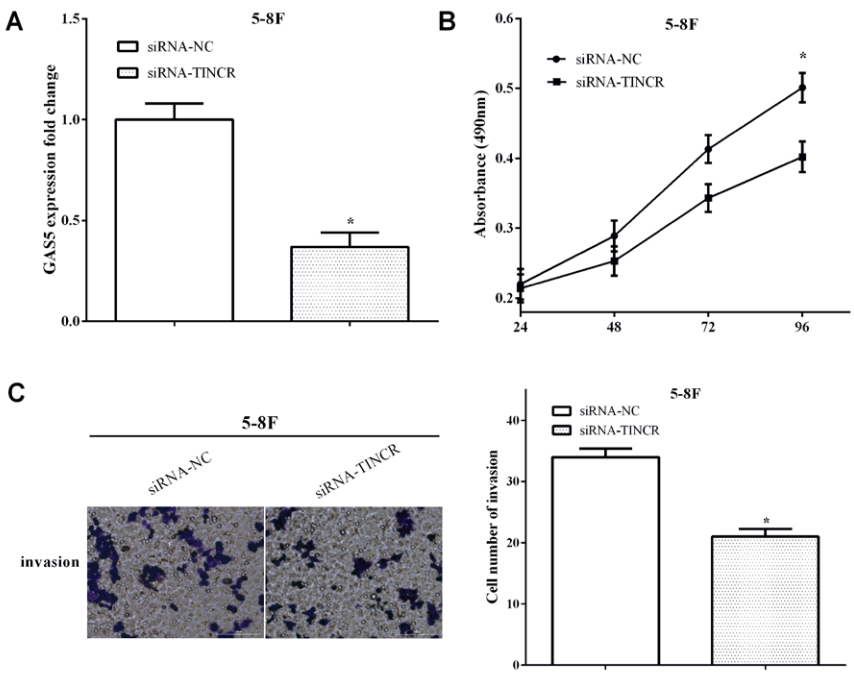


Fig. 2. *Overexpression of TINCR could promote the proliferation and invasion of NPC cells.* ***A****) The transfection efficiency of knocking down TINCR was measured using RT-qPCR.* ***B****) Knocking down of TINCR could significantly suppress the proliferation of 5-8F cells.* ***C****) Knocking down of TINCR could significantly inhibit the migration of 5-8F cells (200×magnification).*

LncRNA TINCR serves as a sponge of miR-31 to suppress its expression

In this study, downregulation of TINCR was found to promote the proliferation and invasion of NPC cells, but its underlying mechanism remains unclear. StarBase (http://www.starbase.com) was used for bioinformatics analysis, and the results showed that TINCR contained a potential target site of miR-31 (Fig. 3A). In order to further verify that TINCR can directly bind to miR-31, we performed a dual luciferase reporter gene test. The results showed that miR-31 mimic reduced the luciferase activity of wild type TINCR, but had no significant effect on the luciferase activity of the mutant TINCR ($P<0.05$) (Fig. 3B). Thus, the expression of miR-31 in tissues was detected, and it was found that the expression of miR-31 in NPC tissues was lower than that in the adjacent tissues ($P<0.05$) (Fig. 3C). After that, RT-qPCR results showed that the expression of TINCR in NPC tissue was negatively correlated with the expression of miR-31 ($P<0.05$) (Fig. 3D). These results indicated that miR-31 was a downstream target of TINCR, and its expression may be negatively regulated by TINCR.

TINCR promotes 5-8F cell proliferation and invasion via sponging miR-31

In order to explore the functions of miR-31 in NPC, the expression of miR-31 was calculated in cell lines, and miR-31 was found to be low expressed in NPC 5-8F cells compared with nasopharyngeal epithelial cell line NP69 ($P<0.05$) (Fig. 4A). The expression of miR-31 was up-regulated after knocking down TINCR in 5-8F cells ($P<0.05$) (Fig. 4B).

Combined with the above analysis, appropriate

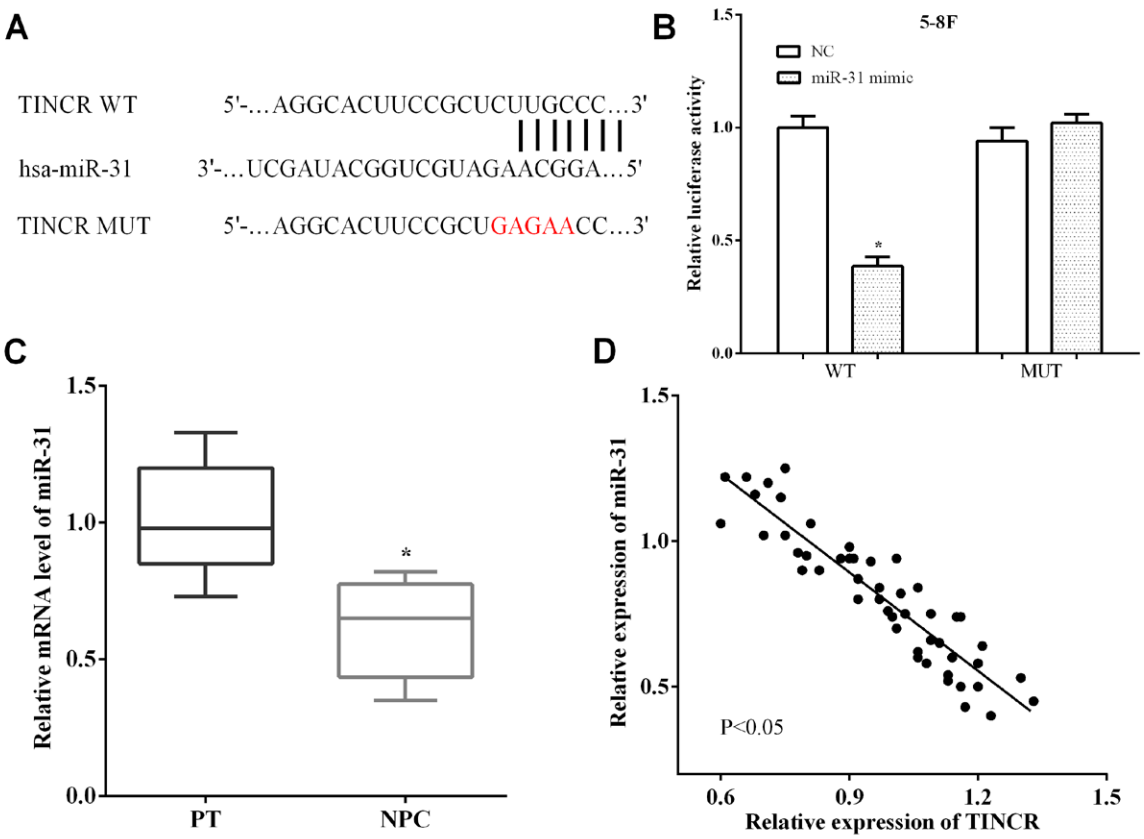


Fig. 3. *LncRNA TINCR serves as a sponge of miR-31 to suppress its expression. **A)** TINCR contained a potential target site for miR-31. **B)** The luciferase reporter gene assay was performed to verify TINCR binding to miR-31. **C)** The expression ratio of miR-31 in NPC tissues was lower than the adjacent tissues. **D)** The expression of TINCR negatively correlated with the expression of miR-31 in NPC tissues. PT, paracancerous tissues; NPC, nasopharyngeal carcinoma; WT, wild type; MUT, mutate type.*

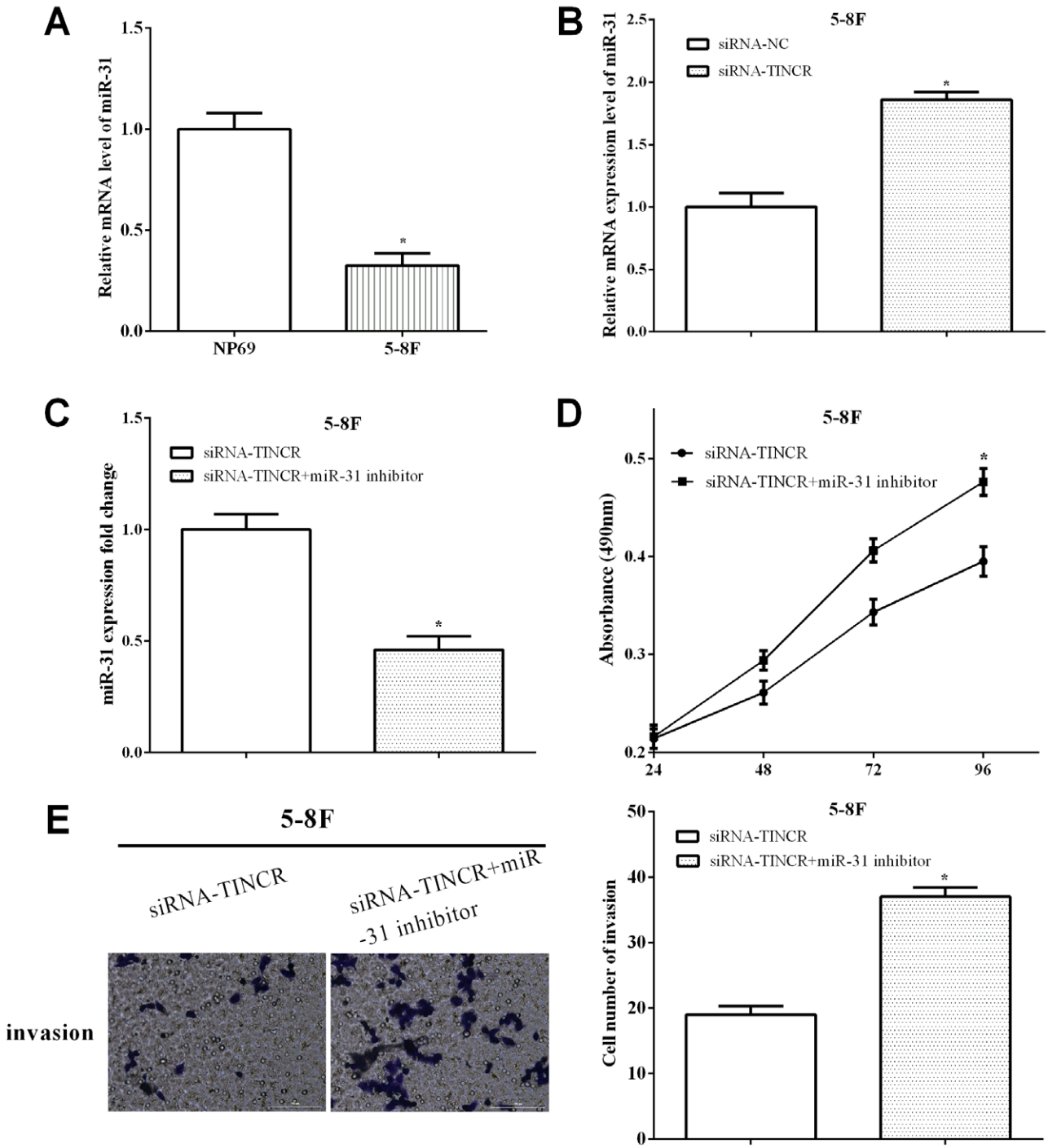


Fig. 4. *TINCR promotes 6-8F cell proliferation and invasion via sponging miR-31.* ***A)*** *MiR-31 was low expressed in NPC cell line 5-8F compared with normal NP69 cells.* ***B)*** *The expression of miR-31 was up-regulated after knocking down the expression of TINCR in 5-8F cells.* ***C)*** *The miR-31 inhibitor was transfected in TINCR low expressed 5-8F cells.* ***D)*** *Co-transfected with siRNA-TINCR and miR-31 inhibitor in 5-8F cells enhanced cell proliferation. E) miR-31 inhibitor promoted cell invasion compared to only transfected with siRNA-TINCR (200×magnification).*

rescue experiments were performed. The 5-8F cells with low expression of TINCR were transfected with the miR-31 inhibitor, and the transfection efficiency was measured by using RT-qPCR ($P<0.05$) (Fig. 4A). In addition, CCK-8 and Transwell assays were used for measuring cell proliferation and invasion. As expected, co-transfection of siRNA-TINCR and miR-31 inhibitor in 5-8F cells promoted cell proliferation ($P<0.05$) and invasion ($P<0.05$) compared to only transfected with siRNA-TINCR (Fig. 4 B, C). It was proved that overexpression of miR-31 can reverse the promotion of TINCR on the proliferation and invasion in 5-8F cells.

DISCUSSION

Previous studies have shown that TINCR has a potential role in carcinogenesis (8). However, the biological role of TINCR in various types of human tumors has not been explored. In addition, there are few reports on the expression of TINCR in nasopharyngeal carcinoma. Here, the expressions of TINCR were examined in tissues and cells, and the roles of TINCR in NPC cells were calculated. TINCR served as a tumor suppressive effect in several cancers (9). TINCR could inhibit cell proliferation and promote cell apoptosis of colorectal cancer (10). In this study, TINCR was found to be overexpressed in NPC tissues and cell lines, compared to the normal tissues and immortalized normal nasopharyngeal epithelial cells. Consistent with previous studies, we discovered that knocking down of TINCR inhibited cell proliferation and invasion.

MicroRNAs (miRNAs) are a group of small non-coding RNAs with a length of 21 to 25 nucleotides (11). MiR-31 has been confirmed as a direct target of TINCR, and it could be negatively regulated by TINCR via competitive endogenous RNA (ceRNA) mechanism (12). Consistent with the above findings, we discovered that TINCR directly binds to miR-31 and enhances the expression of miR-31 by silencing of TINCR. In addition, the expression of TINCR is negatively correlated with the expression of miR-31 in NPC tissues. MiR-31 could partially restore the functions of TINCR on cell proliferation and invasion. However, only one cell line was used for the experiment, which may have limitations. In addition, the small number of clinical cases may cause certain errors in the results.

In summary, this study indicates that knocking down TINCR inhibits cell proliferation and migration by directly targeting miR-31. This study provides novel insights into TINCR in NPC and may help improve the development of nasopharyngeal cancer treatment.

REFERENCES

1. Chua MLK, JTS Wee, EP Hui, ATC Chan. Nasopharyngeal carcinoma. Lancet (London, England) 2016; 387:1012-24.
2. Chang ET, HO Adami. The enigmatic epidemiology of nasopharyngeal carcinoma. Cancer epidemiology, biomarkers & prevention : a publication of the American Association for Cancer Research, cosponsored by the American Society of Preventive Oncology 2006; 15:1765-77.
3. Necsulea A, M Soumillon, M Warnefors, et al. The evolution of lncRNA repertoires and expression patterns in tetrapods. Nature 2014; 505:635-40.
4. Zhao H, Z Xie, G Tang, S Wei, G Chen. Knockdown of terminal differentiation induced ncRNA (TINCR) suppresses proliferation and invasion in hepatocellular carcinoma by targeting the miR-218-5p/DEAD-box helicase 5 (DDX5) axis. J Cell Physiol 2020.
5. Hou A, Y Zhang, Y Zheng, Y Fan, H Liu, X Zhou. LncRNA terminal differentiation-induced ncRNA (TINCR) sponges miR-302 to upregulate cyclin D1 in cervical squamous cell carcinoma (CSCC). Hum Cell 2019; 32:515-21.
6. Jia Z, J Peng, Z Yang, J Chen, L Liu, D Luo, P He. Long non-coding RNA TP73-AS1 promotes colorectal cancer proliferation by acting as a ceRNA for miR-103 to regulate PTEN expression. Gene 2019; 685:222-29.
7. Zheng J, Y Huang, Y Li, et al. lncRNA-TINCR Functions as a Competitive Endogenous RNA to Regulate the Migration of Mesenchymal Stem Cells by Sponging miR-761. Biomed Research Int 2020; 2020:9578730.
8. Liu Y, Y Du, X Hu, L Zhao, W Xia. Up-regulation of

ceRNA TINCR by SP1 contributes to tumorigenesis in breast cancer. BMC cancer 2018; 18:367.

9. Dong H, J Hu, K Zou, et al. Activation of LncRNA TINCR by H3K27 acetylation promotes Trastuzumab resistance and epithelial-mesenchymal transition by targeting MicroRNA-125b in breast Cancer. Mol Cancer 2019; 18:3.
10. Zhang X, J Yao, H Shi, B Gao, L Zhang. LncRNA TINCR/microRNA-107/CD36 regulates cell proliferation and apoptosis in colorectal cancer via PPAR signaling pathway based on bioinformatics analysis. Biol Chem 2019; 400:663-75.
11. Chen L, J Song, J Cui, J Hou, X Zheng, C Li, L Liu. microRNAs regulate adipocyte differentiation. Cell Biol Int 2013; 37:533-46.
12. Liu Y, Y Wang, X He, S Zhang, K Wang, H Wu, L Chen. LncRNA TINCR/miR-31-5p/C/EBP-α feedback loop modulates the adipogenic differentiation process in human adipose tissue-derived mesenchymal stem cells. Stem Cell Res 2018; 32:35-42.

LETTER TO THE EDITOR

Analysis of ultrasonic diagnostic indexes of fetuses with coarctation of aorta

X-D. Zheng[1], Y-L. Bi[2], L-M. Zhang[1], Y-G. Xing[3], X-Z. Wang[4] and Z-N. Wang[5]

[1]Department of Ultrasound, Maternity and Child Health Care of Zaozhuang, Zaozhuang, China; [2]Operation Room, The People's Hospital of Zhangqiu Area, Jinan, China; [3]Department of Ultrasound, The People's Hospital of Zhangqiu Area, Jinan, China; [4]Department of Nutrition, The People's Hospital of Zhangqiu Area, Jinan, China; [5]Special Inspection Department, Qingdao Women and Children's Hospital, Qingdao, China

Received August 23, 2020 – Accepted November 18, 2020

To the Editor,

Coarctation of the aorta (CoA) refers to aortic lumen stenosis from the innominate artery to the first intercostal artery. Aortic stenosis exists between the left subclavian artery and the ductus arteriosus among 90% of children, and 8% of the children with congenital heart malformations have aortic stenosis (1). The prognosis of CoA fetus is very poor, and the incidence of circulatory failure and death is significantly increased when the ductus arteriosus is closed, therefore it is of great importance to improve the prognosis of fetus with CoA by early diagnosis and treatment (2). Moreover, accurate prenatal diagnosis can not only improve the prognosis of CoA fetus, but also to well prepare parturients and their families. However, fetal CoA is often associated with other intracardiac malformations, and clinical diagnosis is difficult. Especially in the third trimester of pregnancy, the arteries and pulmonary arteries are widened, and the aorta is relatively narrow, leading to higher false positive diagnosis rate of coarctation (3).

In recent years, prenatal diagnosis technology of CoA has gradually improved and popularized thanks to the continuous improvement of the performance of ultrasound equipment. As a means of non-invasive diagnosis, ultrasound can directly and comprehensively display the hemodynamic information, structure of the heart and large vessels, and is of great significance for the diagnosis of the heart (4). In this study, the ultrasonic diagnostic indexes were analyzed in order to improve the accuracy of clinical diagnosis of fetuses with CoA.

MATERIALS AND METHODS

The clinical data of 122 children with suspected CoA and successful delivery in the Maternity and Child Health Care Hospital of Zaozhuang from January 2017 to January 2020 were analyzed using retrospective analysis. The maternal ages were 20-42 years, with an average of (29.23 ±5.18) years. The gestational weeks of the parturients were 21-39 weeks (average 31.18 ±4.66) weeks. Written informed consent was obtained from the parents or the legally authorized representative according to Declaration of Helsinki. This study was approved by the Ethics Committee of Maternity and Child Health Care of Zaozhuang.

Inclusion criteria: a) varying degrees of stenosis from the ascending aorta to the aortic isthmus, and the inner diameter was similar to that of the adjacent superior vena

Key words: coarctation of aorta; hemodynamics; ultrasound diagnosis

Corresponding Author:
Dr Zhenna Wang,
Special Inspection Department,
Qingdao Women and Children's Hospital,
217 Liaoyang West Road,
Shibei District, Qingdao 266000, China
e-mail: qi024x@163.com

0393-974X (2020)
Copyright © by BIOLIFE, s.a.s.
This publication and/or article is for individual use only and may not be further reproduced without written permission from the copyright holder.
Unauthorized reproduction may result in financial and other penalties
DISCLOSURE: ALL AUTHORS REPORT NO CONFLICTS OF INTEREST RELEVANT TO THIS ARTICLE.

cava; b) isthmus stenosis of aortic arch; c) the diameter ratio of pulmonary artery to aortic exceeded 1.5; d) the right ventricle was larger than the left ventricle in the four-chamber section of the heart, and the ratio of transverse diameter of the two ventricles was more than 1.3; e) the curvature of the aortic arch became smaller, stiff and abnormal; f) Singleton pregnancy; g) The data of ultrasonic examination were complete.

Exclusion criteria: a) Fetuses with intrauterine growth restriction, fetal hypoxia; b) Puerpera with complications of pregnancy-induced hypertension, gestational diabetes, and thyroid disease, etc; c) Fetuses with chromosomal abnormalities and acute extracardiac events; d) Fetuses with persistent arrhythmia.

The ultrasound parameters and flow velocity indexes of CoA fetus and normal fetus were retrospectively analyzed, and the correlation, sensitivity and specificity between each index and CoA were analyzed by ROC curve.

Ultrasonic parameters included: Z value of right ventricular diameter (RV Z); Z value of left ventricular diameter (LV Z); Right ventricular diameter/left ventricular diameter (RV/LV); Z value of main pulmonary artery diameter (MPA Z); Z value of ascending aorta diameter (AAO Z); main pulmonary artery diameter/ ascending aorta diameter (MPA/AAO); Z value of aortic isthmus (AI Z); Z value of descending aorta diameter (DA Z); Z value of ascending aorta (AO Z); aortic isthmus/ descending aorta diameter (AI/DA); aortic isthmus/aortic diameter(AI/AO); Z value=(actual data-average data)/ standard deviation.

Ultrasonic velocity parameters included: pulmonary artery velocity/aortic velocity (PAv/AOv); systolic velocity of aortic arch/Systolic velocity of ductus arteriosus (ARvs/ DAvs); diastolic velocity of aortic arch/diastolic velocity of ductus arteriosus (ARvd/DAvd); systolic velocity of middle cerebral artery/systolic velocity of internal segment of umbilical artery (MCAvs/inUAvs); diastolic velocity of middle cerebral artery/ diastolic velocity of

Table I. *Comparison of the ultrasound parameters of the two groups of fetuses*

Parameters	CoA(n=65)	Control(n=57)	*t*	*p*
Mother's age(age)	28.67±5.51	29.93±4.89	1.952	0.053
Gestational week (week)	30.13±4.82	33.78±4.55	2.421	0.017
RV Z	0.98±1.02	1.31±1.04	2.263	0.039
LV Z	-1.83±0.78	-1.05±0.64	2.383	0.019
RV/LV	1.16±0.31	1.27±0.29	1.741	0.078
MPA Z	0.43±0.30	0.34±0.22	1.602	0.087
AAO Z	-2.00±0.45	-1.00±0.31	4.137	0.005
MPA/AAO	1.93±0.43	1.62±0.29	2.419	0.018
AI Z	-3.40±1.17	-1.46±1.12	2.175	0.041
DA Z	-1.34±1.38	1.12±0.75	4.763	0.003
AO Z	-2.06±1.18	-1.33±1.51	2.319	0.025
AI/DA	0.62±0.33	1.07±0.25	2.293	0.027
AI/AO	0.48±0.09	0.62±0.18	3.929	0.007

internal segment of umbilical artery(MCAvd/inUAvd); resistance index of middle cerebral artery/resistance index of internal segment of umbilical artery(MCA_{RI}/$inUA_{RI}$); pulsation index of middle cerebral artery/pulsation index of internal segment of umbilical artery(MCA_{PI}/$inUA_{PI}$).

Statistical analysis

The data were expressed by mean ± standard deviation. The statistical analysis was performed by SPSS24.0 statistical software. Comparison between groups was performed by *t*-test. ROC curve was used to analyze the correlation, sensitivity and specificity between each index and CoA. The statistical significance of intergroup difference was defined by $p < 0.05$.

RESULTS

Comparisons between the two groups of fetuses

As shown in Table I, the gestational weeks of the fetus in the CoA group were less than those in the control group, and the values of RVZ, LVZ, AAOZ, AIZ, DAZ, AOZ, AI/DA and AI/AO in the CoA group were lower than those in the control group. However, the MPA/AAO value in the CoA group was higher than that in the control group ($p<0.05$). The values of MAC_{RI}/$inUA_{RI}$ and MAC_{PI}/ $inUA_{PI}$ of fetuses in theCoA group were significantly lower than those in control group ($p<0.05$) (Table II). In the correlation analysis between ultrasonic diagnostic indexes and CoA, the values of RV Z, LV Z, AAO Z, AI Z, DA Z, AO Z, AI/DA, AI/AO, MAC_{RI}/$inUA_{RI}$, MAC_{PI}/ inA_{PI} were negatively correlated with CoA, while MPA/AAO value was positively correlated with CoA ($p < 0.05$).

Table III. *Correlation analysis of various ultrasound diagnostic indexes and CoA*

Indexes	*r*	*p*
RV Z	-0.608	0.038
LV Z	-0.741	0.021
AAO Z	-0.485	0.004
AI Z	-0.364	0.019
DA Z	-0.848	0.037
AO Z	-0.531	0.043
AI/DA	-0.044	0.374
AI/AO	-0.791	0.030
MPA/AAO	0.846	0.022
MAC_{RI}/$inUA_{RI}$	-0.734	0.024
MAC_{PI}/$inUA_{PI}$	-0.653	0.033

Table II. *Comparison of ultrasound flow rate parameters of two groups of fetuses*

Parameters	CoA (n=65)	Control (n=57)	*t*	*p*
PA_v/AO_v	1.07±0.50	0.83±0.16	1.618	0.085
AR_{vs}/DA_{vs}	0.88±0.15	0.95±0.15	1.952	0.053
AR_{vd}/DA_{vd}	1.01±0.32	0.80±0.28	1.741	0.078
MAC_{vs}/$inUA_{vs}$	0.62±0.33	0.63±0.24	1.583	0.091
MAC_{vd}/$inUA_{vd}$	0.85±0.63	0.45±0.22	1.819	0.067
MAC_{RI}/$inUA_{RI}$	0.91±0.20	1.15±0.28	2.365	0.021
MAC_{PI}/$inUA_{PI}$	0.98±0.39	1.62±0.65	2.276	0.031

Table IV. *Comparison of the sensitivity and specificity of various ultrasound diagnostic indicators in the diagnosis of CoA*

parameters	Sensitivity（95%CI）	Specificity（95%CI）	AUC（95%CI）	*p*
Gestational week	0.781（0.674～0.883）	0.476（0.342～0.617）	0.657（0.554～0.756）	0.006
RV Z	0.567（0.432～0.708）	0.798（0.687～0.901）	0.621（0.516～0.745）	0.033
LV Z	0.716（0.554～0.884）	0.623（0.467～0.786）	0.691（0.567～0.821）	0.009
AAO Z	0.615（0.487～0.745）	0.834（0.721～0.934）	0.734（0.645～0.833）	0.001
AI Z	0.902（0.823～0.991）	0.354（0.191～0.523）	0.632（0.487～0.765）	0.040
DA Z	0.554（0.432～0.695）	0.897（0.789～1.002）	0.694（0.574～0.810）	0.006
AO Z	0.809（0.554～1.002）	0.834（0.675～0.978）	0.913（0.814～1.005）	0.001
AI/DA	0.607（0.465～0.083)	0.945（0.845～1.018）	0.781（0.504～1.009）	0.030
AI/AO	0.636（0.223～0.097）	0.921（0.334～1.132）	0.515（0.345～0.778）	0.002
MPA/AAO	0.699（0.457～0.893）	0.923（0.783～1.564）	0.545（0.227～0.983）	0.021
$MAC_{RI}/inUA_{RI}$	0.522（0.417～0.789）	0.583（0.174～0.904）	0.939（0.143～1.556）	0.001
$MAC_{PI}/inUA_{PI}$	0.344（0.171～0.894）	0.503（0.332～0.984）	0.844（0.171～0.905）	0.010

In the comparison of sensitivity and specificity of different ultrasonic diagnostic indexes for CoA diagnosis, the sensitivity and specificity of most alone used ultrasonic diagnostic indexes were less than 80%, among which the specificity of AI Z value and AO Z value were relatively higher (Table IV). Therefore, comprehensive evaluation and combination with other parameters such as gestational weeks could improve the sensitivity and specificity of ultrasonic diagnosis.

DISCUSSION

CoA is a common clinical congenital acute cardiovascular disease, which is often associated with other intracardiac malformations (5). Some studies have reported that the accuracy of ultrasound in the diagnosis of fetal heart malformation or congenital heart disease is over 90% (6). However, if only the absolute value of the aorta diameter is used to diagnose CoA, the false positive rate and false negative rate will be higher (7). Therefore, Z value was used to judge the degree of fetal CoA in the current study (8).

In the present paper, the results showed that the values of $MAC_{RI}/inUA_{RI}$ and $MAC_{PI}/inUA_{PI}$ in the CoA group were significantly lower than those in the control group. Moreover, when examining fetuses with severe CoA, the transverse aortic arch could not be clearly distinguished from the amputation of the aortic arch, which affected the diagnosis. Herein, the diagnostic performance of each index was further investigated, and results indicated that the sensitivity and specificity of the most ultrasonic diagnostic indexes were less than 80%.

To sum up, it was still difficult to diagnose the occurrence of CoA only by single ultrasound diagnostic index. Therefore, in order to improve the clinical diagnosis rate of fetal CoA, other indicators should be combined. In addition, combination

with the known bi-directional blood flow signal of isthmus and the presence of aortic arch dysplasia in previous studies can also provide accurate reference information for CoA prognosis. The sample size collected in this study was relatively small, and there is need to increase the sample size for further in-depth research.

REFERENCES

1. Meng QH, Guo Y, Zhang DN, Zhang Q, Li Y, Bian H. Tongsaimai reverses the hypertension and left ventricular remolding caused by abdominal aortic constriction in rats. J Ethnopharmacoly 2020; 246(1):112-54.
2. Song S, Liu L, Yu Y, et al. Inhibition of BRD4 attenuates transverse aortic constriction- and TGF-beta-induced endothelial-mesenchymal transition and cardiac fibrosis. J Mol Cell Cardiol. 2019; 127:83-96.
3. Wu J, Liu Y, Wang M, et al. The value of three-section of aortic arch in ultrasonic diagnosis of coarctation of fetal aorta. Chin J Perinat Med 2019; (9):669-72.
4. Lei Q, Wei XC, Xu JD, Chai YF, Zeng S, Xu GM, Fan D. Echocardiographic evaluation of cardiac remodeling in minimally invasive transverse coarctation of aorta in mice. Western Med 2019; 31(4):503-507.
5. Zheng RH, Bai XJ, Zhang WW, et al. Liraglutide attenuates cardiac remodeling and improves heart function after abdominal aortic constriction through blocking angiotensin II type 1 receptor in rats. Drug Des Devel Ther 2019; 13 (6):2745-57.
6. Daniel AR, Mark JA, Timothy DC, et al. Distinct Phenotypes Induced by Three Degrees of Transverse Aortic Constriction in Mice. Sci Rep 2019; 9(1):5844.
7. Wang SM, Sun F, Shi XB, Yu HR, Bian H, Ma CS. Z value method to evaluate the prevalence and related factors of proximal aortic dilatation. Chin J Geriatr 2018; 37 (6):670-75.
8. Zhang XH, Dong FQ, Wang K, Wang YY. Prenatal ultrasonographic diagnosis of coarctation of aorta and related study. Chin J Medical Ultras (Electronic Edition) 2018; 15 (12): 909-11.

LETTER TO THE EDITOR

Montelukast sodium combined with budesonide for cough variant asthma in children

AH. Li[1], YH. Gao[2], YM. Liu[3], YQ. Hu[4], H. Wei[5] and SQ. Lv[1]

[1]Department of Pharmacy, Weifang People's Hospital, Weifang, China; [2]Department of Pediatrics, Jiyang People's Hospital, Jinan, China; [3]Department of Cardiac function, Qingdao Central Hospital, Qingdao University, Qingdao, China; [4]Department of Endocrinology, The People's Hospital of Zhangqiu Area, Jinan, China; [5]Department of Ward, The People's Hospital of Zhangqiu Area, Jinan, China

Received May 22, 2020 - Accepted November 18, 2020

To the Editor,

Cough variant asthma (CVA), also known as occult asthma and allergic cough, is a common respiratory disease in children and belongs to a special type of asthma (1). The clinical symptoms mainly include long-term repeated dry cough. It is characterized as a persistent disease, with high recurrence rate and low cure rate, leading to a risk of asthma (2). Generally, the average physical functions of children are weaker than adults, and the delay of treatment may cause life-threatening complications (3). Therefore, timely and accurate diagnosis is of particular importance for therapy in the early stage.

Montelukast is a potent and selective leukotriene receptor antagonist non-steroidal anti-inflammatory drug (4), which can selectively inhibit the activity of leukotriene polypeptide in airway smooth muscle, as well as effectively prevent and inhibit the increase of vascular permeability caused by leukotriene, airway eosinophil (EOS) infiltration and bronchospasm. It specifically reduces airway cellular and non-cellular inflammatory substances caused by allergen stimulation as well as inhibiting airway hyperresponsiveness induced by allergens. Montelukast sodium employs its high affinity for the cysteyl leukotriene-1 receptor to selectively suppress the binding of cysteyl leukotriene to the cysteyl leukotriene-1 receptor to mediate airway hyperresponsiveness and lung function (5).

MATERIALS AND METHODS

Eighty children diagnosed with CVA were selected for the study and randomly divided into a combined treatment group and a control group, with 40 patients in each group. There were 23 males and 17 females in the control group, with an average age of (4.65±1.29) years. In the combined treatment group, there were 22 males and 18 females, with an average age of (5.18±1.35) years. The study was reviewed and approved by the hospital committee and all parents or guardians of the patients signed the informed consent.

Diagnostic criteria

According to the Guidelines for the Diagnosis and Treatment of Chronic Cough in Chinese Children revised by the Respiratory Group Chronic Cough Group of the Pediatrics Branch of the Chinese Medical Association in 2013, CVA is profiled as continuous cough more than 4 weeks, symptoms of dry cough, night or early morning attacks, worsened cold cough, clinically no infection symptoms or antibacterial drugs for a long time ineffective.

Key words: montelukast sodium; budesonide; CVA in children

Corresponding Author:
Dr Suqin Lv,
Department of Pharmacy,
Weifang People's Hospital,
151 Guangwen Street,
Weifang 261041,China
e-mail: mtp9bh@163.com

0393-974X (2020)
Copyright © by BIOLIFE, s.a.s.
This publication and/or article is for individual use only and may not be further reproduced without written permission from the copyright holder.
Unauthorized reproduction may result in financial and other penalties
DISCLOSURE: ALL AUTHORS REPORT NO CONFLICTS OF INTEREST RELEVANT TO THIS ARTICLE.

The treatment with bronchodilators was adopted to relieve cough symptoms. The lung ventilation function was normal, and the bronchial provocation test was airway hyperresponsiveness. An allergic disease or positive family history can be diagnosed using an allergen test. Chronic cough symptoms from other conditions were excluded.

Treatment

All children were given conventional treatments, such as anti-asthma, anti-cough, anti-infection, and phlegm elimination. In the control group, patients were treated with budesonide aerosol inhalation, 1 m/time, 2 times/d, 6-8 hours apart, 1 month/course, for a total of 4 courses. In the combined treatment group, the therapy adopted in the control group was combined with montelukast sodium. Under 5 years old, the dosage was 4 mg/time, while for the patients 5 years old and above, the dosage was 5 mg/time, for a total of 4 courses of treatment.

Lung function indicators were measured before and after treatment in the two groups, including forced vital capacity (FVC), forced expiratory volume in the first second (FEV1), and the ratio of the two (FEV1/FVC), and the peak night and day expiratory flow (PEF). Significant effect: the cough and other symptoms of the child basically disappeared within 14 days of receiving treatment, and lungs showed no obvious positive signs after examination, and there were no signs of recurrence after 6 months of follow-up. Effective: cough and other symptoms disappeared within 1 month after treatment, and lungs did not show obvious positive signs after examination, and there was no sign of recurrence after 6 months of follow-up. Ineffective: cough symptoms and other symptoms did not disappear within 1 month after receiving treatment, and lungs showed obvious positive signs after examination.

Statistical analysis

The data obtained in this study were analyzed using statistical software SPSS17.0. Counting data were expressed as percentages and *Chi*-squared test was used. The data were expressed as mean ± standard deviation of three independent biological experiments. Comparison between groups was performed using independent sample *t*-test. In the group comparison, paired sample *t*-test was used, and $P < 0.05$ indicated that the difference was statistically significant.

RESULTS

The time of cough relief and disappearance in the combined treatment group was significantly shorter than that of the control group ($P < 0.05$) (Table I). The total effective rate of the combined treatment group was 92.86%, which was significantly elevated compared with the control group of 69.05% ($P < 0.05$) (Table II).

There was no significant difference in pulmonary function indexes between the two groups before treatment ($P > 0.05$). After treatment, the pulmonary function indexes of the two groups increased significantly ($P < 0.05$), and the lung function in the patients from the combined treatment group was significantly improved compared to that in control group ($P > 0.05$) (Table III).

DISCUSSION

CVA is a clinically specific bronchial asthma with a high incidence in children (6, 7). CVA presents the characteristics of high response and chronic airway inflammation, suggesting that the clinical treatment should target the control of chronic airway inflammation, and it is particularly critical to reduce airway hyperresponsiveness (8). Therefore, early and effective treatment is of great significance for improving the prognosis of such patients.

Montelukast sodium combined with budesonide in the treatment of CVA can effectively improve lung function of patients, improve clinical effectiveness, and facilitate timely recovery (9). In this study, the combined treatment significantly shortened the time of cough relief and disappearance. The total effective rate of treatment was also higher than that of the control group, indicating a favorable clinical effectiveness in the treatment of CVA. The lung function of patients who received therapy of montelukast sodium combined with budesonide was markedly improved after evaluating indexes such as FEVl and FVC, compared to patients who received

single budesonide nebulized inhalation therapy.

In summary, the combined clinical effect of montelukast sodium and budesonide in the treatment of CVA is comparatively favorable to single use of budesonide, which provides new insights for the future treatment against CVA in clinical practice.

REFERENCES

1. Wang Y, Pengyu Z, Jiejun T, Zhiwei L, Wanying Q, Lujia L, Zhijun L. Therapeutic effects of Kangzhi syrup in a guinea pig model of ovalbumin-induced CVA. Evid Based Complement and Alternat Med 2018:1-11.
2. Nakajima T, Nishimura Y, Nishiuma T, Kotani Y, Funada Y, Nakata H, Yokoyama M. Characteristics of patients with chronic cough who developed classic asthma during the course of CVA: a longitudinal study. Respiration 2005; 72:606-11.
3. Zhou J, Zhao X, Zhang X, et al. Values of fractional exhaled nitric oxide for cough-variant asthma in children with chronic cough. J Thorac Dis 2018; 10:6616-23.
4. Ozkan E, Akyuz C, Sehirli AO, Topaloglu U, Ercan F, Sener G. Montelukast, a selective cysteinyl leukotriene receptor 1 antagonist, reduces cerulein-induced pancreatic injury in rats. Pancreas 2010; 39:1041-46.
5. Peng J, Zhou H, Kuang G, Xie L, Tian T, Liu R. The selective cysteinyl leukotriene receptor 1 (CysLT1R) antagonist montelukast regulates extracellular matrix remodeling. Biochem Biophys Res Commun 2017; 484:474-79.
6. Fujimura M, Ogawa H, Nishizawa Y, Nishi K. Comparison of atopic cough with CVA: is atopic cough a precursor of asthma? Thorax 2003; 58:14-18.
7. Li W, Ban C, Zhang J, Hu Y, Han B, Han B. Correlation study of CVA and mycoplasma pneumonia infection in children. Pak J Pharm Sci 2017; 30:1099-102.
8. Corrao WM. Pearls and pitfalls in the diagnosis of CVA. Allergy Asthma Proc 2018; 39:466-67.
9. Shin J, Oh SJ, Petigara T, et al. Comparative effectiveness of budesonide inhalation suspension and montelukast in children with mild asthma in Korea. J Asthma 2019; 1-11.

LETTER TO THE EDITOR

Correlation between CT small airway parameters, T-lymphocyte subsets and MMP-9 level in patients with bronchial asthma

J.Y. Hou[1], X.N. Wang[2], G. Qiu[3], D.L. Gao[4] and Y. Wang[4]

[1]Department of Radiology, Changle County People's Hospital, Weifang, Shandong Province, China;
[2]Medical Laboratory Division, Changle County People's Hospital, Weifang, Shandong Province, China;
[3]Division of respiratory medicine, Changle County People's Hospital, Weifang, Shandong Province, China;
[4]Department of blood transfusion, Changle County People's Hospital, Weifang, Shandong Province, China

Received August 16, 2020 – Accepted November 20, 2020

To the Editor,

Bronchial asthma is a chronic airway inflammation mainly involving eosinophils (Eos), lymphocytes and mast cells (1). T lymphocyte disorders of $CD3^+$ and $CD8^+$ can not only promote the infiltration of inflammatory cells, but also accelerate tissue damage, affecting the tolerance of bronchial mucosa (2). Matrix metalloproteinase-9 (MMP-9), as a member of the matrix metalloproteinases family, plays an important role in inflammatory cell migration and matrix remodeling in asthma (3). Studies have shown that MMP-9 is highly expressed in the airway, sputum and other aspects of asthma patients (4).

Based on the relationship above, some scholars have proposed that asthma can be treated by regulating T-lymphocyte subsets and MMP-9 level in asthmatic patients. However, the main symptoms of asthma are airway inflammation and multistage airway changes, especially small bronchioles with inner diameter less than 2 mm (referred to as small airway). In order to explore the correlation among T-lymphocyte subsets, MMP-9 level and clinical outcome of asthma treatment, 30 patients who were diagnosed with bronchial asthma who had undergone CT examination were selected for this study.

MATERIALS AND METHODS

In this study, 30 patients with bronchial asthma treated in the Changle County People's Hospital, Weifang, Shandong from June 2019 to December 2019 were selected, including 10 males and 20 females aged 27-80 years with an average age of 56 years, and the course of disease was 1-62 years with an average course of 10 years. The inclusion criteria were: over 18 years of age, and met the diagnostic criteria for asthma in GINA (Global Initiative for Asthma) (5); no other serious diseases, and no other respiratory diseases such as pneumonia or chronic obstructive pulmonary disease; complete laboratory examination data, imaging data and clinical data, and normal intelligence and cognitive level. The study was approved by the hospital ethics committee, and all patients voluntarily participated in the study and signed the informed consent.

Two radiologists were selected to measure the patients' small airway parameters, and the final result was the average of the two measurements. The patients took a supine position and inhaled deeply. The American GE 750 HD CT scanner was used to scan the patients from the bottom of the lung to the apex of the lung, with the tube voltage was set at 120 kVp and the tube current

Keywords: bronchial asthma; CT small airway parameters; T-lymphocyte subsets index; MMP-9 level; correlation study

Corresponding Author:
Dr Y. Wang,
Department of Blood Transfusion,
Changle County People's Hospital,
No.278 Limin Street, Changle County,
Weifang City, 262400, Shandong Province, China
Tel.: +860536-6222822
e-mail: wangxiaona1980@163.com

0393-974X (2020)
Copyright © by BIOLIFE, s.a.s.
This publication and/or article is for individual use only and may not be further reproduced without written permission from the copyright holder.
Unauthorized reproduction may result in financial and other penalties
DISCLOSURE: ALL AUTHORS REPORT NO CONFLICTS OF INTEREST RELEVANT TO THIS ARTICLE.

at 125-210 mA. Standard algorithm was used for image reconstruction with a layer thickness of 0.625 mm. At the same time, Airway Analysis software (American GE Company) was used to measure the small airway at the distal end of the grade 6 bronchi (inner diameter<2 mm), and the small airway contour was adjusted with 1000 HU of window width and -600HU of window level. The airway measurements were generated by computer. Small airways measurements included the branch in the posterior basal segment of the lower right lung lobe, the branch in the apical segment of the upper lobe, the branch outside the lateral segment of the middle lobe, the branch in the basal segment of the lower left lung lobe, the branch in the posterior apical segment of the upper lobe and the branch in the anterior lingual segment of the upper lobe. After the average value of the above six small airway parameters was calculated, $LD_{correction}$ (cavity diameter), $Ai_{correction}$ (cavity area), $WT_{correction}$ (airway wall thickness), and WA% (percentage of airway wall area) were obtained by body surface area correction (6).

5 ml of peripheral venous blood samples were taken from patients under fasting condition in the morning and placed in heparin sodium anticoagulant tubes. 100 μl of the whole blood extracted and treated with anticoagulation was selected and added to the test tubes containing CD3-FITC, CD4-FITC and CD8-PE antibodies (American CytoFLEX company), respectively, which were then incubated in the dark for 25 minutes, rinsed with PBS for two times and incubated for 30 min with FITC-labeled secondary antibodies. After washing with PBS for 3 times, a flow cytometry (American CytoFLEX company) was used to detec T-lymphocyte subsets.

For determination of inflammatory factors (MMP-9 and Eos) in induced sputum, induced sputum obtained by an ultrasonic nebulization inhaler (Jiangsu Kangxin Medical Equipment Co., Ltd.) was collected in the patients, mixed evenly with equal volume of dithiothreitol (4%) and incubated at 37°C for 30 min. After centrifugation for 5 minat a speed of 200 r/min, MMP-9 level in the supernate was determined by enzyme-linked immunosorbent assay (ELISA) according to the instructions of the kit (American R&D Company). At the same time, Wright-Giemsa staining method was used to determine Eos content, and the staining result of Eos was pink (Giemsa stain, Shanghai Ming Bo Biological Technology Co., Ltd.).

EvaluationiIndexes

Intraclass correlation coefficient (ICC) was used to evaluate whether the small airway parameters independently determined by the two radiologists had consistency. ICC<0.40 represented poor consistency, 0.40≤ICC≤0.75 represented relatively good consistency and ICC>0.75 represented good consistency. T-lymphocyte subsets in peripheral blood of patients with bronchial asthma were recorded, including $CD3^+$, $CD4^+$, and $CD8^+$. Inflammatory factors in included sputum were also recorded, including MMP-9 and Eos.

Statistical analysis

Relevant materials and data in this paper were processed and analyzed by statistical software SPSS20.0. Measurement data were measured by *t*-test, expressed by ($\bar{x}$±s), and correlation analysis was performed with Spearman correlation test. The difference was statistically significant when $p < 0.05$.

RESULTS

The CT small airway parameters independently determined by the two radiologists had good consistency, with ICC value of 94.9%. The CT small airway parameters were the average value of the measurement results of the radiologists, including $LD_{correction}$ mean (1.30±0.12) mm, $Ai_{correction}$ mean (1.35±0.28) mm, $WT_{correction}$ mean (0.95±0.13) mm, and WA% mean (82.95±4.03)%.

The results of T-lymphocyte subsets detected by a flow cytometry are shown in Fig. 1. Enzyme linked immunosorbent assay (ELISA) and Wright-Giemsa staining method were used to detect MMP-9 and Eos (%), and the results are shown Fig. 2.

Correlation analyses

WA% was positively correlated with $CD3^+$ (%), $CD4^+$ (%) and $CD3^+/CD4^+$ (r=0.508, r=0.551, r=0.453, P<0.05). There was no significant correlation between parameters ($LD_{correction}$, $Ai_{correction}$ and $WT_{correction)}$ and $CD3^+$ (%), parameters and $CD4^+$ (%), parameters and $CD3^+/CD4^+$ (P > 0.05). $LD_{correction}$ and $Ai_{correction}$ were positively correlated with $CD8^+$(%) (r=0.534, r=0.551, P<0.05). $WT_{correction}$ was negatively correlated with $CD8^+$(%) (r=-0.488,

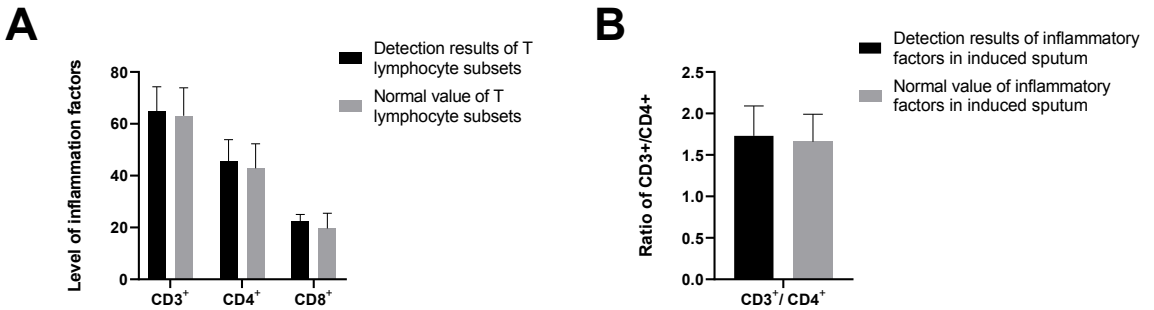


Fig. 1. *Detection of T-lymphocyte subsets. **A)** Expression level of $CD3^+$, $CD4^+$ and $CD8^+$ of all patients compared with normal value. **B)** Ratio of $CD3^+$ /$CD4^+$ of all patients compared with normal value.*

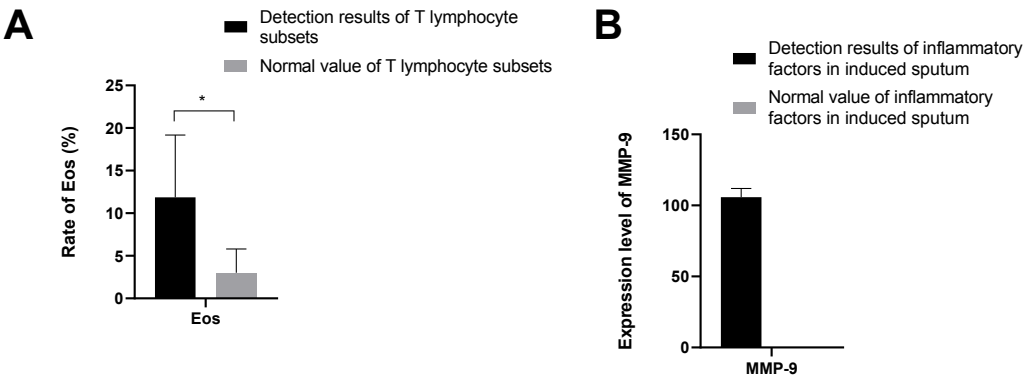


Fig. 2. *Detection of inflammatory factors in induced sputum. **A)** Rate of Eos of all patients compared with normal value (*means P<0.05). **B)** Expression level of MMP-9 of all patients compared with normal value.*

P<0.05). There was no significant correlation between WA% and $CD8^+$ (%) (P > 0.05, Table I).

$LD_{correction}$ and $Ai_{correction}$ were negatively correlated with Eos (%) (r=-0.842, r=-0.840, P<0.05). There was no significant correlation between parameters ($WT_{correction}$ and WA%) and Eos (%) (P > 0.05). WA% was positively correlated with MMP-9 (r=0.637, P<0.05). There was no significant correlation between parameters ($LD_{correction}$, $Ai_{correction}$ and $WT_{correction)}$ and MMP-9 (P > 0.05, Table II).

DISCUSSION

Clinical studies have shown that a variety of cells and cell groups are involved in the pathogenesis of bronchial asthma. T lymphocytes are the most prominent cell group in human immune function, and their immune response imbalance is the main mechanism to trigger asthma (7-9). Moreover, Eos, as the main effector cell of bronchial mucosal injury, also participates in the pathogenesis of asthma, which mainly causes bronchial mucosal injury by releasing granule proteins and producing inflammatory mediators (10). When asthma occurs, lymphocytes and Eos cells increase, resulting in excessive production of MMP-9, which leads to the destruction of epithelial basement membrane and endothelium. The arrival of inflammatory cells at the site of inflammation will then lead to further development of inflammation, and can easily cause airway hyperresponsiveness (11).

The results of this study showed that WA% was positively correlated with $CD3^+$, $CD4^+$ and $CD3^+$/

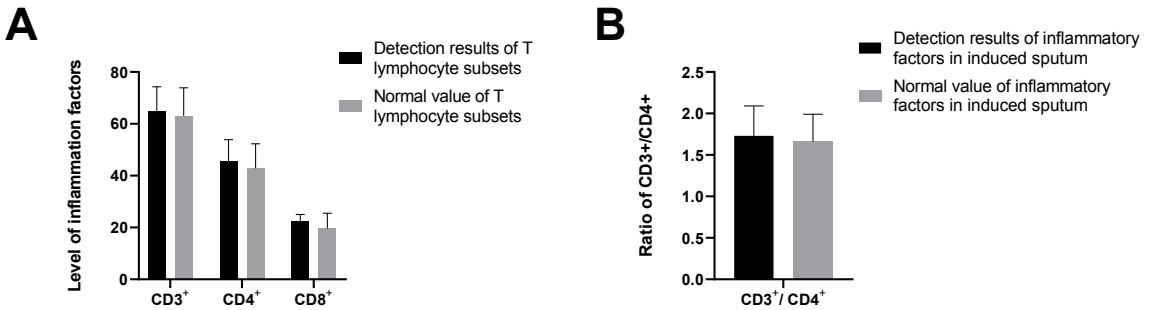


Fig. 1. *Detection of T-lymphocyte subsets. **A)** Expression level of $CD3^+$, $CD4^+$ and $CD8^+$ of all patients compared with normal value. **B)** Ratio of $CD3^+$ /$CD4^+$ of all patients compared with normal value.*

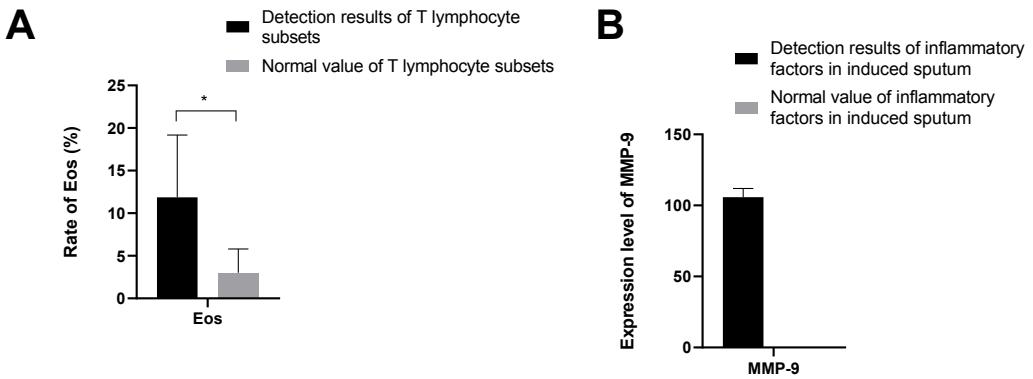


Fig. 2. *Detection of inflammatory factors in induced sputum. **A)** Rate of Eos of all patients compared with normal value (*means P<0.05). **B)** Expression level of MMP-9 of all patients compared with normal value.*

P<0.05). There was no significant correlation between WA% and $CD8^+$ (%) (P > 0.05, Table I).

$LD_{correction}$ and $Ai_{correction}$ were negatively correlated with Eos (%) (r=-0.842, r=-0.840, P<0.05). There was no significant correlation between parameters ($WT_{correction}$ and WA%) and Eos (%) (P > 0.05). WA% was positively correlated with MMP-9 (r=0.637, P<0.05). There was no significant correlation between parameters ($LD_{correction}$, $Ai_{correction}$ and $WT_{correction)}$ and MMP-9 (P > 0.05, Table II).

DISCUSSION

Clinical studies have shown that a variety of cells and cell groups are involved in the pathogenesis of bronchial asthma. T lymphocytes are the most prominent cell group in human immune function, and their immune response imbalance is the main mechanism to trigger asthma (7-9). Moreover, Eos, as the main effector cell of bronchial mucosal injury, also participates in the pathogenesis of asthma, which mainly causes bronchial mucosal injury by releasing granule proteins and producing inflammatory mediators (10). When asthma occurs, lymphocytes and Eos cells increase, resulting in excessive production of MMP-9, which leads to the destruction of epithelial basement membrane and endothelium. The arrival of inflammatory cells at the site of inflammation will then lead to further development of inflammation, and can easily cause airway hyperresponsiveness (11).

The results of this study showed that WA% was positively correlated with $CD3^+$, $CD4^+$ and $CD3^+$/

Table I. *Analysis of correlation between CT small airway parameters and T-lymphocyte subsets*

T-lymphocyte subsets	$LD_{correction}$	$Ai_{correction}$	$WT_{correction}$	WA%
$CD3^+$（%）	-0.203（0.455）	-0.081（0.761）	0.198（0.459）	0.508（0.043）
$CD4^+$（%）	-0.208（0.408）	-0.455（0.056）	0.312（0.184）	0.551（0.016）
$CD3^+$/ $CD4^+$	-0.101（0.693）	-0.025（0.912）	0.334（0.152）	0.453（0.044）
$CD8^+$（%）	0.534（0.018）	0.551（0.016）	-0.488（0.028）	-0.457（0.058）

Values in parentheses are P values

Table II. *Analysis of correlation between small airway parameters and induced sputum inflammatory factors*

T-lymphocyte subsets	$LD_{correction}$	$Ai_{correction}$	$WT_{correction}$	WA%
$CD3^+$（%）	-0.203（0.455）	-0.081（0.761）	0.198（0.459）	0.508（0.043）
$CD4^+$（%）	-0.208（0.408）	-0.455（0.056）	0.312（0.184）	0.551（0.016）
$CD3^+$/ $CD4^+$	-0.101（0.693）	-0.025（0.912）	0.334（0.152）	0.453（0.044）
$CD8^+$（%）	0.534（0.018）	0.551（0.016）	-0.488（0.028）	-0.457（0.058）

Values in the parentheses are P values

$CD4^+$. $LD_{correction}$ and $Ai_{correction}$ were positively correlated with $CD8^+$, while $WT_{correction}$ was negatively correlated with $CD8^+$. These indicate that peripheral blood T-lymphocyte subsets are correlated with airway remodeling. Furthermore, the results showed that $LD_{correction}$ and $Ai_{correction}$ were negatively correlated with Eos, while WA% was positively correlated with MMP-9, which was similar to the results of FAN Yan-ping (12) et al.

In conclusion, peripheral blood T-lymphocyte subsets, induced sputum Eos and MMP-9 level in patients with bronchial asthma can affect partial CT small airway parameters, which provides a reference for the treatment of bronchial asthma.

ACKNOWLEDGEMENTS

This work was funded by Weifang Science and Technology Development Project 2018YX108; Weifang City Health Commission Chinese Medicine Research Project 2019 (Third Category) No. 2019-3-001.

REFERENCES

1. Yang X, Zeng Q, Göktas E, et al. T-lymphocyte subset distribution and activity in patients with glaucoma. Invest Ophthalmol Vis Sci 2019; 60(4):877-88.
2. Doras C, Petak F, Bayat S, Badat A, Von Guarnier. C, Eigenmann P, Habre W. Lung responses in murine models of experimental asthma: value of house dust mite over ovalbumin sensitization. Respir Physiol Neurobiol 2018; 247:43-51.
3. Konietzke P, Weinheimer O, Wielpütz MO, et al Quantitative CT detects changes in airway dimensions and air-trapping after bronchial thermoplasty for severe asthma. Eur J Radiol 2018;107:33-38.
4. Zou F, Zhang J, Xiang G, Jiao H, Gao H. Association of matrix metalloproteinase 9 (MMP-9)

polymorphisms with asthma risk: a meta-analysis. Can Respir J 2019; 2019:9260495.
5. Matsushita S, Yamashiro T, Matsuoka S, Yagihashi K, Nakajima Y. The association between bronchial wall CT attenuation and spirometry in patients with bronchial asthma. Acad Radiol 2019; 26(7):960-66.
6. Bodienkova GM, Boklazhenko EV, Bodienkova SG, Beygel EA. Comparative characteristics of cytokine and IgE levels in patients with bronchial asthma of professional and non-professional genesis. Biomed Khim 2018; 64(4):376-79.
7. Shi G, Zhao JW, Sun XX, Ma JF, Wang P, He FC, Ming L. TIPE2 is negatively correlated with tissue factor and thrombospondin-1 expression in patients with bronchial asthma. Exp Ther Med 2018; 15(4):3449-54.
8. Huijuan Xu, Mei Song, Zhaofan Lin. Serum levels of IL-33 and S1P in patients with bronchial asthma and their clinical significance. China Med Hera 2019; 016(016):87-90.
9. Rodrigo-Muñoz JM, Cañas JA, Sastre B, et al. Asthma diagnosis using integrated analysis of eosinophil microRNAs. Allergy 2019; 74(3):507-517.
10. Li HZ, Gao ZY, Huang W, et al. Effects of Fritillariae Cirrhosae Bulbus on MMP-2,MMP-9 and TIMP-1 in murine asthma model. China J Chin Mater Med 2017; 42(21):4180-86.
11. Chen LY, Tang Y, Zhang L, et al. Detection of interleukin-22 in peripheral blood of patients with bronchial asthma and its clinical significance. J Jilin Univ 2017; 43(2):349-52.
12. Fan YP, Yi JQ, WU Min. Relationship between Serum MMP-9,Gal-3,TGF-β1 and Pulmonary Function in Children with Bronchial Asthma. J Modern Lab Medicine 2017; 004(032):76-79.

LETTER TO THE EDITOR

Diagnosis and treatment of two patients with novel coronavirus pneumonia combined with acute stress disorder

X-Y. Duan[1*], S-R. Lu[2*], G-Q. Yan[3*], R. Qiu[4] and M-W. Liu[5]

[1]Department of Tuberculosis Diseases, Changpo Hospital of Third People's Hospital of Kunming City, Taiping Town, Anning City, China; [2]Department of Respiratory and Critical Care, Third People's Hospital of Kunming City, Guandu District, Kunming, China; [3]Department of Science and Education, First Affiliated Hospital of Kunming Medical University, Wuhua District, Kunming, China; [4]Department of Respiratory and Critical Care, Suining Central Hospital, Chuanshan District, Suining, China; [5]Department of Emergency Medicine, First Affiliated Hospital of Kunming Medical University, Wuhua District, Kunming, China

Received September 15, 2020 – Accepted November 25, 2020

[*]These Authors contributed equally to this work

To the Editor,

Acute stress disorder (ASD) or the acute psychogenic response is a transient dysphrenia caused by sudden egregious strong and stressful life events (1). Symptom development has an explicit correlation with stressor and events. Even with variations in clinical findings, ASD can be divided into two types: psychomotor inhibition, which is accompanied with a certain degree of disturbance of consciousness and even stupor state; and psychomotor excitement, which is accompanied with fear and autonomic nerve system symptoms. In emotional disorder, anxiety or depression is relatively common and involves severe injury to the physical and psychological health of patients. Therefore, early diagnosis, symptomatic treatment, and improvement of disease conditions and emotional states are conducive to patient rehabilitation (2).

The novel coronavirus pneumonia (COVID-19) was declared as an internationally public health emergency by the World Health Organization (WHO). This disease is caused by the novel severe acute respiratory syndrome coronavirus 2 (SARS-CoV-2), which has never been previously discovered in humans, and involves human-to-human transmission and family infection (3). In the early stages, patients develop fever, hypodynamics, and dry cough, breathing difficulties, respiratory distress syndrome or septic shock, incorrigible metabolic acidosis, and coagulation dysfunction (4). Given the extremely strong infectivity of the pathogen, crowds are generally susceptible, and the epidemic develops rapidly. COVID-19 exhibits a certain fatality and may cause severe psychological stresses triggering various psychological and physiological responses in patients. Patients with COVID-19 experience severe pulmonary disease and have high infectivity. Radical therapy is necessary to rapidly control the disease, relieve symptoms, and decrease the negative and impulsive emotions of patients and the infection risk of other medical staffs.

This study discussed a psychiatric intervention

Key words: novel coronavirus pneumonia; acute stress disorder; psychological intervention; citalopram; abidor

Corresponding Author:
Dr Ming-wei Liu,
Department of Emergency Medicine,
First Affiliated Hospital of Kunming Medical University,
295 Xichang Road, Wuhua District, Kunming,
Yunnan Province,650032, China
e-mail: lmw2004210@163.com

0393-974X (2020)
Copyright © by BIOLIFE, s.a.s.
This publication and/or article is for individual use only and may not be further reproduced without written permission from the copyright holder.
Unauthorized reproduction may result in financial and other penalties
DISCLOSURE: ALL AUTHORS REPORT NO CONFLICTS OF INTEREST RELEVANT TO THIS ARTICLE.

strategy for patients with combined COVID-19 and ASD in isolation wards on the basis of the diagnosis and treatment of two special cases.

MATERIALS AND METHODS

This study was approved by the Kunming medical University Research Ethics Boards. The trial was registered in the Chinese Clinical Trials Registry (ChiCTR-IOR-17020107), on January 14, 2020. Written informed consent for participation was obtained from the patients or their relatives.

Case 1

Patient 1 was a 46-year-old male admitted to Sichuan Suining Central Hospital in China on February 15, 2020 due to "cold intolerance, fever, and muscular stiffness in the previous 8 days." One week before admission, the patient dined with his brother and sister-in-law who were both diagnosed with COVID-19 one day prior to his diagnosis. According to physical examination, the patient had conscious mind; showed no yellow stain of the skin sclera, palpable swelling superficial lymph node, pressing pain, or swelling on lower limbs; presented rebound tenderness, muscular tension, and soft abdomen; and was unable to finish cardiopulmonary stethoscope. According to the chest Computer Tomography (CT) in the local hospital, multiple plaques and lamellar shadow were observed in both lungs, thus indicating interstitial changes. Viral pneumonia was considered, and further diagnosis was necessary (Fig. 1). Blood routine examination, coagulation function, biochemistry analysis, myocardial enzyme, and respiratory pathogen antibody were negative. On February 15, the patient was tested positive according to Centers for Disease Control and Prevention (CDC) novel coronavirus nucleic acid in Suining City. After hospitalization, he was diagnosed with COVID-19 after the discussion of COVID-19 experts in Suining City. On February 16, the patient was given 0.2 g of abidor (three times a day) orally and provided with an intravenous drip of 0.5 g of ribavirin (once/day) and fluid infusion to maintain electrolyte balance and thymosins to enhance immunity. On February 17, the medical staff noticed the suicidal behavior of the patient on 00:05. He broke the clinical thermometer and stabbed himself, inflicting an approximately 5 mm-depth and 3 mm-wide wound. The wound was sterilized and bound with sterilized bandages. The patient was unwilling to state the reasons of suicide. Medical staff strengthened communication and psychiatric nursing to prevent suicide and accidents. During the psychiatric interview with a psychosomatic consultant, the patient did not cooperate, waited for a long time, and often answered questions with simple words. He expressed that he could not accept the fact that he and his family were diagnosed with COVID-19, he was depressed and felt guilty for the infection of his family, and did not show other emotions. He reflected that his suicidal behavior yesterday was based on impulse and denied having negative thoughts and emotional problems previously. At present, he had no depression, suicidal intentions, or plans. The patient had no similar symptoms and no psychiatry or psychological treatment records, after eliminating the organic mental disorders, dissociative (conversion) disorder, mental disorder caused by drug or psychoactive drug substances or depression, and was therefore diagnosed with ASD. For ASD intervention, every dangerous item in the isolation ward was strictly controlled, and inspection tours were increased, especially at night. The supervising physician and nurses provided the patient with supportive and encouraging communication and explained the disease to relieve his emotional responses. The patient was asked to take 1 mg of estazolam before sleeping every night. After 3 days, his emotion improved remarkably, and he stopped taking estazolam. The patient experienced stuffy discomfort at the middle and upper abdomen, and a suspicious punch-through wound was observed. According to abdominal CT examination at emergency treatment, a columnar high-density shadow was found in the middle and upper abdomen, which was close to the anterior gastric wall in local region. The longest diameter was approximately 9 cm. Foreign matter was suspected (Fig. 1). After repeated questions, the patient confessed that he had stabbed a mercurial thermometer below the xiphoid on the morning of January 17. With suspicion of foreign matter in the abdomen, an abdominal laparotomy under combined spinal–epidural anesthesia was performed to remove the abdominal foreign matter, and abdominal drainage was performed on the morning of February 20. During the operation, a 2 mm-irregular perforating wound was found below the xiphoid, and the omentum majus approximately 1 cm away from the greater curvature was destroyed and

formed a local 4 cm×3 cm hematoma. Thermometer residue of approximately 9 cm in size was found in the omental bursa. The mercury head of the thermometer was missing, and no evident anomalies were found after the examination of posterior gastric wall, colon transversum and its mesentery, and small intestine and its mesentery. Moreover, no hematocele, pus substance, and food debris were detected in the abdomen. After the operation, the patient lay on the bed without a pillow for 6 h and was prohibited from drinking and eating. Levofloxacin was stopped, and piperacillin tazobactam was used to prevent infection. Other symptomatic treatments, such as fluid supplementation and pain relief, were also administered. Tetanus antitoxin was injected, and the local dressing of the surgical wound was frequently changed. On February 22, the highest body temperature was 37.3°C, and no coughing, expectoration, cold intolerance, anhelation, chest distress and pain, abdominal pain and diarrhea, and fever was detected since then. On February 23, the patient defecated on himself. According to CT reexamination, multiple sheet-like plaques with interstitial changes were found in both lungs. These findings conformed to the imaging characteristics of viral pneumonia. However, lesion absorption was decreased compared with that in previous observation, and clinical symptoms were considered in the treatment. The mesentery at the middle and upper abdomen was swollen, and local soft tissues on the right antetheca were thickened. However, no primary intraperitoneal foreign body was observed. On February 19, 2020, the patient tested positive for the novel coronavirus antibody test in the hospital; negative for deep sputum novel coronavirus nucleic acid test on February 20, 22, and 23; negative for stool novel coronavirus nucleic acid test on February 24; negative in three successive respiratory novel coronavirus nucleic acid tests (interval: at least 1 day); and negative in stool novel coronavirus nucleic acid test. Lung lesion was absorbed significantly according to lung CT examination (Fig. 2). At present, the body temperature of the patient has been normal for 4 days, and his respiratory

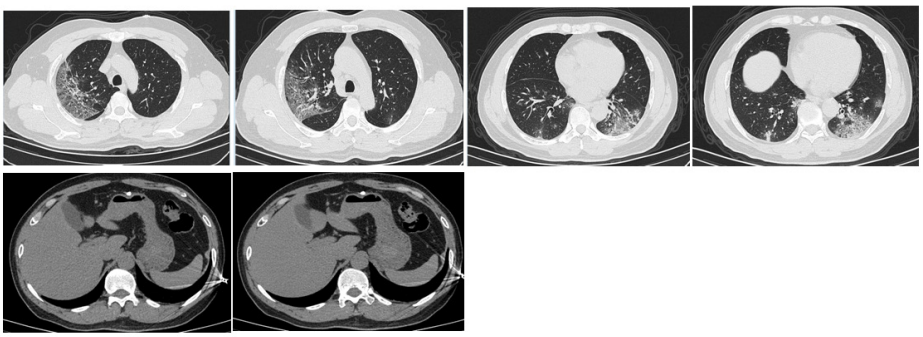


Fig. 1. *Lung CT images of patient 1 before treatment. Multiple plaques and sheet shadows with interstitial changes in the two lungs. High density foreign bodies in the abdominal cavity. Viral pneumonia is considered, and further diagnosis is required.*

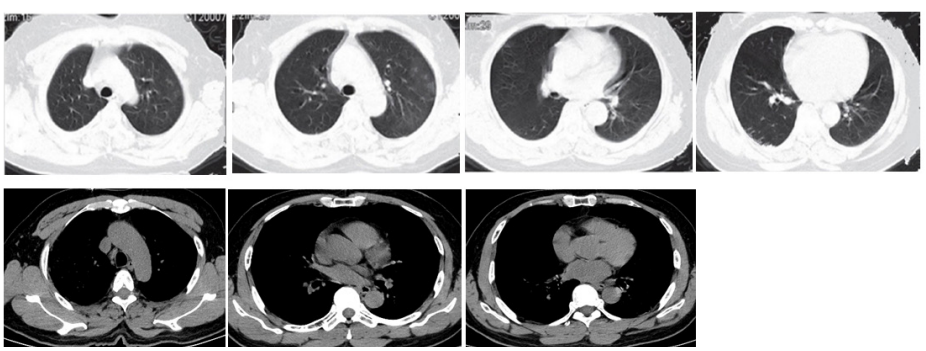


Fig. 2. *Lung CT images of patient 1 after treatment. Clear lesion absorption in the two lungs.*

symptoms were all completely relieved, blood routine examination, coagulation function, biochemistry analysis, and myocardial enzyme were negative. The patient was removed from isolation and discharged on February 26, 2020. No anomalies were discovered from blood routine reexamination, biochemistry, chest CT, respiratory sample, and stool novel coronavirus nucleic acid tests at 2 weeks after the discharge.

Case 2

Patient 2 is a 67-year-old male admitted for quarantine in the Kunming Third Hospital in Yunnan Province on January 26, 2020 who had been isolated for 2 weeks because his family members were diagnosed with COVID-19. During this period, he became nervous, insomniac, and malaise. On the 12th day of isolation, the patient had fever, weakness, coughing, and chest distress. According to further blood routine examination, the WBC, HGB, PLT, NEUT%, LYMPH%, and L# of the patient were 6.6×10^9/L, 153 g/L, 174×10^9/L, 51.5%, 38.1%, and 1.23×10^9/L, respectively. Coagulation function, biochemistry analysis, respiratory pathogen antibody, and myocardial enzyme were negative, ESR was 47 mm/h. Blood novel coronavirus nucleic acid test was negative. Nasopharyngeal swab nucleic acid test was positive. Lung CT revealed multiple flake consolidation shadows on the outer belts of the two lungs, accompanied by local ground glass density shadows mainly in the inferior lobes of both lungs (Fig. 4). After consultation with local CDC COVID-19 experts, the patient was finally diagnosed with "COVID-19." He was given 0.2 g of abidor orally (three times a day) and administered an intravenous drip of 0.5 g of ribavirin (once/day), fluid infusion to maintain electrolyte balance, and thymosins to improve immunity on January 27, 2020. After hospitalization, the patient experienced various physical discomforts, including conscious palpitation, chest distress, and breathing difficulties, which were inconsistent with ECG, oxyhemoglobin saturation, and electrocardiograph monitoring. The patient also suffered from sleep disorder manifested by difficulty in falling asleep and easily woken



Fig. 3. *Lung CT images of patient 2 before treatment. Multiple sheet-like consolidation shadows in the outer belts of the two lungs, and local ground glass density shadows mainly in the lower lobes of the two lungs.*

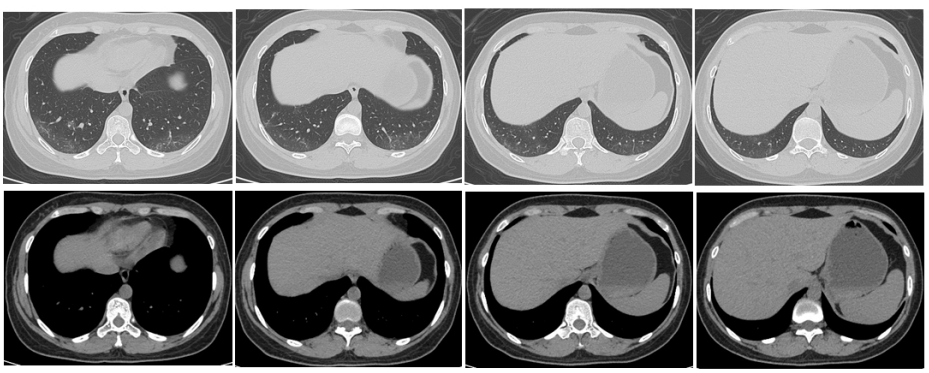


Fig. 4. *Lung CT images of patient 2 after treatment. Clear lesion absorption in the two lungs.two lungs, and local ground glass density shadows mainly in the lower lobes of the two lungs.*

up. On the second day of hospitalization, a psychiatrist recognized anxiety and excessive worry during rounds of the wards but found no evidence of dysphoria, pessimism, or desperation. The patient denied his emotional symptoms and refused to take psychiatric drug intervention, except for sleeping drugs. The psychiatrist offered supportive psychotherapy and a prescription of zolpidem to improve his sleeping condition. On the third day of hospitalization, the condition of patient considerably intensified. He became enraged, frequently attracted medical staff, and claimed "no cure." He was very pessimistic and in despair. The patient even pulled off the insulating clothing of the medical staff during raging, thus severely exposing them to the infection. According to the psychiatry department, the patient had clear consciousness, contact cooperation, tidy presence, and complete orientation. He did not exhibit hallucination, illusion, or sensory perception disorder and presented connected thinking. Moreover, the patient was anxious, walked around in the ward, and showed depression, pessimism, desperation, poor self-perception, and intensified malaise. Although he still had willpower, he lost self-consciousness. The patient had no history of similar symptoms, psychiatric or psychological treatment. After eliminating the organic mental disorders, dissociative (conversion) disorder, metal disorder caused by drug or psychoactive drug substances and depression, he was therefore diagnosed with "ASD". Since the patient had no self-consciousness, he refused all emotional symptoms and treatment for desperation and acted negatively toward any intervention. Psychological intervention was employed, but the patient refused, resulting in poor effect. The staff requested the psychiatrist to control the anxiety and depression symptoms of the case patient and to report the progress to the command center. To rapidly control the symptoms, the psychiatrist prescribed 20 mg of citalopram in the morning and 5 mg of olanzapine tablets at night. After 2 days of continuous follow-up visits, the sleeping quality and emotions of the patient significantly improved. His chest distress, palpitation and weakness symptoms were improved, except for some coughing and expectorations. To relieve his anxiety and depression and address his current poor physical health, the patient was prescribed with 5 mg of olanzapine tablets every night for 3 days, which was then decreased to 2.5 mg every night. The patient could recognize his emotional problems on the 7th day and began to accept psychological intervention. During this situation, olanzapine tablets were stopped, but the 20 mg of phthalein/day was continued until the 14th day. The patient maintained a stable emotion and showed no physical discomfort. At the 14th day of hospitalization, the COVID-19 condition of the patient was relieved. The blood routine reexamination, coagulation, and biochemistry analysis showed no anomalies. The patient was positive according to the novel coronavirus antibody test, and his body temperature was normal for 5 days with completely relieved respiratory symptoms on February 11, 2020. Moreover, the patient tested negative in three successive respiratory novel coronavirus nucleic acid tests (February 11, 13 and 15, 2020) and negative in stool novel coronavirus nucleic acid test. Furthermore, the lung lesion was absorbed significantly according to the lung CT examination. The patient was removed from isolation and discharged (Fig. 4). No anomalies were discovered from the blood routine reexamination, biochemistry, chest CT, respiratory sample, and stool novel coronavirus nucleic acid tests at 2 weeks after discharge.

DISCUSSION

Given that patients with COVID-19 have partial infectivity and cannot comply with the treatment, the emotional responses of patients to ASD may influence medical staff and thereby increase their exposure risks (5-7). Hence, ASD treatment must relieve the symptoms and aid patients to immediately overcome anxiety and fear and recover the psychological equilibrium state regarding the uniqueness of COVID-19 so that patients can comply with quarantine and treatment.

Both patients met the diagnosis standards of ASD in the 10th revised version of International Disease Classification (8). For patient 1, since he is relatively young and without severe lung infection and breathing difficulties and good oxygen saturation, benzodiazepines drugs, such as estazolam and alprazolam tablets, were administrated after full assessment, which controlled his anxiety and depression symptoms well. For patient 2, the patient was older and had lung diseases, resulting in a high risk of using benzodiazepines. Citalopram shows high safety (9, 10). In addition to anxiety and depression, this patient was enraged and unreasonable, which

were against effective psychological intervention. Therefore, a small-dose of olanzapine combined with citalopram was selected because it can rapidly and effectively relieve the clinical symptoms of patients and reduce the risk of depression, thus satisfying the demands for clinical treatment. In addition to mental symptoms, positive anti-virus treatment was adopted (11, 12). Hence, both patients with SARS-CoV-2 in this study were administrated with a combination of arbidol and ribavirin and were cured under this therapy, indicating that the combination of arbidol and ribavirin may effectively treat SARS-CoV-2 infection.

In conclusion, patients with COVID-19 and ASD develop impulsive, pessimistic, and self-harming behaviors, in addition to anxiety, depression, and sleep disorders. Clinical treatment must be extensively performed, and psychological intervention must be administered immediately. Considering that COVID-19 has strong infectivity and causes the rapid expansion of lung lesion, antiviral treatment is suggested while managing the psychological stress disorders of patients. However, sample size can be further expanded, and research conclusions can further be confirmed by multi-center control studies.

ACKNOWLEDGEMENTS

The study received a Research Grant [Grant No. 2017FE468(-032)] from Yunnan Applied Basic Research Project-Union Foundation. The authors are grateful for the excellent technical assistance provided by Prof. Lan-fang Qin and Xu Liu.

REFERENCES

1. Astill Wright L , Sijbrandij M , Sinnerton R , Lewis C, Roberts NP , Bisson JI . Pharmacological prevention and early treatment of post-traumatic stress disorder and acute stress disorder: a systematic review and meta-analysis. Transl Psychiatry 2019; 9(1):334.
2. Douglas KM , Groves S , Porter RJ , et al . Traumatic imagery following glucocorticoid administration in earthquake-related post-traumatic stress disorder: A preliminary functional magnetic resonance imaging study. Aust N Z J Psychiatry 2019; 53(12):1167-78.
3. Colaneri M, Seminari E, Piralla A, et al. COVID19 IRCCS San Matteo Pavia Task Force. Lack of SARS-CoV-2 RNA environmental contamination in a tertiary referral hospital for infectious diseases in Northern Italy. J Hosp Infect 2020; 105(3):474-76.
4. Luan J, Lu Y, Jin X, Zhang L. Spike protein recognition of mammalian ACE2 predicts the host range and an optimized ACE2 for SARS-CoV-2 infection. Biochem Biophys Res Commun 2020; 526(1):165-69.
5. Mazzella Ebstein AM, Joseph SJ, Hernandez M. Psychological stress and pancreatic cancer patients: a qualitative systematic review protocol. JBI Database System Rev Implement Rep 2020; 18(3):576-82
6. Roberts NP, Kitchiner NJ, Kenardy J, Lewis CE, Bisson JI. Early psychological intervention following recent trauma: a systematic review and meta-analysis. Eur J Psychotraumatol 2019; 10(1):1695486
7. Bell TM , Vetor AN , Zarzaur BL. Prevalence and treatment of depression and posttraumatic stress disorder among trauma patients with non-neurological injuries. J Trauma Acute Care Surg 2018; 85(5):999-1006
8. Bryant RA. The Current Evidence for Acute Stress Disorder. Curr Psychiatry Rep 2018; 20(12):111.
9. Kheirabadi GR, Yousefian Z, Zargar F, Bahrami M, Maracy MR. Citalopram and metacognitive therapy for depressive symptoms and cognitive emotion regulation in patients with major depressive disorder: A randomized controlled trial. J Educ Health Promot 2020; 9:6
10. Nejati S, Khakpai F, Zarrindast MR. Synergistic effect between citalopram and citicoline on anxiolytic effect in non-sensitized and morphine-sensitized mice: An isobologram analysis. Brain Res 2020; 1734:146701
11. Lu H. Drug treatment options for the 2019-new coronavirus (2019-nCoV). Biosci Trends 2020; 14(1):69-71.
12. Wang Y, Ding Y, Yang C, et al. Inhibition of the infectivity and inflammatory response of influenza virus by Arbidol hydrochloride in vitro and in vivo (mice and ferret). Biomed Pharmacother 2017; 91:393-401.

LETTER TO THE EDITOR

Effects of luteolin in different doses on the cardiomyocyte apoptosis in rats with myocardial ischemia reperfusion

JP. Li[1*], R. Yan[2*], PL. Ma[1], P. Fu[3], HT. Tian[4] and LL. Wang[4]

[1]Department of Anesthesiology, Qingdao Hospital of Traditional Chinese Medicine, Qingdao Hiser Hospital, Qingdao, China; [2]ECG Room, Yantaishan Hospital, Yantai, China; [3]Department of Anesthesiology, Qingdao Fuwai Cardiovascular Hospital, Qingdao, China; [4]Department of Anesthesiology, Jining NO.1 People's Hospital, Affiliated Jining NO.1 People's Hospital of Jining Medical University, Jining Medical University, Jining, China

Received September 15, 2020 – Accepted November 27, 2020

[*]These Authors contributed equally to this work

To the Editor,

Myocardial ischemia (MI) is a common clinical disease with complex pathogenesis and a high fatality rate (1). The most effective way to reduce the damage of MI is to restore tissue perfusion. However, the ischemic myocardium will induce a series of functions, structure, metabolism and electrophysiological characteristics of myocardial cells and other aspects of the damage after the restoration of blood reperfusion, which will further aggravate the myocardial ischemia-reperfusion injury (MIRI) (2). Cardiomyocyte apoptosis is the main factor of myocardial cell death in the early stage of MI, and ischemia-reperfusion injury accelerates its apoptosis (3). Studies have shown that the effective components of traditional Chinese medicine could prevent and control MIRI through a variety of mechanisms, showing multi-target effect and reflecting the overall characteristic advantages of traditional Chinese medicine (4). Luteolin is one of the most abundant secondary metabolites in plants and has various pharmacological activities (5). Luteolin has been reported to have antioxidant, antimicrobial, anti-inflammatory, chemoprevention, chemotherapy, cardioprotection, anti-diabetic, neuroprotective and anti-allergic properties (6). In this study, based on the establishment of MIR model in rats, the changes of myocardial infarction rate, myocardial cell apoptosis and some biochemical indexes were detected to evaluate the protective effects of luteolin in different doses on myocardium after ischemia-reperfusion in rats. Luteolin may be a potential candidate for the prevention and treatment of cardiovascular disease.

MATERIALS AND METHODS

Experimental animals and treatment of animals

Forty male SD rats (body weight 200-250g) were purchased from the Affiliated Qingdao Hiser Hospital of Qingdao University. All rats were fed adaptively for 1 week and prior to the experiment. Forty rats were randomly divided into 4 groups (n=10 in each), namely sham operation group (sham), ischemia-reperfusion (IR) model group (model), luteolin low-dose group (LD), and luteolin high-dose group (HD), respectively.

Key words: luteolin; myocardial reperfusion; myocardial ischemia; apoptosis; rats

Corresponding Author:
Dr Lulu Wang,
Department of Anesthesiology, Jining NO.1 People's Hospital,
Affiliated Jining NO.1 People's Hospital of Jining Medical University,
Jining Medical University,
Jining 272000, China
e-mail: zly9cx@163.com

0393-974X (2020)
Copyright © by BIOLIFE, s.a.s.
This publication and/or article is for individual use only and may not be further reproduced without written permission from the copyright holder.
Unauthorized reproduction may result in financial and other penalties
DISCLOSURE: ALL AUTHORS REPORT NO CONFLICTS OF INTEREST RELEVANT TO THIS ARTICLE.

The sham group was given 0.5% sodium carboxymethyl cellulose (CMC-Na, 10ml/(kg·d) once a day) for 5 days without ischemia-reperfusion treatment. The model group was fed with 0.5% CMC-Na (10ml/(kg·d) once a day) for 5 days, then underwent ischemia for 30 min, and reperfusion for 120 min. The luteolin-treated group was intragastrically administered with 10 mg/(kg·d) and 50 mg/(kg·d) once a day, respectively. The rest of the operation in the luteolin-treated group was the same as the model group. All animal procedures were approved by the Ethics Committee of the Affiliated Qingdao Hiser Hospital of Qingdao University.

Establishment of myocardial ischemia reperfusion model

A model of myocardial ischemia reperfusion (MIR) was made by ligating the left anterior descending (LAD) coronary artery of the rats. The rats were anesthetized with 3% pentobarbital sodium. Electrodes were inserted subcutaneously in the extremities to monitor the electrocardiogram. A small animal ventilator was connected to control breathing. An incision was made approximately 0.5 cm from the left margin of the sternum at the third and fourth intercostal spaces on the left side of the rat to fully expose the heart. The LAD coronary artery was ligated with surgical thread. After 30 min, the ligation was released and myocardial reperfusion was performed for 120 min. When the ST segment of the electrocardiogram was obviously raised, the myocardial color of the ligation site was darkened. During reperfusion, the ST segment dropped by more than $^{1}/_{2}$, and the color of myocardium turned red, indicating that the construction of MIR model was successful. Coronary arteries were not ligated after threading in the sham group.

Detection of correlation index

The heart was removed and rinsed with phosphate buffered saline (PBS) then quickly placed maintained at -20°C for 5 min. Then in the direction parallel to the atrioventricular sulcus, the left ventricle was transected into thin slices of 1~2mm thickness. Slices were put into 1% TTC dye solution for 15~30 min in a 37°C water bath thermostat to avoid light. After the reaction was completed, the myocardial slices were taken out and fixed in 10% formalin solution for about 24 h. Then they were scanned with a scanner. The non-infarcted area was brick red, and the infarcted area was off-white. The plane area quadrature method was used to calculate the myocardial infarction rate: myocardial infarction rate (%) = infarct area/total left ventricular area × 100%.

Cardiomyocyte apoptosis was detected strictly according to the instructions of In Situ Cell Death Detection Kit, POD kit (Roche, Switzerland). After dewaxing and hydration, the sections were treated with 10 mmol proteinase K for 15 min. The slides were immersed in the TUNEL reaction mixture and incubated at 37°C for 60 min in the dark. Then incubation with POD reaction solution was performed in the dark for 30 min at 37°C. The blue nuclear staining was normal cells, and the brown nuclear staining was apoptotic cells (positive cells). The slides were analyzed with an optical microscope. For each sample, 8 areas were randomly selected to count and calculate the average apoptotic cells. Cardiomyocyte apoptosis rate (%) = average total number of positive cells/average total number of cells × 100%. After 120 min of IR, 6 ml of blood was taken from the abdominal aorta. Then the blood was left for 30 min, and centrifuged at 3000 r/min for 10 min at 4°C to separate serum. The contents of CK and LDH in serum were determined by chemical colorimetry according to the kit instructions (TSZ, USA). After separating the serum, the enzyme-linked immunosorbent assay (ELISA) was used for TNF-α and IL-6 detection according to the instructions of the TNF-α and IL-6 kits (TSZ, USA). The myocardial tissue of each group was made into a 10% homogenate. Superoxide dismutase (SOD) activity, malondialdehyde (MDA) content and GSH/GSSG ratio in the rat myocardial tissue were detected according to the manufacturer's instructions (TSZ, USA).

Statistical analysis

SPSS 13.0 software was used to analyze the experimental data. The measurement data was expressed as mean ± standard deviation ($\bar{x}\pm s$). The significance of the difference between the groups was compared by one-way ANOVA. $P < 0.05$ was considered statistically significant.

RESULTS

Effects of luteolin on serum CK and LDH activities

Compared with the sham group, the serum CK and LDH activities of the rats in the model group were significantly increased (Table I, $P< 0.05$).

However, the serum CK and LDH activities in the luteolin groups were obviously decreased *versus* the Model group, especially in the HD group (Table I, $P< 0.05$). The results showed that luteolin could inhibit the release of MIR rat serum LDH and CK. It confirmed that the rat model of MIRI was successfully established.

Table I. *Result of the activity of LDH and CK in serum of rats in each group ($\bar{x}\pm s$ U/mL)*

Group	LDH	CK
Sham	1.396±0.275	0.695±0.095
Model	4.810±0.716[a]	1.981±0.106[a]
LD	3.633±0.501[ab]	1.602±0.114[ab]
HD	2.308±0.420[abc]	0.942±0.108[abc]

[a]: compared with sham examination, P < 0.05.
[b]:compared with model group, p<0.05. [c]: compared with LD group, p<0.05.

Table II. *Result of the SOD activity, MDA content and GSH/GSSG ratio of myocardial tissue in isolated heart of rats in each group ($\bar{x}\pm s$)*

Group	TNF-α (ng/L)	IL-6 (pg/mL)
Sham	19.614±1.633	8.807±0.818
Model	69.195±5.584[a]	19.622±1.634[a]
LD	53.997±4.255[ab]	14.609±1.614[ab]
HD	39.169±3.521[abc]	11.174±1.008[abc]

[a]: compared with sham examination, P < 0.05.
[b]:compared with model group, p<0.05. [c]: compared with LD group, p<0.05.

Effect of luteolin on the rate of myocardial infarction

Compared with the sham group, the model group had severe ischemia of isolated heart muscle and the rate of myocardial infarction (Fig. 1, $P< 0.05$). Compared with the model group, the isolated myocardial ischemia state was improved and the myocardial infarction rate was significantly reduced of rats in the LD and HD groups (Fig. 1, $P< 0.05$). The above changes in the HD group were more obvious than those in the LD group (Fig. 1, $P< 0.05$).

Effect of luteolin on apoptosis of cardiac myocytes

Compared with the sham group, the model group's cardiac myocyte apoptosis rate increased significantly (Fig. 2, $P< 0.05$). It was significantly reduced in the luteolin treatment group compared with Model group, and the reduction in the HD group was more obvious (Fig. 2, $P< 0.05$).

Effect of luteolin on inflammation

As shown in Table II, the content of proinflammatory cytokines TNF-α and IL-6 in the model and luteolin groups were significantly increased compared with the sham group ($P< 0.05$), while they were significantly reduced in LD and HD group compared to the model group ($P< 0.05$). The change in the HD group was more obvious than that in LD group ($P< 0.05$). These results suggest that luteolin could decrease the levels of TNF-α and IL-6 in MIR rats.

Effect of luteolin on SOD activity, MDA content and GSH/GSSG ratio in myocardial tissue

Compared with the sham group, the SOD

Table III. *Result of the SOD activity, MDA content and GSH/GSSG ratio of myocardial tissue in isolated heart of rats in each group ($\bar{x}\pm s$)*

Group	SOD (U/mg·prot)	MDA (μmol/kg·prot)	GSH/GSSG ratio
Sham	10.141±0.426	265.840±20.448	37.101±0.718
Model	1.121±0.337[a]	639.735±16.529[a]	16.845±0.825[a]
LD	3.426±0.309[ab]	566.387±18.977[ab]	29.929±1.022[ab]
HD	7.826±0.279[abc]	456.405±17.335[abc]	23.261±1.103[abc]

[a]: compared with sham examination, P < 0.05. [b]: compared with model group, p<0.05. [c]: compared with LD group, p<0.05.

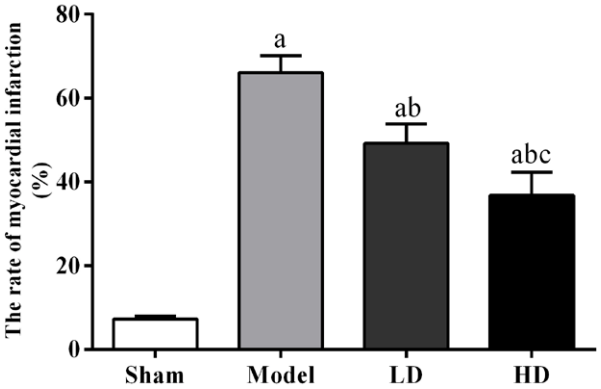


Fig. 1. *Result of the myocardial infarction rate in heart of rats in each group.* ***a)*** *p<0.05, compared with sham group.* ***b)*** *p<0.05, compared with model group.* ***c)*** *p<0.05, compared with LD group.*

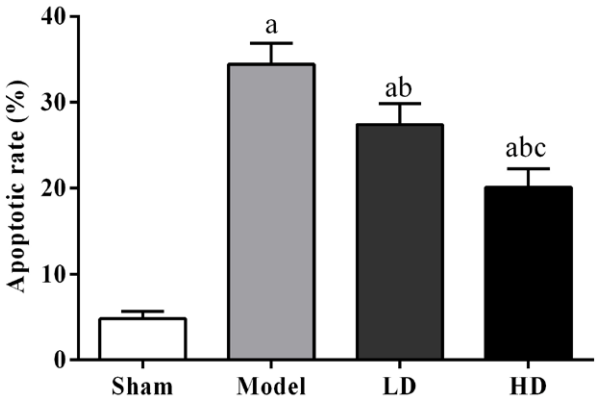


Fig. 2. *Result of the apoptosis rate of cardiac muscle cell in heart of rats in each group.* ***a)*** *p<0.05, compared with sham group.* ***b)*** *p<0.05, compared with model group.* ***c)*** *p<0.05, compared with LD group.*

activity and GSH/GSSG ratio in the isolated heart muscle tissue of the model group was significantly reduced, while the MDA content was significantly increased (Table III, $P< 0.05$). Compared with the model group, the SOD activity and the GSH/GSSG ratio increased significantly while the MDA content decreased obviously in isolated cardiac muscle tissue of rats treated by luteolin, especially in the HD group (Table III, $P< 0.05$).

DISCUSSION

Cardiomyocyte apoptosis is one of the major causes of MIRI. Myocardial cell damage can lead to changes in cell membrane permeability, thus a large amount of myocardial enzymes are released into the blood. (7). The results of this study showed that the myocardial infarction rate and the myocardial cell apoptosis rate were decreased in the luteolin group compared to the model group, especially in high-dose luteolin, indicating that luteolin could alleviate MIR.

MIRI also could cause inflammatory response. Wu et al. found that osthole inhibited the release of inflammatory factors IL-6, IL-1β and TNF-α to slow down myocardial cell injury in MIR rats (8). The results of this study showed that luteolin could significantly reduce the content of IL-6 and TNF-α in MIRI rats, and more significantly in the high concentration group. The antioxidant enzyme system, such as SOD, removes small amounts of free radicals from the body under normal circumstances (9). When the ischemic and hypoxic tissue restores blood supply, oxidative stress in the myocardial tissue reduces the antioxidant enzymes and releases a large amount of oxygen free radicals (10). This study found that the myocardial tissue MDA content was notably decreased, SOD content and GSH/GSSG ratio were obviously increased in the luteolin group compared with the model group, especially in the high-dose group.

In summary, luteolin has a significant improvement effect on MIRI, mainly manifested as reducing myocardial infarction rate and myocardial cell apoptosis, reducing the release of myocardial isoenzymes LDH and CK, and reducing the level of oxidative stress and inflammation. Taken together, these results suggested that the improvement effect of luteolin on myocardium might be related to its antioxidant and anti-apoptotic activities, but the role of luteolin in MIRI needs to be confirmed by further experiments and clinical studies.

ACKNOWLEDGEMENTS

This study was funded by Key Research and Development Projects in Shandong (2018GSf118216), Development Plan of Medical

and Health Science and Technology (Projects) in Shandong province (2017WS524), Qingdao Medical Scientific Research Guidance Plan (2017-WJZD068, 2017-WJZD140, 2018-WJZD136), Supported by Qingdao Outstanding Health Professional Development Fund, and Shandong Medical and Health Science and Technology Development Plan Project (2015WS0316).

REFERENCES

1. Weiwei C, Runlin G, Lisheng L, et al. Outline of the report on cardiovascular diseases in China, 2014. Eur Heart J Suppl 2016; 18:F2-11.
2. Yu L, Li F, Zhao G, et al. Protective effect of berberine against myocardial ischemia reperfusion injury: role of Notch1/Hes1-PTEN/Akt signaling. Apoptosis 2015; 20:796-810.
3. Badalzadeh R, Mokhtari B, Yavari R. Contribution of apoptosis in myocardial reperfusion injury and loss of cardioprotection in diabetes mellitus. J Physiol Sci 2015; 65:201-15.
4. Liu Q, Li J, Wang J, Li J, Janicki JS, Fan D. Effects and mechanisms of Chinese herbal medicine in ameliorating myocardial ischemia-reperfusion injury. Evid Based Complementary Alternat Med 2013; 2013:925625.
5. Kisang K, Young-Sook K, Seung-Whan K, Yu K, Kyung-Ho L, O-Yu K. Luteolin-induced apoptosis through activation of endoplasmic reticulum stress sensors in pheochromocytoma cells. Mol Med Rep 2017; 16:380-86.
6. Luo Y, Shang P, Li D. Luteolin: a flavonoid that has multiple cardio-protective effects and its molecular mechanisms. Front Pharmacol 2017; 8:692.
7. Zheng Q, Bao XY, Zhu PC, Qiang T, Zheng GQ, Yan W. Ginsenoside Rb1 for myocardial ischemia/reperfusion injury: preclinical evidence and possible mechanisms. Oxid Med Cell Longev 2017; 2017:1-14.
8. Wu J, Yang Y, Xun N, Zeng L, Tang H. Osthole attenuates myocardial ischemia/reperfusion injury in rats by inhibiting apoptosis and inflammation. Am J Transl Res 2018; 10:1109-16.
9. Woźniak D, Dryś A, Matkowski A. Antiradical and antioxidant activity of flavones from Scutellariae baicalensis radix. Nat Prod Res 2015; 29:1567-70.
10. Sykiotis GP, Bohmann D. Stress-activated Cap'n'collar transcription factors in aging and human disease. Sci Signal 2010; 3:re3.

LETTER TO THE EDITOR

High expression of KPNA2 promotes colorectal cancer development by activating the PI3K/AKT pathway

B. Huang[1*], H. Luo[1*] and XB. Guo[2]

[1]Department of General Surgery, Institute of surgery Research Daping Hospital, Army Medical University, Chongqing, China; [2]Department of Gastrointestinal Surgery, The Second Affiliated Hospital of Guangzhou Medical University, Guangzhou, Guangdong Province, China

Received September 30. 2020 – Accepted November 27, 2020

*These Authors contributed equally to this work

To the Editor,

Colorectal cancer (CRC) is a malignant tumor that originates from the glandular epithelium of the large intestine and can occur in various segments of the large intestine (1). The specific cause of CRC is unclear, however, it has been reported that the incidence of CRC is mainly related to people's lifestyle, environment, and diet. Some types of CRC may be more related to genetic factors (2). In addition, the prognosis of CRC patients is related to tumor stage. The 5-year survival rate of CRC patients after radical surgery is approximately 50-70% (3). Therefore, finding effective targets for early diagnosis is of great significance for improving survival rates.

Recently, it has been reported that karyopherin α2 (KPNA2) regulates malignant behaviors in human cancers. KPNA2 over-expression was found to be a potential marker for the prognosis and therapeutic sensitivity of CRC patients (4). KPNA2 was also reported to be a reliable marker for identifying patients with high-risk stage II CRC (5). In addition, KPNA2 has been reported to promote cell migration and invasion in epithelial ovarian cancer by inducing epithelial-mesenchymal transition (EMT) via Akt/GSK-3β/Snail activation (6). However, the relationship between KPNA2 and the PI3K/AKT pathway in CRC has not been reported in previous studies. Therefore, the present study explored the regulatory mechanism of KPNA2/PI3K/AKT pathway in CRC. At the same time, the effects of KPNA2 on cell proliferation, migration and invasion in CRC were also investigated.

MATERIALS AND METHODS

Clinical tissue samples

CRC tissues and adjacent tissues (at least 5 cm from the edge of the tumor) were obtained from 92 patients. No patient had received other treatment prior to surgery. The clinicopathological characteristics of these patients were analyzed and are shown in Table I. The study was approved by the Ethics Committee of Institute of surgery Research Daping Hospital, Army Medical University., and all patients signed informed consents.

The difference of KPNA2 expression between CRC tissues and normal tissues was analyzed by Box plots. GEPIA (http://gepia.cancer-pku.cn/) is an interactive web server for analyzing gene expression from TCGA data. The screening conditions were colon adenocarcinoma (COAD), KPNA2 and boxplot.

Key words: KPNA2; colorectal cancer; proliferation; cell metastasis; PI3K/AKT

Corresponding Author:
Dr Xiongbo Guo,
Department of Gastrointestinal Surgery,
The Second Affiliated Hospital of Guangzhou Medical University,
No. 250 Changgang Dong Road, Haizhu District, Guangzhou,
510260, Guangdong Province, China
Tel.: +86 13544313514
e-mail: rangkow2128@163.com

0393-974X (2020)
Copyright © by BIOLIFE, s.a.s.
This publication and/or article is for individual use only and may not be further reproduced without written permission from the copyright holder.
Unauthorized reproduction may result in financial and other penalties
DISCLOSURE: ALL AUTHORS REPORT NO CONFLICTS OF INTEREST RELEVANT TO THIS ARTICLE.

Cell culture and transfection

The normal colon epithelial cell line NCM460 and CRC cell lines (SW620, HCT116) were purchased from BeiNa Biotechnology (BNCC, Beijing, China). The cells were seeded in RPMI-1640 medium with 10% fetal bovine serum (FBS) and incubated at 37°C under an atmosphere with 5% CO_2.

Short hairpin RNAs (shRNA) for KPNA2 (sh-KPNA2), scrambled oligonucleotides (sh-NC), KPNA2 vector (pcDNA-KPNA2) or empty pcDNA3.1 vector (pcDNA-NC) were purchased from GenePharma (Shanghai, China). Next, they were transfected into SW620 cells using Lipofectamine 3000 (Invitrogen, CA, USA), respectively. SW620 cells were seeded in a 6-well plate and incubated in infection medium with the siRNAs and vectors for 12 h. The medium was then replaced with fresh complete medium. The cells were screened with puromycin (Shanghai GeneChem Co., Ltd.) at a dose of 2μg/ml after 72 h transfection. The transfection efficiency was confirmed by RT-qPCR. SW620 cells with pcDNA-KPNA2 were treated with 10 μM PI3K inhibitor (LY294002, Selleck Chemicals) for 24 h to block the PI3K/AKT pathway.

Quantitative real-time PCR

TRIZOL reagent (Invitrogen, CA, USA) was used to isolate total RNA, and the PrimeScript RT Kit (Takara, Dalian, China) was applied to reverse transcribe KPNA2 into cDNA. RT-qPCR assay was performed using Real-time PCR mixture assays (Takara) in CFX96 real-time PCR detection system (Bio-Rad Laboratories, Inc.). GAPDH was used as an internal control for KPNA2. The relative expression of KPNA2 was analyzed using the $2^{-\Delta\Delta Cq}$ method. The primers used in qPCR were as follows: forward 5'-CAA GGC TGT GGT AGA TGG-3' and reverse, 5'-GCG GCA AAG ATT AGA AAG-3' for KPNA2; forward, 5'-CAA TGA CCC CTT CAT TGACC-3' and reverse, 5'-GAC AAG CTT CCC GTT CTC AG-3' for GAPDH.

Western blot analysis

RIPA lysis buffer (Beyotime) was used to obtain protein samples. Next, the proteins were separated by using 10% SDS-PAGE. The protein sample was blocked with 5% skim milk and transferred to the PVDF membrane. The protein sample was incubated with Bax (rabbit polyclonal antibody; dilution, 1:500; cat. no. 137321), Bcl-2 (rabbit polyclonal; dilution, 1:500; cat. no. ab45171), E-cadherin (rabbit monoclonal; dilution, 1:1,000; cat. no. ab1416; Abcam), N-cadherin (rabbit polyclonal; dilution, 1:1,000; cat. no. ab18203; Abcam), vimentin (rabbit monoclonal; dilution, 1:1,000; cat. no. ab217673; Abcam), PI3K (rabbit monoclonal; dilution, 1:1,000; cat. no. ab32089; Abcam), p-PI3K (rabbit monoclonal; dilution, 1:1,000; cat. no. ab154598; Abcam), AKT (rabbit polyclonal; dilution, 1:1,000; cat. no. ab8805; Abcam), p-AKT (rabbit monoclonal; dilution, 1:1,000; cat. no. ab81283; Abcam), KPNA2 (rabbit polyclonal; dilution, 1:1,000; cat. no. ab70160) and GAPDH (rabbit monoclonal, dilution, 1:1,000; cat. no. ab181602) primary antibodies (Abcam, Shanghai, China) at 4°C overnight. The protein sample was then incubated with the secondary antibody (mouse anti-rabbit, dilution, 1:2,000; cat. no. 58802; Abcam) for 1 h. Finally, the protein bands were evaluated using the ECL kit (Beyotime, Shanghai, China).

Assays

MTT assay was used to measure cell proliferation. SW620 cells were seeded in 96-well plates. The transfected cells were incubated for 24, 48, 72 and 96 h, respectively. Then, the cells were incubated with MTT solution (Sigma, USA) for 4 h at 37°C. The absorbance at 490 nm was detected with a spectrophotometer.

The transfected cells (500 cells/well) were seeded in a 6-well plate. Then, the cells were placed in a cell incubator for 7-14 days, and the cell status was observed every 3 days. When macroscopic colonies appeared in the petri dish, the culture was terminated. The supernatant was discarded and carefully washed twice with PBS and 4% paraformaldehyde was added to fix the cells for 15 min. Then the fixative was removed, and the colonies were stained with GIMSA staining solution for 30 min. Finally, colonies were counted.

The transfected SW620 cells (4×10^3 cells/well) on a glass petri dish were incubated overnight at 37°C until the cells reach 90% confluence. Then, a straight scratch was made with a plastic pipette tip. After 48 h, the wound gap was observed under an inverted light microscope. Finally, the wound was imaged at 0 and 48 h.

The capacity for cell migration was assessed using Transwell chambers (8 μm diameter; Corning Inc., Corning, NY, USA). After the transfected SW620 cells were cultured

for 48 h, the cells were resuspended in RPMI-1640 without FBS. In total, 100 μL of suspension (5×10^3 cells/well) were placed in the upper chamber. The lower chamber was added with RPMI-1640 medium with 10% FBS. At 24 h after inoculation, non-migratory cells were gently removed, and the migratory cells were fixed with 100% methanol, stained with 0.5% crystal violet, washed with PBS, and imaged using an inverted microscope (Olympus Corporation, Tokyo, Japan). The Transwell invasion assays were similar to the migration assay except that the chambers were precoated with Matrigel (BD Biosciences).

Statistical analysis

The experimental data were analyzed using Graphpad Prism 6 software. Data are expressed as mean ± SD. Student's *t*-test and one-way ANOVA were used to analyze the differences between two or multiple groups. The relationship between KPNA2 expression and clinicopathological characteristics of CRC patients was analyzed using *Chi*-squared test. $P < 0.05$ was considered statistically significant.

RESULTS

KPNA2 is upregulated in CRC tissues and cells

Firstly, the GEPIA database (http://gepia.cancer-pku.cn/) was used to predict the expression of different genes in CRC. Box plot analysis showed that KPNA2 expression was increased in CRC tissues compared with normal tissues ($P < 0.05$, Fig. 1A). In order to verify the above results, this study also detected the expression of KPNA2 in 92 CRC tissues by RT-qPCR. Compared with normal tissues, KPNA2 was upregulated in CRC tissues ($P < 0.01$, Fig. 1B). At the same time, KPNA2 expression was found to be higher in CRC cell lines SW620 and HCT116 compared with the normal colon epithelial NCM460cell line ($P < 0.05$, Fig. 1C). The expression of KPNA2 was highest in SW620 CRC cells, therefore, SW620 cells were used for further experiments in this study. In addition, the relationship between abnormal expressions of KPNA2 and clinical features in CRC patients was analyzed. The tumor size, TNM stage and lymph node metastasis of CRC patients were related to the abnormal expression of KPNA2 ($P < 0.05$, Table I). Based on these results, we conclude that KPNA2 may play an important role in the tumorigenesis of CRC.

KPNA2 promotes cell viability in CRC

In order to explore the function of KPNA2 in the development of CRC, sh-KPNA2 or sh-NC

Table I. *Correlation between the clinicopathologic characteristics and KPNA2 expression in CRC*

Characteristics	Number of Cases (n=92)	KPNA2		P-value
		High	Low	
Age (years)				0.54
≥ 60	44	28	16	
<60	48	33	15	
Gender				0.43
Male	47	32	15	
Female	45	29	16	
Tumor size (cm)				0.04*
≥ 5	50	36	14	
<5	42	25	17	
TNM stage				0.03*
I + II	62	39	23	
III + IV	30	22	8	
Lymph node metastasis				0.02*
No metastasis	59	39	20	
Metastasis	33	22	11	

*Statistical analyses were performed by the χ2 test. TNM: tumor node metastasis; *P<0.05 was considered significant.*

was transfected into SW620 CRC cells. Compared with the sh-NC group, the expression of KPNA2 in the sh-KPNA2 group was significantly reduced ($P < 0.01$, Fig. 2A). Next, MTT assay showed that down-regulation of KPNA2 significantly inhibited cell proliferation in SW620 cells ($P < 0.01$, Fig. 2B). Similarly, the colony formation assay showed that knockdown of KPNA2 significantly inhibited the clone formation capacity in SW620 cells compared with the sh-NC group ($P < 0.05$, Fig. 2C). In addition, the effect of KPNA2 on pro-apoptotic protein Bax and anti-apoptotic protein Bcl-2 was investigated in SW620 cells. Western blot analysis indicated that Bax expression was increased in the sh-KPNA2 group, and Bcl-2 expression was reduced in SW620 cells with sh-KPNA2 ($P < 0.05$, Fig. 2D). These results indicate that knockdown of KPNA2 can inhibit cell viability in CRC.

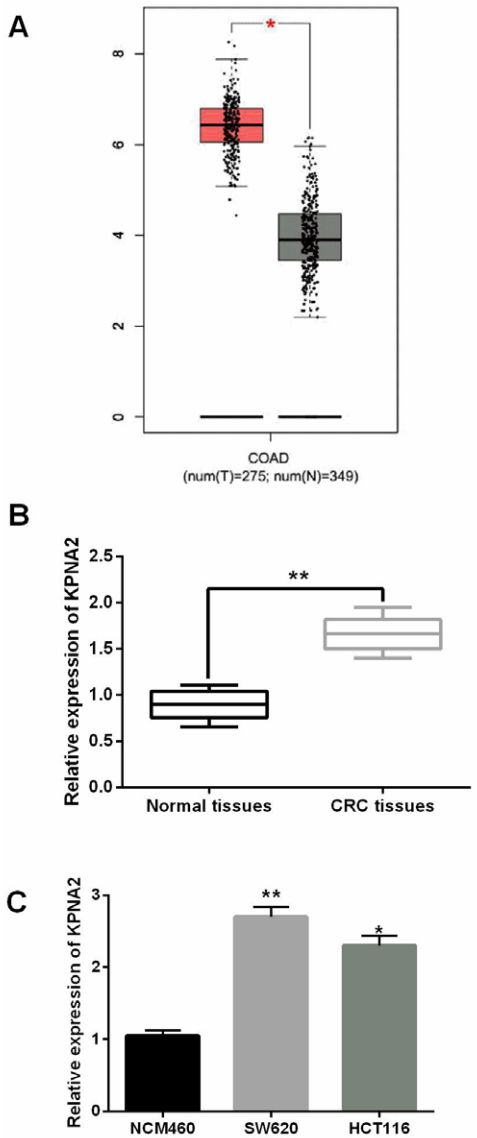


Fig. 1. *KPNA2 is upregulated in CRC tissues and cells. **A**) Expression level of KPNA2 in CRC tissues n=375) and normal tissues n=349) analyzed in TGCA database. **B**) KPNA2 expression was detected in CRC tissues and normal tissues n=92) by RT-qPCR. **C**) KPNA2 expression in SW620 and HCT116 CRC cell lines and normal colon epithelial cell line NCM460. *P < 0.05, **P < 0.01*

KPNA2 promotes cell metastasis and EMT in CRC

Next, the effect of KPNA2 on cell migration and invasion was investigated in CRC cells. Wound healing assay showed that downregulation of KPNA2 significantly reduced the scratch healing ability of SW620 cells ($P < 0.05$, Fig. 3A). Compared with the sh-NC group, Transwell assay showed that KPNA2 knockdown significantly inhibited cell migration and invasion in SW620 cells ($P < 0.01$, Fig. 3 B, C). Then, the effect of KPNA2 on EMT was investigated in SW620 cells by detecting the expression of E-cadherin, N-cadherin and Vimentin. Western blot analysis showed that the expression of E-cadherin was increased by downregulation of KPNA2, while N-cadherin and Vimentin expressions were decreased by KPNA2 downregulation in SW620 cells ($P < 0.05$, Fig. 3D). Collectively, KPNA2 silencing inhibits cell migratory and invasive abilities and EMT in CRC.

Overexpression of KPNA2 activates the PI3K/AKT pathway in CRC cells

In order to explore the underlying mechanism of KPNA2 in the progression of CRC, the relationship between KPNA2 and PI3K/AKT pathway was investigated in SW620 cells. After transfection of pcDNA-NC or pcDNA-KPNA2, the protein expression of PI3K/AKT pathway components was detected in CRC cells. Then, SW620 cells with pcDNA-NC and pcDNA-KPNA2 were treated with PI3K inhibitor (10 μM, LY294002) for 24 h. The protein expression of PI3K/AKT pathway components was also detected. Western blot analysis showed that the upregulation of KPNA2 promoted p-PI3K and p-AKT expressions in SW620 cells. At the same time, PI3K inhibitor significantly reduced

the expression levels of p-PI3K and p-AKT in SW620 cells. However, pcDNA-KPNA2 restored the decreased expression of p-PI3K and p-AKT induced by PI3K inhibitor ($P < 0.01$, Fig 4A). These results indicate that the upregulation of KPNA2 can activate the PI3K/AKT pathway in CRC cells. Next, MTT and Transwell assays were performed to preliminarily explain the functional mechanism of the KPNA2/PI3K/AKT pathway. We found that the upregulation of KPNA2 promoted the proliferation, migration and invasion of SW620 cells. However, PI3K inhibitor can attenuate the promoting effect of KPNA2 on cell proliferation, migration and invasion ($P < 0.05$, Fig 4 B-D). In summary, upregulation of KPNA2 can promote cell viability and metastasis in CRC by activating the PI3K/AKT pathway.

DISCUSSION

In this study, the expression of KPNA2 was increased in CRC tissues and cells. We also found that the abnormal expression of KPNA2 was related to tumor size, TNM stage and lymph node metastasis in CRC patients. More importantly, it was found that

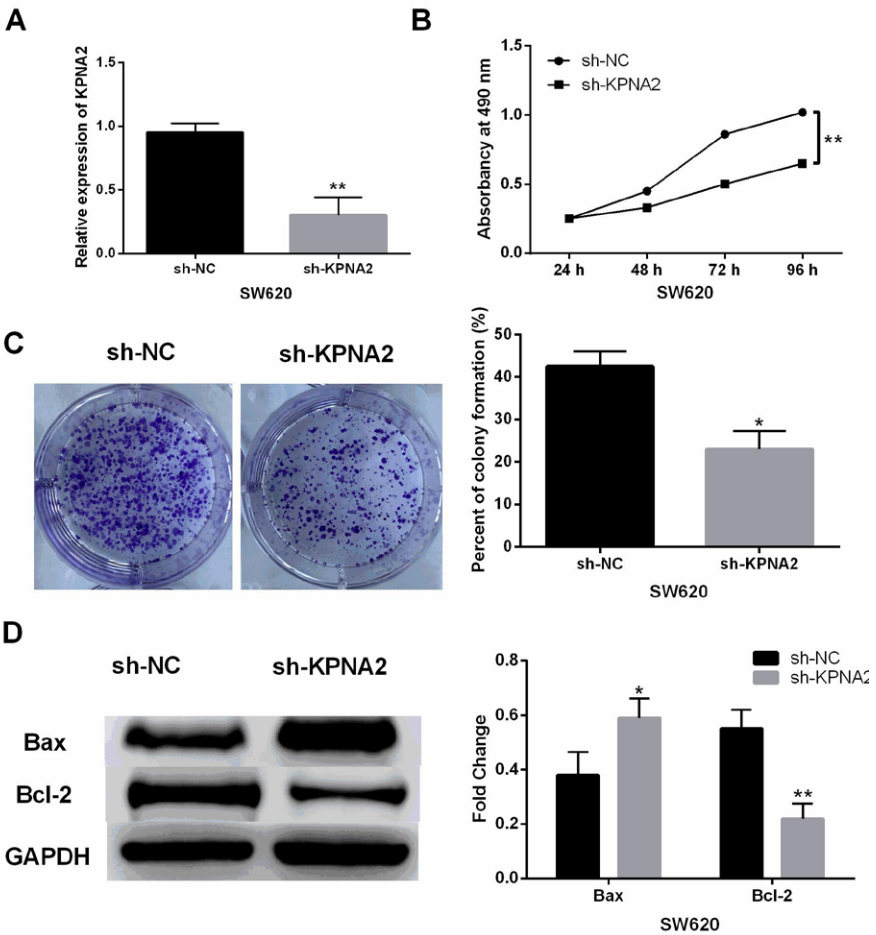


Fig. 2. *KPNA2 promotes cell viability in CRC.* ***A****) KPNA2 expression in SW620 cells with sh-KPNA2 or sh-NC.* ***B****) Cell proliferation was detected in SW620 cells with sh-KPNA2 or sh-NC by MTT assay.* ***C****) Colony formation capacity of SW620 cells with sh-KPNA2 or sh-NC D) Apoptosis-related proteins Bcl-2/Bax) was detected in SW620 cells with sh-KPNA2 or sh-NC by Western blot analysis. *P < 0.05, **P < 0.01*

knockdown of KPNA2 inhibited cell proliferation in CRC. Downregulation of KPNA2 promoted Bax expression and reduced Bcl-2 expression in SW620 cells. In addition, downregulation of KPNA2 can inhibit cell migration, invasion and EMT in CRC. All these results suggest that KPNA2 acts as a tumor promoter in the progression of CRC.

Similarly to our study, it has been reported that KPNA2 expression is a novel diagnostic and prognostic factor for CRC (7). In addition, KPNA2 expression in CRC tumors and lymph node metastasis specimens was higher than that in normal tissues (8). More importantly, Wip1 cooperated with KPNA2 to regulate cell proliferation and migration

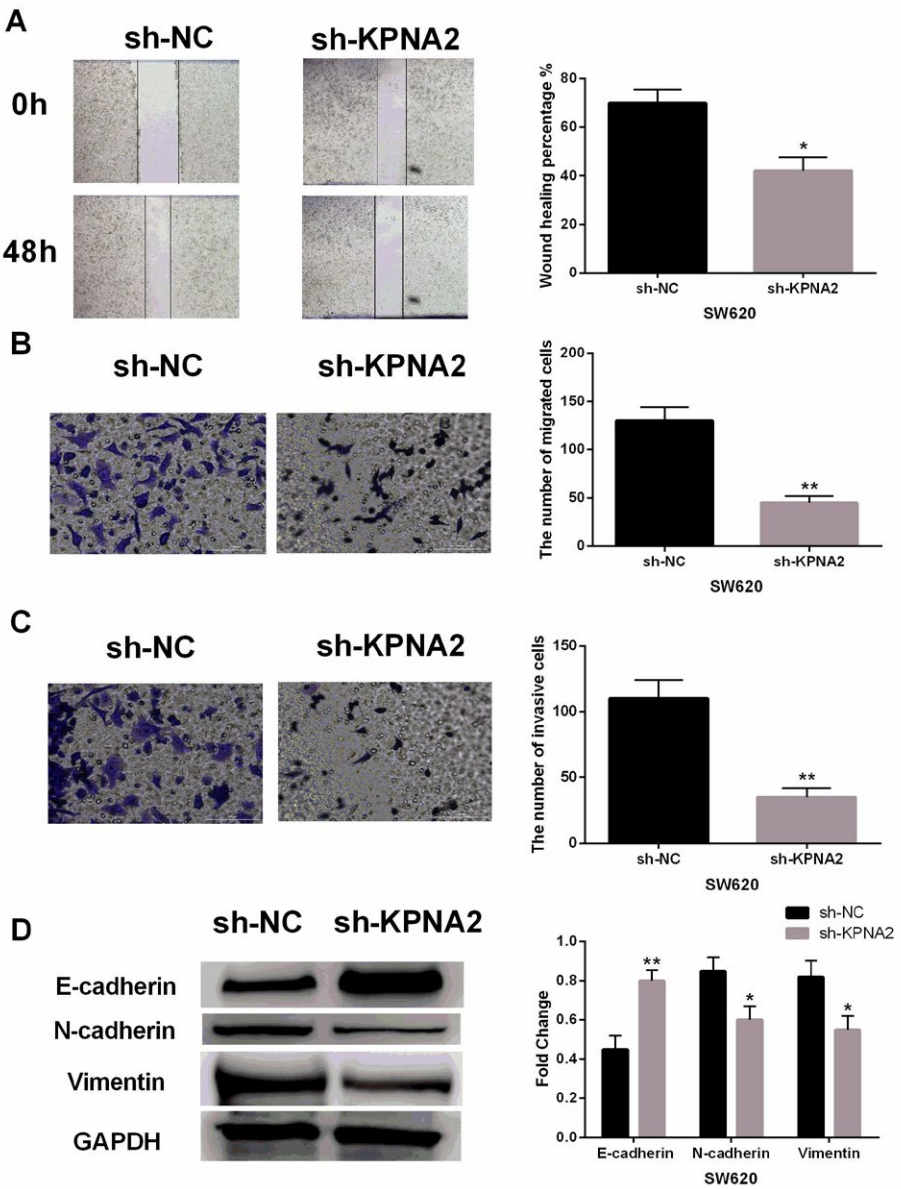


Fig. 3. *KPNA2 promotes cell metastasis and EMT in CRC.* ***A)*** *Cell migration was detected in SW620 cells with sh-KPNA2 or sh-NC by Wound healing assay.* ***B, C)*** *Cell migration and invasion were detected in SW620 cells with sh-KPNA2 or sh-NC by Transwell assay.* ***D)*** *E-cadherin, N-cadherin and Vimentin expression was detected in SW620 cells with sh-KPNA2 or sh-NC by Western blot analysis. *P < 0.05, ** P <0.01*

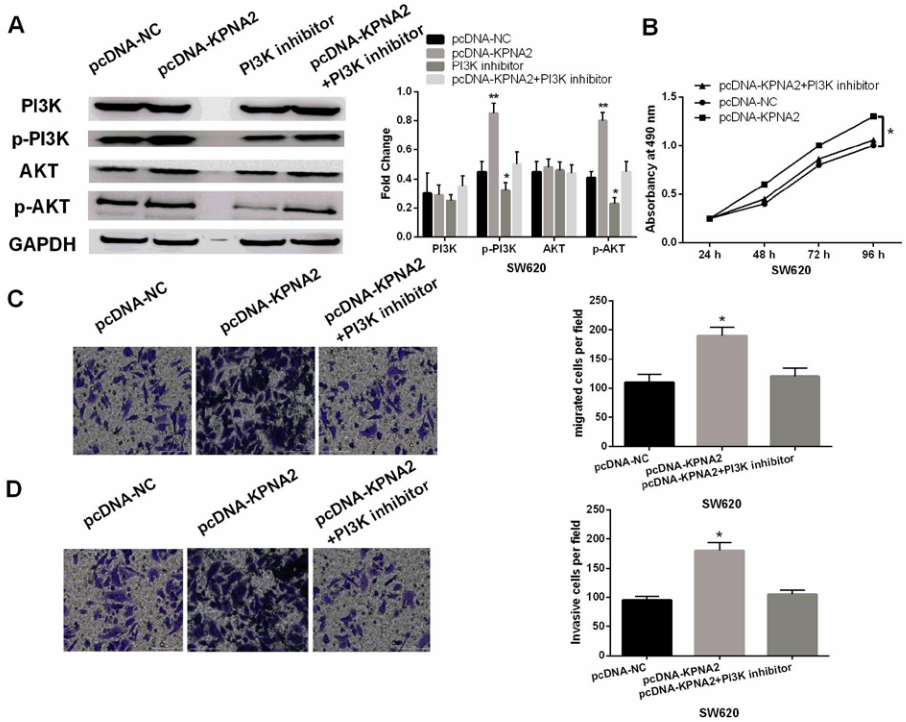


Fig. 4. *KPNA2 regulates the PI3K/AKT pathway in CRC cells.* ***A)*** *PI3K, AKT, p-PI3K and p-AKT expression was detected in SW620 cells with pcDNA-NC, pcDNA-KPNA2, PI3K inhibitor or pcDNA-KPNA2+PI3K inhibitor by Western blot analysis.* ***B, C, D)*** *Cell proliferation, migration and invasion were assessed in SW620 cells with pcDNA-NC, pcDNA-KPNA2, or pcDNA-KPNA2+PI3K inhibitor. *P < 0.05, ** P <0.01*

in CRC (9). A similar inhibitory effect of KPNA2 silencing in CRC was also detected in the present study. In addition, we also found that KPNA2 silencing inhibited EMT in CRC, which has not been reported in previous studies.

In this study, upregulation of KPNA2 promoted cell viability and metastasis in CRC by activating the PI3K/AKT pathway. Similarly, FOXCUT promoted cell proliferation and invasion by activating the FOXC1/PI3K/AKT pathway in CRC (10). These findings indicate that KPNA2 may promote the development of CRC through activation of the PI3K/AKT pathway. However, this study lacks *in vivo* experiments, therefore, *in vivo* experiments should be performed in the future to verify our results.

REFERENCES

1. Courtney RJ, Paul CL, Carey ML, et al. A population-based cross-sectional study of colorectal cancer screening practices of first-degree relatives of colorectal cancer patients. BMC Cancer 2013; 13:13.
2. Bray F, Ferlay J, Soerjomataram I, Siegel RL, Torre LA, Jemal A. Global cancer statistics 2018: GLOBOCAN estimates of incidence and mortality worldwide for 36 cancers in 185 countries. CA Cancer J Clin 2018; 68:394-424.
3. Kong JC, Guerra GR, Pham T, et al. Prognostic impact of tumor-infiltrating lymphocytes in primary and metastatic colorectal cancer: a systematic review and meta-analysis. Dis Colon Rectum 2019; 62:498-508.
4. Takada T, Tsutsumi S, Takahashi R, et al. KPNA2 over-expression is a potential marker of prognosis and therapeutic sensitivity in colorectal cancer patients. J Surg Oncol 2016; 113:213-17.
5. Jeong D, Kim H, Ban S, et al. Karyopherin alpha-2 is a reliable marker for identification of patients with high-risk stage II colorectal cancer. J Cancer Res Clin Oncol 2017; 143:2493-503.

6. Huang L, Zhou Y, Cao X, Lin J, Zhang L, Huang S, Zheng M. KPNA2 promotes migration and invasion in epithelial ovarian cancer cells by inducing epithelial-mesenchymal transition via Akt/GSK-3β/Snail activation. J Cancer 2018; 9:157-65.
7. Yu L, Wang G, Zhang Q, et al. Karyopherin alpha 2 expression is a novel diagnostic and prognostic factor for colorectal cancer. Oncol Lett 2017; 13:1194-200.
8. Zhang Y, Zhang M, Yu F, Lu S, Sun H, Tang H, Peng Z. Karyopherin alpha 2 is a novel prognostic marker and a potential therapeutic target for colon cancer. J Exp Clin Cancer Res 2015; 34:145.
9. Wang P, Zhao Y, Liu K, et al. Wip1 cooperates with KPNA2 to modulate the cell proliferation and migration of colorectal cancer via a p53-dependent manner. J Cell Biochem 2019; 120:15709-18.
10. Zhang X, Yi S, Xing G, Wu H, Zhu Y, Guo X, Zhang L. FOXCUT promotes the proliferation and invasion by activating FOXC1/PI3K/AKT pathway in colorectal cancer. Cancer Manag Res 2020; 12:6269-78.

LETTER TO THE EDITOR

Clinical experience of extracorporeal shockwave treatment on diaphyseal forearm non-union: effects on healing and bone density

A. Notarnicola[1,2], M. Baglioni[1], I. Covelli[1,2], FP. Bianchi[3], L. Moretti[1], G. Maccagnano[1,2] and B. Moretti[1,2]

[1]Orthopedics Section, Department of Medical Sciences of Basis, Neurosciences and Organs of Sense, Faculty of Medicine and Surgery, University of Study of Bari, General Hospital, Bari, Italy; [2]Course of Motor and Sports Sciences, Department of Medical Sciences of Basis, Neurosciences and Organs of Sense, Faculty of Medicine and Surgery, University of Study of Bari, Bari, Italy; [3]Department of Biomedical Sciences and Human Oncology, Faculty of Medicine and Surgery, University of Study of Bari, General Hospital, Bari, Italy

Received April 7, 2020 – Accepted October 9, 2020

To the Editor,

Within 3-6 months after trauma the failure to respect physiological bone healing times is a possible eventuality and occurs in about 8% of cases of diaphyseal fractures (1). According to the literature, fracture healing is associated with an increase in bone mineral density (BMD), with values of at least 75% of the contralateral segment (2). Dual-energy X-ray absorptiometry (DXA) is an effective method for monitoring early local bone response, already at 3 weeks. In an animal model after Extracorporeal Shockwave Therapy (ESWT) on femur osteotomy, significant increases in callus size, bone mineral density and bone tissue formation have been found (3).

The initial interpretation of shock wave (SW) application and regenerative effects on bone tissue is a mechanical stimulation comparable to the micro-damage of a fracture (4). This mechanical stimulation on fracture is responsible for a subperiosteal hematoma, which should increase the volume of trabecular bone and cancellous bone in the first 2 weeks and, subsequently, a periosteal reaction with neo-cortical formation. According to recent literature, SWs are responsible for a mechanotransduction stimulation which may guarantee the transformation of the mechanical stimulation into biochemical signals. Osteogenesis is due to multiple endogenous pathways (5). SWs are able to improve the differentiation of stem cells into an osteogenetic line by inducing a RANKL/OPG ratio reduction with inhibition of osteoclastogenesis on osteoblasts, thus causing osteocyte death. In effect, the RANKL/OPG ratio reduction is able to modify sclerostin signalling so improving the efficacy of osteoblasts. In fact, these cells are able to produce more osteoid tissue and neo-cortex (6). Finally, SWs are responsible for angio- and lymphogenesis effects, and for inflammation modelling.

Due to the biological effects on bone tissue, ESWT is indicated for the treatment of delayed union (7). The success rate in terms of bone healing, documented by continuity of the cortical bone, ranges from 50 to 80% (7). A C-type grade of recommendation (level of evidence III) is identified. The aim of the present study is to quantify the quantitative modifications in bone fracture healing before and after ESWT.

Key words: fractures; delayed union; non-union; shock waves; densitometry

Corresponding Author:
Angela Notarnicola, M.D. Ph.D.,
Orthopedics Section, Department of Medical Sciences of Basis, Neurosciences and Organs of Sense, Faculty of Medicine and Surgery, University of Study of Bari, General Hospital, Bari,
Piazza Giulio Cesare n.11, 70124, Bari, Italy
Tel./Fax: +39 0805592938
e-mail: angelanotarnicola@yahoo.it

0393-974X (2020)
Copyright © by BIOLIFE, s.a.s.
This publication and/or article is for individual use only and may not be further reproduced without written permission from the copyright holder.
Unauthorized reproduction may result in financial and other penalties
DISCLOSURE: ALL AUTHORS REPORT NO CONFLICTS OF INTEREST RELEVANT TO THIS ARTICLE.

MATERIALS AND METHODS

This is an observational prospective study. For two years, 20 patients affected by delayed union or non-union of diaphyseal forearm fracture, who had undergone ESWT were enrolled. The study was approved by the local Ethics Committee and written consent was obtained from the patients. The following were used as inclusion criteria: patients affected by diaphyseal forearm fracture which showed delay or non-union linked to unsuccessful results of fracture treatment after the open reduction internal fixation with an extra-articular LCP plate (1/3 tubular plate and screws 2.5 mm, DePuy Johnson); SW treatment carried out by our Orthopedic Unit; requirement of X-ray and clinical evaluation for patient management. Exclusion criteria were: unstable fractures (not properly stabilized with plate); patients aged <18 years; neurological deficits with functional impairment of the area; the presence of endocrine-metabolic pathologies (hyperparathyroidism, chronic renal failure, etc.); incomplete follow-up.

The diagnosis of delayed union was confirmed by the absence of bone callus formation on X-ray images four months after the fracture. Non-union (or pseudoarthrosis) was diagnosed in patients, with no signs of bone union at 6 months following the fracture or most recent surgery. For each patient, the epidemiological data (age, gender) anthropometric data (weight, height, BMI), smoking habit (yes/no), anatomical site of delayed or non-union (radium or ulna), any previous treatment at least 4 weeks after the fracture (non-steroidal anti-inflammatory drugs, cortisone, vitamin D integration) were recorded. The detected fracture data were: trauma time and range of bone healing in order to define delayed union (from 3 to 6 months) or non-union (> 6 months), type of trauma (high or low impact), closed or open fracture, diastases (gap expressed as mm). Previous pulsed electromagnetic field (PEMF), information relating to the treatment of SW [Energy Density Flux (EDF), number of cycles] were recorded.

Each patient was followed-up for a period of 6 months after ESWT in order to evaluate the effect of SWs on bone healing. This represents the primary endpoint of the study. The assessment times were: at the time of recruitment (T0), 2 months after treatment (T1) then at 4 months (T2) and 6 months (T3). Possible adverse effects were monitored: hematomas, ecchymosis, hyperalgesia, rupture of metal devices. X-ray images were analyzed at all the time-points for each patient enrolled. A bony union was defined as the union where the callus is bridging the fracture site in more than three-fourths of the bone circumference on both anteroposterior and lateral views of the X-ray. The delayed consolidation of fracture was defined as the presence of less than three closed corticals. Furthermore, according to Weber-Cech classification, atrophic non-union was defined as the radiographical absence of callus across the fracture gap. Hypertrophic non-union was diagnosed as obvious callus formation without sclerosis at the end of the bone healing physiological process. Oligotrophic non-union, however, was diagnosed when there was the combination of atrophic and hypertrophic conditions and so incomplete callus formation. A fracture was considered healed if the closure of at least 3 out of 4 cortices was found on X-ray. The results of radiographic assessments were based on the consensus of two independent orthopedic surgeons blinded to patient profiles. In the case of a discrepancy, a third surgeon was called for a further assessment. A district DXA exam was conducted at T0 and T3. For unhealed fractures, the DXA exam was scheduled before starting another therapy.

ESWT

All patients were treated with ESWT at our Orthopedic Unit. ESWT was applied using a shock wave device (Minilith SL1, Storz Medical, Tägerwilen, Swiss) equipped with in-line ultrasound-guidance Aloka SSD 900 (Aloka Co., Ltd. Tokyo, Japan) set on the delivery of 4000 impulses at an energy flux density (EDF) between 0.08 and 0.17 mJ/mm^2. The probe focused the treatment on the area of fracture. The impulse frequency was 240/min. Visualization of non-union was carried out under ultrasound guide. The patients were followed-up for six months until fracture healing. In the case of failure of ESWT at the first cycle another ESWT was delivered. A maximum of 3 cycles of treatment was given, at 2-month intervals and then surgery was adopted.

Bone mineral density measurement by DXA scans

Bone mineral density (BMD) of calluses was determined using DXA in a high-resolution mode (Hologic Horizon, 35 Crosby Drive Bedford, MA, 01730 USA). The region of interest (ROI) was centered on the fracture gap. Point types were marked out to exclude artifacts from the fixation plate. The entire contralateral bone without fracture was

used as an internal control. DXA equipment was calibrated using a lumbar spine phantom and following the Hologic guidelines. All scanning and analyses were performed by the same operator to ensure consistency. The precision error (per cent coefficient of variation with repositioning) of DXA measurement is 1% for BMD. The BMD value was expressed in gr/cm^2 (Fig. 1).

Statistic analysis

The compiled forms were put into a database using Office Excel and analysed using Stata MP16 software. Continuous variables were expressed in mean ± standard deviation and range, the categorical variables as proportions, with the indication of the 95% confidence interval (95% CI). The normality of continuous variables was assessed using the Skewness and Kurtosis test and for those not normally distributed, where possible, a normalization model was set. Continuous variables were compared across multiple times using the Friedman test, between two times using the student *t*-test for paired data (parametric) or the Wilcoxon sign rank test (non−parametric). Univariate and multivariate logistic regression was used to evaluate the association between the healing finding (yes/no) and the demographic variables, the characteristics of the fracture and the treatment; the Odds Ratio (OR) were calculated, with an indication of 95% CI. A value p value <0.05 was considered significant for all tests.

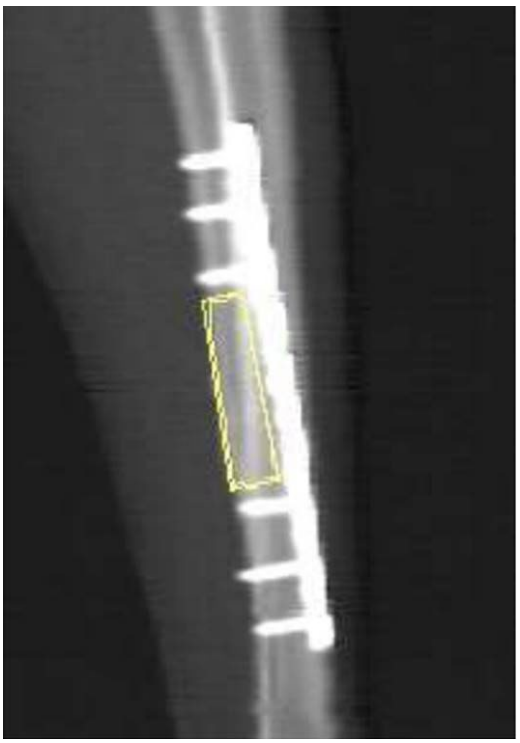


Fig. 1. *DXA image studied the fracture gap and excluded the fixation plate.*

Table I. *Baseline characteristics of sample.*

Variable	Value
Males; n (%)	14 (70.0)
Age; average± SD (range) (years)	44.9±14.5 (18-67)
Weight (Kg)	76.1±18.1 (50-122)
Height (cm)	174.1±10.9 (150-189)
BMI (kg/m^2)	24.9±4.0 (17.2-34.2)
Smokers; n (%)	8 (42.1)
Use of NSAIDs; n (%)	6 (30.0)
Use of corticosteroids; n (%)	1 (5.0)

RESULTS

The study group was made up of 20 subjects, 6 women (30%) and 14 men (70%). The mean age of the group was 44.9±14.5 years (range: 18-67), BMI 24.9±4.0 kg/cm2 (range: 17.2-34.2). The characteristics of the patients are described in Table I.

In 55% of the cases, radium was involved, in 45% ulna; 65% of the fractures were on the right, 35% on the left. The range from the traumatic event to the start of the SW was 7.5±4.2 months (range 4-20). 85% of the fractures were caused by high impact trauma, 75% were a closed fracture, and the mean value of diastasis was 2.5±1.7 mm (range: 0-7). 70% of the fractures were hypertrophic, 30% atrophic. 55% of the patients had to undergo CEMPs for an average of 24.1±31.6 days (range: 0-90). 45% of the patients took vitamin D supplementation. The number of SW cycles was 1.2±0.5 (range: 1-3), with an average EDF of 0.14±0.03 mJ/mm2 (range: 0.08-0.17 mJ/mm2). During the SW treatment sessions and at the follow-ups, no patient reported adverse reaction linked to the treatment. The study population was divided into two subgroups according to the treatment outcome. Group A (n = 4) included the cases with no complete bone union. Group B (n = 16) included the subjects with complete bone union. At T1 sixteen patients presented three closed corticals, and the data remained constant at T2 and T3. The values of the number of closed corticals and ROI, by detection time, are shown in Table II (Fig. 2). In 16/20

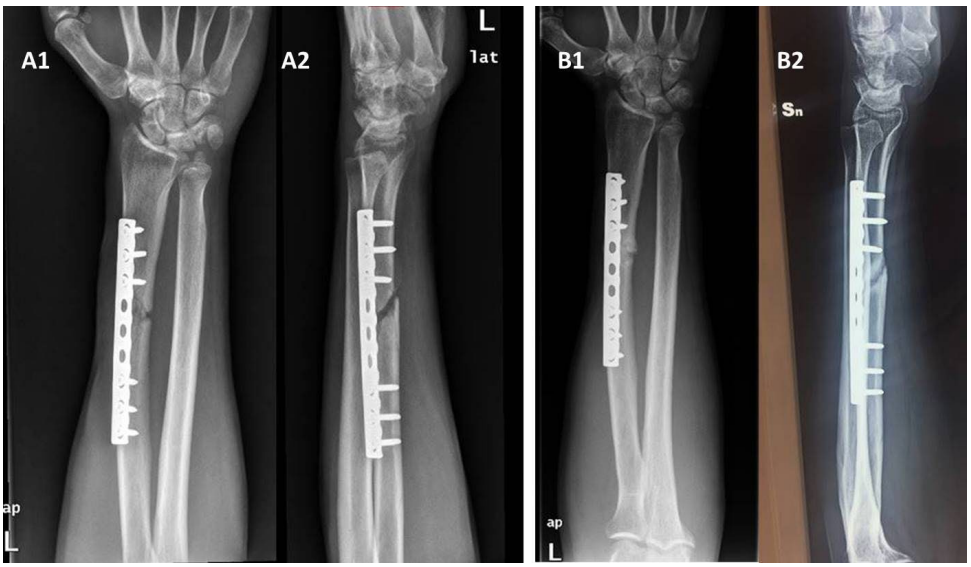


Fig. 2. *The X-ray images of a 54-year-old male showing the non-union of the left radial fracture. Before ESWT (T0) there were two open cortices in the two projections (A1 and A2). After 6 months (T3) three cortices were closed (B1 and B2).*

Table II. *Mean± SD and range of variables number of closed cortex and ROI, by detection time.*

Variable	T0	T1	T2	T3	p-value
n. of closed cortex	1.5±0.8 (0-1)	2.7±0.8 (0-3)	2.7±0.8 (0-3)	2.7±0.8 (0-3)	0.004
Fracture site ROI BMD (g/cm2)	0.47±0.15 (0.23-0.80)	-	-	0.48±0.15 (0.25-0.85)	0.162
BMD of the ROI of the contralateral seat ROI BMD (g/cm2)	0.20±0.08 (0.08-0.37)	-	-	0.20±0.08 (0.08-0.37)	0.006

(80%; 95% CI = 56.3-94.3%) treated patients there was evidence of functional recovery and bone healing.

A statistically significant difference emerged with the comparison of the pre-treatment (3.9±2.8; range: 0-8) and post-treatment (2.7±2.5; range: 0-7; p = 0.010) VAS value. Univariate and multivariate analysis did not show statistically significant associations between the healing finding (yes/no) and the determinants in analysis (p> 0.05).

DISCUSSION

In this study, by monitoring healing through the observation of the progressive closure of the callus, bridging the fracture site, it was verified that 80% of the consolidation defects of diaphyseal forearm fractures healed after SW treatment within 6 months. It was found that the density at the fracture site was greater than in the healthy contralateral segment and

there were no significant changes after ESWT. While there is no experience to date on fresh fractures, it could be reasonable to use SWs on "iatrogenic fractures", i.e. osteotomies, because these are considered likely sites of non-union, eventually even in young high-demanding patients who undergo hip replacement for sequelae of hip dysplasia (8, 9). According to the literature, there are no differences between the various types of focused generators (electromagnetic, piezoelectric, electrohydraulic) (10). Osteoporosis is not a contraindication to SW treatment, and the association with antiresorptive drugs could improve the healing effects (11). It has been found that the densitometric response was the same in cases that healed after ESWT and in cases that did not heal. These results are consistent with a previous clinical study that monitored the effects of SWs in treatment of pseudo arthrosis with bone scintigraphy: after 2 weeks, there was a significant increase in bone metabolism, both in patients with complete recovery and in those with treatment failure (12).

The present study has some limitations. Firstly, the absence of randomization, as there was no control group. Secondly, the small number of patients could potentially confound the clinical results. Thirdly, the treatment success was determined at 6 months after ESWT, a longer term follow-up may have been useful. Fourthly, only the X-ray method was used to identify fracture healing, while neither a CT scan nor a scintigraphy was performed. However, these evaluation methods are commonly accepted and considered appropriate according to clinical practice and literature.

In conclusion, ESWT is an effective method for delayed fracture healing and pseudarthrosis. In the literature, SW application in recent fractures improves densitometric values. However, the present study did not demonstrate an improvement of densitometric values. Therefore, the restorative effects may be more linked to the interaction with the collagen ultrastructure, the transmembrane molecular flows and the endocytoplasmic pathways that regulate nuclear functions than with effects on the structural and mechanical strength characteristics of the bone. Further investigations are needed to assess this hypothesis.

ACKNOWLEDGEMENTS

The authors thank Brian John Molloy B.A. for language revision.

REFERENCES

1. Ekegren CL, Edwards ER, de Steiger R, Gabbe BJ. Incidence, Costs and predictors of non-union, delayed union and mal-union following long bone fracture. Int J Environ Res Public Health 2018; 15(12).
2. Chotel F, Braillon P, Sailhan F, et al. Bone stiffness in children: part II. Objectives criteria for children to assess healing during leg lengthening. J Pediatr Orthop 2008; 28(5):538-43.
3. Chen YJ, Kuo YR, Yang KD, Wang CJ, Huang HC, Wang FS. Shock wave application enhances pertussis toxin protein-sensitive bone formation of segmental femoral defect in rats. J Bone Miner Res 2003; 18:2169–79.
4. D'Agostino MC, Frairia R, Romeo P, et al. Extracorporeal shockwaves as regenerative therapy in orthopedic traumatology: a narrative review from basic research to clinical practice. J Biol Regul Homeost Agents 2016; 30(2):323-32.
5. Tamma R, dell'Endice S, Notarnicola A, et al. Extracorporeal shock waves stimulate osteoblast activities. Ultrasound Med Biol 2009; 35(12):2093-100.
6. Ogden JA, Toth-Kischkat A, Schultheiss R. Principles of shock wave therapy. Clin Orthop Relat Res 2001; 387:8-17.
7. Romeo P, Gigliotti S, Notarnicola A, et al. Extracorporeal shock wave therapy in bone healing disorders. Biological basis and operative applications. GIOT 2017; 43:205-210.
8. Grappiolo G, La Camera F, Della Rocca A, Mazziotta G, Santoro G, Loppini M. Total hip arthroplasty with a monoblock conical stem and subtrochanteric transverse shortening osteotomy in Crowe type IV dysplastic hips. Int Orthop 2019; 43(1):77-83.
9. Rollo G, Solarino G, Vicenti G, Picca G, Carrozzo M, Moretti B. Subtrochanteric femoral shortening osteotomy combined with cementless total hip replacement for Crowe type IV developmental dysplasia: a retrospective study. J Orthop Traumatol.

2017; 18(4):407-13.
10. Notarnicola A, Iannone F, Maccagnano G, Lacarpia N, Bizzoca D, Moretti B. Chondrocytes treated with different shock wave devices. Muscles Ligaments Tendons J. 2017 10; 7(1):152-56.
11. Lama A, Santoro A, Corrado B, et al. Extracorporeal shock waves alone or combined with raloxifene promote bone formation and suppress resorption in ovariectomized rats. PLoS One 2017 3; 1 2(2):e0171276.
12. Czarnowska-Cubała M, Gwoździewicz K, Studniarek M, Lasek J. Predictive role of scintigraphy (BS) in bone union induction using extracorporeal shock wave treatment (ESWT). J Orthop 2013; 10(2):70-3.

LETTER TO THE EDITOR

Effectiveness of powder air polishing on natural and artificial dental surfaces: *in-vitro* study

A. Chiesa[1,2], M. Mignani[1], C. Preda[1,2], F. Esposito[1,2], N. Buonocunto[3], AM. Genovesi[1,4] and S. Cosola[1,5]

[1]Tuscan Stomatologic Institute, Versilia General Hospital, Lido di Camaiore, Italy; [2]Study Center for Multidisciplinary Regenerative Research, Guglielmo Marconi University, Rome, Italy; [3]Private practitioner, Pisa, Italy; [4]Unicamillus International Medical University, Rome, Italy; [5]Department of Stomatology, University of Valencia, Valencia, Spain

Received May 25, 2020 – Accepted October 16, 2020

To the Editor,

The professional oral hygiene session has the purpose of promoting the eubiosis of the oral cavity. During the session, the bacterial biofilm is removed, the microbiological balance is restored, and the patient is supported in his own daily oral hygiene. Motivation and oral hygiene instructions allow the patient to maintain a correct routine for his oral health using a sonic or other automatic toothbrush and interdental cleaning tools.

During the One Stage Full Mouth Disinfection (OSFMD) session, polishing is the step following sonic/ultrasonic instrumentation. Its main goal is to remove residual biofilm and any extrinsic stains from the dental surface, making it smooth and shiny. Tooth polishing can be carried out with engine-driven or air-powder polishers. The first method includes the use of abrasive paste and brushes/rubber cups mounted on a dental unit hand piece. Air powder polishing devices, instead, can attach directly to the air/water connector of the dental unit, and their function is to propel abrasive powders onto dental surfaces by an air/water jet. The second method is the most common procedure nowadays and is supported by scientific evidence. Throughout life, a person can undergo conservative therapies, prosthetic therapies of single or multiple elements, up to Implant-prosthetic rehabilitation (1). In particular, during deplaquing procedure, air polishing powders can come into contact with implant connections, prosthesis and conservative restorations (2).

How do dental materials react to this procedure? Can the abrasive powders roughen dental surface and therefore expose it to a quicker bacterial biofilm colonization (3, 4)? The purpose of this study is to verify the effectiveness of air polishing, evaluating whether different powders can modify artificial or natural teeth surfaces by analyzing them before and after the treatment through images of Scanning Electron Microscope (SEM).

MATERIALS AND METHODS

This is an *in-vitro* study performed at the Tuscan Stomatologic Institute. An air polishing device (MyLunos®: Dürr Dental SE) was used at the maximum power of the compressed air and with the maximum water-flow. The nozzle was positioned at a distance of 3 mm from the tested surface at the angle of 70° for 5 seconds. For this study two different perio-polishing powders were tested: glycine and trehalose. Both powders were tested in two different grain sizes, for the glycine granulometries

Key words: titanium, zirconia, trehalose, glycine, air polishing

Corresponding Author:
Dr Alessandro Chiesa,
Tuscan Stomatologic Institute,
Versilia General Hospital, Lido di Camaiore, Italy
Tel.: +39 3495760516
Fax: +39 0584618414
e-mail: alessandro.chiesa@hotmail.it

0393-974X (2020)
Copyright © by BIOLIFE, s.a.s.
This publication and/or article is for individual use only and may not be further reproduced without written permission from the copyright holder.
Unauthorized reproduction may result in financial and other penalties
DISCLOSURE: ALL AUTHORS REPORT NO CONFLICTS OF INTEREST RELEVANT TO THIS ARTICLE.

of ~65µm and ~25µm were used, and for the trehalose granulometries of ~65µm and ~30µm were used. Seven different materials were tested (Fig. 1):

- composite resins;
- laboratory composite resins;
- lithium disilicate;
- feldspathic ceramic;
- chrome-cobalt:
- zirconia;
- titanium.

For each tested material, four blocks were produced with a surface between 0.5 and 1 cm^2 for a total of 28 samples. A rubber cup placed on a hand piece was used to polish all surfaces. To analyze and take pictures of metal-

Table I. *Twenty-eight blocks tested with 2 different perio-polishing powders (Glycine and Trehalose) at 2 different grain sizes (65 µm and 30 µm).*

IMG	MATERIAL	POWDER	SEM OBSERVATION T0 –T1
1	COMPOSITE RESIN	GLYCINE 65 µm	?
2	COMPOSITE RESIN	GLYCINE 25 µm	
3	COMPOSITE RESIN	TREHALOSE 65 µm	
4	COMPOSITE RESIN	TREHALOSE 30 µm	?
5	LABORATORY COMPOSITE RESIN	GLYCINE 65 µm	
6	LABORATORY COMPOSITE RESIN	GLYCINE 25 µm	
7	LABORATORY COMPOSITE RESIN	TREHALOSE 65 µm	
8	LABORATORY COMPOSITE RESIN	TREHALOSE 30 µm	NV
9	LITHIUM DISILICATE	GLYCINE 65 µm	
10	LITHIUM DISILICATE	GLYCINE 25 µm	
11	LITHIUM DISILICATE	TREHALOSE 65 µm	?
12	LITHIUM DISILICATE	TREHALOSE 30 µm	
13	FELDSPATIC CERAMIC	GLYCINE 65 µm	
14	FELDSPATIC CERAMIC	GLYCINE 25 µm	
15	FELDSPATIC CERAMIC	TREHALOSE 65 µm	
16	FELDSPATIC CERAMIC	TREHALOSE 30 µm	NV
17	COBALT-CHROME	GLYCINE 65 µm	
18	COBALT-CHROME	GLYCINE 25 µm	
19	COBALT-CHROME	TREHALOSE 65 µm	
20	COBALT-CHROME	TREHALOSE 30 µm	
21	ZIRCONIA	GLYCINE 65 µm	
22	ZIRCONIA	GLYCINE 25 µm	
23	ZIRCONIA	TREHALOSE 65 µm	
24	ZIRCONIA	TREHALOSE 30 µm	
25	TITANIUM	GLYCINE 65 µm	
26	TITANIUM	GLYCINE 25 µm	
27	TITANIUM	TREHALOSE 65 µm	
28	TITANIUM	TREHALOSE 30 µm	
		NO CHANGE	
		CHANGES ON THE SURFACE	
		NOT EVALUABLE	NV
		DIFFICULT IN EVALUATION	? ?

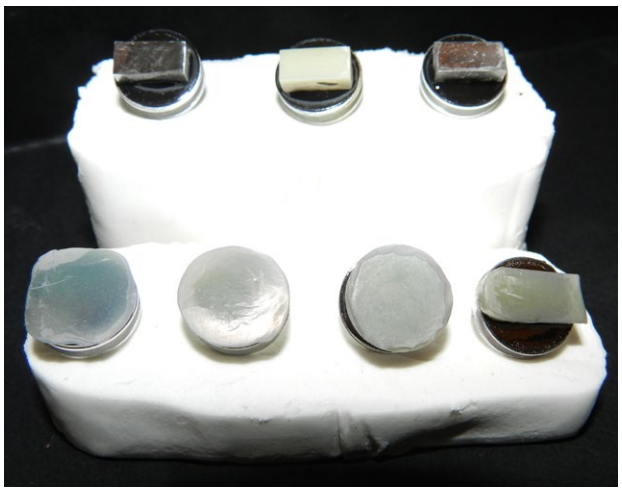


Fig. 1. *One block for each tested material with a surface between 0.5 and 1 cm².*

free samples with the SEM, they were covered with a microlayer metal called "coating"(5).

Test procedure

A total of 28 block samples were grouped to have four blocks for each of the seven materials tested, listed in the previous paragraph. Each material had 2 blocks corresponding to 2 different perio-polishing powders (glycine and trehalose) and 2 blocks corresponding to 2 different grain sizes (65 µm and 30 µm). At T0 the image acquisition was performed by SEM and selected by the same operator. A second operator used the polish device for all blocks. Immediately after this procedure (T1), the post-treatment image acquisition was performed again by SEM. The image comparison and evaluation of the perio-polishing powders treatment was performed by a third operator.

RESULTS

The results of the treatment on 28 samples are shown in Table I. Out of 28 comparisons in 2 cases, one lithium disilicate and one feldspatic ceramic (block n. 8 and n. 16), the evaluation was not possible because the images were not interpretable. Excluding these two blocks, 18 out of the other 26 analyzed samples were lesion-free and presented a smooth surface, including the following materials: feldspatic ceramic, chrome-cobalt, zirconia and titanium. In 8 images at T1 there was evidence of a surface change. On the surface of blocks n. 1, 4 and 11 an abrasion could be observed, a concave dent-like lesion could be observed on the surface of blocks n. 5, 6, 7 and 11 while a lot of scratch-like grooves could be observed on the surface of block ns. 10 and 12. Materials reacted in different ways to powder exposure: composite resin showed an abrasion-like lesion; the laboratory composite resin showed dent-like lesion; lithium disilicate showed grooves and in one case, a dent. Type and size of the powder did not affect the appearance of the lesions since these occurred with trehalose and glycine of both 65 µ and 25/30 µ. The change could either be attributed to the impact of the air/dust/water mixture or it may have been already present on the surface before the test. The rubber polishing performed on the blocks may have not removed all imperfections. This doubt arises from the presence of a concavity in the shots both in T0 and in T1 on the zirconia tiles, therefore, block ns. 21, 22 and 23 were not taken into consideration. The representative images of T0/T1 comparisons are shown in Fig. 2.

DISCUSSION

The results of this study evaluated how the surface of the tested materials was modified by air polishing with glycine -65m and -25m and with trehalose -65m and -30m. After the therapy, a reduction of the bacterial biofilm was recorded in all the analyzed groups and a change in the surface could be noticed depending on the surface treated. The use of powders modifies the surface, altering it, therefore making it rougher and consequently subject to a more rapid colonization by the bacterial biofilm. The results highlight how materials reacted differently: composite resin suffered an abrasion, laboratory composite was dented, lithium disilicate was scratched and in one case, dented (6). The type of powder and granulometry used did not affect the observed lesions since these occurred with both trehalose and glycine, with both 65m and 25/30m. The results clearly show how it is not possible to establish whether the surface alteration can be related to the impact of the air-powder-water mixture or not (7-9). It is important to remember that in clinical protocols larger granulometries are mostly used for

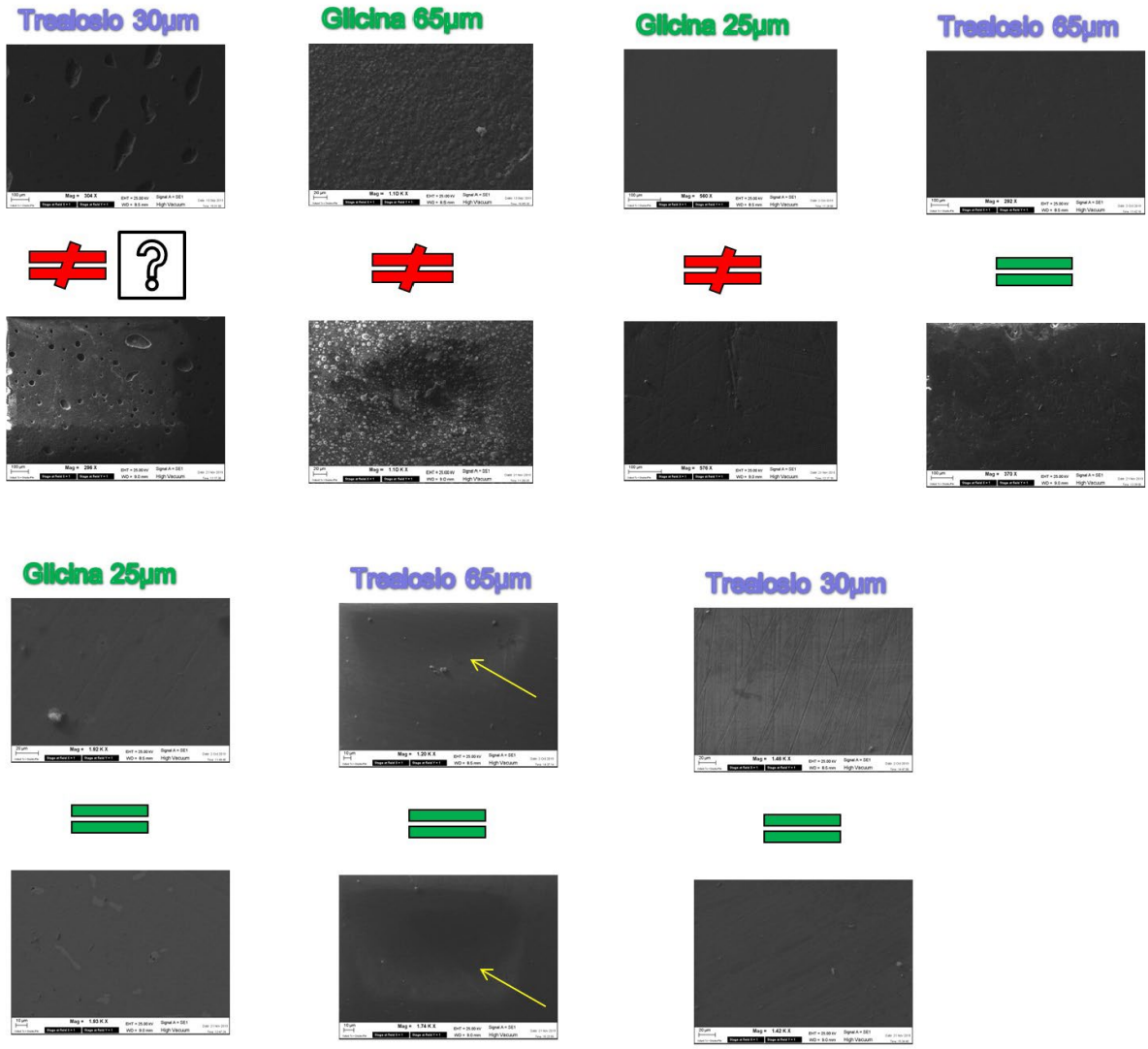


Fig. 2. *Resin, laboratory composite resin, lithium disilicate, feldspatic ceramic, chrome-cobalt, zirconia and titanium.*

supra-gingival air polishing, while smaller ones are preferred for sub-gingival air polishing (10, 11).

Comparing the concavities on the zirconia tile numbers 21, 22, 23, it was possible to observe these imperfections both at T0 and at T1, and for this reason they were not evaluated as damaged (Table I). Using the device at a distance of 3 mm and in a static way may cause a surface alteration regardless of the type of powder. The impact angle (70°, almost vertical) influence may also have been relevant; in fact, the powders tend to release almost all their kinetic energy at the impact point.

This study certainly presents some limitations regarding image evaluation and comparison:

- uneven surfaces;
- exposure duration not electronically regulated;
- visual and non-instrumental observation of the surfaces;
- images compared with different zoom and scale;
- lack of reference points in T0 and T1.

Our conclusion is that there are no differences in results between glycine and trehalose using this type of air polishing device. Eighteen out of 26 samples showed no significant morphologic difference

on their surfaces, 8 samples, instead, presented lesions on their surfaces with both materials and granulometries. Furthermore, the granulometry did not influence morphological alterations of block surfaces. This could be caused by the distance of the air polishing device from the surface treated.

Images taken by SEM highlight that if the device is used at a distance of 3 mm, with an inclination of 70° and with a static application, it modifies the surface of lithium disilicate and composite resin blocks. Other material block surfaces are not altered by the device with these parameters. The use of powders for stain and plaque removal on lithium disilicate and composite resin cannot be excluded, but this test shows that careful attention to distance, inclination and movement of the device must be considered (12).

The adhesion of biofilm after air polishing requires further studies and should take into consideration not only visible alteration of the surface, but also its roughness. As a matter of fact, a match between surface alteration and roughness augmentation could promote biofilm adhesion, thus generating a plaque-related pathology.

ACKNOWLEDGEMENTS

The authors would like to acknowledge the director of Istituto Stomatologico Toscano, Prof. Ugo Covani who allowed this *in-vitro* study and Julija Atanasova for the English revision as professional translator.

REFERENCES

1. Barnes CM, Covey D, Watanabe H, Simetich B, Schulte JR, Chen H. An in vitro comparison of the effects of various air polishing powders on enamel and selected esthetic restorative materials. J Clin Dent 2014; 25(4):76-87.
2. Moharrami M, Perrotti V, Iaculli F, Love RM, Quaranta A. Effects of air abrasive decontamination on titanium surfaces: A systematic review of in vitro studies. Clin Implant Dent Relat Res 2019; 21(2):398-421.
3. Biazussi BR, Perrotti V, D'Arcangelo C, et al. Evaluation of the effect of air polishing with different abrasive powders on the roughness of implant abutment surface: an in vitro study. J Oral Implantol 2019; 45(3):202-206.
4. Giacomelli L, Salerno M, Derchi G, Genovesi A, Paganin PP, Covani U. Effect of air polishing with glycine and bicarbonate powders on a nanocomposite used in dental restorations: an in vitro study. Int J Periodontics Restorative Dent 2011; 31(5):e51-e56.
5. Ermetici M, Segù M, Butera A. Comparison to the scanning electron microscope of professional dental hygiene methods on metal-free layered structures and metal-free monolithic structures processed by different polymerization cycles. Minerva Stomatol 2014; 63(6):189-202.
6. Bühler J, Amato M, Weiger R, Walter C. A systematic review on the effects of air polishing devices on oral tissues. Int J Dent Hyg 2016; 14(1):15-28.
7. Flemmig TF, Arushanov D, Daubert D, Rothen M, Mueller G, Leroux BG. Randomized controlled trial assessing efficacy and safety of glycine powder air polishing in moderate-to-deep periodontal pockets. J Periodontol 2012; 83(4):444-452.
8. Lu H, He L, Zhao Y, Meng H. The effect of supragingival glycine air polishing on periodontitis during maintenance therapy: a randomized controlled trial. Peer J 2018; 6:e4371. Published 2018 Feb 12.
9. Müller N, Moëne R, Cancela JA, Mombelli A. Subgingival air-polishing with erythritol during periodontal maintenance: randomized clinical trial of twelve months. J Clin Periodontol 2014; 41(9):883-89.
10. Kruse AB, Akakpo DL, Maamar R, et al. Trehalose powder for subgingival air-polishing during periodontal maintenance therapy: A randomized controlled trial. J Periodontol 2019; 90(3):263-270. doi:10.1002/JPER.17-0403.
11. Kruse AB, Maamar R, Akakpo DL, et al. Effects of subgingival air-polishing with trehalose powder on oral biofilm during periodontal maintenance therapy: a randomized-controlled pilot study. BMC Oral Health 2020; 20(1):123.
12. Tastepe CS, Lin X, Donnet M, Wismeijer D, Liu Y. Parameters that improve cleaning efficiency of subgingival air polishing on titanium implant surfaces: an in vitro study. J Periodontol 2017; 88(4):407-14.

LETTER TO THE EDITOR

Carboxytherapy with oxygen propulsion treatment of cellulite is more effective in women not affected by periodontal disease

A. Scarano[1], D. Amuso[2], M. Amore[2], G. Ferraro[3], E. L. Iorio[1], A. Sbarbati[4], F. Lorusso[1] and M. Petrini[1]

[1]Department of Medical, Oral and Biotechnological Sciences, University G. d'Annunzio of Chieti-Pescara, Chieti, Italy; [2]Department of Medical, Oral and Biotechnological Sciences, University G. d'Annunzio of Chieti-Pescara, Chieti, Italy; [3]Department of Plastic, Reconstructive and Aesthetic Surgery, University of Campania "Luigi Vanvitelli", Naples, Italy; [4]Department of Neurosciences, Biomedicine and Movement Sciences, Anatomy and Histology Section, University of Verona, Verona, Italy

Received June 12, 2020 – Accepted October 22, 2020

To the Editor,

Cellulite is an unesthetic condition that affects about 80-90% of post-pubertal women, but also men can be affected. The multifactorial aetiology of this problem comprises genetic predisposition, gender, anatomical and hormonal factors, deficiencies in lymphatic drainage, vascular/inflammatory alterations, and lifestyle. In particular, the peripheral circulatory and metabolic failure could enhance an increased proliferation of fibroblast, with the consequent formation of fibrosis around the adipocytes (1). Cellulite should not be considered only as a cosmetic problem, and to find the best treatment, metabolic and circulatory conditions should also be analyzed (2). A wide range of treatments, both invasive and non-invasive, have been described for cellulite, however, they usually are costly, time-consuming as it is necessary to repeat many sessions, and do not permit the total eradication of the problem. The outcomes of cellulite treatments aim at not only improving the surface texture of the skin, but also enhancing a reduction of the circumference of the part of the body treated.

Periodontal disease is a multifactorial, chronic, inflammatory pathology, and, with a prevalence of 20–50%, represents the sixth most predominant condition worldwide (3). Recent evidence has shown an association between waist circumference and waist-to-height ratio and periodontal pocketing, and BMI was correlated with prevalence, extent, and severity of periodontitis (4). Many studies have shown that periodontal disease is associated with increased odds for other systemic pathologies such as hypertension, diabetes, metabolic syndrome, and heart disease (5). The primary aim of this study is to evaluate whether carboxytherapy, enriched with oxygen propulsion, is an efficient tool for the treatment of cellulite, intended as a circumference reduction of the different areas of the body treated. We also hypothesized that cellulite and periodontal disease, sharing a common systemic inflammatory condition, could affect each other. The secondary aim is to evaluate whether the presence of periodontal disease and the treatment with the non-surgical periodontal therapy could affect the outcomes of carboxytherapy

Key words: cellulite; carboxytherapy; oxygen propulsion; periodontal disease; Skin barrier; periodontitis; NSPT

Corresponding Author:
Prof. Antonio Scarano, D.D.S., M.D.
Department of Medical, Oral and Biotechnological Sciences,
University of Chieti-Pescara,
Via Dei Vestini 31, 66100 Chieti, Italy
Tel.: +39 08713554084 - Fax: +3908713554099
e-mail: ascarano@unich.it

0393-974X (2020)
Copyright © by BIOLIFE, s.a.s.
This publication and/or article is for individual use only and may not be further reproduced without written permission from the copyright holder.
Unauthorized reproduction may result in financial and other penalties
DISCLOSURE: ALL AUTHORS REPORT NO CONFLICTS OF INTEREST RELEVANT TO THIS ARTICLE.

MATERIALS AND METHODS

The present study was based in a private practice in Modena (MO), in full accordance with ethical principles, including the World Medical Association Declaration of Helsinki (https://www.wma.net/wp-content/uploads/2018/07/DoH-Oct2008.pdf) and the additional requirements of Italian law. All patients signed consent to treatment with carboxytherapy. Sixty female patients were recruited for the clinical trial. The inclusion criteria of the study protocol comprised the presence of cellulite. The exclusion criteria were age under 18 years, severe systemic diseases, cancer, radiotherapy or chemotherapy treatment, uncompensated diabetes.

Cellulite evaluation

Before initiating the treatment, standardized photographs were taken of all participants to assess the severity of the cellulite. Then the circumference of the waist, belly, hip, legs (right LEGR, and left LEGF) and right knee were measured (t0).

Periodontal evaluation and treatment

Dental evaluation comprehended clinical and radiographical evaluation of the teeth and the jaws (t0). A UNC periodontal probe was used to evaluate the periodontal status of the patients: periodontal pocket depth (PPD), the clinical attachment level (CAL), the presence of plaque and bleeding were evaluated at 6 points for all teeth, excluding third molars.

Treatment protocol

The treatment was started by using a carboxytherapy device (CarboBes, Terni, Italy). For subcutaneous injections of carbon dioxide gas and oxygen, a 30 gauge/0.3 × 15 microlance needle directed at 45° was used and the depth of infusion was 10–15 of carbon dioxide with oxygen. Several points, medium, medial, anterior and posterior, for both the right and left waist, hip, legs, and knee were used. The infusion velocity was 30 cc/min, with a total of gas administrated equal to 400 cc for each thigh for 20–30 min. The cycle of treatment consisted of twelve sessions of carboxytherapy with oxygen propulsion with an interval of 7 days between each session.

After 7 days from the completion of the first cycle of sessions (t1), the waist, hip, leg, and knee circumferences were measured. Then, patients with a diagnosis of periodontal disease were subjected to oral hygiene instruction and non-surgical periodontal treatment (NSPT) by the use of ultrasound tips and manual curettes in periodontal pockets greater than 4 mm. Teeth considered hopeless were extracted.

After 7 days, the second cycle of carboxytherapy with oxygen propulsion was performed only on periodontal patients who had been subjected to NSPT. Seven days after the completion of the second cycle of sessions (t2), the waist, hip, legs and knee circumferences were analyzed.

Non-surgical periodontal therapy

Non-surgical periodontal therapy (NSPT) was performed by means of ultrasonic tips and manual curettes in order to remove supragingival and subgingival debris. Patients were instructed to perform oral hygiene manoeuvres, as previously described (6).

Statistical analysis

SPSS for Windows version 21 (IBM SPSS Inc., Chicago, IL, USA) performed the statistical analysis of the data. The Shapiro-Wilk test was performed to evaluate the normality of the data distribution. The study groups were compared by Student's paired (dependent variables) and unpaired *t*-test (independent variables). A p-value 0.05 was considered statistically significant. Analysis of variance (ANOVA) and the LSD test were used to compare different groups based on age decades.

RESULTS

The average body mass index (BMI), which ranged between 21 (normal weight) and 31 (obesity class 1), remained stable during the study. In particular, 26 patients were classified as "normal weight", 33 "overweight" and 1 "class 1 obesity". Periodontal disease was diagnosed in 14 patients. T-test of baseline values (Table I) of patients, stratified for the presence or absence of periodontitis, showed homogeneity of the sample: the only significant difference was the age (p=0.014): patients with periodontitis were older (mean age 53 years) than those with a healthy periodontium (mean age 45 years). Baseline values of BMI of the included population were

stratified in age decades as follows (Fig. 1):

- 3 patients in the 20/30 decade
- 14 patients in the 30/40 decade
- 15 patients in the 40/50 decade
- 14 patients in the 50/60 decade
- 14 patients in the 60/70 decade

ANOVA analysis of baseline values stratified for age decades showed that the population analyzed was homogeneous for all parameters except for BMI (p=0.002), which increased with age.

In the whole population (60 patients) the first cycle of treatment (t1) promoted a significant mean reduction of the circumference for all the measurement points (Fig. 1). Waist, belly, hips, thighs, and knees showed a statistically significant decrease in the measured circumference after the treatment, p<0.01. The skin texture also showed a reduction of the superficial roughness. ANOVA analysis found no significant intra- or intergroup differences concerning the effect of 1 cycle of treatment, stratified for the age decade (p>0.05) and BMI (p>0.05).

However, if we consider these results stratified for the presence or absence of periodontitis, we can see that 1 cycle of treatment had very positive effects on people with periodontal health (46), with a significant reduction of all circumferences measured (p<0.05). On the contrary, patients affected by periodontitis (14) had no positive effects after 1 cycle of treatment (Table II Fig. 2). After t1, 2 patients dropped out of the periodontitis group, so only 12

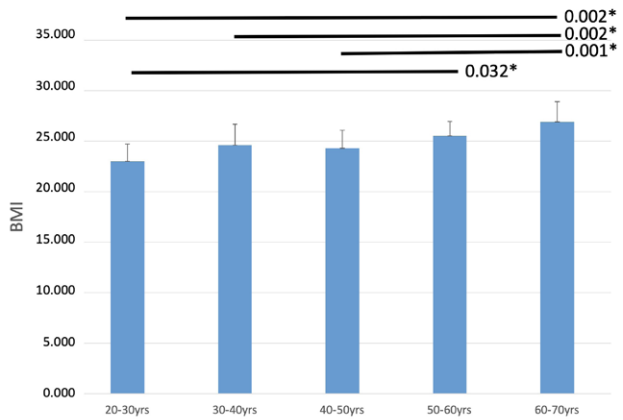


Fig. 1. *Baseline values of BMI of the included population (n=60 patients), stratified in age decades. LSD analysis (significance= p<0.05)*

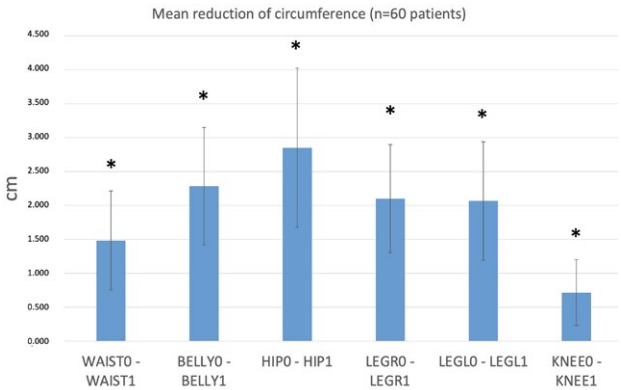


Fig. 2. *Mean differences of the circumferences, before (t0) and after (t1) the first cycle of treatment in the whole population.* Student's paired t-test *(*significance= p<0.05).*

patients completed the protocol up to t2. After the second cycle of treatment, t2, a significant reduction of the belly, hip, legs, and knee was recorded also in periodontal patients (Table III).

In periodontal patients, 1 cycle of treatment was not effective in promoting a decrease of circumferences of any of the areas analyzed in this study. On the contrary, after the second cycle of treatments, there was a significant improvement in all parameters (Table III). There were no significant differences between patients with a healthy periodontium after 1 cycle of treatment (t1) and periodontal patients after two cycles (t2) for all parameters analyzed in this study, p>0.05.

DISCUSSION

Carboxytherapy is microinjections of CO_2 in subcutaneous tissues that, causing local hypercapnia, stimulates the increase of blood flow and viscosity and the production of VEGF that promotes neoangiogenesis (7). The novelty is that after the induction of a state of hypercapnia, with the consequent increase of blood flow and microcirculation, we proceeded with oxygen profusion, increasing the bioavailability of this gas that is fundamental for living cells. In this way we could contrast some of the most important etiologic factors of cellulite, that are local hypoxia and ischemia of the adipose tissue (1). A significant reduction of waist, belly, hip, thigh and knee circumference

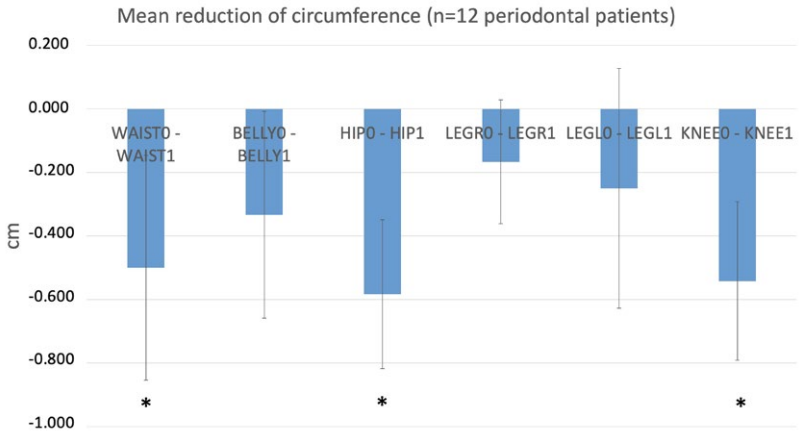


Fig. 3. *Mean differences of the circumferences, before (t0) and after (t1) the first cycle of treatment in the periodontal population. Student's paired t-test (*significance= p<0.05).*

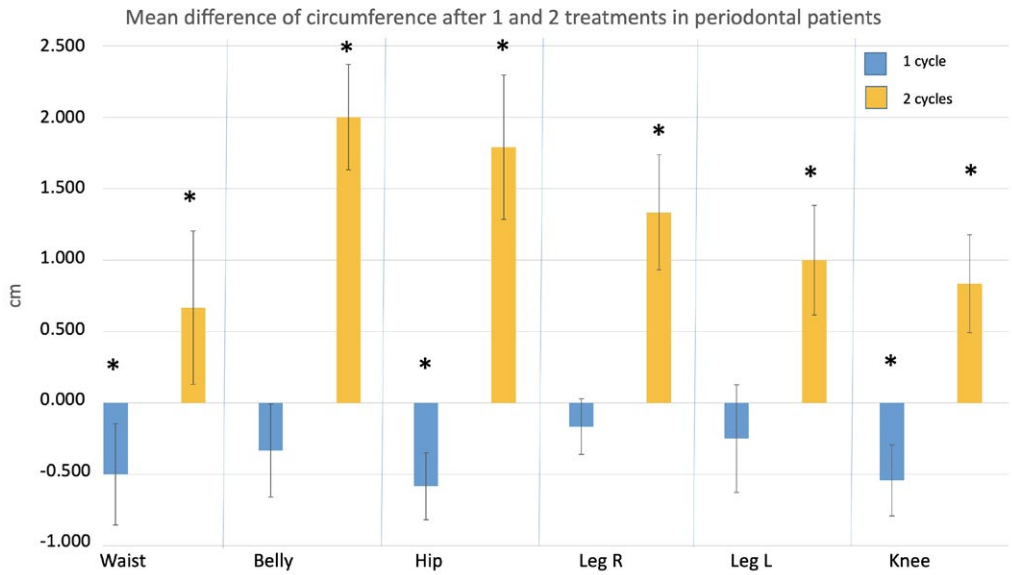


Fig. 4. *Different effects of 1 and 2 cycles of treatment in patients with periodontitis; baseline values (n=12 patients). Student's paired t-test (*significance= p<0.05)*

was recorded at the end of the treatment in the whole population. These data are in accordance with previous studies, in which carboxytherapy promoted a significant reduction of leg and thigh circumferences, a decrease of cellulite severity scale and the histological analysis confirmed the lipolytic effects of this treatment (7, 8) . Interestingly, patients with periodontitis had no benefits after 1 cycle of treatment and results were statistically significant ($p<0.05$). It is important to highlight that considering the small number of the sample, these data should be considered as preliminary and need to be confirmed by further investigations. A hypothetic explanation of these results could be the systemic inflammation caused by the presence of periodontal pathogens in patients affected by periodontal disease, that has been shown by many studies to have increased levels of blood markers such as CRP (5). The effect of periodontal disease on systemic inflammation is so crucial as to have negative effects also on glycaemic control and on the levels of glucoregulatory hormones (9, 10). The effects of

Table I. *Baseline values of patients stratified for periodontitis.*

Baseline values of patients stratified for periodontitis		N	Mean values	St. Dev.	p-value
AGE	NO PERIODONTITIS	46	45.739	10.690	**0.014***
	PERIODONTITIS	14	53.143	11.461	
HEIGHT	NO PERIODONTITIS	46	162.739	5.591	0.116
	PERIODONTITIS	14	165.500	5.906	
WEIGHT	NO PERIODONTITIS	46	66.959	6.608	0.071
	PERIODONTITIS	14	70.807	7.669	
BMI	NO PERIODONTITIS	46	24.870	1.939	0.115
	PERIODONTITIS	14	25.857	2.282	
WAIST t0	NO PERIODONTITIS	46	75.370	4.668	0.993
	PERIODONTITIS	14	75.357	5.638	
BELLY t0	NO PERIODONTITIS	46	81.913	5.054	0.659
	PERIODONTITIS	14	82.643	6.404	
HIP t0	NO PERIODONTITIS	46	97.174	5.942	0.298
	PERIODONTITIS	14	95.357	4.584	
LEG Right t0	NO PERIODONTITIS	46	55.457	3.770	0.444
	PERIODONTITIS	14	54.571	3.736	
LEG Left t0	NO PERIODONTITIS	46	49.500	2.994	0.448
	PERIODONTITIS	14	48.786	3.286	
KNEE t0	NO PERIODONTITIS	46	37.957	2.221	0.625
	PERIODONTITIS	14	38.286	2.091	

*Student's unpaired t-test (*significance= $p<0.05$).*

Table II. *Different effects of 1 cycle of treatment in patients with and without periodontitis; baseline values (n=60 patients) versus t1 in different groups.*

AVERAGE DIFFERENCE OF CIRCUMFERENCE AFTER 1 TREATMENT		N	St. Dev.	p-value
WAIST	NO PERIODONTITIS	46	1.03979	**p<0.001***
	PERIODONTITIS	14	.67937	
BELLY	NO PERIODONTITIS	46	1.11965	**p<0.001***
	PERIODONTITIS	14	.69929	
HIP	NO PERIODONTITIS	46	1.55604	**p<0.001***
	PERIODONTITIS	14	.47463	
LEG RIGHT	NO PERIODONTITIS	46	1.04604	**p<0.001***
	PERIODONTITIS	14	.42582	
LEG LEFT	NO PERIODONTITIS	46	1.32388	**p<0.001***
	PERIODONTITIS	14	.69929	
KNEE	NO PERIODONTITIS	46	.77436	**p<0.001***
	PERIODONTITIS	14	.49862	

*Student's unpaired t-test (*significance= $p<0.05$).*

Table III. *Different effects of 1 and 2 cycles of treatment in patients with periodontitis; baseline values (n=12 patients).*

	Paired t-Test		
	Mean difference	St. dev.	Sig. (2-code)
WAIST0 - WAIST2	0.66667	1.07309	0.054
WAIST1 - WAIST2	1.16667	0.68534	**0.000***
BELLY0 - BELLY2	2.000000	0.738549	**0.000***
BELLY1 - BELLY2	2.33333	0.49237	**0.000***
HIP0 - HIP2	1.79167	1.01036	**0.000***
HIP1 - HIP2	2.37500	0.93237	**0.000***
LEGR0 - LEGR2	1.33333	0.80716	**0.000***
LEGR1 - LEGR2	1.50000	0.76871	**0.000***
LEGL0 - LEGL2	1.00000	0.76871	**0.001***
LEGL1 - LEGL2	1.25000	0.83937	**0.000***
KNEE0 - KNEE2	0.83333	0.68534	**0.001***
KNEE1 - KNEE2	1.37500	0.48265	**0.000***

*Student's unpaired t-test (*significance= $p<0.05$).*

periodontitis that induce hormonal changes is very important, also because they share this function in common with adipocytes, the main actors in cellulite, that have endocrine functions and relationships with inflammatory diseases and insulin resistance (9). The confirmation of our hypothesis is that after the NSPT (t2), the effects of carboxytherapy and oxygen propulsion on circumference measurements were similar to those on patients without periodontitis. Indeed, the effect of non-surgical periodontal therapy in patients with periodontitis is a decrease of systemic markers of inflammation (11, 12).

REFERENCES

1. Rossi ABR, Vergnanini AL. Cellulite: a review. J Eur Acad Dermatology Venereol 2000; 14:251-62. doi:10.1046/j.1468-3083.2000.00016.x.
2. Tokarska K, Tokarski S, Woźniacka A, Sysa-Jędrzejowska A, Bogaczewicz J. Cellulite: a cosmetic or systemic issue? Contemporary views on the etiopathogenesis of cellulite. Adv Dermatology Allergol 2018; 35:442-46. doi:10.5114/ada.2018.77235.
3. Eke PI, Borgnakke WS, Genco RJ. Recent epidemiologic trends in periodontitis in the USA. Periodontol 2000 2020; 82:257-67. doi:10.1111/prd.12323.
4. Kangas S, Timonen P, Knuuttila M, Jula A, Ylöstalo P, Syrjälä A-MH. Waist circumference and waist-to-height ratio are associated with periodontal pocketing-results of the Health 2000 Survey. BMC Oral Health 2017; 17:48. doi:10.1186/s12903-017-0336-y.
5. Sanz M, Marco del Castillo A, Jepsen S, et al. Periodontitis and cardiovascular diseases: Consensus report. J Clin Periodontol 2020; 47:268-88. doi:10.1111/jcpe.13189.
6. Graziani F, Palazzolo A, Gennai S, et al. Interdental plaque reduction after use of different devices in young subjects with intact papilla: A randomized clinical trial. Int J Dent Hyg 2018;16:389-96. doi:10.1111/idh.12318.
7. Sant'Ana EMC, Pianez LRG, Custódio FS, Guidi RM, de Freitas JN. Effectiveness of carboxytherapy in the treatment of cellulite in healthy women: a pilot study. Clin Cosmet Investig Dermatol 2016; 9:183-90. doi:10.2147/CCID.S102503.
8. Eldsouky F, Ebrahim HM. Evaluation and efficacy of carbon dioxide therapy (carboxytherapy) versus mesolipolysis in the treatment of cellulite. J Cosmet Laser Ther 2018; 20:307-12. doi:10.1080/14764172.2017.1400175.
9. Solini A, Suvan J, Santini E, et al. Periodontitis affects glucoregulatory hormones in severely obese individuals. Int J Obes 2019; 43:1125-29. doi:10.1038/s41366-018-0253-4.
10. Graziani F, Gennai S, Solini A, Petrini M. A systematic review and meta-analysis of epidemiologic observational evidence on the effect of periodontitis on diabetes An update of the EFP-AAP review. J Clin Periodontol 2018; 45:167-87. doi:10.1111/jcpe.12837.
11. Piattelli A, Scarano A, Piattelli M. Detection of alkaline and acid phosphatases around titanium implants: a light microscopical and histochemical study in rabbits. Biomaterials 1995; 16(17):1333-38. doi: 10.1016/0142-9612(95)91049-5.
12. Graziani F, Cei S, Orlandi M, et al. Acute-phase response following full-mouth versus quadrant non-surgical periodontal treatment: A randomized clinical trial. J Clin Periodontol 2015; 42:843-52. doi:10.1111/jcpe.12451.

LETTER TO THE EDITOR

A bioprogressive approach for post-acute rehabilitation in elderly COVID-19 survivors

R. Saggini[1-2], T. Paolucci[1], A. Bramanti[2] and R.G. Bellomo[3]

[1]Unit of Physical Medicine and Rehabilitation, G. D'Annunzio University of Chieti-Pescara, Department of Oral Medical Science and Biotechnology (DSMOB), Italy; [2]Centro per Neurolesi "Bonino Pulejo," IRCSS, Messina, Italy; [3]Department of Biomolecular Sciences, University of Urbino Carlo Bo, Urbino, Italy

Received June 23, 2020 – Accepted October 27, 2020

To the Editor,

The recent COVID-19 pandemic has the potential to cause significant physical and mental damage in older people (1, 2). Also, the rise in the prevalence of comorbid chronic conditions and the aging of the world's population have increased the number of people who have been affected by COVID, effecting low survival rates. COVID-19 represents the pandemic of the century, with approximately 3.5 million cases and 250,000 deaths worldwide as of May 2020. Survivors report short-term and medium-term sequelae with respect to reduced pulmonary function (restrictive pattern), polyneuropathy, and sometimes poor lower and upper extremity strength and low functional capacity (myopathy) (3).

Overall, this postural biomechanical dysfunction syndrome is characterized by postural alterations and imbalance, with the loss of strength of the deep muscles of the spine and a myofascial syndrome that is related to alterations in muscle rheological parameters. These conditions include an increase in stiffness and a reduction in elasticity, which also occur in peripheral compressive neuropathies. Furthermore, patients emerge from prolonged periods of immobility and, during recovery, a forced posture is triggered, with mutation of the sacrum and lumbar straightening, increased kyphosis, and anteposition of the head. At the same time, the near-constant use of personal protective equipment, such as masks, has led to an increase in energy expenditure that is associated with a reduction in respiratory capacity due to contracture of the diaphragm.

Subsequently, surviving COVID-19 patients need a comprehensive, integrated rehabilitation plan that includes a multidisciplinary and interdisciplinary team for all of these clinical aspects and rehabilitative dysfunctions. Moreover, optimizing one's function, at all ages, is a major global public health goal, particularly in the elderly (4). After recovery from COVID-19, patients manifest several functional impairments across many bio-psycho-social domains, and considering the physiological characteristics of the elderly, the pathological features of respiratory diseases, and the psychosocial disorders that existed prior to the COVID-19 epidemic, we suggest, as a recommended rehabilitative approach, a bioprogressive and sensorimotor rehabilitation plan with advanced physical energy, such as very-low-intensity and -frequency magnetic fields, focal vibration, and specific motor exercises. The use of an extremely low magnetic field (ELF-MF) is a potentially new treatment and preventive method with regard to biofilm, related to

Key words: COVID-19; rehabilitation; subacute care; infectious disease

Corresponding Author:
Dr Teresa Paolucci,
University G. D'Annunzio Chieti,
Department of Medical and Oral Sciences and Biotechnologies,
Viale Abruzzo 322,
66100 CH, Chieti-Pescara, Italy
email: teresa.paolucci@unich.it

0393-974X (2020)
Copyright © by BIOLIFE, s.a.s.
This publication and/or article is for individual use only and may not be further reproduced without written permission from the copyright holder.
Unauthorized reproduction may result in financial and other penalties
DISCLOSURE: ALL AUTHORS REPORT NO CONFLICTS OF INTEREST RELEVANT TO THIS ARTICLE.

chronic infections, such as pulmonary disease, and for countering posttraumatic stress disorder (5, 6). A rehabilitation plan that implements motor exercises in terrestrial and aquatic microgravity environments improves automatic and cognitive processes and enhances attentional strategies, facilitating the integration of proprioceptive, visual, and vestibular information.

A bioprogressive rehabilitative approach, with the assistance of modern technological developments, such as microgravity-producing devices and techniques, enables personalized and targeted therapeutic approaches to be established, which appear to be the most effective in the rehabilitation and prevention of neuro-myo-sensory disorders that compromise the homeostatic body harmony, particularly in old age (7). For example, a rehabilitative program that combines a dynamic antigravity postural system (SPAD) and a vibration sound system (ViSS) for postural instability has shown efficacy in improving postural attitude and balance in patients with Parkinson's disease (8).

Furthermore, the oscillations that are produced by mechanical vibration activate proprioceptors (mainly Pacinian corpuscles and muscle spindles) and afferent nerve fibers, inducing long-term potentiation of the segmental levels and central circuits, increasing neuronal cortical excitability and the ability to produce enhanced muscle peak and the strength of muscle contractions. In this context, physical exercise should be specific for resistance or strength and flexibility to create better adaptive responses in aging patients, especially in post-COVID rehabilitation. Within the bio-progressive-integrated rehabilitation approach, thermal medicine and health resort-based rehabilitation can also become valid allies in the post-COVID patient in the outpatient setting (10).

The bioprogressive and multisensory rehabilitation plan, tailored to COVID patients, could reduce postural biomechanical syndrome and significantly improve the kinetic and kinematic actions that are related to segmental and global body movements during static and dynamic motion. Such integrated rehabilitation methods represent a future challenge for the outpatient management of COVID patients, meriting future research in this area.

REFERENCES

1. Feng F, Tuchman S, Denninger JW, Fricchione GL, Yeung A. Qigong for the prevention, treatment, and rehabilitation of COVID-19 infection in older adults [published online ahead of print, 2020 May 15]. Am J Geriatr Psychiatry 2020;10.1016/j.jagp.2020.05.012. doi:10.1016/j.jagp.2020.05.012.
2. Sheehy LM. Considerations for postacute rehabilitation for survivors of COVID-19. JMIR Public Health Surveill 2020; 6(2):e19462. doi:10.2196/19462.
3. Herridge MS, Moss M, Hough CL, et al. Recovery and outcomes after the acute respiratory distress syndrome (ARDS) in patients and their family caregivers. Intensive Care Med 2016; 42:725-38.
4. Heinemann AW, Feuerstein M, Frontera WR, et al. Rehabilitation Is a Global Health Priority. BMC Health Serv Res 2020;20(1):143. doi:10.1186/s12913-020-4962-8.
5. Di Bonaventura G, Pompilio A, Crocetta V, et al. Exposure to extremely low-frequency magnetic field affects biofilm formation by cystic fibrosis pathogens. Future Microbiol. 2014; 9(12):1303-1317. doi:10.2217/fmb.14.96.
6. Paolucci T, Pezzi L, Centra AM, Giannandrea N, Bellomo RG, Saggini R. Electromagnetic field therapy: a rehabilitative perspective in the management of musculoskeletal pain – a systematic review, J Pain Res. 2020; 13:1385–1400. doi: 10.2147/JPR.S23177.
7. Pokorski M, Barassi G, Bellomo RG, Prosperi L, Crudeli M, Saggini R. Bioprogressive Paradigm in Physiotherapeutic and Antiaging Strategies: A Review. Adv Exp Med Biol. 2018;1116:1-9. doi:10.1007/5584_2018_281.
8. Di Pancrazio L, Bellomo RG, Franciotti R, et al. Combined rehabilitation program for postural instability in progressive supranuclear palsy. NeuroRehabilitation. 2013;32(4):855-860. doi: 10.3233/NRE-130909.
9. Masiero S, Maccarone MC, Agostini F. Health resort medicine can be a suitable setting to recover disabilities in patients tested negative for COVID-19 discharged from hospital? A challenge for the future. Int J Biometeorol 2020;64(10):1807-1809. doi: 10.1007/s00484-020-01947-4.

LETTER TO THE EDITOR

Efficacy of a nasal spray containing N-acetylcysteine in hypertonic solution in the treatment of non-allergic chronic rhinitis with goblet cell metaplasia

E. Maffezzoni[1], M. Notargiacomo[2], S. Agostini[3] and M. Gelardi[4]

[1]Rhinocytoallergology Unit, Istituto Figlie di San Camillo, Cremona, Italy; [2]Otorhinolaryngology Unit, Melzo Hospital, Milan, Italy; [3]Scientific Direction, Pharma Line, Milan, Italy; [4]Unit of Otolaryngology, University of Foggia, Foggia, Italy

Received June 29, 2020 – Accepted October 29, 2020

To the Editor,

Continued exposure to exogenous irritants, such as tobacco smoke, air pollutants, substances dispersed in the workplace, and endogenous irritants (hydrochloric acid, pepsin), as in gastroesophageal and laryngopharyngeal reflux, initiates inflammatory processes in the mucous membranes of the upper respiratory tract, leading to their chronic status. The chronic inflammatory process that characterizes chronic rhinitis results in a progressive remodelling of the nasal mucosa. This can lead to goblet cell metaplasia, a condition in which there is an increase in distribution of goblet cells in the nasal cavity at nasal cytology. The altered integrity of the nasal mucosa leads to a progressive impairment of mucociliary clearance which favours bacterial colonization and the onset of infections, which further support the inflammatory status. This generates a vicious circle with mutual reinforcement of inflammation and metaplasia. Chronic rhinitis with goblet cell metaplasia is characterized by nasal obstruction, rhinorrhoea, sneezing, itching, post-nasal drip, facial pain and anosmia or hyposmia.

Nasal cytology is a useful, cost-effective and easily applicable diagnostic method to better classify the various rhinitis phenotypes. It makes it possible to quantify cell populations in the nasal mucosa to better discriminate pathological conditions and to assess the effect of the therapeutic strategy undertaken (1, 2). The clinical trial started in early May 2019 and was completed in mid-December 2019. Its purpose was to evaluate the efficacy of a medical device containing 3% buffered hypertonic saline and 6% N-acetylcysteine (NAC) compared to the efficacy of a nasal spray containing only 3% hypertonic saline in the treatment of patients who have non-allergic chronic rhinitis with cytological diagnosis of goblet cell metaplasia.

MATERIALS AND METHODS

Tested medical device

Viscoflu® Nasal Spray (VNS - Pharma Line S.r.l. Milan, on the market since July 2018) is a medical device containing 3% hypertonic saline solution (NaCl), with controlled pH, and 6% N-acetylcysteine. The product is indicated to facilitate fluidification and removal of stagnant mucous secretions or purulent mucus in nasal cavities and paranasal sinuses, improving the symptoms and course of acute, subacute and chronic inflammation of the airways. The effectiveness of this product was compared to the effectiveness of a nasal spray containing only 3% hypertonic saline solution (NaCl) (HSS). The two products were made available free of charge by Pharma Line (Milan).

Key words: chronic rhinitis; goblet cell metaplasia; nasal cytology; N-acetylcysteine; hypertonic saline solution; topical therapy

Corresponding Author:
Matteo Gelardi, MD
Unit of Otolaryngology,
University of Foggia,
Viale L. Pinto, Foggia, Italy
Tel.: +39 3393286982
e-mail: matteo.gelardi@unifg.it

0393-974X (2020)
Copyright © by BIOLIFE, s.a.s.
This publication and/or article is for individual use only and may not be further reproduced without written permission from the copyright holder.
Unauthorized reproduction may result in financial and other penalties

Assessed subjects

Eighty patients (41 men, 39 women), with an average age of 43.3 years (minimum age 18, maximum age 76), with chronic rhinitis or rhinosinusitis with goblet cell metaplasia were evaluated. Patients were divided into two groups of 40 patients each: a group treated with VNS (19 men, 21 women) and a group treated with HSS (22 men, 18 women). The demographic and medical history data of the patients enrolled in the study are shown in Table I.

Adult male and female subjects suffering from chronic non-allergic rhinitis with cytological diagnosis of goblet cell metaplasia were included in the study. Subjects with proven sensitivity to one or more components of VNS or HSS, with active infections, malignant diseases and/or nasal polyposis were excluded from the study. Those who had taken drugs for the treatment of rhinopathy in the four weeks prior to the start of the application of the two nasal sprays were also excluded. Patients were enlisted with their personal identification data and signed regular informed consent to both the proposed therapy and the processing of personal data. At the time of enrolment, a medical history form was completed for each patient with all the data collected and a form to be completed at the next check-up was attached.

Study design

This is a prospective and comparative clinical study. Two treatment arms were created to which patients were randomly assigned. The subjects belonging to the VNS group and the subjects belonging to the HSS group were

Table I. *The two groups of patients treated were homogeneous in demographic and medical history characteristics as well as in regard to the signs and symptoms of the disease and the outcome of the rhinocytogram in basal conditions.*

Variable	VNS (n=40)	HSS (n=40)	p-value
Age in years, average±SD	42.7 ± 13.9	44.1 ± 15.8	0.669
Sex, %F (n)	52.5 (21)	45.0 (18)	0.655
Chronic rhinitis diagnosis*, % (n)	90.0 (36)	92.5 (37)	1.000
Smoking, % yes (n)	12.5 (5)	15.0 (6)	1.000
Familiarity**, % yes (n)	50.0 (10)	40.0 (8)	0.751
Rhinocytogram, median [25° - 75°]			
Neutrophils	2 [0 – 3]	1 [0 – 3]	0.566
Lymphocytes	1 [0 – 2]	1 [0 – 1]	0.386
Goblet cells	3 [3 – 4]	3 [3 – 3]	0.260
*Bacteria***	2 [0 – 2.3]	0 [0 – 2]	0.075
Turbinate hypertrophy, median [25° - 75°]	3 [3 – 3]	3 [3 – 3]	0.936
TNSS**, median [25° - 75°]	7 [6.8 – 9]	6 [5 – 8]	0.271
Fibrorhinoscopy**, % (n)			
Serous catarrhal rhinorrhoea	15 (3)	40 (8)	0.133
Serum-mucosal rhinorrhoea	20 (4)	25 (5)	
Serum-purulent rhinorrhoea	65 (13)	35 (7)	

**The remaining subjects suffered from chronic rhinosinusitis: 10% in the VNS group and 7.5% in the HSS group. ** For familiarity rate, bacterial count, TNSS and fibrorhinoscopy, data are only available for 20 patients in each treatment group.*

checked on two occasions: at the start of the application of VNS or HSS (T0) and after 10 days of application of VNS or HSS (T1). From the moment of the start of the application of the assigned product (T0) and in the following days (T0 to T1), the subjects applied the assigned product in the measure of 2 deliveries per nostril 3 times a day, for 10 consecutive days.

Assessment

At the time of enrolment, subjects underwent an accurate medical history with evaluation of allergies, symptoms, smoking, occupation, familiarity with allergic and non-allergic nasal diseases, operations undertaken and ongoing therapies. Data were also collected by means of a physical examination: deviation of the nasal septum, lower turbinate hypertrophy, presence or absence of polyps, presence of catarrhal, serous or purulent rhinorrhoea. Finally, data were collected through nasal cytological examination: confirmation of goblet cell metaplasia, presence of bacterial biofilm, nasal epithelium appearance. At the time of enrolment, the two groups of patients were homogeneous in terms of signs and symptoms (Table I).

All patients underwent a sample collection through scraping technique both at T0 and T1. Each sample underwent cytological examination, which was carried out by spreading the sample over a glass slide and staining it with the May Grunwald - Giemsa method. All the slides were observed under 100, 400, 1000 magnifications to count the cellular inflammatory (neutrophils and lymphocytes) and mucin-producing elements and the presence of any bacteria. The outcome of the nasal cytological examination was evaluated by using the classification shown in Table II (3). In addition, all patients were assessed for turbinate hypertrophy by scoring from 0 to 3 in accordance with the Mladina classification, depending on the presence and severity of this sign (4).

A sample of 20 patients treated with VNS and 20 patients treated with HSS was evaluated by using, as a method of symptom detection, the Total Nasal Symptom

Table II. *Quantitative classification of nasal cytological examination results.*

Cell type	Description	Quantity	Classification
Neutrophils and lymphocytes	None	0	0
	Sporadic	0.1 – 1%	½+
	A Few scattered cells, small groups	1.1 – 5%	1+
	In discreet numbers, large groups	5 – 15%	2+
	Large cellular clusters that do not occupy the entire field	15 – 20%	3+
	Large cellular clusters occupying the entire field	>20%	4+
Goblet cells	None	0	0
	From rare to few cells	1 -24%	1+
	In a significant number	25 - 49%	2+
	In large numbers	50 - 74%	3+
	Lots of cells scattered all over the field	75 – 100%	4+
Bacteria	None	Not standardized	0
	Sporadic cell cluster		1+
	In a significant number		2+
	Many easily visible cells		3+
	Bacteria in the entire field		4+

Score (TNSS), which assigns a 4 point rating (from 0 to 3), depending on the presence and intensity of the symptoms the patient is experiencing, among the following 4 nasal symptoms: nasal obstruction, rhinorrhoea, nasal itching and sneezing (5). The remaining sample of 20 patients treated with VNS and 20 patients treated with HSS, which was not evaluated by using TNSS, underwent fibrorhinoscopy to assess rhinorrhoea. A scale commenting the increasing severity of the rhinorrhoea detected was used: absence of rhinorrhoea, catarrhal rhinorrhoea, serum-mucosal rhinorrhoea, serum-purulent rhinorrhoea or purulent rhinorrhoea.

All investigations were conducted both at the start of application (T0) and after 10 days of regular application of the nasal spray assigned to each patient (T1). Patients were also asked to express an opinion on the tolerability and degree of satisfaction with the therapy they underwent, scoring from 0 to 4, with the emoticons system: worsening (0), unchanged situation (1), moderate improvement (2), good improvement (3), great improvement (4). Finally, reports of any adverse effects attributable to the application of the nasal sprays tested were collected.

Statistical analysis

The descriptive statistics were used for the summary presentation of patient cohort characteristics in terms of median and percentiles [25° - 75°] or frequencies, when deemed appropriate. The differences in baseline conditions between the two treatment groups were assessed by *t*-test or the corresponding non-parametric test in the case of continuous variables and by Fisher's exact test in the case of frequencies. The effect of the treatment was evaluated against the variation in the result between the T1 and T0 visits and the significance of the differences was determined by applying Mann-Whitney's non-parametric test for paired data in the case of the

Table III. *Medians of cell count, of the score attributed to turbinate hypertrophy according to the Mladina classification and of the score given to the TNSS at the time of initiation of therapy (T0) and after 10 days of nasal spray application (T1), median of variations for each parameter investigated and statistical significance of the variations.*

Rhinocytogram	Treatment	T0 Median [25° - 75°]	T1 Median [25° - 75°]	p-value	T1-T0 Median [25° - 75°]
Neutrophils	VNS	2 [0; 3]	1 [0; 2]	p < 0.0001	-1 [-1.3; 0]
	HSS	1 [0; 3]	1 [0; 2]	p = 0.009	0 [-1; 0]
Lymphocytes	VNS	1 [0; 2]	0.5 [0; 1]	p < 0.0001	-0.5 [-1; 0]
	HSS	1 [0; 1]	1 [0; 1]	p = 0.773	0 [0; 0]
Goblet cells	VNS	3 [3; 4]	1 [1; 2]	p < 0.0001	-2 [-2; -1.5]
	HSS	3 [3; 3]	3 [2; 3]	p < 0.0001	-1 [-1; 0]
Bacteria*	VNS	2 [0; 2.3]	1 [0; 1]	p = 0.002	-1 [-1; 0]
	HSS	0 [0; 2]	0 [0; 1.3]	p = 0.346	0 [0; 0]
Turbinate hypertrophy	VNS	3 [3; 3]	2 [1; 2]	p < 0.0001	-1 [-2; -1]
	HSS	3 [3; 3]	2 [2; 3]	p < 0.0001	-1 [-1; 0]
TNSS	VNS	7 [6.8; 9]	3 [2; 4]	p < 0.0001	-4 [-5.3; -3]
	HSS	6 [5; 8]	4 [3; 5.3]	p = 0.0001	-2 [-4; -1]

The values shown in the table are expressed as medians of the measures collected, based on the classification shown in Table II, for all subjects at T0 and T1. The square brackets indicate the values of the 25th and 75th percentile. (*) Bacterial cells were present at T0 in 8 patients treated with HSS and 12 patients treated with VNS.

comparison between T1 and T0 and for unpaired data in the case of the comparison of the variations between the two treatment groups. In all the analyses carried out the results are considered statistically significant for $p < 0.05$.

Statistical analysis was performed by using the R software version 3.6.1 for Windows (R Core Team; 2013. A language and environment for statistical computing. R Foundation for Statistical Computing, Vienna, Austria).

RESULTS

Cytological examination

Treatment with VNS and treatment with HSS resulted in a significant reduction in neutrophils ($p < 0.0001$ and $p = 0.009$ respectively). Treatment with VNS resulted in significantly greater neutrophil reduction than that induced by HSS (-1 [-1.3; 0] *vs*

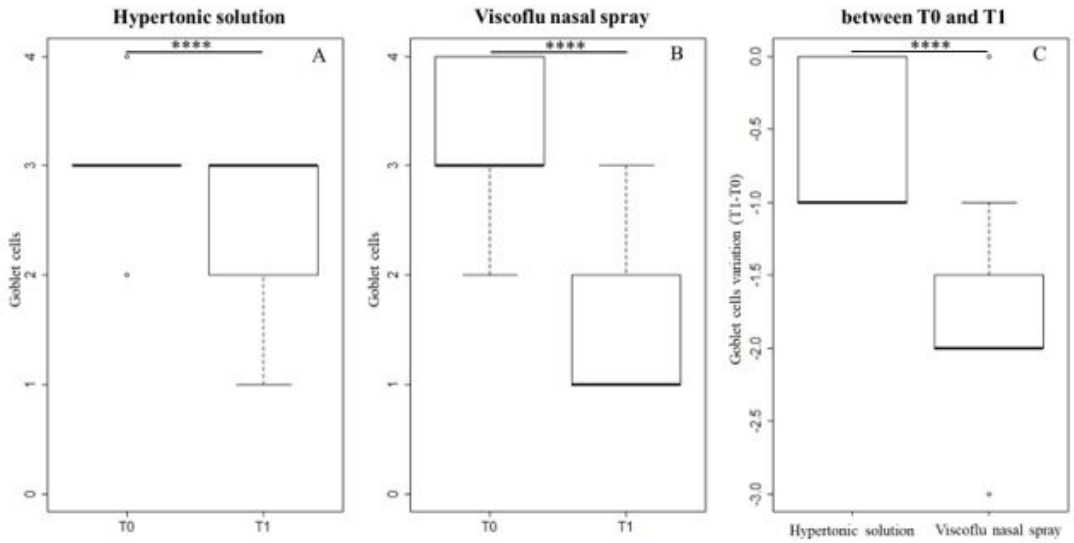


Fig. 1. *Both treatments resulted in significant neutrophil reduction (**A, B**). Treatment with VNS resulted in a significantly greater reduction in neutrophils than that induced by HSS (**C**). All the graphs use Tukey's representation; * $p < 0.05$; ** $p < 0.01$; **** $p < 0.0001$.*

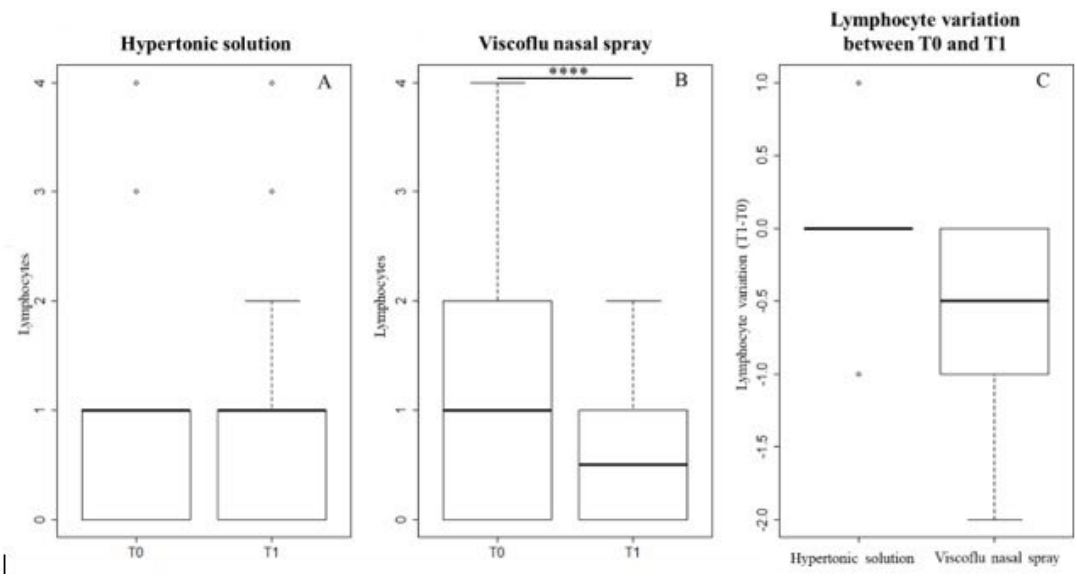


Fig. 2. *Lymphocyte reduction was significant only in subjects treated with VNS (**B**) and averaged -0.5 [-1; 0]. Treatment with HSS did not result in a statistically significant reduction in lymphocytes (**A**). Treatment with VNS resulted in a significantly greater reduction in lymphocytes than that induced by HSS (**C**). All the graphs use Tukey's representation; **** $p < 0.0001$.*

0 [-1; 0]; p = 0.01) (Table III, Fig. 1 A, B, C). The reduction in lymphocytes was significant only in subjects treated with VNS (p < 0.0001) and on average was -0.5 [-1; 0]. Treatment with HSS did not result in a statistically significant reduction in lymphocytes (Table III, Fig. 2 A, B, C). Both treatments induced a significant reduction in the number of goblet cells (p < 0.0001). Treatment with VNS resulted in a significantly greater reduction in the number of goblet cells than that induced by HSS (-2 [-2; -1.5] vs -1 [-1; 0]; p < 0.0001) (Table III, Fig. 3 A, B, C). Bacterial reduction was significant only in subjects treated with VNS (p = 0.002) and on average was -1 [-1; 0]. Treatment with HSS did not result in a statistically significant bacterial reduction (Table III).

Turbinate hypertrophy

Both treatments induced a statistically significant reduction in turbinate hypertrophy (p < 0.0001). In patients treated with VNS the reduction was greater than that induced by HSS and the difference between the two results is statistically significant (-1 [-2; -1] vs -1 [-1; 0]; p = 0.0001; Table III).

Total Nasal Symptom Score

Treatment with VNS and treatment with HSS resulted in a statistically significant reduction in the TNSS score (p < 0.0001 and p = 0.0001 respectively), but in subjects treated with VNS the effect was significantly greater than that measured in subjects treated with HSS (-4 [-5.3; -3] *vs* -2 [-4; -1]; p = 0.029; Table III)

Fibrorhinoscopy

Treatment with VNS resulted in rhinorrhoea improvement in 95% of patients under treatment, while HSS resulted in rhinorrhoea improvement in 40% of patients under treatment. The effect of VNS on the rhinorrhoea profile, evaluated by fibrorhinoscopy, was significantly greater than that induced by treatment with HSS alone (p < 0.001).

Satisfaction

Subjects in both treatment groups were satisfied (p = 0.435) and reported moderate to good improvement (VNS: good improvement 40%; moderate improvement 45%; unchanged 15%. HSS: good improvement 35%; moderate improvement 30%; unchanged 35%). The data on patient satisfaction is in line with what was observed in the evaluation of the other parameters.

Reported adverse effects

None of the patients in the two groups complained

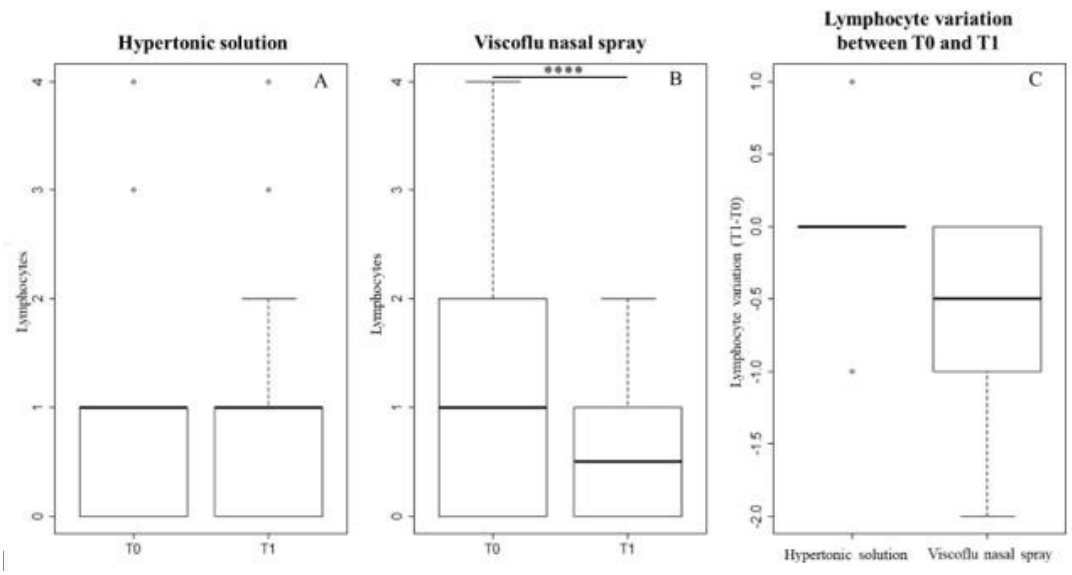


Fig. 3. *Both treatments induced a significant reduction in goblet cells (**A, B**). Treatment with VNS resulted in a significantly greater reduction in the number of goblet cells than that induced by HSS (**C**). All the graphs use Tukey's representation; **** p < 0.0001.*

of adverse effects attributable to the application of nasal sprays during the 10-day treatment. No patient stopped applying nasal spray.

DISCUSSION

In addition to basic research literature, there is extensive literature available on the clinical use of saline solution: it cleanses the mucous membranes, removes secretions, physiologically mobilizes the surface gel layer, increases hydration in the sol layer, improves mucociliary function and removes inflammatory mediators. It is recommended as an adjuvant treatment in the management of rhinitis and rhinosinusitis (6), as it is effective, safe, cost-effective and easy to use. NAC has a proven mucolytic action, stimulates glutathione biosynthesis and has antioxidant activity (7). Studies show that NAC has anti-inflammatory activity and the ability to counteract the formation of bacterial biofilms (8, 9).

No clinical studies were identified in the literature in which a combination of hypertonic saline solution and NAC was tested for topical use in the treatment of non-allergic chronic rhinitis with goblet cell metaplasia. A recent retrospective clinical study demonstrated the efficacy of this combination in the topical treatment of chronic rhinosinusitis without polyposis, with early recurrence after Functional Endoscopic Sinus Surgery (FESS) (10).

The present clinical study shows a significant improvement in the rhino-cytological profile of the nasal mucosa of patients who have non-allergic chronic rhinitis with a cytological diagnosis of goblet cell metaplasia and who applied a nasal spray containing HSS or VNS for 10 consecutive days. VNS has been shown to be significantly more effective than HSS in reducing the number of goblet cells, neutrophils, lymphocytes and bacteria, and in reducing turbinate hypertrophy, TNSS score and rhinorrhoea. This result can be supposedly attributed to the synergistic action between the 3% hypertonic saline solution and 6% NAC. VNS proved safe and well tolerated: in the 10 days of product intake, no patient reported adverse events and no patient discontinued therapy.

VNS can therefore be considered a valid aid in the treatment of the most frequent nasal-sinus diseases, especially in those with a high irritative component accompanied by a strong mucous reaction. In conclusion, the use of VNS can be recommended for its significant mucolytic activity, for its ability to restore surface ciliary activity at the epithelium level and for the modulation of inflammation, which are essential processes for the optimisation of nasal-sinus defensive functions.

CONFLICT OF INTEREST

Enrico Maffezzoni, Mario Notargiacomo and Matteo Gelardi declares that they have no commercial associations (e.g. consultancies, stock ownership, equity interest, patent/licensing arrangement etc.) that might pose a conflict of interest in connection with the submitted article. Stefano Agostini is an employee of Pharma Line.

ACKNOWLEDGEMENT

The authors sincerely thank Nica Carbonara for her valuable contribution in the initial phases of this study.

REFERENCES

1. Gelardi M. Atlante di citologia nasale per la diagnosi differenziale delle rinopatie. Edi Ermes. Milano 2012.
2. Gelardi M, Fiorella ML, Russo C, Fiorella R, Ciprandi G. Role of nasal cytology. Int J Immunopathol Pharmacol 2010; 23(1 Suppl):45-94.
3. Gelardi M, Iannuzzi L, Quaranta N, Landi M, Passalacqua G. Nasal cytology: practical aspects and clinical relevance. Clin Exp Allergy 2016; 46:785-92.
4. Mladina R. The role of maxillar morphology in the development of pathological septal deformities. Rhinology 1987; 25(3):199-205.
5. Downie SR, Andersson M, Rimmer J et al. Symptoms of persistent allergic rhinitis during a full calendar year in house dust mite-sensitive subjects. Allergy 2004; 59(4):406-14.
6. Hermelingmeier KE, Weber RK, Hellmich M, Heubach CP, Mosges R. Nasal irrigation as an adjunctive treatment in allergic rhinitis: a systematic

review and meta-analysis. Am J Rhinol Allergy 2012; 26(5):e119–e125.
7. Mokhtari V, Afsharian P, Shahhoseini M et al. A Review on Various Uses of N-Acetyl Cysteine. Cell J 2017; 19(1):11-17.
8. Dinicola S, De Grazia S, Carlomagno G et al. N-acetylcysteine as powerful molecule to destroy bacterial biofilms: a systematic review. European Review for Medical Oxidative Medicine and Cellular Longevity and Pharmacological Sciences 2014; 18(19):2942-48.
9. Macchi A, Terranova P, Castelnuovo P. Recurrent acute rhinosinusitis: a single blind clinical study of N-acetylcysteine vs ambroxol associated to corticosteroid therapy. Int J Immunopathol Pharmacol 2012; 25(1):207-17.
10. Zanetti L, Valetti L, Bettoni L, Agostini S. Efficacy of a nasal spray containing N-acetylcysteine in hypertonic saline solution in the treatment of chronic rhinosinusitis, with early recurrence after Functional Endoscopic Sinus Surgery. Farmaci 2019; 18(3):1-8.

LETTER TO THE EDITOR

Assessment of eosinophilic nasal inflammation in patients with severe asthma and nasal polyposis before and after six months of therapy with Benralizumab

E. Buonamico[1], S. Dragonieri[1], P.I. Sciancalepore[2], P. Carratù[1], G.E. Carpagnano[1], O. Resta[1] and M. Gelardi[3]

[1]Respiratory Diseases, University of Bari, Bari, Italy; [2]Otolaringology, University of Bari, Bari, Italy; [3]Otolaringology, University of Foggia, Foggia, Italy

Received May 27, 2020 – Accepted October 30, 2020

To the Editor,

Numerous studies have indicated a strong relationship between chronic rhinosinusitis with nasal polyposis (CRNP) and eosinophilic severe asthma (ESA) (1). Indeed, typical histopathological findings such as airway remodeling, eosinophilic infiltration, T-helper recruitment and IL-5 production are evident in both CRNP and ESA (1). International guidelines suggest that patients with ESA may require add-on biological therapy consisting in a monoclonal antibody to be selected between currently available anti-interleukin (IL)-5 and anti-IL-5 receptor agents (2). In particular, Benralizumab is an eosinophil-depleting anti IL-5 receptor biologic drug which has been previously shown to be effective in preventing ESA exacerbations, improving lung function and symptom control (3) and oral corticosteroid sparing (4). Moreover, Benralizumab showed to be successful in reducing nasal polyps and ameliorating nasal symptoms (3).

Nasal cytology is an easy, cheap and safe diagnostic procedure which allows the assessment of normal and pathological features of nasal mucosa by identification and count of cell types and morphology (5). Viral infections, allergic rhinitis, vasomotor rhinitis and overlapping forms are easily discriminated by nasal cytology, which can aid to set a proper therapeutic approach (5). It is plausible that examination of nasal eosinophils, instead of sputum, might be useful for the diagnosis and monitoring of eosinophil-positive rhinitis as well as severe asthma.

To date, no studies have investigated the effect of biologic agents on nasal cells in rhinosinusitis and nasal polyps. Based on the above, the aim of our study was to evaluate the influence of Benralizumab on nasal eosinophils in a group of patients with coexisting CRNP and ESA.

MATERIALS AND METHODS

Patients

In the current pilot study 10 patients (6 females, 4 males; mean age 48.9±10.1) affected by severe eosinophilic asthma and history of documented nasal polyposis and chronic rhinosinusitis were enrolled. All participants were eligible for biologic therapy, according to the most recent guidelines (2). Patients were enrolled from the outpatient clinic of Respiratory diseases and Otolaringology departments of the University hospital Policlinico in Bari, Italy. Exclusion criteria were the following: poor inhaler technique and/or non-adherence to treatment, history of smoking, comorbidities such as neoplasms, cardiac or renal

Key words: nasal citology; eosinophils; severe asthma; nasal polyposis; Benralizumab

Corresponding Author:
Dr Silvano Dragonieri,
Department of Respiratory Diseases,
University of Bari, Piazza Giulio Cesare 11
70124 Bari, Italy
Tel.: +39 0805593215
e-mail: silvano.dragonieri@uniba.it

0393-974X (2020)
Copyright © by BIOLIFE, s.a.s.
This publication and/or article is for individual use only and may not be further reproduced without written permission from the copyright holder.
Unauthorized reproduction may result in financial and other penalties
DISCLOSURE: ALL AUTHORS REPORT NO CONFLICTS OF INTEREST RELEVANT TO THIS ARTICLE.

failure, diabetes mellitus and presence of eosinophilic lung diseases such as acute or chronic eosinophilic pneumonia and Churg-Strauss syndrome.

This research was conducted in accordance with the guidelines for good clinical practice and the ethical principles originating in the Declaration of Helsinki. Nasal cytology is a routine tool in the workup of sinus-nasal diseases as it is regularly performed at our institutions for clinical purposes. Cases were retrospectively evaluated, therefore there was no need to require a formal approval by the ethics committee. All participants signed informed consent.

Study design

The study subjects were observed over a 6-month period, as part of their routine care. At baseline (T1) all patients were carefully evaluated at the Respiratory diseases outpatient clinic, and performed pre- and post-bronchodilator pulmonary function tests, according to the most recent recommendations (ATS/ERS 2019). Moreover, symptom control was assessed by the Asthma Control Test (ACT). After evaluating inclusion and exclusion criteria, add-on therapy with Benralizumab was prescribed if the patient was eligible.

Before the first injection of biologic therapy, no later than 7 days from the first pulmonological evaluation, all subjects were visited at the Otholaringology outpatient clinic and underwent anterior rhinoscopy and nasal cytology. Within 7 days from the visit, the patients returned to the Respiratory Disease unit and the first dose of Benralizumab was administered as indicated in the drug data sheet. Successive injections of biologic therapy were performed in the Respiratory Disease outpatient clinic and the subjects were carefully evaluated for symptoms. After 6 months from first injection (T2), the patients underwent a new pulmonological and otholaringological visit and repeated exactly the same procedures as at T1.

Nasal cytology

Nasal cytology includes sampling, processing and microscope reading. Sampling requires the collection of cells from the surface of the middle portion of the inferior turbinate using a sterile disposable curette. The procedure is performed under anterior rhinoscopy, with an appropriate light source, and is completely painless. The sample obtained is immediately smeared on a glass slide, air-dried and stained with May-Grünwald-Giemsa (MGG) for 30 min. The stained sample was examined by optical microscopy with a 1000x objective with oil immersion (Fig. 1). Fifty fields are considered the minimum number to identify a sufficient number of cells. The count of each cell type was expressed by a semi-quantitative grading as previously described (5). Samples were examined blindly by two different investigators and the mean of the two measurements was considered for analysis.

Nasal endoscopy

The diagnosis of nasal polyposis was made using a fiberoptic endoscope (Vision Science- ENT 2000 of 3.4 mm diameter) Nasal polyp endoscopic 4-grade classification proposed by Meltzer was adopted (6).

Statistical analysis

Being a pilot study, sample size estimation was not calculated. Statistical analysis was performed by GraphPad

Table I. *Clinical and functional characteristics of patients at T1 and T2.*

Parameter	T1	T2	p
FEV1 pre L	1.6±0.7	1.8±0.4	ns
FVC pre L	2.6±0.9	2.7±0.5	ns
FEV1 post L	2.1±0.8	2.3±0.5	ns
FVC post L	3.1±1.1	3.1±0.7	ns
ACT	15.2±3.9	21.3±3.1	<0.05
Blood eosinophils(cells/μL)	576.3±235.8	0	<0.01
Nasal eosinophils (% total)	10.5±9.1	0	<0.01
Nasal neutrophils (%total)	13.1±11.3	0	<0.01
Nasal mast cells (%total)	2.3±1.5	3.5±2.3	ns
Nasal polyps (n)	4.2± 1.9	2.1±2.0	<0.05

Prism software, version 5.03. Continuous variables were expressed as mean±standard deviation. Categorical variables were expressed as frequency and percentage. Student's *t*-test was used to compare lung function values and ACT score between T1 and T2. Non-parametric Wilcoxon signed-rank test was used to compare the level of blood and nasal eosinophilic infiltration between T1 and T2. For all cases, $p<0.05$ was considered as significant.

RESULTS

Clinical and functional parameters are show in Table I**.** No significant differences were reported in terms of lung function values between T1 and T2. In particular, mean pre- and post-brochodilator FEV1 were higher at T2 compared to T1 although the statistical significance was not reached. ACT score was significantly improved ($p<0.05$) after 6 months of therapy with Benralizumab, and a complete suppression of blood eosinophils was observed at T2 ($p<0.01$). The number of polyps was also significantly reduced between T2 and T1 ($p<0.05$).

Nasal cytology analysis between T1 and T2 showed a full depletion of nasal eosinophils after 6 months of biological therapy ($p<0.01$, Fig. 2). Similarly, we observed a zeroing of nasal neutrophils at T2, in comparison with T1 ($p<0.01$). Finally, no significant differences in terms of nasal mast cells were reported between T1 and T2.

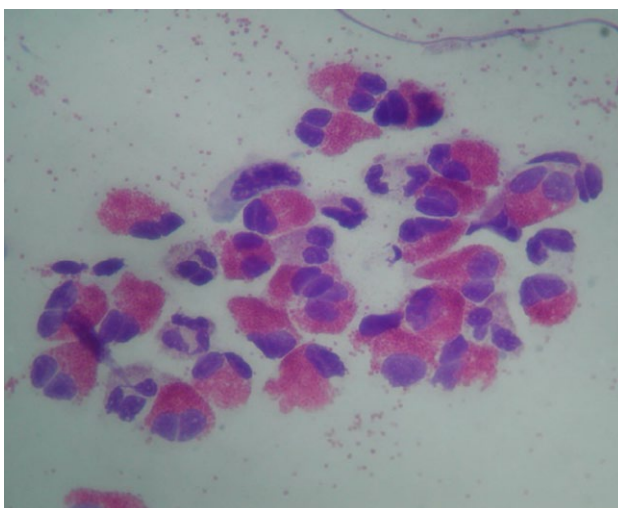


Fig. 1. *Cytological nasal sample under microscope at high-power magnification showing numerous eosinophils, partly degranulated, with absence of ciliated epithelial cells. (MGG; 1000x magnification)*

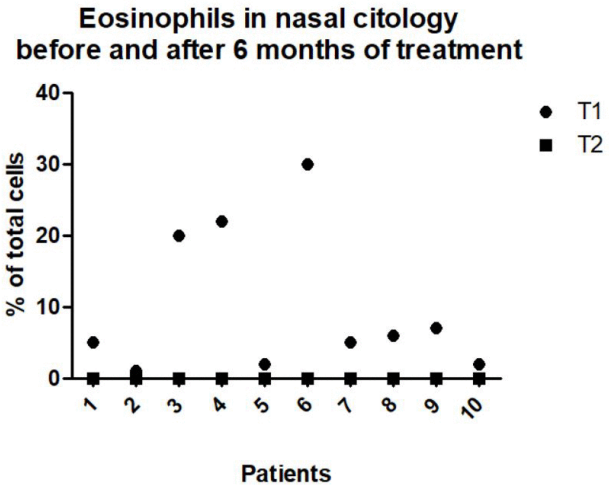


Fig. 2. *Percentage of nasal eosinophils before and after 6 months of treatment with Benralizumab.*

DISCUSSION

In the present study, we demonstrated that nasal eosinophilia is significantly reduced after six months of biological therapy with Benralizumab in a group of patients with concurrent severe eosinophilic asthma and chronic rhinosinusitis with polyposis. To the best of our knowledge, this is the first study which specifically investigated the effect of biological treatment on nasal cytology. Interestingly, we observed a relevant effect of Benralizumab on nasal eosinophils and on nasal polyps, which were present in all the patients. Our study extends the findings of a very recent case report by Pelaia et al, who observed a fast and striking therapeutic effect in a female patient with severe eosinophilic asthma and nasal polyposis (7). This effect of Benralizumab must be highlighted since nasal polyposis is one of the most frequent comorbidities of severe asthma. Nasal polyps are characterized by eosinophilic infiltration of polyp tissue (8), and the manifestation of nasal polyps is one of the most consistent predictive elements for a positive therapeutic response to therapy with Benralizumab (9).

We may therefore hypothesize that the notable improvements in terms of symptoms and nasal

polyposis observed in our population were related to Benralizumab-induced fast resolution of type-2 airway eosinophilic inflammation. Indeed, Benralizumab, which binds with high affinity to the α subunit of IL-5 receptor and suppresses eosinophils and basophils by inducing apoptosis via enhanced antibody-dependent cell-mediated cytotoxicity, is known to lower eosinophil counts in airway (sub-mucosa) and sputum, and deplete eosinophils in bone marrow and peripheral blood (10). Unsurprisingly, the above findings were reflected in the nasal mucosa, as assessed by our data. Moreover, we observed a total reduction of nasal neutrophils after 6 months of biologic-therapy. A recent study revealed that activated neutrophil granulocytes show a T-cell priming capacity and an ability to enhance eosinophil migration, thus affecting the course of inflammation in allergic rhinitis (11).

Given that no patients had infectious rhinosinusitis at either T1 or T2, which could have explained a difference in the number of neutrophil granulocytes, our above-mentioned findings might derive from a direct effect of therapy with Benralizumab. Undoubtedly, further investigations are warranted to clarify the effect of biologic therapy on nasal and systemic neutrophils.

The strengths of our study were the strict selection of ESA and CRNP patients, using broadly accepted guidelines (2) and the reliability of our measurements of nasal cytology, made by well-trained personnel in a fully equipped laboratory. The limitations of the current study were the limited number of enrolled patients, without a sample size estimation. Unquestionably, our findings originating from this pilot study necessitate further investigations with larger populations. Additionally, we did not perform direct correlation between nasal and sputum eosinophils, which is warranted in future studies. The latter is essential, since induced sputum analysis can be difficult to perform on particular types of patients such as children or those with very severe lung function parameters (12). Therefore, nasal cytology, being non invasive, cheap and easily repeatable, if validated may be considered not only as part of the rhino allergologic diagnostics (5), but an alternative to sputum for diagnosis and therapeutic response monitoring of patients with concomitant chronic rhinosinusitis with polyposis and severe eosinophilic asthma.

ACKNOWLEDEGMENTS

This study was independent and entirely financed by University of Bari.

REFERENCES

1. Ponikau JU, Sherris DA, Kephart GM, Kern EB, Gaffey TA, Tarara JE, Kita H. Features of airway remodeling and eosinophilic inflammation in chronic rhinosinusitis: is the histopathology similar to asthma? J Allergy Clin Immunol 2003; 112:877-82.
2. Global Initiative for Asthma, 2019. Update, www.ginasthma.org
3. Bleecker ER, FitzGerald JM, Chanez P, et al. Efficacy and safety of Benralizumab for patients with severe asthma uncontrolled with high-dosage inhaled corticosteroids and long-acting β2-agonists (SIROCCO): a randomised, multicentre, placebo-controlled phase 3 trial. Lancet 2016; 388:2115-27.
4. Nair P, Wenzel S, Rabe KF, et al. Oral glucocorticoid-sparing effect of Benralizumab in severe asthma. N Engl J Med 2017; 376:2448-58.
5. Gelardi M, Landi M, Ciprandi G. Nasal cytology: a Precision Medicine tool in clinical practice. Clin Exp Allergy 2018; 48:96-97.
6. Meltzer EO, Hamilos DL, Hadley JA, et al. Rhinosinusitis: developing guidance for clinical trials. Rhinosinusitis initiative. J Allergy Clin Immunol 2006; 118:S17-61.
7. Pelaia C, Busceti MT, Vatrella A, et al. Effects of the first three doses of Benralizumab on symptom control, lung function, blood eosinophils, oral corticosteroid intake, and nasal polyps in a patient with severe allergic asthma. SAGE Open Med Case Rep 2020; 8:2050313X20906963.
8. Newton JR, Ah-See KW. A review of nasal polyposis. Ther Clin Risk Manag 2008; 4:507-12.
9. Bleecker ER, Wechsler ME, FitzGerald JM, Menzies-Gow A, Wu Y, Hirsch I, Goldman M, Newbold P, Zangrilli JG. Baseline patient factors impact on the clinical efficacy of Benralizumab for severe asthma

Eur Respir J 2018; 52:1800936
10. Laviolette M, Gossage DL, Gauvreau G, et al. Effects of Benralizumab on airway eosinophils in asthmatic patients with sputum eosinophilia. J Allergy Clin Immunol 2013; 132:1086-96.
11. Arebro J, Ekstedt S, Hjalmarsson E, et al. A possible role for neutrophils in allergic rhinitis revealed after cellular subclassification. Sci Rep 2017; 7:43568
12. Murayama N, Murayama K. Nasal Discharge Eosinophils in childhood asthma patients as a predictive factor for persistent asthma mediators Inflamm 2018; 2018:2563978.

LETTER TO THE EDITOR

Anti-SARS CoV2 antibody testing in healthcare workers: comparison between rapid-cassette tests, ELISA and CLIA methods

L. Pistelli[1*], C. Sitzia[2*], M. Carrara[1], S. Borlini[1], M. Tejada[3], G. Sammarco[3], C. Fulceri[3], R. Valaperta[3], P. Giubbilini[3], R. Rigolini[3], B. Rampoldi[3], M. Cornetta[3], S. Mazza[3], S.D. Corino[3], A. Pettinato[3], S. Ferrari[3], C. Paduraru[3], A. Moroni[3], B. Jance[4], E. Costa[3] and M.M. Corsi Romanelli[2,3]

[1]Residency Program in Clinical Pathology and Clinical Biochemistry, University of Milan, Milan, Italy; [2]Department of Biomedical Sciences for Health, University of Milan, Milan, Italy; [3]Service of Laboratory Medicine 1-Clinical Pathology, I.R.C.C.S. Policlinico San Donato, San Donato Milanese, Milan, Italy; [4]Residency Program in Clinical Pathology and Clinical Biochemistry, University of Study of Florence, Florence, Italy

Received July 27, 2020 – Accepted November 9, 2020

[*]These authors equally contributed to this work

To the Editor,

Early diagnosis of SARS-CoV-2 infection is extremely important for effective management and treatment of patients. The gold standard for the diagnosis of infection is qRT-PCR analysis on respiratory samples. However pre-analytical variables – specimens and techniques of sample collection – and analytical variables - extraction and detection of viral nucleic acids – affect the sensitivity of the test that varies from 99 to 70% (1).

Serological analysis could be an easier, low time-consuming method to improve sensitivity and to investigate asymptomatic subjects who do not meet the appropriate criteria for RT-PCR testing. Sensitivity of serologic tests could be very high (2), however it could be affected by the timing of sampling. In particular, IgM could be detected 3 days after symptom onset and reach 95-100% of sensitivity in 12 days, while IgG could be detected as early as 4 days post-infection (2, 3), and IgM and IgG often coexist (3, 4). Specificity could be influenced by cross-reaction with other coronavirus strains. Despite all these limitations, serologic tests are easy to perform, low-cost and do not require skilled personnel. Indeed rapid-cassette tests could represent, once validated, a powerful tool to immediately obtain an indicative result when rapidity is fundamental as in an emergency. Knowledge of the analytical performance of commercial methods is of critical importance for the correct interpretation of the results. To date, a multitude of commercially available kits exist.

Here, we show the comparison of analytic performance of two different rapid-cassette tests with the ELISA method. Finally, we compared the obtained results with an FDA-approved fully automatized CLIA method to further validate the obtained data. The study was performed on a population of healthcare workers to evaluate the feasibility and the validity of these tests for application in healthcare surveillance or in large-scale screening.

Key words: Covid-19; Antibody testing; rapid-cassette tests; ELISA; CLIA

Corresponding Author:
Clementina Sitzia MD,
Department of Biomedical Sciences for Health,
University of Milan,
Via Luigi Mangiagalli, 31
20133 Milan, Italy
Tel.: +39 02 50315384/50315387
e-mail: clementina.sitzia@unimi.it

0393-974X (2020)
Copyright © by BIOLIFE, s.a.s.
This publication and/or article is for individual use only and may not be further reproduced without written permission from the copyright holder.
Unauthorized reproduction may result in financial and other penalties
DISCLOSURE: ALL AUTHORS REPORT NO CONFLICTS OF INTEREST RELEVANT TO THIS ARTICLE.

MATERIALS AND METHODS

Study population

The study was conducted at the IRCCS Policlinico San Donato of Milan (Italy). Samples were collected from 9th March 2020 to 13th May 2020. Serum samples from healthy donors collected in April 2018 were used as negative controls, representing pre-COVID-19 background immunity. Each patient gave written informed consent. This study was performed in accordance with the International Conference on Harmonisation of Good Clinical Practice guidelines, the Declaration of Helsinki (2008) and the European Directive 2001/20/EC.

Seventy-four voluntary healthcare workers (49 females and 25 males, mean age: 45.28 years), were included in the study. The subjects had performed nasopharyngeal swabs during sanitary surveillance or because of the onset of symptoms (41 RT-PCR +, 33 RT-PCR-), and 42 serum samples were collected before May 2018 which represented negative control of background immunity. Blood samples were collected within 4-8 weeks after performing nasopharyngeal swabs (mean 28.77 days SD: 23.11 days Min-Max: 0-81 days).

Cassette rapid IgG/IgM Test

Rapid tests were performed on serum samples after separation by centrifugation at 9000 rpm 9 minutes from freshly collected blood venous specimens. Cellex rapid cassette is a lateral flow chromatographic immunoassay, formed by a coloured pad, that contains SARS-CoV-2 recombinant antigens. Briefly 10µl of freshly isolated serum were dispensed in the sample well and 2 drops of sample diluent were immediately added. The results were read after 15-20 minutes. Declared sensitivity and specificity were 93.75% and 96.40%. Cross-reactivity is denied for principal infectious agents such as influenza A virus, adenovirus, respiratory syncytial virus, HBV, HCV, chlamydia pneumonia, cytomegalovirus etc., but positive results may be due to past or present infection with non-SARS-CoV-2 coronavirus strains HKU1, NL63, OC43 or 229E.

Zhejiang Orient Gene is a lateral flow chromatographic immunoassay. The cassette is analogue to Cellex Cassette. Briefly 5µl of freshly isolated serum was dispensed in the sample well and 2 drops of sample buffer were immediately added. Results were read after 10 minutes. Declared sensitivity and specificity were 87.9% and 100% for IgM and 97.2% and 100% for IgG. Interference of elevated title of rheumatoid factor is reported.

ELISA tests

EDI (Epitope Diagnostics, San Diego, CA) COVID-19 IgG ELISA kit utilizes the microplate-based enzyme immunoassay technique. Microplate was coated with COVID-19 recombinant full-length nucleocapsid protein. Cross-reactivity is denied for principal infectious agents such as influenza A and B virus, adenovirus, respiratory syncytial virus, HCV and ANA presence. Declared sensitivity and specificity was 100% and 100%, respectively.

EDI (Epitope Diagnostics, San Diego, CA) COVID-19 IgM ELISA kit utilizes the "IgM capture method" on microplate-based enzyme immunoassay technique. A microplate was coated with an anti-human IgM specific antibody. A horseradish peroxidase (HRP) labelled recombinant COVID-19 antigen was added to each well. Cross-reactivity is denied for principal infectious agents such as influenza A and B virus, adenovirus, respiratory syncytial virus, HCV and ANA presence. Declared sensitivity and specificity was 45% and 100%, respectively. For both IgM and IgG, negative (NC) and positive (PC) controls were added. Positive cut-off was calculated on the basis of ROC curve.

Chemiluminescent method

SARS-CoV-2-IgG (Abbott, Ireland) is a chemiluminescent microparticle immune assay for qualitative assessment of IgG anti-nucleocapsid protein of SARS-CoV-2 in human serum on Architect analyser. Analyses were performed following the manufacture's instruction. Intensity of chemiluminescent reaction is measured as relative light units (RLU) that are directly correlated to the amount of SARS-CoV-2-IgG. The results are compared to RLU of the calibrator and transformed as a calculated Index (S/C): the cut-off is 1.4 Index (S/C).

Cross-reactivity for non-SARS-CoV-2 coronavirus strain was not evaluated, Cross-reactivity for principal infectious was excluded (see detailed datasheet from the manufacturer). The manufacturer declared that the positive percentage agreement was 100% following the analysis of sera after 14 days from the onset of symptoms. On the contrary, negative percentage agreement was 99.63% following the analysis of sera both from the pre-COVID19

era (before January 2019) and from subjects with other respiratory infections. Anti-human IgG do not recognize human IgM, IgA or ovine IgG. Interference of elevated title of rheumatoid factor is reported.

Statistical analysis

Sensitivity, specificity, accuracy, and ROC curve analysis were performed with Prism Graph Pad Software.

RESULTS

Rapid-cassette tests performance comparison

Seventy-four subjects (49 females and 25 males, mean age: 45.28 years) belonging to healthcare personnel of IRCCS Policlinico San Donato Hospital in Milan, Italy were screened. Both medical doctors, nurses and technical personnel were included. Firstly, the presence of simultaneous IgM or IgG responses were screened through rapid tests of two different companies, Cellex and Zhejinang Orient Gene.

Comparable results were obtained with both tests. In particular sensibility was 85.4% (95%CI 70.8-94.4), specificity was 90.91% (95%CI: 75.6-98.1) and accuracy was 87.8% for Cellex IgG, and sensitivity was 85.4% (95%CI: 70.8-94.43), specificity 87.88.6% (95%CI: 71.8-96.6) and accuracy 86.5%, respectively, for Cellex IgM. Sensitivity was 90.2% (95%CI: 76.9-97.3), specificity was 87.9% (95%CI: 71.8-96.6) and accuracy was 89.2% for Orient Gene IgG and 73.2% (95%CI: 57.1-85.8), 90.9% (95%CI: 75.7-98.1) and 81.2%, respectively, for Orient Gene IgM.

False positive subjects (3 on Cellex and 4 on Orient Gene) were observed according to IgM or IgG with both rapid tests. One hypothesis is a cross-reaction with other non-SARS-CoV-2 coronavirus strains such as HKU1, NL63, OC43 or 229E, or these subjects could be true positives turned negative to qRT-PCR, due to timing of analysis or due to low sensitivity of qRT-PCR. Deeper investigation revealed positivity to ANA and rheumatoid factor in one subject, a possible interferent.

Rapid-cassette tests showed positivity of both IgM and IgG in the majority of samples, however in some samples, IgM were undetectable while IgG were still present, possibly reflecting recovery. In fact, the time window of sampling covered 2-3 months post-infection.

Accordance between the two rapid tests was excellent (Accordance: 0.970, K Cohen: 0.936) on both IgM and IgG. All negative control samples collected before May 2018 resulted negative with both rapid tests.

Comparison of rapid-cassette tests with immune-enzymatic method

Screening was repeated on 33 of 74 samples through immune-enzymatic method. Results are shownas ROC curve in Fig. 1. According to the data,

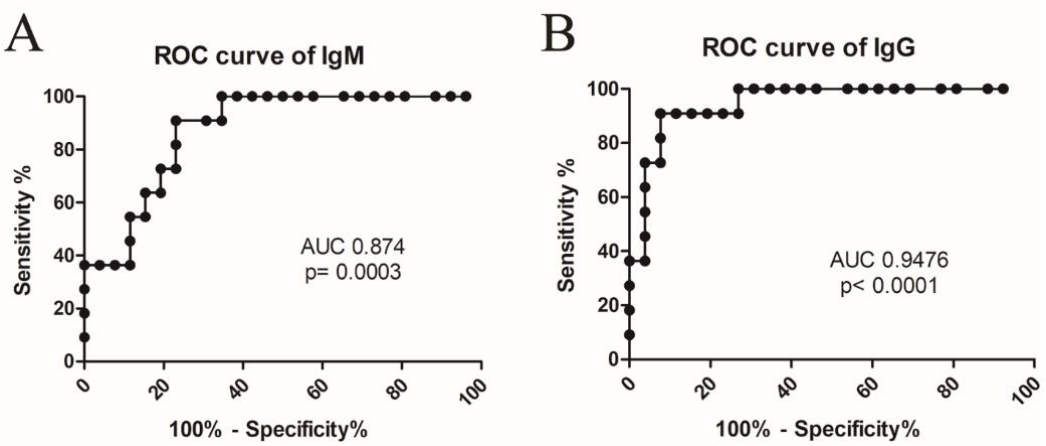


Fig. 1. *Graphs showing ROC curves of IgM (**A**) and IgG (**B**) of ELISA method.*

ROC curve of IgM showed a moderate performance (AUC=0.874, p=0.00038), optimal cut-off is 0.1870 Abs, estimated by Youden Index, it allowed a specificity of 76.92% and a sensitivity of 90.91% (Fig. 1A). IgG analysis showed a high performance according to AUC= 0.947 p=<0.0001, allowing a sensitivity of 90.91% and a specificity of 92.31% with a cut-off 0.1105 Abs (Fig. 1B).

Total agreement between ELISA and rapid test was excellent for IgG (Agreement: 0.970; k Cohen: 0.933) and, similarly to rapid-cassette tests; ELISA IgG did not avoid cross-reaction with other non-Sars-Cov-2 viruses. Total agreement between ELISA and rapid test was moderate for IgM (Agreement: 0.697; k Cohen: 0.289).

Comparison of rapid-cassette and ELISA with CLIA method

The results obtained were finally confirmed by using the CLIA method, designed to detect anti-nucleocapsid protein. Sensitivity was 85.37% (95% CI: 70.8-94.4) and specificity was 96.9% (95% CI:84.2-99.9), accuracy was 90.549%. Total agreement with ELISA was 97% (K Cohen: 0.93). Furthermore, CLIA confirmed positivity of one subject that was positive to both rapid-cassette and ELISA suggesting a false negative result of RT-PCR. Total agreement with rapid-cassette Cellex was excellent, 94.6% (K Cohen: 0.892). Total agreement with rapid-cassette Orient Gene was excellent 90.5% (K Cohen: 0.811). One negative control sample collected before May 2018 resulted positive with CLIA method.

DISCUSSION

The spreading of Covid-19 disease has represented a major challenge for healthcare systems worldwide. Furthermore, the degree of symptoms can vary, with a proportion of pauci/asymptomatic patients. In this sense, rapid recognition of new infections is of critical importance, and RT-PCR detects directly viral RNA in a brief time window, whilst serologic tests record both active and previous infections. Here, we showed that serological monitoring of antibody responses could be a reliable low-cost method to screen a large mass of individuals, such as workers in industries or travellers in airports. These methods are rapid (answer in 10 minutes), easy to perform, and do not require skilled personnel, thus allowing to screen a large number of samples (a limit of molecular analysis). The results demonstrate that the rapid tests analysed have good analytical performance, with the majority of subjects showing positive response within 3 weeks, accordingly to the literature (4). Rapid Zhejiang Orient Gene cassette has been independently evaluated by another group (5) and the results showed the same IgM sensitivity, probably due to timing of sampling, but higher sensitivity. ELISA analysis confirmed the results obtained by rapid-cassette in terms of sensitivity, but presented higher specificity. Finally, the CLIA method increased specificity up to 97%. However, a positive serological test always requires - independently from the method – to perform molecular analysis, so that specificity will be increased anyway. Conversely, to avoid false negative at first screening remains of critical importance. In synthesis, CLIA automatized methods are the best choice whenever it is possible (and easy) to collect venous blood samples and time-to-answer is not a limitation. On the other hand, rapid tests are better when non-skilled personnel have to test high numbers of people in a short time – for example to monitor passengers in airports, or workers in large industries.

ACKNOWLEDGEMENTS

The authors received specific funding for this work from the Italian Ministry of Health.

REFERENCES

1. Wang W, Xu Y, Gao R., et al. Detection of SARS-CoV-2 in different types of clinical specimens. Jama 2020; doi:10.1001/jama.2020.3786.
2. Zainol Rashid Z, Othman SN, Abdul Samat MN. Aòi UK, Wonk KK. Diagnostic performance of COVID-19 serology assays. Malays J Pathol 2020; 42(1):13-21.
3. Lee C.Y, Lin RTP, Renia L, Lis FPNg. Serological approaches for COVID-19: epidemiologic perspective on surveillance and control. Front immunol 2020; 11:879. doi:10.3389/fimmu.2020.00879.
4. Long QX, Liu BZ, Deng, HJ. et al. Antibody responses

to SARS-CoV-2 in patients with COVID-19. Nat Med 2020; 26:845-48, doi:10.1038/s41591-020-0897-1.

5. Hoffman T, Nissen K, Krambrich J, et al. Evaluation of a COVID-19 IgM and IgG rapid test; an efficient tool for assessment of past exposure to SARS-CoV-2. Infect Ecol Epidemiol 2020; doi:10.1080/20008686.2020.1754538.

LETTER TO THE EDITOR

Primary care experience on Rinfodim 3® in children with recurrent respiratory infections

E. Poggi[1], A. Giannattasio[1], M.E. Cartosio[1], R. Campus[1] and G. Ciprandi[2]

[1]Pediatric Primary Care, ASL 3 Genovese, Genoa, Italy; [2]Allergy Clinic, Villa Montallegro, Genoa, Italy

Received July 28, 2020 – Accepted November 9, 2020

To the Editor,

Respiratory infections (RI) are very common among children and contribute substantially to pediatric morbidity; antibiotic use/overuse for RI management is also very frequent in the clinical practice. Many factors may be involved in promoting and/or causing RRI, including age (for a relative immaturity of the immune system), early attending at day care centres and preschool, air and home pollution, passive tobacco smoking, low socioeconomic level, and atopy. Prevention of RRI is therefore an important public health challenge. RI treatment is generally based on symptomatic medications (e.g. acetaminophen), anti-inflammatory drugs (namely corticosteroids), and antibiotics, even though frequently prescribed empirically. However, the better way to manage RRI could be their prevention; in this regard, many attempts have been tried using natural compounds, including probiotics, micronutrients, vitamins, and oligo-elements (1).

The FAO/WHO Expert Committee has defined probiotic strains as "live microorganisms which, when consumed in appropriate amounts in food, confer a health benefit on the host". Probiotics are widely used in daily practice and may be associated with other compounds exerting additional immune-modulatory activity. In this regard, Rinfodim 3® is a multicomponent dietary supplement containing: *Lactobacillus rhamnosus* GG ATCC 53103, docosahexaenoic acid (DHA), and vitamin D3. These components exert relevant activities in the immunomodulation and resolution of inflammation. There is robust evidence concerning these effects (2-4).

Based on this background, we tested the hypothesis that Rinfodim 3® could prevent RI acting on different steps of the immune response. Therefore, the current real-world study aimed to evaluate the prevention activity of Rinfodim 3® in children prone to RRI and managed in a primary care setting.

MATERIALS AND METHODS

One hundred eighty-six children with RRI were enrolled in the current study. All patients were evaluated by a primary care paediatrician. The inclusion criteria were: i) age between 2 and 6 years, ii) both sexes, and iii) history of RRI in the past year. The exclusion criteria were: i) congenital or acquired immunodeficiency, ii) craniofacial abnormalities, iii) sleep apnoea syndrome, iv) Down syndrome, v) chronic disease (including metabolic disorders, cystic fibrosis, cancer, etc.), vi) clinically relevant passive smoking; and vii) previous (last 3 months) or current administration of drugs able to interfere with the study (e.g. immunomodulators, homoeopathic therapy, or systemic corticosteroids for at least 2 consecutive weeks). The study was conducted according to the Declaration of Helsinki, and the parents or legal tutors, after receiving complete information on the study, gave their written informed consent to participate.

All children were treated with standard treatment

Key words: recurrent respiratory infection; immune system; Lactobacillus rhamnosus GG ATCC 53103; docosahexaenoic acid; vitamin D3; children; real-world; primary care

Corresponding Author:
Giorgio Ciprandi, MD
Via P. Boselli 5,
16146 Genoa, Italy
Tel.: + 39 10 35338120
e-mail: gio.cip@libero.it

0393-974X (2020)
Copyright © by BIOLIFE, s.a.s.
This publication and/or article is for individual use only and may not be further reproduced without written permission from the copyright holder.
Unauthorized reproduction may result in financial and other penalties
DISCLOSURE: ALL AUTHORS REPORT NO CONFLICTS OF INTEREST RELEVANT TO THIS ARTICLE.

for any infection that occurred during the observation period. The children were randomly and consecutively subdivided into two groups at baseline. The first group (93 children) was supplemented with Rinfodim 3® 1 mL/day up to 2 years of age or 2 mL/day after 2 years of age for 3 consecutive months and considered as Active arm. The second group (93 children) was treated as needed with the standard therapy alone and considered as Control arm. Rinfodim 3® is a multicomponent dietary supplement, available as an oral solution, containing *Lactobacillus rhamnosus* GG ATCC 53103 $1x10^9$ CFU/mL, docosahexaenoic acid of microalgal origin 100 mg/mL, and vitamin D3 400 IU/mL.

The primary outcome was the change in the number of RI between the previous year and the current study period. RI was diagnosed based on the symptoms reported by the parents, as previously defined in detail (5). Briefly, the RI diagnosis was made when at least 2 symptoms or fever (axillary temperature ≥38°C), in addition to one other symptom (see below), were present for at least 48 hours. The considered symptoms were: mucopurulent rhinorrhoea, stuffy or dripping nose or both, sore-throat, cough (dry or productive), otalgia (earache), fever, dyspnoea, and mucopurulent secretion. RI was classified as upper respiratory infection (URI), including the common cold, rhinosinusitis, pharyngitis, otitis, and laryngitis, or lower respiratory infection (LRI), including tracheitis, bronchitis, and pneumonia.

Secondary outcomes were: i) the change in the number of URI and LRI during the study period; ii) the use of antibiotics (number of cycles), inhaled corticosteroids (ICS) evaluated as number of cycles, and oral corticosteroids (OCS) evaluated as treatment days; iii) the severity of respiratory symptoms assessed by a conventional score (0=absent; 1=mild; 2=moderate; 3=severe; 4=very severe), concerning 5 symptoms, including nasal itching, sneezing, rhinorrhoea, nasal congestion, and restless sleep, evaluated as a sum of each score and named T5SS (total of five symptom scores), and sleep disorder (i.e. snoring); iv) the parents' perception of respiratory symptoms severity, treatment effectiveness, and sleep quality, measured by the visual analogue scale (VAS) according to the methods described in a previous study (6); and v) the number of days lost of school attendance or working days of the parents.

All children were visited at baseline, after the 3-month treatment period (D 90), and after a 3-month follow-up (D 180). The study was conducted between October 2018 and June 2019. Demographic and clinical characteristics were described using means with SDs for continuous data (i.e. age) or as absolute frequency and percentages for categorical data (i.e. frequency of children with allergic sensitization). Any statistically significant difference in the mean values of each continuous variable was evaluated with the Wilcoxon signed-rank test (comparison between pre and post) or with Mann U Whitney test (comparison between Control arm *vs* Active arm), respectively. Kruskal-Wallis test was used to compare data for >2 groups followed by Dunn's correction for multiple comparisons. *Chi*-squared test or the Fisher's Exact test in case of expected frequencies less than 5 was used to compare categorical data. Statistical analyses were performed using GraphPad Prism software, GraphPad Software Inc, CA, USA.

RESULTS

Table I reports the demographic and clinical data and the outcomes in the two groups of children with RRI at baseline. The groups were not homogeneous only for two parameters concerning the previous year: upper respiratory infections were significantly ($p<0.0001$) more frequent in Active arm than in Control arm, whereas inhaled corticosteroid cycles were significantly ($p=0.003$) higher in Control arm.

Concerning the primary outcome, Active arm had a significantly ($p<0.0001$) greater change in the number of URI than Control arm, namely children of Active arm had a mean reduction of 4 URI whereas children in Control arm had a reduction of 2 URI during the study period (Fig. 1). This was true also considering LRI ($p=0.012$), namely, children in Active arm had a mean reduction of 0.36 LRI, but children in Control arm had only 0.04 (Fig. 1). Consistently, the intragroup analysis showed that children in Active arm had a significant reduction of both URI and LRI ($p<0.0001$ and 0.0002 respectively), whereas children in Control arm had a significant reduction only for URI ($p<0.0001$) as shown in Table II.

Control arm had a significantly greater change in antibiotic use than Active arm ($p=0.002$) as shown in

Fig. 2A. There was no significant difference between the active and control arm in the change in oral corticosteroid use, even though a better trend was reported in Active arm (p=0.66, Fig. 2B); differently, the active arm had a significantly greater change in inhaled corticosteroid use as compared to control arm (p = 0.0006) as reported in Fig. 2C. The intragroup analysis showed that children in Active arm had a significant reduction of the number of antibiotic and ICS cycles as well as OCS treatment days (p<0.0001, 0.03, and <0.0001 respectively); children in Control arm had a significant reduction of only antibiotic cycles (p<0.0001) as reported in Table II.

Children in Active arm had a significant reduction of symptom severity, scored by T5SS, during the follow-up period (p<0.0001), whereas children in Control arm had a significant worsening of symptoms severity (p<0.0001); the intergroup comparison showed a significant difference at both D90 and D180 (p<0.05 and <0.0001 respectively), as reported in Fig. 3A and Table III. Moreover, Active arm had a decreasing change whereas Control arm had an increasing change, with a significant difference between groups (p<0.0001) as reported in Fig. 3B.

The parents of children in Active arm perceived less severe respiratory symptoms, assessed by VAS, than the parents in Control arm both after the 3-month treatment period and at the follow-up visit (p<0.0001 for both) as reported in Fig. 3C. However, even though the change in VAS for respiratory symptom severity was higher in Active arm than in Control arm, this difference did not reach the statistical significance (Fig. 3D). The intragroup analysis showed that there was a significant reduction of VAS

Table I. *Demographic and clinical data in the Control arm and Active arm, at baseline.*

	Control arm	Active arm	P value
Age (years), [mean (SD)]	3.94 (1.08)	4.10 (1.45)	0.59
Gender (m, f)	49 m, 44 f	45 m, 48 f	0.74
Feeding (Yes), [No. (%)]			
Breastfeeding	76 (81.72%)	80 (86.02%)	0.40
Mixed	9 (9.68%)	4 (4.3%)	
Formula	8 (8.6%)	9 (9.68%)	
Familiar atopy (Yes), [No. (%)]	15 (16.13%)	21 (22.58%)	0.35
Allergen sensitization (Yes), [No. (%)]	13 (13.98%)	11 (11.83%)	0.66
School attendance (Yes), [No. (%)]	86 (92.47%)	85 (91.4%)	0.79
Concomitant symptomatic drugs (Yes), [No. (%)]	35 (37.63%)	31 (33.33%	0.54
Respiratory infections and treatments in the previous year			
Upper respiratory infection (No.), [mean (SD)]	6.39 (1.53)	8.45 (1.98)	**< 0.0001**
Lower respiratory infection (No.), [mean (SD)]	0.45 (0.70)	0.58 (0.94)	0.63
Antibiotic cycles (No.), [mean (SD)]	2.39 (1.28)	2.25 (1.44)	0.31
Inhaled corticosteroid cycles (No.), [mean (SD)]	3.57 (1.70)	3.14 (2.94)	**0.003**
Oral corticosteroid treatment (days), [mean (SD)]	0.51 (0.75)	0.99 (2.30)	0.07

Table II. *Intragroup comparison between data at baseline (i.e. in the previous year) and at day 180 (i.e. at the end of the follow-up period) in Control arm and in Active arm.*

	Control arm			Active arm		
	Baseline	Day 180	P value*	Baseline	Day 180	P value*
Upper respiratory infection (No.)	6.39 (1.53)	4.52 (1.65)	<0.0001	8.45 (1.98)	4.00 (2.06)	<0.0001
Lower respiratory infection (No.)	0.45 (0.70)	0.41 (0.53)	0.57	0.58 (0.94)	0.22 (0.49)	0.0002
Antibiotic cycles (No.)	2.39 (1.28)	1.07 (1.15)	<0.0001	2.25 (1.44)	1.48 (1.21)	<0.0001
Oral corticosteroid treatment (days)	0.51 (0.75)	0.49 (0.75)	0.71	0.99 (2.30)	0.50 (3.00)	0.031
Inhaled corticosteroid cycles (No.)	3.57 (1.70)	3.59 (1.86)	0.71	3.14 (2.94)	1.88 (1.57)	<0.0001

*All data are reported as mean (SD); *Wilcoxon signed rank test*

Table III. *Intragroup comparison between data at day 90 (after 90-day treatment) and at day 180 in Control arm and in Active arm.*

	Control arm			Active arm		
	After 90 day-treatment period	At the end of the 90 day-follow-up period	P value*	After 90 day-treatment period	At the end of the 90 day-follow-up period	P value*
T5SS (score)	12.15 (3.16)	16.63 (4.03)	<0.0001	10.55 (1.95)	5.80 (2.62)	<0.0001
VAS of respiratory symptoms (score)	5.77 (1.24)	5.48 (1.32)	0.045	3.80 (2.03)	2.77 (2.70)	0.0048
Sleep disorder (score)	2.98 (0.81)	2.53 (1.02)	0.0003	2.15 (0.74)	1.10 (0.80)	<0.0001
VAS of sleep quality (score)	4.62 (1.20)	4.22 (1.14)	0.0020	6.36 (1.43)	6.81 (1.53)	0.003
VAS of disease improvement (score)	3.63 (1.05)	4.12 (1.60)	0.030	4.99 (2.75)	6.57 (1.84)	<0.0001
School absence (no.)	3.26 (4.62)	2.00 (3.25)	0.008	4.48 (3.52)	1.38 (1.88)	<0.0001
Working days loss (no.)	2.11 (2.71)	1.42 (2.29)	0.023	2.28 (2.14)	1.07 (1.70)	<0.0001

*All data are reported as mean (SD); *Wilcoxon signed rank test*

in both groups (p=0.045 and 0.0048, respectively), as shown in Table III.

The severity of sleep disorder significantly diminished in both arms (p=0.0003 and p<0.0001, respectively) as shown in Table III. Children in Active arm had less severe sleep disorder than children in Control arm both after the 3-month treatment period and at the follow-up visit (p<0.001 for both), as reported in Fig. 4A. At the end of the follow-up period, sleep disorder was significantly lower in children in Active arm than in Control arm (p<0.001), and the reduction in sleep disorder severity was higher in children in Active arm than in Control arm, (p<0.0001), as shown in Fig. 4B.

The parents of children in Active arm perceived better sleep quality, assessed by VAS, than the parents in Control arm both after the 3 month-treatment period and at the follow-up visit (p<0.0001 for both) as reported in Fig. 4C. The change in VAS for sleep quality was positive in Active arm, but negative in the Control arm, with a significant difference (p<0.0001), as shown in Fig. 4D. The intragroup analysis showed that there was a significant increase of VAS in Active arm (p=0.003), but a significant decrease in Control

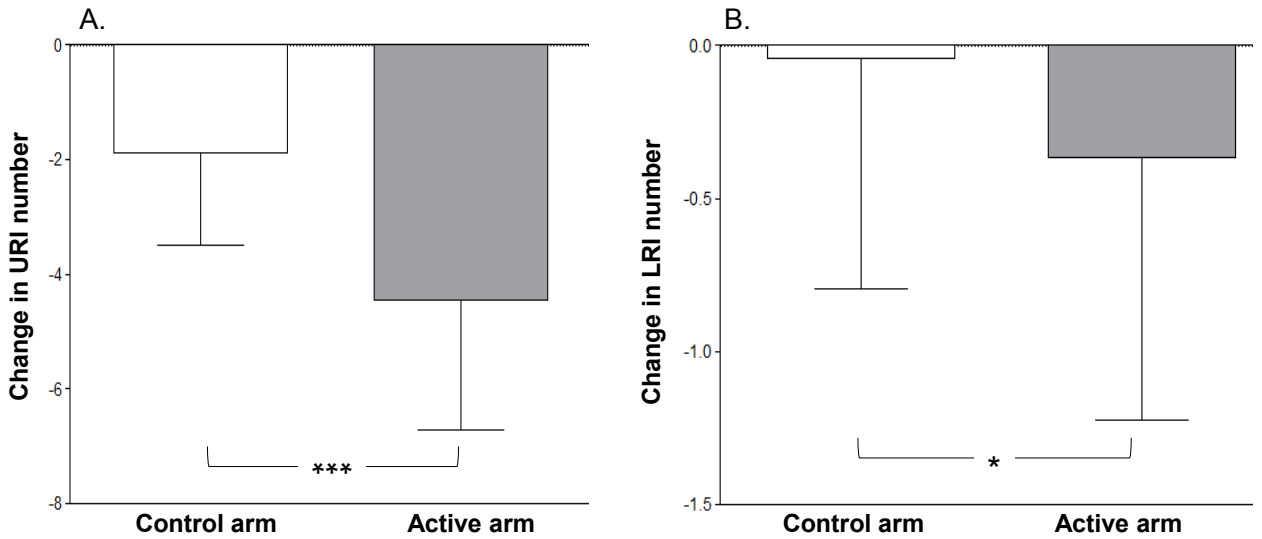


Fig. 1. *Changes in the upper respiratory infection (URI, **A**) and the lower respiratory infection (LRI, **B**) number in the Control Arm or the Active Arm. The change was calculated as the difference between the number of respiratory infections during the 180-day study period (i.e. the number of respiratory infections during the 90-day treatment period + the number of respiratory infections during the 90-day follow-up period) and the number of respiratory infections in the previous year. Data are reported as mean and vertical bars represent standard deviation. * = p<0.05; *** = p<0.001 (Mann Whitney test)*

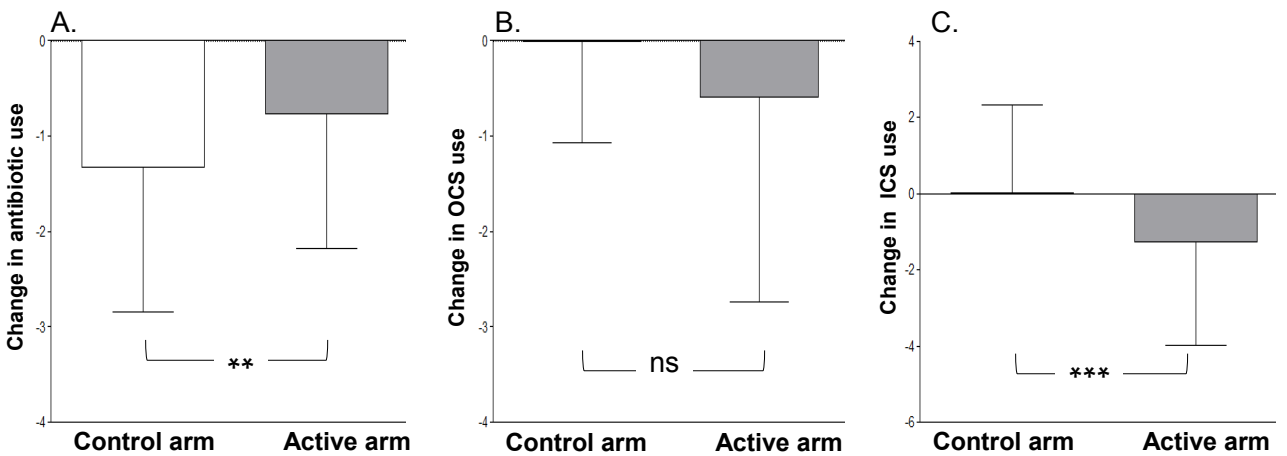


Fig. 2. *Changes in the use of antibiotics (**A**), oral corticosteroids (**B**) or inhaled corticosteroids (**C**) in the Control Arm or Active Arm. The change was calculated as the difference between the number of cycles/days of treatment during the 180-day study period (i.e. the number of cycles/days during the 90-day treatment period + the number of cycles/days during the 90-da -follow-up period) and the number of cycles/days of treatment in the previous year. Data are reported as mean and vertical bars represent standard deviation. * = p<0.05; ** = p<0.01; *** = p<0.001 (Mann Whitney test)*

arm (p=0.002), as shown in Table III.

The parental perception of disease improvement, assessed by VAS, was significantly better in Active arm than in Control arm both after the 3 month-treatment period and at the follow-up visit (p<0.0001 for both) and significantly improved between D 90 and D 180 in Active arm alone (p<0.0001), as shown in Fig. 5A. Consistently, the change in perception

of disease improvement was significantly greater in Active arm than in Control arm ($p<0.05$) as shown in Fig. 5B. The intragroup analysis showed that both Active arm and Control arm had a significant increase ($p<0.0001$ and 0.03, respectively) as reported in Table III.

The change in school absence was generally greater in Active arm, but without significant difference (Fig. 5C). The intragroup analysis showed that there was a significant reduction in both groups ($p<0.0001$ and 0.008, respectively) as reported in Table III. The change in working days loss was significantly greater in Active arm than in Control arm ($p<0.0001$), as shown in Fig. 5D. The intragroup analysis showed that there was a significant reduction in both groups ($p<0.0001$ and 0.023, respectively) as reported in Table III.

No clinically relevant adverse event was reported in children supplemented with Rinfodim 3®.

DISCUSSION

The current outcomes demonstrated that Rinfodim 3® supplementation was able to significantly reduce the number of RI episodes. In particular, the primary outcome of the study was achieved concerning both upper and lower RI: in fact, children supplemented with Rinfodim 3® had 4 fewer URI and 0.5 LRI than

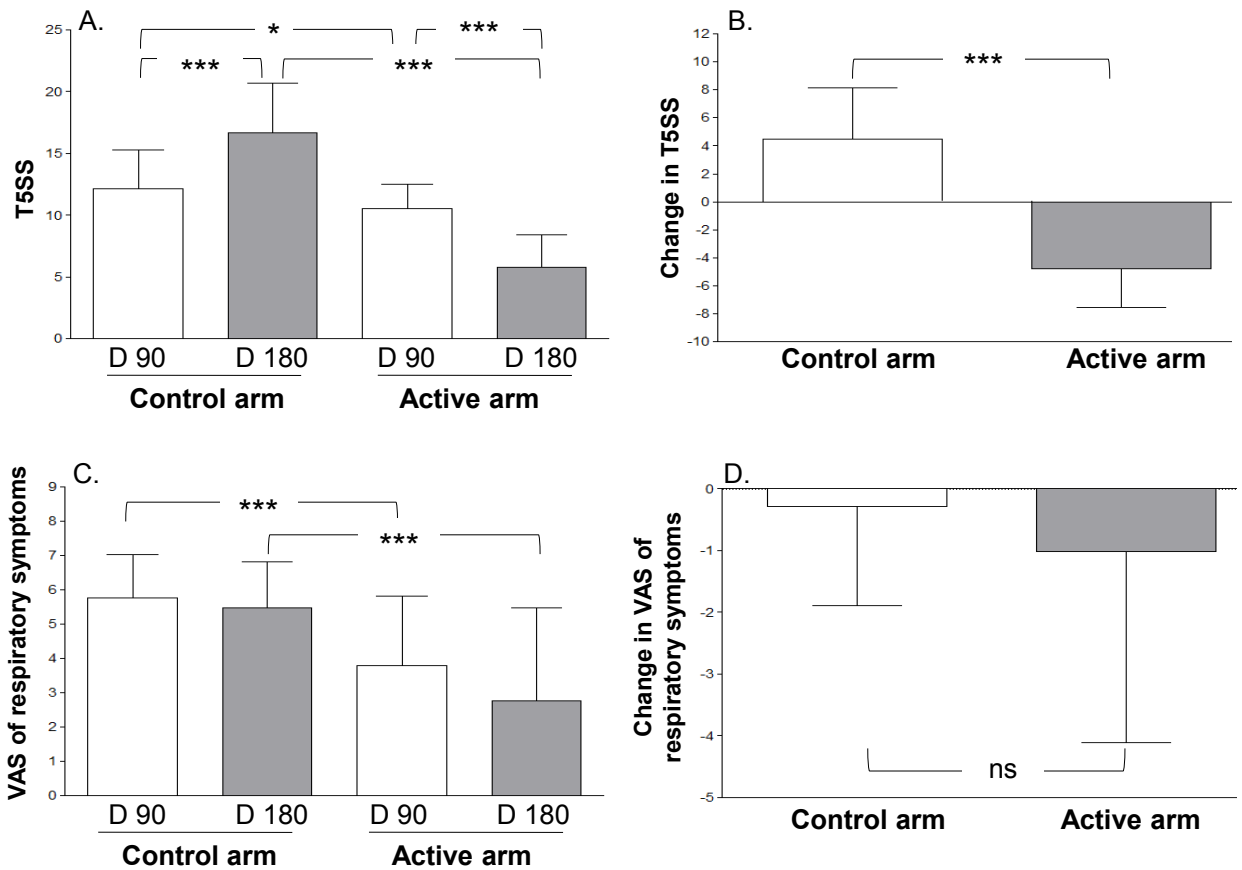


Fig. 3. *Panel **A** and panel **C** report T5SS and VAS of respiratory symptoms evaluated after 90-day treatment and at the end of the 90-day follow-up in Control Arm or Active Arm. Panel **B** and panel **D** show changes in T5SS and VAS in Control Arm or Active Arm. The change was calculated as the difference between score evaluated at the end of the follow-up period (day 180) and score evaluated at the end of the treatment period (day 90). Data are reported as mean and vertical bars represent standard deviation. * = $p<0.05$; *** = $p<0.001$ (Panels A and C: Kruskal-Wallis test followed by Dunn's Multiple Comparison Test; panel B and panel D: Mann Whitney test)*

the previous year. This finding represents a remarkable success as it has clinically relevant consequence regarding clinical, pharmacoeconomic, and social aspects. This result is further supported by the secondary outcomes obtained with the supplementation that are consistent with the primary outcome. In particular, Rinfodim 3® significantly reduced the use of inhaled corticosteroids but did not affect antibiotic use, probably because supplemented children had a more severe RI history. However, the supplementation of the multi-component compound significantly reduced the respiratory symptom severity just after the treatment period, such as during the first 90 days. Moreover, it has to be noted that at the end of the follow-up period, the children in Control arm significant worsened, whereas the children in Active arm progressively improved. This finding was consistent with the parental perception, measured by VAS, of respiratory symptoms. Remarkably, the parents' perception of treatment effectiveness, sleep problems, and sleep quality, was significantly favourable for the supplementation. Moreover, the use of the supplementation significantly reduced school absence and loss of working days. Finally, the multicomponent compound was well tolerated by all children.

These findings could be explained by the complex mechanism of action of Rinfodim 3®. The components exert several positive effects that

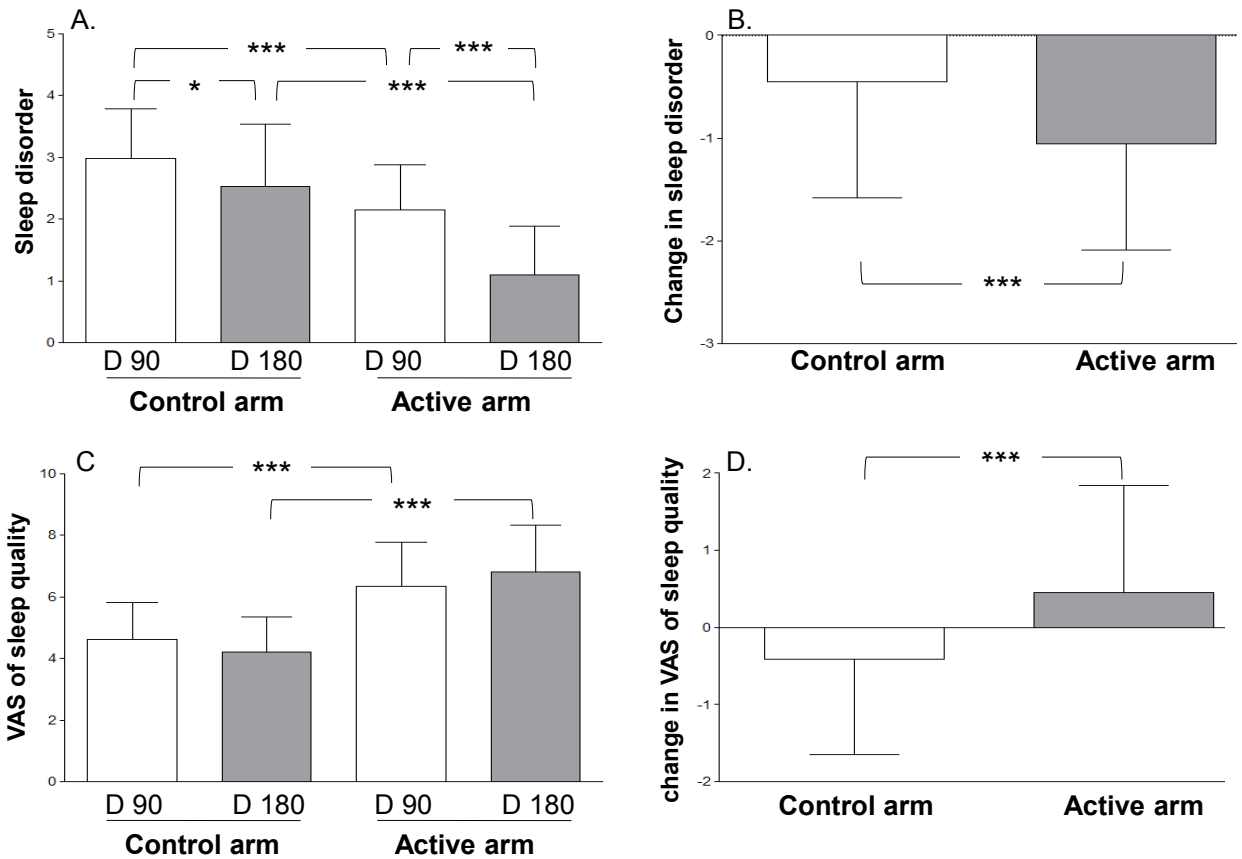


Fig. 4. *Panel **A** and panel **C** report severity of sleep disorder and VAS of sleep quality evaluated at the end of the 90-day treatment period and at the end of the 90-day follow-up period in Control Arm or Active Arm. Panel **B** and panel **D** show changes in sleep disorder severity and VAS of sleep quality in Control Arm or Active Arm. The change was calculated as the difference between score evaluated at the end of the follow-up period (day 180) and score evaluated at the end of the treatment period (day 90). Data are reported as mean and vertical bars represent standard deviation. * = p<0.05; *** = p<0.001 (Panels A and C: Kruskal-Wallis test followed by Dunn's Multiple Comparison Test; panel B and panel D: Mann Whitney test)*

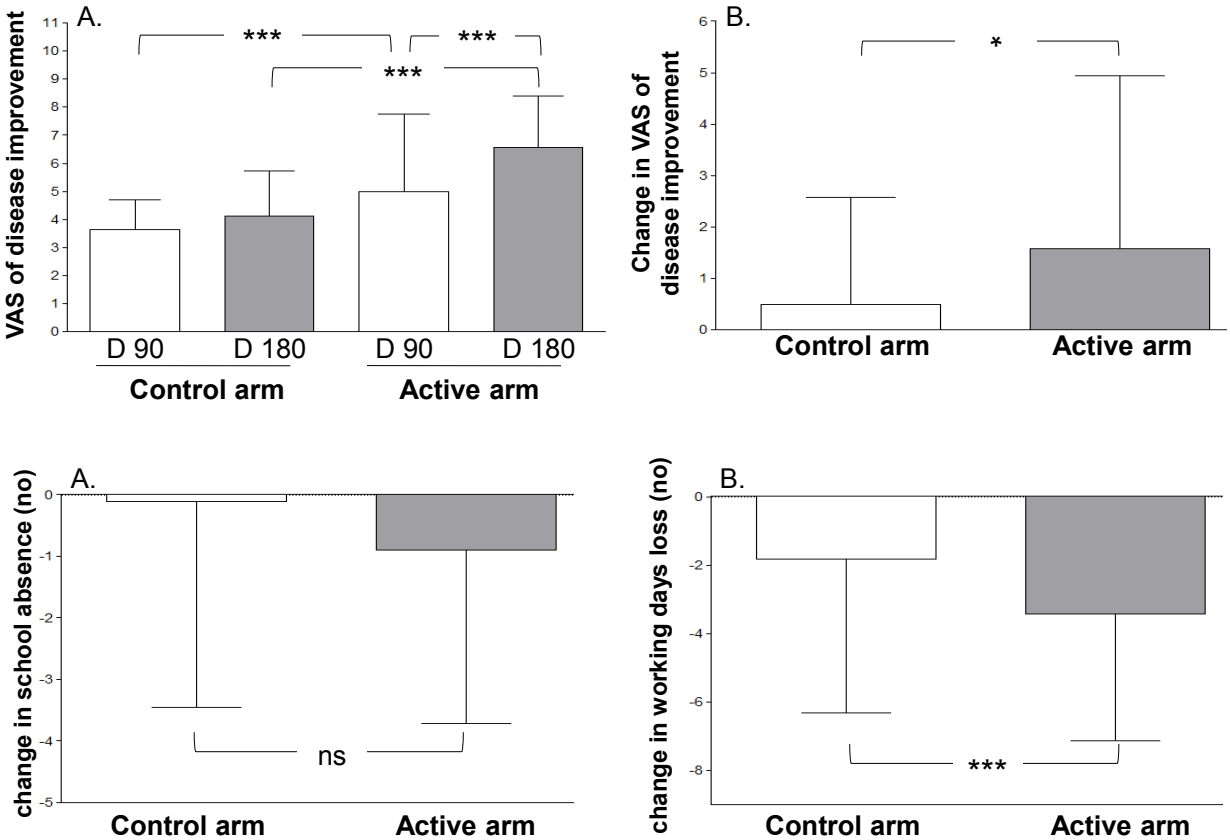


Fig. 5. *Panel **A** reports VAS of disease improvement evaluated after 90-day treatment period and at the end of the 90-day follow-up period in Control Arm or Active Arm. Panel **B** shows changes in VAS of disease improvement in Control Arm or Active Arm. Panel **C** and panel **D** show changes in school absence and working days lost in Control Arm or Active Arm. The change was calculated as the difference between score evaluated at the end of the follow-up period (day 180) and score evaluated at the end of the treatment period (day 90). Data are reported as mean and vertical bars represent standard deviation. * = $p<0.05$; *** = $p<0.001$ (Panels A: Kruskal-Wallis test followed by Dunn's Multiple Comparison Test; panel B, C, and D: Mann Whitney test).*

could be summarized in two principal mechanisms: modulation of the immune system (exerted mainly by *Lactobacillus rhamnosus* and Vitamin D) and anti-inflammatory activity (exerted mainly by DHA). Moreover, synergistic mechanisms have been described between probiotics and vitamin D, namely probiotics increase the expression of the VDR target genes, such as antimicrobial peptide cathelicidin, regulating and controlling immune-mediated inflammation (7). These documented mechanisms explain the complex activities played by the multicomponent supplementation and could be involved in the obtained findings.

However, the present study has some limitations, including the open design, the lack of documented infections diagnosis, and the absence of mediator measurement. Thus, further studies should be designed to answer these unmet needs. On the other hand, the current study was performed in a real-world setting, such as paediatric primary care. Increasing attention has been paid to real-world studies as they may provide information more adherent to the daily practice than randomized controlled trials that involve selected patient populations that rarely mirror the real situation (8).

In conclusion, the current real-world study demonstrated that Rinfodim 3® supplementation in children with RRI might safely prevent RI and reduce their impact on clinical, pharmacoeconomic, and social aspects.

REFERENCES

1. Lanzilli G, Falchetti R, Cottarelli A, Macchi A, Ungheri D, Fuggetta MP. In vivo effect of an immunostimulating bacterial lysate on human B lymphocytes. Int J Immunopathol Pharmacol 2006; 19:551-59.
2. Capurso L. Thirty years of Lactobacillus rhamnosus GG a Review. J Clin Gastroenterol 2019; 53 (Suppl. 1):S1-S41.
3. Richard C, Lewis ED, Field CJ. Evidence for the essentiality of arachidonic and docosahexaenoic acid in the postnatal maternal and infant diet for the development of the infant's immune system early in life. Appl Physiol Nutr Metab 2016; 41:461-75.
4. Saggese G. Vitamin D in pediatric age: consensus of the Italian Pediatric Society and the Italian Society of Preventive and Social Pediatrics, jointly with the Italian Federation of Pediatricians. Italian Journal of Pediatrics 2018; 44:51.
5. Ameli F, Ciprandi G. Sinerga may prevent recurrent respiratory infections in allergic children. J Biol Reg 2019; 33:601-7.
6. Barberi S, D'Auria E, Bernardo L, Pinto F, Pietra B, Ciprandi G. Hypertonic saline monotherapy in children with perennial allergic rhinitis: a pilot study. J Biol Res 2016; 30:271-75.
7. Choi KYG, Napper S, Mookherjee N. Human cathelicidin LL-37 and its derivative IL-19 regulate interleukin-32-induced inflammation. Immunology 2014; 142:68-80.
8. Sherman RE, Anderson SA, Dal Pan GJ, Gray GW, Gross T, Hunter NL, et al. Real-world evidence—what is it and what can it tell us? N Engl J Med 2016; 375:2293-97.

JOURNAL OF BIOLOGICAL REGULATORS & HOMEOSTATIC AGENTS Vol. 34, no. 6, 2375-2378 (2020)

LETTER TO THE EDITOR

Orthodontic appliances in patients allergic to nickel

D. Lucarelli[1,2], A. Stabilini[2], A. De Filippis[1,2], V. D'Avola[1,2], E. Mainardi[1,2] and L. Esposito[1]

[1]Department of Biomedical, Surgical and Dental Sciences, School of Dentistry, University of Milan, Milan, Italy; [2]Fondazione IRCCS Cà Granda, Ospedale Maggiore Policlinico, Milan, Italy

Received October 6, 2020 – Accepted November 16, 2020

To the Editor,

In recent years there has been an increase in the incidence of allergies, contact dermatitis and sensibilization to nickel and resin (PMMA) in patients wearing orthodontic appliances (1). The use of orthodontic resins and stainless steel devices requires a long permanence in the oral cavity, direct contact with tissues and therefore requires their proper adaptation to the biological environment (2-4). Nickel is a metal contained in stainless steel while resins are polymers obtained by the addition or condensation of substances ad high molecular weight; both are used for the realization of the most orthodontic appliances (3).

The biocompatibility of materials in orthodontics represents an emerging problem, especially for the spread in the population of fashion piercing that can cause an increase in sensitization to nickel. The most used metals for the production of orthodontic appliances are the 18/8 stainless steels, containing 18% of chromium and 8% of nickel, and the super-elastic alloy NiTi, containing 50% of nickel. Both nickel and chromium can cause hypersensitivity that usually occurs with widespread itching, eczema, vesicles, hives and flaking. In severe cases, respiratory symptoms may be detected, such as asthma and gastrointestinal disorders. Nickel is an ubiquitous substance that can be found in ornamental metal objects, especially in jewelry, kitchen utensils, cosmetic products, detergents, and hair dyes, as well as in numerous foods.

The incidence of allergies to metals is found in 1% of men and in 10% of women. Piercing, on the ears or on other areas of the body, is considered one of the major trigger factors of this sensitization. It has been shown that once hypersensitivity occurs, all surfaces of the oral mucosa may be involved. The diagnosis of allergy is made with a skin test (patch test) which consists of placing on the skin a patch containing calibrated slowly-released quantities of the material to be tested for sensitivity. The test is positive if, on the removal of the patch, there are red areas with itchy vesicles.

These issues have led to the search for alternative materials for the realization of orthodontic appliances. The purpose of this work is to show the use of titanium orthopedic devices in patients with allergy to resin and nickel. Furthermore, the aim is to underline the resolution of problems, such as stomatitis and perilabial dermatitis, that can occur with the use of traditional acrylic resin and steel tools.

MATERIALS AND METHODS

Sixty patients from the Department of Orthodontics of the IRCCS of Milan, who needed a first orthognatodontic

Key words: nickel allergy; titanium; orthodontic resins allergy

Corresponding Author:
Dr Andrea Stabilini,
Ospedale Maggiore Policlinico,
Via Francesco Sforza 35,
20122. Milano (Mi), Italy
Tel.: +39 0255032520 - Fax: +39 0255032520
e-mail: andrea.stabilini@gmail.com

0393-974X (2020)
Copyright © by BIOLIFE, s.a.s.
This publication and/or article is for individual use only and may not be further reproduced without written permission from the copyright holder.
Unauthorized reproduction may result in financial and other penalties
DISCLOSURE: ALL AUTHORS REPORT NO CONFLICTS OF INTEREST RELEVANT TO THIS ARTICLE.

visit and orthopedic therapy (such as rapid palatal expander and morfocorrector), were recruited. Informed consent was given by all patients or, if minors, by their parents or legal representatives, before being recruited in this work. Each patient had undergone a dental, dermatological anamnesis and a two patch test to check hypersensitivity to materials. The first test was performed before the treatment phase while the second one year later.

The first test carried out highlighted the nickel sensitivity in 8 patients, 2 males and 6 females, showing sexual dimorphism. The second patch test confirmed the results of the previous test, highlighting 37 positivity, again emphasizing the sexual dimorphism with a prevalence of nickel sensitization much higher in women (25) than in men. The familiarity of the patients who presented positivity at the first test was assessed: 7 out of 8 patients presented a familiar anamnesis positivity. Of the 37 patients who were positive at the second test, 34 presented positive familiarity. A significant correlation between familiarity atopy and nickel sensitization was therefore identified. In patients with this problem, two devices were tested: the morphocorrector and the rapid palate expander, both constructed entirely in titanium.

The construction phases of the device were:

• taking silicone impressions with double impression technique and model development;

• duplication of models in refractory for titanium;

• waxing for the carrying out of mergers;

• coating;

• construction of the merger;

• printing and polishing of the structure;

• laser welding, titanium mergering.

The master model, obtained from the development of impressions, was duplicated and poured using the specific Ultra type coating with "spiniello", that avoids the formation of Alfacase (impurities present in the fusions). The smelter with the Rematitan Dentaurum system was used to obtain mechanically valid structures with full biocompatibility features. On the model, an extention of 1 mm was constructed in the anterior and lateral vestibular fornix, depending on the prescription of the morphocorrector (I, II, III Class).

The models were mounted in an articulator with average values and we proceeded with the waxing phase on the vestibular fornix, which were made of titanium, similarly to the traditional processing for a resin and steel morphocorrector. The 1.5-mm thick preformed cylindrical wax was modeled for the construction of the palatal bar; 1.2mm-thick preformed wax was used for the the occlusal stops on the molars, for the upper vestibular arch and the activation loops in the canine area, for the inferior vestibular arch, for the connectors, for the activation loops between the lower anterior vestibular shields and the lateral vestibular shields. Finally, the anterior vestibular "pelotes" were modeled. Once the modeling process was completed, the wax structures were removed and with the preparation phase for the fusion was started.

The coating was carried out by applying a plastic support cone to the primary modeling. The casting cylinder was placed and fixed on the appropriate support where the coating mass was cast (Ultra type). After 2 hours from the setting and hardening, the cylinder was put in the preheating furnace.

The electronically programmed Rematitan smelter machine was used for titanium processing. The pure titanium ingot was put in a copper crucible. The oxygen was completely aspirated and replaced with type C Argon gas. The melting point of the titanium was reached through a voltaic arc at approximately 1700°C. The casting by pressure drop occurs in hundredths of a second with a remarkable temperature changing. A first radiographical check was made of the fused structure for any porosity that could weak the different parts, failing or fracturing during the orthodontic treatment. Subsequently, the printing, polishing, cleaning and finishing of titanium structures was initiated. A second radiographic control of the melted structure was then carried out.

The morphocorrector was used in patients with skeletal class II and III open bite disorder. Construction of the circuit breaker was made with a screw made entirely of titanium (Dentaurum), the Rematitan fusion system and the laser welding technology (Dentaurum Desktop) to match the screw in titanium with the titanium arms (5, 6). The use of laser welding is essential to obtain a monometallic structure that avoids electro-galvanic effects and gives adequate mechanical characteristics.

The critical area for unloading orthopedic forces, applied on the upper maxilla, is the joining area between the titanium arms and the titanium screw. Currently, titanium bands are not available on the market (5), and for this reason, crowns in melted titanium were used to anchor the expander to the dental elements. For the production

phases of rapid palatal expander, the model was obtained from the impression made of silicone materials. Then the model was duplicated and poured with the material used as a refractory for titanium castings. On this model a wax-up of all structures was made. After placing a spacer paint on the molars, we modeled on them the caps and, with the use of waxes for casting channels, we modeled the joint arms to the screw and the extension arms in the canine area. Finally we positioned the screw adapting waxes in the areas where subsequently we made the

At the end of this process, the preparation of the fusion was carried out, channeling all the waxes with the main casting channel. The model was inserted in refractory with all the waxes in the casting box. The dryer phase was made and, subsequently, the fusion. The structures obtained were roughed down. The surfaces were uniformed and satinized to complete the polishing of the structure. The arms and the screw of junction in titanium were welded onto the model obtained. The rapid palatal expander was cemented in the oral cavity using an orthodontic glass-ionomeric cement and the caps and the extension arms have been fixed with a light-curing composite. Activations were carried out two times a day for 2 weeks to obtain an orthopedic action on the maxilla with the restoration of the nasal respiratory function (6, 7). At the end of these 2 weeks, the central screw was locked with a titanium welding wire. The contention phase lasted for 6 months.

RESULTS

The structure of both the morphocorrector and the rapid palatal expander showed high resistance, in particular in moments of maximum mechanical stress, i.e., during the activations. No breakages or cracks occurred in the castings. There was no allergic reaction in the patients treated, confirming the hypoallergenic properties of titanium. In the sensitized patients there was the total regression of the symptomatology, and in subjects with a history of nickel allergy there was no allergic reaction.

DISCUSSION

It is already known that the phenomenon of corrosion inside the oral cavity is the basis of allergies. This event determines the release of ions which are the allergens that could activate the cell-mediated reaction mechanisms responsible for allergic manifestations. The biocompatibility of the materials is directly dependent on the corrosive phenomenon (2, 3). The opinion of the Authors is that if an alloy or a metal does not allow the release of ions, it will not have an action of damage or destruction on the cellular DNA. The oxidation state is very important for the reactivity of the ions, which can also confer a carcinogenic action. Nickel and PMMA are among the most common allergens in orthodontics, which are the main components of orthodontic appliances (8).

Titanium is a light noble metal with a low thermal conductivity. The stability of this metal to corrosion (biocompatibility) is linked to the ability to form oxides on its surface, reacting with oxygen. This process creates a film that gives chemical inertia to the material, self-limiting the oxidation process (passivation). Sensitization to nickel occurs in about 30% of the population. Often this phenomenon goes unnoticed because there is a certain tolerance threshold in a large number of patients, who often do not show any apparent symptoms. However, the inflammatory phenomena are actually due to cell-mediated reactions and therefore to phenomena of sensitization to nickel (9-12). This could be due to the fact that the amount of nickel needed to determine a hypersensitive reaction is different for each subject, furthermore, there can be a protective action by salivary secretions and crevicular fluids. Titanium allows to create appliances with good mechanical strength, light and totally hypoallergenic.

Resins are polymers obtained by addition or condensation of high molecular weight substances. Among the acrylic resins, the most used is methyl-methacrylate. Finished products rarely cause allergies that can arise through contact with not completely polymerized resins, which are able to release monomers derived from the incomplete processing of the product. The substance that could be responsible for the allergenic power seems to be the excess of methacrylate residual monomer that remains on the surface because of an incomplete polymerization of the autopolimerizing acrylic resins or because of incorrect procedures in thermopolymerizing resins.

In the present study, light-curing resins were used but, in sensitized subjects, there was no improvement or disappearance of allergic reactions. Allergic reactions appear 24-48 hours after the exposure to the allergen factor and they can be located in the contact areas (primary lesions) or extend into nearby areas or appear at long-distance (secondary lesions). The titanium devices used gave excellent results, thanks to their property of forming superficial oxides, blocking the oxidation phenomena and, therefore, the corrosion phenomena.

Today, the difficulties of processing titanium-cast structures have been solved by new laboratory techniques, such as the Rematitan Dentaurum system, that allows to obtain mechanically valid structures with biocompatibility characteristics. The results of this study allow us to confirm the anallergic property of titanium and propose it as an alternative material in subjects with a history of allergy to metals and resins.

REFERENCES

1. Abate A, Cavagnetto D, Fama A, Matarese M, Lucarelli D, Assandri F. Short term effects of rapid maxillary expansion on breathing function assessed with spirometry: a case-control study. Saudi Dental J 2020; doi.org/10.1016/j.sdentj.2020.09.001
2. Abate, A, Cavagnetto D, Fama, A, Matarese, M, Bellincioni F, Assandri F. Efficacy of operculectomy in the treatment of 145 cases with unerupted second molars: a retrospective case–control study. Dent J 2020; 8:65.
3. Maspero C, Fama, A, Cavagnetto D, Abate A, Farronato M. Treatment of dental dilacerations. J Biol Regul Homeost Agents 2019; 33.5:1623-28.
4. Farronato G, Giannini L, Galbiati G, Pisani L, Mortellaro C, Maspero C, Verification of the reliability of the three-dimensional virtual presurgical orthodontic diagnostic protocol. J Craniofac Surg 2014; 25:2013-16.
5. Farronato G, Giannini L, Galbiati G, Maspero C. Comparison of the dental and skeletal effects of two different rapid palatal expansion appliances for the correction of the maxillary asymmetric transverse discrepancies. Minerva Stomatol 2012; 61(3):45-55.
6. Maspero C, Abate A, Bellincioni F. et al. Comparison of a tridimensional cephalometric analysis performed on 3T-MRI compared with CBCT: a pilot study in adults. Prog Orthod 2019; 20.1: 40.
7. Maspero C, Farronato M, Bellincioni F, Annibale A, Machetti J, Abate A, Cavagnetto D. Three-Dimensional evaluation of maxillary sinus changes in growing subjects: a retrospective cross-sectional study. Materials 2020; 13:1007.
8. Maspero C, Cavagnetto D, Abate A, Cressoni P, Farronato M. Effects on the facial growth of rapid palatal expansion in growing patients affected by juvenile idiopathic arthritis with monolateral involvement of the temporomandibular joints: a case-control study on posteroanterior and lateral cephalograms. J Clin Med 2020; 9(4):1159.
9. Maspero C, Abate A, Cavagnetto D, El Morsi M, Fama A, Farronato M. Available technologies, applications and benefits of teleorthodontics. a literature review and possible applications during the COVID-19 pandemic. J Clin Med 2020; 9:1891.
10. Maspero C, Farronato M, Bellincioni F. et al. Assessing mandibular body changes in growing subjects a comparison of CBCT and reconstructed lateral cephalogram measurements. Sci Rep 2020; 10:11722.
11. Maspero C, Galbiati G, Perillo L, Favero L, Giannini, L. Orthopaedic treatment efficiency in skeletal Class III malocclusions in young patients: RME-face mask versus TSME. Eur J Paediatr Dent 2012; 13.3:225-30.
12. Maspero C, Abate A, Cavagnetto D, Fama A, Stabilini, A, Farronato G, Farronato M. Operculectomy and spontaneous eruption of impacted second molars: a retrospective study. J Biol Regul Homeost Agents 2019; 33(6):1909.

Extraction socket healing in leukemic patients: a preliminary radiographic evaluation

C. Bertoldi[1], L. Generali[1], A. Forabosco[1], D. Zaffe[2], M. Ferrari[3] and F. Narni[4]

[1]Department of Surgery, Medicine, Dentistry and Morphological Sciences with Transplant Surgery, Oncology and Regenerative Medicine Relevance, University of Modena and Reggio Emilia, Modena, Italy; [2]Department of Biomedical, Metabolic and Neural Sciences, University of Modena and Reggio Emilia, Modena, Italy; [3]Private Practice, Carpi MO, Italy; [4]Department of Medical and Surgical Sciences for Children and Adults, Division of Haematology and Hemopoietic Stem Cell Transplant Program, University Hospital of Modena, Italy

Received August 19, 2020 – Accepted November 16, 2020

To the Editor,

Hematopoietic stem cell transplantation (HSCT) is an essential treatment for patients with malignant hematological diseases such as acute and chronic leukemias (1-3). Three chemotherapy cycles are routinely used to prepare for the treatment. Autologous or allogeneic bone marrow transplantation is recommended to consolidate remission, and transplantation has to be performed within a few months (1). An infection during chemotherapy for hematologic malignancy can be life-threatening, therefore the elimination of odontogenic foci is recommended before initiation of chemotherapy (1), however complete elimination is sometimes impossible because of time limitations and a problematic lack of criteria for deciding appropriate dental management before myelosuppressive chemotherapy (2, 4).

Tooth extraction is recommended for severe dental diseases or when conservative treatments are not completely predictive. Such pre-HSCT dental treatments are anticipated to decrease the risk of local and systemic odontogenic infections during patient immunosuppression. Some studies have established dental intervention protocols and analyzed sequelae and complications for patients with hematologic malignancy, including indications and contraindications for dental extraction (1, 3, 5). No information, however, is currently available on the alveolar healing process after tooth extraction in acute myelogenous leukemia (AML)-patients. Only the healing of the surgical wound (socket healing, in this case) is a guarantee of avoiding side effects and complications.

The aim of this preliminary study is to evaluate, by means of subtractive radiology, the alveolar healing of extraction sockets in AML patients. The study is aimed to establish whether, in leukemic patients who are candidates to HSTC, bone tissue healing is compromised after tooth extraction in comparison with healthy individuals and to define the ideal timing of surgical intervention in relation to leukemic therapy.

MATERIALS AND METHODS

Screening

This study was performed at the Unit of Dentistry and Oral-Maxillofacial Surgery of Modena University Hospital from January 2006 to December 2008. All the

Key words: oral rehabilitation; bone regeneration; socket healing; subtractive radiology; leukemia; chemotherapy

Corresponding Author:
Prof. Carlo Bertoldi,
Dipartimento Chirurgico, Medico, Odontoiatrico e di Scienze Morfologiche con Interesse Trapiantologico, Oncologico e di Medicina Rigenerativa, Università di Modena e Reggio Emilia, Via del Pozzo 71, 41124, Modena, Italy
Tel.: +39 0594224101 - Fax: +39 0594224795
e-mail: carlo.bertoldi@unimore.it

0393-974X (2020)
Copyright © by BIOLIFE, s.a.s.
This publication and/or article is for individual use only and may not be further reproduced without written permission from the copyright holder.
Unauthorized reproduction may result in financial and other penalties
DISCLOSURE: ALL AUTHORS REPORT NO CONFLICTS OF INTEREST RELEVANT TO THIS ARTICLE.

selected patients signed the informed consent detailing all procedures of the treatment, as requested by Helsinki protocols.

The study was a two-branch design: the control cohort (CC) considered healthy patients, particularly ruling out bone disease (6, 7), whilst the test cohort (TC) considered ALM-affected patients. Moreover, they had to satisfy the following inclusion criteria: over 18 years of age, non-pregnant or lactating, non-smokers, not undergoing antibiotic or anti-inflammatory therapy and no recent suffering from relevant affective symptoms (e.g. anxiety, depression) or personality disorders in lifetime medical history (8). In particular, the study concerned only mandibular monoradicular teeth. Sites needing two or more adjacent extractions were excluded. The full-mouth plaque score (FMPS) and the full-mouth bleeding score (FMBS), had to be maintained ≤20% (measured at 4 aspects per tooth) in all the patients.

For the CC, healthy patients were chosen from a list of patients who underwent at least one tooth extraction that matched the criteria of selection. CC patients having at least one periodontal hopeless tooth were grouped as CC1, while patients needing at least one dental root extraction were grouped as CC2. The TC comprised patients suffering from AML diagnosed at the Division of Haematology and Hemopoietic Stem Cell Transplant Program and assigned to the Section of Dentistry and Maxillofacial Surgery, University of Modena and Reggio Emilia, for the evaluation of dental status of all patients. The screening consisted of clinical examination of the hard and soft oral tissues and radiographic survey, including periapical films for symptomatic teeth. The extraction of teeth that could represent a source of septic complication where any other less aggressive treatment would not be predictable, was performed (1, 3, 5).

Operative protocol

The same team carried out all clinical evaluations during the pre-surgical, surgical and post-surgical phases. Descriptive criteria were used to classify the initial appearance of tissue changes during the therapy and final healing results (9).

Haematologists generally referred TC patients to the dental and oral- maxillofacial unit for pre-therapeutic assessment of their dental condition and provided information about diagnosis, regimen and schedule of chemotherapy, myelosuppression grade of chemotherapy, and other details (1-3, 5). Alveolar sites were clinically and radiographically (orthopantomography and periapical radiographs) examined.

A complete radiographic study was performed before surgical interventions by the surgical protocol. In particular, periapical radiographs were taken with standardized projection geometry using a Rinn individual film holder by a single clinical examiner. An acrylic stent was prepared for each patient from chalk models and, after tooth extraction, in correspondence to the teeth that would be extracted a radiopaque rod of well-known length was inserted in the stent. The rod represented as a benchmark index to evaluate the baseline alveolar width and depth dimension and then regenerative activity. The film holder was particularized by an adaptation. The biteblock of the Rinn film holder was embedded in a double bite impression consisting of a silicon bite. This device always permitted to cog in the same manner the film holder, allowing reproducible, comparable and reliable evaluations of periapical radiographs. Immediately after the extraction, a baseline periapical radiograph was taken, scanned and digitalized using a Polaroid SprintScan 35-mm slide scanner connected to a PC. A line joining the highest bone crest, mesial and distal to the socket (taken from the sagittal projection of each periapical radiograph), was plotted for each periapical post-extractive radiograph after the digitalization. As a result, the plotted line had a particular length, slope and, primarily, a fixed spatial relation with the rod (and the stent) that permitted to replace it in exactly the same position in the following periapical radiographs. The measure between the more coronal radiolucent part of the socket and the plotted line following the axial plane of the socket (Fig, 1) was recorded on each post-surgical radiograph. The data were considered both numerically and as a percentage ratio of the alveolar whole depth and surface (100% immediately after surgery). In particular, percentage ratios were used to perform a comparison among the cohorts at following times from immediate post-surgical phase.

Immediately after tooth or residual root extraction (T0-baseline), 15 days after (T1), 30 days after (T2) and 45 days after (T3), a periapical radiograph was taken using the acrylic stent and film holder individually prepared for each patient. The results from periapical radiographs following the post-surgical phase were obtained in the same way as previously described. The landmark was

represented by the rod and, consequently, by the plotted line (the line joining the highest bone crest, mesial and distal to the socket) and the more coronal radiolucent part of the socket on the way to recovery, always following the socket axial plane.

Alignment of the post-surgical baseline (T0) and the following (T1, T2 and T3) images was made using the aforesaid references. Following selection of the socket area for all the patients in the 3 groups (CC1, CC2 and TC) on the images, the T1-image was subtracted from the corresponding T0 image, the T2 from T1 and T0, and the T3 image from T2, T1 and T0 using an image analysis software (ImageJ-NIH). Changes between images were depicted as a lightened area for an increase in alveolar bone mass. The resulting lightened areas were measured (using ImageJ) and reported as numerical data and calculated the percentage value with respect to that of the entire socket (at T0). Statistical comparisons were performed on linear and area recorded data.

In T0 images, the residual socket depth (RSD) and the residual socket area (RSA), measured between the plotted line and more coronal radiolucent part of the socket, but not as a percentage (it would have been 100% in all events) were considered. The regeneration percentage was considered at T1, T2 and T3 comparison analyses. If 100% is represented by the entire depth and area of the residual socket measured at T0, the depth regeneration percentage (DRP) is the decrease per cent of the residual socket depth. The area regeneration percentage (ARP) is the decrease per cent of the residual socket area measured at T1, T2 or T3 (Fig. 1). It represents the reciprocal of the direct measurements because it considers the regenerated part and not the share to be regenerated and standardizes the defects to 100% which are different from each other as absolute metrical value. The regeneration percentage was used for cross-comparisons between the 3 cohorts of patients, while, in the same cohort, only metric values were considered in the longitudinal comparisons between the different phases (T0-T1-T2-T3), to avoid 0% at T0.

Surgical procedure

The attending dental hygienist provided oral hygiene instruction to maintain a plaque index lower than 20%. According to the authors' established dental intervention protocol for patients, teeth with marginal periodontitis and probing depth greater than 8 mm, severe mobility or with dental caries involving the endodontic canal (hopeless teeth or roots) were removed. All dental extractions were performed under local anaesthesia with prophylactic antibiotic administration. The extractions were performed by flapless operation following the same alveolar bone conservative criteria scheduled in post-extractive implantology. In particular, any injury or removal of the healthy alveolar ridge was accurately avoided and supra-crestal soft tissue was preserved. Absorbable suture by means of a copolymer of lactic and glycolic acid (Vicryl® -Ethicon) was carried out to increase gingival stabilization and haemostasis.

Periapical radiographic projections (X-Safe 70, Castellini, Bologna, Italy) were taken immediately after surgery (T0 – baseline) and repeated after 15 (T1), 30 (T2) and 45 (T3) days. A 0.12% chlorexidine mouthwash, 10 ml 3 times per day was prescribed for 45 days post-surgery. Antibiotic therapy (Bassado® - doxycycline – 100 mg twice daily – Pharmacia Upjhon, Nerviano, Italy) for 4 consecutive days, starting from the day before the surgery was carried out.

Statistical analysis

Statistical analysis was performed using the non-parametric Kruskal–Wallis test for the comparison of the 3 cohorts of patients (CC1, CC2 and TC) at each phase (T0, T1, T2 and T3), and the Friedman test for repeated measures on the same cohort along the 4 phases. The χ^2 test (nominal data) was applied to compare the gender distribution between the three treated cohorts (10). Both the Kruskal–Wallis and Friedman test were followed by Student-Newman-Keuls multiple comparison test if the former tests resulted significant (10). For all measured variables, the null hypothesis (H_0) of no difference among groups was rejected for a critical significance level of $p < 0.05$.

RESULTS

Fifteen patients, (5 females and 10 males), ranging in age from 20 to 55 years (mean ± standard deviation: 35.8±10.11) were selected and completed the 45-day follow-up period. Ten healthy individuals formed the control cohort (CC), five of whom, aged between 32 and 50 years (39.4±3.311), requiring extractions of periodontally hopeless teeth, formed the CC1. The other 5 patients, aged between 29 and 55

years (43.6±10.43) needing residual root extractions, formed CC2. Both the control cohorts were formed by three males and two females, so the control cohort (CC) was formed by 6 males and 4 females). The test cohort (TC), contained three males and two females, aged 25–51 years (40.2±9.471. Five patients had acute myeloid leukaemia (AML, subtypes M2-M4).

A total of 15 sockets was considered for analyses. The patients considered showed a normal blood count. The surgical procedure was successful without serious complications in almost all patients. No infection, alveolitis, dehiscence or neurovascular injuries were observed. A satisfactory post-surgical course was achieved in all the patients. No statistically significant differences were found among groups for age (p=0.7) and gender (p=1).

At T0 (baseline) phase, the RSD and RSA were respectively 18.8±3.6 mm and 124.7±25.8 mm^2 in CC1, 21.4±2.4 mm and 140.3±15.5 mm^2 in CC2, and 18.8±5.1 mm and 123.7±23.5 mm^2 in TC. No statistically significant differences were found among groups for RSD (p=0.4) and RSA (p= 0.5).

At T1 phase, in CC1, RSD and RSA were respectively 17±3.8 mm and 115.2±27.3 mm^2, while DRP and ARP were respectively 10.1±3.9% and 8±3.1%. In CC2, RSD and RSA were respectively 17.8±1.9 mm and 121.5±12.7 mm^2, while DRP and ARP were 16.7±3% and 13.3±2.4%. In TC, RSD and RSA were respectively 16.8±4.4 mm and 112.8±29.7 mm^2, while DRP and ARP were respectively 10.2±7.5% and 8.5±5.3%. No statistically significant differences were found among groups for RSD (p=0.8), RSA (p= 0.7), DRP (p=0.09) and ARP (p=0.09).

At T2 phase, in CC1, RSD and RSA were respectively 11.8±2.6 mm and 88.7±20.8 mm^2, while DRP and ARP were 37±7.9% and 29.2±6.2%. In CC2, RSD and RSA were respectively 12.4±1.8 mm and 93.7±12.6 mm^2, while DRP and ARP were respectively 42.2±2.5% and 33.3±2.9%. In TC, RSD and RSA were respectively 15±4.2 mm and 102.9±27.9 mm^2, while DRP and ARP were 19.9±11.9% and 16.7±7.3%. No statistically significant differences were found among groups for RSD (p=0.4) and RSA (p= 0.6). DRP and ARP resulted significant at Kruskal-Wallis test (p=0.007)

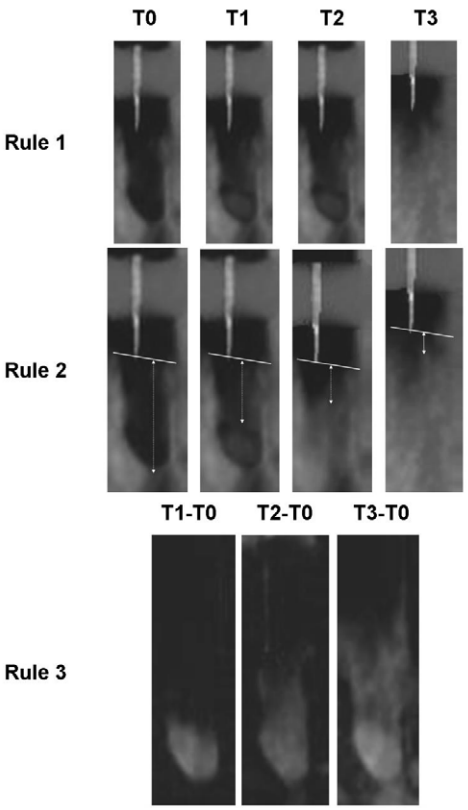


Fig. 1. *Periapical X-ray - Schematic figure showing the measurements performed by the radiopaque rod inserted in the acrylic stent (Rule 1 – raw periapical x-ray), the rod (of well-known length and embedded in an acrylic stent) was positioned in parallel with to the long axis of the tooth allowing reproducible, comparable and reliable radiologic periapical evaluations performed by a biteblock of Rinn film holder embedded in a silicon double bite (Rule 1). Immediately after the extraction at baseline (T0) and at each phase (T1, T2 & T3) periapical radiograph was taken, scanned and digitalized. A line joining the highest bone crest, mesial and distal to the socket (taken from the sagittal projection of each periapical radiograph), was plotted for each periapical post-extractive radiograph after the digitalization (white line - Rule 2 - Linear and Area measurement). The axial lineal measurement was taken from the more coronal radiopaque area of the residual socket to the plotted line on the axial plane (white double arrow). The area measurement regarded the socket area defined coronally by the white plotted line and then the area bordered the socket perimeter and deeply edged the newly formed bone (Rules 2 and 3). The reciprocal of direct linear and area measurements represented the regenerated part and gave its origin to the subtractive radiology (Rule 3). The regeneration percentage was used for cross-comparisons between the 3 patient cohorts while only metric values in the longitudinal comparisons between the different phases (T0-T1-T2-T3) within the same cohort were considered.*

so Student-Newman-Keuls multiple comparison test was performed showing a lower regeneration percentage in TC for both DRP and ARP.

At T3 phase, in CC1, RSD and RSA were respectively 9.6±11.5 mm and 66.7±14.3 mm^2, while DRP and ARP were respectively 48.3±6.5% and 46.6±6.3%. In CC2, RSD and RSA were respectively 10.2±11.6 mm and 69.4±11 mm^2, while DRP and ARP were respectively 52.6±2.7% and 50.8±2.6%. In TC, RSD and RSA were respectively 9.2±2.9 mm and 62.6±19.1 mm^2, while DRP and ARP were respectively 51.4±6.5% and 49.7±6.3%. No statistically significant differences were found among groups for RSD (p=0.8) and RSA (p= 0.9), DRP (p=0.5) and ARP (p=0.5).

The CC1 longitudinal analysis resulted significant both for RSD (p=0.002) and RSA (p=0.002) at Friedman test. An increasing regeneration share was observed step by step from T0 to T3. However, only comparing not subsequent phases (T0 *vs* T2, T1 *vs* T3, etc.) a statistically significant result (Student-Newman-Keuls multiple comparison) for both RSD and RSA was observed.

The CC2 longitudinal analysis resulted significant both for RSD (p=0.002) and RSA (p=0.002) at Friedman test. An increasing regeneration share was observed step by step from T0 to T3. As before, only comparing not subsequent phases (T0 *vs* T2, T1 *vs* T3, etc.) a statistically significant result (Student-Newman-Keuls multiple comparison) for both RSD and RSA was observed.

The TC longitudinal analysis resulted significant for both RSD (p=0.005) and RSA (p=0.002) at Friedman test. An increasing regeneration share was

Table I. *Raw data with mean and staandard deviation of the radiological measurements of the patients considered in the study.*

	T0			T1				T2				T3			
CC1	pt	RSD	RSA	RSD	RSA	DRP	ARP	RSD	RSA	DRP	ARP	RSD	RSA	DRP	ARP
	1	18	117.5	16	107.1	11.1	8.8	11	81.5	38.9	30.7	9	60.8	50	48.3
	2	13	84.8	11	74.4	15.4	12.2	9	64.2	30.8	24.3	8	53.3	38.5	37.1
	3	22	153.6	21	148.4	4.5	3.6	15	117.6	31.8	25.1	12	90.6	45.5	43.9
	4	21	137	19	126.6	9.5	7.6	14	101	33.3	26.3	10	67.7	52.4	50.6
	5	20	130.5	18	120.1	10	8	10	79	50	39.4	9	61.2	55	53.1
	M	**18.8**	**124.7**	**17.0**	**115.3**	**10.1**	**8.0**	**11.8**	**88.7**	**37.0**	**29.2**	**9.6**	**66.7**	**48.3**	**46.6**
	SD	**±3.6**	**±25.8**	**±3.8**	**±27.3**	**±3.9**	**±3.1**	**±2.6**	**±20.8**	**±7.9**	**±6.2**	**±1.5**	**±14.3**	**±6.5**	**±6.3**
CC2	pt	RSD	RSA	RSD	RSA	DRP	ARP	RSD	RSA	DRP	ARP	RSD	RSA	DRP	ARP
	1	18	120.3	15	104.4	16.7	13.3	10	78.1	44.4	35	8	55.8	55.6	53.7
	2	23	150.1	20	134.5	13	10.4	14	103.8	39.1	30.9	11	74.5	52.2	50.4
	3	20	127.6	17	112.4	15	11.9	11	82.3	45	35.5	9	59.8	55	53.1
	4	22	146.8	18	125.6	18.2	14.5	13	99.4	40.9	32.3	11	75.9	50	48.3
	5	24	156.6	19	130.7	20.8	16.6	14	105.1	41.7	32.9	12	81	50	48.3
	M	**21.4**	**140.3**	**17.8**	**121.5**	**16.7**	**13.3**	**12.4**	**93.7**	**42.2**	**33.3**	**10.2**	**69.4**	**52.6**	**50.8**
	SD	**±2.4**	**±15.5**	**±1.9**	**±12.7**	**±3.0**	**±2.4**	**±1.8**	**±12.6**	**±2.5**	**±1.9**	**±1.6**	**±11.0**	**±2.7**	**±2.6**
TC	pt	RSD	RSA	RSD	RSA	DRP	ARP	RSD	RSA	DRP	ARP	RSD	RSA	DRP	ARP
	1	20	135.5	18	18	10	8	16	114.1	20	15.8	9	63.5	55	53.1
	2	12	78.3	11	11	8.3	6.6	9	62.9	25	19.7	5	34.2	58.3	56.3
	3	17	110.9	17	17	0	2	17	105.4	0	5	10	66.8	41.2	39.8
	4	19	124	15	15	21	16.7	13	93.5	31.6	24.6	9	60.9	52.7	50.9
	5	26	169.7	23	23	11.5	9.2	20	138.8	23.1	18.2	13	87.8	50	48.3
	M	**18.8**	**123.7**	**16.8**	**16.8**	**10.2**	**8.5**	**15.0**	**102.9**	**19.9**	**16.7**	**9.2**	**62.6**	**51.4**	**49.7**
	SD	**±5.1**	**±33.5**	**±4.4**	**±4.4**	**±7.5**	**±5.3**	**±4.2**	**±27.9**	**±11.9**	**±7.3**	**±2.9**	**±19.1**	**±6.5**	**±6.3**

T0: Baseline; T1: 15-days after surgery; T2: 30-days after surgery; T3: 45-days after surgery; CC1: control cohort -1 patients; CC2: control cohort-2 patients; TC: test cohort patients; pt: series of patients for each cohort; RSD: residual socket depth; RSA: residual socket area; DRP: depth regeneration percentage; ARP: area regeneration percentage; M: mean; SD: standard deviation.

observed step by step from T0 to T3. However, only comparing not subsequent phases (T0 *vs* T2, T1 *vs* T3, etc.), with the exception of the RSD comparison of T0 *vs* T2, a statistically significant result (Student-Newman-Keuls multiple comparison) for both RSD and RSA was observed. The raw data with mean and standard deviation of the radiological records are reported in Table I.

DISCUSSION

In the present study, all the TC patients had already started chemotherapy and the median time from the last chemotherapy (consolidation phase) to the following conditioning phase (severe myelosuppression and persistent immunodeficiency - that constituted the third therapeutic phase) was two months. This was the entire period of time available for dental evaluation, treatment and alveolar recovery.

The RSD and RSA trend was similar for CC1 and TC without statistical significance among groups. However, CC1 is formed by periodontally diseased patients and periodontal disease produces the hindering of periodontal and bone regeneration (6). On the contrary, at T2 phase (30 days after surgery) both DRP and ARP resulted significantly lower in TC, showing a lower regeneration percentage in TC than in CC1 and CC2. Both the DRP and ARP showed a similar regeneration trend for CC1 and CC2 which is deeply different from TC in T2 phase.

The longitudinal analyses of RSD, RSA, DRP and ARP showed an increasing regeneration share, step by step, proceeding from T0 to T3. However, statistical significance was only observed in the comparisons of phases distant at least one phase between them and, in the TC case, with the exception of T2 with T0. At T3 phase, regeneration was alike among cohorts. Due to its high accuracy, it was decided to employ digital subtraction radiography to evaluate bone tissue changes in post-extraction sockets (11, 12). No previous studies exist regarding bone healing in extraction sockets in acute leukemic patients.

In conclusion, the healing process and the regenerative potential of post-extractive sockets seems to be affected by the leukemic condition during the 30 days after the extraction. Although a longer healing time seems to be necessary for the regenerative process to occur, the final result is identical to that observed in healthy patients 45 days after surgery. Because the scanty average lapse of time from consolidation phase and conditioning phase, it is momentous to make the best use of the available time to avoid devoting only 1 month for tooth extraction and healing.

REFERENCES

1. Akashi M, Kishimoto M, Kusumoto J, Yakushijin K, Matsuoka H, Komori T. Delayed socket healing after dental extraction in patients undergoing myelosuppressive chemotherapy for hematological malignancy: incidence and risk factors J Oral Maxillofac Surg 2018; 76:2057-65.
2. Elad S, Thierer T, Bitan M, Shapira MY, Meyerowitz C. A decision analysis: the dental management of patients prior to hematology cytotoxic therapy or hematopoietic stem cell transplantation. Oral Oncol 2008; 44:37-42.
3. Yamagata K, Onizawa K, Yanagawa T, et al: A prospective study to evaluate a new dental management protocol before hematopoietic stem cell transplantation. Bone Marrow Transpl 2006; 38:237-42.
4. Monari E, Cuoghi A, Bellei E, Bergamini S, Lucchi A, Tomasi A, Cortellini P, Zaffe D, Bertoldi C. Analysis of protein expression in periodontal pocket tissue: a preliminary study. Proteome Sci 2015; 13:33. doi: 10.1186/s12953-015-0089-y.
5. Tsuji K, Shibuya Y, Akashi M, et al. Prospective study of dental intervention for hematopoietic malignancy. J Dent Res 2015; 94:289-96;
6. Bertoldi C, Monari E, Cortellini P, Generali L, Lucchi A, Spinato S, Zaffe D. Clinical and histological reaction of periodontal tissues to subgingival resin composite restorations. Clin Oral Investig 2020; 24:1001-11.
7. Bertoldi C, Pradelli JM, Consolo U, Zaffe D Release of elements from retrieved maxillofacial plates and screws. J Mater Sci Mater Med 2005; 16:857-61
8. Bertoldi C, Venuta M, Guaraldi G et al. Are periodontal outcomes affected by personality

patterns? A 18-month follow-up study. Acta Odontol Scand 2018; 76:48-57

9. Bertoldi C, Bergamini S, Ferrari M et al. Comparative proteomic analysis between the gingival crevicular fluid and the corresponding periodontal pocket: a preliminary study. J Biol Regul Homeost Agents 2019; 33:9838-46.
10. Consolo U, Bertoldi C, Zaffe D. Intermittent loading improves results in mandibular alveolar distraction osteogenesis. Clin Oral Implants Res 2006; 17:179-87.
11. Bertoldi C, Zaffe D, Consolo U. Polylactide/ polyglycolide copolymer in bone defect healing in humans. Biomaterials 2008; 29:1817-23.
12. Ortman LF, Dunford R, McHenry K, Illausman E. Subtraction radiography and computer assisted densitometric analysis of standardized radiographs: a comparison study with 125-I absorptiometry. J Periodontal Res 1985; 20: 644-51.

LETTER TO THE EDITOR

Dystrophic rhinitis: etiopathogenetic mechanisms and therapeutic strategy for functional recovery

L. Maiolino[1], I. La Mantia[1], C. Grillo[1], Ct. Grillo[1] and G. Ciprandi[2]

[1]Clinica Otorinolaringoiatrica – Università degli Studi di Catania, Catania, Italy; [2]Allergy Clinic, Casa di Cura Villa Montallegro, Genoa, Italy

Received October 13, 2020 – Accepted November 23, 2020

To the Editor,

Dystrophic rhinitis is characterized by a progressive alteration of the mucosal trophism, associated with a reduction in the muciparous glands' functional activity and consequent reduction in mucus production (1). Dystrophic rhinitis symptoms include anosmia, epistaxis, sneezing, crusted intranasal formations, pharyngeal irritation, and breathing discomfort (2). Many treatments have been proposed to relieve local symptoms, among which, a new multi-component medical device seems to be promising, as it contains D-panthenol, hyaluronic acid (HA), vitamin E, vitamin A, and biotin.

D-panthenol is the alcohol analog of pantothenic acid (vitamin B_5) and is a provitamin of B_5; it improves hydration, reduces inflammation, and accelerates mucosal wound healing (3). D-panthenol readily penetrates the mucous membranes (including the intestinal mucosa), quickly oxidized to pantothenic acid. It is also used in the biosynthesis of coenzyme A, which controls a wide range of enzymatic reactions. HA is a fundamental component of the connective tissue, and can modulate the inflammatory response, cellular proliferation, and remodeling of the extracellular matrix (4). Moreover, HA has important lubricant and moisturizing properties.

Vitamin E, such as tocopherol, is a fat-soluble antioxidant that can protect the polyunsaturated fatty acids in the membrane from oxidation, regulate the production of reactive oxygen species, reactivate nitrogen species, and modulate signal transduction, as well as exerting eutrophic activity and immune stimulation (5). Vitamin A, a retinoid, is an essential micronutrient for the body and is associated with the proper functioning of the visual system, maintenance of epithelial integrity, red cell production, growth and development, and immune and reproductive functions (6). In particular, topical application stimulates epithelial growth, fibroblasts, granulation tissue, angiogenesis, collagen synthesis, epithelialization, and fibroplasia. These activities concur to repair the mucosal wound. Biotin, such as vitamin H, is a water-soluble B-complex vitamin and is well-known as a co-factor for five essential carboxylases; biotin exerts anti-inflammatory and immunomodulatory activities, relevant in repairing mechanisms of mucosal damage (7). Therefore, the current study investigated this multi-component medical device's role in relieving nasal discomfort in patients with dystrophic rhinitis.

MATERIALS AND METHODS

This study enrolled 40 patients of both sexes (19 males), aged between 18 and 75 years; all patients presented signs and

Key words: dystrophic rhinitis; treatment; D-panthenol; hyaluronic acid; vitamin A; vitamin E; biotin

Corresponding Author:
Prof. Giorgio Ciprandi,
Allergy Clinic,
Casa di Cura Villa Montallegro,
Genoa, Italy
e-mail: gio.cip@libero.it

0393-974X (2020)
Copyright © by BIOLIFE, s.a.s.
This publication and/or article is for individual use only and may not be further reproduced without written permission from the copyright holder.
Unauthorized reproduction may result in financial and other penalties
DISCLOSURE: ALL AUTHORS REPORT NO CONFLICTS OF INTEREST RELEVANT TO THIS ARTICLE.

symptoms typical of dystrophic rhinitis. Inclusion criteria were: i) adult age, ii) dystrophic rhinitis diagnosis, iii) wash-out of at least 15 days for any medications affecting nasal symptoms, such as antihistamines, systemic and/or topical corticosteroids, nasal decongestants, hyaluronic acid, NSAIDs, or other anti-inflammatory drugs; and iv) more than one month after surgery on the nasal area. Exclusion criteria included nasal anatomic defects, allergic rhinitis, immune and/or immunodeficiency diseases, congenital or acquired, acute febrile illness (> 38°C), clinical conditions that may interfere with the evaluation of the safety and efficacy of the product under investigation, such as nasal polyps, cystic fibrosis, kidney disease and/or dialysis, alcohol abuse or other drug addiction, psychological conditions incompatible with participation in the research, concomitant cancer, or treatment with immunosuppressive drugs.

The diagnosis of dystrophic rhinitis was performed according to validated criteria, such as a history of 2 or more clinical features for six months and more prolonged, including patient-reported recurrent epistaxis or episodic anosmia; or physician-documented nasal purulence, nasal crusting, chronic inflammatory disease of the upper airway, or two or more sinus surgeries (8). The study was performed according to the Helsinki Conference's ethical rules, and the internal review board approved the procedure. Each patient signed informed consent.

At baseline (T0), the investigators performed: anamnestic assessment, administering a specific questionnaire, with subjective evaluation scale by visual analogic scale (VAS) of nasal discomfort, nasal obstruction, nasal dryness, hyposmia/anosmia, and presence of nasal crusts, epistaxis, and pharyngitis. VAS measured the disease's impact on the quality of life, sleep quality, and daily habits. Investigators performed nasal endoscopy and anterior rhinomanometry. The score obtained by the VAS was categorized in 5 severity grades: 0= absent; 1-2= mild; 3-5= moderate; 6-8= severe; 9-10= very severe. All patients sprayed into the nose the multi-component medical device (Rinocross®; DMG Italia, Pomezia, Italy): two puffs per nostril twice a day for one month. At the end of the treatment (T1), investigators re-evaluated the patients performing the same procedures. The statistical analysis was performed using the *chi*-squared test. With a p-value less than 0.05, the differences were selected as significant, and Graphpad analyzed data.

RESULTS

Baseline data

At T0, 10 (25%) patients had mild nasal dystrophy, 13 (32.5%) moderate, 9 (22.5%) intense, and 8 (20%) severe nasal dystrophy. Eleven (27.5%) patients had mild reduction of nasal airflow (700-870 cm^3/sec), 17 (42.5%) had moderate (500-700 cm^3/sec), and 12 (30%) severe nasal obstruction (300-500 cm^3/sec). Nasal discomfort was considered mild by 7 (17.5%) patients, moderate by 19 (47.5%), intense by 8 (20%), and severe by 6 (15%) patients. Nasal obstruction was evaluated as mild by 9 (22.5%) patients, moderate by 15 (37.5%), intense by 9 (22.5%), and severe by 7 (17.5%) patients. Nasal dryness was considered mild by 7 (17.5%) patients, moderate by 19 (47.5%), intense by 10 (25%), and severe by 4 (10%) subjects. Olfaction impairment was evaluated mild by 11 (27.5%) patients, moderate by 17 (42.5%), intense by 8 (20%), and severe by 4 (10%) patients. Crusting was evaluated mild by 5 (12.5%) patients, moderate by 20 (50%), intense by 3 (7.5%), and severe by 12 (30%) patients. Sore throat was evaluated mild by 25 (62.5%) patients and moderate by 15 (37.5%) patients. Epistaxis was considered mild by 18 (45%) patients, moderate by 15 (37.5%), and intense by 7 (17.5%) patients. With regard to the quality of life (QoL), 12 (30%) patients reported a mild QoL impairment, 14 (35%) moderate, 6 (15%) intense, and 8 (20%) severe QoL impairment. Sleep quality was considered mildly compromised by 18 (45%) patients, moderately by 16 (40%), and intensely by 6 (15%) patients. The impact on life habit was considered mild by 28 (70%) patients, and moderate by 12 (30%) patients.

End of treatment data

The endoscopy showed 18 (45%) patients had no signs of nasal dystrophy, 15 (37.5%) mild dystrophy, and 7 (17.5%) moderate dystrophy. The anterior rhinomanometry showed that 18 (45%) patients had a mild reduction of nasal airflow, 12 (30%) moderate, and 10 (25%) intense reduction.

Fifteen (37.5%) patients reported no nasal discomfort, 16 (40%) moderate, 5 (12.5%) intense, and 4 (10%) severe nasal discomfort. Twenty-two

(55%) patients reported no nasal obstruction, 13 (32.5%) moderate, and 5 (12.5%) intense nasal obstruction. Regarding nasal dryness, 18 (45%) patients reported mild symptom, 11 (27.5%) moderate, 7 (17.5%) intense, and 4 (10%) severe nasal dryness.

Considering olfactory dysfunction, 19 (47.5%) patients had mild symptom, 12 (30%) moderate, 8 (20%) intense, and 1 (2.5%) anosmia. Twenty-three (57.5%) patients reported nasal crusting, 11 (27.5%) moderate, 3 (7.5%) intense, and 3 (7.5%) severe crusting. Concerning sore throat, 32 (80%) patients had a mild symptom, and 8 (20%) moderate pharyngeal complaints. Epistaxis was considered mild by 24 (60%) patients, and moderate by 16 (40%) patients. Quality of life was considered mildly impaired by 20 (50%) patients, moderately by 18 (45%), and intensely by 2 (5%) patients. Sleep was considered mildly disturbed by 22 (55%) patients, moderately by 16 (40%), and intensely by 2 (5%) patients. Life habit was impaired mildly in 33 (82.5%) patients, and moderately in 7 (17.5%) patients.

Between times comparison

Nasal endoscopy findings significantly improved ($p=0.008$), nasal airflow significantly increased ($p=0.007$), nasal discomfort significantly diminished ($p=0.009$), nasal obstruction significantly reduced ($p=0.01$), nasal dryness significantly improved ($p=0.008$), nasal crusting significantly diminished ($p<0.0001$), olfaction significantly improved ($p<0.0001$), sore throat significantly improved ($p=0.009$), and epistaxis significantly diminished ($p=0.008$). The treatment did not modify the quality of life, quality of sleep, and life habits.

DISCUSSION

Several endogenous and exogenous pathogenic mechanisms cause nasal mucosa dystrophy, which is associated with multiple functional alterations of the nose. Patients with nasal dystrophy present a series of signs and symptoms that can be particularly disturbing, so much as to alter the quality of life, sleep, and life habits. Consequently, the therapeutic strategy should be addressed to relieve symptoms and improve the patient's personal and social lifestyle (9). Moreover, the multifactorial etiology should be adequately investigated and consequently treated (10). Several compounds have been tested on patients with dystrophic rhinitis, but clear evidence of efficacy still lacks, as provided by a recent meta-analysis (11). Therefore, the current study was designed to investigate the efficacy and safety of a new multi-component medical device on a group of patients with dystrophic rhinitis. The rationale of its use is based on the documented activities exerted by the single components, including repairing, antioxidant, anti-inflammatory, moisturizing, and hydrating the damaged mucosa (12). Namely, these substances exert a synergistic effect on the restoration of a normal eutrophysm of the nasal mucosa, ensuring the supply of nutritional elements, stimulating the turnover, and epithelial regeneration. The overall analysis of the data obtained highlighted a progressive clinical improvement in most patients after the treatment. Notably, the symptom severity markedly diminished after only one month of topical application of the medical device. There was also a non-significant trend for personal and social aspects. Probably, a longer duration of treatment could obtain significant outcomes.

Furthermore, no side effects or adverse events were observed, which is an important point as it confirms the safety of the topical administration of the multi-component medical device. The present study has some limitations, including the open design, the lack of biomarker assessment, and the limited number of enrolled patients. Consequently, further studies should be addressed to unmet needs.

In conclusion, the current study provided preliminary findings that supported the efficacy and safety of a new multi-component medical device in treating patients with dystrophic rhinitis.

REFERENCES

1. Hildenbrand T, Weber RK, Brehmer D. Rhinitis sicca, dry nose and atrophic rhinitis: a review of the literature. Eur Arch Otorhinolaryngol 2011; 268(1):17-26.
2. Dutt SN, Kameswaran M. The etiology and

management of atrophic rhinitis. J Laryngol Otol 2005; 119(11):843-52.
3. Proksch E, de bony R, Trapp S, Boudon S. Topical use of dexpanthenol: a 70th-anniversary article. J Dermatol Treat 2017; 28:766-73.
4. Gelardi M, Taliente S, Fiorella ML, et al. Ancillary therapy of intranasal T-LysYal for patients with allergic, nonallergic, and mixed rhinitis. J Biol Reg Homeost Agents 2016; 30:99-106.
5. Khadangi F, Azzi A. Vitamin E - The Next 100 Years. IUBMB Life 2019;71(4):411-415
6. Polcz ME, Barbul A. The role of vitamin A in wound healing. Nutr Clin Pract 2019; 34(5):695-700.
7. Mock DM. Biotin: From nutrition to therapeutics. J Nutr 2017; 147(8):1487-92.
8. Banks TA, Gada SM. Atrophic rhinitis. Allergy Asthma Proc 2013; 34(2):185-87.
9. Lee JY, Byun JY. Primary atrophic rhinitis. Otolaryngol Head Neck Surg 2010; 143(4):601-2.
10. Hildenbrand T, Weber RK, Brehmer D. Rhinitis sicca, dry nose and atrophic rhinitis: a review of the literature. Eur Arch Otorhinolaryngol 2011; 268(1):17-26.
11. Mishra A, Kawatra R, Gola M. Interventions for atrophic rhinitis. Cochrane Database Syst Rev 2012; (2):CD008280.
12. Ciprandi G. Treatment of nonallergic perennial rhinitis. Allergy 2004; 56(S76):16-23.

LETTER TO THE EDITOR

Oral breathers and related malocclusion

G. Galbiati[1,2], A. De Filippis[1,2], V. D'Avola[1,2], E. Mainardi[1,2] and L. Esposito[1,2]

[1]Department of Biomedical, Surgical and Dental Sciences, School of Dentistry, University of Milan, Milan, Italy; [2]Fondazione IRCCS Cà Granda, Ospedale Maggiore Policlinico, Milan, Italy

Received September 11, 2020 – Accepted November 23, 2020

To the Editor,

The harmony between the various components of the stomatognathic system is strictly correlated with a correct growth and development (1). Respiratory function is particularly influenced by certain jaw skeletal conditions because of anatomical proximity and functional connections between the oral cavity and the upper aerodigestive tract (2). The resistance of nasal cavities is strictly related also to nasal cycle (1). Most Authors link respiratory function to facial growth pattern (3-6). The upper aerodigestive tract is of primary importance for breathing. During inspiration, the air flow is diverged in the nasal valve region, whose concave shape disperses the air over all the surface of the turbinates and the paranasal sinuses (4). As the air flow speed increases, because of irregularities on the nasal cavity surfaces, the flow becomes turbulent. These two steps are responsible for the three major changes to air quality: purification, humidification and heating.

Hypertrophy of the pharyngeal tonsil or its idiopathic growth make a physiological nasal respiration difficult or impossible (7). Nose breathing is linked to a physiological eugnathic growth, mouth breathing to malocclusion. Mouth breathing is a well-known bad oral habit. This mode of respiration is detrimental (8). The breathed air travels very quickly through the oral cavity, not making it possible for the changes that physiologically occur in the nasal and paranasal cavities such as heating and humidification (9,10).

The aim of this work is to analyze oral breathing, its clinical local and systemic effects and benefits of rapid palatal expansion (RPE) on respiratory function.

MATERIALS AND METHODS

Search strategy

The systematic review of the literature was conducted through the use of the Medline database (www.ncbi.nim.nih.gov/pubmed). The key words chosen were "oral habit, malocclusion". Regarding the articles found, only those included between 2005 and 2020 were selected. Using the limit options, only the articles referring to "Humans" were considered. Some articles were then added from non-indexed journals. A limitation of the review was that meta-analysis of data was not possible because of the heterogeneity of study designs and of technological tools assessed.

RESULTS

Local effects of mouth breathing

Mouth breather children very often present gingival inflammation, higher incidence of caries, and altered maxillofacial development (11, 12). The facial appearance of mouth breathing children is "*facies adenoidea*" (10). Common skeletal findings

Key words: oral breathers; stomatognathic system; malocclusion

Corresponding Author:
Dr. Guido Galbiati,
Ospedale Maggiore Policlinico,
Via Francesco Sforza 35,
20122 Milano (Mi), Italy
Tel.: +39 0255032520 - Fax: +39 0255032520
e-mail: guido.galbiati@unimi.it

0393-974X (2020)
Copyright © by BIOLIFE, s.a.s.
This publication and/or article is for individual use only and may not be further reproduced without written permission from the copyright holder.
Unauthorized reproduction may result in financial and other penalties
DISCLOSURE: ALL AUTHORS REPORT NO CONFLICTS OF INTEREST RELEVANT TO THIS ARTICLE.

include narrow elongated face, mandibular and maxillary retrognathism, hyperdivergence, decreased nasopharyngeal sagittal dimension and maxillary transverse hypoplasia (11). Mouth-breathing may cause excessive drying of teeth and gingiva and produce an imbalance of soft tissue forces. Dental findings include open bite, periodontal inflammation and increased development of caries. Eye bags, atypical deglutition and phonetic alterations are often present (12). Intense oral ventilation can cause mucosal dehydration and thermal changes (2). The xerostomic effect is usually limited to the anterior maxillary and mandibular areas. This dryness increases the susceptibility of the gingivae to chronic inflammation and the teeth to caries (6). Inhaled air, not moistened nor heated due to its rapid passage in the oral cavity, promotes the inflammation of Waldeyer ring and hypertrophy of the adenoids. Moreover, oral respiration may cause lung and bronchial infections (3, 12). Maxillo-facial altered growth makes the face appear longer and narrower, increases maxillo-mandibular divergence and causes mandibular and maxillary retrognathism, diminished sagittal nasopharyngeal dimension and transverse maxillary deficit (10).

These patients often present lip and chin strain, often associated with labial incompetence, which may favor the establishment of atypical swallowing. Asymmetrical muscular hypotonia, in particular of the buccinator and zygomatic muscle, can determine the so-called "facial flaccidity", which gives an aging look to a child's face (3, 8). Eye bags, asymmetrical eye position and dyslalias are often associated (5,11).

It is widely documented in literature that premature aging is more evident at the level of the face, as there are numerous muscles with delicate functions (6). The mandible keeps a low posture to maintain a half-open mouth that is needed to allow air flow. This posture promotes mandibular clockwise growth, that leads to skeletal open bite and posterior teeth hyper-eruption, anterior vertical face height keeps increasing, and posterior vertical face height appears reduced (4). As a consequence, facial muscles increase lateral pressure on the jaws, and this pressure is not counterbalanced by the tongue, that keeps a low postural position to allow air flow through the mouth (3).

Systemic effects of mouth breathing

Episodes of hypoxia and hypercapnia are common. In fact, these patients have reduced pulmonary volumes (about one-third reduction) compared to nasal breathers (3). A significant nasal obstruction, as in mouth breathing mode, results in an attempt to overcome this obstruction by increasing the inspiratory effort through the accessory muscles of inspiration. Difficulties with functional capacity and compromised respiratory system may damage lung ventilation with lower thoracic expansibility and, consequently, a weakness of the respiratory muscles may develop. Diaphragmatic excursion is limited, the chest is underdeveloped with a reduction of its circumference and with large intercostal spaces, falling shoulders associated with forward head posture and increased lumbar lordosis are connected to muscular hypotonia (9).

Chronic hypoxemia may manifest as a delay in growth, in neurological development and in motor development. Children may present cold and pale skin, asthenic appearance and, in severe cases, a pathological increase in eritropoietin that may favor thrombosis (11). Circulatory vasoconstriction of the variable degree of pulmonary circulation due to hypoxia and hypercapnia is frequent at the circulatory level which, in severe cases, may cause right heart failure, pulmonary edema and congestive decompensation (5). Long and troublesome digestive processes are frequent (4). Mouth breathers, in fact, do not perform an adequate chewing since the mouth must be emptied quickly to ensure air flow (9). Food is then swallowed while not adequately chewed nor adequately mixed with saliva resulting more difficult to digest (7).

Frequent episodes of cerebral vasodilatation due to hypercapnia, with a consequent increase in cerebral spinal fluid pressure, result in weakness, apathy, irritability and daytime drowsiness. These symptoms are due to reduced REM sleep phases present in mouth breathers' sleep, as documented by EEG studies (4-6). They are characterized by frequent psychological and cognitive alterations, poor concentration and easy tiring, that can jeopardize academic performance (3, 9). These factors, combined with an under-development of

the cranio-maxillofacial area, can cause a sense of insecurity in these children, giving them a feeling of inadequacy towards their peers (11).

Expansion of the palate and respiratory function

RPE has an orthopedic action, it corrects bone and dental defects, and it can also promote a physiological nasal breathing by decreasing nasal airway resistances. Respiratory resistances encountered while breathing through the nose are greater than when breathing through the mouth and RPE can help overcoming the first boundary on the instauration of a physiological nasal breathing (7). Various studies have investigated RPE and its effect on the upper aero-digestive and respiratory tract.

Also Surgically Assisted Rapid Palatal Expansion (SARPE) determines significant improvements (9). Furthermore, the passage to a nasal respiratory pattern induced by the RPE could favor a reduction of the aerobic and anaerobic pathogenic microorganisms in the oropharynx, reducing the risk of infections (4). The RPE may also prevent changes induced in the maxillo-facial area by changes in the respiratory pattern. The increase in airway size and the consequent decrease of the cranial-cervical angle may lead to an alteration of the cervical posture (12).

Optimization of respiratory function has a positive effect on craniofacial growth (10). After the establishment of a correct nasal respiration, the nasomaxillary complex undergoes an advancement and a clockwise rotation thus increasing posterior airway space diameter. According to Maspero et al. both nasopharynx and oropharynx increase their volume (9). Piriform opening increases by about 2 mm and the septum also increases its length. Furthermore, an enlargement of the medial meatus occurs due to an inclination of the lateral walls of the nasal cavities. The RPE is a simple and reliable method to correct transverse hypoplasia of the maxilla; moreover, it can facilitate the establishment of a correct nasal breathing (7). However, some authors point out that it is not always able to reduce nasal air resistance (8).

In conclusion, the sole purpose of improving respiration cannot be considered enough to perform a rapid maxillary expansion (5). It can also be combined with a myofunctional therapy to educate the neuromuscular system and transfer learned mechanisms to an unconscious level (12).

DISCUSSION

Mouth breathing has an etiopathogenetic role in the development of certain malocclusion (open bite, mandibular skeletal class II, etc.), but it also represents a secondary event of transversal deficiency of the upper jaw (1). An early diagnosis requires accurate medical history, specific instrumental and radiological investigations. Anamnesis evaluates the possible presence of bad habits (thumb sucking, atypical deglutition) and pathologies associated with oral respiration (asthma, allergy, etc) (9). Instrumental aids in diagnosis are represented by endoscopy, rhinoscopy, olfactometry and rhinomanometry, the latter being the most used nowadays (11). Most significant radiological exams are Cone-Beam Computed Tomography (CBCT) and Magnetic Resonance Imaging (MRI) scans, however, latero-lateral and posterior-anterior teleradiography of the skull already give preliminary information (6). Latero-lateral teleradiography gives information on degree of airway patency and on the possible presence of hypertrophy of adenoid or palatine tonsils (9). Posterior anterior teleradiography gives information on the patency of nasal and paranasal cavities, on the anatomy of the septum and of the upper jaw (10).

REFERENCES

1. Maspero C, Giannini L, Riva R, Tavecchia M.G, Farronato G. Nasal IC analysis. Mondo Ortodontico 2009; 34(5):263-68.
2. McNamara JA Jr, Lione R, Franchi L, Angelieri F, Cevidanes LH, Darendeliler MA, Cozza P. The role of rapid maxillary expansion in the promotion of oral and general health. Prog Orthod. 2015; 16:33.
3. Almuzian M, Ju X, Almukhtar A, Ayoub A, Al-Muzian L, McDonald JP. Does rapid maxillary expansion affect nasopharyngeal airway? A prospective Cone Beam Computerised Tomography (CBCT) based study. Surgeon 2018; 16(1):1-11.

4. Farronato G, Giannini L, Galbiati G, Pisani L, Mortellaro C, Maspero C. Verification of the reliability of the three-dimensional virtual presurgical orthodontic diagnostic protocol. J. Craniofac. Surg. 2014; 25:2013-16.
5. Farronato G, Giannini L, Galbiati G, Maspero C. Comparison of the dental and skeletal effects of two different rapid palatal expansion appliances for the correction of the maxillary asymmetric transverse discrepancies. Minerva Stomatol 2012; 61:45-55.
6. Zheng W, Zhang X, Dong J, He J. Facial morphological characteristics of mouth breathers vs. nasal breathers: A systematic review and meta-analysis of lateral cephalometric data. Exp Ther Med 2020; 19(6):3738-50.
7. Kiliç N, Oktay H. Effects of rapid maxillary expansion on nasal breathing and some naso-respiratory and breathing problems in growing children: a literature review. Int J Pediatr Otorhinolaryngol 2008; 72(11):1595-601.
8. Maspero C, Cavagnetto D, Abate A, Cressoni P, Farronato M. Effects on the facial growth of rapid palatal expansion in growing patients affected by juvenile idiopathic arthritis with monolateral involvement of the temporomandibular joints: a case-control study on posteroanterior and lateral cephalograms. J Clin Med 2020; 9:1159.
9. Maspero C, Abate A, Cavagnetto D, El Morsi M, Fama A, Farronato M. Available technologies, applications and benefits of teleorthodontics. a literature review and possible applications during the COVID-19 pandemic. J. Clin Med 2020; 9:1891.
10. Maspero C, Farronato M, Bellincioni F, et al. Assessing mandibular body changes in growing subjects: a comparison of CBCT and reconstructed lateral cephalogram measurements. Sci Rep 2020; 10:11722.
11. Niu X, Di Carlo G, Cornelis MA, Cattaneo PM. Three-dimensional analyses of short- and long-term effects of rapid maxillary expansion on nasal cavity and upper airway: A systematic review and meta-analysis. Orthod Craniofac Res. 2020; 23(3):250-76.
12. Koletsi D, Makou M, Pandis N. Effect of orthodontic management and orofacial muscle training protocols on the correction of myofunctional and myoskeletal problems in developing dentition. A systematic review and meta-analysis. Orthod Craniofac Res. 2018; 21(4):202-15.

LETTER TO THE EDITOR

Obstructive sleep apnea syndrome

L. Giannini[1,2], L. Garavelli[1,2], E. Mainardi[1,2], A. De Filippis[1,2] and L. Esposito[1,2]

[1]*Department of Biomedical, Surgical and Dental Sciences, School of Dentistry, University of Milan, Milan, Italy;* [2]*Fondazione IRCCS Cà Granda, Ospedale Maggiore Policlinico, Milan, Italy*

Received September 16, 2020 – Accepted November 27, 2020

To the Editor,

Respiratory disorders during sleep, or Sleep-Disordered Breathing (SDB), constitute a broad spectrum of clinical disorders, represented, by increasing gravity, from simple snoring, Upper Airway Resistance Syndrome (UARS), to Obstructive Sleep Apnea Syndrome (OSAS) (1, 2). Clinical manifestations of these disorders include night snoring, waking headache, daytime drowsiness, and decreased cognitive performance. Symptoms evolve depending on the severity of respiratory obstruction.

In simple snoring, the only disturbance is the habitual night snoring, which mainly involves the sphere of social relations. The individual presents himself in excellent psychophysical condition (1-4). The syndrome of increased resistance of the upper airways in addition to snoring is associated with excessive daytime sleepiness, while in the syndrome of obstructive sleep apnea entails headache on awakening and progressive fatigue that also leads to asthenia. Drowsiness can reach levels that interfere with the patient's everyday activity.

Failure to recognize this condition is particularly serious, as obstructive apnea syndrome during sleep is indiscriminately associated with an increased risk of high blood pressure, cardiovascular disease, daytime sleepiness, road accidents, home and work accidents, and a reduction in cognitive and work capacity with an overall deterioration in the quality of life. For all these reasons, this syndrome is now a real socio-economic problem, therefore strategies are needed to reduce its prevalence and limit its consequences (4-7). These objectives can be achieved by strengthening prevention measures and planning an effective therapeutic approach, preceded by a valid diagnostic process, capable of connecting the condition once it has been established, to improve the quality of life of the patient and to stop the evolution towards long-term complications (8-12).

The purpose of this work is to carry out a systematic review of the literature on obstructive sleep apnea syndrome, highlighting its prevalence, incidence, risk factors, diagnosis, and therapy, with particular reference to orthodontic therapy.

MATERIALS AND METHODS

A systematic review of the literature on obstructive sleep apnea syndrome was conducted through the use of the Medline database (www.ncbi.nim.nih.gov/pub-med). The key words used were: "SDB" sleep-disordered breathing and "OSAS" obstructive sleep apnea syndrome. The articles that provided information about etiology, diagnosis, treatment options, and results were therefore considered. Of the articles found, only those between 1980 and 2020 were selected. Using the limits options, only articles referring to "humans" were considered. Several articles published in unindexed

Key words: obstructive sleep apnea syndrome; respiratory disorders; mandibular advancement device. c pap

Corresponding Author:
Dr Lucia Giannini, DDS,
Postgraduate Specialist in Orthodontics
Ospedale Maggiore Policlinico, Via Francesco Sforza 35,
20122. Milano (Mi), Italy
Tel.: +39 0255032520 - Fax: +39 0255032520
e-mail: luciamariachiaragiannini@gmail.com

0393-974X (2020)
Copyright © by BIOLIFE, s.a.s.
This publication and/or article is for individual use only and may not be further reproduced without written permission from the copyright holder.
Unauthorized reproduction may result in financial and other penalties
DISCLOSURE: ALL AUTHORS REPORT NO CONFLICTS OF INTEREST RELEVANT TO THIS ARTICLE.

journals and some considerations from relevant texts were also added.

RESULTS

From the analysis of the literature and the comparison of the studies conducted by the different Authors, important discrepancies emerge in terms of sample stratification and diagnosis thresholds according to the apnea/hypopnea index. Studies based on a very restrictive definition of the sample population, which only considers individuals with moderate or severe disease who require a continuous positive airway pressure (CPAP) prescription, report a prevalence of 0.5% in the male population of the United States (average age 48.2 years) with Body Mass Index (BMI) of 24.9 kg/m^2 and 1.5% in a population with an average age of 52 years and BMI of 27.1 kg/m^2. In Italy, the prevalence rates of OSAS have only been partially defined. A 1989 study of Italian males aged between 30 and 69 years showed a prevalence of 2.7% of individuals with an Apnea/Hypopnea Index (AHI) value of at least 10/hour and a history of habitual snoring. This estimate rises to 3.5-5% among males in the 40-59 age group. The most recent data obtained from the International Literature Review suggest that the prevalence of OSAS is 2-4% in males and 1-2% in females of average age (3). These are significant values, especially considering that prevalence of obstructive apnea syndrome during sleep is highly underestimated. Even in countries where this condition is widely known, a large percentage of symptomatic individuals remain undiagnosed. Recent estimates attest to more than 5% of adults in Western countries suffer from undiagnosed OSAS and are candidates for treatment. In the United States in 1997, a study on 4,925 adults estimated that 82% of males and 92% of females with moderate or severe OSAS had not yet received diagnosis.

Table I. *OSAS etiology*

Anatomical factors
- adipose filling of the submucosa
- macroscopic anatomical abnormalities
- microscopic anatomical abnormalities
Physiological functional factors
- reduction in activity of the pharyngeal muscles during sleep with a consequent increased resistance to the passage of air
Pathological functional factors
- excessive reduction in activity of the pharyngeal muscles during sleep
- decreased reflexes during sleep

Risk factors and etiology

To date, the interventions have been aimed at reducing body weight, also due to the epidemic spread, especially in Western countries, of food behavior anomalies and the consequent development of alterations in body mass. The causes of OSAS are of anatomical and functional/neurological nature: structural abnormalities, present even during wakefulness, can, however, become obstructive only during sleep due to the characteristic physiological changes in muscle tone; functional abnormalities, unlike structural ones, are present only during sleep (1). The etiology of OSAS is therefore multi-factorial (Table I).

The role of sleep

Sleep plays a two-fold role in OSAS pathophysiology. On the one hand, by reducing muscle tone at the level of the first airways, particularly during REM sleep, the genesis of apnoic/hypopnoic phenomena is an important contributing factor. On the other hand, it suffers the consequences of obstructive events to which the body responds with micro-awakenings that, although they do not reach the level of consciousness, they superficialize sleep and, by far exceeding their physiological number during REM sleep, impoverish it both in quantity and in quality, producing daytime hypersomnolence

and alterations of modulated activities during this phase of sleep, in particular endocrine functions, resulting in a systemic interest of the organism.

Diagnosis

The typical symptoms of the syndrome should therefore be sought, before starting a patient with a suspicion of OSAS on the instrumental diagnostic pathway, with particular regard to habitual snoring (every night) and persistent (for at least 6 months), to respiratory sleep breaks reported by the partner, to awakenings with a feeling of suffocation in a snoring subject (not necessarily habitual), and to daytime drowsiness, possibly quantified through subjective and objective assessment tests (Table II). Useful for diagnostic guidance and possible differential diagnoses is the objective examination with the evaluation of Body Mass Index, abdominal circumference and neck, craniofacial ratios, nasal patency, oral cavity (dentition and tongue), oropharynx, and finally the recording of blood pressure and respiratory, cardiovascular and neurological objectivity, in order to reveal any conditions. Sleep studies represent the reference diagnostic procedures, among which traditional polysomnography, despite changes in reproducibility between night and night in the same subject, is the gold standard for OSAS diagnosis and for the objective evaluation of therapeutic results.

Table II. *Signs and symptoms of obstructive sleep apnea*

Typical
- snoring
- daytime sleepiness
- difficulty concentrating
- unrefreshing sleep
Frequent
- morning headache
- choking during sleep
- testimony of apneas
- irritability and/or personality change
- restless sleep
- nocturia
Uncommon
- secondary hypogonadism (decreased libido, impotence)
- enuresis

The role of orthodontic therapy

The selection criteria proposed by American Sleep Disorders Association (ASDA**)** are only polysomnographic and non-clinical criteria. Although most literature agrees with the limits of obstructive apnea symptoms in patients with initial AHI > 50 values, some authors, including Pancer and Coll. first (1999), support the efficacy of this type of therapy in treating patients with severe OSAS (3). In these cases, however, it is recommended to limit the use of the devices to those who do not run a serious risk to life if they suspend the use of CPAP and to those whose severity suggests tracheostomy as the only therapy. Contraindications relating to the use of an oral device as a first-choice treatment remain, however, cases of severe OSAS with excessive daytime hypersomnolence and marked desaturation of oxygen in the night. The presence of incongruous conservative or prosthetic restorations is also a contraindication of the application of Mandibular Advancement Devices (MAD) and a proper restoration before the application of the device is therefore indicated (9).

Therapeutic success is instead associated with a high percentage of cases of young subjects, who have a thin neck, low BMI, and prevalent or exclusive positionality of respiratory events (supine position). Significant improvements occur in the case of OSAS related to small and/or retruded jaw.

In 2002, Petit and Coll. reported an incidence of 34% of primary contraindications to the use of MAD in 100 patients examined who had carried out a polysomnographic study for a suspected respiratory disorder during sleep:

- insufficient number of teeth for each dental arch (minimum 8 teeth per arch);
- untreated periodontal diseases or excessive dental mobility;
- dysfunctional temporomandibular joint (TMJ) symptoms and/or severe malocclusion. TMJ

pathologies that represent a contraindication are joint and muscle pain, the presence of joint noises, and the limitations in the opening or protruding path of the jaw, need be evaluated individually, but they do not necessarily constitute a contraindication;
- limited mandible protrusion (< 6 mm);
- limited opening of the mouth (< 25 mm).

DISCUSSION

The search for a therapeutic scheme that can effectively respond to the need to heal as many patients as possible still animates a lively scientific debate, open on several fronts, favored by the very nature of the syndrome. The versatility of the symptoms and signs with which OSAS presents itself to the observer from time to time has made the syndrome a subject of study for many specialists. It has been addressed in the recent story of medicine by neurologists specialised in the study of sleep-related pathology, by pneumologists and otolaryngologists, the latter being responsible for the introduction of surgical therapeutic options. The figure of the maxillofacial surgeon has more recently entered the panorama of the management of obstructive sleep apnea syndrome, but his contribution seems to occupy an increasingly important role.

It is now clear that this pathology, given the multisystemic involvement of the organism that characterizes it, is not the subject of one or a few of the specialists mentioned above, but all, with the addition of cardiologists, must be involved in a multidisciplinary diagnostic and therapeutic strategy in the effort to achieve satisfactory therapeutic results in the care of patients suffering from OSAS.

The orthodontist currently plays a major role in managing OSAS and preventing patients from developing snoring. First of all, the help of teleradiography of the skull and cephalometric tracing can identify patients at risk and those who need to undergo further checks. Early diagnosis is crucial in preventing or treating any medical complications when they are at an early stage. Furthermore, the orthodontist also has a role in the treatment of patients suffering from this syndrome: among the therapeutic options, in selected patients, the use of an oral device (comparable to a functional device but to be worn only at night) can be chosen, which is the exclusive competence of the dentist concerning selection and follow-up. Finally, the orthodontist can also intervene in the pre- and post-surgical phase in subjects who must undergo maxillofacial surgery.

Moreover, OAs, and especially MAD, present a viable therapeutic alternative for patients with mild-moderate OSAS or for patients with severe OSAS who cannot tolerate CPAP treatment, as many studies claim. The multidisciplinary approach, therefore, allows better management of MAD therapy and significantly improves the effectiveness of the treatment. Since OSAS is a clinical condition that can seriously compromise the quality and lifespan of those who suffer from it, it is necessary to carry out an early diagnosis and therapeutic programming in order to allow the subject to re-establish his physiological functions. Epidemiological data show a prevalence of 2-4% in the population aged between 20-60 years and a mortality 4 years after diagnosis of 20%, describing the extent of a phenomenon that could become a major health and social problem in the near future. The high costs to public health related to the management of patients with this syndrome and the associated conditions, including cerebral and cardiovascular diseases, road and work accidents, and mood disorders, require the need, on the one hand, to raise awareness among the medical community to promote the recognition of the syndrome that still too often remains unknown and, on the other hand, to arrive at the definition of a diagnostic and therapeutic process that allows effective multidisciplinary classification and treatment for the greater number of patients.

REFERENCES

1. Abate A, Cavagnetto D, Fama A, Matarese M, Lucarelli D, Assandri. F. Short term effects of rapid maxillary expansion on breathing function assessed with spirometry: a case-control study. Saudi Dental Journal 2020; 8(3):65.
2. Flores-Mir C, Korayem M, Heo G, Witmans M, Major MP, Major PW. Craniofacial morphological

characteristics in children with obstructive sleep apnea syndrome: a systematic review and meta-analysis. J Am Dent Assoc 2013;144(3):269-77.

3. Lanteri V, Farronato M, Ugolini A et al. Volumetric changes in the upper airways after rapid and slow maxillary expansion in growing patients: a case-control study. Materials 2020; 13:22-39.
4. Aubertin G, Schröder C, Sevin F, Clouteau F, Lamblin MD, Vecchierini MF. Diagnostic clinique du syndrome d'apnées obstructives du sommeil de l'enfant [Obstructive sleep apnea-hypopnea syndrome in children: Clinical diagnosis]. Arch Pediatr 2017; 24(S1):S7-S15.
5. Baik UB, Suzuki M, Ikeda K, Sugawara J, Mitani H. Relationship between cephalometric characteristics and obstructive sites in obstructive sleep apnea syndrome. Angle Orthod 2002 r;72(2):124-34.
6. Farronato G, Maspero C, Esposito L, Briguglio E, Farronato D, Giannini L. Rapid maxillary expansion in growing patients. Hyrax versus transverse sagittal maxillary expander: a cephalometric investigation. Eur J Orthod 2011; 33(2):185-9.
7. Defabjanis P. Impact of nasal airway obstruction on dentofacial development and sleep disturbances in children: preliminary notes. J Clin Pediatr Dent 2003; 27(2):95-100.
8. Farronato G, Giannini L, Galbiati G, Maspero C. Modified Hyrax expander for the correction of upper midline deviation: a case report. Minerva Stomatol 2011; 60(4):195-204.
9. Marino A, Malagnino I, Ranieri R, Villa MP, Malagola C. Craniofacial morphology in preschool children with obstructive sleep apnoea syndrome. Eur J Paediatr Dent 2009; 10(4):181-84. .
10. Favero L. La distalizzazione molare con il pendulum. Quintessenza Edizioni.
11. Abate A, Cavagnetto D, Fama A, Matarese M, Bellincioni F, Assandri F. Efficacy of operculectomy in the treatment of 145 cases with unerupted second molars: a retrospective case–control study. Dent J 2020; 8:65.
12. Remy F, Bonnaure P, Moisdon P, Burgart P, Godio-Raboutet Y, Thollon L, Guyot L. Preliminary results on the impact of simultaneous palatal expansion and mandibular advancement on the respiratory status recorded during sleep in OSAS children. J Stomatol Oral Maxillofac Surg 2020; S2468-7855(20)30171-3.

LETTER TO THE EDITOR

Conservative treatment of hip osteoarthritis; comparison between three medium/high molecular weight hyaluronic acid injections and two injections of HYADD®4: a randomized controlled double-blind study

N. Setaro, P. Luciani, L. Farinelli and A. Gigante

Department of Clinical and Molecular Science, School of Medicine, Università Politecnica delle Marche, Ancona, Italy

Received September 25, 2020 – Accepted November 27, 2020

To the Editor,

Osteoarthritis (OA) is the most common joint disease in humans. In the literature there are numerous studies on the infiltrative treatment of OA of the knee (1), while there are fewer studies that analyse the infiltrative treatment in hip OA. Hip OA treatment with hyaluronic acid (HA) has proven to be safe and well tolerated with a low complication rate reported by patients (1). Moreover, the use of ultrasound (US) guidance favors an improved and accurate delivery of the injected product (2). Clinical benefit of HA intra-articular injections for OA may rely on different mechanisms of action: mechanical viscosupplementation of the joint, the reestablishment of joint homeostasis by inducing endogenous HA production (3), anti-inflammatory effects and cell stimulation. However, its effectiveness and durability depend largely on the length of its chains and molecular weight (4). HA-based products can be divided into three categories: low/medium molecular weight (LMMW) (MW < 1,000,000 Da); medium/high MHMW (MW between 1,000,000 and 3,000,000 Da) and cross-linked MW (MW > 3,000,000 Da) (4). A new type of HA has been introduced on the market; it is a hexadecylammide of highly purified natural sodium hyaluronate (HYADD®4) obtained by bacterial fermentation (Hymovis®; Fidia Farmaceutici, Abano Terme,Italy). The efficacy and safety of this product has been so far only demonstrated in the treatment of conditions affecting the knee joint through some clinical and preclinical studies. In one of these studies Hymovis® was shown to significantly delay cartilage degeneration, reduce synovial hyperplasia and increase high molecular weight HA synthesis by chondrocytes in a rabbit model with anterior cruciate ligament rupture (5).

The primary aim of the present study was to compare the infiltrative treatment with this new type of reticular HA, compared to infiltrative treatment with medium/high molecular weight HA (MHMW-HA) for the treatment of hip OA. The secondary aim of the study was to evaluate the safety in terms of occurrence of adverse events of these therapeutic approaches in treating hip OA.

MATERIALS AND METHODS

This is a double blind randomised controlled study which was approved by the institutional ethics review board of Università Politecnica delle Marche, Ancona, Italy.

Key words: hip; osteoarthritis; hyaluronic acid; injection; ultrasound guide; orthopedic; conservative treatment; molecular weight

Corresponding Author:
Nicola Setaro, MD
Department of Clinical and Molecular Sciences,
Università Politecnica delle Marche
Via Tronto 10/ 60126, Ancona, Italy
Tel.: +39 071 5963346 - Fax: +39 071 5963341
e-mail: nicola.setaro@libero.it

0393-974X (2020)
Copyright © by BIOLIFE, s.a.s.
This publication and/or article is for individual use only and may not be further reproduced without written permission from the copyright holder.
Unauthorized reproduction may result in financial and other penalties
DISCLOSURE: ALL AUTHORS REPORT NO CONFLICTS OF INTEREST RELEVANT TO THIS ARTICLE.

Patients

Patients affected by primary OA of the hip were enrolled in the study, and all signed informed consent for participation. The radiological classification was performed by anteroposterior pelvic radiography according to the Kellgren-Lawrence (K-L) grading scale (6). The main study inclusion criteria were: patients affected with primary hip OA grade 3 on K-L scale and aged over 40 years. The main study exclusion criteria were: bilateral hip OA; avascular necrosis of the femur head; rheumatoid arthritis; malignancies; and previous hip injuries. Between January 2017 and March 2019 64 patients were recruited. Patients were randomly assigned to one of the two groups. One group (MHMW-HA group; 32 patients) was subjected to 3 intra-articular injections of medium-high molecular weight hyaluronic acid (MHMW-HA) Hyalubrix® 30 mg which is a sterile, non-pyrogenic, viscoelastic solution manufactured with hyaluronic acid sodium salt, obtained by bacterial fermentation from a fraction of high molecular weight (>1500 kDa). The other group (HYADD®4 group) (32 patients) was subjected to 2 intra-articular injections (one every 7 days) of Hymovis® which is a sterile, non-pyrogenic hydrogel manufactured with HYADD®4 derivative of HA obtained by controlled chemical synthesis, with a molecular weight between 500 and 730 kDa. In Hymovis®, 2% of the carboxy radicals on the glucuronic acid present in the polysaccharide chain are conjugated with aliphatic amine (hexadecylamine). This chemical structure makes the three-dimensional lattice of Hymovis® particularly hygroscopic, and forms a hydrogel with excellent viscoelastic, lubricating, and rheological properties, capable of remaining longer inside the joint (7).

Infiltrative technique

Intra-articular injections were performed without anesthesia, on a sterile field, under ultrasound guidance, using a special 7.5 MHz linear probe and a 20G spinal needle (9 or 15 cm in length, depending on the size of the patient). Before the injection, the presence of intra-articular effusion was evaluated (when it was present it was aspirated before injecting the study product). The needle was introduced into the anterior capsule, at the level of the femoral head. Once in contact with the femoral head, the needle was retracted by about 1 mm e the product was injected into the hip joint. Verification of its presence in the intra-articular space was observed by real-time monitoring. The procedure thus performed it usually allows the patient to get up and leave a few minutes after the treatment with the advice to apply ice 2-3 times during the same day.

Follow-up

Each patient underwent a clinical evaluation prior to treatment and then 1, 3, 6 and 12 months after treatment. The clinical evaluation consisted of the subjective global pain assessed by VAS pain score. The intensity of pain, walking capacity and activities of daily life were assessed by the Lequesne algofunctional index. The Western Ontario and McMaster Universities Osteoarthritis index (WOMAC) were also used. Moreover, any adverse events were recorded after each injection and for the entire duration of the study. Double blinding was ensured thanks to a blinded evaluator; the evaluator who performed the clinical evaluation was different from the injector who performed the injections.

Statistical analysis

We calculated that a sample size of 64 patients (32 for each group) would be appropriate for the analysis of the primary outcome, with an estimated effect size of 0.5, 80% of power and two-sided significance levels of 0.05. Values±Standard Deviation (SD) are given as mean±SD. The differences between the two groups of patients for continuous variables were assessed using an unpaired Student's *t*-test or Mann–Whitney test according to the characteristics of the data distribution. A Student *t*-test was used to test pre- and post-operative values±SD of continuous variables. The differences for categorical variables were tested with the *Chi*-squared test. A value of p value <0.05 was considered significant.

RESULTS

Among the 64 patients who participated in the study, 37 were women and 27 were male. The two groups of patients were compared for age, side affected and body mass index (Table I). All injections in both groups were unilateral. The results of the pre-treatment and after 1, 3, 6, 12 months of treatment assessment scales are reported in Table II.

In the MHMW-HA group, the improvement in terms of VAS score, WOMAC score and Lequesne

index could be observed until 3 months after treatment. In contrast the VAS, WOMAC and Lequesne scores showed a reversal of the trend after 6 and 12 months from the treatment; however, the post-treatment results remained better than those pre-treatment. The VAS range was between 6.2±1.5 pretreatment and 4.6±1.5 after 3 months of treatment; WOMAC score values improved from 53.9±5.3 pretreatment to 76.6±5.5 after 3 months of treatment; Lequesne index values improved from 10.7±2.1 pretreatment to 5.1±1.04 after 3 months of treatment.

In the HYADD®4 group, the improvement trend was linear until the sixth month of treatment in terms of WOMAC score and Lequesne index, while the improvement trend of VAS score was linear until the third month of treatment. However, as in the other group, the post-treatment VAS, WOMAC and Lequesne score values remained better than those pre-treatment. In this group the range of the VAS, WOMAC score and Lequesne index was, respectively, from the pre-treatment value of 6.5±1.4, 52.3±5.7 and 11.03±2.04 to a value of 4.2±1.9 after 3 months of treatment for the VAS, and 79.7±5.7 and 4.6±1.5 after 6 months of treatment for the WOMAC and Lequesne.

At the beginning of the study, the mean baseline values of the VAS score, the WOMAC score and the Lequesne index showed no statistically significant differences between the two groups. Likewise, no statistically significant difference was found between the average scores of the two groups at 1 and 3 months after treatment. However, after 6 and 12 months of treatment, statistically significant differences were observed between the two groups in all three assessment scales ($p < 0.05$). In particular,

Table I. *Comparison of age, side affected and body mass index between the two groups.*

	Mean age	Dominant limb	Body mass index
MHMW-HA	62.5±11.4	59%	26.2±3.7
HYADD®4	65.4±10.7	54%	27.9±2.8
p value	0.5	0.2	0.3

Table II. *Clinical outcomes in the MHMW-HA and HYADD®4-HA groups before viscosupplementation and after 1, 3, 6 and 12 months of follow-up.*

	Pretreatment	1 month	3 months	6 months	12 months
VAS MHMW-HA HYADD®4	6.2±1.5 6.5±1.4	4.8±1.9 4.4±2.01	4.6±1.5 4.2±1.9	5.1±1.4 4.3±1.5	5.7±1.1 4.9±1.5
WOMAC score MHMW-HA HYADD®4	53.9±5.3 52.3±5.7	74.2±4.8 75.0±5.1	76.6±5.5 78.9±4.8	68.8±5.5 79.7±5.7	58.6±4.3 62.5±4.7
Lequesne index MHMW-HA HYADD®4	10.7±2.1 11.03±2.04	5.9±1.02 6.2±1.5	5.1±1.04 4.8±1.1	6.8±1.4 4.6±1.5	9.1±2.08 7.9±2.4

the HYADD®4 group showed better outcomes than the MHMW-HA group. Both groups showed a statistically significant clinical improvement already after one month of treatment. No adverse events were observed in either of the two groups during the study period nor after 1, 3, 6 and 12 months of follow-up.

DISCUSSION

Comparison between 2 injections of HYADD4 and 3 MHMW-HA injections showed a statistically significant difference ($p < 0.05$) of the HYADD®4 treatment at 6 and 12 months in all scores evaluated. Furthermore, the greater efficacy of HYADD®4 was also clinically confirmed by the reduction in pain and disability reported by patients. Viscosupplementation has been considered for a long time one of the best conservative treatment for knee OA while its use in the treatment of hip OA was only suggested later (1). HA stimulates various cellular activities, such as migration and proliferation of condrocytes and it also has an anti-inflammatory effect, reducing the expression of various pro-inflammatory cytokines, and relieves pain by acting directly on nociceptors (8). One retrospective study showed that ultrasound-guided HA injection seems to delay total hip replacement in symptomatic hip OA (9). On the contrary, there are very few studies on the long-term effectiveness of this treatment or which formulations of HA give the best results in terms of pain reduction and normal activities resumption (10). Ghosh et al. showed that HAs within an MW range between 0.5 and 1.0 MDa partially restore the rheological properties of synovial fluid and the metabolism of synovial fibroblasts in animal models. These biological activities of HA could explain the reported long-term clinical benefits of this therapy (11). HAs with high molecular weight, including cross-linked HA, are characterized by a greater resistance to degradation compared to LMW HA, resulting in longer persistence in the joint. To our knowledge, the present randomised controlled study is the first to evaluate the effectiveness of a new type of HA constituted of hexadecylammide of highly purified natural sodium hyaluronate (HYADD®4) in the treatment of hip OA. The composition of the product should improve the lubrication and shock absorption function of the synovial fluid, protecting the cartilage from mechanical injuries. These properties combined with the prolonged permanence of the product within the joint could allow a shorter treatment with only 2 injections, reducing risks and discomfort related to the frequency of the procedure. The results of the present randomized controlled study show that 2 intra-articular injections of HYADD®4, performed under ultrasound guidance, represent a safe and effective treatment for osteoarthritis of the hip.

REFERENCES

1. Gigante A, Callegari L. The role of intra-articular hyaluronan (Sinovial) in the treatment of osteoarthritis. Rheumatol Int 2011; 31(4):427-44.
2. Migliore A, Tormenta S, Laganà B, Piscitelli P, Granata M, Bizzi E, et al. Safety of intra-articular hip injection of hyaluronic acid products by ultrasound guidance: an open study from ANTIAGE register. Eur Rev Med Pharmacol Sci 2013; 17(13):1752-59.
3. Nguyen C, Lefèvre-Colau M-M, Poiraudeau S, Rannou F. Evidence and recommendations for use of intra-articular injections for knee osteoarthritis. Ann Phys Rehabil Med 2016; 59(3):184-89.
4. Rayahin JE, Buhrman JS, Zhang Y, Koh TJ, Gemeinhart RA. High and low molecular weight hyaluronic acid differentially influence macrophage activation. ACS Biomater Sci Eng 2015; 1(7):481-93.
5. Mainil-Varlet P, Schiavinato A, Ganster MM. Efficacy evaluation of a new hyaluronan derivative HYADD® 4-G to maintain cartilage integrity in a rabbit model of osteoarthritis. Cartilage 2013; 4(1):28-41.
6. Kellgren JH, Lawrence JS. Radiological assessment of osteo-arthrosis. Ann Rheum Dis 1957; 16(4):494-502.
7. Priano F. Early efficacy of intra-articular HYADD® 4 (Hymovis®) injections for symptomatic knee osteoarthritis. Joints 2017; 5(2):79-84.
8. Moskowitz RW. Hyaluronic acid supplementation. Curr Rheumatol Rep 2000; 2(6):466-71.
9. Migliore A, Bella A, Bisignani M, et al. Total hip replacement rate in a cohort of patients affected by symptomatic hip osteoarthritis following intra-articular sodium hyaluronate (MW 1,500-

2,000 kDa) ORTOBRIX study. Clin Rheumatol 2012; 31(8):1187-96.
10. Lieberman JR, Engstrom SM, Solovyova O, Au C, Grady JJ. Is intra-articular hyaluronic acid effective in treating osteoarthritis of the hip joint? J Arthroplasty 2015; 30(3):507-11.
11. Ghosh P, Guidolin D. Potential mechanism of action of intra-articular hyaluronan therapy in osteoarthritis: are the effects molecular weight dependent? Semin Arthritis Rheum 2002; 32(1):10-37.